Control of adipocyte differentiation and metabolism by mitogen-activated protein kinase (MAPK)-interacting kinases (MNKs)

James Edward Merrett

A dissertation submitted to The University of Adelaide in candidature for the degree of Doctor of Philosophy in the Faculty of Sciences

February 2020

THE UNIVERSITY of ADELAIDE

Department of Molecular and Biomedical Science
School of Biological Sciences
The University of Adelaide

Contents

List of Tables 10

List of Figures 11

List of Appendices 14

Abstract 15

Declaration 16

Acknowledgements 17

Dedication 18

Abbreviations 19

Chapter 1 Introduction 21

Study preface 22

MAPK-interacting kinases (MNKs) 22

Structure and activity of the MNKs 22

MNK isoforms in humans 22

Subcellular localisation 23

MAPK signalling pathways 25

Overview of MAPK signalling 25

Biological functions of the MNKs 27

eIF4E and mRNA translation initiation 27

Oncology and cell transformation 30

Additional MNK substrates 30

MNK2-specific protein activities 31

Development of small molecule MNK inhibitors 31

Adipose tissue development 32

Overview of adipose tissue function 32

Origin and lineage commitment of adipocytes 33

Transcriptional regulation of adipogenesis 33

CCAAT/enhancer binding protein (C/EBP)-β and δ 34

CCAAT/enhancer binding protein-α (C/EBPα) 36

C/EBP homologous protein (CHOP) 36

Translational regulation of C/EBPβ 37
Translational regulation of C/EBPα 37
Peroxisome proliferator-activated receptor-γ (PPARγ) 38
Transcriptional pathway of adipogenesis 42
MAPK signalling and adipogenesis 42
ERK pathway 42
p38 MAPK pathway 43
The rising obesity epidemic and the need for new solutions 44
MNKs are implicated in metabolic disease 44
Weight gain 44
Glucose uptake and diabetes 44
Diet-induced obesity and adipogenesis 45
Study hypotheses and aims 46
Aim 1 46
Aim 2 46
Aim 3 46
Chapter 2 Materials and Methods 48
Tissue culture methods 49
Cell lines 49
Culture media and growth conditions 49
Sub-culturing 49
Trypan Blue exclusion 49
Cryo-preservation of cells 49
Resuscitation of cryopreserved cells 50
Animal studies 50
Isolation of mouse embryonic fibroblasts (MEFs) 50
Maintenance of MEFs 51
3T3-L1 pre-adipocyte differentiation 51
Oil Red O (ORO) Staining 51
Quantification of Oil Red O Staining by Image J 52

Gene silencing by small interfering RNA (siRNA) 52
siRNA efficacy testing 53
Metabolic assays 53
Molecular biology methods 54
RNA isolation from cell cultures 54
RNA isolation from tissues 54
Reverse transcription 55
Real time-qPCR (RT-qPCR) using SYBR Green 55
Primer efficiency testing 57
RT-qPCR using TaqMan gene expression assays 57
RT-PCR of cdc2-like kinase (*Clk*) pre-mRNA 59
Extraction of protein 60
Bradford protein assay 60
Pouring gels for sodium dodecyl sulphate–polyacrylamide gel electrophoresis (SDS-PAGE) 61
Western blot 61
Re-probing membranes 63
DNA extraction 63
Routine PCR 63
Agarose gel electrophoresis 64
Sanger sequencing 65
Bacterial transformation 65
Mini-preparation of plasmid DNA 66
Midi-preparation of plasmid DNA 66
Identification of DNA response element binding sites 66
Chromatin immunoprecipitation (ChIP) 66
Assessing protein-protein interactions 70
Cell cycle and size analysis 70
Statistics 71
CRISPR-Cas9 genetic editing methods 71
Construction of GeneART CRISPR-EGFP vector 71

Single guide RNA (sgRNA) design and selection 72
Annealing, phosphorylation and ligation of sgRNAs 72
Screening vectors with successfully ligated sgRNA 74
Nucleofection of sgRNA-GeneART CRISPR vectors 74
Fluorescence-activated cell sorting (FACS) of $CD4^+/EGFP^+$ cells 75
Screening of *Mknk2*-KO clones 75
Chapter 3 MNKs and eIF4E in 3T3-L1 pre-adipocyte differentiation 76
Introduction 77
Results 79
Expression of MNK1/2 in 3T3-L1 pre-adipocytes 79
Analysis of adipogenic factor expression in 3T3-L1 pre-adipocytes 79
Analysis of ERK1/2, protein kinase B (PKB) and mTORC1 signalling in 3T3-L1 pre-adipocytes 80
Interim Conclusion 80
Analysis of early gene expression in 3T3-L1 pre-adipocytes using individual components of the adipogenic induction medium 83
Interim Conclusion 84
Identification of CREs and GREs in *Cebpb, Cebpd, Mknk1* and *Mknk2* 84
Occupancy of CREB and GR at CRE and GREs in *Cebpb, Cebpd, Mknk1* and *Mknk2* 86
Interim Conclusion 95
Regulation of *Mknk2* expression by terminal differentiation factors 95
Interim Conclusion 99
Efficacy of *Mknk1/2* small interfering RNAs (siRNAs) 99
Relative activity of MNK isoforms in 3T3-L1 pre-adipocytes 101
Interim Conclusion 101
Effect of CGP57380 on 3T3-L1 pre-adipocyte differentiation 101
Interim Conclusion 106
MNK-I1: a thienopyrimidine derivative and candidate MNK inhibitor 106
Efficacy of MNK-I1 in 3T3-L1 pre-adipocytes 106
Effect of CGP57380 and MNK-I1 on mTORC1 signalling 109

Interim Conclusion 109
Effect of MNK-I1 on 3T3-L1 pre-adipocyte differentiation 110
Interim Conclusion 115
Refinement of MNK-I1 inhibitor treatment period 115
Effect of MNK-I1 pre-treatment on 3T3-L1 pre-adipocyte differentiation 116
Effect of MNK-I1 on CREB and GR expression and activation 118
Effect of MNK-I1 pre-treatment on terminal adipocyte differentiation 123
Interim Conclusion 123
Effect of MNK-I1 on C/EBPβ phosphorylation 123
Identification of C/EBP response elements on *Cebpa* and *Pparg* gene promoters and the effect of MNK-I1 on occupancy of C/EBPβ 124
Identification of PPAR response element on *Cebpa* promoter and effect of MNK-I1 on occupancy of PPARγ 124
Effect of MNK-I1 on the auto-regulatory expression of *Cebpa* 130
Effect of MNK-I1 on the occupancy of C/EBPα in *Pparg1* and *2* 130
Interim Conclusion 130
Events preceding C/EBPα and PPARγ expression in adipogenesis 130
Effect of MNK-I1 on MCE 131
Analysis of cell cycle factor expression during G1 to S-phase transition 131
Effect of MNK-I1 on RB hyper-phosphorylation and D-cyclin expression 136
Interim Conclusion 138
Alternative splicing and cell cycle progression 138
Regulation of CLK1/4 expression through alternative splicing 139
Dosage of TG003 in 3T3-L1 pre-adipocytes 139
Effect of TG003 on 3T3-L1 adipocyte differentiation 142
Comparison of MNK and CLK inhibition on 3T3-L1 adipocyte differentiation 142
Interim Conclusion 145
Comparison of CLK and MNK inhibition on MCE 145
Effect of TG003 on D-cyclin expression 148
Interim Conclusion 148

Efficacy of *Clk1/4* siRNA....148
Delineating the cause of impaired differentiation: requirement for selective MNK inhibitors....154
Efficacy of MNK-7g, ETC-206 and eFT508 in 3T3-L1 pre-adipocytes....154
Effect of MNK-7g, ETC-206 and eFT508 on auto-inhibitory regulation of CLK1/4....157
Interim Conclusion....158
Effect of selective MNK inhibition on 3T3-L1 pre-adipocyte differentiation....158
Effect of MNK-7g on pre-adipocyte differentiation....159
Interim Conclusion....159
Discussion....166
Chapter 4 Role of MNK2 in 3T3-L1 pre-adipocyte differentiation....171
Introduction....172
Results....173
Expression analysis of MNK1/2 in mouse adipose tissue (AT)....173
Interim Conclusion....176
MNK2-KO CRISPR/Cas9 gene editing strategy....176
Construction of GeneART CRISPR-EGFP vector....179
Annealing and ligation of sgRNA oligonucleotide duplexes....179
Generation of single-cell $CD4^+$/$EGFP^+$ 3T3-L1 colonies....179
Interim Conclusion....179
External PCR screening of 3T3-L1-2KO colonies....180
Internal PCR screening of 3T3-L1-2KO colonies....183
Interim Conclusion....185
Analysis of P-eIF4E levels in 3T3-L1-2KO clones....185
Validation of 3T3-L1-2KO genotype by Sanger sequencing....185
Interim Conclusion....186
Assessment of 3T3-L1-2KO differentiation potential....187
Interim Conclusion....189
Effect of clonal selection on adipogenic propensity....191
Interim Conclusion....192
Effect of CRISPR-Cas9 methodology on adipogenic propensity....194

Interim Conclusion 194
Analysis of CRISPR-Cas9 off-targets induced by sgRNAs 197
Interim Conclusion 199
Analysis of non-responsive 3T3-L1-2KO clone (1-6B) 199
Interim Conclusion 200
Analysis of impaired 3T3-L1-2KO clones (1-7B and 4-8E) 200
Interim Conclusion 204
Interim Conclusion 205
Analysis of normal differentiation 3T3-L1-2KO clones (2-11D and 4-11F) 205
Interim Conclusion 205
Analysis of enhanced differentiation 3T3-L1-2KO clones (2-2E and 4-7C) 210
Interim Conclusion 210
Effect of siMknk2 on adipogenesis and lipid accumulation 210
Interim Conclusion 213
Discussion 218
Chapter 5 MNKs in adipocyte and lipid metabolism 222
Introduction 223
Results 224
Adipocytes and the balance of energy metabolism 224
Effect of MNK2 knockdown on metabolic gene expression 225
Interim Conclusion 231
Effect of siMknk2 on metabolic protein expression 232
Interim Conclusion 232
Effect of si*Mknk2* on the rate of lipolysis 235
Effect of individual si*Mknk2* on metabolic gene expression 235
Interim Conclusion 238
Gene expression changes in MNK-2KO and double KO (DKO) adipocytes 238
Interim Conclusion 241
Effect of eFT508 on metabolic gene expression 241
Effect of eFT508 on metabolic protein expression and lipolysis 241

Interim Conclusion 246
Effect of si*Mknk1* on metabolic gene expression 246
Interim Conclusion 249
Regulation of ChREBP expression and glucose uptake by MNK2 249
Effect of individual siRNA on ChREBP expression and glucose uptake 252
Interim Conclusion 252
Role of MNK2 in the regulation of glycolytic flux 252
Interim Conclusion 253
Regulation of ChREBP nuclear translocation by MNK2 253
Interim Conclusion 255
Prediction of MNK2 protein interactions 258
Interim Conclusion 261
Metabolic changes induced by si*Mknk2* post-adipogenesis 261
Interim Conclusion 262
Discussion 267
Chapter 6 Discussion, Future Perspectives and Limitations 271
Key findings and future work 272
Future perspectives 277
Limitations 278
Appendices 281
References 304

List of Tables

Table 2-1: SilencerSelect siRNA assays. 53
Table 2-2: QuantiNova Reverse Transcription Program 55
Table 2-3: Components required for Fast SYBR mastermix assembly. 56
Table 2-4: Fast SYBR RT-qPCR cycling conditions. 56
Table 2-5: Primers used for RT-qPCR gene expression analyses. 57
Table 2-6: TaqMan assay probes used for RT-qPCR gene expression analyses. 58
Table 2-7: Components required for Fast TaqMan mastermix assembly. 59
Table 2-8: TaqMan RT-qPCR cycling conditions. 59
Table 2-9: Primers used for *Clk* splicing product analyses. 59
Table 2-10: Components required for *Clk* PCR primer mastermix assembly. 59
Table 2-11: Thermocycler reaction conditions for *Clk* splicing product amplification. 60
Table 2-12: Formulation of SDS acrylamide/bis-acrylamide gels used for PAGE 61
Table 2-13: Primary antibodies used for detection of proteins by Western blot. 62
Table 2-14: Secondary antibodies used for fluorescent detection of primary antibody 63
Table 2-17: Assembly of components for routine PCR reactions 63
Table 2-18: Thermocycling conditions for routine PCR. 64
Table 2-19: PCR primer sequences, their required annealing temperature and extension times. 64
Table 2-20: Assembly of components required for Sanger sequencing of purified DNA. 65
Table 2-21: Sanger sequencing primer sequences. 65
Table 2-22: Antibodies used for ChIP. 68
Table 2-23: RT-qPCR cycling conditions used for ChIP 68
Table 2-24: Primers used for enrichment of protein-bound DNA regions. 69
Table 2-25: *Eco*RI and *Age*I restriction digestion 71
Table 2-26: Ligation of EGFP CDS into GeneART CRISPR backbone. 72
Table 2-27: Single-guide RNA (sgRNA) sequences selected for the KO of *Mknk2*. 72
Table 2-28: sgRNAs oligonucleotide sequences. 72
Table 2-29: Assembly of components for annealing of sgRNA oligonucleotides. 73
Table 2-30: Thermocycling conditions for annealing of sgRNA oligonucleotides. 73
Table 2-31: Assembly of components for *Bae*I linearisation of GeneART CRISPR vector. 73
Table 2-32: Assembly of components for ligation of sgRNA into GeneART CRISPR vector. 74
Table 2-33: Assembly of components for sequential *Bae*I and *Eco*RI restriction digestion. 74
Table 4-1: Summary of 3T3-L1 *Mknk2*-KO genomic screening. 184
Table 4-2: sgRNA off-targets as predicted *in silico*. 197
Table 5-1: Comparison of *in vitro* and *in vivo* effects of MNK2 knockdown. 239

List of Figures

Figure 1-1: Structural domain features of MNK1/2. 24
Figure 1-2: Mitogen-activated protein kinase (MAPK) signalling pathways....26
Figure 1-3: Assembly of the mRNA translation initiation complex. 28
Figure 1-4: Regulation of mRNA translation initiation by mTORC1. 29
Figure 1-5: Adipogenic transcriptional cascade. 41
Figure 1-6: Aspects of adipocyte biology that are to be investigated in this study. 47
Figure 3-1: Overview of MNK1/2 and adipogenic factor expression during 3T3-L1 adipogenesis. 82
Figure 3-2: Control of early adipogenic signalling by components of the adipogenic induction medium. 85
Figure 3-3: Identification of CREB and GR binding sites on the *Cebpb* promoter. 88
Figure 3-4: Identification of CREB and GR binding sites on the *Cebpd* promoter. 90
Figure 3-5: Identification of CREB and GR binding sites on the *Mknk1* promoter. 92
Figure 3-6: Identification of CREB and GR binding sites on the *Mknk2* promoter. 94
Figure 3-7: Identification of PPARγ and C/EBP binding sites on the *Mknk2* promoter. 98
Figure 3-8: Efficacy of *Mknk1/2* small interfering RNA (siRNA). 100
Figure 3-9: Basal and stimulated activity of MNK1/2 in 3T3-L1 pre-adipocytes. 103
Figure 3-10: Effect of CGP57380 on 3T3-L1 pre-adipocyte differentiation. 105
Figure 3-11: Efficacy, stability and specificity of MNK-I1 in 3T3-L1 pre-adipocytes. 108
Figure 3-12: Effect of MNK-I1 on 3T3-L1 pre-adipocyte differentiation. 112
Figure 3-13: Effect of MNK-I1 on early 3T3-L1 pre-adipocyte differentiation. 113
Figure 3-14: Effect of MNK-I1 on terminal adipogenesis in 3T3-L1 pre-adipocytes. 114
Figure 3-15: Refinement of MNK-I1 treatment period during 3T3-L1 pre-adipocyte differentiation. 117
Figure 3-16: Effect of MNK-I1 pre-treatment on 3T3-L1 pre-adipocyte differentiation. 120
Figure 3-17: Effect of MNK-I1 pre-treatment on terminal adipogenesis in 3T3-L1 pre-adipocytes. 122
Figure 3-18: Effect of MNK-I1 on C/EBPβ phosphorylation and promoter occupancy. 126
Figure 3-19: Effect of MNK-I1 on PPARγ promoter occupancy. 128
Figure 3-20: Effect of MNK-I1 on C/EBPα promoter occupancy. 129
Figure 3-21: Effect of MNK-I1 on mitotic clonal expansion (MCE). 134
Figure 3-22: Analysis of cell cycle factor expression by adipogenic stimuli. 135
Figure 3-23: Effect of MNK-I1 on cell cycle factor expression. 137
Figure 3-24: *Clk1/4* alternative splicing and dosage of TG003 in 3T3-L1 pre-adipocytes. 141
Figure 3-25: Effect of TG003 on 3T3-L1 pre-adipocyte differentiation. 144
Figure 3-26: Comparing the effect of TG003 and MNK-I1 on 3T3-L1 pre-adipocyte differentiation. 147

Figure 3-27: Effect of TG003 and MNK-I1 on MCE. 150
Figure 3-28: Efficacy of *Clk1/4* siRNA. 152
Figure 3-29: Efficacy and specificity of MNK-7g, ETC-206 and eFT508 in 3T3-L1 pre-adipocytes. 156
Figure 3-30: Effect of MNK inhibition on auto-inhibitory regulation of *Clk1/4*. 157
Figure 3-31: Effect of ETC-206 on 3T3-L1 pre-adipocyte differentiation. 160
Figure 3-32: Effect of eFT508 on 3T3-L1 pre-adipocyte differentiation. 162
Figure 3-33: Effect of MNK-7g on 3T3-L1 pre-adipocyte differentiation. 163
Figure 3-34 Effect of MNK-7g on terminal adipogenesis in 3T3-L1 pre-adipocytes. 165
Figure 4-1: *Mknk1/2* adipose tissue expression analysis. 175
Figure 4-2: CRISPR-Cas9 *Mknk2* gene KO approach. 178
Figure 4-3: Genomic screening of *Mknk2*-KO in 3T3-L1 clones. 182
Figure 4-4: Levels of P-eIF4E in 3T3-L1-2KO clones. 187
Figure 4-5: Comparison of 3T3-L1-2KO adipogenic propensity. 191
Figure 4-6: Effect of clonal derivation on 3T3-L1 adipogenic propensity. 193
Figure 4-7: Effect of CRISPR-Cas9 methodology on 3T3-L1 adipogenic propensity. 196
Figure 4-8: Adipogenic differentiation of non-responsive clone (1-6B). 201
Figure 4-9: Adipogenic differentiation of impaired clone (1-7B). 202
Figure 4-10: Adipogenic differentiation of impaired clone (4-8E). 203
Figure 4-11: Cell cycle factor expression during differentiation of impaired clone (1-7B) 206
Figure 4-12: Cell cycle analysis of impaired clone (1-7B) during MCE 207
Figure 4-13: Adipogenic differentiation of normal clone (2-11D). 208
Figure 4-14: Adipogenic differentiation of normal clone (4-11F). 209
Figure 4-15: Adipogenic differentiation of enhanced clone (2-2E). 211
Figure 4-16: Adipogenic differentiation of enhanced clone (4-7C). 212
Figure 4-17: Effect of *Mknk2* siRNA knockdown on 3T3-L1 adipogenesis. 215
Figure 4-18: Comparison of individual si*Mknk2* on 3T3-L1 adipogenesis. 217
Figure 5-1: Lipogenic and lipolytic pathways in adipocytes. 226
Figure 5-2: Effect of si*Mknk2* on metabolic gene expression during 3T3-L1 adipogenesis 228
Figure 5-3: Effect of si*Mknk2* on metabolic protein expression during 3T3-L1 adipogenesis. 234
Figure 5-4: Effect of individual si*Mknk2* on metabolic gene expression. 237
Figure 5-5: Effect of eFT508 on metabolic gene expression during 3T3-L1 adipogenesis. 243
Figure 5-6: Effect of eFT508 on metabolic protein expression during 3T3-L1 adipogenesis. 245
Figure 5-7: Effect of si*Mknk1* on metabolic gene expression during 3T3-L1 adipogenesis 248
Figure 5-8: Effect of si*Mknk2* on glucose metabolism in 3T3-L1 adipocytes. 251
Figure 5-9: Effect of si*Mknk2* on lactate production in 3T3-L1 adipocytes. 254
Figure 5-10: Identification of ChoRE elements in ChREBP-responsive genes. 257
Figure 5-11: Predicted protein interactions with MNK2. 260

Figure 5-12: Inducible effects of si*Mknk2* on metabolic gene expression. 264
Figure 5-13: Regulation of 3T3-L1 adipocyte metabolism by MNK2.....266
Figure 6-1: Graphical abstract of thesis findings.....280

List of Appendices

Appendix 1: Generation of GeneART CRISPR-EGFP vector. 282
Appendix 2: Sanger sequencing alignment of the EGFP CDS and flanking regions of the GeneART CRISPR-EGFP vector. 283
Appendix 3: Ligation of *Mknk2* E4 and *Mknk2* E5 sgRNAs into GeneART CRISPR vectors. 284
Appendix 4: Verification of sgRNA cloning. 286
Appendix 5: Sanger sequencing alignment of Clone 1-6B. 287
Appendix 6: Sanger sequencing alignment of Clone 1-7B. 288
Appendix 7: Sanger sequencing alignment of Clone 1-8E. 289
Appendix 8: Sanger sequencing alignment of Clone 2-2E. 290
Appendix 9: Sanger sequencing alignment of Clone 3-2G. 291
Appendix 10: Sanger sequencing alignment of Clone 4-7C. 292
Appendix 11: Sanger sequencing alignment of Clone 4-8E. 293
Appendix 12: Sanger sequencing alignment of Clone 4-11F. 294
Appendix 13: Off-targets of sgRNA *Mknk2* E4. 295
Appendix 14: Off-targets of sgRNA *Mknk2* E5. 300

Abstract

The mitogen-activated protein kinase (MAPK)-interacting kinases (MNKs) are a family of serine/threonine protein kinases that are activated downstream of the ERK1/2 (extracellular regulated kinase) and p38α/β MAPK pathways. The MNKs are encoded on separate genes, *Mknk1* and *Mknk2*, giving rise to two proteins in mice, MNK1 and MNK2, respectively. The MNKs have previously been implicated in metabolic disease and shown to regulate weight gain in mice in response to an energy-rich high-fat diet (HFD). In particular, MNK2-knockout (KO) mice are protected from HFD-induced weight gain and therefore, MNK2 is proposed to regulate adipose tissue expansion. Adipose tissue acts as a stable, long term energy reserve that can be readily mobilised, and plays an important role in regulating whole-body energy homeostasis. It is suggested that MNK activity may be required for the differentiation of new fat cells (adipocytes) and increasing adipocyte lipid storage; however, the function and underlying mechanisms of the MNKs in these processes are yet to be determined.

Using the well-established mouse 3T3-L1 *in vitro* model of adipogenesis, the role of the MNKs in adipocyte differentiation (adipogenesis) and lipid storage was investigated. Inhibition of MNK activity using specific inhibitors failed to impair adipogenesis or lipid accumulation, suggesting MNK activity is not required for adipocyte differentiation and does not regulate lipid storage. Despite this, expression analysis revealed MNK2 to be the predominant isoform in adipose depots. Therefore, to investigate the role of MNK2 specifically in these processes, a 3T3-L1-2KO cell model was generated using CRISPR-Cas9 and small-interfering RNA (siRNA)-mediated knockdown of *Mknk2* was also used. Intriguingly, the knockdown of MNK2 was found to decrease lipid accumulation in adipocytes, suggesting non-catalytic functions of MNK2 regulate adipocyte metabolism.

It was revealed that MNK2 likely regulates the levels of two major lipogenic transcription factors, ChREBP (carbohydrate response element binding protein) and LPIN1 (Lipin-1), through novel protein-protein interactions. These factors are largely responsible for activating expression of genes in synthetic processes that promote lipid storage in adipocytes, namely *de novo* lipogenesis (DNL) and triglyceride synthesis. The knockdown of MNK2 also increases the expression of HSL (hormone-sensitive lipase) which increases the breakdown (lipolysis) of stored triglyceride. Herein, a model in which the knockdown of MNK2 *in vitro* accounts for a significant reduction in adipocyte lipid accumulation is proposed.

These findings identify MNK2 as a regulator of adipocyte metabolism and reveal some of the underlying MNK2-driven mechanisms that promote adipose tissue expansion. The development of an MNK2-targeted therapy may therefore be a useful intervention for reducing weight caused by excessive nutrient intake.

Declaration

I certify that this work contains no material which has been accepted for the award of any other degree or diploma in my name in any university or other tertiary institution and, to the best of my knowledge and belief, contains no material previously published or written by another person, except where due reference has been made in the text. In addition, I certify that no part of this work will, in the future, be used in a submission in my name for any other degree or diploma in any university or other tertiary institution without the prior approval of the University of Adelaide and where applicable, any partner institution responsible for the joint award of this degree.

I give permission for the digital version of my thesis to be made available on the web, via the University's digital research repository, the Library Search and also through web search engines, unless permission has been granted by the University to restrict access for a period of time.

I acknowledge the support I have received for my research through the provision of an Australian Government Research Training Program Scholarship.

…… …….

James Edward Merrett Date

Acknowledgements

This PhD would not have been possible without the support of a number of people; I wish to duly acknowledge these individuals and their contribution to this Thesis.

Chris, thank you for the opportunity to undertake my PhD in your laboratory, and your guidance, insight and support throughout. I was reassured by your belief in my abilities, the confidence you shared for my project and the direction in which I chose to lead it. I am also incredibly grateful for Peter and the dedication you have shown as my co-supervisor; your perspective, encouragement and counsel have been most helpful and reassuring.

I am greatly indebted to Kirk for your supervision during the early stages of my project and instilling in me the technical knowledge, skills and attributes of a good scientist. I will carry these things with me forever in my career going forward. I would also like to thank Claire for the work that you did that preceded my project and for your early guidance in the laboratory.

This PhD has not been an easy ride and I would not be where I am today without the support of my close friends: Nick, Anna, Jodie and Soni. Thank you for your emotional support, encouragement and always being there as a shoulder to lean on.

I would also like to acknowledge my dear friends and colleagues Wan Xian and Lauren for being there from what seems like the very beginning. You have been most helpful and supportive as laboratory assistants and am grateful for the fun times we had working together.

I want to acknowledge the support that I have received from fellow students: Roman, Shuye, Sanuja, Andrew and Julian; navigating this PhD journey together has made it more endurable and enjoyable.

To my parents, I am indebted for the support you have provided me during this time. Thank you to my brothers for having faith in my abilities and helping to put things in perspective, and to Grandma and Grandpa for your inspiring and unwavering support; it has been a pleasure to see your genuine and keen interest in my research. To Nan, I am grateful for the times we spent together that always served as a pleasurable momentary distraction from the rigours of my PhD. The optimism you hold for my future has been an inspiration and helped carry me through.

A special thank you to Sophie for your encouragement and careful proof-reading of this manuscript.

Lastly, I am forever grateful for Catherine and Jeni. Thank you for being there when I needed you most and navigating me through some difficult periods. I am a stronger and finer person because of you.

Dedication

For Claire Weekes; your incredible insight, wisdom and scientific endeavour

Abbreviations

4E-BP	eIF4E-binding protein
AGPAT	acyl-glycerophosphate acyltransferase
ATGL	adipose triglyceride lipase
C/EBP	CCAAT/enhancer binding protein
C/EBPRE	C/EBP response element
cAMP	cyclic adenosine monophosphate
Cas9	CRISPR-associated protein 9
CDK	cyclin-dependent kinase
cDNA	complementary DNA
ChIP	chromatin immunoprecipitation
CHOP	C/EBP homologous protein
ChoRE	carbohydrate response element
ChREBP	carbohydrate response element binding protein
CLK	cdc2-like kinase
CRE	cAMP response element
CREB	cAMP response element-binding protein
CRISPR	clustered regularly interspaced short palindromic repeats
DAG	diacylglycerol
DEX	dexamethasone
DGAT	diacylglycerol-acyltransferases
DMSO	dimethyl sulfoxide
DNL	*de novo* lipogenesis
DSB	double-stranded break
EGFP	enhanced green fluorescent protein
eIF4E	eukaryotic initiation factor 4E
ERK	extracellular regulated kinase
FA	fatty acid
FABP4	fatty acid binding protein 4
FACS	fluorescence-assisted cell sorting
FASN	fatty acid synthase
FFA	free-fatty acid
GPAT	glycerol-3-phosphate acyltransferase
GR	glucocorticoid receptor
GRE	glucocorticoid response element
HFD	high-fat diet
HSL	hormone-sensitive lipase
IBMX	3-isobutyl-1-methylxanthine

LAP	liver-enriched transcriptional activator protein
LIP	liver-enriched inhibitory protein
LPIN1	lipin 1
MAG	monoacylglycerol
MAPK	mitogen-activated protein kinase
MCE	mitotic clonal expansion
MEFs	mouse embryonic fibroblasts
MGL	monoacylglycerol lipase
MK2	MAPK-activated protein kinase 2
MNK	MAPK-interacting kinase
mRNA	messenger RNA
MSC	mesenchymal stem cell
mTORC1	mammalian target of rapamycin complex 1
ORO	oil red o
PAGE	polyacrylamide gel electrophoresis
PBS	phosphate-buffered saline
PCR	polymerase chain reaction
PKA	cAMP-dependent protein kinase / protein kinase A
PLIN1	perilipin 1
PPARγ	peroxisome proliferator-activated receptor gamma
PPARE	peroxisome proliferator-activated receptor response element
PTRF	polymerase I and transcript release factor
RB	retinoblastoma
ROSI	rosiglitazone
RT-PCR	reverse-transcription PCR
RT-qPCR	real-time quantitative PCR
SDS	sodium dodecyl sulphate
SDS-PAGE	SDS-polyacrylamide gel electrophoresis
sgRNA	single guide RNA
siRNA	small interfering RNA
SREBP	sterol regulatory element-binding protein
SRSF	serine- and arginine-rich splicing factor
TAG	triacylglycerol / triglyceride
TNFα	tumor necrosis factor alpha
WT	wildtype

Chapter 1
Introduction

Study preface

The ability to sense and respond to changes in the extra- and intra-cellular environment is essential for regulating changes in gene expression, which in turn is critical for maintaining the normal functioning of cells and organisms. The ability of cells to respond to changes in nutrient level, growth factors, hormones, as well as cell stress, requires the integration of coordinated signalling networks. Dysregulated cell signalling can lead to dysfunction and cellular abnormalities, which may ultimately lead to diseases, notably cancers. The mitogen-activated protein kinase (MAPK)-interacting kinases (MNKs), which are downstream effectors of pathways regulating growth, proliferation, differentiation and stress, have been implicated in metabolic disease and in mediating adverse responses to high-fat feeding [1–3]. In this Thesis, the role of the MNKs in driving these responses, specifically in adipocytes was investigated.

MAPK-interacting kinases (MNKs)

Structure and activity of the MNKs

A two-hybrid and novel kinase screen used to identify extracellular regulated kinase (ERK) 1/2 substrates ultimately led to the discovery of the MNKs [4,5]. MNK1 and MNK2 are serine/threonine kinases and encoded on separate genes in mice, *Mknk1* and *Mknk2*, respectively. The kinases exhibit similarity in their primary sequence (78% homology) and contain similar structural motifs: an N-terminal basic amino acid region that mediates localisation, a catalytic kinase domain; and an MAPK-binding domain in their carboxy-termini (Figure 1-1) [5].

The MNKs are activated by phosphorylation of two threonine residues in their T-loop activation domain (Thr197/Thr202) as catalysed by ERK or p38 MAPK [5–7] (Figure 1-1). MNK1/2 share similar N-terminal regions that consist of a polybasic sequence involved in binding to eIF4G [8] but they differ in their C-termini MAPK-binding domains that facilitate interactions with ERK and p38 MAPK [9,10]. MNK1 binds both ERK and p38 MAPK, which strongly induce its low basal activity [9]. In contrast, MNK2 binds strongly only to only activated ERK and this is thought to be responsible for its constitutive high basal activity, which is not further enhanced by stimuli [10]. MNK1/2 are responsible for phosphorylating eukaryotic initiation factor 4E (eIF4E) [7,8,11,12], which is the only *in vivo* validated substrate of the MNKs [13].

MNK isoforms in humans

In humans, alternative splicing gives rise to two isoforms from each gene: MNK1a / MNK1b and MNK2a / MNK2b [14,15]. Mice are thought to express only the longer ‘a’ isoform and for simplicity these forms will be henceforth referred to as MNK1 and MNK2. MNK1b and MNK2b, are truncated at their C-termini and lack a MAPK-binding domain, making them poor substrates for ERK and p38 MAPK, which account for their low basal activity [10,14]. Nevertheless, MNK1b

is able to phosphorylate eIF4E *in vitro* and *in vivo* independent of MAPK signalling and may therefore be important for maintaining MNK activity in the absence of stimuli [14]. Serine- and arginine-rich splicing factor (SRSF) 1 is reported to control the alternative splicing of *Mknk2* in human cells, since SRSF1 over-expression increases the expression of MNK2b and causes a corresponding decrease in MNK2 [16].

Subcellular localisation

MNK1 and MNK2 are both mainly cytoplasmic, albeit for different reasons: MNK1 possesses a consensus nuclear export signal (NES) that ensures its localisation is primarily cytoplasmic; however, a critical residue of the NES is absent from MNK2 and it is actually mainly localised to the cytoplasm because its C-terminus apparently impedes access to its nuclear localisation signal (NLS) [10] (Figure 1-1). In contrast, MNK1b and MNK2b are predominantly nuclear, since they possess an NLS that binds α-importin but lack an NES [10]. Given their different sub-cellular localisations, it is not surprising that MNK2 splice variants have been reported to perform distinct functions [17].

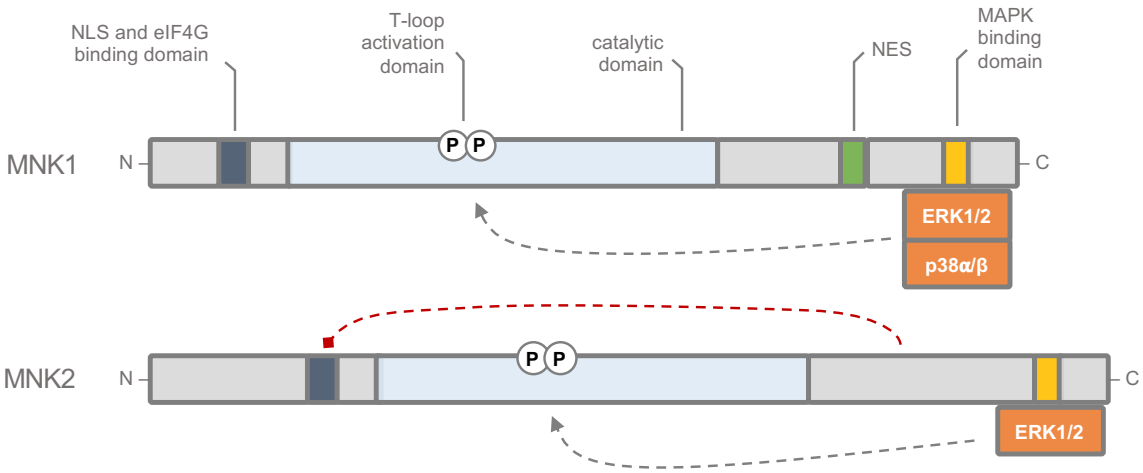

Figure 1-1: Structural domain features of MNK1/2.

Common features of MNK1/2 include an N-terminal NLS which also functions as an eIF4G binding domain, a central catalytic kinase domain and a C-terminal MAPK binding domain. MNK1 binds both ERK1/2 and p38 MAPK, whereas MNK2 binds only ERK1/2. MNK1/2 are activated by phosphorylation in their T-loop activation domain, which are catalysed by p38 or ERK1/2 MAPK (grey-dotted line). MNK1 contains a consensus NES which accounts for its cytoplasmic localisation; however, MNK2 does not contain a NES, rather unique features in its C-terminus are thought to occlude access of nuclear transport factors to its N-terminal NLS (red dotted-line) constraining MNK2 to the cytoplasm. Abbreviations: NLS: nuclear localisation signal; NES: nuclear export signal; MAPK: mitogen-activated protein kinase; ERK: extracellular regulated kinase.

MAPK signalling pathways

Overview of MAPK signalling

MAPKs are a family of serine/threonine protein kinases that are activated by external signals and regulate fundamental cellular processes, including growth, proliferation, differentiation and apoptosis. In mammals, MAPKs have been characterised into six distinct groups: the ERK1/2, ERK3/4, ERK5, ERK7/8, Jun N-terminal kinase (JNK)1/2/3 and the p38 MAPK isoforms α/β/γ(ERK6)/δ. MAPK signalling pathways are arranged in three-tiered kinase modules in which an MAPK becomes activated upon phosphorylation by an MAPK kinase (MAPKK), which in turn is activated when phosphorylated by an MAPKKK (Figure 1-2).

ERK1/2 is the best studied MAPK pathway in mammals (Figure 1-2). ERK1/2 is activated in response to growth factors and mitogens which, through receptor tyrosine protein kinases (RTPKs), triggers guanosine triphosphate (GTP) loading of the Ras GTPase. This recruits Raf kinases to the membrane for activation. Activated Raf (MAPKKK) activates MEK1/2 (MAPKK), which subsequently phosphorylate and activate ERK1/2 (MAPK). Active ERKs phosphorylate a wide range of cytoplasmic and nuclear targets, including kinases, phosphatases, transcription factors and cytoskeletal proteins [18]. In particular, ERK1/2 bind to, phosphorylate and activate the MNKs [4,5,8].

Sustained, though not transient, ERK1/2 signalling promotes proliferation through two distinct mechanisms: (1) the stabilisation of c-Fos [19] which upregulates genes involved in G1-S phase entry [20]; and (2) the down-regulation of anti-proliferative genes that have the ability to suppress S phase entry through an AP-1-dependent mechanism [19]. Sustained ERK activation increases the activity of the MNKs, notably MNK1, and consequently elevates P-eIF4E [5,12].

Cells can be subjected to many environmental stresses, including hypoxia, inflammation and cellular energy stress caused by dysregulated energy production, in addition to pharmacological stresses caused by pharmaceutical and oncology treatments [21]. JNK and p38 MAPK are stress-activated MAPK pathways and, in contrast to ERK1/2, largely seem to counteract proliferative signalling by displaying tumour-suppressive effects [21]. It is important to note that while p38α/β bind to and activate MNK1 (Figure 1-2), neither MNK1/2 binds JNK [4]. Given the upstream regulation of MNK1/2, it can be appreciated how activation of different MAPK nodes can result in selective activation of MNK1 and/or MNK2 and therefore elicit distinct biological responses.

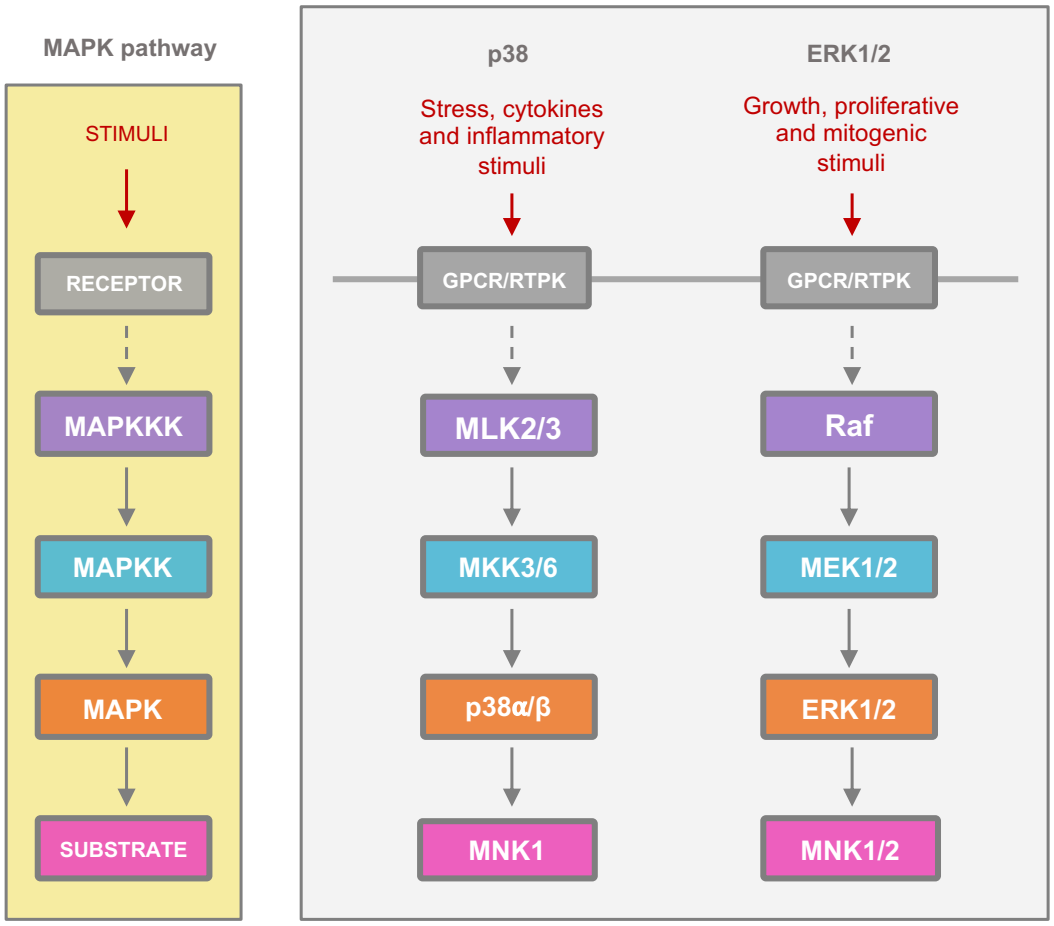

Figure 1-2: Mitogen-activated protein kinase (MAPK) signalling pathways.

MAPK signalling pathways are organised into hierarchical domains. MAPK signalling pathways are responsive to external stimuli which are detected by receptors, typically G-protein-coupled receptors and receptor-tyrosine protein kinases. These receptors transduce signals through various modulator proteins (dashed arrows) which ultimately activate a kinase signalling cascade, beginning with MAPK kinase kinase (MAPKKK). Activated MAPKKK subsequently activates a MAPK kinase (MAPKK), which in turn activates a MAPK. MAPKs are responsible for phosphorylating a number of diverse substrates. The p38 MAPK and ERK1/2 pathways, responsible for phosphorylating and activating MNK1/2, as shown. MNK1 is activated by both p38 and ERK1/2; however, MNK2 is only activated by ERK1/2. p38 MAPK signalling is activated by stress inducing stimuli and is transduced through mixed lineage kinase (MLK) 2/3 and MAPKK (MKK) 3/6. ERK1/2 signalling is activated by growth, proliferative and mitogenic stimuli and is transduced through Raf and MAPKK (MEK) 1/2. For simplicity, not all MAPKKK and MAPKK-identified factors are shown.

Biological functions of the MNKs

eIF4E and mRNA translation initiation

eIF4E is an essential component of the cap-dependent mRNA translation machinery (reviewed in [22]) and is regulated by MNK phosphorylation at Ser209 [7,8,11,12]. eIF4E binds to the 5′-5′ m^7GpppG cap-structure at the 5′-end of eukaryotic messenger RNA (mRNA) which is necessary for the recruitment of scaffolding protein eIF4G, among other factors, to assemble the translation initiation complex required for mRNA translation (reviewed in [23]) (Figure 1-3). MNK1/2 bind to a docking site on eIF4G which facilitates the phosphorylation of eIF4E by bringing substrate and kinase into close proximity [7,24,25]. The interaction of MNKs with eIF4G is thought to significantly enhance eIF4E phosphorylation [24]; however, Ser209 phosphorylation is not essential for general protein synthesis or cap-dependent mRNA translation, and mice in which MNK1/2 have been homozygously knocked-out display normal cell growth and development [13].

eIF4E is considered to be the rate-limiting factor involved in the recruitment of ribosomes to the mRNA [22]. The availability of eIF4E to engage with the translational machinery is considered critical for the regulation of translation initiation: eIF4E binds to a set of inhibitory proteins known as eIF4E-binding proteins (4E-BPs) via a site that overlaps with that used by eIF4G [26–28]. Binding of eIF4E to unphosphorylated 4E-BPs prevents formation of functional translation initiation complexes with eIF4G and thus inhibits cap-dependent translation (Figure 1-4). 4E-BP1 is the best studied 4E-binding protein and is phosphorylated at multiple residues by the mammalian target of rapamycin complex 1 (mTORC1), a multi-subunit protein kinase [29]. Hyper-phosphorylation, caused by activation of mTORC1 signalling, causes 4E-BP1 to dissociate from eIF4E, enabling eIF4G to bind and form active initiation complexes (Figure 1-4). Phosphorylation of 4E-BP1 is blocked by inhibitors of mTORC1, which prevent the release of 4E-BP1 from eIF4E and promote the formation of inactive translation initiation complexes, thereby impairing cap-dependent translation [29].

The biological significance of the phosphorylation of eIF4E (P-eIF4E) remains an ongoing, unresolved and contentious issue in the field of mRNA translation. However, it is generally accepted that phosphorylation of eIF4E reduces its binding affinity for capped RNA [30]. It is proposed that the phosphate group on Ser209 may negatively interact with phosphate groups on the RNA backbone [31], which release eIF4E from the initiation complex, perhaps enabling it to initiate another round of mRNA translation and/or recruit other mRNAs into active polyribosomes [30,32]. Phosphorylation of eIF4E may regulate the translation of specific mRNAs in response to certain stimuli [13], whilst overexpression of eIF4E has been shown to facilitate the translation of mRNAs containing excessive secondary structure in their 5’ untranslated regions (UTRs) [33].

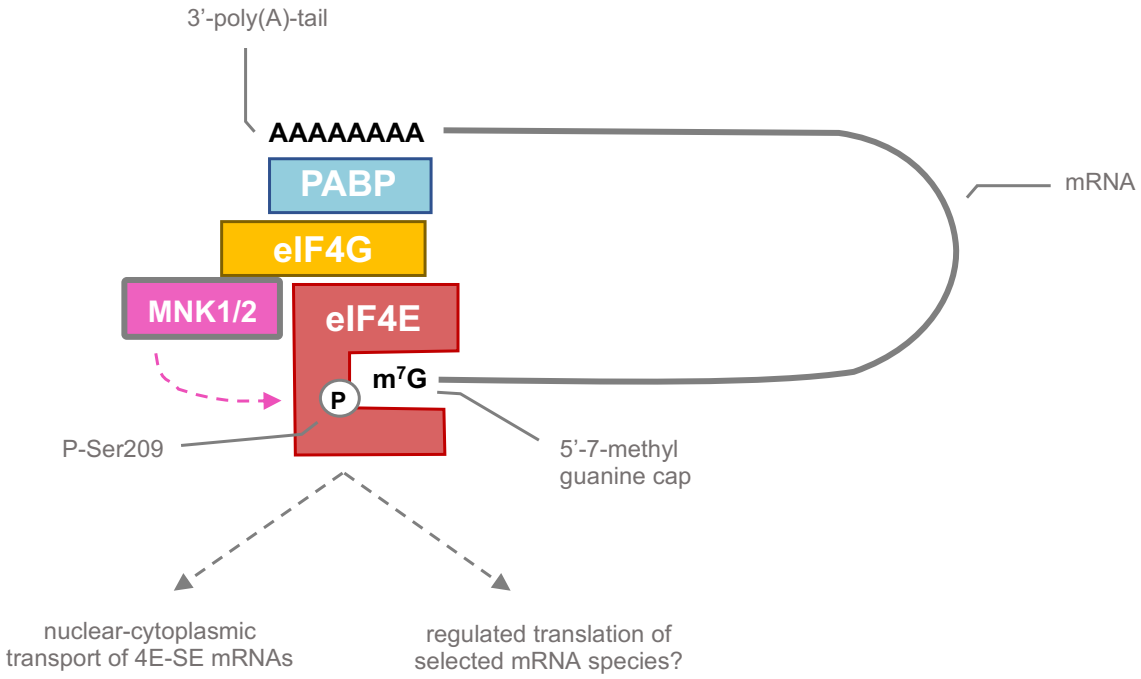

Figure 1-3: Assembly of the mRNA translation initiation complex.

The cap-binding protein eIF4E binds to the 7-methyl guanine (m^7G) cap of eukaryotic mRNAs. The scaffold protein eIF4G binds both eIF4E and poly(A)-binding protein (PABP), which loops the mRNA and is necessary for functional initiation complex assembly. MNK1/2 bind to a docking site on eIF4G which enhances the phosphorylation of eIF4E at Ser209.

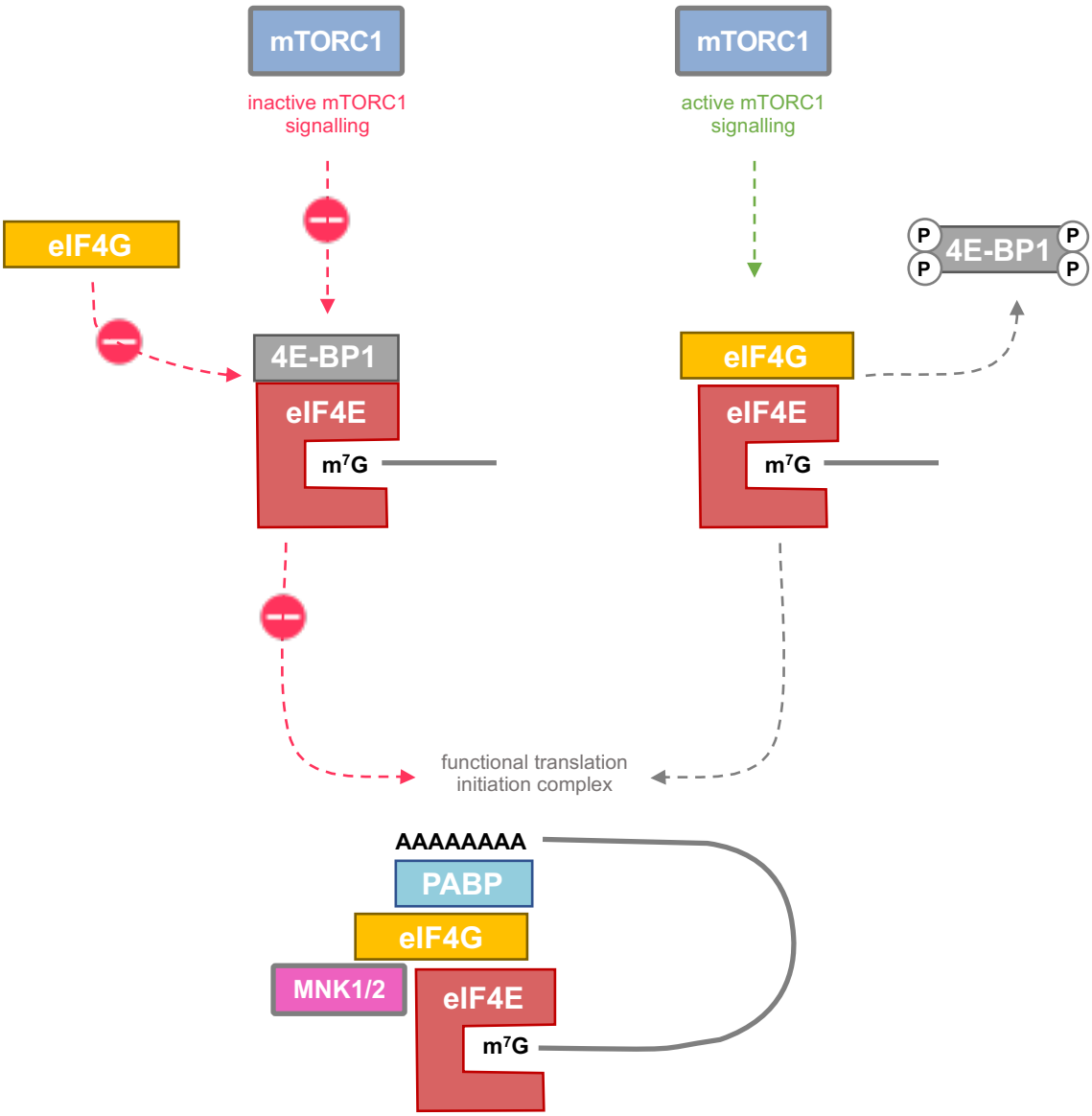

Figure 1-4: Regulation of mRNA translation initiation by mTORC1.

When mTORC1 signalling is inactive, such as under nutrient-deprived conditions, hypo-phosphorylated 4E-BP1 binds eIF4E, preventing the binding of eIF4G and thus formation of functional translation initiation complexes. When mTORC1 signalling is activated, 4E-BP1 becomes hyper-phosphorylated which disrupts its binding to eIF4E. eIF4G is now able to bind eIF4E and form functional initiation complexes to promote mRNA translation and protein synthesis.

Furthermore, inhibiting MNK activity (eIF4E phosphorylation) with the MNK inhibitor CGP57380 preferentially enhances the translation of mRNAs containing a cap and 5' terminal RNA duplex [34]. Together these studies suggest a potential role of eIF4E in affecting the RNA unwinding abilities of the initiation complex, although it is unclear how this could be regulated by Ser209 phosphorylation. A recent paper suggests that phosphorylation of eIF4E may affect certain mRNAs through modulation of the association of mRNAs with the RNA helicase, eIF4A [35].

Oncology and cell transformation

There has been intense interest in the functions of the MNKs in cancers as Ser209 phosphorylation has been shown to promote oncogenic transformation (see, e.g. [36,37]) and aberrant P-eIF4E levels have been observed in many human cancers, and are correlated with disease severity, and associated with metastasis and poor survival [37,38] (reviewed in [32]). eIF4E phosphorylation has been shown to *enhance* cellular transformation *in vitro* [39], and mice expressing non-phosphorylatable eIF4E are resistant to tumorigenesis in a model of prostate cancer [37], suggesting P-eIF4E is actually *required* for oncogenic transformation. In support of this, P-eIF4E has been demonstrated to enhance the nuclear-cytoplasmic export of certain growth-promoting mRNAs, including *Cyclin D1* [39], which are discriminated by a ~100 nt sequence in the 3'UTR known as the eIF4E sensitivity element (4E-SE) [40].

Additional MNK substrates

Beyond eIF4E, there are reports of additional MNK substrates, although *in vivo* data are still lacking. Tumor necrosis factor α (TNFα) is implicated in various inflammatory diseases and its mRNA is tightly regulated by AU-rich elements (ARE) in its 3'UTR [41]. TNFα production is regulated by p38 and ERK pathways [42,43], which are upstream of the MNKs. MNK1 was found to phosphorylate the ARE-binding protein, hnRNPA1, which decreased its affinity for TNFα mRNA and thereby promoted its translation [44]. The MNKs have also been reported to phosphorylate the polypyrimidine tract-binding protein-associated splicing factor (PSF), which also binds to TNFα mRNA [45]. However, the physiological significance of MNK-mediated phosphorylation of PSF remains to be established.

Sprouty2 (Spry2) belongs to a family of proteins that negatively regulate downstream signalling of receptor tyrosine kinases [46,47]. Two separate studies report that MNK1 phosphorylates Spry2 on Ser112 and Ser121 [48,49]. This phosphorylation stabilises the Spry2 protein and thereby enhances its ability to inhibit growth factor signalling [48]. Therefore, MNK-mediated stabilisation of Spry2 may prolong its ability to inhibit downstream signalling, for example, through ERK.

Cytosolic phospholipase A2 (cPLA2) is involved in the production of eicosanoids, which are important secondary messengers in inflammation, immunity and regulation of the central

nervous system [50]. MNK1 was shown to phosphorylate cPLA2 on Ser727, which reportedly enhances its enzymatic activity [51]. However, MNKs' role in the physiological regulation of cPLA2 remains unclear.

MNK2-specific protein activities

Like many other kinases [52], MNK2 has several functions that are independent of its catalytic activity, and which are regulated through protein-protein interactions. In particular, MNK2 has been reported to interact with mammalian target of rapamycin complex 1 (mTORC1) to inhibit the phosphorylation of the downstream mTORC1 target, p70S6K (70-kDa ribosomal protein S6 kinase) [53]. Specific interactions with oestrogen receptor β (ERβ) have also been reported; ERβ specifically binds MNK2b, but not MNK2 or MNK1 [15]. It is proposed the interaction with MNK2b may lead to the phosphorylation of ERβ and/or alter its transactivation activity, but this is yet to be determined [53]. As mentioned earlier, MNK2 also interacts with eIF4G, which enhances eIF4E phosphorylation [7]. Finally, MNK2 has been reported to phosphorylate plectin [54], a cytoskeletal-associated protein that interacts with microtubules, intermediate filaments and the actin microfilaments [55]. MNK2-mediated phosphorylation of plectin was found to attenuate its interactions with intermediate filaments, suggesting MNK2 may regulate cytoskeletal integrity [54].

Development of small molecule MNK inhibitors

The inhibition or knockout (KO) of MNKs shows promising therapeutic potential in oncology, especially as the MNKs are not essential for viability or development [13], and so the development of MNK inhibitors has attracted substantial interest and led to the discovery of several compounds which block MNK activity *in vitro* and in cells. The MNKs belong to a group of Ca^{2+}/calmodulin-modulated protein kinases [56]. In place of the otherwise strictly conserved Asp-Phe-Gly (DFG) motif found in all other kinases, the MNKs contain an Asp-Phe-Asp (DFD) motif, which exhibits a conformation that obstructs ATP binding [57]. The crystal structure of MNK1, in its inactive, auto-inhibited state has been solved; it shows that the Phe residue of the DFD motif resides in a hydrophobic pocket near the ATP-binding site which causes it to flip-out, resulting in an inactive DFD-out conformation [58]. A similar situation applies to MNK2, although it does not adopt an auto-inhibited conformation [57]. Such DFD-out conformations are not competent to bind ATP and this is a feature not generally observed in other kinases. Like many other kinases, the MNKs contain a so-called 'gatekeeper residue', (Phe159 in MNK2), and a residue just N-terminal of the DFG motif (Cys225 in MNK2) which can be targeted to develop favourable stereo-electronic interactions with inhibitors to improve kinase selectivity [59]. These residues are conserved in MNK1 (Phe124 and Cys190) [59]. It is therefore apparent that the MNKs are architecturally distinct from other protein kinases, which has important implications for drug discovery and design.

Although many protein kinase inhibitors are ATP-competitive, inhibitors that bind the inactive structures of protein kinases can also be valuable, particularly if they stabilise structures that impede their activation. Such compounds have been described for the MNKs [58,60]; however, since MNK2 is basally phosphorylated and active [61], such inhibitors may be less useful for MNK2.

The first two reported and so far, most widely-used MNK inhibitors are CGP57380 [62] and cercosporamide [63]. However, both compounds exert several off-target effects. For instance, CGP57380 inhibits CK1, BRSK2 and MKK1 to a similar extent as the MNKs [64], while cercosporamide actually shows greater potency against PRK2, MRK2 and IKKε than the MNKs [65]. Later, a thienopyridine derivative, MNK-I1, was shown to inhibit the MNKs at low micromolar concentrations in cells and exhibit superior specificity relative to CGP57380 and cercosporamide [64,65]. Wang's group have designed and synthesised a variety of pyrimidine derivatives as potent MNK inhibitors [66,67]. In addition, several compounds that target the inactive forms of the MNKs, with higher potency against MNK2 than MNK1, have been identified [60]. More recently, an MNK-selective inhibitor of the same molecular scaffold as MNK-I1 was identified, which possessed similar potency against MNK1, but higher selectivity against MNK2. This new inhibitor also requires a less complicated synthesis process than MNK-I1 [68]. Notably, a number of MNK inhibitors have entered clinical trials for cancer treatment: BAY1143269 [69] is in phase I trial in the U.S. against locally advanced or metastatic solid tumours; and eFT508 [59] has been tested in several U.S. clinical trials (up to phase II) against diverse types of tumours, including colorectal cancer, breast cancer and lymphoma.

Adipose tissue development

Overview of adipose tissue function

In animals, highly integrated systems have evolved to promote storage during periods of energy abundance and conversely to mobilise stores during periods of energy deprivation and demand [70]. Excessive nutrient intake relative to expenditure produces a metabolic state that promotes energy storage; in the context of adipose tissue, this results in adipocyte hyperplasia and hypertrophy [71]; hyperplasia involves stem cell recruitment to the adipocyte lineage and results in increased adipocyte number, whereas hypertrophy involves the expansion of existing adipocyte triglyceride (TAG) stores. Given adipose tissue is fundamental for regulating whole-body energy homeostasis, it is not surprising that dysregulation or perturbation of adipose function can cause disease (reviewed in [72]). Sustained and rapid expansion of adipose tissue can be problematic; if vascularisation cannot keep pace with expansion, oxygen supply to adipocytes can become limited, leading to hypoxic regions of adipose tissue which promote inflammation. Infiltration of inflammatory mediators such as TNFα and immune cells are thought to contribute to the development of adipocyte insulin resistance in adipocytes (and other cell/tissues) and thus to

type-2 diabetes. Excess or dysregulated adipose tissue expansion largely underpins the development of chronic diseases; understanding the pathways that regulate adipocyte hypertrophy and hyperplasia is therefore of paramount importance.

Origin and lineage commitment of adipocytes

Adipocytes are derived from pluripotent mesenchymal stem cells (MSCs) which have the capacity to develop into several cell types, including adipocytes, myocytes, chondrocytes and osteocytes [70,71]. These stem cells reside in the vascular stroma of adipose tissue as well as the bone marrow which, when appropriately stimulated, i.e. through excessive nutrient intake, undergo a multi-step process of commitment to the adipocyte lineage [70,71]. Commitment to the adipocyte lineage gives rise to pre-adipocytes which, when induced, undergo multiple rounds of mitosis (mitotic clonal expansion; MCE) and then differentiate into adipocytes, a process termed 'adipogenesis'. MCE precedes expression of genes that give rise to the adipocyte phenotype and is considered a prerequisite for terminal adipocyte development [73], as discussed below.

Adipocyte lineage commitment is regulated by a network of extracellular signalling factors that impinge on the promoters of lineage-specific transcription factors [70]. The balance of these signalling molecules determines the developmental pathway, since activation of one pathway often inhibits another. Bone morphogenic protein (BMP) signalling has been implicated in the commitment phase: specifically, exposure of stem cells to BMP2 and BMP4 gives rise to pre-adipocyte-like cells [74–76]. The downstream targets of BMP signalling are cytoskeleton-associated proteins, and it is thought their differential regulation may determine the ability of stem cells to commit to the adipocyte lineage through cell shape regulation [77].

The Wnts comprise a family of secreted signalling glycoproteins that mediate their effect through the frizzled receptor and low-density-lipoprotein (LDL)-related protein 5/6 [78]. During lineage commitment of stem cells, Wnt signalling is activated, which stabilises β-catenin, a transcription factor, allowing it to accumulate in the nucleus where it acts as a coactivator of the lymphoid-enhancing factor and T-cell factor (Lef/Tef). This in turn triggers the transcription of downstream genes such as *c-Myc* and *Cyclin D1,* which promote progression through the cell cycle [79].

Transcriptional regulation of adipogenesis

Following commitment to the adipocyte lineage, a population of pre-adipocytic cells progress through a synchronous and highly orchestrated program of adipogenesis. Established pre-adipocyte cell models have been indispensable for the study and identification of key transcription factors that regulate adipogenesis: 3T3-L1 pre-adipocytes are the most widely-used model as they faithfully recapitulate the events that occur during *in vivo* adipogenesis [80–82]. Established protocols have been developed to initiate the differentiation of pre-adipocytes; inducers that activate the insulin [83], glucocorticoid and cyclic adenosine monophosphate

(cAMP)-signalling pathways [84] initiate a phase of early transcription, which is followed by synchronous entry into the cell cycle and several rounds of mitosis (MCE). Upon exit from the cell cycle, cells lose their fibroblastic morphology, accumulate triglyceride and acquire the metabolic features and appearance of adipocytes [80–82,85]. Triglyceride accumulation is closely correlated with an increased rate of *de novo* lipogenesis (DNL) and a coordinate rise in expression of the enzymes of fatty acid and triacylglycerol (TAG) biosynthesis [83,84,86]. Rosiglitazone (ROSI), a thiadiazol used as a diabetic treatment that enhances insulin sensitivity [87], is now routinely used for adipogenic induction as it significantly enhances the conversion of pre-adipocytes to adipocytes [88]. The program of adipogenesis involves the coordinated and temporal expression of a number of key transcriptional regulators, (Figure 1-5) which are discussed in detail below.

CCAAT/enhancer binding protein (C/EBP)-β and δ

Three members of the CCAAT/enhancer binding protein (C/EBP) family have been strongly implicated in adipogenesis; namely C/EBPα, C/EBPβ and C/EBPδ [89]. All three contain a DNA-binding domain and an adjacent C-terminal leucine zipper domain, which permits homo- or hetero-dimerisation with other C/EBP family members, a prerequisite for DNA binding [90]. Although C/EBPα was the first C/EBP isoform to be implicated as a principal player in adipogenesis [91–95], it later became apparent that its expression was preceded by that of two other C/EBP isoforms [89,96].

C/EBPβ and C/EBPδ are the most-rapidly induced factors of adipogenesis and increase quickly following induction of adipogenesis (<4 h) [97]. C/EBPβ and C/EBPδ are the direct targets of cAMP- and glucocorticoid signalling, respectively [89,96]. Over-expression of C/EBPβ, but not C/EBPδ, promotes adipogenesis in the absence of any adipogenic inducers, indicating C/EBPβ plays a key role in the initiation of adipogenesis [96]. C/EBPδ lacks a stretch of basic amino acids common to both C/EBPα and C/EBPβ and is thought to bind DNA less avidly than its counterparts, which may explain its lower adipogenicity [89]. *In vivo*, C/EBPβ is thought to be expressed at low levels and occupy so-called DNA 'hot-spots' prior to induction, to prime the chromatin for subsequent remodelling [98,99]. At these hot-spots, C/EBPβ is associated with histone deacetylase 1 (HDAC1)-containing repressor complexes; however, upon glucocorticoid treatment, becomes acetylated in a GCN5-dependent manner and causes the dissociation of the HDAC1 repressor [100]. In turn, the local chromatin environment is opened up, which facilitates the recruitment of chromatin-remodelling factors and primes genes for their expression.

C/EBPβ has been shown to be required for adipogenesis in cell culture [97,101–103]; however, the individual KO of C/EBPβ or C/EBPδ has little effect on adipose tissue accumulation *in vivo* [103]. Only mice lacking expression of both C/EBPβ and C/EBPδ have markedly reduced adipose

mass, suggesting some synergy and redundancy may operate between these factors [103]. In C/EBPβ$^{-/-}$ C/EBPδ$^{-/-}$ mice, the reduction in adipose tissue mass was attributed to a reduction in adipocyte cell number, suggesting these factors may play an important role in promoting cell proliferation [100].

As mentioned earlier, upon adipogenic induction, growth-arrested pre-adipocytes re-enter the cell cycle and undergo about two rounds of mitotic division [73]. MCE is a required step in adipogenesis, since blocking cell cycle progression through various means prevents differentiation [73,97,104,105]. Indeed, C/EBPβ$^{-/-}$ mouse embryonic fibroblasts (MEFs) are unable to undergo MCE or differentiate into adipocytes, suggesting C/EBPβ is a prerequisite for MCE and therefore adipogenesis [102]. Moreover, ectopic expression of a dominant negative C/EBPβ isoform (A-C/EBPβ) containing a leucine zipper but lacking functional DNA-binding and transactivation domains disrupts both MCE and adipocyte differentiation [105]. When A-C/EBPβ is expressed conditionally in the adipose tissue of mice, animals become devoid of white adipose tissue, strongly suggesting C/EBPβ is required for adipogenesis *in vivo* [106].

Following 16-20 h of adipogenic induction, C/EBPβ and C/EBPδ become associated with centromeres, which is thought to be important for traversing the G1-S phase checkpoint [97]. C/EBPβ and C/EBPδ lack DNA binding activity when initially expressed and only become competent to bind DNA when phosphorylated [101]. C/EBPβ is phosphorylated sequentially, first by MAPK at Thr188, then much later by glycogen synthase kinase-3β at Thr179 or Ser184 [101]. This dual phosphorylation is thought to induce a conformational change that renders the leucine zipper of monomeric C/EBPβ accessible for dimerisation [107].

Retinoblastoma (RB) is a critical regulator of cell cycle progression (reviewed in [108]) and is essential for adipogenesis [109]. RB directly interacts with C/EBPβ *in vitro* and in cells, which enhances its DNA-binding and transactivation activity [109,110]. C/EBPβ interacts with RB during a defined window and only in differentiating cells. Three isoforms of C/EBPβ have been suggested: one inactivated prior to interaction with RB; a second transiently complexed with RB during differentiation; and a third activated after dissociation from RB [109]. In support of this, hypo-phosphorylated RB (6 h after induction) binds C/EBPβ, whereas hyper-phosphorylated RB (18 h after induction) does not [111]. The interaction of hypo-phosphorylated RB with C/EBPβ inactivates its DNA-binding activity, whereas maximal DNA-binding activity occurs when RB and C/EBPβ are no longer associated (i.e. upon RB hyper-phosphorylation). This suggests the RB-C/EBPβ interaction is essential for coupling the initiation of differentiation with cell cycle progression [111].

CCAAT/enhancer binding protein-α (C/EBPα)

Adipogenesis is characterised by increased expression of C/EBPα [94,95,112,113] and its inducible ectopic expression is sufficient to drive adipogenesis in the absence of hormonal stimulation [112]. Furthermore, C/EBPα has been demonstrated to transactivate the expression of adipose-specific genes directly, including fatty acid-binding protein 4 (FABP4) [93], stearyl CoA desaturase (SCD1) [114] and insulin-responsive glucose transporter 4 (GLUT4) [92], and is therefore considered a master regulator of the adipogenesis program. In support of this, blocking C/EBPα expression inhibits the expression of adipose-specific mRNA and accumulation of TAG [94,95]. In support of *in vitro* studies, C/EBPα-deficient mice fail to accumulate lipid and die shortly after birth due to the inability to produce and store glucose in adipocytes, suggesting that adipose tissue maturation requires C/EBPα [115].

C/EBPα is anti-mitotic, and so its constitutive expression during adipogenesis actually precludes their propagation and inhibits differentiation [112]. Typically, expression of C/EBPα occurs as cells exit mitosis [116] at which time it becomes associated with centromeres [97], which is thought to drive cells out of MCE. The temporal expression of C/EBPα, which is regulated by the delayed acquisition of C/EBPβ DNA binding activity, as mentioned above, is further evidence that MCE is required for adipogenesis. The binding of the negative regulators AP-2α [117] and Sp1 [118,119] to the *Cebpa* promoter are additional mechanisms that help prevent the premature expression of C/EBPα. AP-2α and Sp1 levels are down-regulated upon entry into MCE [117,118], which permits the binding of C/EBPβ and C/EBPδ to the C/EBP response element (C/EBPRE) in the proximal promoter of *Cebpa* and induce C/EBPα expression [96,113].

Once expressed, C/EBPα co-ordinately activates the expression of adipocyte genes in concert with peroxisome proliferator-activated receptor gamma (PPARγ). C/EBPα also self-promotes its own expression, which is thought to maintain adipocyte gene expression in terminally differentiated adipocytes [113,120–123].

C/EBP homologous protein (CHOP)

C/EBP homologous protein (CHOP) was identified from a cDNA library based on its ability to interact with the C/EBP C-terminal leucine zipper domain [124]. In contrast to other C/EBP isoforms, the DNA-binding domain of CHOP is inactive; therefore, ‘inactive’ heterodimers are formed upon hetero-dimerisation with other C/EBP isoforms, which are unable to activate transcription. [124]. CHOP is normally expressed in G1 growth-arrested pre-adipocytes to prevent the premature binding of C/EBPβ and C/EBPδ to DNA, and is down-regulated upon entry into MCE [125]. However, when CHOP is ectopically expressed it blocks adipogenesis [126], strongly supporting its role as a dominant negative regulator of C/EBP proteins.

Translational regulation of C/EBPβ

As discussed above, C/EBPβ activity is regulated at different levels, including transcription, phosphorylation and protein-protein interactions. Whilst interactions among C/EBP family members are known to occur [127], C/EBPβ is also reported to interact with glucocorticoid receptor (GR) [128], cAMP response element-binding protein (CREB) [129] and nuclear factor-kappa B (NF-kB) [130]. The resulting hetero-dimeric complexes have altered DNA binding selectivity, allowing expression of different target genes to be modulated.

C/EBPβ, also known as liver-enriched transcriptional activator protein (LAP) following its discovery in hepatocytes [131], is also regulated at the level of translation. Three C/EBPβ isoforms are translated from alternative start sites on a single intronless gene, and are referred to as LAP, LAP* and LIP (liver-enriched inhibitory protein) [132]. C/EBPβ-LIP lacks the N-terminal transactivation domain and acts as a dominant negative inhibitor of C/EBPβ function either by occupying binding sites on target gene promoters or by forming transcriptionally inactive heterodimers with other C/EBP isoforms. In support of this, ectopic expression of C/EBPβ-LIP inhibits adipocyte differentiation [133]. Unsurprisingly, the LAP/LIP ratio regulates the relative transcriptional activity of target genes, with higher ratios resulting in significantly higher transactivation of target genes and *vice versa* [96,132,134]. This is supported by the fact that over-expression of C/EBPβ-LAP accelerates and increases adipogenesis [96,133,135]. In human adipose progenitors it was shown that the protein stability of C/EBPβ isoforms is differentially regulated throughout adipogenesis: C/EBPβ-LIP protein steady-state levels decrease considerably faster than C/EBPβ-LAP, whilst the half-life of C/EBPβ-LIP is significantly shorter than that of C/EBPβ-LAP [133]. The regulated proteolytic degradation of C/EBPβ isoforms is an important part in the differentiation program, since constitutive overexpression of C/EBPβ-LAP actually leads to down-regulation of certain adipogenic regulators during later stages of adipogenesis [133]. Therefore, the decline in C/EBPβ expression and up-regulation of C/EBPα that are typically observed during adipogenesis are critical to ensure that later stages of differentiation proceed correctly.

Translational regulation of C/EBPα

Two C/EBPα isoforms, referred to as p42 and p30, are translated from alternative start sites, the latter of which is located 351 bp down-stream of the first start codon [120,136]. The p30 isoform is truncated in its N-terminus and lacks a potent transactivation domain [136]. Consequently, the p42 isoform is a stronger transcriptional activator than p30 [136], but p30 nevertheless retains its ability to transactivate the expression of adipocyte genes [120]. The anti-mitotic activity of C/EBPα is contained within the N-terminal 12 kDa of p42 [120]; therefore, the expression of p42 appears to be essential for driving cells out of MCE. The p42/p30 ratio is also reported to increase

during the course of adipogenesis [120], but the functional consequence(s) of this is yet to be determined.

Peroxisome proliferator-activated receptor-γ (PPARγ)

PPARγ is a member of the nuclear receptor superfamily and is regarded as the master-regulator of adipogenesis, as supported by a large body of *in vitro* and *in vivo* evidence. A series of gain-of-function experiments showed that ectopic PPARγ expression in fibroblasts is able to induce adipogenesis and give rise to mature adipocytes [137]. The importance of PPARγ as the master regulator of adipogenesis is perhaps best demonstrated by the fact that it induces adipogenesis even in the absence of C/EBPα, but the converse is not possible (i.e. C/EBPα is unable to drive adipogenesis in the absence of PPARγ) [138]. Although PPARγ is sufficient to induce adipogenesis in the absence of C/EBPα, adipocytes differentiated under such conditions have abnormally low insulin sensitivity [139]. Therefore, C/EBPα is considered important for establishing insulin sensitivity in adipocytes [139].

PPARγ is expressed as two isoforms which are generated by alternative promoter usage [140–143]. PPARγ2 is 30 amino acids longer than PPARγ1 and is the main isoform in adipocytes [140]. PPARγ1 is expressed in a range of different tissues whereas PPARγ2 is almost exclusively expressed in adipose tissue [140,142]. PPARγ1 is just as capable of inducing adipogenesis as PPARγ2 [144], however, PPARγ2-deficient mice are insulin-resistant, suggesting PPARγ2 may play a selective role in regulating insulin sensitivity [145].

Since KO of PPARγ is embryonically lethal [146], KO models using novel strategies to overcome lethality were developed to study its function. In these models, PPARγ-deficient mice completely failed to develop adipose tissue, further supporting the master-regulatory function of PPARγ in adipose tissue development [146,147]. Moreover, conditional hypomorphic expression of PPARγ in white adipose tissue resulted in mice with severe lipodystrophy and hyperlipidaemia [148]. More recently, selective deletion of the PPARγ2 isoform in obese and insulin-resistant (*ob/ob*) mice led to decreased fat mass, severe insulin resistance and dyslipidaemia [149].

PPARγ is directly induced by the binding of C/EBPβ and C/EBPδ to a C/EBPRE identified in its proximal promoter [150–153]. Ectopic expression of C/EBPβ-LAP alone or treatment with dexamethasone cannot induce adipogenesis, but together, are capable of inducing PPARγ expression and stimulating adipogenesis [150]. Interestingly, ectopic expression of the dominant negative C/EBPβ-LIP isoform blocks adipogenesis but not the glucocorticoid-induced expression of PPARγ1, suggesting PPARγ expression is dependent on both C/EBPβ and an initial exposure to glucocorticoids [134]. It is proposed that C/EBPδ (a target for GR) may synergise and form

heterodimers with C/EBPβ to enhance the expression of PPARγ to the levels required for complete adipogenesis [151].

PPARγ contains an N-terminal domain involved in ligand-independent activation function (AF1), a DNA-binding domain, and a C-terminal ligand-binding domain involved in its ligand-dependent activation function (AF2) [154]. PPARγ binds as an obligate heterodimer with the retinoid X receptor (RXR) [155] to DNA sequences that conform to a consensus motif containing two imperfect direct repeats of the sequence AGGTCA, separated by a single nucleotide [156]. Like other members of the nuclear receptor superfamily, PPARγ transcriptional activity is modulated by ligand binding. PPARγ binds DNA even in the absence of ligand, which in this conformation favours interactions that recruit chromatin-modifying enzymes such as histone deacetylases to repress transcription [154]. Activation of PPARγ by ligands appears to occur during early adipogenesis and is dependent on C/EBPβ and cAMP signalling [134]. The binding of ligand to PPARγ induces a conformational change which favours interactions with coactivators such as histone acetyltransferases (HATs), including CREB-binding protein (CBP), P300, and the Mediator complex, which promote gene transcription [154]. In the absence of ligand, recruitment of HATs and Mediator can still occur but is instead mediated through the AF1 domain [157]. Although the physiologically-relevant endogenous ligand(s) have yet to be identified, derivatives of long-chain fatty acids and a number of synthetic ligands have been shown to promote differentiation in a dose-dependent manner in PPARγ2-overexpressing cells [137]. More recently, a class of pharmaceutical known as thiazolidinediones (TZDs) has been developed as direct agonists of PPARγ. These drugs act as potent insulin sensitisers and are used in the management of diabetes to increase peripheral glucose disposal and decrease fasting free fatty acid (FFA) [157]. As mentioned earlier, TZDs are now a routine addition to the adipogenic induction medium when studying adipogenesis *in vitro* [88].

The increased expression of PPARγ activates the expression of adipocyte target genes as well as C/EBPα [134,158,159], which itself binds to the C/EBPRE in PPARγ to provide a stable, self-reinforcing regulatory loop [158]. A large number of genes involved in lipogenesis and insulin sensitivity contain PPAR response elements (PPARE's) responsible for binding PPARγ [160]. However, less than 10% of the PPARγ binding sites are located close to promoters, with many sites located in distal intergenic regions and about half in intronic regions [157]. Despite this, chromatin conformation capture analyses suggest that distant binding sites may loop to the promoter and therefore be important for gene regulation [161].

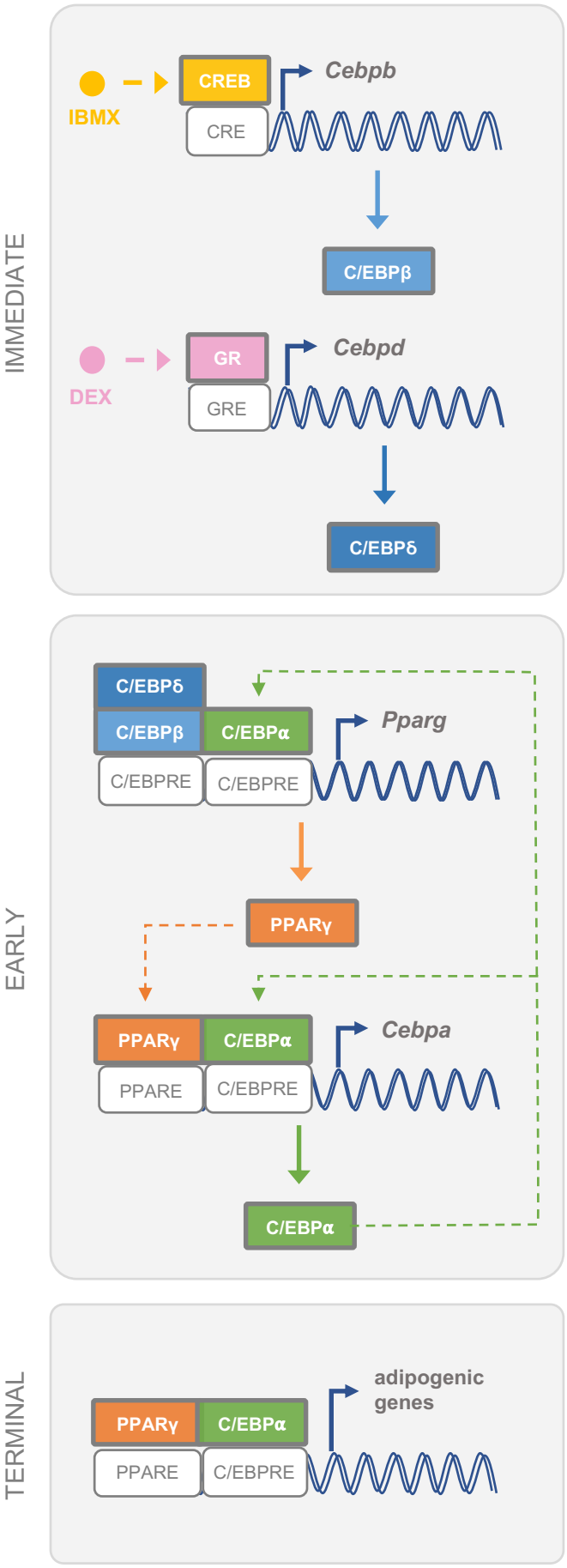
IMMEDIATE
IBMX
CREB
Cebpb
CRE
C/EBPβ
DEX
GR
Cebpd
GRE
C/EBPδ
EARLY
C/EBPδ
C/EBPβ
C/EBPα
Pparg
C/EBPRE
C/EBPRE
PPARγ
PPARγ
C/EBPα
Cebpa
PPARE
C/EBPRE
C/EBPα
TERMINAL
PPARγ
C/EBPα
adipogenic genes
PPARE
C/EBPRE

Figure 1-5: Adipogenic transcriptional cascade.

Stimulation of adipocyte differentiation with IBMX and DEX results in the immediate and direct upregulation of C/EBPβ and C/EBPδ through the binding of CREB and GR to the respective response elements in their promoters. C/EBPβ and C/EBPδ together bind to response elements in the promoter of *Pparg* and the expression of PPARγ in turn, transactivates expression of *Cebpa*. C/EBPα binds to response elements in *Pparg* and its own promoter to provide a stable, self-reinforcing regulatory loop. During the terminal phase of adipogenesis, PPARγ and C/EBPα bind to their respective response elements in concert to induce the expression of adipogenic genes.

PPARγ and C/EBPα function as the key transcriptional regulators of adipogenesis. These two factors induce the expression of each other [154] and genome-wide profiling has demonstrated that 30–60% of PPARγ binding sites in murine and human adipocytes are also bound by C/EBPα [162,163]. PPARγ binding sites are strongly enriched in the vicinity of genes induced in adipogenesis, including genes involved in fatty acid and glucose metabolism [164]. Intriguingly, there is a striking and almost complete overlap between C/EBPα and C/EBPβ binding sites in mature adipocytes, indicating that C/EBP homo- and hetero-dimers might bind interchangeably [162].

Transcriptional pathway of adipogenesis

As outlined above, the consensus transcriptional pathway of adipogenesis involves the sequential activation of PPARγ expression by C/EBPβ and C/EBPδ [150–153], which in turn activates C/EBP α and the expression of adipocyte genes in concert with PPARγ [134,158,159] (Figure 1-5). However, it is important to note that alternative pathways have been proposed: some suggest that C/EBPβ first induces the expression of C/EBPα and that these factors together regulate PPARγ [70,71]; others suggest that C/EBPβ and C/EBPδ simultaneously control the expression of both C/EBPα and PPARγ [64]. Despite this, it is clear that a concerted and highly-coordinated transcriptional cascade regulates adipogenesis.

MAPK signalling and adipogenesis

As mentioned earlier, MAPK signalling pathways regulate many essential cellular processes and have a well-defined key role in connecting extra-cellular signals to the activation of transcription factors in the nucleus. Many *in vitro* and *in vivo* studies have specifically implicated ERK and p38 MAPK pathways in adipogenesis, as discussed below.

ERK pathway

ERK signalling is activated by mitogens and growth factors and consequently this pathway is important for regulating the cell cycle and proliferation (reviewed in [165]). As a result, the ERK pathway is of particular relevance given adipose tissue expansion is governed by hyperplasia, the proliferation of stem-cell progenitors and their subsequent differentiation into adipocytes.

Early gain-of-function studies investigating the potential links between ERK signalling and adipogenesis found that ERK positively regulates adipogenesis [166]. Moreover, anti-sense RNA knockdown of ERK1/2 demonstrated that ERKs are indeed required for adipogenesis [167]. However, it became clear that the function of ERK during adipogenesis is more complex when it was revealed that ERK phosphorylates PPARγ, which negatively decreased ERK's transactivation activity and inhibits adipogenesis [168,169]. It is therefore proposed that ERK function is regulated in a temporal manner during adipogenesis, that is, turned on during early proliferative

steps and shut-down at later stages to avoid PPARγ phosphorylation. In support of this, inhibition of ERK activity during MCE was found to block adipogenesis [73], whilst ERK activity is down-regulated during the terminal phase of adipogenesis, when PPARγ is induced [73]. The requirement for ERK activity during early adipogenesis was later attributed to its ability to phosphorylate C/EBPβ [101], which is required for the dimerisation and DNA binding of this transcription factor. This appears to be a specific function of ERK2, since C/EBPβ is a preferential substrate for ERK2, relative to ERK1 [170].

KO of ERK2 is embryonically lethal in mice, making it difficult to study its role in development [171]. In contrast, ERK1$^{-/-}$ mice are viable, fertile and of normal size, despite showing defective thymocyte maturation [172]. ERK1$^{-/-}$ mice exhibit impaired adipogenesis and consequently have decreased adiposity and fewer adipocytes than wildtype (WT) counterparts, suggesting ERK1 regulates adipocyte differentiation [173]. Notably, these mice are also resistant to diet-induced obesity and insulin resistance when challenged with a high-fat diet (HFD) [173]. The activity and expression of ERK1 and ERK2 are differentially regulated during the differentiation of human mesenchymal stem cells (hMSCs). However, the temporal function of ERK1/2 activity during hMSC differentiation appears to be complex as inhibition of ERK1/2 during either early or later stages of differentiation leads to adipogenic defects [174]. However, the effect of selective inhibition of ERK1/2 was not evaluated, presumably because suitable inhibitors are not available. Nevertheless, it is apparent that ERK1/2 activity is important for hMSC adipogenic differentiation, but future work is required to evaluate the specific role of ERK2 specifically in adipogenesis.

p38 MAPK pathway

The p38 MAPK is reported to play a positive role in adipogenesis, since its inhibition during early adipogenesis decreases adipocyte formation [175–177]. Moreover, constitutive activation of the p38 MAPK pathway is sufficient to induce adipogenesis in 3T3-L1 in the absence of hormonal stimuli [176]. However, this is contradicted in human pre-adipocytes, where inhibition of p38 MAPK activity has only moderate effects on differentiation and lipid metabolism [178], whilst another report suggests p38 MAPK activity actually inhibits adipogenesis by phosphorylating CHOP [179]. In another study, p38 MAPK was found to phosphorylate nuclear factor of activated T cells (NFATc4) which impaired its nuclear translocation [180]. NFATc4 is a transcription factor implicated in adipogenesis, with binding elements located in relevant adipocyte target genes, including PPARγ [180,181]. The p38 MAPK-mediated phosphorylation of NFATc4 is therefore thought to regulate adipogenesis negatively. Given the conflicting functions of p38 MAPK in adipogenesis, greater clarification is needed. In particular, a p38 MAPK-deficient mouse model would be of great use but given that these mice are only viable for a short time after birth developmental studies would be difficult [182].

The rising obesity epidemic and the need for new solutions

The incidence of overweight and obesity, defined by measures of body mass index between 25.0–29.99 and > 30.00 kg/m^2, respectively, are increasing rapidly in Australia [183] and globally [184]. As of 2017-18, approximately 12.5 million Australian adults (or 67%) were overweight or obese [185]. Being overweight and obesity are major risk-factors for developing several chronic diseases, including cardiovascular disease, hypertension, type-2 diabetes and certain types of cancers; and contributed around 8% of the total disease burden in Australia in 2015 [186]. People who are overweight or obese have higher rates of death and difficulty in managing chronic disease [185]. Chronic diseases are generally complex and require long-term and persistent management. They present as a major burden and financial liability to health systems, as well as those affected, their families and carers. As the 'obesity epidemic' continues to worsen, as predicted, particularly in developing countries, so will the cost to health budgets. By 2025, the cost of obesity to Australia is expected to be in the order of $21 billion [187]. Not only is it therefore economically sensible to address the rising incidence of overweight and obesity, but unnecessary suffering could be potentially alleviated by prevention. Ultimately, excessive caloric intake coupled with insufficient exercise are causing the rise in prevalence of being overweight or obese. By increasing our understanding of the underlying mechanisms that lead to weight gain (i.e. adipose tissue expansion), lifestyle interventions or novel therapeutic strategies may be identified which could be applied to those at risk [187].

MNKs are implicated in metabolic disease

Weight gain

The potential link between MNKs and metabolic disease was first documented in a patent application in which the authors disclosed a link between the human MNK genes, particularly variants of MNK2 (MNK2a and MNK2b) and the regulation of body weight [2]. Specifically, ectopic expression of MNK2 in transgenic mice led to increased body weight, suggesting MNK2 promotes weight gain. This was despite *in vitro* analysis which showed that ectopic MNK2 expression decreased insulin-stimulated lipid synthesis and the uptake of FFAs. To account for this discrepancy, it was suggested that MNK2 may regulate thermogenesis. Therefore, it was claimed that MNK2 variants may be involved in metabolic diseases such as obesity and diabetes mellitus.

Glucose uptake and diabetes

In an earlier patent, it was disclosed that over-expression of the MNK2b isoform negatively regulates glucose uptake in differentiated 3T3-L1 adipocytes [1]. In support of this, small interfering RNA knock-down of MNK2 led to an increase in the activity of a glucose response elements in various gene reporter assays. Interestingly, MNK2b overexpression also led to decreased activity of sterol regulatory element-binding protein (SREBP) response elements,

suggesting MNK2b may negatively regulate lipid metabolism. It was therefore proposed that inhibiting the expression or activity of MNK2b could potentially be used as prophylaxis or indeed therapy of diseases associated with insulin resistance, specifically type-2 diabetes.

Diet-induced obesity and adipogenesis

In an attempt to address these claims and understand the role of MNKs in metabolic disease, a recent study employed the use of MNK1- and MNK2-knockout (KO) mice in a model of diet-induced obesity [3]. In this study, the MNKs were found to be crucial in mediating adverse biological responses to a HFD: MNK2-KO mice had fewer but larger adipocytes, which did not increase further in size on a HFD. Consequently, MNK2-KO mice gained less weight than WT animals on a HFD; in contrast, MNK1-KO animals on a HFD gained weight similar to WT animals. Metabolic phenotyping suggests there is no reduction in energy intake or increase in energy expenditure to account for the decreased mass of MNK2-KO mice (unpublished data). Therefore, the major inference is that MNK2 may be important for regulating the development of new adipocytes and adipocyte metabolism. In support of this, when adipogenesis was assayed in 3T3-L1 cells in the presence of the MNK inhibitor CGP57380, lipid accumulation was substantially inhibited along with the expression of key adipogenic genes, suggesting MNK activity plays a role in adipocyte differentiation [3].

MNK2-KO mice also displayed better glucose tolerance and insulin sensitivity compared to WT mice on a HFD although these improvements were more striking in MNK1-KO mice [3]. However, our lab recently observed a somewhat different phenotype in MNK1-KO mice housed in a different animal facility and consuming a slightly different HFD, placing this finding in some doubt (unpublished data). Despite this, it was recently shown that mice lacking expression of both MNK1 and MNK2 (MNK-DKO) exhibit even greater and more robust protection from diet-induced obesity than MNK2-KO mice when challenged with a HFD (unpublished data). These findings suggest that the combined activity of MNK1 and MNK2 may be important for regulating weight gain. However, the roles of individual MNK isoforms requires clarification and the underlying mechanisms are yet to be determined.

Study hypotheses and aims

Given the implication of MNKs in metabolic disease, as evidenced in early patents [1,2], and their role in mediating weight gain in response to a HFD [3], the MNKs are strongly implicated in regulating the expansion of adipose tissue. This thesis will address three broad aims, as detailed below and summarised in Figure 1-6.

Aim 1

Hypothesis: MNKs regulate the development of new adipocytes from precursors (adipogenesis) given that MNK2-KO mice appear to have fewer adipocytes and an MNK inhibitor impairs adipogenesis *in vitro*.

The aim is to explore the requirement for MNK catalytic activity in 3T3-L1 adipogenesis using a number of specific inhibitors.

Aim 2

Hypothesis: MNK2 regulates adipogenesis and metabolism given that MNK2-KO mice have blunted weight gain and exhibit the greatest protection from diet-induced obesity.

The aim is to investigate the role and underlying mechanisms of MNK2 in adipogenesis and adipocyte metabolism using a 3T3-L1 MNK2-KO cell line and siRNA-mediated knockdown of *Mknk2*.

Aim 3

Catalytic activity is only one aspect of kinase function. Hypothesis: Non-catalytic interactions of MNK2 may regulate aspects adipocyte biology.

The aim is to assess possible non-catalytic functions of MNK2 pertaining to adipocytes and understand how they regulate adipocyte metabolism mechanistically.

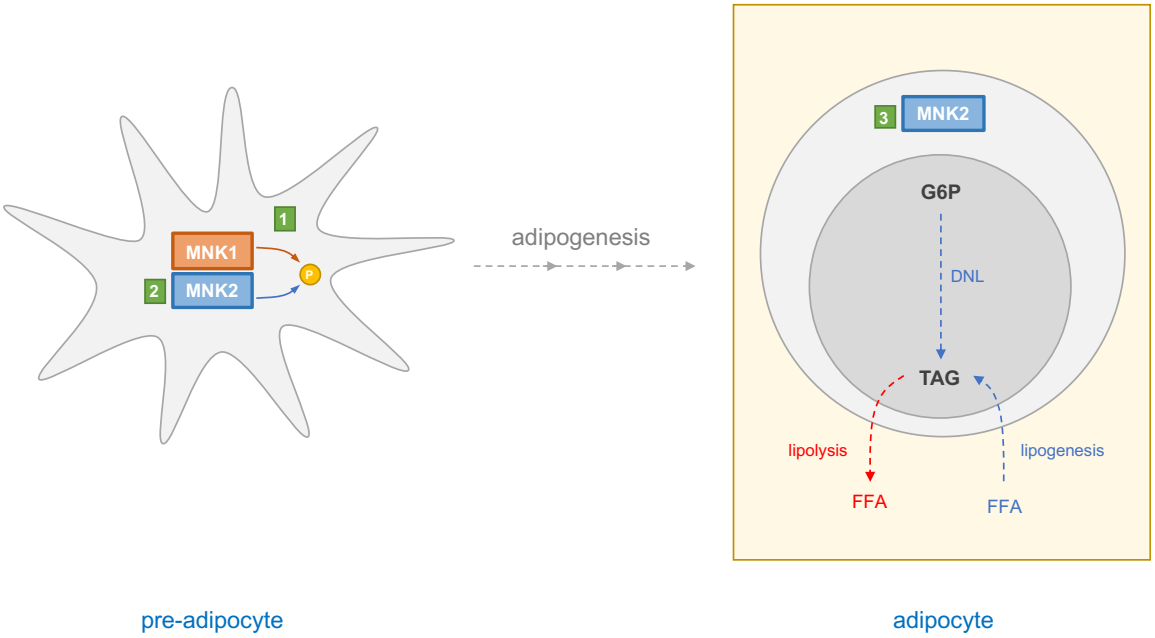

Figure 1-6: Aspects of adipocyte biology that are to be investigated in this study.

Aim [1] will explore the requirement for MNK catalytic activity in 3T3-L1 adipogenesis (i.e. phosphorylation of eIF4E, as depicted by (P)). Aim [2] will investigate specifically, the role and underlying mechanisms of MNK2 in adipogenesis, whilst Aim [3] will assess possible non-catalytic roles of MNK2 pertaining to adipocytes and their metabolism. Abbreviations: FFA: free fatty acid; G6P: glucose-6-phosphate; TAG: triacylglycerol; DNL: *de novo* lipogenesis.

Chapter 2
Materials and Methods

Tissue culture methods

Cell lines

Murine 3T3-L1 embryonic fibroblasts (ATCC; CL-173) used in this study were generously provided by Yeeshim Khew-Goodhall from the Centre for Cancer Biology (SA Pathology, Adelaide).

Culture media and growth conditions

Cells were maintained in high glucose Dulbecco's modified eagle medium (DMEM) (Invitrogen; 11995-065) supplemented with 10% foetal bovine serum (FBS) (Invitrogen; 10099-141) and 1% penicillin-streptomycin (Invitrogen; 15140-122) and grown at 37°C in a humidified incubator with 5% CO_2. Cultures were maintained in sterile 0.2 μm vented tissues culture flasks (Corning; 25, 75 or 175 cm^2). When required for experimentation cells were plated into appropriately sized culture dishes (Corning; 30 mm, 60 mm, 100 mm ∅) or plates (Corning; 6-well, 12-well, 24-well, 48-well or 96-well) at the required density.

Sub-culturing

3T3-L1 cells were strictly sub-cultured at 75-85% confluence every 2-3 days since maintenance at high growth densities lowers their adipogenic propensity. Cells were sub-cultured by aspirating the growth medium, washing once with sterile phosphate-buffered saline (PBS) and detaching adherent cells with TrypLE Express dissociation reagent (Invitrogen; 12605-028) (2 mL per 75 cm^2) for 2-5 min at 37°C. Detached cells were resuspended in growth medium and then split into new culture flasks containing fresh medium. If cell counts were required, the resuspended cells were transferred to 50 mL tubes (Falcon) and centrifuged at 850 rpm for 5 min to pellet cells. Following centrifugation, the majority of growth media was aspirated, and cells resuspended in the remaining volume (< 1 mL). Cell counts were performed as described below.

Trypan Blue exclusion

An equal volume of resuspended cells (20 μL) was mixed with Trypan Blue (Sigma; T6146) solution (0.4% w/v). Ten μL of this suspension was transferred to each chamber of a haemocytometer; the average number of cells per large square was then counted to calculate the concentration of cells as follows:

$$Concentration\left(\frac{cells}{ml}\right) = avg\ no.\ cells\ (per\ large\ square)\ \times\ 2\ (dilution\ factor) \times 10^4$$

Cryo-preservation of cells

Cells to be cryo-preserved were grown to 75-85% confluence. Growth media was aspirated, then cells washed once in PBS and detached with TrypLE Express. Detached cells were resuspended in growth media, transferred to a 50 mL tube and centrifuged at 850 rpm for 5 min. Growth media was aspirated completely, and cells were then gently resuspended in cryo-preservation media

(70% DMEM, 20% FBS, 10% DMSO). The cell suspension was gently mixed prior to aliquoting 0.5 mL to each cryo-tube. The cryo-tubes were transferred to a rate-controlled freezing chamber at –80°C for at least 24 h. Cryo-tubes were then transferred to a liquid nitrogen storage chamber for long-term cryo-preservation.

Resuscitation of cryopreserved cells

Cryopreserved cells were thawed quickly in a 37°C water bath, then added to a flask containing pre-warmed growth media. Following overnight incubation at 37°C, the growth medium was aspirated and replenished.

Animal studies

MNK1-KO, MNK2-KO and WT mice, previously developed on a C57BL/6 background [13], were housed in the South Australian Health and Medical Research Institute (SAHMRI) Bioresources Facility and maintained under a 12-h light/dark cycle (lights on at 07:00 h) at a constant temperature of 19-23°C with food and water available *ad libitum*. At four-weeks, mice were allocated to groups fed either an HFD (42% energy from lipid, 23% from protein, 35% from carbohydrate) (Specialty Feeds; SF15-095) or a chow diet (18% energy from fat, 24% from protein, 58% from carbohydrate) (Envigo) for a further 16-weeks. Diets were γ-irradiated at Steritech (Victoria, Australia) prior to delivery to the Bioresources Facility. At post-mortem, tissues and organs were dissected, snap-frozen, and stored at –80 °C until required for protein or RNA extraction. All experimental procedures involving mice were approved by the SAHMRI Animal Ethics Committee (approval numbers: SAM181, SAM324) and conducted in accordance with the South Australian Animal Welfare Act (1985) and Australian Code for the Care and Use of Animals for Scientific Purposes (2013).

Isolation of mouse embryonic fibroblasts (MEFs)

MEFs from MNK1-KO, MNK2-KO, and WT counterparts were prepared from mouse embryos on Day E13.5 – 14.5. Mice were sacrificed by CO_2 asphyxiation, and the abdominal area was dissected to expose the uterus (containing embryos). The uterus was removed and submerged in 70% ethanol, followed by a wash in cold PBS. In a biosafety cabinet, the embryos were popped out of their sacs and separated from the placenta. The foetuses were sacrificed by removing the head with a scalpel. Any blue and/or dark areas of blood were carefully removed from the foetuses and discarded. The foetuses were then transferred to a 50 mL tube and washed twice with 30 mL PBS. The washed foetal tissue was transferred to a 100 mm dish and shredded continuously using a scalpel for at least 12 min. The shredded tissue was collected into a 50 mL tube and digested with 7.5 mL of trypsin/EDTA (0.05%) (Invitrogen; 25300-054) at 37 °C for 5 min. The suspension was mixed by pipetting up and down, and the incubation repeated two more times. DNA was digested by the addition of 200 μL DNase I (10 mg/ml) (NEB; M0303S) and 15 mL of DMEM, incubated at 37°C for 5 min. The cells were centrifuged at 1000 rpm for 5 min,

resuspended in fresh growth media and then distributed to 15 cm plates, depending on the number of embryos harvested (3 embryos/plate). The final growth media volume was 30 mL per plate. After 24 h the growth media was aspirated and replenished. Cells were cultured until confluent (2-3 days), then cryo-preserved in MEF cryopreservation media (40% FBS, 10% DMSO, 50% DMEM).

Maintenance of MEFs

MEFs were maintained as described for 3T3-L1 pre-adipocytes, in *Culture media and growth conditions* and not used beyond passage 5.

3T3-L1 pre-adipocyte differentiation

For adipogenesis studies, 3T3-L1 pre-adipocytes were seeded at a density of 3.5 x 10^4 cells/cm^2, typically in six-well plates. Cells were grown to two-days post-confluence (Day 0) at which point the media was replaced with growth media freshly supplemented with 350 nM insulin, 500 μM 3-isobutyl-1-methylxanthine, 0.5 μM dexamethasone and 2 μM rosiglitazone (differentiation media). On day 3, the media was replaced with growth media supplemented with 350 nM insulin (maintenance media). The maintenance media was replenished every three-days until the cells were utilised for experimentation or the end-point of differentiation was reached (typically Days 9 or 10).

When assaying the effect of MNK inhibitors on adipocyte differentiation, compounds were added at the time of cell seeding (pre-treatment) and supplemented at each change of media, unless indicated otherwise. When assaying the effect of siRNA-mediated knockdown on adipocyte differentiation, cells were transfected 24 h after seeding, then re-transfected three-days post-induction, unless indicated otherwise; see *Gene silencing by small interfering RNA (siRNA)*.

Oil Red O (ORO) Staining

Typically, lipid staining was performed on differentiated adipocytes cultured in six-well plates. Volumes of 1 mL/well were used in this instance or otherwise scaled up or down, depending on the size of the culture vessel. Cells were stained at the end stage of differentiation, unless indicated otherwise. Growth media was first aspirated, then cells were washed twice with ice-cold PBS. Under a chemical fume-hood, cells were fixed in 10% formalin for 30 min with shaking.

Formalin was then removed from the wells and washed twice with Milli-Q water. Cells were washed with 60% isopropanol for 5 min with shaking whilst a working solution of ORO was prepared by mixing three-parts ORO stock (0.35% (w/v) in isopropanol) to two-parts Milli-Q water. This solution was mixed and then left undisturbed for 10 min, then filtered using a 0.2 μm filter. The 60% isopropanol was aspirated completely; the filtered ORO working solution was then added for 20 min with shaking. ORO was removed from each well which were then washed five-times with reverse osmosis (RO) water to remove residual unbound stain. Cells remained in

RO water for subsequent imaging. Six representative images were taken (per well) on the ZEISS Axio Cert A1 inverted microscope (ZEISS) using a 5X or 10X objective lens.

Following imaging, the amount of lipid staining (per well) was assayed semi-quantitatively by eluting the ORO in 100% isopropanol for 5 min with shaking. The absorbance at 490 nm was measured using the GloMax Discoverer (Promega).

Quantification of Oil Red O Staining by Image J

ORO-stained images were quantified using a macro script in Image J (NIH). Initially, the image files were converted to an RGB stack and the Green (slice 2) channel selected. The image threshold was adjusted so that red pixels corresponding to ORO were selected. The total threshold area was measured using the %Area statistic. The macro script was applied to batch analysis so that multiple image files could be analysed simultaneously. Six images (fields of view) were analysed per sample, unless indicated otherwise, and %Area was used to calculate the total lipid content relative to the control sample (100%).

Macro:

```
run("RGB Stack");
setSlice(2);
setAutoThreshold();
getThreshold(min, max)
setThreshold(0, 127);
run("Set Measurements...", "area area_fraction limit display redirect=None decimal=3");
run("Measure");
selectWindow("Results");
```

Gene silencing by small interfering RNA (siRNA)

SilencerSelect siRNA (ThermoFisher) were used to silence protein expression in 3T3-L1 cells (Table 2-1). siRNA was transfected using Lipofectamine RNAiMAX Transfection Reagent (Invitrogen; 13778150) in a 1:3 ratio, according to the manufacturer's instructions, except that reagent and siRNA dilutions were made in serum and antibiotic-free DMEM (Invitrogen; 11995-065), not Opti-MEM. siRNA directed against *Gapdh* was used as a positive transfection control whereas Negative Control No.1 siRNA with scrambled nucleotide composition (*Scrambled*) was used as a negative control. Where more than one siRNA was directed against a single gene, the molar ratio of each siRNA was proportioned so that the total molar ratio remained the same.

Table 2-1: SilencerSelect siRNA assays.

siRNA	Catalog. No.	Assay No.
***Mknk1* #1**	4390771	s69877
***Mknk1* #2**		s69878
***Mknk2* #1**		s69880
***Mknk2* #2**		s69881
Clk1		s64055
Clk4		s64060
Gapdh	4390849	
Scrambled	4390844	

siRNA efficacy testing

siRNA gene silencing efficacy was assayed after 48 and 96 h by Western blot where appropriate antibodies were available and/or by RT-qPCR using primers spanning exons in the 3'-end of mRNA (Table 2-5)

Metabolic assays

For all metabolic assays, 3T3-L1 cells were seeded in 96-well assay plates, transfected with or without siRNA as appropriate, and subjected to adipogenic differentiation, as described above.

Glucose uptake was measured using the Glucose Uptake-Glo Assay (Promega; J1341), and following the manufacturer's recommendations. Briefly, cells were serum-starved prior to the assay by incubation in serum-free DMEM (SF-DMEM) overnight. On the day of the assay (Day 9), cells were treated with SF-DMEM without glucose (Invitrogen; 11966-025, with 1 mM sodium pyruvate), supplemented with insulin (0.01, 0.1, 1, 10 or 100 nM) for 1 h. Cells were then treated with 1 mM 2-deoxyglucose (2DG), diluted in PBS for 10 min at room temperature. The assay was conducted according to the manufacturer's recommendations. Luminescence, corresponding to the amount of 2-DG uptake, was recorded using the GloMax Discoverer (Promega) with 0.3- to one-second integration.

Lipolysis was measured using the Lipolysis Assay Kit (Abcam; ab185433). On Day 9, cells were washed twice with Lipolysis Wash Buffer, then stimulated with or without 100 nM isoproterenol (in sterile water) for 3 h. The assay was conducted according to the manufacturer's recommendations. Absorbance at 570 nm was measured using the GloMax Discoverer (Promega) and glycerol concentration was determined using a standard curve.

Lactate levels were assayed using the L-Lactate Assay Kit (Abcam; ab65330) in media collected from differentiating adipocytes (Day 6). Media samples were first diluted 1:1000 in assay buffer,

then 2 μL of this dilution was assayed in duplicate in black polystyrene microplates (Corning; CLS3631). The assay was conducted according to the manufacturer's recommendations for a fluorometric assay. Fluorescence output (ex/em:520/580 nm) was measured using the GloMax Discoverer (Promega). L-Lactate concentration was determined using a standard curve and adjusted to the relevant dilution factor.

Molecular biology methods

RNA isolation from cell cultures

RNA was routinely harvested from cells grown in six-well plates using TRI Reagent (Sigma; T9424). Growth media was aspirated from cell monolayers, then lysed directly with TRI Reagent (1 mL/10cm^2) for 5 min to permit complete dissociation of nucleoprotein complexes. The lysate was then pipetted up and down and transferred to a microfuge tube.

Chloroform (0.2 mL) was added per 1 mL of TRI Reagent used in lysis, vortexed for 15 secs then incubated for 2-5 min at room temperature. Samples were centrifuged at 4 ºC for 15 min at >12,000 x g, separating the mixture into a lower red phenol-chloroform, interphase, and colourless upper aqueous phase. Four-hundred μL of the aqueous phase (containing RNA) was transferred to a new tube, to which 0.5 mL of isopropanol was added, vortexed thoroughly then placed at –20ºC overnight. The following day, RNA was precipitated by centrifugation for 30 minutes at >12,000 × g at 4°C. Supernatant was removed and the pellet washed with 1 mL 75% ethanol, vortexed and centrifuged for 5 min at >12,000 × g at 4°C. Supernatant was removed and the pellet left to air-dry. When completely dry, the pellet was resuspended in 50 μL of RNase-free water and mixed by repeated pipetting. Yield and purity were assayed on a Nanodrop 8000 Spectrophotometer (ThermoFisher). RNA was used immediately or stored at – 20ºC until required.

RNA isolation from tissues

To isolate RNA from tissues, 50-100 mg of snap-frozen mouse tissue was homogenised in 1 mL of TRI Reagent (Sigma) on ice with a rotor-stator homogeniser (Qiagen; TissueRuptor). Samples containing excessive fat content were centrifuged at 12,000 x g for 5 min at 4ºC and supernatant transferred to a new tube. All samples were then incubated for 5 min at room temperature to allow complete dissociation of nucleoprotein complexes.

Chloroform (0.2 mL) was then added to each sample, per 1 mL of TRI Reagent used in lysis. The samples were shaken vigorously for 60 sec then incubated for 2-5 min at room temperature. Samples were centrifuged for 15 min at >12,000 x g at 4 ºC; 400 μL of the aqueous phase was then transferred to a new tube. An equal volume of 70% ethanol was added to reach a final concentration of 35%, after which samples were processed using the PureLink RNA Mini Kit (ThermoFisher; 12183025), according to the manufacturer's recommendations. Briefly, samples

were transferred to a Spin Cartridge and centrifuged at 12,000 x g for 30 sec. The Spin Cartridge was washed once with Wash Buffer I, followed by two washes in Wash Buffer II, at 12,000 x g for 30 sec. RNA was eluted from the Spin Cartridge membrane in 30 μL of RNase-free water at 12,000 x g for 2 min. Yield and purity were assayed on a Nanodrop 8000 Spectrophotometer (ThermoFisher). RNA was stored at – 20 °C until required.

Reverse transcription

Reverse transcription (RT) was carried out using the QuantiNova Reverse Transcription Kit (Qiagen; 205413) which combines an efficient procedure for RT and genomic DNA (gDNA) removal. In the first step of the two-stage protocol, template RNA (1 μg) and RNase-free water were assembled in PCR reaction tubes to a final volume of 13 μL. Two μL of gDNA Removal Mix was then added to reach a final volume of 15 μL. Tubes were capped, briefly microfuged and then placed in a thermocycler (BioRad; 1709703) with the heated lid switched off. Stage 1 of the cycle was run, as detailed in Table 2-2. Subsequently, a mastermix containing 1 μL RT Enzyme and 4 μL RT mix was prepared per reaction. Five μL of this mastermix was dispensed to each sample which was then returned to the thermocycler for Stage 2 of the program (Table 2-2).

At the completion of the program, complementary DNA (cDNA) was diluted 1:10 with 180 μL Milli-Q water. cDNA was then immediately ready for use in down-stream applications. cDNA was stored at –20°C and freeze-thaw cycles were kept to a minimum.

Table 2-2: QuantiNova Reverse Transcription Program

Step	Temp (°C)	Time (min)	Stage
gDNA removal	45	2	1
Pause	4	Hold	
Annealing	25	3	2
Reverse transcription	45	10	
Inactivation of reaction	85	5	
Infinite hold, end of program	4	Hold	

Real time-qPCR (RT-qPCR) using SYBR Green

Quantitative gene expression analysis was performed using Fast SYBR Green Master Mix (Applied Biosystems; 4385617) on the StepOnePlus Real-Time PCR System (Applied Biosystems). RT-qPCR reactions were performed in MicroAmp Fast Optical 96-Well Reaction Plates (0.1 mL) (Applied Biosystems; 4346907) using gene-specific primers (Table 2-5) assembled in 18 μL of RT-qPCR mastermix (Table 2-3) and 2 μL of cDNA. Reaction plates were assayed using the cycling conditions detailed in Table 2-4. Melt curve analysis was performed on all assays to assess gene amplification specificity.

Primers were designed by ProbeFinder software (Roche), or manually using Primer3 software to anneal to exons spanning one or more introns, where possible, to distinguish between amplified cDNA and potential contaminating DNA. Primers were tested for their amplification efficiency and specificity as detailed below. All reactions were performed in triplicate. Relative gene expression was calculated using $2^{-\Delta\Delta Ct}$. A panel of reference genes were assessed for their stability across the adipogenic program, according to [188]. *Nono* and *Hprt* were selected as the internal reference genes as they were the most stable.

The relative expression of *Mknk1* and *Mknk2* in mouse tissues was calculated using $2^{-\Delta Ct}$. The geometric mean of *B2m* and *Hprt* was used as the internal reference.

Table 2-3: Components required for Fast SYBR mastermix assembly.

Component	Volume (μL)	[Final]
Forward primer (5 μM)	0.8	200 nM
Reverse primer (5 μM)	0.8	200 nM
Fast SYBR Green Mastermix (2x)	10.0	1x
RNase-free water	6.4	

Table 2-4: Fast SYBR RT-qPCR cycling conditions.

Step	Temp (°C)	Time (sec)	Cycles
DNA polymerase activation	95	20	Hold
Denature	95	3	40
Anneal and extend	60	30	

Table 2-5: Primers used for RT-qPCR gene expression analyses.

Gene	F Primer (5'-3')	R Primer (5'-3')
Acaca	TGCCTCTGAGAACCCGAAAC	GCCAATCCACTCGAAGACCA
B2m	CTGCTACGTAACACAGTTCCACCC	CATGATGCTTGATCACATGTCTCG
Cebpa	AAACAACGCAACGTGGAGAC	AGTTCACGGCTCAGCTGTTC
Cebpb	CTGCGGGGTTGTTGATGT	ATGCTCGAAACGGAAAAGGT
Cebpd	GCAGCCCCAAAAGCCAGTAAT	GATCAGGGAAGGGGTTGGAA
Clk1	CTTTAGGTGAAGGTGCTTTCG	CAGCTTCACAGTATCTATCCACATTT
Clk4	AGCGGATCTTAGGACCCATC	TGAACTATGCTCGTCCCAATC
Eif4e	TGTGAAAACAGAGATGCAGTCA	GCGTGGGACTGATAACCAAT
Fabp4	GGATGGAAAGTCGACCACAA	TGGAAGTCACGCCTTTCATA
Gapdh	GGGTTCCTATAAATACGGACTGC	CCATTTTGTCTACGGGACGA
Hprt	ACATTGTGGCCCTCTGTGTG	TTATGTCCCCCGTTGACTGA
Lpin1	AAGAGGAAAGCAAGCCTGAA	GGCTGCTCTCCGGTATTGT
Mknk1	GATTCCTCTGAGACTCCAAGTTAA	ACGCTTCTTCTTCCTCCTCTT
Mknk2	CCAGTGCCAGGGACATAGG	GCCACGCATCTTCTCAAACA
Nono	TGCTCCTGTGCCACCTGGTACTC	CCGGAGCTGGACGGTTGAATGC
Plin1	TGTACAGGGTGCCAGCAA	TCTGCAGGCCAACTCATTG
Pnpla2	GTGCATATGCCCTTTCCTGT	TTCTGATCTCTCCCAAGGTTCT
Pparg	TCCGTGATGGAAGACCACTCGCAT	CAGCAACCATTGGGTCAGCTCTTG

Primer efficiency testing

Primer pairs were assessed for amplification efficiency by generating a dilution series of cDNA covering four dilution points (undiluted, 1:5, 1:25, 1:125) and performing RT-qPCR analysis, as detailed above. Average Ct values were plotted against quantity (1, 0.2, 0.04, 0.008) on an X-log scale. A linear regression was performed, and the slope of the curve was then used to determine amplification efficiency according to:

$$\text{Efficiency (\%)} = \left(10^{\frac{-1}{slope}} - 1\right) \times 100$$

Primers with efficiencies between 90-110% were considered efficient.

RT-qPCR using TaqMan gene expression assays

Quantitative gene expression analysis was performed using TaqMan Fast Advanced MasterMix (Applied Biosystems) on a 7500 Fast Real Time PCR System (Applied Biosystems). RT-qPCR reactions were performed in MicroAmp Fast Optical 96-Well Reaction Plates (0.1 mL) (Applied Biosystems; 4346907) using pre-designed TaqMan assay probes (Table 2-6), (Invitrogen) assembled in 8 μL of RT-qPCR mastermix (Table 2-7) and 2 μL of cDNA. Reaction plates were

assayed using the program detailed in Table 2-8. All reactions were performed in triplicate. Relative gene expression was determined using $2^{-\Delta\Delta Ct}$; the geometric mean of *Nono* and *Hprt* was used as the internal reference.

Table 2-6: TaqMan assay probes used for RT-qPCR gene expression analyses.

Gene	Assay ID
Acaca	Mm01304257_m1
Acacb	Mm01204671_m1
Acly	Mm01302282_m1
Agpat9	Mm04211965_m1
B2m	Mm00437762_m1
Cd36	Mm00432403_m1
Chrebpa	Mm02342723_m1
Chrebpb	Mm04931160_m1
Dgat1	Mm00515643_m1
Dgat2	Mm00499536_m1
Fasn	Mm0062319_m1
Gapdh	Mm99999915_g1
Hprt	Mm03024075_m1
Ldha	Mm01612132_g1
Lipe	Mm00495349_m1
Lpin1	Mm00550511_m1
Lpl	Mm00434764_m1
Mgll	Mm0449274_m1
Nono	Mm00834875_g1
Pck1	Mm01247058_m1
Pdha	Mm00468675_m1
Plin1	Mm00558672_m1
Pnpla2	Mm00503040_m1
Ppargc1	Mm01208835_m1
Sfrp5	Mm01194236_m1
Slc2a4	Mm00436615_m1
Srebf1	Mm00550338_m1

Table 2-7: Components required for Fast TaqMan mastermix assembly.

Component	Volume (μL)	[Final]
TaqMan gene expression assay (20x)	0.5	1x
TaqMan Fast Advanced Mastermix (2x)	5.0	1x
RNase-free water	2.5	

Table 2-8: TaqMan RT-qPCR cycling conditions.

Step	Temp (°C)	Time (sec)	Cycles
UNG Incubation	50	120	Hold
Polymerase Activation	95	20	Hold
Denature	95	3	40
Anneal and extend	60	30	

RT-PCR of cdc2-like kinase (Clk) pre-mRNA

CLK splicing was assessed by PCR of cDNA samples using primers specific for the *Clk* splicing products (Table 2-9). PCR reactions were assembled in PCR reaction tubes according to Table 2-10 and transferred to a thermocycler using the conditions detailed in Table 2-11. PCR products were then analysed by agarose gel electrophoresis (2%); *see* Agarose gel electrophoresis.

Table 2-9: Primers used for *Clk* splicing product analyses.

Splicing Target	F Primer (5'-3')	R Primer (5'-3')
Clk1 E3-5	TGACTACATGGGCTACGAGC	TGCATTCCACCACTTTTCCG
Clk1 I3R	TAAACACAGGAGTCGCCACC	ACTTTAGTACCCTGTGGCCA
Clk1 I4R	GGATGATGAGGAGGGTCACC	TGATCGATGCATTCCACCACT
Clk4 E3-5	AGCAGCCCTAAGAGAAAGCG	TGCCGTGATCAATGCACTCT
Clk4 I3R	AGCAGCCCTAAGAGAAAGCG	ATTTTCCCCTCAGCACCCAG
Clk4 I4R	GGATGATGAGGAGGGTCACC	TGCCGTGATCAATGCACTCT

Table 2-10: Components required for *Clk* PCR primer mastermix assembly.

Component	Volume (μL)	[Final]
Forward primer (10 μM)	0.5	200 nM
Reverse primer (10 μM)	0.5	200 nM
OneTaq Hot Start Quickload Mastermix (2x)	12.5	1x
RNase-free water	10.5	
cDNA template	1	

Table 2-11: Thermocycler reaction conditions for *Clk* splicing product amplification.

Step	Temp (ºC)	Time (sec)	Cycles
Initial denaturation	94	30	Hold
Denaturation	94	15	30
Annealing			
E3-5	54	15	
I3R/ I4R			
Hprt	53		
Extension			
E3-5	68	90	
I3R/ I4R		30	
Hprt		15	
Final Extension	68	300	1
Hold, end of program	4	Indefinite	Hold

Extraction of protein

3T3-L1 and MEFs cell monolayers were harvested on ice in RIPA lysis buffer (50 mM Tris-HCl, pH 7.5, 150 mM NaCl, 1% (v/v) NP-40 (IGEPAL CA-630), 1% (v/v) sodium deoxycholate, 0.1% (v/v) sodium dodecyl sulphate (SDS), 1 mM ethylenediaminetetra-acetic acid (EDTA), 50 mM β-glycerophosphate, 0.5 mM $NaVO_3$, 0.1% (v/v) 2-mercaptoethanol and protease inhibitors (Roche; 11836170001)).

Lysates were scraped and collected into microfuge tubes. Insoluble material was removed by centrifugation at >12,000 x g for 10 min at 4 °C. Cleared supernatants were transferred to new tubes. Protein content was determined by the *Bradford protein assay* and lysates prepared to equal concentrations.

Bradford protein assay

Bradford Protein Dye Reagent Concentrate (BioRad; 5000006) was diluted 1:5 in Milli-Q water and set side to warm to room temperature. BSA protein standards were prepared by serial dilution in the same buffer used to prepare cell lysates. Protein content was assayed in duplicate, in clear 96-well assay plates (Corning). To reduce the concentration of agents that interfere with the dye, protein samples and standards were first diluted 1:10 in Milli-Q water prior to addition of the dye. One μL of protein sample was assayed in 250 μL of Bradford dye reagent. The plate was incubated for 5 min at room temperature, then absorbance was measured at 600 nm using the GloMax Discoverer (Promega). Protein concentration was determined from the Standard Curve.

Pouring gels for sodium dodecyl sulphate–polyacrylamide gel electrophoresis (SDS-PAGE)

When separating proteins 10 – 130 kDa in size, 13.5-0.36% acrylamide/bis-acrylamide resolving gels were cast in a Mini-PROTEAN Tetra Handcast System (Bio-Rad) according to Table 2-12. When separating proteins larger than 120 kDa, the amount of acrylamide and bis-acrylamide was reduced and 10.0-0.2% acrylamide/bis-acrylamide gels were cast. Once stacking gels were set, 5.0-0.13% stacking gels were cast on top.

Table 2-12: Formulation of SDS acrylamide/bis-acrylamide gels used for PAGE.

		10 – 130 kDa		> 120 kDa	
		[Final]		[Final]	
[Stock]	**Component**	**Resolving**	**Stacking**	**Resolving**	**Stacking**
40 %	Acrylamide	13.5 %	5.0 %	10.0 %	5.0 %
2 %	Bis-acrylamide	0.36 %	0.13 %	0.1 %	0.13 %
1.5 M	Tris-HCl pH 8.8	380 mM		380 mM	
1 M	Tris-HCl pH 6.8		125 mM		125 mM
20 %	SDS	0.1 %	0.1 %	0.1 %	0.1 %
10 %	APS	0.05 %	0.05 %	0.05 %	0.05 %
100 %	TEMED	0.1 %	0.1 %	0.1 %	0.1 %

Abbreviations: APS: ammonium persulfate; TEMED: N,N,N',N'-tetramethylethane-1,2-diamine

Western blot

Cell lysates were heated at 95°C for 5 min in Sample Buffer (5x) (500 mM Tris–HCl pH6.8, 10% (v/v) SDS, 20% (v/v) glycerol, 0.12% (w/v) bromophenol blue, 5% (v/v) 2-mercaptoethanol). Twenty μg of protein, alongside 1 μL Precision Plus Protein Ladder Dual Colour (Bio-Rad) was subjected to SDS-PAGE, using gels prepared above in Running Buffer (25 mM Tris, 192 mM glycine, 0.1% SDS, pH 8.3) at 180V for 60 min using the Mini-PROTEAN Tetra Cell System (BioRad), followed by electrophoretic transfer to 0.45 μm nitrocellulose membranes (BioRad; 1620115) in Transfer Buffer (5 mM Tris, 192 mM glycine, 20% (v/v) methanol, 0.02% (v/v) SDS, pH 8.3) at 100V for 65 min using the Mini Trans-Blot Cell System (Bio-Rad). Membranes were then blocked in PBS-0.05% Tween20 (PBST) containing 5% (w/v) skim milk powder for 30-60 min at room temperature. Membranes were probed with primary antibody prepared at the appropriate dilution in PBST with 5% BSA (Sigma) (w/v) (Table 2-13) overnight at 4°C. Thereafter, membranes were washed (3 x 5 min) in PBST and then incubated with fluorescently tagged secondary antibody for 1 h, diluted in PBST as detailed in Table 2-14. Membranes were washed in PBST (3 x 5 min), then visualised using the Odyssey Quantitative Imaging System (LI-COR).

Table 2-13: Primary antibodies used for detection of proteins by Western blot.

Abbreviations: M: mouse, R: Rabbit.

Target	Dilution	Species	Catalog. No.	Supplier
eIF4E	1:1000	R	CST-9742	Cell Signaling
P-eIF4E (Ser209)	1:1000	R	PA-44528G	ThermoFisher
rpS6	1:1000	M	sc-74459	Santa-Cruz
P-rpS6 (Ser240/244)	1:1000	R	CST-2215	Cell Signaling
ERK	1:1000	R	CST-9102	Cell Signaling
P-ERK (Thr202/Tyr204)	1:1000	R	CST-4370	Cell Signaling
PKB	1:1000	R	CST-4685	Cell Signaling
P-PKB (Ser473)	1:500	R	CST-9271	Cell Signaling
4EBP1	1:1000	R	CST-9644	Cell Signaling
P-4EBP1 (Ser65)	1:500	R	CST-9451	Cell Signaling
ACTIN	1:5000	M	A2228	Sigma
GAPDH	1:5000	M	G8795	Sigma
C/EBPα	1:500	R	CST-2295	Cell Signaling
C/EBPβ	1:500	R	sc-150	Santa-Cruz
P-C/EBPβ (Thr188)	1:500	R	CST-3084	Cell Signaling
C/EBPδ	1:500	R	CST-2318	Cell Signaling
CHOP	1:500	M	CST-2895	Cell Signaling
PPARγ	1:1000	R	CST-2443	Cell Signaling
SREBP1	1:500	M	MA-516124	ThermoFisher
GLUT4	1:1000	M	CST-2213	Cell Signaling
CD36	1:500	R	CST-14347	Cell Signaling
PLIN1	1:1000	R	CST-9349	Cell Signaling
LPIN1	1:1000	R	CST-14906	Cell Signaling
FABP4	1:1000	R	CST-3544	Cell Signaling
ATGL	1:1000	R	CST-2439	Cell Signaling
HSL	1:1000	R	CST-18381	Cell Signaling
FASN	1:1000	R	CST-3180	Cell Signaling
MNK1	1:1000	R	CST-2195	Cell Signaling
MNK2	1:1000	R	ab-84345	Abcam
CCND1	1:1000	R	CST-2978	Cell Signaling
CCND2	1:1000	R	CST-3741	Cell Signaling
CCND3	1:1000	M	CST-2936	Cell Signaling
RB	1:1000	M	CST-9309	Cell Signaling
P-RB (Ser780)	1:1000	R	CST-8180	Cell Signaling
P-RB (Ser807/811)	1:1000	R	CST-8516	Cell Signaling
$p27^{kip}$	1:500	R	sc-776	Santa-Cruz
GR	1:1000	R	CST-12041	Cell Signaling
CREB	1:500	R	CST-9197	Cell Signaling
P-CREB (Ser133)	1:500	R	CST-9198	Cell Signaling

Table 2-14: Secondary antibodies used for fluorescent detection of primary antibody.

Secondary Antibody	Dilution	Catalog. No.	Supplier
Goat anti-Rabbit IgG (H+L) DyLight 680 Conjugated	1:20,000	35568	Invitrogen
Goat anti-Mouse IgG (H+L) DyLight 800 Conjugated	1:20,000	35521	Invitrogen

Re-probing membranes

Membranes were immersed briefly in Milli-Q water to saturate the membrane, then incubated overnight at 4°C with appropriate primary antibody. Membranes were developed as described above. No stripping or additional blocking was performed.

DNA extraction

DNA was extracted using QuickExtract DNA Extraction Solution (Lucigen; QE0905T), following the manufacturer's recommendations. Briefly, cell monolayers were harvested from growth plates using TrypLE Express, then centrifuged at 200 x g for 5 min at room temperature. Cell pellets were then lysed in QuickExtract solution (50 μL/24-well), vortexed for 15 sec, incubated at 65°C for 6 min, vortexed, then incubated at 98°C for 2 min. DNA concentration and purity were measured on the Nanodrop 8000 (ThermoFisher). DNA was then ready for use in downstream applications.

Routine PCR

Routine PCR reactions were assembled using OneTaq HotStart QuickLoad MasterMix with Standard Buffer (NEB; M0488) according to the manufacturer's instructions (Table 2-17). The cycling conditions outlined in Table 2-18 were used unless stated otherwise and all reactions were performed in a thermocycler (BioRad; 1709703). Annealing temperatures for primer pairs were determined using the NEB T_m calculator (tmcalculator.neb.com) and the required extension times were calculated at 1 min/kb, as detailed in Table 2-19.

Table 2-17: Assembly of components for routine PCR reactions.

Component	Quantity
Forward primer (10 μM)	200 nM
Reverse primer (10 μM)	200 nM
OneTaq Hot Start QuickLoad Mastermix (2x)	1x
DNA template	10 – 100 ng
Nuclease-free water	to 25 or 50 μL

Table 2-18: Thermocycling conditions for routine PCR.

Step	Temp (°C)	Time	Cycles
Initial denaturation	94	30 sec	Hold
Denaturation	94	30 sec	30
Annealing	variable[1]	15 – 30 sec	
Extension	68	1 min/kb[2]	
Final Extension	68	5 min	1
Hold, end of program	4	Indefinite	Hold

[1] Annealing temperature was determined using NEB T_m calculator, as detailed in Table 2-19.

[2] See Table 2-19 for required extension time.

Table 2-19: PCR primer sequences, their required annealing temperature and extension times.

Primer	Sequence (5'-3')	Annealing Temp (°C)	Extension Time (sec)
pX458 F	ACCCTGATCCACCAGAGCAT	56	60
pX458 R	TAGTTA**ACCGGT**CTTGTACAGCTCGTCCATGC		
Ext F	AACAGGGGCAGAATCCTTTCGA	56	60
Ext R	AACATGGAGTGATCAAGGGCCA		
Int F	GAAGGTGAGCTGCAGAGAGC	53	10
Int R	CTGCAGCTGATAGACATCTGG		

Flanking *Age*I restriction site sequence is **bold underlined**.

Agarose gel electrophoresis

UltraPure Agarose (ThermoFisher) powder was dissolved, 1% or 2% (w/v), in 1x Tris-acetate-EDTA buffer (40 mM Tris, 20 mM acetic acid, 1 mM EDTA) with heating in a microwave oven. GelRed Nucleic Acid Gel Stain (Biotium; 41003) was diluted 1:10,000 in the molten agarose solution just prior to casting. Once set, wells were loaded with nucleic acid sample either directly (if using QuickLoad PCR Mastermix) or mixing with 6x DNA Gel Loading Dye (Invitrogen; R0611). Samples were run alongside a 100 bp DNA ladder (Invitrogen; 15628019), for products less than 2,500 bp, or a GeneRuler 1kb DNA ladder (ThermoFisher; SM0314) for products >2,500 bp. Gels were run for the required duration, usually for 60 min at 100V, then visualised using the ChemiDoc XRS+ system (Bio-Rad).

Sanger sequencing

Purified DNA (PD) template (plasmid or PCR product) was pre-mixed with the appropriate sequencing primer and nuclease-free water to a final volume of 12 μL, according to Table 2-20 Samples were submitted to the Australian Genome Research Facility (AGRF, Adelaide) for BDT labelling, purification and Sanger sequencing. Table 2-21 lists the sequencing primers used.

Table 2-20: Assembly of components required for Sanger sequencing of purified DNA.

Component	Quantity
Purified DNA (PD) template	
PCR Product 200 – 400 bp	6 - 12 ng
PCR Product 400 – 600 bp	12 - 18 ng
PCR Product 600 – 800 bp	18 - 30 ng
Plasmid, Double-stranded	600 - 1500 ng
Sequencing primer	10 pmol (0.8 pmol/µL)
Nuclease-free water	to 12 μL

Table 2-21: Sanger sequencing primer sequences.

Primer	Sequence (5'-3')	DNA template	Application
sgRNA Seq F	GCATATACGATACAAGGCTGTTAG	GeneART CRISPR vector	Verify ligated sgRNA sequence, forward direction
sgRNA Seq R	AGAAAAAAGCACCGACTCG		Verify ligated sgRNA sequence, reverse direction
Sel Cas Seq F	TGACAAATCTGGGCGCACCTGC		Verify EGFP/CD4 coding sequence, forward direction
Sel Cas Seq R	GGGACCGAACCCCGCGTTTATG		Verify EGFP/CD4 coding sequence, reverse direction
Mknk2 Seq F	AACAGGGGCAGAATCCTTTCGA	*Mknk2*-KO clones	Analyse *Mknk2* sequence of *Mknk2*-KO clones, forward direction
Mknk2 Seq R	AACATGGAGTGATCAAGGGCCA		Analyse *Mknk2* sequence of *Mknk2*-KO clones, reverse direction

Bacterial transformation

Chemically competent DH5α *Escherichia coli* were thawed on ice, gently mixed by flicking, then aliquoted into pre-chilled microfuge tubes (50 μL per transformation). The required volume of DNA (2-5 μL ligation mixture, 10-100 ng plasmid DNA or 100 pg pUC19 positive control) was pipetted into the cell suspension, mixed by gentle flicking and incubated on ice for 30 min. Cells were then heat-shocked at 42°C for exactly 30 sec and immediately returned to ice for 2-5 min; 950 μL of Luria Broth (LB) or Super Optimal Broth (SOB) was added to each sample prior to incubation at 37°C with shaking for up to 60 min. Varying volumes (50-200 μL) of the outgrowth broth were spread over LB-agar plates supplemented with 50 μg/mL carbenicillin, then incubated at 37°C for 16-18 h overnight.

Mini-preparation of plasmid DNA

Colonies were picked from LB-agar plates and used to inoculate polypropylene round-bottom capped tubes (FisherScientific; 14-959-11A) containing 5 mL LB and 50 μg/mL carbenicillin. Tubes were incubated at 37°C with rotation for 16-18 h overnight. Purified plasmid DNA was prepared using the NucleoSpin Plasmid Kit (Macherey-Nagel; 740588-250), following the manufacturer's recommendations. Plasmid DNA was eluted in 50 μL of Milli-Q water, then purity and quantity were assessed using the Nanodrop 8000 (ThermoFisher).

Midi-preparation of plasmid DNA

Plasmid DNA (from mini-preparation) was transformed into chemically competent DH5α *E. coli,* as described above. A single colony was picked from the transformation plate and used to inoculate a polypropylene round-bottom capped tube containing 5 mL LB and 50 μg/mL carbenicillin. The tube was incubated at 37°C with rotation for 6-8 h. Subsequently, 200 μL of this inoculation was transferred to a flask containing 200 mL LB and 50 μg/mL carbenicillin, which was incubated for 16-18 h at 37°C with shaking.

Plasmid DNA was prepared using the NucleoBond Xtra Midi Kit (Macherey-Nagel; 740410-50), following the manufacturer's recommendations. Plasmid DNA was eluted in 50-100 μL of Milli-Q water, and purity and quantity were assessed using Nanodrop 8000 (ThermoFisher). Plasmid identity was verified by *Agarose gel electrophoresis* and *Sanger sequencing*, as required.

Identification of DNA response element binding sites

Publicly accessible chromatin immunoprecipitation (ChIP)-sequence (ChIP-seq) data was extracted from ChIP-atlas (chip-atlas.org) using the 'Peak Browser' function. Briefly, ChIP-seq data for the antigen of interest was pulled from all cell types using a threshold significance of 100. The data were analysed using the Integrative Genomics Viewer (IGV) software (v2.0) (Broad Institute, California), aligned to the mouse NCBI37/mm9 genome assembly (July 2007). Enrichment peaks for the antigen of interest were analysed within ± 10 kb of a given gene's transcription start site. The corresponding regions were analysed on a genome browser (benchling.com) and putative binding sequences were identified using the available consensus sequence data. All reported transcription start site locations are referenced to the mouse NCBI37/mm9 genome assembly (July 2007).

Chromatin immunoprecipitation (ChIP)

3T3-L1 cells were seeded at a density of 3.5 x 10^4 cells/cm^2 in 100 mm culture dishes (Corning; 430167) and differentiated as detailed previously. At the desired time of analysis, proteins were cross-linked to DNA by the addition of 37% formaldehyde (Sigma; F8775) to a final concentration of 1% (270 μL/10 mL media) for 10 min at room temperature with shaking. One-M glycine was added to a final concentration of 125 mM (1.25 mL/10 mL media) to quench the

formaldehyde and incubated for 5 min at room temperature, with shaking. The media was then aspirated, and cells rinsed twice with ice-cold PBS. Adherent cells were scraped in 1 mL PBS, supplemented with protease inhibitor cocktail (Roche), and centrifuged at 1000 × g for 5 min at 4°C. Supernatant was removed and the cell pellet was lysed in 400 μL ChIP lysis buffer (50mM HEPES-KOH, pH 7.5, 140 mM NaCl, 1mM EDTA, pH8, 1% Triton X-100, 0.1% sodium deoxycholate, 0.1% SDS, 1 x protease inhibitor cocktail). Lysates were sonicated on ice for 3 min (in 30 sec bursts; 30 sec breaks between bursts) using an ultrasonic processor (Sonics; VCX130PB) at 30% amplitude. Following sonication, cell debris was pelleted by centrifugation at 8000 × g for 10 min at 4°C and the supernatant, containing chromatin, was transferred to a new tube. Chromatin was subsequently diluted with 600 μL RIPA buffer (50 mM Tris-HCl pH 8, 150 mM NaCl, 2 mM EDTA, 1% NP-40 (IGEPAL), 0.5% sodium deoxycholate, 0.1% SDS, 1 x protease inhibitor cocktail), and pre-cleared with 20 μL ChIP-grade Protein G Magnetic Beads (Cell Signaling Technology; 9006) for 2 h at 4°C with rotation. Magnetic beads were pelleted using a magnetic separation rack, and pre-cleared chromatin was transferred to a new tube. To serve as the input control, 1% of chromatin was removed from each sample and stored at –20°C.

Immunoprecipitating antibodies were then added to the appropriate chromatin samples and incubated overnight at 4°C with rotation, as detailed in Table 2-22. The following day, immune complexes were collected by adding 20 μL ChIP-grade Protein G Magnetic Beads to each sample and incubating for 2 h at 4°C with rotation. Immune complexes were pelleted using a magnetic separation rack, then washed three-times with 1 mL Low Salt Wash Buffer (20 mM Tris-HCl, pH 8, 150 mM NaCl, 2 mM EDTA, 1% Triton X-100, 0.1% SDS) for 5 min at 4°C with rotation. This was followed by a final wash with 1 mL High Salt Wash Buffer (20 mM Tris-HCl, pH 8, 500 mM NaCl, 2 mM EDTA, 1% Triton X-100, 0.1% SDS).

Chromatin was then eluted in 150 μL Elution Buffer (100 mM $NaHCO_3$, 1% SDS) for 30 min at 65°C with shaking (1200 rpm). Magnetic beads were pelleted and the supernatant containing eluted chromatin was transferred to a new tube. At this point, Elution Buffer was also added to each of the 1% input samples. Cross-links were reversed by adding 6 μL 5M NaCl and 2 μL Proteinase K (NEB; P8107S) to all samples, which were then incubated at 65°C overnight. DNA was purified using QIAquick PCR clean-up kit (Qiagen; 28106), following the manufacturer's instructions. DNA was eluted in 50 μL of Elution Buffer.

Table 2-22: Antibodies used for ChIP.

Target	Dilution	Species	Catalog.	Supplier
C/EBPα	1:100	R	CST-2295	Cell Signaling
C/EBPβ	1:100	R	sc-150	Santa-Cruz
P-CREB	1:100	R	CST-9198	Cell Signaling
GR	1:100	R	CST-12041	Cell Signaling
IgG	1:1000	R	CST-2729	Cell Signaling
PPARγ	1:100	R	CST-2443	Cell Signaling

qRT-PCR was performed as described previously; see *Real-time quantitative PCR*. Eluted chromatin was used as the template using the cycling conditions, detailed in Table 2-23. Protein enrichment was calculated using the 'percent input method' whereby signals obtained from each immunoprecipitation were expressed as a percentage of the total input chromatin.

Primers were designed manually using Primer3 Plus (primer3plus.com) to flank the putative DNA binding site(s) of the relevant protein (Table 2-24). All primers were tested for their amplification efficiency and specificity using sonicated chromatin as the template.

$$\% \text{ Input} = 1\% \times 2^{(\text{C[T] 1\% Input Sample} - \text{C[T] IP Sample})}$$

Table 2-23: RT-qPCR cycling conditions used for ChIP.

Step	Temp (°C)	Time (sec)	Cycles
DNA polymerase activation	95	180	Hold
Denaturation	95	15	40
Annealing and extension	60	60	

Table 2-24: Primers used for enrichment of protein-bound DNA regions.

Gene promoter, type of response element and the distance from transcription start site are indicated. Regions where no specific enrichment was expected are indicated as NEG (negative).

Protein	DNA Region	F Primer (5'-3')	R Primer (5'-3')
CREB	*Cebpb* CRE -60/106	CCCCGCGTTCATGCAC	CCACTTCCATGGGTCTAAAGGC
	Cebpb CRE -2343/2398	CATGGCCTATTGAGCAAAGAACC	ACCTCATCACAGAGCTTGGC
	Cebpd CRE -41	AAACCGCACAAACAGGAAGGAG	ACCGCCGCCTTTTCTAGC
	Mknk1 CRE -60	AGTGAACTGGCCTTGCTTCTC	GTCGAGAACGCGGAAGAGG
	Mknk2 CRE -372	AAGGGGAGATTCCGAGGGAAG	AGCCTCTCCACACAGTCCTC
GR	*Cebpb* GRE +20	GCGCCGCCTTATAAACCTC	CAGGCGGTGCATGAACG
	Cebpb GRE -1161	GCTAGCGTCTTACCCTTTCCC	CAACCTTCGGTGTTATCTGCTGAG
	Cebpd GRE -98	TCCGCCTTTGCTATGTCTGAAG	ACTCCTTGCCTTCCCTCCTTC
	Mknk1 GRE -142	CTGCCCTCAGGTTTACAAGAACTC	AGAAGCAAGGCCAGTTCACTG
	Mknk2 GRE -86	ACCAGTCTCCGCCTTTCTCAG	TAAGCTCCGCCCCTTAAACG
	Mknk2 GRE -1883	TCTGACAGCCAAGTACGTCTTC	TGGTGCCTATAGGGTGAACATC
	Mknk2 GRE -3270	GTCAGTGTCCTATGCTTGGGATTG	CTTATGTGGTGTGATCTGGTGAGG
C/EBPα	*Mknk2* C/EBPRE -1204/1258	CAGGGGATAGAACTTCAGCTCAAG	CTCTTACATGTGTCCCAGGAATGG
	Cebpa C/EBPRE -203/227	GATCTCTCTCCACTAGCACTATGC	TTTTATAGAGGGTCGGGCATCG
	Pparg C/EBPRE -269/289	TTGGCCAAATACGTTTATCTGGTG	GCGTGAACTGTACAGTAGTTGG
	Pparg C/EBPRE -3997/4006	GCACCTTTTATGAGTTCTCTGTGG	GGGGTGGCCCTTTAATATAGGTATG
C/EBPβ	*Mknk2* C/EBPRE -264/290	AACACGGCTGCGCACTTC	GGCTGCAGTCGAGTATCTTTTCAC
	Mknk2 C/EBPRE -1204/1258	CAGGGGATAGAACTTCAGCTCAAG	CTCTTACATGTGTCCCAGGAATGG
	Cebpa C/EBPRE -203/227	GATCTCTCTCCACTAGCACTATGC	TTTTATAGAGGGTCGGGCATCG
	Pparg C/EBPRE -269/289	TTGGCCAAATACGTTTATCTGGTG	GCGTGAACTGTACAGTAGTTGG
	Pparg C/EBPRE -3997/4006	GCACCTTTTATGAGTTCTCTGTGG	GGGGTGGCCCTTTAATATAGGTATG

PPARγ	*Mknk2* PPARE -1975	ATGTTCACCCTATAGGCACCAG	TGGGAGCCTAGCTTGTAAACAG
	Mknk2 PPARE -3348	CCATAGAGGAAGAACTGAGACAGC	GGCAGAGCATGTGTCTATTGTACC
	Mknk2 PPARE -3993	CCATAGAGGAAGAACTGAGACAGC	GGCAGAGCATGTGTCTATTGTACC
	Cebpa PPARE -125	GATCTCTCTCCACTAGCACTATGC	TTTTATAGAGGGTCGGGCATCG
	Fabp4 PPARE -2945	TGGGAACAGCCTGGCTTG	CAGGCAAAGGTTAGAAGGATGC
	Fabp4 PPARE -5376	GCTGTGACACTTCCACTAGTGAAC	CCAGAGAGAAGGGATTGTAGTCAG
NEG	*Cebpb* NEG -12460	TTCCTCAACCTCCTGTCTTGTCTC	GAACTGTACAGCATTCCTGACCAG
	Cebpd NEG -1378	GTTGGCGGGTTTCTGAATACAC	CTGGGTCCACTCACTACGTTTATG
	Mknk1 NEG -6325	GTGGCTTCACCTTTACACATTACC	TTTGTACCTCTGCCCTCTGCTC
	Mknk2 NEG -4862	GAGTCAACATGGCAGGCTAAAC	GGAGAAGAGAAATATAGGCTTGGG
	Cebpa NEG -3111	GCTTGGAGGAAGACATACATGCTG	AGGCGACCTAGGACCTTTAAATAC
	Pparg NEG -17510	CCAGGTCTACCTTTTGACATCTCC	CCAGAGAAGCCAGTGACAATACAG
	Fabp4 NEG -1424	CTCAGGCTTCCTACTGGATAAGAC	GGCTAATCGCTTGAGAACATGTC

Assessing protein-protein interactions

Potential interaction partners of MNK2 were assessed using the STRING database (string-db.org). Searching the database summarised the network of predicted associations with murine MNK2 based on experimental, co-expression, text-mining, neighbourhood and co-occurrence evidence sources. Default search settings were applied.

Cell cycle and size analysis

Propidium iodide (PI) staining was used to analyse cell cycle stage of differentiating pre-adipocytes. At the required time, cells were washed in PBS and collected into FACS tubes using TrypLE Express. Cells were pelleted at 900 rpm for 5 min, then resuspended in 300 μL by repeated pipetting. Cells were then fixed in 700 μL 100% MeOH (–80ºC), added drop-wise with vortexing. Cells were incubated at 4ºC for at least 30 min, or for several days prior to staining.

Cells were centrifuged at 900 rpm for 5 min, then resuspended in 300 μL PI Staining Buffer (16 μg/mL PI, 10 μg/mL RNase A, PBS). Cells were stained for 30 min at room temperature in the dark and PI signal intensity was analysed on a BD FACSCantoII Flow Analyser (BD Biosciences) (15,000 gated events per sample) using BD FACSDiva Software (BD Biosciences).

Statistics

All values are given as mean ± standard error of the mean (SEM). Differences between two groups were assessed using unpaired two-tailed t-tests, unless otherwise specified; comparisons between multiple groups were performed by one or two-way ANOVA. All statistical analysis was performed using GraphPad Prism (v8) for Macintosh.

CRISPR-Cas9 genetic editing methods

Construction of GeneART CRISPR-EGFP vector

The coding sequence (CDS) for enhanced green fluorescent protein (EGFP) in vector pX458, which included a flanking *Eco*RI site, was amplified by PCR using pX458 F and R primers (Table 2-19). The amplified PCR product was then purified using the QIAquick PCR Purification Kit (Qiagen; 28106), according to the manufacturer's recommendations. The EGFP CDS and GeneART CRISPR-CD4 vector were subsequently digested with *Eco*RI-HF and *Age*I-HF, according to Table 2-25.

Table 2-25: *Eco*RI and *Age*I restriction digestion.

Component	Volume (μL)	[Final]
Purified DNA		
EGFP CDS	30 μL	
GeneART CRISPR-CD4	5 μg	
NEB CutSmart Buffer (10x)	5	1x
***Age*I-HF**	2	20 units
***Eco*RI-HF**	2	20 units
milliQ water	to 50 μL	
Incubate at 37°C for 60 min		
Heat-inactivate at 65°C for 20 min		

The digestion products were analysed by *Agarose gel electrophoresis*, and the products corresponding to the GeneART CRISPR vector backbone (~8.5 kb) and EGFP CDS (~0.7 kb) were gel-purified using the GeneJET Gel Purification Kit (ThermoFisher; K0691).

The purified vector backbone and EGFP CDS were subsequently ligated at 16°C overnight using 3:1 and 6:1 insert:vector molar ratios (Table 2-26). Five μL of the ligation reaction was transformed into DH5α competent cells, as detailed previously. Plasmid DNA was prepared from transformed colonies as detailed previously; see *Mini-preparation of plasmid DNA,* and then screened by *Eco*RI and *Age*I restriction enzyme digestion (Table 2-25) and gel electrophoresis to identify plasmids with successfully ligated EGFP CDS. Vectors with successfully ligated EGFP were validated by *Sanger sequencing*.

Table 2-26: Ligation of EGFP CDS into GeneART CRISPR backbone.

Component	(3:1)	(6:1)	[Final]
***Eco*RI-*Age*I GeneART CRISPR backbone**	15 fmol	15 fmol	
***Eco*RI-*Age*I EGFP CDS**	45 fmol	90 fmol	
T4 DNA Ligation Buffer (10x)	2 μL	2 μL	1x
T4 DNA Ligase	1 μL	1 μL	1 unit
milliQ water	to 20 μL	to 20 μL	
Assemble components, then incubate at 16°C overnight			

Single guide RNA (sgRNA) design and selection

sgRNAs for *Mknk2* were designed using the 'CRISPR sgRNA' design module on Benchling (benchling.com). The module ranked sgRNAs based on both their specificity and on-target efficiency. sgRNAs with the highest ranked on-target efficiency satisfying the requirements of the KO approach were selected (Table 2-27).

Table 2-27: Single-guide RNA (sgRNA) sequences selected for the KO of *Mknk2*.

sgRNA	Sequence (5'-3')	PAM
***Mknk2* E4**	CTACTGACAGCTTCTCAGGC	AGG
***Mknk2* E5**	GTTGGTGATGAGATTGACAC	AGG

Abbreviations: PAM: protospacer adjacent motif.

Annealing, phosphorylation and ligation of sgRNAs

For ligation of sgRNA into GeneART CRISPR vectors, single-stranded oligonucleotides corresponding to the sgRNA sequence and its reverse complement were synthesised (Table 2-28). Oligonucleotides were specially-designed with 3' overhangs to facilitate ligation.

Table 2-28: sgRNAs oligonucleotide sequences.

Specially-designed 3' overhangs are bold underlined.

Oligonucleotide	Sequence (5'-3')
***Mknk2* E4 Top**	CTACTGACAGCTTCTCAGGC**GTTTT**
***Mknk2* E4 Bottom**	GCCTGAGAAGCTGTCAGTAG**CGGTG**
***Mknk2* E5 Top**	GTTGGTGATGAGATTGACAC**GTTTT**
***Mknk2* E5 Bottom**	GTGTCAATCTCATCACCAAC**CGGTG**

Oligonucleotides were phosphorylated and annealed in a thermocycler using the components and reaction conditions outlined in Tables 2-29 and 2-30, respectively. The annealed products were then diluted 1:200 to acquire a concentration of 0.1 pmol/μL.

Table 2-29: Assembly of components for annealing of sgRNA oligonucleotides.

Component	Volume (μL)	[Final]
Top strand oligo (200 μM)	1	20 μM
Bottom strand oligo (200 μM)	1	20 μM
T4 DNA Ligation Buffer (10x)	1	1x
T4 Polynucleotide Kinase (PNK)	1	1 unit
milliQ water	6	

Table 2-30: Thermocycling conditions for annealing of sgRNA oligonucleotides.

Step	Temp (°C)	Time (min)
Phosphorylation	37	30
Annealing	95	Ramp-down 5°C min^{-1} to 25°C
	25	

Prior to ligation of sgRNAs, the appropriate GeneART CRISPR vector was linearised by *Bae*I restriction digestion, overnight at 25°C (Table 2-31), then gel-purified from a 1% agarose gel using the GeneJET Gel Extraction Kit (ThermoFisher; K0691) according to the manufacturer's instructions. Annealed oligonucleotides (sgRNAs) were then ligated into the linearised GeneART CRISPR vector at 16°C overnight (Table 2-32). Five μL of the ligation reaction was transformed into DH5α competent cells, as detailed previously. Plasmid DNA was prepared from transformed colonies as detailed previously; see *Mini-preparation of plasmid DNA*.

Table 2-31: Assembly of components for *Bae*I linearisation of GeneART CRISPR vector.

Component	Volume (μL)	[Final]
GeneART CRISPR vector	2-6 μg	
NEB CutSmart Buffer (10x)	10	1x
***Bae*I**	5	50 units
S-adenosyl-methionine (SAM) (320 μM)	12.5	40 μM
milliQ water	to 100 μL	
Assemble components, then incubate at 25°C overnight		

Table 2-32: Assembly of components for ligation of sgRNA into GeneART CRISPR vector.

Component	Volume (μL)	[Final]
Linearised GeneART CRISPR vector	100 ng	15 fmol/μL
Annealed oligos (sgRNA) (0.1 pmol/μL)	2	100 fmol/μL
T4 DNA Ligation Buffer (10x)	1	1x
T4 DNA Ligase	1	1 unit
milliQ water	to 10 μL	
Assemble components, then incubate at 16°C overnight		

Screening vectors with successfully ligated sgRNA

To identify plasmids with successfully ligated sgRNA, sequential *Bae*I and *Eco*RI restriction digestion was performed on DNA mini-preparations (Table 2-33), and then analysed by gel electrophoresis.

Table 2-33: Assembly of components for sequential *Bae*I and *Eco*RI restriction digestion.

Component	Volume (μL)	[Final]
GeneART CRISPR-sgRNA ligated plasmid	500 ng	
NEB CutSmart Buffer (10x)	1.5	1x
***Bae*I**	0.5	5 units
SAM (320 μM)	1.88	40 μM
milliQ water	to 15 μL	
Incubate at 25°C for 15 min		
***Eco*RI-HF**	0.5	5 units
Incubate at 37°C for 15 min		

Nucleofection of sgRNA-GeneART CRISPR vectors

Undifferentiated 3T3-L1 cells were simultaneously transfected with EGFP-*Mknk2*-E5 and CD4-*Mknk2*-E4 vectors using the SE Cell Line 4D-Nucleofector X Kit L (Lonza; V4XC-1024), and following the '4D-Nucleofector Protocol for undifferentiated 3T3-L1 cells' (Lonza Knowledge Database). Briefly, 3T3-L1 cells at ~80% confluence were collected from T175 flasks using TrypLE Express. One μg of each vector was aliquoted to the bottom of a microfuge tube, after which 1.0 x 10^6 cells, resuspended in 4D-Nucleofector solution with supplement, was added. The entire contents of the tube were transferred to a Nucleocuvette Vessel and placed into the retainer of the 4D-Nucleofector X Unit (program CM137). After the program run, cells were resuspended with pre-warmed growth medium (400 μL) and mixed by gentle pipetting using the kit-supplied pipette. Cells were then transferred to new growth flasks (T175) and incubated for 48 h.

Fluorescence-activated cell sorting (FACS) of $CD4^+/EGFP^+$ cells

Forty-eight h post-nucleofection, 3T3-L1 cells were collected from T175 flasks using TrypLE Express, washed once in PBS, then resuspended in Flow Cytometry Staining Buffer (1 x PBS, 5 mM EDTA) and incubated with anti-CD4 antibody (BD Pharmingen; 555347) for 30 min at 4ºC, covered from light. $CD4^+/EGFP^+$ cells were sorted individually into 96-well plates using a FACSAriaIII Fusion Cell Sorter (BD Biosciences) and FACSDiva 8.0 Software (BD) at the Australian Cancer Research Foundation (ACRF) Flow and Laser-Scanning Facility (SAHMRI). Plates were monitored daily thereafter for growth and single-cell colony formation. Colonies were progressively sub-cultured to 24-well plates, six-well plates and eventually to T25 flasks. To reduce any adverse effects on adipocyte differentiation propensity, care was taken to minimise cell-cell contact and to ensure colonies were sub-cultured prior to reaching confluence.

Screening of Mknk2-KO clones

DNA from $CD4^+/EGFP^+$ single-cell colonies was harvested, amplified by PCR using External (Ext) and Internal (Int) primers, as detailed in Table 2-17 to 2-19, and analysed by gel electrophoresis. Clones satisfying both screening measures, were analysed by Sanger sequencing using the Ext amplicon as the DNA template and sequencing primers detailed in Table 2-19.

Chapter 3
MNKs and eIF4E in 3T3-L1 pre-adipocyte differentiation

Introduction

Over the decades, substantial interest in eIF4E and the MNKs has largely focused on their role in cellular transformation and cancer where the control of protein translation is important for cell growth, proliferation and survival (reviewed in [189]). However, the MNKs are also implicated in a broad array of other biological functions, including cellular responses to inflammation, [190], cytokine production [191], and more recently, in mediating adverse responses to high-fat feeding in mice [3]. In the latter study, MNK1/2 were reported to mediate aspects of cell metabolism in distinct ways. MNK2-KO mice were protected from weight gain, whilst MNK1-KO mice displayed improved insulin and glycaemic responses when challenged with an HFD [3]. On a regular chow diet, MNK2-KO mice had fewer but larger adipocytes than their WT counterparts, suggesting a deficiency in the development of new adipocytes. Furthermore, adipocytes from MNK2-KO mice failed to increase in size on an HFD, consistent with their blunted weight gain, suggesting a deficiency in fat storage or lipid metabolism more generally. MNK1-KO mice were not protected from HFD-induced weight gain; however, improvements were observed in insulin sensitivity and glucose tolerance. These findings suggest MNK2 plays a distinct role from MNK1 in adipocyte biology in terms of the development of new adipocytes and in the metabolism of mature adipocytes.

Adipocyte development, a process termed *adipogenesis*, has been widely studied for more than four decades using 3T3-L1 pre-adipocytes [82]. Growth-arrested 3T3-L1 fibroblasts rapidly differentiate into mature, functional, lipid-laden adipocytes following exposure to a cocktail of 3-isobutyl-1-methylxanthine (IBMX), dexamethasone (DEX) and insulin (INS), which can be further enhanced by the addition of rosiglitazone (ROSI), a thiazolidinedione and PPARγ agonist [88].

MAPK signalling (p38 and ERK1/2) is involved in regulating various aspects of adipogenesis (reviewed in [192]) and activating the MNKs [5–7]. Whilst MNK1 activity is induced by p38 MAPK and ERK1/2 signalling, MNK2 has high basal activity due to its tight association with ERK1/2, and its activity is not further enhanced by stimuli [7,61]. MNK2 is reported to be the predominant MNK isoform in adipose tissue [3]; however, the expression and activity of MNKs in differentiating pre-adipocytes is not well-established. Understanding the expression of MNKs may provide new insights into the control of adipocyte differentiation and the integration of the early signalling events.

Given the MNKs are activated downstream of MAPK signalling, it is hypothesised that MNK activity is important for adipogenesis. The role of MNK activity in adipocyte development was first investigated using CGP57380 [3], a low potency, ATP-competitive MNK1/2 inhibitor. When assayed in 3T3-L1 pre-adipocytes, CGP57380 inhibited the accumulation of lipid and substantially inhibited the expression of key adipogenic genes, PPARγ, C/EBPα, SREBP1c, GLUT4 and CD36, at both 3 and 6 days of the program. These data suggest that MNKs play a role in the

differentiation of 3T3-L1 cells into adipocytes and indicate that they may also play a role in adipocyte differentiation *in vivo* [3]. However, one caveat is that whilst CGP57380 targets MNKs, it also inhibits CK1, BRSK2 and MKK1 with similar potency [64]. This is a common limitation of ATP-competitive inhibitors, arising from the similarity between ATP binding sites in different protein kinases. CGP57380 is not a specific inhibitor of the MNKs and thus results obtained from its use in cell-based assays are difficult to interpret unambiguously [64]. Increasing interest in developing MNK therapeutics for oncology has driven the development of new classes of MNK inhibitor (reviewed in [189]). An MNK inhibitor containing a thieno[2,3-d]pyrimidine scaffold, MNK-I1, has increased targeting specificity and greater potency than CGP57380 [65]. A key question was whether MNK-I1 similarly affects adipocyte differentiation like CGP57380.

The only *in vivo* validated substrate of the MNKs is eIF4E, which is phosphorylated at Serine 209 [8,11]. It is not known whether the impaired adipocyte differentiation due to inhibition of MNK activity is due to the lack of P-eIF4E (i.e. dependent on the phosphorylation of eIF4E) or whether another MNK substrate(s) is involved. This is quite plausible given there have been several reports of additional MNK substrates [44,45,48,49,51], although none have been validated *in vivo*.

This Chapter aimed to evaluate the expression and activity of MNKs in 3T3-L1 pre-adipocytes and provide new insights into the early steps in the control of adipocyte development. Additionally, given eIF4E is a physiologically relevant substrate of the MNKs, this Chapter also assessed whether P-eIF4E or MNK activity more generally is required for adipogenesis using a number of specific MNK inhibitors.

Results

Expression of MNK1/2 in 3T3-L1 pre-adipocytes

To assess the relevance of MNKs as factors involved in the regulation of adipocyte differentiation, MNK1 and MNK2 expression was assessed by RT-qPCR and Western blot in differentiating 3T3-L1 murine pre-adipocytes. RNA and protein were collected from two-day post-confluent, growth-arrested pre-adipocytes (Day 0) prior to adipogenic induction, after which samples were collected at regular intervals over a period of nine days. *Mknk2* levels were induced in the first 3 h of adipogenic induction, increasing four-fold after 6 h, suggesting *Mknk2* is increased by hormone induction (Figure 3-1A). Thereafter, *Mknk2* expression progressively increased and was highest in mature, differentiated adipocytes on Day 9, consistent with the fact MNK2 is the predominant isoform in adipose tissue [3]. In contrast, *Mknk1* levels fell two-fold within 3 h of adipogenic induction and remained at that level throughout adipogenesis (Figure 3-1A); this was not reflected in reduced MNK1 protein levels, suggesting that MNK1 is stably expressed throughout adipogenesis (Figure 3-1B). Unfortunately, there is no suitable antibody to assess MNK2 expression; however, given that eIF4E is the physiologically relevant substrate of the MNKs, its phosphorylation (P-eIF4E) was used as a read-out of MNK activity and therefore an indirect measure of MNK expression. P-eIF4E levels were initially reduced from basal levels after adipogenic induction (3- and 6 h) but remained at or above basal levels from 24 h, peaking at Day 6. (Figure 3-1B). The elevation in P-eIF4E levels was consistent with increased *Mknk2* expression, suggesting MNK2 expression is increased during adipogenesis; eIF4E levels remained relatively stable but trended higher over the course of adipogenesis (Figure 3-1B). The apparent increase in eIF4E is consistent with the increased level of protein synthesis occurring during differentiation but was not attributable to increased *Eif4e* transcription, since *Eif4e* levels were mostly stable throughout adipogenesis (Figure 3-1A).

Analysis of adipogenic factor expression in 3T3-L1 pre-adipocytes

The expression of known adipogenic factors was also assessed across the differentiation program. *Cebpb* and *Cebpd,* two immediately-induced transcription factors, were induced within 3 h of adipogenic induction, as reflected in their respective protein levels (Figure 3-1). C/EBPβ remained modestly expressed for 72 h but diminished at Days 6 and 9. In contrast, C/EBPδ levels rapidly decreased at 6 h and remained at a reduced level for 72 h before also falling (Figure 3-1B). *Cebpa* and *Pparg*, the two main drivers of terminal adipogenesis, were induced within 48 h and expression of C/EBPα and PPARγ steadily increased across the differentiation program, reaching maximal levels in mature, differentiated adipocytes on Days 6 and 9 (Figure 3-1A). The expression of PPARγ and C/EBPα drives a program of gene expression that facilitates terminal adipocyte differentiation. One such marker of terminal differentiation is FABP4, which was induced concomitantly with PPARγ and CEBPα after 72 h and reached maximal expression in

mature adipocytes on Day 9 (Figure 3-1B). These findings are consistent with the coordinated and temporal expression profiles of adipogenic factors in differentiating adipocytes [89,96,193].

Analysis of ERK1/2, protein kinase B (PKB) and mTORC1 signalling in 3T3-L1 pre-adipocytes

Given MNKs are activated downstream of ERK1/2 and regulated by mTORC1, activating signalling markers from these pathways were also monitored. The level of activated P-ERK1/2 (Thr202/Tyr204) increased after 24 h of adipogenic induction, remaining elevated until 72 h but then fell significantly by Days 6 and 9 (Figure 3-1B). The P-ERK levels are consistent with a requirement for ERK signalling during the early proliferative phase of adipogenesis, but not terminal adipogenesis [168,169]. P-rpS6 (Ser240/244), used as a readout of mTORC1 signalling, was elevated at 3-, 6-, 48- and 72- h (Figure 3-1B). Lower P-rpS6 levels were, however, recorded at 24 h and on Days 6 and 9. Total levels of 4E-BP1, the availability of which regulates mRNA translation initiation, were elevated in terminally differentiated adipocytes on Day 6 and 9. However, the phosphorylation of 4E-BP1 (P-4E-BP-1), which is a substrate of mTORC1, was not increased relative to total levels of this protein (Figure 3-1B). P-PKB (Ser473) levels, a marker of phosphoinositide 3-kinase (PI3K)/insulin signalling activation, were acutely elevated at 3- and 6-h, but diminished by 24 h, consistent with the effect of insulin in the media and the fact PKB activation is necessary to drive adipogenesis [194–196]. PKB is thought to drive adipogenesis in at least two different ways: (1) through the induction of PPARγ via phosphorylation and inhibition of the forkhead box O (FOXO) family of transcription factors [197,198]; and (2) activation of mTORC1 signalling [199,200], both of which were observed (Figure 3-1B).

Interim Conclusion

Mknk2 (MNK2) expression and P-eIF4E, a readout of MNK activity, are progressively increased during adipogenesis. MNK2 levels are induced and highest in mature, differentiated adipocytes; in contrast MNK1 is stably expressed throughout adipogenesis. *What signalling pathway(s) are responsible for driving Mknk2 expression?*

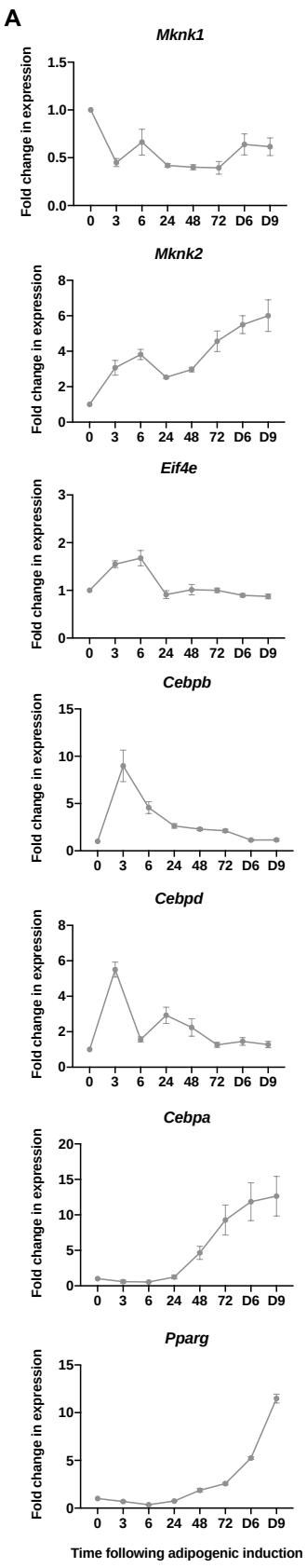
A
Mknk1
Mknk2
Eif4e
Cebpb
Cebpd
Cebpa
Pparg
Fold change in expression
0 3 6 24 48 72 D6 D9
Time following adipogenic induction

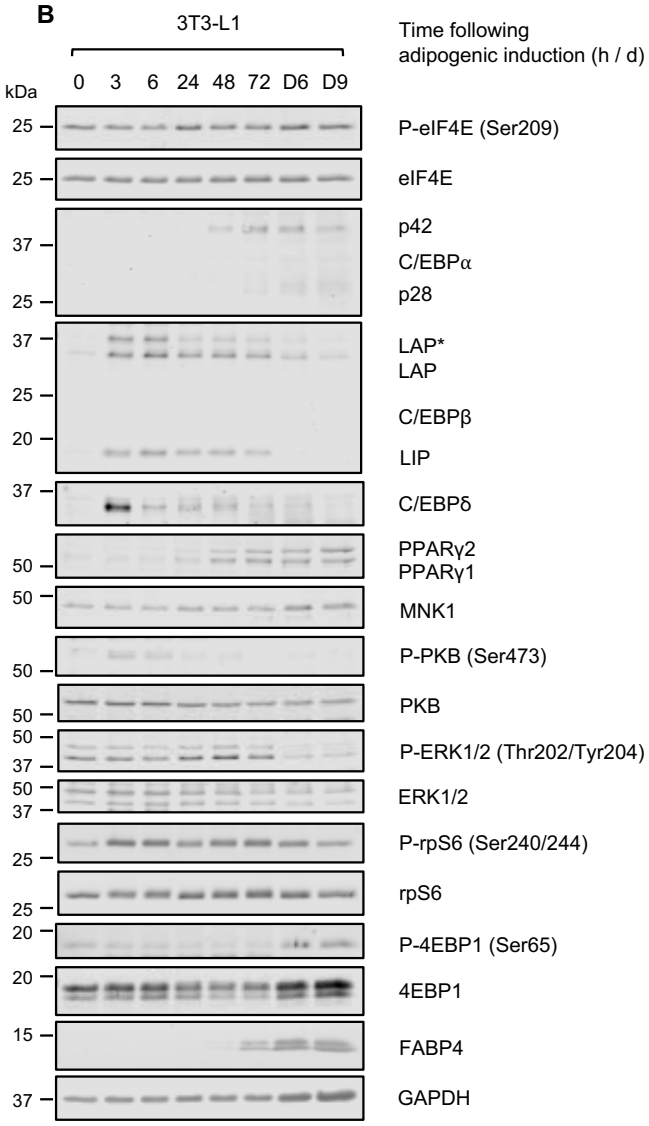
B
3T3-L1
Time following adipogenic induction (h / d)
kDa
0 3 6 24 48 72 D6 D9
P-eIF4E (Ser209)
eIF4E
p42
C/EBPα
p28
LAP*
LAP
C/EBPβ
LIP
C/EBPδ
PPARγ2
PPARγ1
MNK1
P-PKB (Ser473)
PKB
P-ERK1/2 (Thr202/Tyr204)
ERK1/2
P-rpS6 (Ser240/244)
rpS6
P-4EBP1 (Ser65)
4EBP1
FABP4
GAPDH

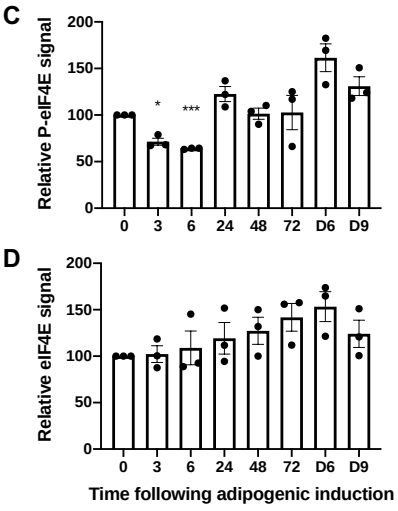
C
Relative P-eIF4E signal
D
Relative eIF4E signal
Time following adipogenic induction

Figure 3-1: Overview of MNK1/2 and adipogenic factor expression during 3T3-L1 adipogenesis.
(A) mRNA levels of *Mknk1*, *Mknk2*, *Eif4e*, *Cebpb*, *Cebpd*, *Cebpa* and *Pparg* were assessed by RT-qPCR at the indicated times. Expression levels were normalised to *Nono* and *Hprt* and represented as fold change with respect to day 0. Data are mean ± SEM; n=3 (B) Cell lysates were harvested at the indicated times and analysed by SDS-PAGE using the indicated antibodies. The levels of (C) P-eIF4E and (D) eIF4E were quantified from (B), relative to day 0. Data are mean ± SEM; n=3; individual data values are plotted; repeated measures (RM) one-way ANOVA (*P < 0.05 **P < 0.01 ***P < 0.001).

Analysis of early gene expression in 3T3-L1 pre-adipocytes using individual components of the adipogenic induction medium

As shown in Figure 3-1, adipogenic induction results in an immediate induction of *Cebpb*, *Cebpd* and *Mknk2*. To understand how early adipogenic signalling promotes this induction, individual components of the adipogenic induction media were used to dissect the signalling pathways involved. Adipogenic induction media includes a cocktail of IBMX, DEX, insulin and ROSI. IBMX is a phospho-diesterase inhibitor and causes an increase in cAMP levels, which in turn activates cAMP-dependent protein kinase (PKA) and thus CREB. Activated CREB translocates to the nucleus and binds to cAMP response elements (CRE's) to activate the expression of target genes. DEX is a glucocorticoid receptor (GR) agonist, which binds to and activates the GR. Ligand-bound GR translocates to the nucleus where it binds to glucocorticoid response elements (GREs) to activate the expression of target genes. Insulin is an anabolic hormone that binds to its extracellular receptor which in turn activates PI3K/PKB signalling which regulate a large number of substrates involved in a diverse array of biological processes [201]. ROSI is a synthetic ligand that agonises PPARγ activity during terminal adipogenesis and is therefore hypothesised not to directly modulate early adipogenic signalling. These components were used either individually, in combination or all together (COCKTAIL) to assess the induction of *Cebpb, Cebpd, Mknk1* and *Mknk2* during early adipogenesis.

As expected, IBMX significantly induced *Cebpb* levels [89,96]. To our surprise, DEX induced an equivalent level of *Cebpb* and further augmented its expression when combined with IBMX (Figure 3-2A). *Cebpb* expression was not further elevated by the addition of insulin or ROSI. This suggests both IBMX and DEX directly induce *Cebpb* and that a combination of the two components augments its expression (Figure 3-2A).

Also as expected, DEX alone directly induced *Cebpd* (Figure 3-2B; [89,96]). IBMX alone was unable to induce *Cebpd*; rather, it diminished the maximal expression of *Cebpd* when combined with DEX (Figure 3-2B). The addition of insulin and ROSI (COCKTAIL) further diminished *Cebpd* expression, suggesting DEX directly induces *Cebpd* and whose levels are modulated by IBMX and potentially also insulin and/or ROSI.

Mknk2 was significantly induced by IBMX but not DEX (Figure 3-2C). However, IBMX and DEX augmented the levels of *Mknk2* when used in combination (Figure 3-2C), similar to *Cebpb*. The addition of insulin and/or ROSI further augmented *Mknk2* levels but neither component was able to induce *Mknk2* expression alone (Figure 3-2C). This suggests that IBMX directly induces *Mknk2* expression which is augmented by glucocorticoid (DEX) and/or insulin stimulation. *Mknk1* expression was unresponsive to IBMX, DEX, insulin, ROSI, and the COCKTAIL (Figure 3-2D), suggesting *Mknk1* expression is regulated independently of the cocktail components.

Interim Conclusion

Cebpb levels are directly induced by IBMX, however, DEX also directly induces *Cebpb* and further augments *Cebpb* levels when combined with IBMX. *Cebpd* levels are directly induced by DEX and its levels are modulated by IBMX and potentially by insulin and/or ROSI. *Mknk2* expression is directly induced by IBMX. DEX appears to augment *Mknk2* levels along with insulin and/or ROSI but these components alone are unable to directly induce *Mknk2. What promoter elements are responsible for the regulation of these genes?*

Identification of CREs and GREs in Cebpb, Cebpd, Mknk1 and Mknk2

Apart from a study mapping the CRE-like elements responsible for CREB-induced *Cebpb* expression [202] and a genome-wide study identifying putative CRE elements based on computational prediction [203], no studies have mapped the transcription factor binding sites on the promoters of *Cebpb*, *Cebpd, Mknk1 or Mknk2*. Publicly accessible ChIP-seq data (https://chip-atlas.org) were therefore used to analyse the enrichment peaks of CREB and GR to locate putative CRE- and GRE-like elements, respectively, in the promoters of the above-mentioned genes.

This analysis identified three GRE-like elements adjacent to the *Cebpb* gene, two of which were proximal (-1161 and -2370) to the transcription start site, with the other one being located in the distal promoter (+20) (Figure 3-3A). The GRE-like elements shared the half-GRE core sequence (RGNACA) [204] (Figure 3-3A). The previously mapped CREs (-60/106) [202], along with additional CRE-like elements (2343/2398), were identified (Figure 3-3A) and shown to contain a half-CRE core sequence (TGACG) [205]. In *Cebpd*, a single CRE- (-41) and GRE-like element (-98) were identified in the proximal promoter (Figure 3-4A). The CRE (-41) shared the half-CRE core sequence (TGACG), whilst the GRE (-98) comprised the full-length consensus sequence, containing two imperfect palindrome 6-bp half-sites separated by three nucleotides (RGNACRnnnWGNNYY), where R=A or G, Y=C or T, W=A or T [204,206] (Figure 3-4A). In *Mknk1*, single CRE- (-60) and GRE-like elements (-142) were identified, sharing the half-CRE (TGACG) and half-GRE (RGNACA) core sequences, respectively (Figure 3-5A). A single CRE-like element, comprised of the half-CRE core sequence, was identified in *Mknk2* (-372) along with three GRE-like elements (-86, -1883, -3270) (Figure 3-6A). The -3270 GRE-like element comprised two imperfect palindromic six bp half-sites separated by three nucleotides, consistent with a full-length GRE element, whilst the -86 and -1883 elements comprised only the half-GRE core sequence (Figure 3-6A). This suggests *Cebpb, Cebpd, Mknk2* - as well as *Mknk1* - contain putative response elements recognised by CREB and GR and may therefore be subject to regulation by their binding. Notably, *Cebpd* and *Mknk2* contain full-length consensus GRE elements, whilst *Mknk1* and *Cebpb* contain only half-GRE elements.

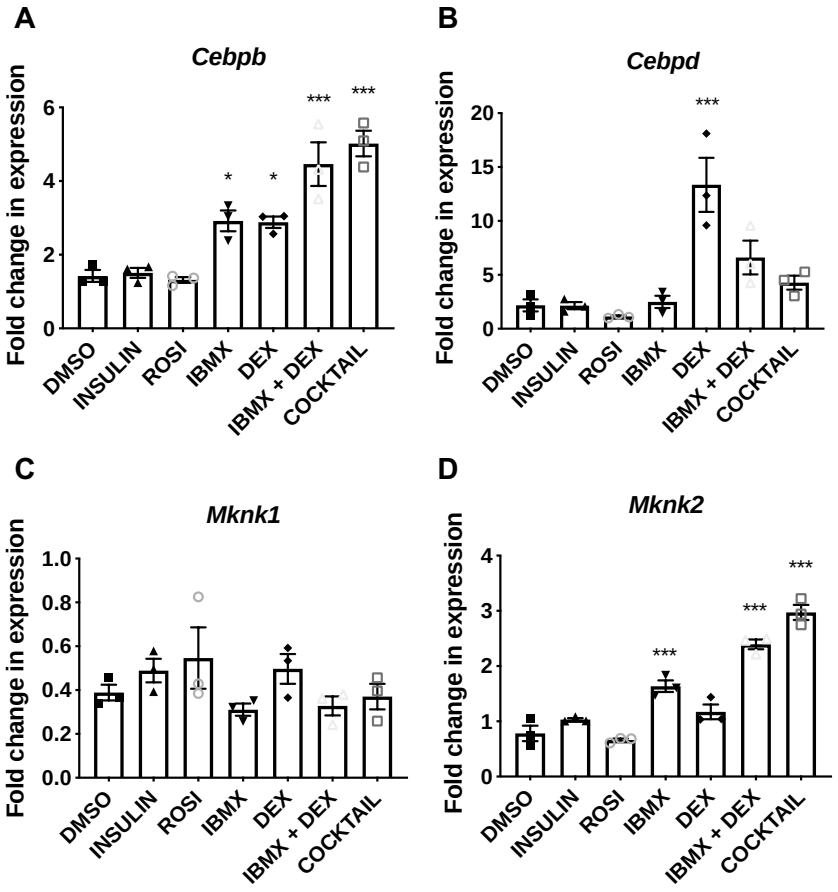

Figure 3-2: Control of early adipogenic signalling by components of the adipogenic induction medium. 3T3-L1 pre-adipocytes were treated with 350 nM insulin, 2µM ROSI, 500 µM IBMX, 0.5 µM DEX or DMSO either individually, in combination IBMX + DEX or all together COCKTAIL, for 3 h after which the mRNA levels of (A) *Cebpb* (B) *Cebpd* (C) *Mknk1* and (D) *Mknk2* were measured by RT-qPCR. Expression levels were normalised to *B2m* and represented as fold change with respect to DMSO. Data are mean ± SEM; n=3; ordinary one-way ANOVA (*P < 0.05 **P < 0.01 ***P < 0.001).

Occupancy of CREB and GR at CRE and GREs in Cebpb, Cebpd, Mknk1 and Mknk2

ChIP assays were performed to enrich for CREB and GR at the CRE- and GRE-like elements following 3 h of adipogenic induction. P-CREB (Ser133) and GR were used as the immunoprecipitating antibodies. In *Cebpb*, P-CREB was most significantly enriched at the -60/106 CRE but also at the -2343/2398 CRE (Figure 3-3B). GR was most significantly enriched at the +20 and -2370 GRE-like elements but less significantly at the -1161 element (Figure 3-3C). This suggests that CREB is likely to regulate *Cebpb* expression through binding at the -60/106 CRE element, consistent with [202], but also, albeit less strongly, at the newly-identified -2343/2398 CRE. Further, GR likely regulates *Cebpb* expression through binding to the +20 and -2370 GRE elements and potentially also the -1161 element.

For *Cebpd*, P-CREB and GR were significantly enriched at the half-CRE (-41) and full-length GRE (-98), respectively (Figure 3-4B and 3-4C), suggesting CREB and GR may regulate *Cebpd* expression through binding to these response elements, consistent with findings from Figure 3-2.

P-CREB was significantly enriched at the *Mknk2* CRE (-372) whilst GR was most significantly enriched at the -1883 half-GRE but less significantly at the -86 half- and -3270 full-length GREs (Figure 3-6B and 6C). This suggests that CREB may regulate expression of *Mknk2* through binding at the -356 CRE whilst GR may regulate expression by binding the -1883 GRE and potentially the -86 and -3270 elements.

Surprisingly, P-CREB and GR were significantly enriched at the -60 half-CRE and -142 half-GRE elements in *Mknk1*, respectively (Figure 3-5B and 5C). This suggests that CREB and GR may regulate the expression of *Mknk1;* however, this contradicts earlier findings which suggest that *Mknk1* is not affected by components of the differentiation induction media (Figure 3-2C).

Across all ChIP assays performed, enrichment was specific to the putative CRE and GRE response elements as there was no significant enrichment in the negative (NEG) non-specific regions of *Cebpb* (-12,460) (Figure 3-3D and 3E), *Cebpd* (-1378) (Figures 3-4D and 4E), *Mknk1* (-6325) (Figures 3-5D and 5E), or *Mknk2* (-4862) (Figures 3-6D and 6E).

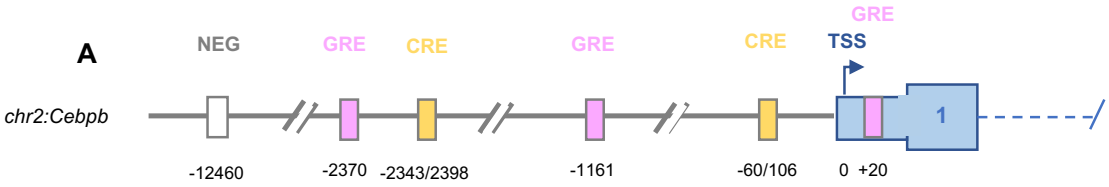

Site	Sequence
GRE +20	GCAC**GGGACC**GGGA
CRE –60/106	**TGACG**CAGCCC-[35]-**TGACG**CGCACC
GRE –1161	CAAG**GGCACA**GGGA
GRE –2370	CTGGGG**AGAACA**ACGATCCTC
CRE –2343/2398	**TGAC**AGGCATG-[55]-CAGCTG**GGTCA**

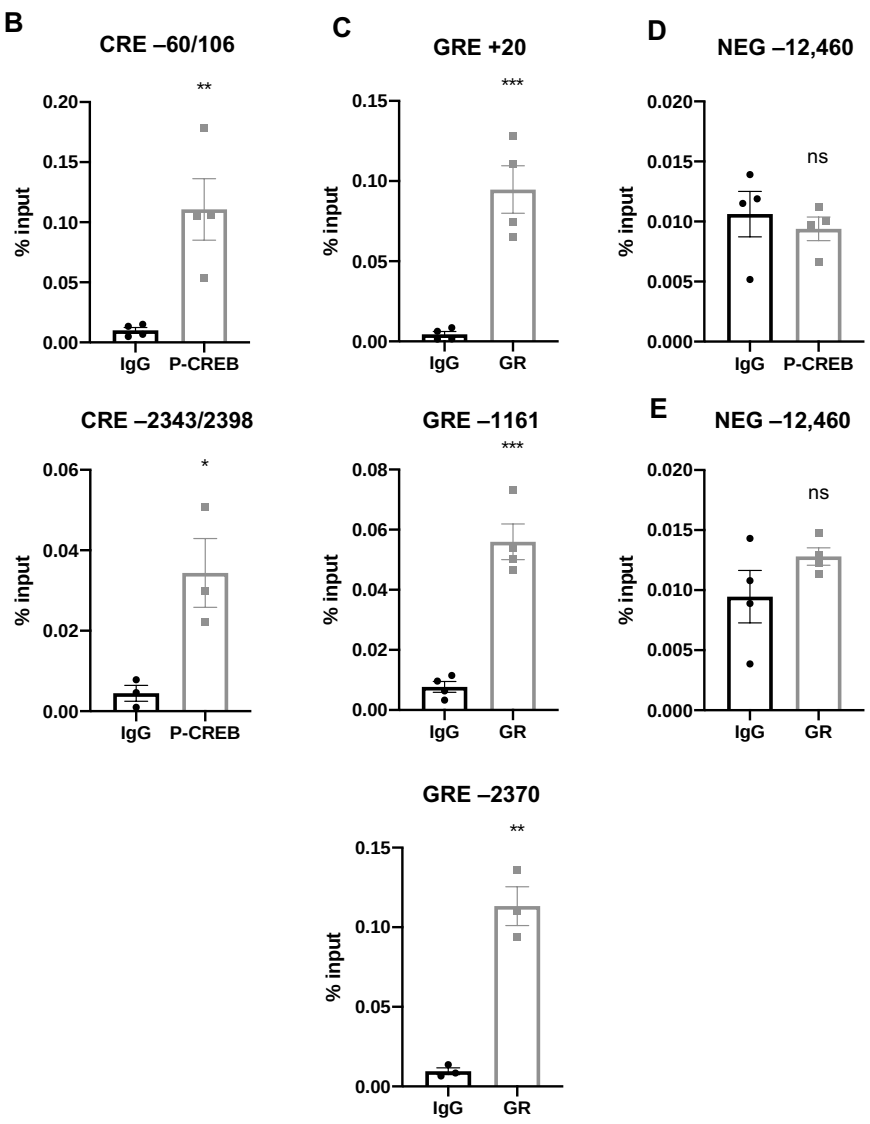

Figure 3-3: Identification of CREB and GR binding sites on the *Cebpb* promoter.

(A) Schematic diagram depicting the genomic position of putative response elements on the *Cebpb* promoter relative to the TSS (chr2:167,514,466). The DNA sequence of the putative response elements are shown: nucleotides corresponding to the core consensus sequence are bold underlined. (B) ChIP assays were performed in 3T3-L1 to assess enrichment of (B) P-CREB at putative CREs and (C) GR at putative GREs after 3 h of adipogenic induction. Enrichment levels are represented as percentage of input chromatin (% input). To assess whether enrichment of (D) P-CREB and (E) GR was specific to the response elements, enrichment was assessed at the corresponding NEG region. Data are mean ± SEM; n=4; unpaired two-tailed t-test (*P < 0.05 **P < 0.01 ***P < 0.001).

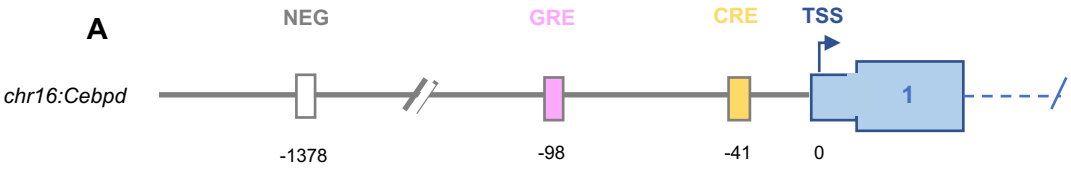

Site	Sequence
CRE –41	CCCAGC**TGACG**CGCACG
GRE –98	CCCAGC**AGCAC**CCCAGTCC**CT**CCCCGC

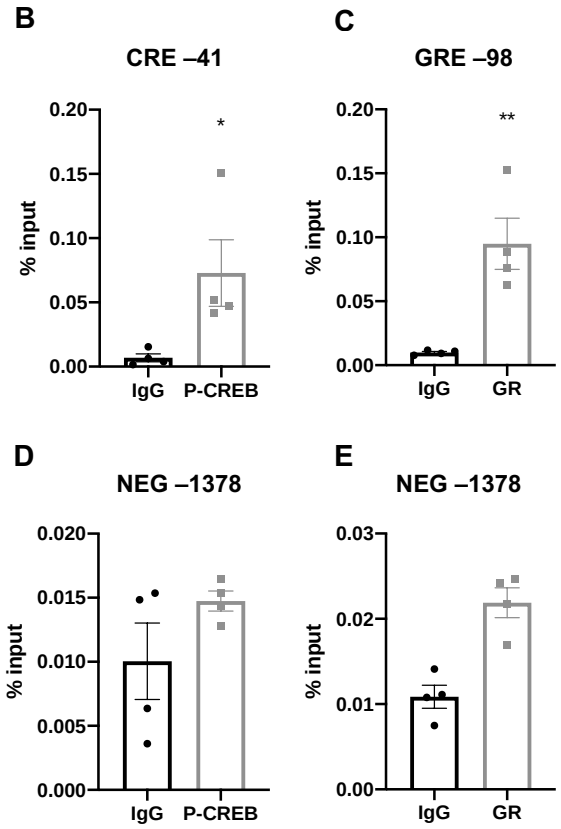

Figure 3-4: Identification of CREB and GR binding sites on the *Cebpd* promoter.

(A) Schematic diagram depicting the genomic position of putative response elements on the *Cebpd* promoter relative to the TSS (chr16:15,887,379). The DNA sequence of the putative response elements are shown: nucleotides corresponding to the core consensus sequence are bold underlined. (B) ChIP assays were performed in 3T3-L1 to assess enrichment of (B) P-CREB at putative CREs and (C) GR at putative GREs after 3 h of adipogenic induction. Enrichment levels are represented as percentage of input chromatin (% input). To assess whether enrichment of (D) P-CREB and (E) GR was specific to the response elements, enrichment was assessed at the corresponding NEG region. Data are mean ± SEM; n=4; unpaired two-tailed t-test (*P < 0.05 **P < 0.01 ***P < 0.001).

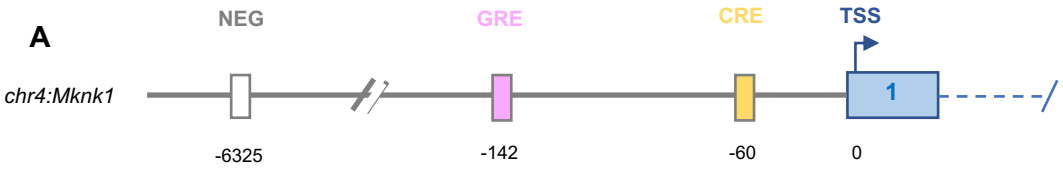

Site	Sequence
CRE –60	CAGGCG**TGAC**TCCTCCC
GRE –142	AACCAG**AGGAC**GCTCTGA

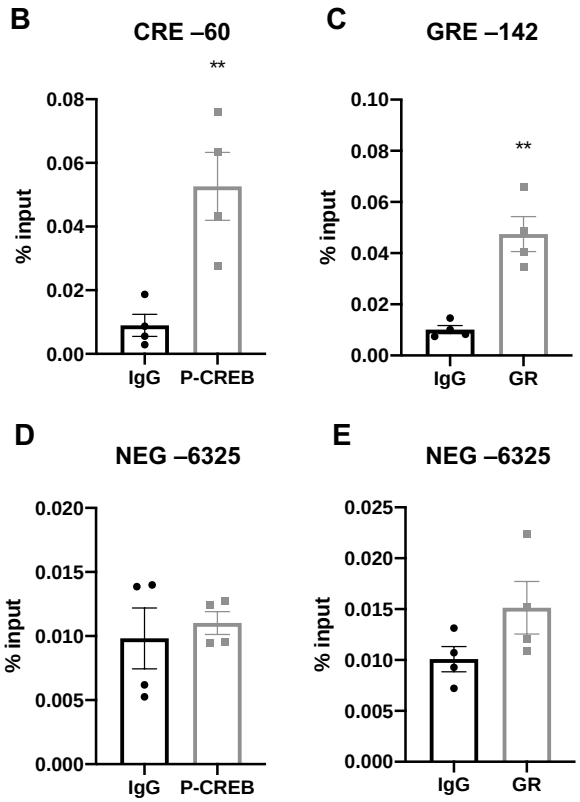

Figure 3-5: Identification of CREB and GR binding sites on the *Mknk1* promoter.

(A) Schematic diagram depicting the genomic position of putative response elements on the *Mknk1* promoter relative to the TSS (chr4:115,511,826). The DNA sequence of the putative response elements are shown: nucleotides corresponding to the core consensus sequence are bold underlined. (B) ChIP assays were performed in 3T3-L1 to assess enrichment of (B) P-CREB at putative CREs and (C) GR at putative GRE's after 3 h of adipogenic induction. Enrichment levels are represented as percentage of input chromatin (% input). To assess whether enrichment of (D) P-CREB and (E) GR was specific to the response elements, enrichment was assessed at the corresponding NEG region. Data are mean ± SEM; n=4; unpaired two-tailed t-test (*P < 0.05 **P < 0.01 ***P < 0.001).

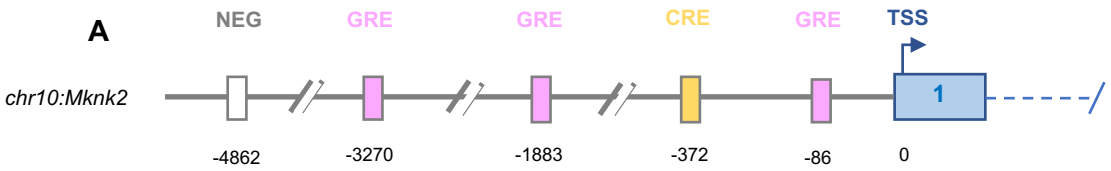

Site	Sequence
GRE –86	TCTCAG**GGAACA**GAGGAG
CRE –372	CCGCG**TGAC**CTGGCTG
GRE –1883	GCCAGTA**GGAACA**GGAAGGG
GRE –3270	ATGGAC**AGAAC**CTGG**TCCTGT**CAGTGT

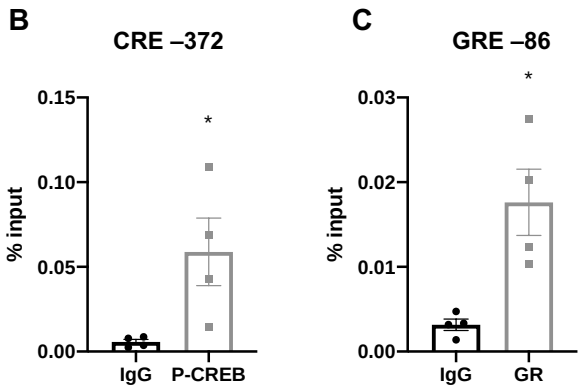

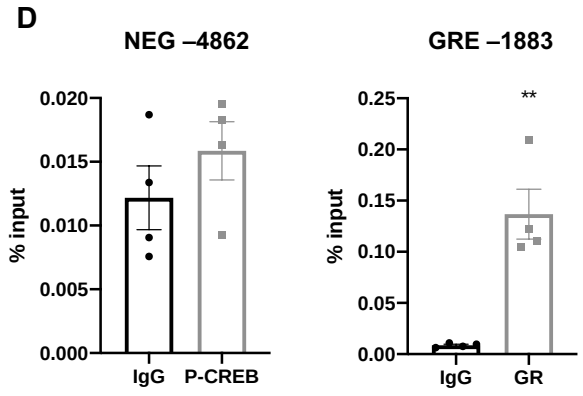

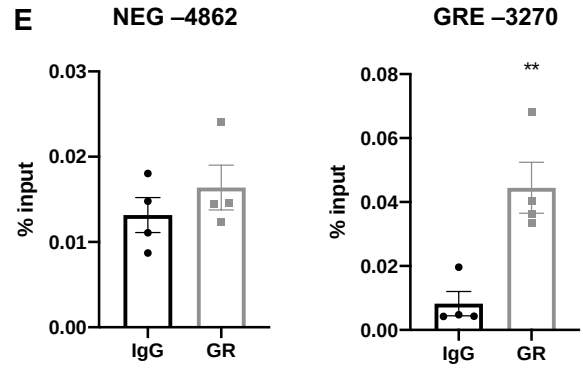

Figure 3-6: Identification of CREB and GR binding sites on the *Mknk2* promoter.

(A) Schematic diagram depicting the genomic position of putative response elements on the *Mknk2* promoter relative to the TSS (chr10:80,139,038). The DNA sequence of the putative response elements are shown; nucleotides corresponding to the core consensus sequence are bold underlined. (B) ChIP assays were performed in 3T3-L1 to assess enrichment of (B) P-CREB at putative CRE's and (C) GR at putative GREs after 3 h of adipogenic induction. Enrichment levels are represented as percentage of input chromatin (% input). To assess whether enrichment of (D) P-CREB and (E) GR was specific to the response elements, enrichment was assessed at the corresponding NEG region. Data are mean ± SEM; n=4; unpaired two-tailed t-test (*P < 0.05 **P < 0.01 ***P < 0.001).

Interim Conclusion

In addition to the already identified CREs, *Cebpb* contains additional response elements for binding CREB at -2343/2398 which is occupied following adipogenic induction. The *Cebpb* promoter also contains three new GREs that are occupied by GR. *Cebpb* expression is therefore suggested to be regulated by both CREB and GR.

A full-length consensus GRE was identified on the promoter of *Cebpd.* This element is occupied by GR following adipogenic induction and is likely to be responsible for *Cebpd* induction. A CRE element was also identified and may be the site at which CREB modulates *Cebpd* levels.

On the promoter of *Mknk2,* three GREs and one CRE were identified. CREB and GR occupied these response elements following adipogenic induction and are therefore likely to be involved in its induction. The *Mknk1* promoter contains a single CRE and GRE which may be constitutively occupied given that *Mknk1* expression is not affected by adipogenic induction media.

Mknk2 is progressively increased during adipogenesis; therefore, what factors are responsible for maintaining its expression?

Regulation of Mknk2 expression by terminal differentiation factors

Given that *Mknk2* is considerably up-regulated and maintained during adipogenesis, it was hypothesised that terminal differentiation transcription factors, such as C/EBPβ, C/EBPα and PPARγ, were responsible for regulating its expression. Publicly accessible ChIP-seq data (https://chip-atlas.org) was used to analyse the enrichment peaks of C/EBPα, C/EBPβ and PPARγ to locate possible C/EBPREs and PPAREs in the promoter of *Mknk2.* The analysis identified two putative C/EBPREs, each containing two CCAAT boxes (-264/290 and -1204/1258) comprising the consensus core sequence (NNGNAAK) where K=T or G [207,208], and three putative PPAREs (-1975, -3348 and -3993) comprising imperfect direct repeats of the consensus core sequence (AGGTCA) separated by a single nucleotide [209] (Figure 3-7A). ChIP assays were performed to enrich for C/EBPβ and C/EBPα at the C/EBPRE elements following 24- and 72- h of adipogenic induction, respectively accounting for their temporal expression.

C/EBPβ was enriched at the -1204/1258 and comparatively less so at the -264/290 C/EBPREs, albeit neither site was significantly enriched (Figure 3-7C). The ChIP-seq analysis predicted C/EBPα occupancy at the -1204/1258 but not the -264/290 C/EBPRE, however, no significant enrichment of C/EBPα was observed at the -1204/1258 element (Figure 3-7D). Likewise, when ChIP assays were performed to assess enrichment of PPARγ after 72 h, there was no significant enrichment at any of the PPARE's (Figure 3-7B), since equivalent levels of enrichment were observed in the NEG non-specific region (-4862) (Figure 3-7E).

Therefore, it is suggested that C/EBPβ is involved in regulating *Mknk2* expression through binding the -1204/1258 and -264/290 C/EBPRE's; however, C/EBPα and PPARγ do not appear to be involved in regulating *Mknk2,* at least after 72 h.

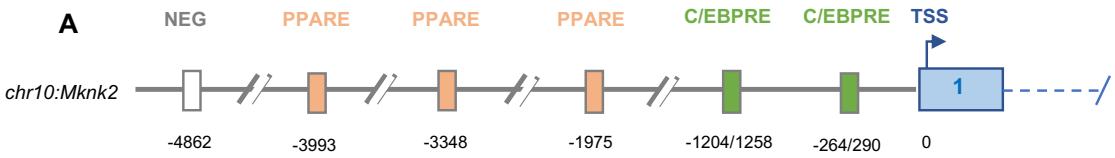

Site	Sequence
C/EBPRE –264/290	TGGCAG**GGGGAAG**GGGAGATTCCG**AGGGAAG**TGGGGC
C/EBPRE –1204/1258	AATTGG**TGGCAA**A-[40]-**CAGGAAT**TGATCC
PPARE –1975	GACAGC**AGGT**TGG**CAGC**TTGCCTGG
PPARE –3348	AGTTATG**GCTGT**C**AGGTC**TGACGAG
PPARE –3993	GACTAG**AGGTCA**C**AAGTC**TGACAAG

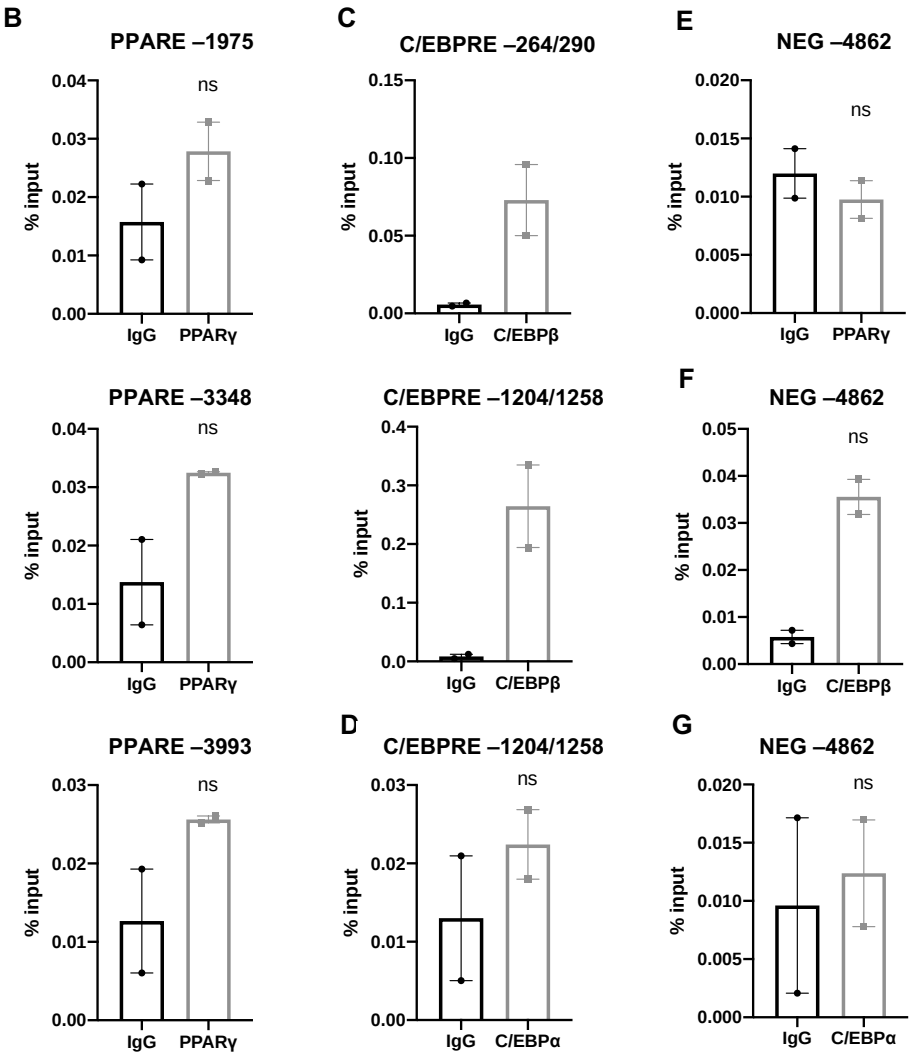

Figure 3-7: Identification of PPARγ and C/EBP binding sites on the *Mknk2* promoter.

(A) Schematic diagram depicting the genomic position of putative response elements on the *Mknk2* promoter relative to the TSS (chr10:80,139,038). The DNA sequence of the putative response elements are shown: nucleotides corresponding to the core consensus sequence are bold underlined. (B) ChIP assays were performed in 3T3-L1 to assess enrichment of (B) PPARγ at putative PPAREs, (C) C/EBPβ and (D) C/EBPα at putative C/EBPREs after (C) 24 h or (B and D) 72 h of adipogenic induction. Enrichment levels are represented as percentage of input chromatin (% input). To assess whether enrichment of (E) PPARγ, (F) C/EBPβ and (G) C/EBPα was specific to the response elements, enrichment was assessed at the corresponding NEG region. Data are mean ± SEM; n=2; unpaired two-tailed t-test (*P < 0.05 **P < 0.01 ***P < 0.001).

Interim Conclusion

The *Mknk2* promoter contains two C/EBPREs that are occupied by C/EBPβ, but not C/EBPα, and three putative PPAREs, which are not occupied by PPARγ. It is suggested the expression of *Mknk2* is likely regulated by C/EBPβ. *What are the relative activities of MNK1/2 in differentiating pre-adipocytes?*

Efficacy of Mknk1/2 small interfering RNAs (siRNAs)

In order to study MNK1/2 and their individual contributions to adipocyte differentiation, siRNAs directed against *Mknk1* (si*Mknk1* #1/#2) and *Mknk2* (si*Mknk2* #1/#2) were used. The siRNAs were assayed individually (#1/#2) or combined (#1+#2). The efficacy of siRNA-mediated knock-down was assayed in 3T3-L1 pre-adipocytes after 72 h by Western blot and RT-qPCR, alongside si*Gapdh* and si*Scrambled,* which were used as positive and negative controls, respectively: si*Gapdh* effectively silenced GAPDH protein and *Gapdh* mRNA expression, indicating the siRNA transfection conditions were acceptable (Figures 3-8A and 8D). si*Mknk1* (#1/#2 and #1+#2) completely abolished MNK1 expression after 72 h, while MNK1 was unaffected by si*Mknk2* (#1/#2 and #1+#2) (Figure 3-8A). As no suitable MNK2 antibody is available, MNK2 expression was assayed by measuring the level of P-eIF4E as a readout of MNK activity, since MNK2 is the main isoform in adipose tissue [3]. si*Mknk2* (#1/#2 and #1+#2) almost completely abolished P-eIF4E (albeit leaving some residual phosphorylation); the residual phosphorylation is attributable to MNK1 since si*Mknk1/Mknk2* used in combination completely abolished P-eIF4E (Figure 3-8A).

Consistent with lowering MNK1 levels, si*Mknk1* (#1/#2 and #1+#2) were effective at silencing *Mknk1* mRNA; however, they reduced *Mknk2* mRNA levels at the same time. *Mknk2* levels were reduced to a greater extent by si*Mknk1* #2 compared to si*Mknk1* #1, whilst si*Mknk1* (#1+#2) resulted in an intermediate level of *Mknk2* mRNA reduction (Figure 3-8C). This indicated some level of siRNA cross-reactivity, which is undesirable in the context of investigating the function of MNK isoforms individually. Consistent with lowering P-eIF4E, si*Mknk2* (#1/#2 and #1+#2) were effective at silencing *Mknk2* mRNA. The same level of *Mknk2* reduction was observed regardless of whether siRNAs were used individually or in combination. However, si*Mknk2* (#1/#2 and #1+#2) appeared to increase *Mknk1* expression: si*Mknk2* #2 increased *Mknk1* levels to a greater extent than si*Mknk2* #1, and the effect was cumulative, since *Mknk1* expression was most elevated when both siRNAs were used in combination (si*Mknk2* #1+#2) (Figure 3-8B). Increased *Mknk1* expression could be a compensatory cellular response to the silencing of *Mknk2* as a mechanism to restore the levels of P-eIF4E.

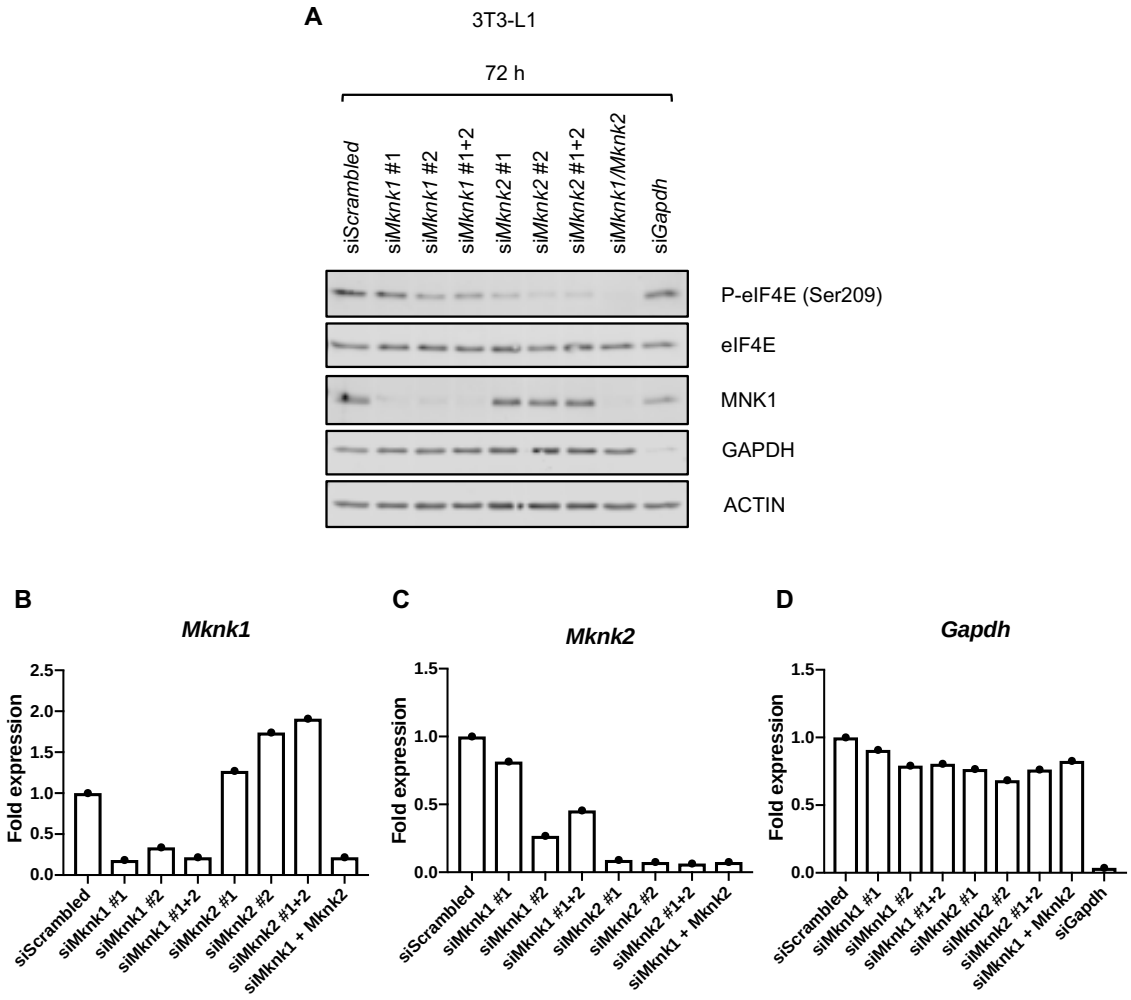

Figure 3-8: Efficacy of *Mknk1/2* small interfering RNA (siRNA).

3T3-L1 pre-adipocytes were transfected with 25 pmol of si*Mknk1* (#1 or #2), siM*knk2* (#1 or #2) individually or in combination, as indicated. When used in combination (si*Mknk1/Mknk2*), 12.5 pmol of each si*Mknk1* #1 and si*Mknk2* #1 were used to keep molar ratios equivalent. si*Scrambled* and si*Gapdh* were used as transfection controls. After 72 h, (A) cell lysates were harvested and analysed by SDS-PAGE using the indicated antibodies; representative immunoblots are shown (n=2); whilst mRNA levels of (B) *Mknk1* (C) *Mknk2* and (D) *Gapdh* were measured by RT-qPCR. Expression levels were normalised to *Nono* and *Hprt* and represented as fold change with respect to si*Scrambled.* Individual data values are plotted (n=1).

Relative activity of MNK isoforms in 3T3-L1 pre-adipocytes

Given the expression profile of MNK1/2 in 3T3-L1 pre-adipocytes, it was important to establish the relative activities of the MNK isoforms. Serum-starved 3T3-L1 cells, silenced for MNK1, MNK2 and MNK1/2 expression by siRNA transfection, were treated with DMSO or the phorbol ester 12-O-Tetradecanoylphorbol-13-acetate (TPA; which activates ERK by stimulating an upstream kinase, protein kinase C) to monitor basal and induced P-eIF4E, respectively. Under basal conditions, P-eIF4E was almost completely abolished in si*Mknk2*, but not si*Mknk1* cells (Figure 3-9). The residual P-eIF4E in si*Mknk2* cells was likely attributable to MNK1 since it was abolished when si*Mknk1/Mknk2* were combined. TPA stimulation of si*Mknk2* cells elevated P-eIF4E beyond basal levels, indicating that MNK1 activity is significantly increased in response to TPA (Figure 3-9). However, TPA stimulation was unable to elevate P-eIF4E levels above basal in si*Mknk1* cells, indicating that, as expected, the high basal activity of MNK2 cannot be further enhanced by stimuli. In si*Mknk1/Mknk2* cells P-eIF4E was completely blocked, as expected. These data suggest that MNK2 is principally responsible for maintaining basal P-eIF4E levels, whilst MNK1 is exclusively responsible for inducible P-eIF4E in 3T3-L1 pre-adipocytes. These findings are consistent with previous reports and the regulatory properties of MNK1/2 [8,12,13,210,211]

Interim Conclusion

MNK2 has high activity and is principally responsible for maintaining basal levels of P-eIF4E in 3T3-L1 pre-adipocytes. MNK1 activity is low under basal conditions but is stimulated by TPA and therefore exclusively responsible for inducible P-eIF4E. *If MNK activity was inhibited what would the effect be on adipogenesis?*

Effect of CGP57380 on 3T3-L1 pre-adipocyte differentiation

The first reported small molecule MNK inhibitor, CGP57380 [62], suffers from substantial drawbacks, in particular relatively low potency and off-target effects [64]. Nevertheless, since it was the only available MNK inhibitor for several years, CGP57380 has been widely used to study the MNKs and contributed to an increased understanding of MNK function. CGP57380 was also the compound that implicated the MNKs in adipocyte differentiation, where it was shown to impair lipid accumulation in mature adipocytes and affect the mRNA expression of both early and late adipogenic factors [3].

To extend the initial analysis performed with CGP57380, the expression of adipogenic transcription factors was measured during 3T3-L1 adipogenesis: two-day post-confluent 3T3-L1 pre-adipocytes were treated with adipogenic induction media in the presence or absence of CGP57380 and monitored over nine-days. CGP57380 effectively inhibited MNK activity in 3T3-L1 cells as it completely blocked P-eIF4E (Figure 3-10A). Whilst CGP57380 did not alter expression of the activating C/EBPβ isoforms (LAP/LAP*) or C/EBPδ, it did increase the level of the inhibitory C/EBPβ-LIP isoform (Figure 3-10A). As a result, the expression of C/EBPα and PPARγ

and their downstream targets: (adipocyte triglyceride lipase (ATGL), Perilipin-1 (PLIN1) and fatty acid-binding protein 4 (FABP4)) were impaired on Day 3 (Figure 3-10A), consistent with the function of C/EBPβ-LIP [3,134]. However, concomitant with the decline in C/EBPβ-LIP expression on Day 6, the levels of C/EBPα, PPARγ, ATGL and PLIN1 were restored and remained so for the remainder of the program (Figure 3-10A). Interestingly, FABP4 levels were not restored and remained impaired on Days 6 and 9 (Figure 3-10A), consistent with the effects of C/EBPβ-LIP over-expression in human white adipose-derived stromal cells (ASCs) [133]. C/EBPβ-LAP/LAP* and -LIP are translated from the same mRNA through a leaky ribosomal scanning mechanism involving two AUG start codons [132]. These data therefore suggest that CGP57380 promotes translation of the C/EBPβ-LIP isoform which lacks the N-terminal transactivation domain. This truncated protein acts in a dominant-negative manner to inhibit C/EBP function, either by occupying binding sites on target gene promoters or by forming inactive heterodimers with other C/EBPβ isoforms [89,132,212]. The early deficiency in adipocyte differentiation is overcome with the decline in C/EBPβ-LIP expression, suggesting that MNK regulates C/EBPβ translation and is necessary to promote C/EBPβ-LAP expression during early adipogenesis.

Oil Red O (ORO) staining was used to measure the accumulation of lipid in differentiated adipocytes on Day 9 (Figure 3-10D). Overall, CGP57380 significantly reduced lipid accumulation (~50%), as quantified from ORO-stained fields of view (Figure 3-10C), consistent with earlier findings [3]. The reduction in lipid accumulation was, however, not reflected in the absorbance (A490) of ORO eluted from stained cells, which showed only a 30% reduction in lipid (Figure 3-10B). This apparent discrepancy is likely attributable to the heterogeneous nature of the differentiated adipocyte population, which is captured more evidently in the quantified fields of view, in contrast to the A490 data which reflects the *sum-total* of lipid content. The reduction in lipid accumulation is suggested to result from impaired adipogenesis rather than a defect in lipid metabolism.

Given the lack of specificity of CGP57380, it was possible that the observed effects on gene expression and lipid accumulation were a result of inhibiting other enzymes in addition to the MNKs [64]. mTORC1 signalling regulates cell metabolism and is also required for adipogenesis [213,214]. Markers of mTORC1 signalling were assessed to determine whether CGP57380 affected this pathway: P-rpS6, a marker of mTORC1 activation was decreased by CGP57380 on Days 1 and 3, whilst it was increased on Day 6. This suggests that CGP57380 can interfere with mTORC1 signalling but does not necessarily mean it is an off-target since MNKs have been implicated in mTORC1 activation [215]. Nevertheless, since CGP57380 affects mTORC1 signalling, it was difficult to distinguish the effects of MNK and mTORC1 inhibition on adipogenesis. These effects were amplified given the relatively low potency of CGP57380 and thus, a more potent inhibitor that does not affect mTORC1 signalling was desired.

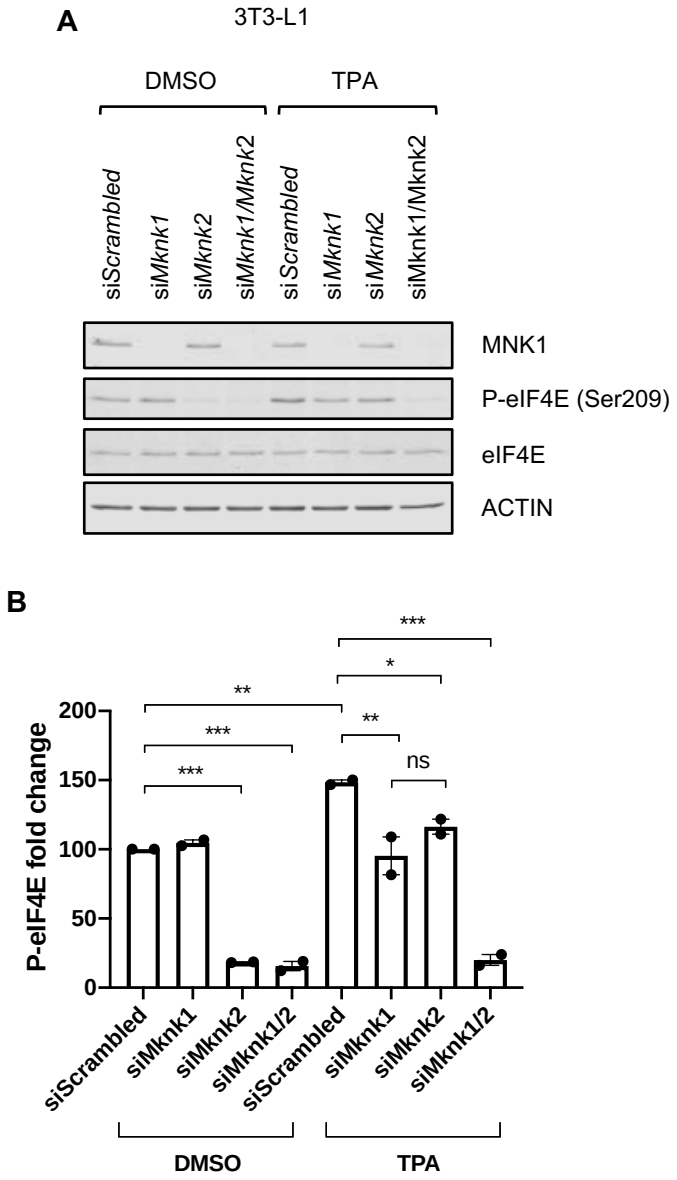

Figure 3-9: Basal and stimulated activity of MNK1/2 in 3T3-L1 pre-adipocytes.

3T3-L1 pre-adipocytes were pre-transfected with 25 pmol of si*Mknk1* (#1), si*Mknk2* (#1) individually or in combination, as indicated. When used in combination, 12.5 pmol of each siRNA was used to keep molar ratios equivalent. Cells were serum-starved overnight for 16 h prior to treatment with 100 mM TPA or equivalent volume of DMSO for 15 min after which (A) cell lysates were harvested and analysed by SDS-PAGE using the indicated antibodies. (B) The level of P-eIF4E was quantified from (A), relative to si*Scrambled*. Data are mean ± SEM; n=2; individual data values are plotted; ordinary one-way ANOVA (*P < 0.05 **P < 0.01 ***P < 0.001).

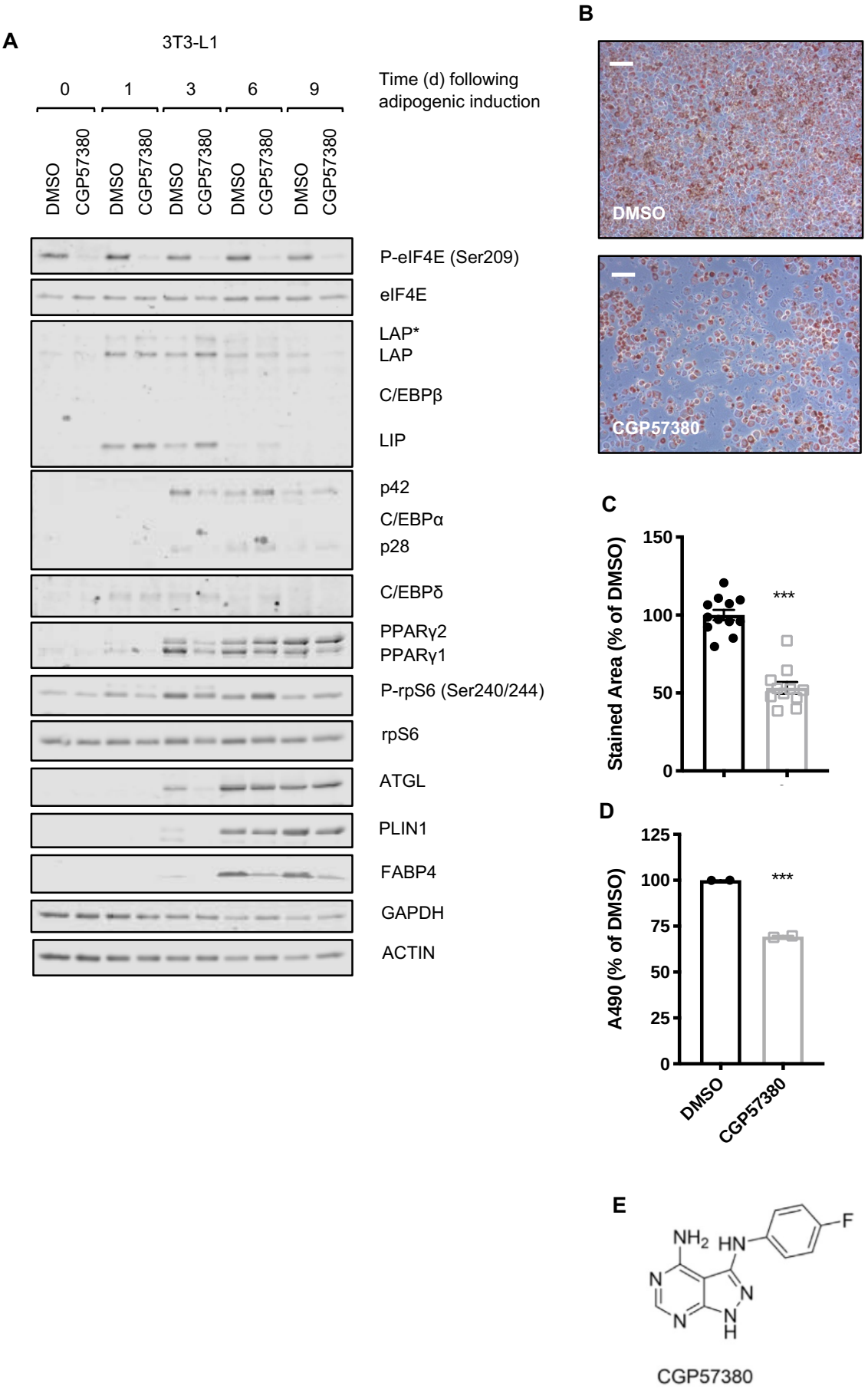
A
3T3-L1
0
1
3
6
9
Time (d) following adipogenic induction
DMSO
CGP57380
P-eIF4E (Ser209)
eIF4E
LAP*
LAP
C/EBPβ
LIP
p42
C/EBPα
p28
C/EBPδ
PPARγ2
PPARγ1
P-rpS6 (Ser240/244)
rpS6
ATGL
PLIN1
FABP4
GAPDH
ACTIN
B
DMSO
CGP57380
C
Stained Area (% of DMSO)
150
100
50
0
***
D
A490 (% of DMSO)
125
100
75
50
25
0
***
DMSO
CGP57380
E
NH2
HN
F
N
N
N
N
H
CGP57380

Figure 3-10: Effect of CGP57380 on 3T3-L1 pre-adipocyte differentiation.

3T3-L1 pre-adipocytes were differentiated with adipogenic induction media in the presence or absence of 20 μM CGP57380 or equivalent volume of DMSO. (A) Cell lysates were harvested at the indicated times and analysed by SDS-PAGE using the indicated antibodies (n=1). (B) Day 9 differentiated adipocytes were stained with ORO to assess lipid accumulation; representative images are shown, scale bar 0.2 μm. (C) Total stained area was quantified from 6 different fields of view from (B) and is represented as percentage stained area relative to DMSO; data are mean ± SEM; individual data values are plotted (n=2); unpaired t-test (*P < 0.05 **P < 0.01 ***P < 0.001) (D) ORO eluted from stained cells was quantified by absorbance (A490) and is represented as percentage absorbance relative to DMSO; data are mean ± SEM; individual data values are plotted (n=2); unpaired t-test (*P < 0.05 **P < 0.01 ***P < 0.001). (E) Chemical structure of CGP57380.

Interim Conclusion

The MNK inhibitor CGP57380 impairs adipogenesis by promoting the translation of C/EBPβ-LIP, which acts in a dominant-negative manner to impair the expression of C/EBPα and PPARγ. In consequence, the expression of downstream targets and lipid accumulation is significantly impaired. However, CGP57380 is non-specific and acutely affects mTORC1 signalling so the inhibitory effects may be a result of inhibiting other kinases.

MNK-I1: a thienopyrimidine derivative and candidate MNK inhibitor

There is considerable interest in the development of more potent and specific MNK inhibitors, particularly for oncological therapy. Thienopyrimidines are reported to be good candidates for pharmaceutical drug development [216] and their efficacy as MNK inhibitors have been documented in patents [217,218]. The thienopyrimidine derivative MNK-I1 [65] is structurally distinct from CGP57380 (Figure 3-10E, 3-11D). MNK-I1 is a more potent and specific inhibitor of the MNKs than CGP57380, inhibiting the activity of MNK1 and MNK2 at micromolar concentrations [65]. MNK-I1 was found to inhibit MNK2 (IC_{50} 0.016 μM) more strongly than MNK1 (IC_{50} 0.023 μM). However, MNK-I1 (1 μM) also strongly affected the activity of several other kinases, including (in order of remaining residual kinase activity) RIPK2 (19%), PHK (23%), BRSK1 (24%), BRSK2 (24%), AMPK (41%), and PRK2 (50%), among others [65]. MNK-I1 has also been used in a follow-up study investigating the role of the MNKs in cancer cell metastasis [219].

Efficacy of MNK-I1 in 3T3-L1 pre-adipocytes

To establish the potency and suitability of MNK-I1 for use in 3T3-L1 cells, a dose-response analysis of was performed to determine the concentration at which MNK activity was completely inhibited. As assessed by P-eIF4E, MNK activity was completely blocked by MNK-I1 at concentrations ≥ 3 μM (Figure 3-11A). To assess whether MNK-I1 had any effects on major cell signalling pathways, the phosphorylation of key signalling proteins was also investigated. MNK-I1 did not affect the phosphorylation of PKB (P-PKB Ser473), rpS6 (P-rpS6 Ser240/244) or 4EBP1 (P-4EBP1 Ser65) at any of the doses tested, suggesting MNK-I1 does not affect PI3K/insulin or mTORC1 signalling (Figure 3-11A). However, the phosphorylation of ERK (P-ERK Thr202/Try204) was increased by MNK-I1 at ≥ 3 μM, suggesting that ERK signalling can be activated by sufficiently high doses of MNK-I1, perhaps via a (hypothetical) feedback loop (Figure 3-11A). Since adipogenic induction requires incubations of three-days between media changes the stability of MNK-I1 in culture media for extended periods was investigated. P-eIF4E levels - monitored at regular intervals over a period of 72 h - did not increase over time, indicating MNK-I1 was still effective, and presumably stable in culture media for extended periods under these conditions (Figure 3-11B).

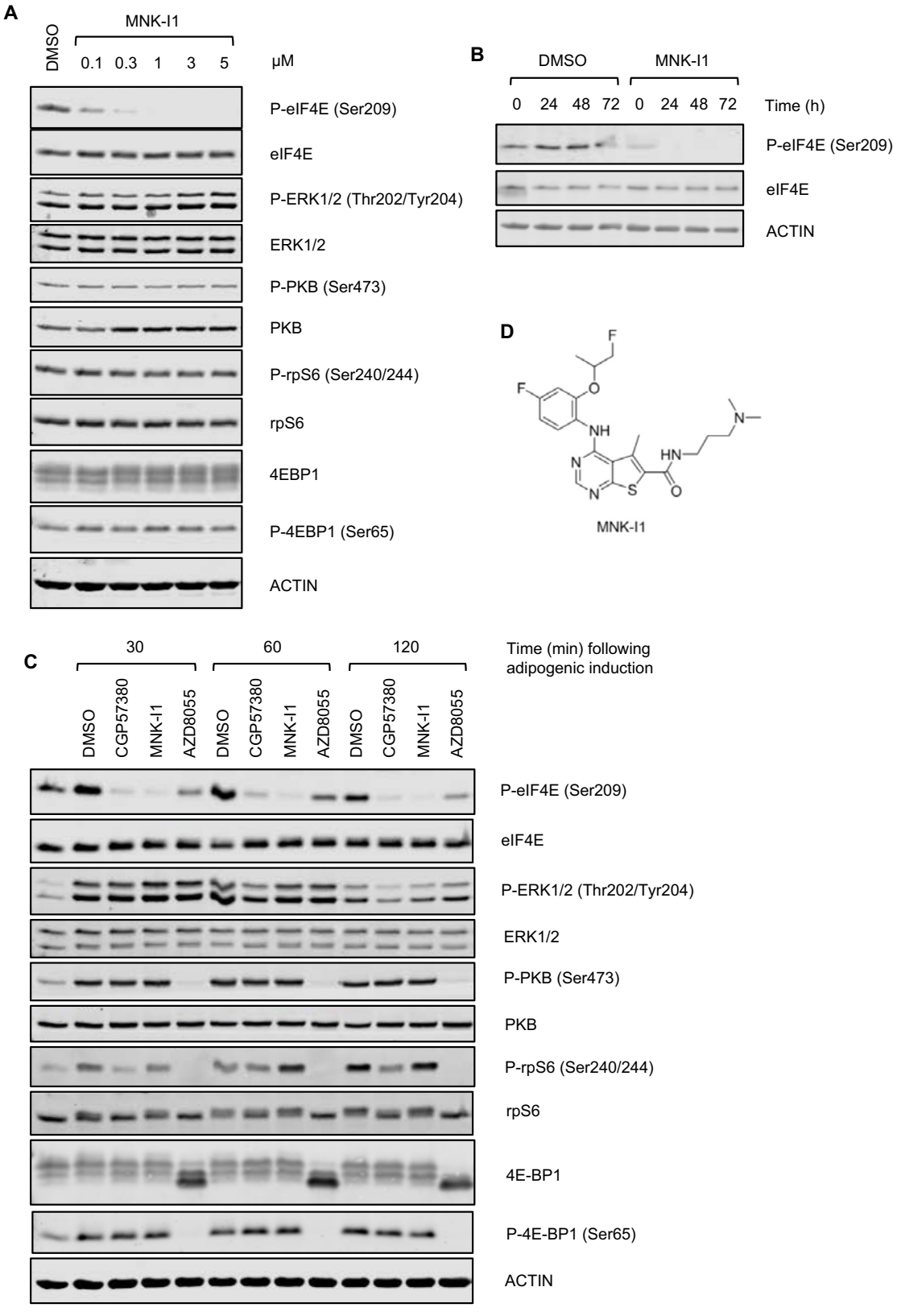
A
DMSO
MNK-I1
0.1 0.3 1 3 5
μM
P-eIF4E (Ser209)
eIF4E
P-ERK1/2 (Thr202/Tyr204)
ERK1/2
P-PKB (Ser473)
PKB
P-rpS6 (Ser240/244)
rpS6
4EBP1
P-4EBP1 (Ser65)
ACTIN
B
DMSO
MNK-I1
0 24 48 72 0 24 48 72
Time (h)
P-eIF4E (Ser209)
eIF4E
ACTIN
D
MNK-I1
C
30
60
120
Time (min) following adipogenic induction
DMSO
CGP57380
MNK-I1
AZD8055
P-eIF4E (Ser209)
eIF4E
P-ERK1/2 (Thr202/Tyr204)
ERK1/2
P-PKB (Ser473)
PKB
P-rpS6 (Ser240/244)
rpS6
4E-BP1
P-4E-BP1 (Ser65)
ACTIN

Figure 3-11: Efficacy, stability and specificity of MNK-I1 in 3T3-L1 pre-adipocytes.

(A) A dose response was performed in 3T3-L1 pre-adipocytes using the indicated concentrations of MNK-I1 or equivalent volume of DMSO. After 2 h, cell lysates were harvested and analysed by SDS-PAGE using the indicated antibodies. (B) Stability of MNK-I1 was assessed by treating 3T3-L1 pre-adipocytes with 3 μM MNK-I1 over a period of 72 h, during which cell lysates were harvested at the indicated times and analysed by SDS-PAGE using the indicated antibodies. (C) 3T3-L1 pre-adipocytes were pre-treated for 1 h with either 20 μM CGP57380, 3 μM MNK-I1 or 1 μM AZD8055, prior to induction with adipogenic induction media for a period of 120 min, during which cell lysates were harvested at the indicated times and analysed by SDS-PAGE using the indicated antibodies. (D) Chemical structure of MNK-I1. For (A), (B) and (C), representative immunoblots are shown (n=3).

Effect of CGP57380 and MNK-I1 on mTORC1 signalling

The effects of CGP57380 and MNK-I1 on mTORC1 signalling were compared alongside AZD8055, a potent mTOR inhibitor [220], during a 120 min period of adipogenic induction. Adipogenic induction resulted in an increase in P-eIF4E (Ser209) which was effectively blocked by MNK-I1, but to a lesser extent by CGP57380, as expected (Figure 3-11C). AZD8055 also blocked P-eIF4E but it was less effective than MNK inhibition (Figure 3-11C). CGP57380 had an immediate and acute effect on mTORC1 signalling, lowering P-rpS6 levels (Ser240/244) within the first 30 min and persisting for the entire 120 min (Figure 3-11C).; however, the effect on mTORC1 was acute, since the levels of phosphorylated 4E-BP1, assessed by its rate of migration on the gel, as well as through a phosphor-specific antibody (Ser65), were not altered by CGP57380. In contrast, MNK-I1 did not affect P-rpS6 levels during the 120 min, nor did it affect 4E-BP1 phosphorylation, suggesting that MNK-I1 does not affect mTORC1 signalling (Figure 3-11C). The mTOR inhibitor AZD8055 completely inhibited mTORC1 activity as assessed by the abolition of P-rpS6 P-4E-BP1 and faster migration of 4E-BP1 (Figure 3-11C). Therefore, the effects of CGP57380 on adipocyte differentiation and lipid accumulation described earlier may not only be due to the impairment of MNK activity, but also to an off-target effect(s) on mTORC1 signalling.

P-PKB (Ser473) was used as a readout of insulin/mTORC2 signalling. Adipogenic induction resulted in an increase in P-PKB, but this was not affected by either CGP57380 or MNK-I1 (Figure 3-11C). P-PKB was completely abolished by AZD8055, as expected (Figure 3-11C). Similarly, adipogenic induction activated ERK1/2, which was impaired by CGP57380 at 60 and 120 min (Figure 3-11C). This suggests that CGP57380 impedes ERK1/2 signalling and may therefore also interfere with MNK activation. In contrast, MNK-I1 and AZD8055 each increased P-ERK1/2 signalling at 30-, 60- and 120 min (Figure 3-11C). As alluded to earlier, the increase in P-ERK1/2 could be due to a (hypothetical) feedback loop.

Interim Conclusion

MNK-I1 is superior to CGP57380 in terms of its potency and specificity in inhibiting MNK activity and does not affect mTORC1 signalling. *What is the effect of MNK-I1 on adipocyte differentiation?*

Effect of MNK-I1 on 3T3-L1 pre-adipocyte differentiation

The effect of MNK-I1 on adipocyte differentiation was investigated by treating two-day post-confluent 3T3-L1 pre-adipocytes with adipogenic differentiation media in the presence or absence of MNK-I1. By Day 9 of the differentiation program, MNK-I1 treatment had significantly inhibited the accumulation of lipid into adipocytes by ~25%, as quantified by ORO-stained fields of view and analysis of total triglyceride content (Figure 3-12B-D). To determine whether the reduction in lipid accumulation was a result of impaired adipogenesis, the gene expression of adipogenic factors was monitored by RT-qPCR (Figure 3-12A). The level of *Cebpb* and *Cebpd* was not significantly affected by MNK-I1, suggesting MNK activity is not required for their expression. Notably, however the level of *Cebpa*, but not *Pparg,* was significantly impaired by MNK-I1 on Day 3, suggesting MNK activity may regulate *Cebpa* transcription. The increase in levels of *Fabp4* and *Pnpla2* but not *Cd36, Lpin1, Acaca or Srebf1* was significantly impaired by MNK-I1 on Day 6 and may be attributable to the reduction in *Cebpa*. This discrepancy in gene expression may reflect redundancy with respect to PPARγ, which is reported to occupy sites on target genes adjacent to C/EBPα [162]. Across the differentiation program, *Mknk2* expression was progressively induced, whilst *Mknk1* expression was initially reduced but remained steady throughout, consistent with earlier findings (Figure 3-1). This suggests that MNK1/2 are differentially expressed and may therefore perform distinct roles in adipocyte differentiation.

Given the physiological function of the MNKs in phosphorylating eIF4E, a key factor in mRNA translation initiation and its regulation, it was hypothesised that key adipogenic proteins may be subject to translational regulation by MNK activity. The expression of adipogenic proteins was therefore monitored over the first 72 h of 3T3-L1 adipogenesis in cells treated with MNK-I1. Adipogenic induction progressively increased the level of P-eIF4E, which, as expected, was completely blocked by MNK-I1 (Figure 3-13). C/EBPβ and C/EBPδ were immediately induced, and their initial induction and expression over the 72 h was not affected by MNK-I1 (Figure 3-13), consistent with their mRNA levels (Figure 3-12A). C/EBPβ-LIP levels were not affected by MNK-I1, in contrast to the effect of CGP57380, suggesting this may be symptomatic of poor inhibitor specificity rather than a genuine effect of the MNKs. C/EBPα and PPARγ were induced at 48- and 24 h, respectively (Figure 3-13). Notably, C/EBPα expression was significantly reduced by MNK-I1, consistent with *Cebpa* mRNA levels (Figure 3-12A), suggesting MNK activity is required for transcription of *Cebpa* and therefore expression of C/EBPα. PPARγ expression, along with *Pparg* mRNA levels were not affected by MNK-I1 (Figure 3-13).

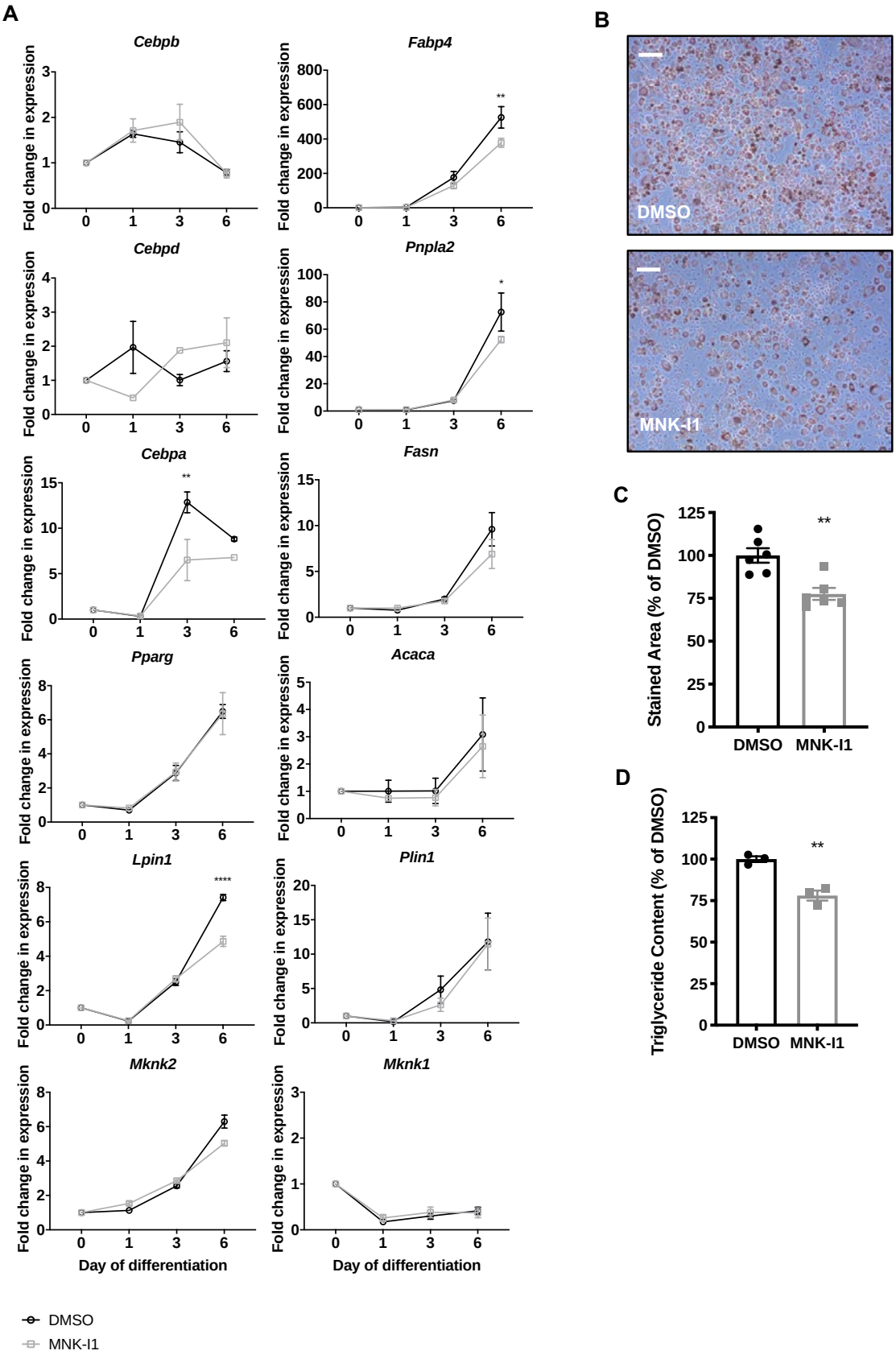
A
Cebpb
Fabp4
Cebpd
Pnpla2
Cebpa
Fasn
Pparg
Acaca
Lpin1
Plin1
Mknk2
Mknk1
Fold change in expression
Day of differentiation
DMSO
MNK-I1
B
DMSO
MNK-I1
C
Stained Area (% of DMSO)
D
Triglyceride Content (% of DMSO)

Figure 3-12: Effect of MNK-I1 on 3T3-L1 pre-adipocyte differentiation.

3T3-L1 pre-adipocytes were differentiated with adipogenic induction media in the presence or absence of 3 μM MNK-I1 or equivalent volume of DMSO. (A) mRNA levels of *Cebpb, Cebpd, Cebpa, Pparg, Lpin1, Fabp4, Pnpla2, Fasn, Acaca* and *Plin1* were assessed by RT-qPCR at the indicated times. Expression levels were normalised to *Nono* and *Hprt* and represented as fold change with respect to day 0. Data are mean ± SEM; (n=2-3); 2-way ANOVA (*P < 0.05 **P < 0.01 ***P < 0.001). (B) Day 9 differentiated adipocytes were stained with ORO to assess lipid accumulation; representative images are shown, scale bar 0.2 μm. (C) Total stained area was quantified from 6 different fields of view from (B) and is represented as percentage stained area relative to DMSO; data are mean ± SEM; individual data values are plotted (n=1); unpaired t-test (*P < 0.05 **P < 0.01 ***P < 0.001). (D) Triglyceride was extracted from Day 9 differentiated adipocytes, quantified and represented as percentage triglyceride content relative to DMSO; data are mean ± SEM; individual data values are plotted (n=3); unpaired t-test (*P < 0.05 **P < 0.01 ***P < 0.001).

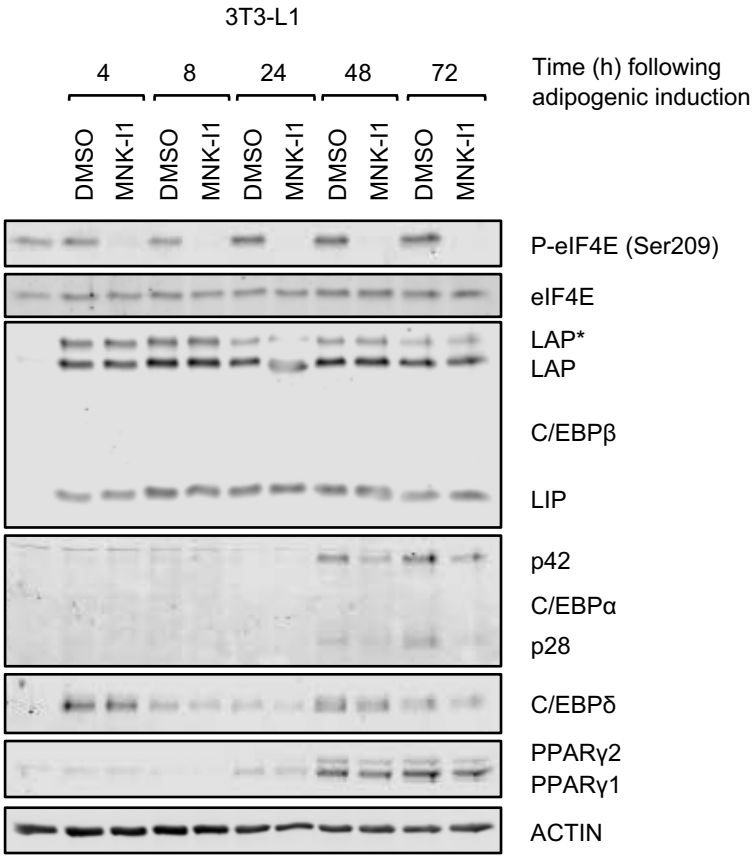

Figure 3-13: Effect of MNK-I1 on early 3T3-L1 pre-adipocyte differentiation.

3T3-L1 pre-adipocytes were differentiated with adipogenic induction media in the presence or absence of 3 μM MNK-I1 or equivalent volume of DMSO for a period of 72 h during which cell lysates were harvested at the indicated times and analysed by SDS-PAGE using the indicated antibodies; representative immunoblots are shown (n=3).

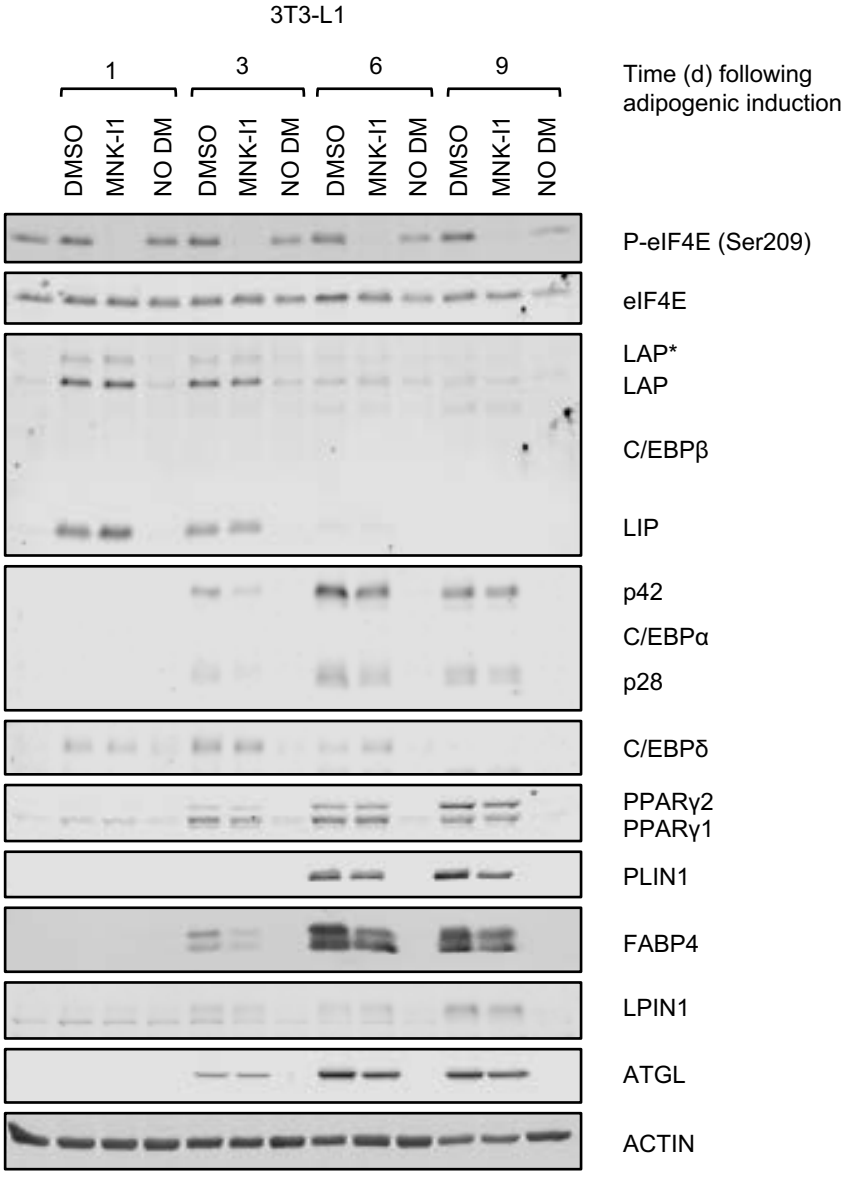

Figure 3-14: Effect of MNK-I1 on terminal adipogenesis in 3T3-L1 pre-adipocytes.

3T3-L1 pre-adipocytes were differentiated with adipogenic induction media in the presence or absence of 3 μM MNK-I1 or equivalent volume of DMSO. Cell lysates were harvested at the indicated times and analysed by SDS-PAGE using the indicated antibodies; representative immunoblots are shown (n=3).

When the analysis was extended to cover the entire adipogenic program, C/EBPα was reduced at Day 6, but not Day 9 (Figure 3-14). C/EBPβ expression, along with PPARγ, was not affected, although MNK-I1 did increase the expression of C/EBPδ on Day 6, relative to control (Figure 3-14). The expression of FABP4, PLIN1, Lipin-1 (LPIN1) and ATGL, was reduced by MNK-I1 on Days 3, 6 and 9 (Figure 3-14), consistent with their respective mRNA levels; PLIN1 was an exception: the specific reduction in C/EBPα levels by MNK-I1 may therefore be the nexus at which this compound impairs adipogenesis. As expected, 3T3-L1 cells treated without induction media (no DM) did not express any of the adipogenic factors assessed (Figure 3-14).

Interim Conclusion

MNK-I1 likely impairs adipogenesis through decreased transcription of *Cebpa* and therefore reduced expression of C/EBPα. This, in turn, decreases expression of downstream target genes and thus C/EBPα may be the nexus at which MNK activity regulates adipogenesis. MNK-I1 does not affect C/EBPβ-LIP or PPARγ expression, suggesting these may be undesirable off-target effects of CGP57380 rather than a genuine effect of the MNKs.

Refinement of MNK-I1 inhibitor treatment period

Hormone-induced adipogenesis initiates a highly-regulated signalling cascade. Therefore, given the function of MNKs as signal-regulated kinases, it was hypothesised that they play an important role in early adipogenesis. To this point cells had been treated with MNK inhibitor *at the time* of adipogenic induction. However, given the signalling events induced by the adipogenic stimuli are immediate, 3T3-L1 pre-adipocytes were treated with MNK inhibitor *prior* to the addition of adipogenic agents to deplete cells of any MNK activity that may potentially continue to promote early signalling events. Adipogenic signalling coordinates re-entry into the cell cycle, a phase known as 'mitotic clonal expansion' (MCE), after which co-expression of PPARγ, C/EBPα and permanent exit from the cell cycle establish an irreversible commitment to adipocyte differentiation [193,221]. Based on the timing of these events, three different inhibitor treatments were proposed:

(1) pre-treatment from the time of seeding (Day –3) to end of differentiation (Day +9)
(2) pre-treatment from time of seeding (Day –3) to post-MCE (Day +3);
(3) treatment from end of MCE (Day +3) to end of differentiation (Day +9).

The expression of adipogenic factors was assessed by Western blot on Days 3 and 6 to compare the effect of the different treatment scenarios on adipogenesis (Figure 3-15). In treatment (1), MNK-I1 caused was a marked impairment in expression of both C/EBPα and PPARγ expression on Days 3 and 6, in addition to CHOP. Whilst MNK-I1 did not affect expression of the activating C/EBPβ (LAP*/LAP) isoforms, it decreased the expression of the inhibitory C/EBPβ-LIP isoform, particularly on Day 3, and elevated C/EBPδ levels by Day 6 (Figure 3-15). This contrasted with

the effect of CGP57380, which increased C/EBPβ-LIP expression as described earlier (Figure 3-10A). The expression of ATGL, LPIN1, PLIN1 and FABP4 was noticeably decreased on Day 6, likely reflecting the lower levels of C/EBPα and PPARγ (Figure 3-15).

As in (1), treatment (2) caused a marked impairment in the expression of C/EBPα and PPARγ, in addition to CHOP and C/EBPβ-LIP on Day 3. However, concomitant with the removal of MNK-I1, these effects did not persist: by Day 6, C/EBPα and PPARγ, but not CHOP levels, had recovered (Figure 3-15). In contrast to (1), C/EBPδ levels were not elevated on Day 6 and the impaired expression of ATGL, LPIN1, PLIN1 and FABP4 was less marked (Figure 3-15). Thus, it appeared the effects of MNK-I1 were somewhat *reversible*.

The expression of C/EBPα, PPARγ, CHOP and C/EBPβ-LIP was not impaired prior to treatment in (3) (Figure 3-15). However, following MNK-I1 addition on Day 3, there was a modest reduction in C/EBPα and FABP4 by Day 6. However, MNK-I1 did not reduce the expression of PPARγ, nor ATGL, LPIN or PLIN1 (Figure 3-15).

In summary, MNK-I1 pre-treatments (1, 2) resulted in significant impairment of C/EBPα and PPARγ expression. However, MNK-I1 withdrawal at Day+3 (2) resulted in the recovery of C/EBPα and PPARγ levels, whilst addition of MNK-I1 post-MCE (3) modestly and selectively reduced C/EBPα expression. This suggests that MNK activity is required prior to adipogenic induction to promote expression of C/EBPα and PPARγ and that MNK activity is also necessary for sustained C/EBPα but not PPARγ expression during terminal adipogenesis.

Effect of MNK-I1 pre-treatment on 3T3-L1 pre-adipocyte differentiation

In light of this, the effect of MNK-I1 was re-assessed across the first 72 h of adipogenesis, this time following *pre-treatment* with MNK-I1 at time of seeding. Impairment of MNK activity at the time of adipogenic induction due to inhibitor pre-treatment was confirmed by the loss of P-eIF4E signal at 0 h (Figure 3-16B). The expression of C/EBPβ was not affected by MNK-I1 pre-treatment, including *Cebpb* mRNA (Figure 3-16A-B), consistent with previous findings with MNK-I1 (Figures 3-13 and 3-14). In contrast, MNK-I1 pre-treatment impaired the induction of C/EBPδ at 3-, 24-, 48- and 72 h, however, *Cebpd* levels were only significantly reduced at 3 h (Figure 3-16A-B). MNK-I1 significantly reduced C/EBPα expression, including *Cebpa* levels at 48- and 72 h (Figure 3-16A-B), consistent but more marked than previous findings (Figure 3-13 and 3-14); MNK-I1 also reduced PPARγ expression at 24-, 48- and 72 h, however this was not reflected in reduced *Pparg* levels (Figure 3-16). This suggests that MNK activity is required to promote the transcription of *Cebpa*, whereas the *Pparg* message may be subject to translational control by the MNKs.

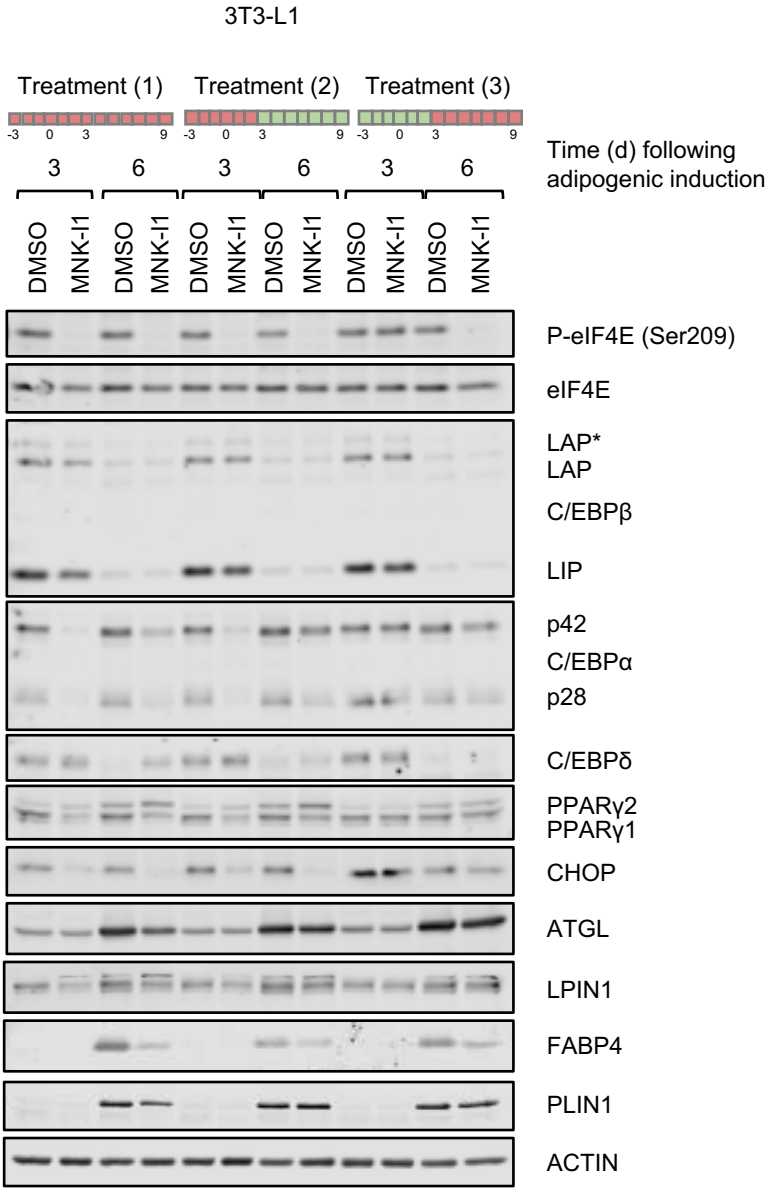

Figure 3-15: Refinement of MNK-I1 treatment period during 3T3-L1 pre-adipocyte differentiation.
3T3-L1 pre-adipocytes were treated with MNK-I1 or equivalent volume of DMSO according to 3 different treatment regimens depicted schematically. Treatment periods, corresponding to days, where MNK-I1 was either present or absent from the media are highlighted in red and green, respectively. Cells were induced with adipogenic induction media on Day 0, after which cell lysates were harvested on Days 6 and 9 and analysed by SDS-PAGE using the indicated antibodies (n=1).

Effect of MNK-I1 on CREB and GR expression and activation

As shown in Figure 3-4, CREB and GR likely regulate expression of *Cebpd* through binding their respective response elements in the *Cebpd* promoter. It was therefore conceivable that the impaired expression of C/EBPδ caused by loss of MNK activity could be due to a reduction in CREB and/or GR expression. In response to adipogenic induction, CREB expression was progressively elevated over the first 72 h of adipogenesis and this was notably impaired by MNK-I1 (Figure 3-16B). The level of activated P-CREB changed in parallel to total CREB, suggesting expression but not activation of CREB is regulated by MNK activity (Figure 3-16B). Adipogenic induction caused a shift in the migration of GR, which slowed its migration through the gel, consistent with its activation by post-translational modification [222]. MNK-I1 did not affect GR levels or migration patterns, suggesting MNK activity does not regulate expression or activation of GR.

Individual adipogenic stimuli were subsequently used to investigate how early CREB expression was affected by MNK-I1 in 3T3-L1 pre-adipocytes (Figures 3-16C and D). IBMX potently induced C/EBPβ expression and modestly induced C/EBPδ, and this was not affected by MNK-I1. This was reflected in both *Cebpb* and *Cebpd* mRNA levels and consistent with earlier findings (Figure 3-2). IBMX did not alter GR migration, suggesting that it does not activate GR, as expected. IBMX increased the level of CREB and activated P-CREB, which was notably impaired by MNK-I1. DEX potently and modestly induced C/EBPδ and C/EBPβ expression, respectively. C/EBPδ, but not and C/EBPβ expression, was affected by MNK-I1, as reflected in their respective mRNA levels (Figure 3-16C), consistent with previous findings (Figures 3-2, 3-16A). DEX induced a band-shift in GR migration suggesting GR was activated by DEX, as expected. However, unlike IBMX, DEX did not increase the levels of CREB or P-CREB, suggesting IBMX is directly responsible for inducing the activation and expression of CREB. IBMX/DEX more potently induced C/EBPβ and C/EBPδ expression more than the individual components themselves, which was also evident with COCKTAIL treatment, consistent with their respective mRNA levels (Figure 3-16C) and previous findings (Figure 3-2). MNK-I1 appeared to reduce the expression of C/EBPβ, although the effect was only slight and may be a transient effect at this timepoint. Notably, the induction of C/EBPδ and CREB with IBMX/DEX and COCKTAIL treatments was significantly impaired by MNK-I1, suggesting MNK activity regulates IBMX-mediated CREB induction.

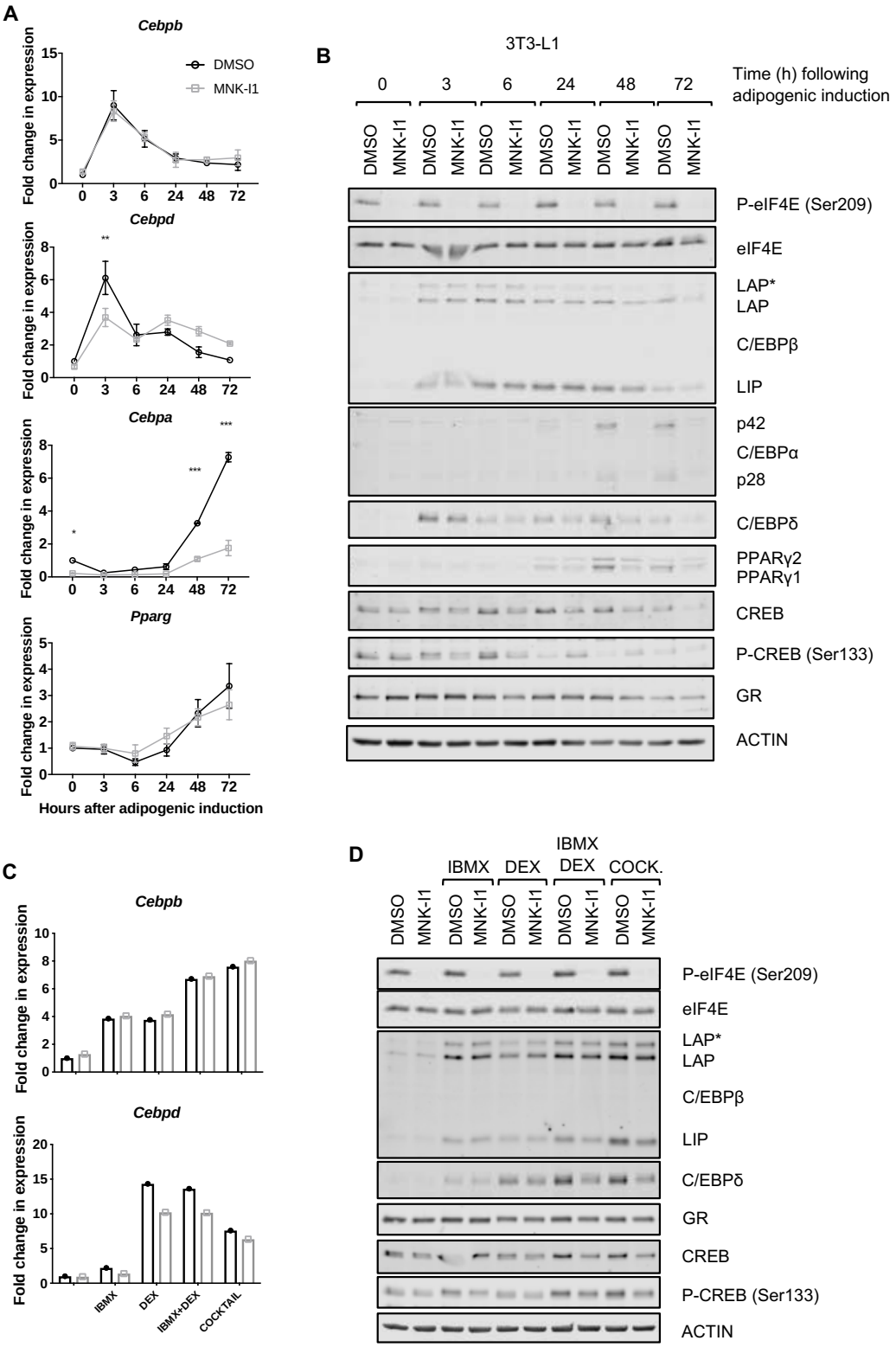
A
Cebpb
Cebpd
Cebpa
Pparg
Fold change in expression
DMSO
MNK-I1
Hours after adipogenic induction
B
3T3-L1
Time (h) following adipogenic induction
P-eIF4E (Ser209)
eIF4E
LAP*
LAP
C/EBPβ
LIP
p42
C/EBPα
p28
C/EBPδ
PPARγ2
PPARγ1
CREB
P-CREB (Ser133)
GR
ACTIN
C
IBMX
DEX
IBMX+DEX
COCKTAIL
D
IBMX
DEX
IBMX DEX
COCK.

Figure 3-16: Effect of MNK-I1 pre-treatment on 3T3-L1 pre-adipocyte differentiation.

3T3-L1 pre-adipocytes were differentiated with adipogenic induction media following pre-treatment with 3 μM MNK-I1 or equivalent volume of DMSO. (A) mRNA levels of *Cebpb, Cebpd, Cebpa* and *Pparg* were assessed by RT-qPCR at the indicated times. Expression levels were normalised to *Nono* and *Hprt* and represented as fold change with respect to Day 0. Data are mean ± SEM; (n=2-3); 2-way ANOVA (*P < 0.05 **P < 0.01 ***P < 0.001). (B) Cell lysates were harvested at the indicated times and analysed by SDS-PAGE using the indicated antibodies; representative immunoblots are shown (n=2). (C) 3T3-L1 pre-adipocytes pre-treated with 3 μM MNK-I1 or equivalent volume of DMSO were stimulated with 500 IBMX and 0.5 μM DEX either individually, in combination (IBMX + DEX) or together with 350 nM insulin and 2μM ROSI (COCKTAIL). After 3 h, the mRNA levels of *Cebpb* and *Cebpd* were analysed by RT-qPCR. Expression levels were normalised to *Nono* and *Hprt* and represented as fold change with respect to DMSO. Data are mean values; (n=1). (D) Cell lysates were also harvested after 3 h and analysed by SDS-PAGE using the indicated antibodies. Representative immunoblots are shown (n=2).

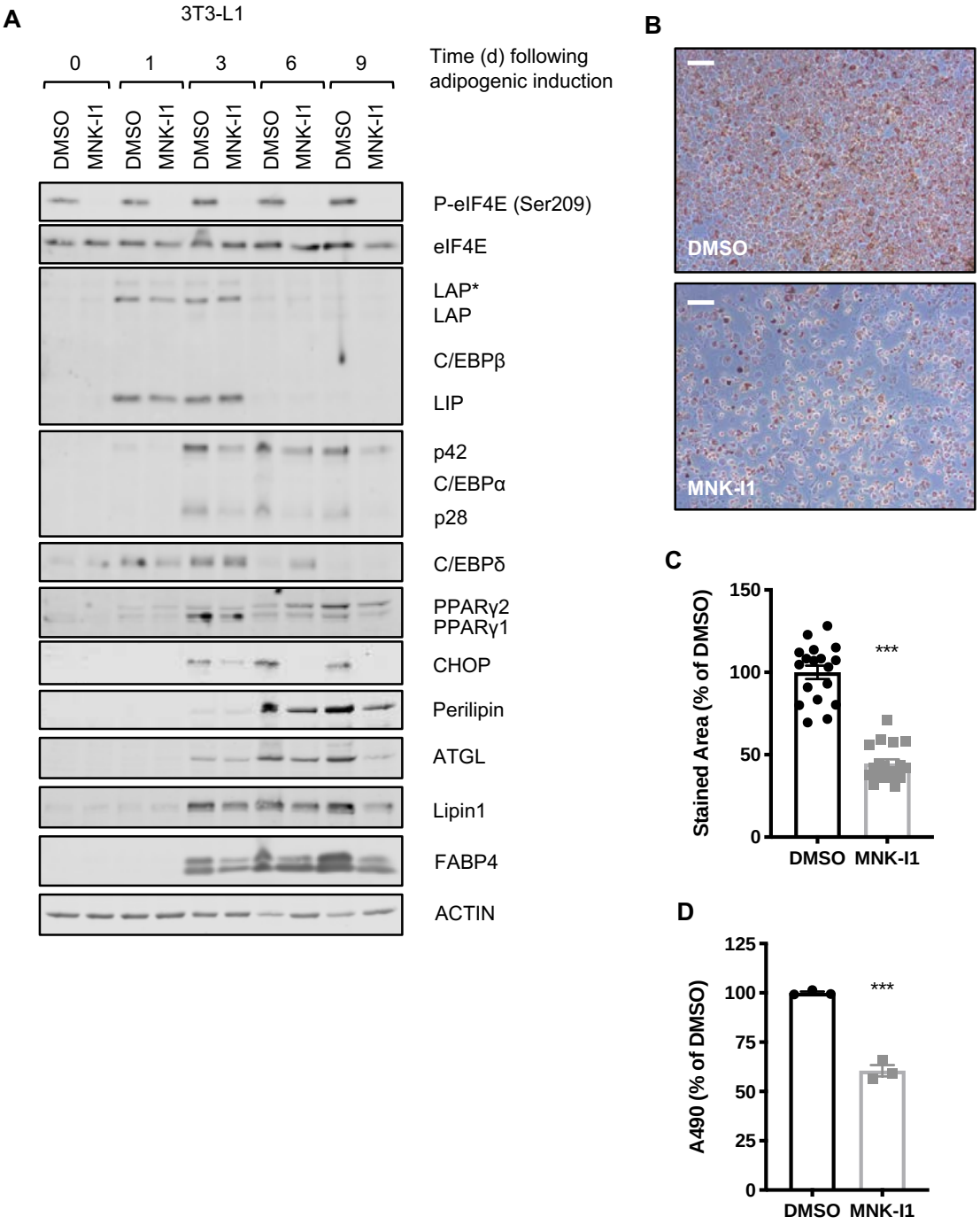
A
3T3-L1
0
1
3
6
9
Time (d) following adipogenic induction
DMSO
MNK-I1
P-eIF4E (Ser209)
eIF4E
LAP*
LAP
C/EBPβ
LIP
p42
C/EBPα
p28
C/EBPδ
PPARγ2
PPARγ1
CHOP
Perilipin
ATGL
Lipin1
FABP4
ACTIN
B
DMSO
MNK-I1
C
Stained Area (% of DMSO)
150
100
50
0
***
DMSO
MNK-I1
D
A490 (% of DMSO)
125
100
75
50
25
0
***
DMSO
MNK-I1

Figure 3-17: Effect of MNK-I1 pre-treatment on terminal adipogenesis in 3T3-L1 pre-adipocytes.
3T3-L1 pre-adipocytes were differentiated with adipogenic induction media following pre-treatment with 3 μM MNK-I1 or equivalent volume of DMSO. (A) Cell lysates were harvested at the indicated times and analysed by SDS-PAGE using the indicated antibodies; representative immunoblots are shown (n=2). (B) Day 9 differentiated adipocytes were stained with ORO to assess lipid accumulation; representative images are shown, scale bar 0.2 μm. (C) Total stained area was quantified from 9 different fields of view from (B) and is represented as percentage stained area relative to DMSO; data are mean ± SEM; individual data values are plotted (n=3); unpaired t-test (*P < 0.05 **P < 0.01 ***P < 0.001) (D) ORO eluted from stained cells was quantified by absorbance (A490) and is represented as percentage absorbance relative to DMSO; data are mean ± SEM; individual data values are plotted (n=3); unpaired t-test (*P < 0.05 **P < 0.01 ***P < 0.001).

Effect of MNK-I1 pre-treatment on terminal adipocyte differentiation

When MNK-I1 pre-treatment was extended to cover the entire adipogenic program, expression of C/EBPα and PPARγ was significantly reduced on Days 3, 6 and 9 (Figure 3-17A). The expression of C/EBPβ was not affected, and C/EBPδ was increased on Day 6 by MNK-I1 pre-treatment (Figure 3-17A), consistent with earlier findings (Figures 3-13 and 3-14). The expression of CHOP was also reduced by MNK-I1 pre-treatment, along with PLIN1, ATGL, LPIN1 and FABP4 on Days 3, 6 and 9 (Figure 3-17). This reduction was more marked with MNK-I1 pre-treatment compared with treatment at the time of induction (Figure 3-14) and is likely attributable to the impaired expression of both C/EBPα and PPARγ.

Lipid accumulation, quantified from ORO-stained fields of view, was significantly reduced by MNK-I1 pre-treatment (~50%) whilst absorbance (A490) of ORO eluted from stained cells was reduced by 40% (Figure 3-17B-E). Lipid accumulation was more significantly reduced with MNK-I1 pre-treatment compared with MNK-I1 treatment at time of adipogenic induction (Figure 3-12B-D). Given that expression of the two major adipogenic transcription factors, C/EBPα and PPARγ, was significantly impaired by MNK-I1, the reduction in lipid accumulation is suggested to result from impaired adipogenesis rather than a defect in lipid metabolism.

Interim Conclusion

MNK-I1 pre-treatment results in more significant impairment of adipocyte differentiation by likely regulating the transcription of *Cebpa* and translation of PPARγ. Consequently, there is a more marked impairment in the expression of downstream adipogenic genes and a greater reduction in lipid accumulation. MNK-I1 pre-treatment appears to impair the IBMX-stimulated induction of CREB, which may account for the reduction in CREB, C/EBPβ and C/EBPδ.

Effect of MNK-I1 on C/EBPβ phosphorylation

The sequence of events leading to terminal adipogenesis involves the regulated induction of C/EBPβ and C/EBPδ, which in turn directly induce the expression of PPARγ and C/EBPα [89,96,150,151,153]. However, some propose that the induction of PPARγ and C/EBPα occurs simultaneously [123], whilst others suggest that C/EBPβ controls the induction of C/EBPα, which together subsequently regulate PPARγ [123,152]. The current consensus proposes a single unified pathway in which C/EBPβ and C/EBPδ induce the expression of PPARγ, which then activates C/EBPα expression, which acts in concert with PPARγ to induce the expression of adipogenic genes [134,159]. In all of the proposed pathways, C/EBPβ is the mutual factor responsible for the induction of PPARγ and C/EBPα. Therefore, given that the expression of C/EBPα and PPARγ was significantly impaired by MNK-I1, it was hypothesised that the DNA binding activity of C/EBPβ may be regulated by MNK activity. C/EBPβ DNA binding activity is regulated by MAPK phosphorylation on Thr188, which primes C/EBPβ for subsequent phosphorylation on Ser184 or

Thr179 by glycogen synthase kinase-3β [101]. The effect of MNK-I1 on the level of P-C/EBPβ Thr188 was assessed over the first 72 h of adipogenic induction: MNK-I1 did not alter P-C/EBPβ Thr188, suggesting the DNA binding activity of C/EBPβ is not regulated by MNK activity (Figure 3-18A).

Identification of C/EBP response elements on Cebpa and Pparg gene promoters and the effect of MNK-I1 on occupancy of C/EBPβ

The functional C/EBP regulatory elements (C/EBPREs) in the promoters of *Cebpa* and *Pparg2* have been previously identified [113,153,208,223]. *Cebpa* (–203/227) and *Pparg2* (–269/289) contain two CCAAT boxes which share the consensus core sequence (NNGNAAK), where K=T or G. Analysis of the *Pparg1* promoter using publicly accessible ChIP-seq data (https://chip-atlas.org) identified two CCAAT boxes (-3997/4006) comprising the consensus core sequence, indicating that *Pparg1* may also be regulated by C/EBPβ (Figure 3-18C). To assess whether occupancy of C/EBPβ at these elements was affected by MNK-I1, ChIP assays were performed following 24 h of adipogenic induction. Whilst C/EBPβ was significantly enriched at the *Cebpa, Pparg1* and *Pparg2* C/EBPREs, it was not significantly affected by MNK-I1 (Figure 3-18D-E). Enrichment of C/EBPβ was specific for the respective C/EBPREs since no significant enrichment was observed at the NEG non-specific regions of *Cebpa* (-3111) (Figure 3-18F) or *Pparg* (-17,510) (Figure 3-18G). This suggests C/EBPβ occupancy on the promoters of *Cebpa* and *Pparg* is not regulated by MNK activity, consistent with findings that the DNA binding activity of C/EBPβ (P-Thr188) was not affected by MNK-I1.

Identification of PPAR response element on Cebpa promoter and effect of MNK-I1 on occupancy of PPARγ

Given that one of the proposed pathways leading to terminal adipogenesis involves the sequential induction of PPARγ by C/EBPβ, which, in turn, activate expression of C/EBPα, it was hypothesised that PPARγ occupancy was reduced on the promoter of *Cebpa*. Analysis of the *Cebpa* promoter using publicly accessible ChIP-seq data (https://chip-atlas.org) identified a PPARE at -125 comprising imperfect direct repeats of the consensus core sequence (AGGTCA) separated by a single nucleotide (Figure 3-18B). The analysis was extended to *Fabp4*, a known target of PPARγ, and identified consensus PPAREs at -2945 and -5376 which would act as positive controls (Figure 3-19A). To assess whether occupancy of PPARγ at these elements was affected by MNK-I1, ChIP assays were performed following 72 h of adipogenic induction. PPARγ was significantly enriched at both PPAREs in *Fabp4* and, surprisingly, this enrichment was significantly enhanced at the -5376 response element by MNK-I1 (Figure 3-19C). PPARγ was not enriched at the *Cebpa* -125 PPARE (Figure 3-19B), as equivalent levels of enrichment were observed in the NEG non-specific region (-1424) (Figure 3-19D). Therefore, it was not possible to assess the occupancy of PPARγ on *Cebpa*.

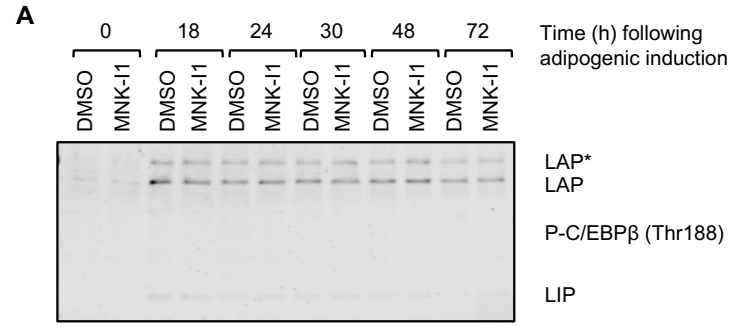

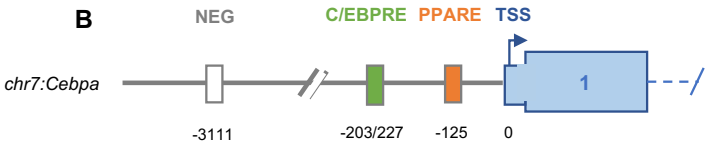

Site	Sequence
C/EBPRE –203/227	TGAGCG**CTGCAAG**CCGGGTTCGC**CTTGCAG**CGCAGG
PPARE –125	CTTGGA**AAGTCA**C**AGGAGA**AGGCGG

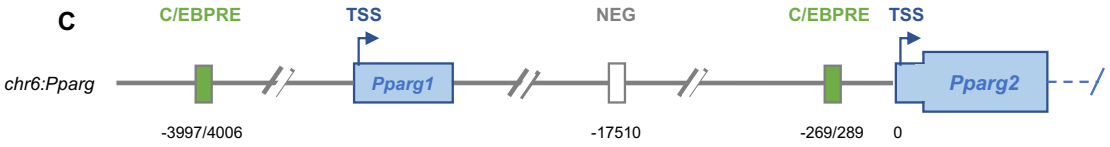

Site	Sequence
C/EBPRE –269/289	ATTTTA**CTGCAAT**TTTAAA**AAGCAAT**CAATAT
C/EBPRE –3997/4006	TGTGGC**TAGTAAG**ACTTACAAAGACAGT**GAGTAAA**CAATGG

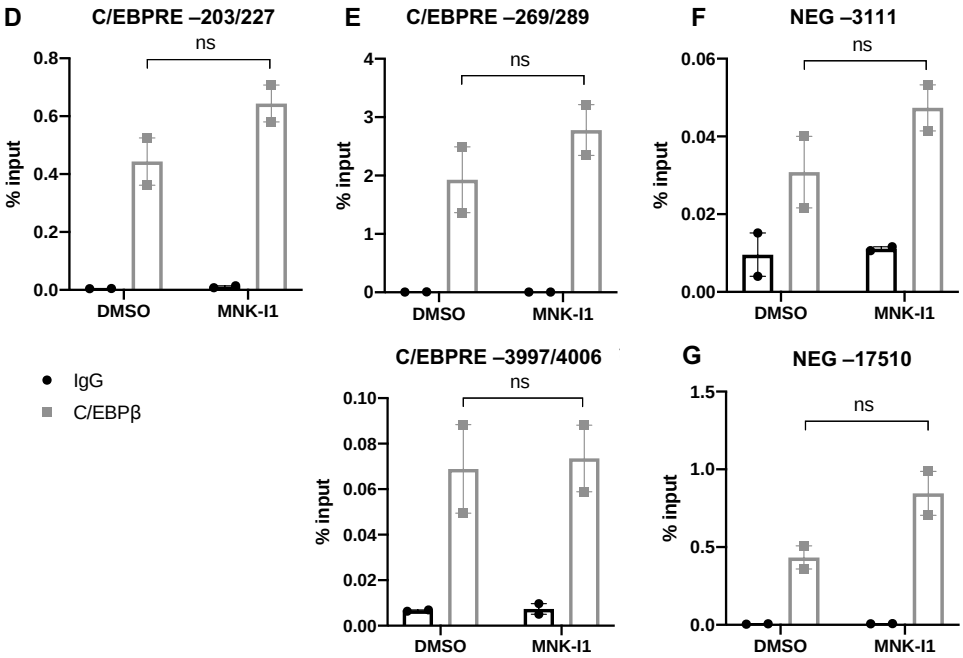

Figure 3-18: Effect of MNK-I1 on C/EBPβ phosphorylation and promoter occupancy.

(A) 3T3-L1 pre-adipocytes were differentiated with adipogenic induction media in the presence or absence of 3 μM MNK-I1 or equivalent volume of DMSO over 72 h during which cell lysates were harvested at the indicated times and analysed by SDS-PAGE using the indicated antibodies; representative immunoblots are shown (n=2). Schematic diagram depicting the genomic position of putative response elements on the (B) *Cebpa* and (C) *Pparg1/2* promoters relative to their TSS (*Cebpa* chr7:35,904,312; *Pparg1* chr6:115,311,167; and *Pparg2* chr6:115,372,010). The DNA sequence of the putative response elements are shown: nucleotides corresponding to the core consensus sequence are bold underlined. ChIP assays were performed in 3T3-L1 to assess enrichment of C/EBPβ at the putative C/EBPREs on the promoter of (D) *Cebpa* and (E) *Pparg1/2* after 24 h of adipogenic induction. Enrichment levels are represented as percentage of input chromatin (% input). To assess whether enrichment of C/EBPβ was specific to the response elements, enrichment was assessed at the corresponding NEG regions of (F) *Cebpa* and (G) *Pparg1/2*. Data are mean ± SEM; n=2; unpaired two-tailed t-test (*P < 0.05 **P < 0.01 ***P < 0.001).

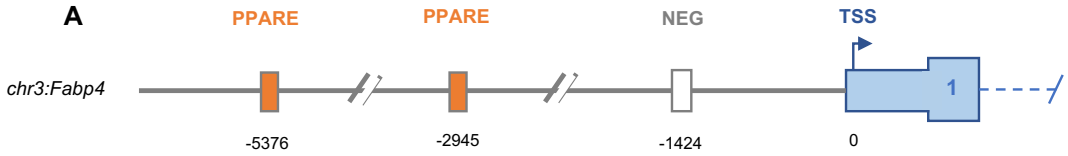

Site	Sequence
PPARE –2945	GGGCTGAGGTCACATCTCAGAATCT
PPARE –5376	AAATGGAGTTCCCAGATGCCTGACA

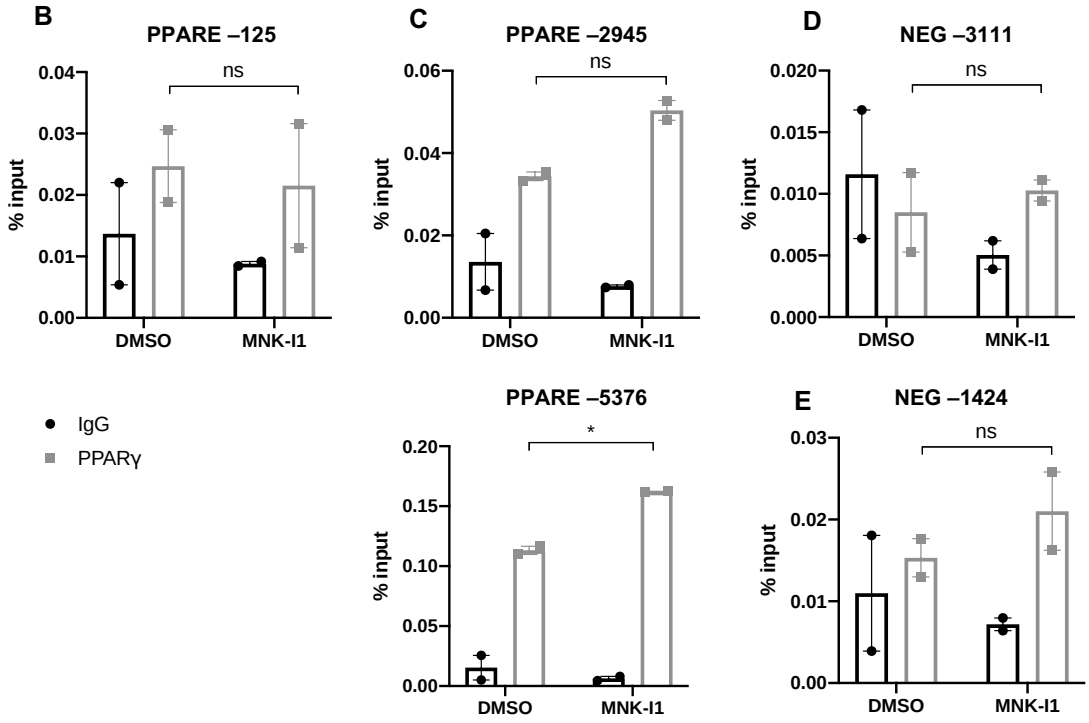

Figure 3-19: Effect of MNK-I1 on PPARγ promoter occupancy.

(A) Schematic diagram depicting the genomic position of putative response elements on the *Fabp4* promoter relative to the TSS (chr3:10,208,576). The DNA sequence of the putative response elements are shown: nucleotides corresponding to the core consensus sequence are bold underlined. ChIP assays were performed in 3T3-L1 to assess enrichment of PPARγ at the putative PPAREs on the promoter of (B) *Cebpa* and (C) *Fabp4* after 72 h of adipogenic induction. Enrichment levels are represented as percentage of input chromatin (% input). To assess whether enrichment of PPARγ was specific to the response elements, enrichment was assessed at the corresponding NEG regions of (D) *Cebpa* and (E) *Fabp4*. Data are mean ± SEM; n=2; unpaired two-tailed t-test (*P < 0.05 **P < 0.01 ***P < 0.001).

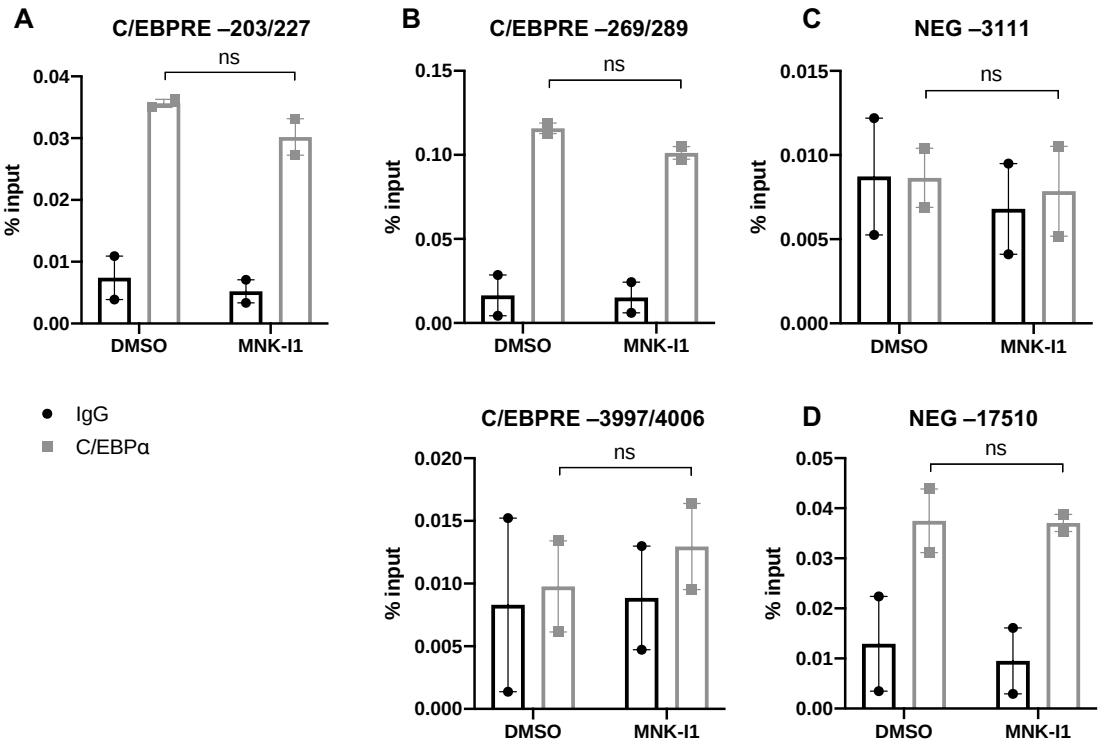

Figure 3-20: Effect of MNK-I1 on C/EBPα promoter occupancy.

ChIP assays were performed in 3T3-L1 to assess enrichment of C/EBPα at the putative C/EBPREs on the promoter of (A) *Cebpa* and (B) *Pparg1/2* after 72 h of adipogenic induction. Enrichment levels are represented as percentage of input chromatin (% input). To assess whether enrichment of PPARγ was specific to the response elements, enrichment was assessed at the corresponding NEG regions of (C) *Cebpa* and (D) *Pparg1/2*. Data are mean ± SEM; n=2; unpaired two-tailed t-test (*P < 0.05 **P < 0.01 ***P < 0.001).

Effect of MNK-I1 on the auto-regulatory expression of Cebpa

The *Cebpa* gene is under the control of a C/EBPα auto-regulatory mechanism that is necessary for maintaining its own expression [113,120–123] and is reported to bind a sequence between -203 and -227 in its own promoter [113]. To determine whether the auto-regulatory mechanism of C/EBPα is modulated by MNK activity, occupancy of C/EBPα was assessed by ChIP after 72 h of adipogenic induction in the presence of MNK-I1. C/EBPα was significantly enriched at the *Cebpa* -203/227 C/EBPRE; however, enrichment was not reduced by MNK-I1, suggesting MNK activity does not regulate C/EBPα auto-regulation (Figure 3-20A). Enrichment was specific to the C/EBPRE since no significant enrichment was observed at the NEG non-specific region of *Cebpa* (-3111) (Figure 3-20C)

Effect of MNK-I1 on the occupancy of C/EBPα in Pparg1 and 2

Given that C/EBPα and C/EBPβ may simultaneously regulate PPARγ expression, it was hypothesised that the occupancy of C/EBPα on the C/EBPREs of *Pparg* was likely to be reduced by MNK-I1. C/EBPα was significantly enriched at the *Pparg2* C/EBPRE (-269/289) as expected [153] but was not significantly affected by MNK-I1 (Figure 3-20B), suggesting that MNK activity likely does not alter the occupancy of C/EBPα on *Pparg2*. C/EBPα was not enriched at the *Pparg1* C/EBPRE (3997/4006) (Figure 3-20B), in contrast to C/EBPβ (Figure 3-18E), suggesting that C/EBPβ, but not C/EBPα is responsible for driving *Pparg1* expression, consistent with [150–152].

Interim Conclusion

MNK-I1 does not affect the phosphorylation of C/EBPβ at Thr188, suggesting its dimerisation and thus DNA binding activity are not regulated by MNK activity. MNK-I1 does not affect the occupancy of C/EBPβ, PPARγ or C/EBPα on the promoter of *Cebpa*, indicating earlier events preceding the induction of C/EBPα may be subject to regulation by the MNKs.

Events preceding C/EBPα and PPARγ expression in adipogenesis

Growth-arrested pre-adipocytes are synchronised into a phase of MCE following hormonal adipogenic induction. The C/EBP proteins intricately regulate mitotic entry and exit based on their temporal expression patterns [73,102,224]. C/EBPβ and C/EBPδ, both pro-mitotic factors, are immediately induced upon hormonal induction and drive entry into mitosis. The expression of C/EBPα, an anti-mitotic factor, is temporally delayed so as not to interfere with mitotic entry [70]. Temporal control of C/EBPα expression is achieved by regulated and delayed phosphorylation of C/EBPβ which is necessary for it to bind DNA [101] and therefore transactivate expression of PPARγ and subsequently C/EBPα. The anti-mitotic activity of C/EBPα, together with a reduction in C/EBPβ and C/EBPδ expression, drives cells out of mitotic expansion and marks the transition to terminal adipocyte differentiation. Disruption of mitosis during this phase of pre-adipocyte differentiation is detrimental to adipogenesis [73]. Given the requisite and

highly synchronised nature of MCE, it was hypothesised that a loss of MNK activity may cause a dysregulation that could explain the impaired adipogenesis phenotype. Consistent with the results obtained thus far, it was hypothesised that the reduced expression of C/EBPα and PPARγ was an indirect effect of earlier events dysregulated during MCE rather than a direct effect

Effect of MNK-I1 on MCE

To investigate mitotic cycling during adipogenesis, pre-adipocytes differentiating in the presence or absence of MNK-I1 were stained with propidium iodide (PI) and analysed by flow cytometry across a period of 42 h (Figure 3-21). MNK-I1 treatment did not alter the proportion of cell cycle populations prior to adipogenic induction (0 h). Concomitant with entry into mitosis after 18 h, there was a shift from G0/1 to S-phase, with the proportion of cells in S-phase (20.90%) significantly reduced by MNK-I1 (11.15%). At 24 h, the proportion of cells in S- (25.15%), and G2-phase (36.05%) increased, whilst MNK-I1 reduced these proportions by approximately half (S-phase: 11.75%; G2-phase: 18.85%). At 30 h, decreases in S-and G2-phase proportions were associated with a corresponding increase in the G0/1 population; however, they were not significantly affected by MNK-I1. At 42 h, cell populations had returned to their pre-induction levels, indicating the end of MCE. Interestingly, MNK-I1 treatment was associated with an increase in the proportion of Sub-G1 cells, although the differences were not statistically significant. Nevertheless, these results suggest that MNK activity is required for cell cycle progression, specifically for the transition from G1 to S-phase during MCE in 3T3-L1 pre-adipocytes.

Analysis of cell cycle factor expression during G1 to S-phase transition

Retinoblastoma (RB) is responsible for regulating entry into S-phase and is part of a critical G1/S checkpoint (reviewed in [108]). The RB family consists of three proteins, RB/p105, p107 and RB2/p130, collectively referred to as 'pocket-proteins'. When hypo-phosphorylated, RB proteins bind to E2F and directly repress gene transcription required for S-phase progression [225]. Cyclin/cyclin-dependent kinase (CDK) complexes are formed during different phases of the cell cycle and are responsible for phosphorylating a distinct set of proteins. The D-cyclins (CCND1, D2 and D3) and their assembly with CDK4 and 6 are responsible for mediating progression through G1/S. The E-Cyclins (CCNE1 and E2) and their assembly with CDK2 mediate additional phosphorylation of RB. The expression of D-cyclins is dependent on mitogenic signalling; CCND1 expression is low in quiescent G0 cells and elevated in response to serum [226,227]. CDK4/6, in complex with D-cyclins, are responsible for phosphorylating RB, which release it from E2F and thereby facilitate transcription of S-phase entry genes. Cyclin E is not regulated by mitogenic signalling; instead, the promoters of both D- and E-cyclins are activated by E2F and it is thought that this auto-regulatory loop governs the accumulation of these products and facilitates the progression of cells through G1 [228,229]. E2F-independent mechanisms also exist to regulate G1/S transition: RB stabilises expression of the $p27^{kip}$ CDK inhibitor by inhibiting its

ubiquitination [230,231], whilst p107 and p130 proteins bind to and inhibit Cyclin E/CDK2 complexes.

RB has been shown to interact with C/EBP isoforms and contain RB-binding motifs similar to the one used by E2F [110]. In particular, it is thought that this interaction is a critical regulator of C/EBPβ DNA binding activity during early adipogenesis [109,110]. C/EBPβ associates with hypo-phosphorylated RB, which inhibits its DNA binding activity; however, when RB is hyper-phosphorylated during G1/S transition, C/EBPβ dissociates from RB which restores its DNA binding activity and permits the progression of differentiation [111]. Furthermore, over-expression of RB inhibits C/EBPβ-mediated transactivation of *Cebpa*, providing further evidence that links RB and the progression of cell cycle with initiation of differentiation [111]. Therefore, it is likely that dysregulation of RB and/or cell cycle progression would have adverse consequences on adipocyte differentiation.

To identify a potential defect in the cell cycle, it was necessary to first understand how the individual adipogenic stimuli regulate mitogenic signalling. Two-day post-confluent 3T3-L1 pre-adipocytes were treated with individual adipogenic stimuli or all stimuli combined (COCKTAIL) and protein expression was monitored after 6- and 24 h (Figure 3-22). There was no immediate increase in P-eIF4E after 6 h, however P-eIF4E levels were elevated by IBMX, DEX, insulin, ROSI and COCKTAIL treatments after 24 h, consistent with earlier findings (Figure 3-1). Insulin and COCKTAIL treatments increased P-rpS6 and P-PKB levels after 6 h, consistent with mTORC2 activation by PI3K/PKB. P-rpS6 but not P-PKB were elevated after 24 h. ROSI acutely elevated P-rpS6 levels after 6 h but this was not maintained after 24 h; activation of mTORC1 by ROSI has been observed previously after prolonged exposure in tissues actively expressing PPARγ [232,233]; 4E-BP1 phosphorylation was not affected by any treatment at 6- or 24 h, although total 4E-BP1 expression was reduced after 24 h of COCKTAIL treatment, consistent with earlier findings (Figure 3-1). This suggests hormone-induced adipocyte differentiation might involve the regulated modulation of 4E-BP1 expression, and is consistent with accelerated adipogenesis observed in 4E-BP1$^{-/-}$ MEFs [234].

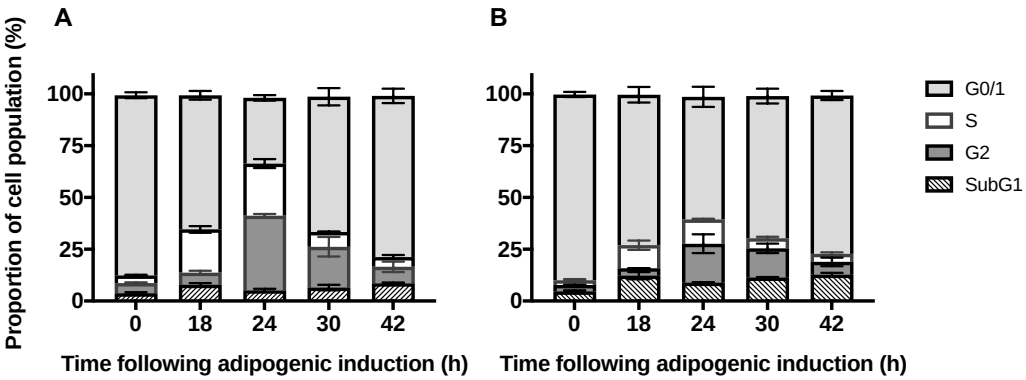

Time (h)	Sub G1	G0/1	S	G2
0	3.70	87.00	3.70	4.95
18	7.85	64.70	**20.90***	5.85
24	5.15	**31.75*****	**25.15****	**36.05*****
30	6.50	65.35	7.10	19.70
42	8.55	77.80	4.75	7.95

Time (h)	SubG1	G0/1	S	G2
0	4.65	89.65	2.30	3.10
18	12.25	72.65	**11.15***	3.55
24	8.80	**59.15*****	**11.75****	**18.85*****
30	11.30	68.65	4.90	14.10
42	12.65	76.50	3.85	6.25

C

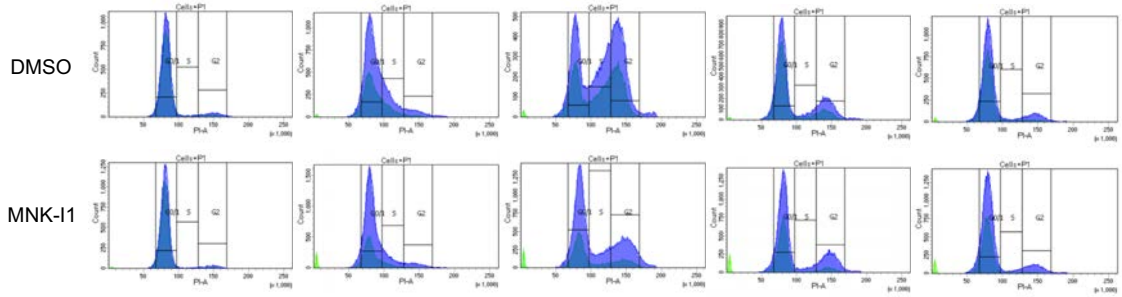

Figure 3-21: Effect of MNK-I1 on mitotic clonal expansion (MCE).

Following pre-treatment with 3 μM MNK-I1 or an equivalent volume of DMSO, 3T3-L1 pre-adipocytes were differentiated with adipogenic induction media for 42 h, during which cells were harvested at the indicated times, stained with propidium iodide (PI) and analysed by flow cytometry. Cells treated with (A) DMSO and (B) MNK-I1 were gated into Sub G1, G0/1, S and G2 populations, the mean proportions (%) of which are graphed (upper) and detailed in the table (lower). Data are mean ± SEM; n=2; statistically significant differences between DMSO and MNK-I1 treatments are highlighted; 2-way ANOVA (*P < 0.05 **P < 0.01 ***P < 0.001). (C) Representative flow cytometry panels of cells treated with DMSO (upper) and MNK-I1 (lower).

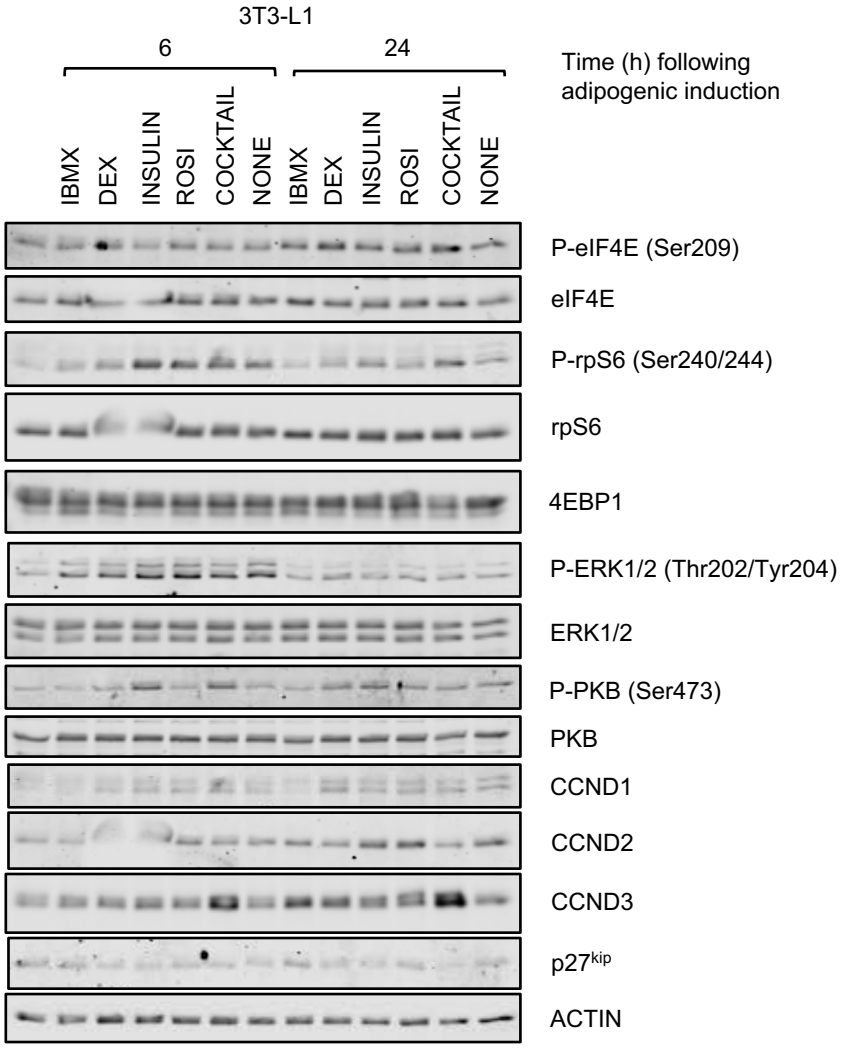

Figure 3-22: Analysis of cell cycle factor expression by adipogenic stimuli.

3T3-L1 pre-adipocytes were stimulated with 500 µM IBMX, 0.5 µM DEX, 350 nM insulin and 2µM ROSI either individually or all together (COCKTAIL). After 6 and 24 h, cell lysates were harvested and analysed by SDS-PAGE using the indicated antibodies (n=1).

Insulin, ROSI, COCKTAIL and growth media replenishment in the absence of hormone inducers (NONE) increased P-ERK1/2 levels after 6 h. The increased P-ERK1/2 levels observed with IBMX, DEX, insulin, ROSI and COCKTAIL treatments are therefore likely attributable to the replenishment of media (containing mitogens) and not the individual stimuli themselves. P-ERK1/2 levels were decreased after 24 h in all treatments, consistent with their regulation during early adipogenesis [168,235]. Similarly, media replenishment (NONE) was sufficient to elevate CCND1 levels after 6 h, consistent with mitogenic activation of CCND1 expression [227]. CCND1 expression levels increased further after 24 h. Interestingly, IBMX impaired CCDN1 expression at 6- and 24 h, suggesting IBMX may modulate MAPK signalling, consistent with the impaired P-ERK1/2 levels observed with IBMX at 6 h. Media replenishment (NONE) along with insulin and ROSI increased CCND2 expression after 24 h. Surprisingly, CCND2 expression was impaired by both IBMX and DEX, and even further by COCKTAIL treatment. Nevertheless, this is consistent with reduced CCND2 expression as cells enter S-phase (Figure 3-22), suggesting that the coordinated action of hormone-stimuli is required to carefully control cell cycle progression. CCND3 expression was elevated by COCKTAIL treatment at 6 h and perpetuated at 24 h; CCND3 expression was also modestly elevated by IBMX and DEX at 24 h but not to the same extent as with COCKTAIL. This suggests that mitogenic stimuli alone (NONE) are insufficient to drive CCND3 expression; rather, CCND3 expression is likely regulated by the coordinated activity of hormone stimuli, most likely IBMX and DEX. Expression of $p27^{kip}$ was reduced after 24 h by DEX, insulin and COCKTAIL treatments, as expected but mitogenic stimuli alone (NONE) did not reduce $p27^{kip}$ levels to the same extent, suggesting that hormonal signalling is required for successful cell cycle progression of 3T3-L1 pre-adipocytes.

Effect of MNK-I1 on RB hyper-phosphorylation and D-cyclin expression

To examine whether loss of MNK activity adversely affected cell cycle progression in growth-arrested 3T3-L1 pre-adipocytes, the expression of cell cycle proteins was investigated following hormone-induced adipogenesis in the presence or absence of MNK-I1 over the course of 96 h (Figure 3-23). RB phospho-specific antibodies were used to assess the level of phosphorylation at Ser780 and Ser807/811. At 18 h, RB was hyper-phosphorylated at Ser780 and Ser807/811 and this was notably inhibited by MNK-I1. The lack of RB phosphorylation was, however, not due to a reduction in D-cyclin levels, as CCDN1 D2 and D3 expression was not affected by MNK-I1. Nevertheless, this suggests MNK activity is required for hyper-phosphorylation of RB and by extension, G1/S transition. By 24 h, RB had returned to a hypo-phosphorylated state, demonstrated by the loss of P-RB Ser780 and Ser807/811 signals.

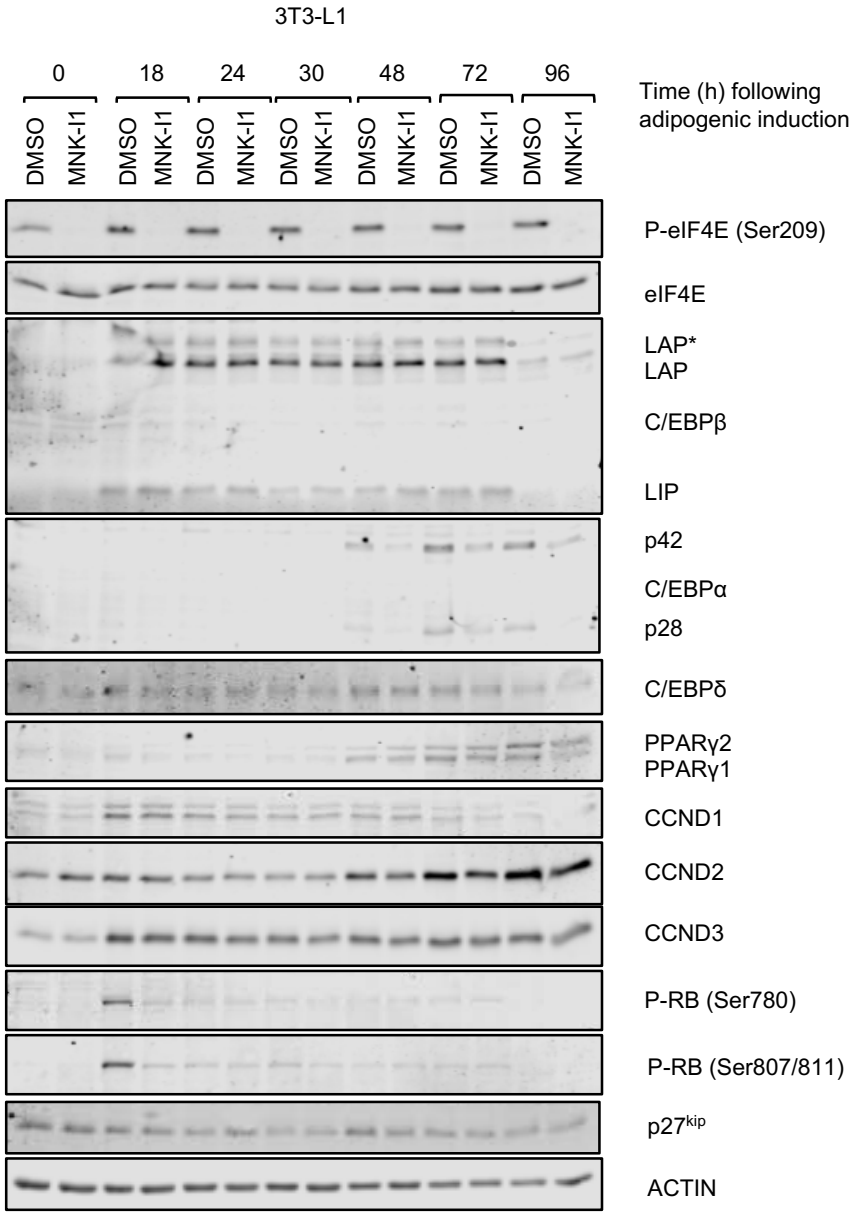

Figure 3-23: Effect of MNK-I1 on cell cycle factor expression.

3T3-L1 pre-adipocytes were differentiated with adipogenic induction media following pre-treatment with 3 μM MNK-I1 or an equivalent volume of DMSO. Cell lysates were harvested at the indicated times and analysed by SDS-PAGE using the indicated antibodies (n=1).

CCND1 and D3 expression was low at quiescence (0 h) but was induced by hormone and/or mitogenic stimuli after 18 h, consistent with previous reports [227]. In contrast, CCND2 was elevated at quiescence and remained at the same level after 18 h, consistent with elevation in contact-inhibited cells [169]. The CDK inhibitor $p27^{kip}$ was elevated in quiescence; $p27^{kip}$, CCND1, D2 and D3 levels were all lowered at 24- and 30 h, consistent with transition into S-phase [104,236]. By 48 h, CCND1 expression was diminished, whereas CCND3 expression remained stable. CCND2 expression progressively increased from 48- to 96 h, however, this increase was notably inhibited by MNK-I1. The increase in CCDN2 was inversely proportional to CCND1, suggesting the D-cyclins may perform distinct roles in adipocyte differentiation. Cyclins have been widely reported to regulate activity of proteins in terminal adipogenesis [237–241], and so elevated expression of CCND2 may allude to a specific function that is yet to be identified. The expression of CCDN2 was induced independently of hormone induction and impaired by MNK-I1, suggesting MNK activity may positively regulate its expression. The expression of C/EBPα and PPARγ, but not C/EBPβ and C/EBPδ, was affected by MNK-I1, consistent with earlier findings (Figures 3-16 and 3-17). In summary, MNK activity appears to be required for RB hyper-phosphorylation and consequently G1/S transition, consistent with Figure 3-21. (Figure 3-21).

Interim Conclusion

MNK-I1 blocks RB hyper-phosphorylation and consequently G1/S transition. The effect of MNK-I1 on G1/S transition is independent of D-cyclin and $p27^{kip}$ expression.

Alternative splicing and cell cycle progression

Alternative splicing is a key gene regulatory mechanism that greatly expands the coding capacity of genomes and the protein diversity of cells. Alternative splicing is required for regulating gene expression during normal development and physiology, and plays a central role in cellular differentiation [242]. Alternative splicing is controlled by a large family of RNA-binding proteins, known as serine and arginine rich (SR) factors, whose activities regulate splice-site selection, among other functions [243]. Protein phosphatases, cdc2-like kinases (CLKs) and other SR protein kinases participate in the sequential phosphorylation and dephosphorylation of SR proteins during the splicing process, which affects their activity, protein-protein interactions and sub-cellular distribution [243–245]. Alternative splicing has been shown to contribute to adipocyte differentiation (reviewed in [246]), and an extensive program of periodic alternative splicing has been linked to cell cycle progression [247]. Many of the periodically-spliced genes important for cell cycle progression are controlled by CLK1, whose levels undergo cell cycle-dependent fluctuations via an auto-inhibitory circuit [247]. Cross-linking and immunoprecipitation (CLIP) assays used to study the interaction between the 5’ mRNA cap and cap-binding protein eIF4E, suggest the association of *Clk1* mRNA with eIF4E is reduced by MNK-I1 (unpublished data). This suggests the phosphorylation of eIF4E may specifically regulate the

translation of *Clk1*. Dysregulated CLK1 expression may affect alternative splicing and therefore cell cycle progression.

Regulation of CLK1/4 expression through alternative splicing

CLK1 and CLK4 are functionally equivalent and share a high degree of homology [248]. CLK1/4 expression is regulated through alternative splicing, which produces full-length catalytically active $Clk1/4^{Full\text{-}length}$ in addition to truncated catalytically inactive isoforms, $Clk1/4^{T1\ (E4S)}$ arising from exon 4 skipping, and $Clk1/4^{T2\ (I3/4R)}$ arising from intron 3/4 retention (Figure 3-24A) [248,249]. Environmental shock such as heat and osmotic stress rapidly reduces $Clk1/4^{T1\ (E4S)}$ and $Clk1/4^{T2\ (I3/4R)}$, shifting the balance to $Clk1/4^{Full\text{-}length}$ [248,249]. Inhibition of CLK activity with the benzothiazole compound TG003 [250] also reduces $Clk1/4^{T1\ (E4S)}$ and $Clk1/4^{T2\ (I3/4R)}$ levels, suggesting that CLK expression is regulated by an auto-inhibitory mechanism to ensure the phosphorylation of SR proteins is maintained [249]. The cis-regulatory elements involved in auto-inhibitory alternative splicing regulation are conserved between *Clk1* and *Clk4* [248].

Dosage of TG003 in 3T3-L1 pre-adipocytes

To investigate the effect of CLK inhibition on adipocyte differentiation, a dose-response analysis for TG003 was initially performed in 3T3-L1 pre-adipocytes. Following 2 h of treatment, RNA was harvested, reverse-transcribed and amplified by PCR using primers to detect the various splicing products (Figure 3-24A). The levels of $Clk1^{T1\ (E4S)}$ and $Clk1^{T2\ (I4R)}$ were effectively reduced by TG003 at ≥ 5 μM (Figure 3-24B). The level of $Clk4^{T1\ (E4S)}$ was effectively reduced at ≥ 1 μM TG003; however, residual levels of $Clk4^{T2\ (I4R)}$ remained at that concentration and were only effectively reduced at ≥ 10 μM (Figure 3-24B). Levels of $Clk1/4^{T2\ (I3R)}$ were reduced at ≥ 0.3 μM but the residual levels that remained could not be lowered further by increased concentrations of TG003, even persisting at 20 μM TG003 (Figure 3-24B). This is, however, consistent with detection of $Clk1^{T2\ (I3R)}$, even with 50 μM TG003 [248]. However, there was no overwhelming shift in $Clk1/4^{Full\text{-}length}$ levels, as shown previously with effective CLK inhibition [248,249]. This may reflect the kinetics of *Clk* expression since only a single timepoint was assessed. Nevertheless, given $Clk1/4^{T1\ (E4S)}$ and $Clk1^{T2\ (I4R)}$ were effectively reduced and consistent with previous studies, 20 μM TG003 was decided as the dosage at which to assay 3T3-L1 adipocyte differentiation.

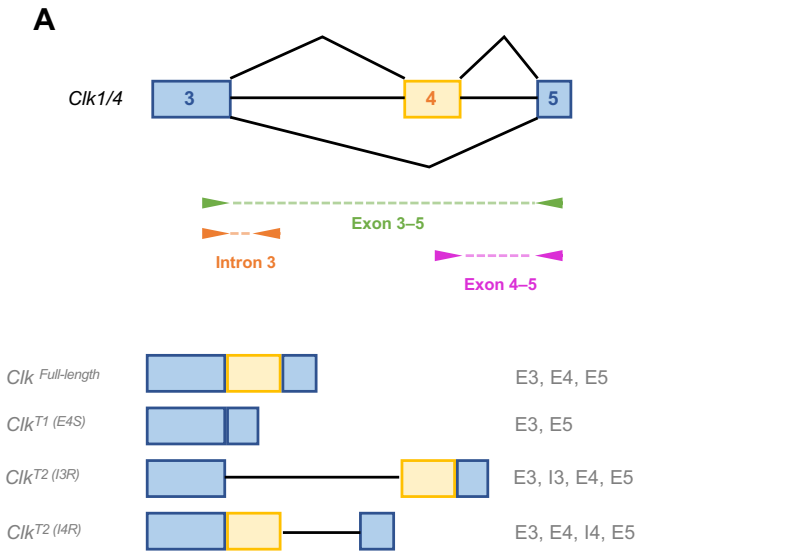
A
Clk1/4
3
4
5
Exon 3–5
Intron 3
Exon 4–5
Clk Full-length
E3, E4, E5
ClkT1 (E4S)
E3, E5
ClkT2 (I3R)
E3, I3, E4, E5
ClkT2 (I4R)
E3, E4, I4, E5

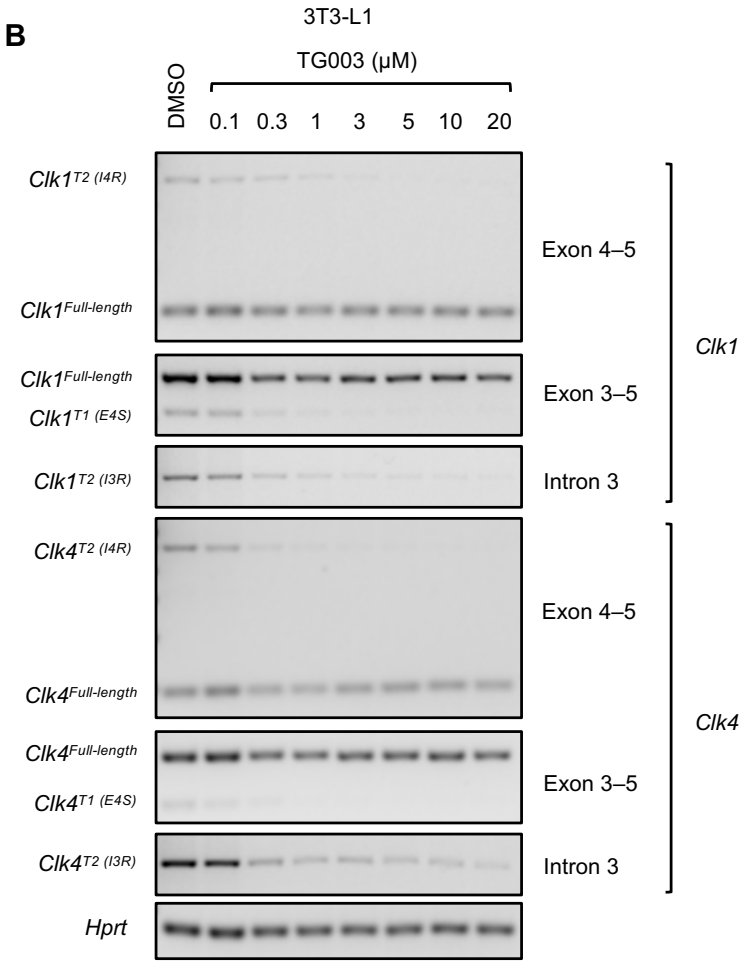
B
3T3-L1
TG003 (μM)
DMSO
0.1 0.3 1 3 5 10 20
Clk1T2 (I4R)
Clk1Full-length
Exon 4–5
Clk1Full-length
Clk1T1 (E4S)
Exon 3–5
Clk1T2 (I3R)
Intron 3
Clk1
Clk4T2 (I4R)
Clk4Full-length
Exon 4–5
Clk4Full-length
Clk4T1 (E4S)
Exon 3–5
Clk4T2 (I3R)
Intron 3
Clk4
Hprt

Figure 3-24: *Clk1/4* alternative splicing and dosage of TG003 in 3T3-L1 pre-adipocytes.

(A) Schematic diagram of *Clk1/4* alternative splicing. Blue and yellow boxes represent constitutive and selective exons, respectively. Intervening introns are represented by a solid straight line connecting the exons 3-4 (intron 3) and 4-5 (intron 4). Possible splicing scenarios are illustrated by diagonal lines. Catalytically active $Clk1/4^{Full\text{-}length}$ is produced when exons 3, 4 and 5 are spliced together. When exons 3 and 5 are spliced together, skipping exon 4 (E4S), the truncated product $Clk1/4^{T1\ (E4S)}$ is produced. If intron 3 or 4 is retained, the truncated $Clk1/4^{T2\ (I3R)}$ or $Clk1/4^{T2\ (I4R)}$ products are produced, respectively. Location of primers used for the detection of various splicing products are shown. Exon 3-5 primers (green) detect $Clk1/4^{Full\text{-}length}$ and $Clk1/4^{T1\ (E4S)}$; Exon 4-5 primers detect $Clk1/4^{Full\text{-}length}$ and $Clk1/4^{T2\ (I4R)}$; Intron 3 primers only detect $Clk1/4^{T2\ (I3R)}$ (B) A dose response of TG003 was performed in 3T3-L1 pre-adipocytes by treating cells with the indicated concentrations of TG003 for 2 h. RNA was harvested and used to amplify *Clk1/4* alternative splicing products by RT-PCR using the indicated primers, which were analysed by agarose gel electrophoresis (n=1).

Effect of TG003 on 3T3-L1 adipocyte differentiation

The effect of CLK inhibition on adipocyte differentiation was investigated by treating two-day post-confluent 3T3-L1 pre-adipocytes with adipogenic differentiation media in the presence or absence of TG003. TG003 effectively reduced *Clk1/4*$^{T1\ (E4S)}$ and *Clk1/4*$^{T2\ (I4R)}$ levels, causing a shift in expression to *Clk1/4*$^{Full\text{-}length}$ throughout differentiation, as expected (Figure 3-25B). *Clk1/4*$^{T2\ (13R)}$ levels were, however, only partially reduced by TG003 (Figure 3-25B), consistent with earlier observations (Figure 3-24). *Clk1/4*$^{Full\text{-}length}$ expression was highest on Day 3, indicating CLK activity is likely most important during this phase of the program (Figure 3-25B). Thereafter, *Clk1/4*$^{Full\text{-}length}$ returned to basal levels, whilst TG003 maintained the shift in elevated *Clk1/4*$^{Full\text{-}length}$ levels (Figure 3-25B).

P-eIF4E levels increased over the course of differentiation but this was not affected by TG003, as expected (Figure 3-25A). C/EBPβ and P-C/EBPβ levels were not affected by TG003 either (Figure 3-25A); rather, TG003 increased the level of C/EBPδ relative to control on Days 4 and 6, consistent with effects observed with MNK-I1 (Figure 3-17 and 3-18). Notably, TG003 reduced the expression of C/EBPα and PPARγ and, consequently, the expression of FABP4 on Days 2 and 3, consistent with the effects of MNK-I1 (Figure 3-17). However, on Day 3, the levels of C/EBPα and PPARγ returned to control levels and on Day 6 were in fact elevated further. This suggests that CLK activity may be required during early adipogenesis to promote C/EBPα and PPARγ expression; thereafter, during terminal adipogenesis, CLK activity becomes redundant and the expression of PPARγ and C/EBPα is restored, presumably through a CLK-independent mechanism. The expression of FABP4 remained reduced on Days 6 and 9, whilst lipid accumulation quantified from ORO-stained fields of view was only modestly reduced by TG003 (~30%) (Figure 3-25C-D). This likely reflects an impairment in adipogenesis caused by the initial reduction in C/EBPα and PPARγ levels.

Comparison of MNK and CLK inhibition on 3T3-L1 adipocyte differentiation

To understand the differences and compare the effects of CLK and MNK inhibition on 3T3-L1 pre-adipocyte differentiation, cells were treated in a head-to-head comparison with either TG003 or MNK-I1. Unexpectedly, MNK-I1 effectively reduced *Clk1/4*$^{T1\ (E4S)}$ and *Clk1/4*$^{T2\ (I4R)}$ levels and caused a shift in expression to *Clk1/4*$^{Full\text{-}length}$ throughout differentiation, suggesting MNK-I1 also inhibits the CLKs in addition to the MNKs (Figure 3-26B). The shift in *Clk1/4*$^{Full\text{-}length}$ and reduction in *Clk1/4*$^{T2\ (I3R)}$ levels was more pronounced with MNK-I1 than with TG003, suggesting MNK-I1 is a more potent inhibitor of the CLKs than TG003 (Figure 3-26B). This cannot be attributed to an on-target indirect effect of MNK inhibition since the use of more specific MNK inhibitors, as discussed later, did not affect *Clk1/4* splicing (Figure 3-30). As shown previously, *Clk1/4*$^{Full\text{-}length}$ levels were highest on Day 3 (Figure 3-26B). Thereafter, *Clk1/4*$^{Full\text{-}length}$ levels returned to basal, whilst TG003 and MNK-I1 maintained the shift in elevated *Clk1/4*$^{Full\text{-}length}$ levels, but was more pronounced with MNK-I1 (Figure 3-26B).

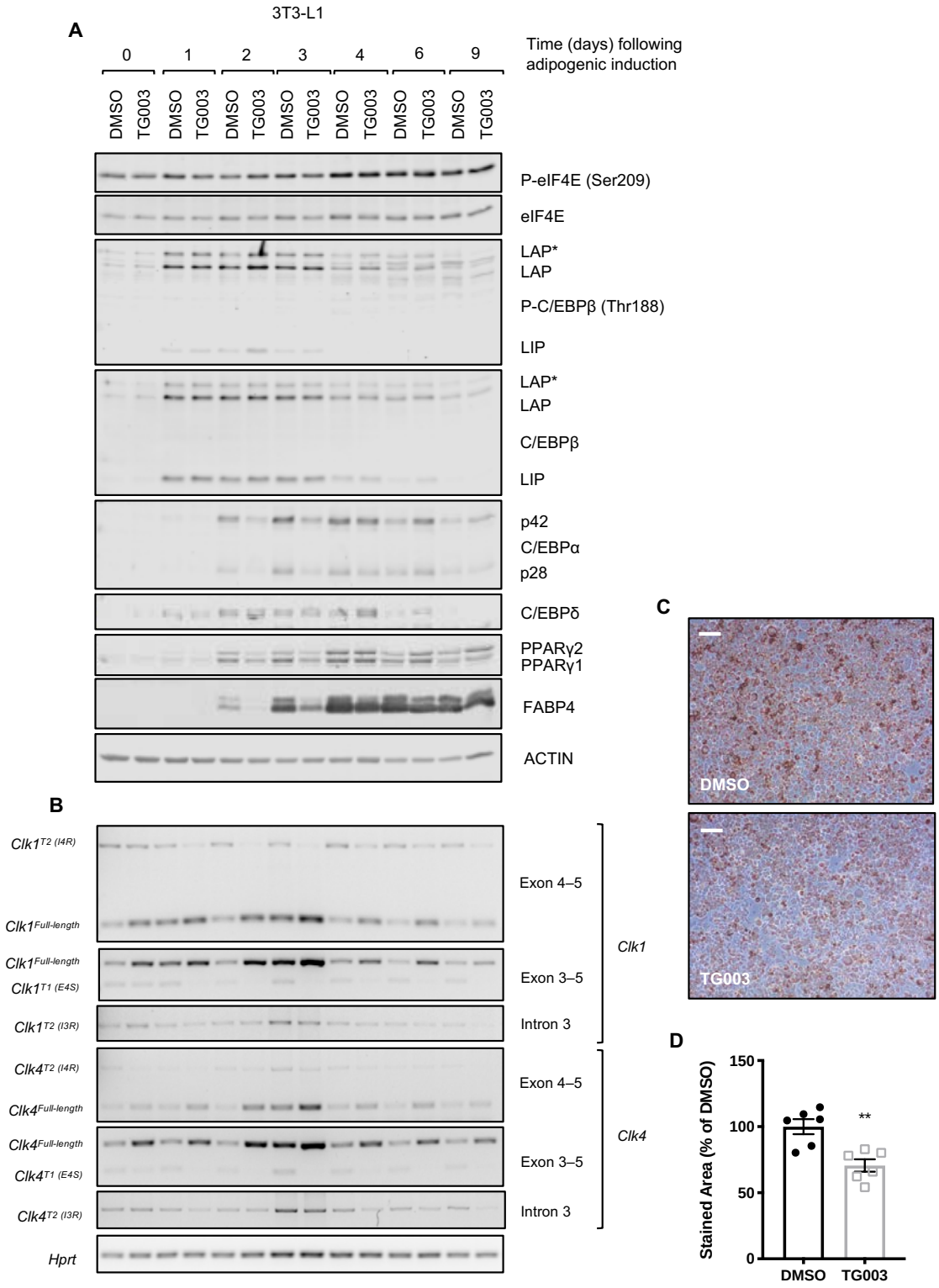
A
3T3-L1
Time (days) following adipogenic induction
0
1
2
3
4
6
9
DMSO
TG003
P-eIF4E (Ser209)
eIF4E
LAP*
LAP
P-C/EBPβ (Thr188)
LIP
LAP*
LAP
C/EBPβ
LIP
p42
C/EBPα
p28
C/EBPδ
PPARγ2
PPARγ1
FABP4
ACTIN
B
Clk1T2 (I4R)
Clk1Full-length
Clk1Full-length
Clk1T1 (E4S)
Clk1T2 (I3R)
Clk4T2 (I4R)
Clk4Full-length
Clk4Full-length
Clk4T1 (E4S)
Clk4T2 (I3R)
Hprt
Exon 4–5
Exon 3–5
Intron 3
Clk1
Exon 4–5
Exon 3–5
Intron 3
Clk4
C
DMSO
TG003
D
Stained Area (% of DMSO)
150
100
50
0
**
DMSO
TG003

Figure 3-25: Effect of TG003 on 3T3-L1 pre-adipocyte differentiation.

3T3-L1 pre-adipocytes were differentiated with adipogenic induction media following pre-treatment with 20 μM TG003 or equivalent volume of DMSO. (A) Cell lysates were harvested at the indicated times and analysed by SDS-PAGE using the indicated antibodies (n=1). (B) RNA was harvested at the indicated times and used to amplify *Clk1/4* alternative splicing products by RT-PCR, which were analysed by agarose gel electrophoresis (n=1). (C) Day 9 differentiated adipocytes were stained with ORO to assess lipid accumulation; representative images are shown, scale bar 0.2 μm. (D) Total stained area was quantified from 6 different fields of view from (C) and is represented as percentage stained area relative to DMSO; data are mean ± SEM; individual data values are plotted (n=1); unpaired t-test (*P < 0.05 **P < 0.01 ***P < 0.001).

Consistent with earlier findings (Figure 3-1B), P-eIF4E levels increased throughout differentiation, and were effectively blocked by MNK-I1 but not TG003 (Figure 3-26A). C/EBPβ and P-C/EBPβ levels were not affected by TG003 or MNK-I1, consistent with previous findings (Figures 3-17, 3-18 and 3-25). TG003 and MNK-I1 did increase expression of C/EBPδ on Day 6 relative to control and this was more pronounced with TG003 (Figure 3-26A). TG003 and MNK-I1 impaired the expression of C/EBPα, PPARγ and FABP4 to a similar extent on Day 3 (Figure 3-26A); however, the expression of C/EBPα and PPARγ was restored on Day 6 with TG003, but remained impaired with MNK-I1 (Figure 3-25A). FABP4 expression remained partially impaired by TG003 on Days 6 and 9 but was more significantly reduced with MNK-I1. Further, lipid accumulation quantified from ORO-stained fields of view and absorbance of ORO eluted from stained cells was more significantly reduced by MNK-I1 (70%) than TG003 (50%) (Figure 3-26 C-E). This is likely a reflection of the differential expression of C/EBPα and PPARγ (Figure 3-26A). This suggests that CLK activity may regulate events preceding C/EBPα and PPARγ expression (i.e. during MCE) and that MNK activity is required later for sustained expression during terminal adipogenesis.

Interim Conclusion

In addition to the MNKs, MNK-I1 potently inhibits the CLKs. Inhibition of the CLKs, whether by TG003 or MNK-I1, is associated with reduced C/EBPα and PPARγ expression during early adipogenesis, suggesting CLK activity may regulate events preceding their expression (i.e. during MCE). C/EBPα and PPARγ levels remain impaired with MNK-I1 but not TG003, suggesting MNK activity is required for sustained C/EBPα and PPARγ expression during terminal adipogenesis.

Comparison of CLK and MNK inhibition on MCE

To determine whether CLK inhibition affected mitotic cycling during MCE in the same manner as MNK-I1, pre-adipocytes differentiating in the presence of TG003 or MNK-I1 were stained with PI and analysed by flow cytometry across a period of 42 h (Figure 3-27). MNK-I1 and TG003 did not alter the proportion of cell cycle populations prior to adipogenic induction (0 h). After 18 h of adipogenic induction, there was a shift from G0/S to S-phase but the proportion of S-phase cells was not significantly reduced by TG003 or MNK-I1, in contrast to earlier findings (Figure 3-21). At 24 h, the proportion of cells in S-phase (24.7%) and G2-phase (18.9%) increased and this was reduced by MNK-I1, consistent with earlier findings that suggest a block in cell cycle progression (Figure 3-21). In contrast, TG003 apparently increased the proportion of cells in G2 (30.2%) whilst maintaining the same proportion of cells in S-phase (26.8%) relative to control. At 30 h, the proportion of cells in G2-phase with TG003 treatment remained elevated (21%) compared to control (10.7%), suggesting TG003 may actually accelerate cell cycle progression in the context of MCE, rather than impair it, in contrast to previous reports [247]. At 42 h, all cell populations had returned to their pre-induction levels, indicating the end of MCE. Unexpectedly, these results suggest that inhibiting CLK activity does not affect the cycling of cells during MCE.

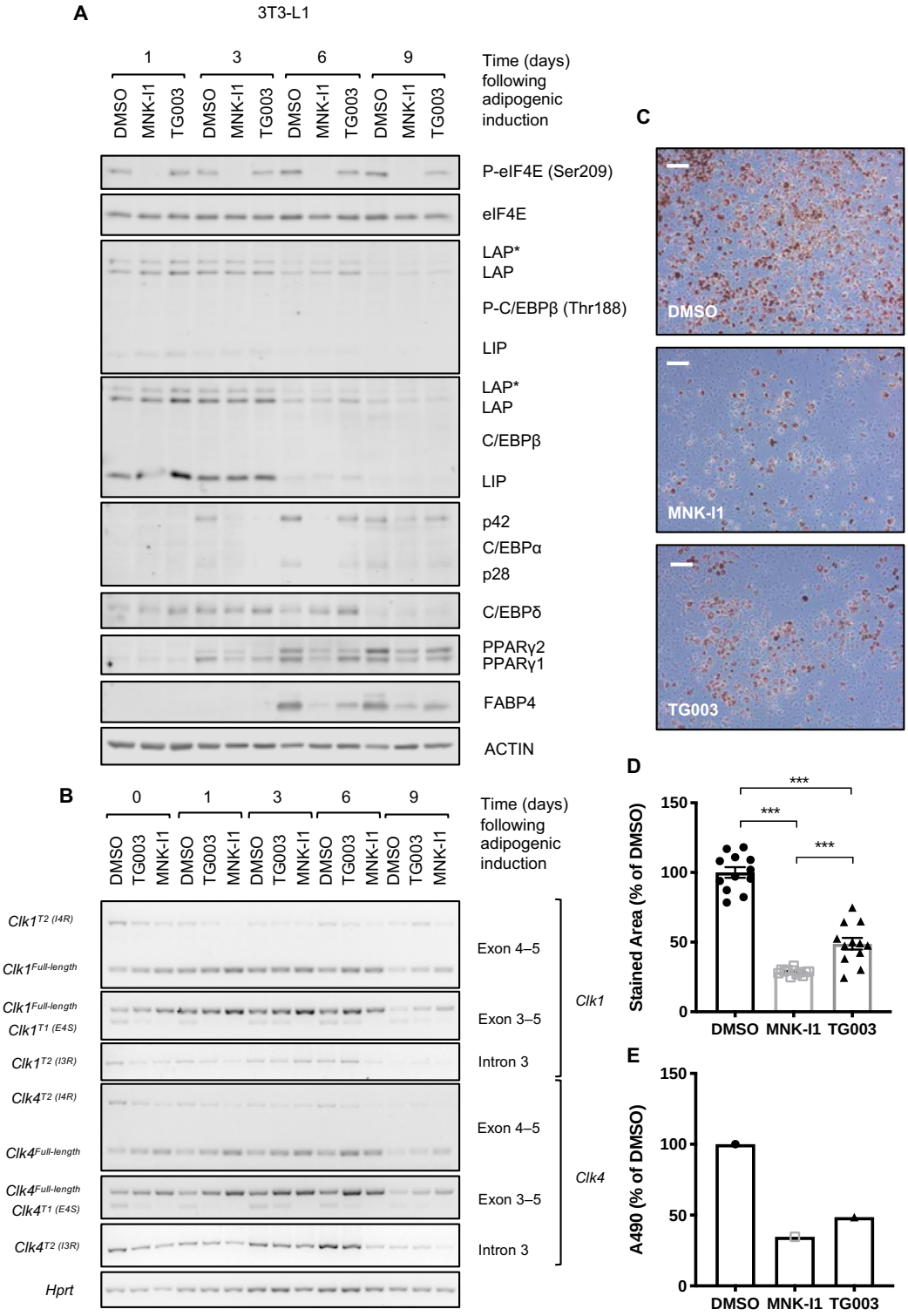
A
3T3-L1
1
3
6
9
DMSO
MNK-I1
TG003
Time (days) following adipogenic induction
P-eIF4E (Ser209)
eIF4E
LAP*
LAP
P-C/EBPβ (Thr188)
LIP
LAP*
LAP
C/EBPβ
LIP
p42
C/EBPα
p28
C/EBPδ
PPARγ2
PPARγ1
FABP4
ACTIN
B
0
1
3
6
9
Time (days) following adipogenic induction
Clk1T2 (I4R)
Clk1Full-length
Clk1Full-length
Clk1T1 (E4S)
Clk1T2 (I3R)
Clk4T2 (I4R)
Clk4Full-length
Clk4Full-length
Clk4T1 (E4S)
Clk4T2 (I3R)
Hprt
Exon 4–5
Exon 3–5
Intron 3
Clk1
Exon 4–5
Exon 3–5
Intron 3
Clk4
C
DMSO
MNK-I1
TG003
D
Stained Area (% of DMSO)
150
100
50
0
***
***
***
DMSO
MNK-I1
TG003
E
A490 (% of DMSO)
150
100
50
0
DMSO
MNK-I1
TG003

Figure 3-26: Comparing the effect of TG003 and MNK-I1 on 3T3-L1 pre-adipocyte differentiation.
3T3-L1 pre-adipocytes were differentiated with adipogenic induction media following pre-treatment with 20 μM TG003, 3 μM MNK-I1 or equivalent volume of DMSO. (A) Cell lysates were harvested at the indicated times and analysed by SDS-PAGE using the indicated antibodies; representative immunoblots are shown (n=3). (B) RNA was harvested at the indicated times and used to amplify *Clk1/4* alternative splicing products by RT-PCR, which were analysed by agarose gel electrophoresis (n=1). (C) Day 9 differentiated adipocytes were stained with ORO to assess lipid accumulation; representative images are shown, scale bar 0.2 μm. (D) Total stained area was quantified from 6 different fields of view from (C) and is represented as percentage stained area relative to DMSO; data are mean ± SEM; individual data values are plotted (n=2); one-way ANOVA (*P < 0.05 **P < 0.01 ***P < 0.001) (E) ORO eluted from stained cells was quantified by absorbance (A490) and is represented as percentage absorbance relative to DMSO; individual data values are plotted (n=1).

Rather, CLK inhibition apparently accelerates cell cycle progression. This phenotype is in complete contrast to that of MNK-I1, suggesting that either (1) the combined activity of MNK and CLK are required for cell cycle progression or (2) MNK-I1 is non-specific and inhibits other kinase(s) required for cell cycle progression.

Effect of TG003 on D-cyclin expression

To investigate the apparent acceleration of cell cycle progression by TG003, the expression of D-cyclins was assessed over the course of differentiation (Figure 3-27E). TG003 increased the expression of CCND1, D2 and D3 relative to control on all days subsequent to adipogenic induction (Figure 3-27E). In contrast, D-cyclin expression was not increased by MNK-I1, which inhibits both CLK and MNK (P-eIF4E) activity. This suggests that CLK inhibition accelerates cell cycle progression through increased D-cyclin expression and that its effect is potentially mediated through P-eIF4E. This is consistent with reports that P-eIF4E promotes the nucleo-cytoplasmic export of *Ccdn1* mRNA [39,40]. *Ccnd2* and *Ccnd3* may therefore also be subject to the same regulation by the MNKs.

Interim Conclusion

TG003 and MNK-I1 have contrasting effects on cell cycle progression: TG003 apparently accelerates cell cycle progression through increased D-cyclin expression, whilst MNK-I1 blocks cell cycle progression through impeding RB phosphorylation. Considering that MNK-I1 is a dual MNK/CLK inhibitor this implies that either: (1) CLK and MNK activity are both required for cell cycle progression; or that (2) MNK-I1 is non-specific and inhibits another kinase(s) required for cell cycle progression.

Efficacy of Clk1/4 siRNA

Given that results obtained with TG003 (Figure 3-27) contradicted previously reported findings in terms of cell cycle progression [247], an siRNA-mediated approach was employed to study the role(s) of *Clk1/*4 in adipocyte differentiation. *Clk1/4* siRNA efficacy was assayed in 3T3-L1 pre-adipocytes after 48- and 96 h by monitoring the levels of alternatively spliced *Clk1/4* by RT-PCR (Figure 3-28A). si*Gapdh* and si*Scrambled,* were used as positive and negative controls, respectively. si*Gapdh* effectively silenced GAPDH protein and *Gapdh* mRNA expression, as assessed by RT-qPCR, indicating the siRNA transfection conditions were acceptable (Figure 3-28B-C). si*Gapdh* did not affect the levels of $Clk1^{Full\text{-}length}$, $Clk4^{Full\text{-}length}$ or any of the truncated splicing products, as expected.

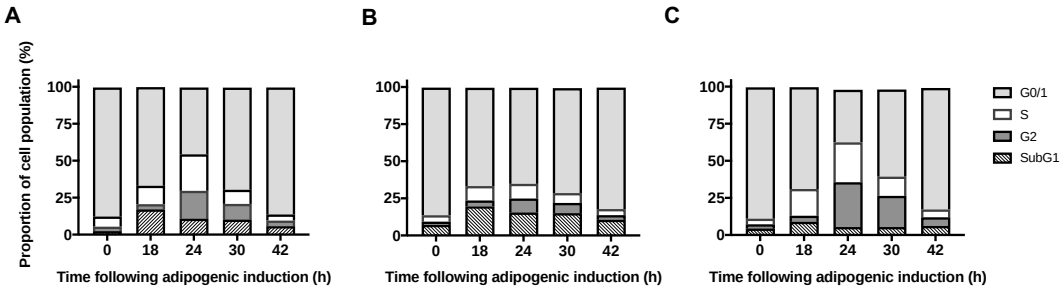

Time (h)	SubG1	G0/1	S	G2
0	2.3	87.3	6.8	3.1
18	17	66.8	**12.4**	3.6
24	10.7	**45.2**	24.7	**18.9**
30	10.1	69.1	9.5	10.7
42	5.7	85.9	4.1	3.8

Time (h)	SubG1	G0/1	S	G2
0	7.1	86	4.3	2.2
18	19.6	66.2	9.7	4
24	15.4	**64.7**	**9.9**	**9.5**
30	15	70.7	6.7	6.9
42	10.5	81.8	4.1	3.2

Time (h)	SubG1	G0/1	S	G2
0	4.3	88.5	3.8	2.9
18	8.9	68.6	18	4.1
24	5.4	**35.5**	26.8	**30.2**
30	5.4	**58.7**	12.9	**21**
42	6.1	81.9	5.3	5.8

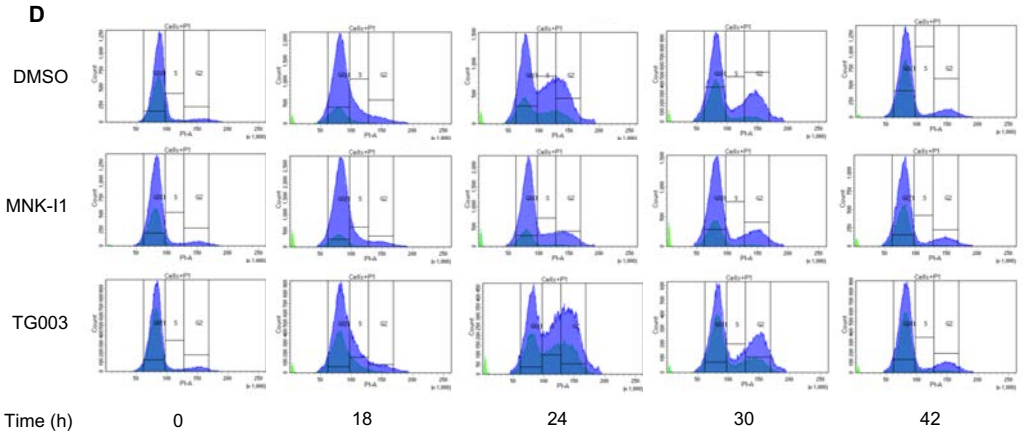

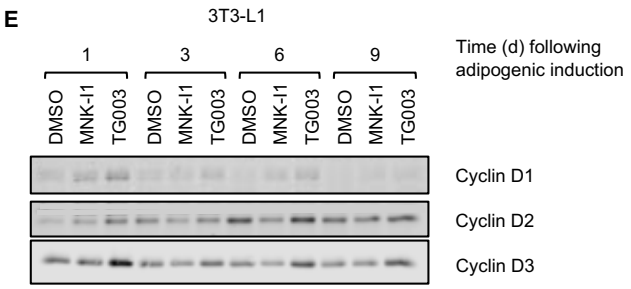

Figure 3-27: Effect of TG003 and MNK-I1 on MCE.

Following pre-treatment with 3 μM MNK-I1, 20μM TG003 or an equivalent volume of DMSO, 3T3-L1 pre-adipocytes were differentiated with adipogenic induction media for 42 h, during which cells were harvested at the indicated times, stained with propidium iodide and analysed by flow cytometry. Cells treated with (A) DMSO, (B) MNK-I1 or (C) TG003 were gated into Sub G1, G0/1, S and G2 populations, the mean proportions (%) of which are graphed (upper) and detailed in the table (lower). Data are mean ± SEM; n=2; statistically significant differences between DMSO and MNK-I1 treatments are highlighted; 2-way ANOVA (*P < 0.05 **P < 0.01 ***P < 0.001). (C) Representative flow cytometry panels of cells treated with DMSO (upper), MNK-I1 (middle) and TG003 (lower).

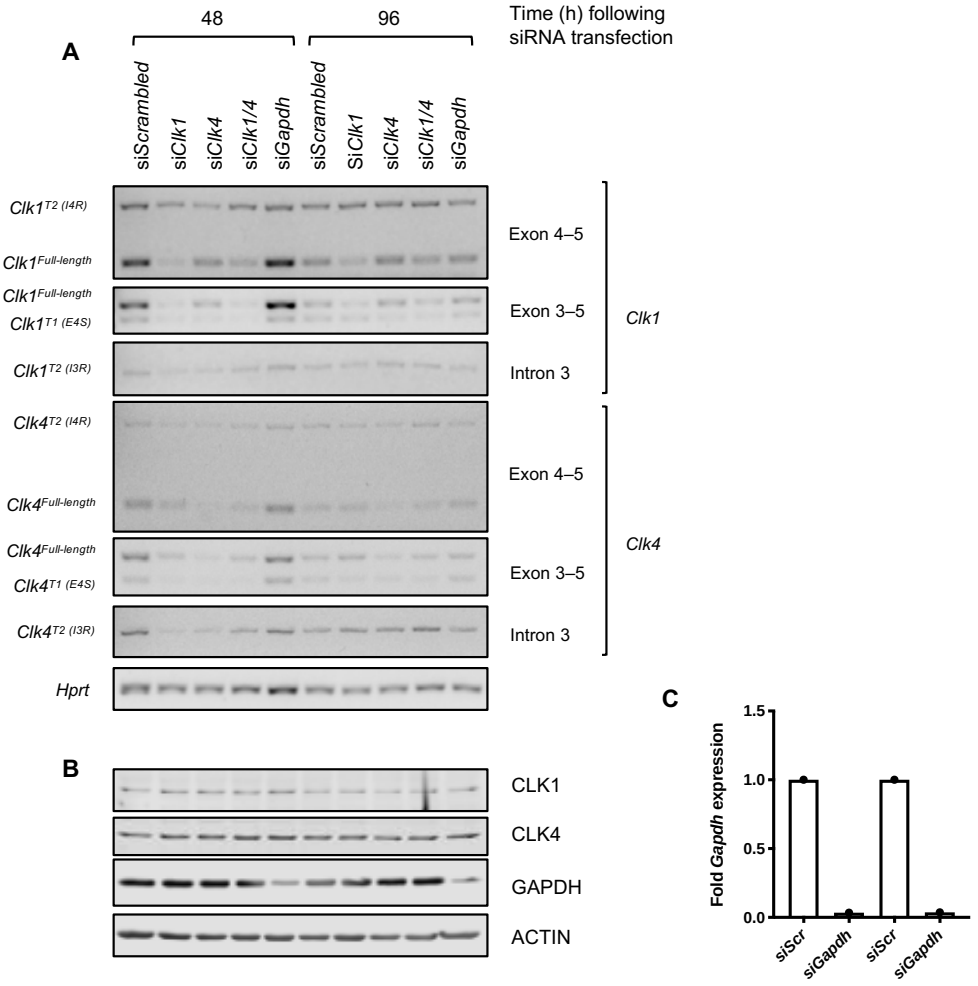

D

```
Clk1 E2    1 ATGAGACATTCAAAGAGAACTTACTGTCCTGACTGGGATGAAAGAGA---     47
             |||.|.|||||.||..|||||.||||||||||.|||||||...|||||
Clk4 E2    1 ATGCGGCATTCCAAACGAACTCACTGTCCTGATTGGGATAGTAGAGAAAG     50

Clk1 E2   48 CTGGGATTATGGAACATGGAGAAGCAGCAGCAGTCACAAAAGAAAGAAGA     97
             |||||...|||.|      ||...|||..|.|||||||||.|.|||||..|
Clk4 E2   51 CTGGGGCCATGAA------AGCTACAGTGGAAGTCACAAACGCAAGAGAA     94

Clk1 E2   98 GATCACATAGCAGCGCCCGTGAGCAAAAGCGCTGCAGG-TACG--ATCAC    144
             |.||.||.|||||..|.|..|||.|.|.||.|||.|.. .||.  ||||.
Clk4 E2   95 GGTCTCACAGCAGTACTCAGGAGAACAGGCACTGTAAACCACATCATCAG    144

Clk1 E2  145 TCCAAAACGACAGACAG    161
             |..|||....|.||..|
Clk4 E2  145 TTTAAAGACTCGGATTG    161

Similarity: 104/167 (62.3%)
```

E

```
Clk1 E5    1 ATGAAATTGTTGATACTTTAGGTGAAGGTGCTTTCGGAAAAGTGGTGGAA     50
             |||||||.||.||.|||||||||||||||.||.||.||.|||||.||.||.
Clk4 E5    1 ATGAAATCGTGGACACTTTAGGTGAAGGAGCCTTTGGCAAAGTTGTAGAG     50

Clk1 E5   51 TGCATCGATCATAAAGT     67
             |||||.|||||.....|
Clk4 E5   51 TGCATTGATCACGGCAT     67

Similarity: 51/67 (76.1%)
```

Figure 3-28: Efficacy of *Clk1/4* siRNA.

3T3-L1 pre-adipocytes were transfected with 25 pmol of si*Clk1* and si*Clk4* either individually or in combination, as indicated. When used in combination (siClk1/4), 12.5 pmol of each siRNA was used to keep molar ratios equivalent. si*Scrambled* and si*Gapdh* were used as transfection controls. After 48 and 96 h: (A) RNA was harvested and used to amplify *Clk1/4* alternative splicing products by RT-PCR, which were analysed by agarose gel electrophoresis (n=1) (B) Cell lysates were harvested and analysed by SDS-PAGE using the indicated antibodies; representative immunoblots are shown (n=2); whilst mRNA levels of (C) *Gapdh* were measured by RT-qPCR. Expression levels were normalised to *Nono* and *Hprt* and represented as fold change with respect to si*Scrambled.* Individual data values are plotted (n=1). *Clk1* and *Clk4* sequences corresponding to (D) Exon 2 and (E) Exon 5 were aligned to assess gene homology, as indicated.

As expected, si*Clk1* effectively reduced the levels of $Clk1^{Full\text{-}length}$, $Clk1^{T1\ (E4S)}$ and $Clk1^{T2\ (13R)}$, whilst only partially reducing $Clk1^{T2\ (I4R)}$ levels, since the latter is predominantly retained in the nucleus [248]; however, si*Clk1* also reduced the levels of $Clk4^{Full\text{-}length}$, $Clk4^{T1\ (E4S)}$, $Clk4^{T2\ (I4R)}$ and $Clk4^{T2\ (13R)}$, albeit not to the same extent, suggesting si*Clk1* cross-reacts with *Clk4* to reduce its expression. si*Clk4* effectively reduced the levels of $Clk4^{Full\text{-}length}$, $Clk4^{T1\ (E4S)}$ and $Clk4^{T2\ (13R)}$ whilst only partially reducing $Clk4^{T2\ (I4R)}$ levels, as expected. The levels of $Clk1^{Full\text{-}length}$, $Clk1^{T1\ (E4S)}$, $Clk1^{T2\ (I4R)}$ and $Clk1^{T2\ (13R)}$ were also reduced by si*Clk4*, suggesting si*Clk4* cross-reacts with *Clk1*, comparable to the cross-reactivity of si*Clk1*. According to the manufacturer, si*Clk1* and si*Clk4* target exons 2 and 5, respectively. Therefore, the sequences of exons 2 and 5 were aligned to determine similarity and assess the likelihood of siRNA cross-reactivity. There was a high degree of identity between the aligned sequences of *Clk1* and *Clk4*: 62.3% for exon 2 and 76.1% for exon 5 (Figure 3-28 D-E). This suggests that there is a high likelihood for si*Clk1* and si*Clk4* to cross-react, consistent with the above-mentioned results.

si*Clk1* and si*Clk4* were combined (si*Clk1/4*) to assess the efficacy in silencing both *Clk1* and *Clk4*. However, si*Clk1/4* was less effective than the individual siRNAs alone in reducing the levels of $Clk1^{Full\text{-}length}$ and $Clk4^{Full\text{-}length}$. This is likely attributable to the fact that only half the molar quantity of each siRNA was present in the combination compared to the individual treatments. Evidently, the reduced molar quantity of siRNA, when used in combination, was not sufficient for effective *Clk1/4* silencing.

Nevertheless, given that si*Clk1* and si*Clk4* effectively reduced the levels of $Clk1^{Full\text{-}length}$ and $Clk4^{Full\text{-}length}$ either directly or through cross-reactivity, the expression of CLK1 and CLK4 was assessed by Western blot (Figure 3-28B). Unexpectedly, CLK1 and CLK4 expression was not reduced by si*Clk1*, si*Clk4* or si*Clk1/4* after 48- or 96 h. According to the antibody supplier (Abcam), the immunogen for the CLK1 antibody shows 77% similarity to CLK4, whilst the immunogen for the with CLK4 antibody shows 57% identity to CLK1. This suggests that there is considerable potential for the antibodies to cross-react and detect expression of the other isoform. Given CLK1 and CLK4 are of similar molecular weights, it was not possible to discriminate between detection of the desired and cross-reactive antigen.

Furthermore, the immunogens for the CLK1 and CLK4 antibodies correspond to residues 124-139 and 107-156, respectively, which are present in the truncated $Clk1/4^{T2\ (I4R)}$ products and therefore detectable by Western blot. Given $Clk1/4^{T2\ (I4R))}$ levels were only partially reduced by si*Clk1* and si*Clk4*, these truncated peptide products may inflate the apparent expression of CLK1 and CLK4, masking the knock-down of CLK1/4 expression. Given the lack of specificity (i.e. cross-reactivity) of si*Clk1* and si*Clk4*, and the difficulties in measuring CLK1/4 knock-down, it was decided not to pursue the study of *Clk1*/4 in adipocyte differentiation.

Delineating the cause of impaired differentiation: requirement for selective MNK inhibitors

To delineate the cause of the impaired differentiation phenotype observed with MNK-I1, it was necessary to find an MNK inhibitor(s) that did not inhibit the CLKs. The use of such an inhibitor(s) would determine whether MNK activity alone is required for pre-adipocyte differentiation. A new range of MNK inhibitors were subsequently acquired: MNK-7g, ETC-206 and eFT508 (Figure 3-29D). MNK-7g is a thienopyrimidine derivative derived from MNK-I1 and is equivalent in terms of overall potency but substantially more potent against MNK2 than MNK1 [68]. ETC-206 is a selective MNK1/2 inhibitor that displays efficacy in a pre-clinical model of blast crisis chronic myeloid leukaemia (BC-CML) [251] whilst eFT508 is a potent and selective MNK1/2 inhibitor in phase II clinical trials for the treatment of lymphoma, colorectal cancer, triple negative breast cancer and hepatocellular carcinoma [59,252]. These inhibitors were subsequently assayed for their efficacy in 3T3-L1 pre-adipocytes.

Efficacy of MNK-7g, ETC-206 and eFT508 in 3T3-L1 pre-adipocytes

Dose-responses were performed in 3T3-L1 cells to determine the concentration at which MNK activity was completely inhibited by MNK-7g, ETC-206 and eFT508. As assessed by P-eIF4E, MNK activity was completely blocked by MNK-7g and ETC-206 at ≥ 3 μM, whilst eFT508 blocked P-eIF4E at ≥ 0.3 μM, and was therefore 10X more potent (Figure 3-29A-C).

To determine whether any of the compounds had effects on major cell signalling pathways, the phosphorylation of key signalling proteins was investigated. MNK-7g increased P-ERK levels at 3 μM and 5 μM, suggesting that ERK signalling can be activated by sufficiently high doses of MNK-7g (Figure 3-29A), perhaps via a (hypothetical) feedback loop, similar to MNK-I1 (Figure 3-11A). eFT508 and ETC-206 only reduced P-ERK levels at ≥ 3 and 5 μM, respectively, well above their effective dosage, suggesting ETC-206 and eFT508 may inhibit a component(s) of the ERK the signalling pathway but only at such doses.

MNK-7g did not affect the levels of P-PKB but reduced P-rpS6 levels at 5 μM, suggesting acute inhibition of mTORC1 signalling at this dose. ETC-206 and eFT508 had no effect on mTORC1 or PKB/PI3K signalling at any of the doses assayed. Importantly, with the exception of MNK-7g, none of the compounds affected ERK, PKB/PI3K or mTORC1 either at or below their effective dosage, indicating the compounds were MNK1/2 selective and appropriate for use.

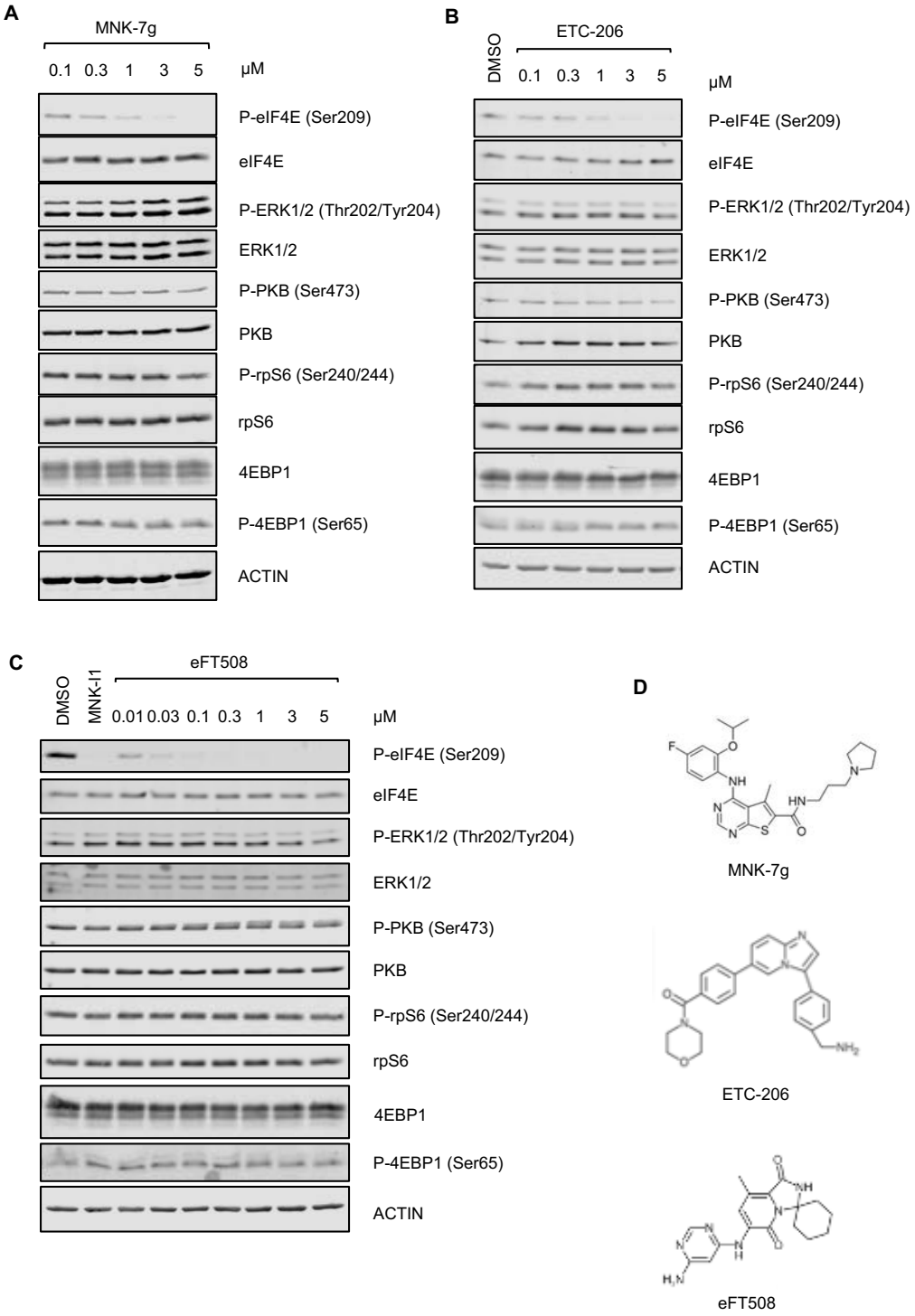
A
MNK-7g
0.1 0.3 1 3 5
μM
P-eIF4E (Ser209)
eIF4E
P-ERK1/2 (Thr202/Tyr204)
ERK1/2
P-PKB (Ser473)
PKB
P-rpS6 (Ser240/244)
rpS6
4EBP1
P-4EBP1 (Ser65)
ACTIN
B
DMSO
ETC-206
0.1 0.3 1 3 5
μM
P-eIF4E (Ser209)
eIF4E
P-ERK1/2 (Thr202/Tyr204)
ERK1/2
P-PKB (Ser473)
PKB
P-rpS6 (Ser240/244)
rpS6
4EBP1
P-4EBP1 (Ser65)
ACTIN
C
DMSO
MNK-i1
eFT508
0.01 0.03 0.1 0.3 1 3 5
μM
P-eIF4E (Ser209)
eIF4E
P-ERK1/2 (Thr202/Tyr204)
ERK1/2
P-PKB (Ser473)
PKB
P-rpS6 (Ser240/244)
rpS6
4EBP1
P-4EBP1 (Ser65)
ACTIN
D
MNK-7g
ETC-206
eFT508

Figure 3-29: Efficacy and specificity of MNK-7g, ETC-206 and eFT508 in 3T3-L1 pre-adipocytes.
Dose responses were performed in 3T3-L1 pre-adipocytes with (A) MNK-7g, (B) ETC-206 and (C) eFT508 using the indicated concentrations of inhibitor or equivalent volume of DMSO; representative immunoblots are shown (n=3). In (C), 3 μM MNK-I1 was included as a positive control. After 2 h, cell lysates were harvested and analysed by SDS-PAGE using the indicated antibodies. (D) Chemical structures of MNK-7g, ETC-206 and eFT508.

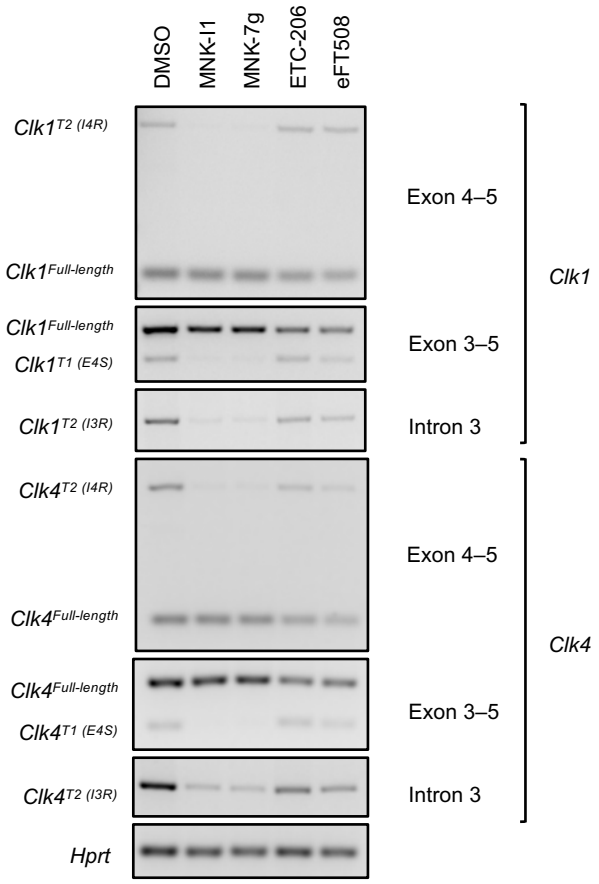

Figure 3-30: Effect of MNK inhibition on auto-inhibitory regulation of *Clk1/4*.

3T3-L1 pre-adipocytes were treated for 2 h with 3 µM MNK-I1, MNK-7g, ETC-206, 0.3 µM eFT508 or equivalent volume of DMSO, after which RNA was harvested and used to amplify *Clk1/4* alternative splicing products by RT-PCR which were analysed by agarose gel electrophoresis (n=1).

Effect of MNK-7g, ETC-206 and eFT508 on auto-inhibitory regulation of CLK1/4

To determine whether the new MNK inhibitor compounds inhibited the CLKs, the levels of alternatively spliced *Clk1/4* were assessed by RT-PCR as a readout of the activation of the CLK auto-inhibitory mechanism (Figure 3-30). MNK-7g reduced $Clk1/4^{T1\ (E4S)}$ and $Clk1/4^{T2\ (I4R)}$ levels, whilst only partially reduced $Clk1/4^{T2\ (I3R)}$ levels (Figure 3-30), similar to MNK-I1 (Figure 3-26B). This suggests that MNK-7g, like MNK-I1, is a potent inhibitor of the CLKs, consistent with their structural similarities [68]. In contrast, the levels of $Clk1/4^{T1\ (E4S)}$, $Clk1/4^{T2\ (I4R)}$ and $Clk1/4^{T2\ (I3R)}$ were only very slightly reduced by ETC-206 and eFT508. The apparent reduction may, however, be due to differences in the PCR amplification efficiency and/or loading of gel lanes, specifically the control (DMSO) lane. Nevertheless, it can be suggested ETC-206 and eFT508 inhibit the CLKs very weakly, if at all, likely because they are both structurally distinct from the thienopyrimidines MNK-I1 and MNK-7g.

Interim Conclusion

MNK-7g is a dual MNK/CLK inhibitor similar to MNK-I1, whereas ETC-206 and eFT508 are selective MNK1/2 inhibitors and only very weakly inhibit the CLKs, if at all. *How does selective MNK1/2 inhibition compare with dual MNK/CLK inhibition during pre-adipocyte differentiation?*

Effect of selective MNK inhibition on 3T3-L1 pre-adipocyte differentiation

ETC-206 and eFT508 do not promote the auto-inhibitory regulation of CLKs, presumably given they are selective for MNK1/2. To determine whether selective MNK1/2 inhibition affects adipocyte differentiation in the same manner as dual CLK/MNK inhibition, two-day post-confluent 3T3-L1 pre-adipocytes were subjected to adipogenic induction in the presence or absence of ETC-206 and eFT508. ETC-206 and eFT508 effectively blocked P-eIF4E, although, as expected, eFT508 was more potent (Figures 3-31A and 3-32A). As the differentiation program progressed, residual P-eIF4E levels progressively increased in ETC-206-treated cells, suggesting the efficacy of ETC-206 was reduced, perhaps due to the increased hydrophobic environment caused by the accumulation of lipid in differentiating adipocytes (Figure 3-31A). The expression of C/EBPβ was not affected by ETC-206 or eFT508 (Figures 3-31A and 3-32A), consistent with the effects of MNK-I1 (Figure 3-17A). ETC-206 did not affect the expression of C/EBPδ. However, eFT508 increased C/EBPδ levels on Days 3 and 6, consistent with the effects of MNK-I1 (Figure 3-17A). Importantly, the expression of C/EBPα, PPARγ and downstream targets FABP4, LPIN1 and PLIN1 was not affected by ETC-206 or eFT508 (Figures 3-31A and 3-32A); in contrast to MNK-I1 (Figure 3-17A). Lipid accumulation and the extent of adipogenesis, quantified from ORO-stained fields of view (Figures 3-31B-C and 3-32B-C), or absorbance of eluted ORO (Figure 3-32D) was not significantly affected by ETC-206 or eFT508, likely because C/EBPα and PPARγ expression was not affected. This suggests that selective inhibition of MNK1/2 does not affect adipogenesis, in contrast to dual MNK/CLK inhibition with MNK-I1. Therefore, it is suggested the combined

activities of CLK/MNK are necessary to promote 3T3-L1 pre-adipocyte differentiation but MNK activity alone is not required for adipogenesis.

Effect of MNK-7g on pre-adipocyte differentiation

Given that MNK-7g, like its derivative, MNK-I1, promotes the auto-inhibitory regulation of CLK, presumably through inhibition of CLK activity, its effect on adipocyte differentiation was assessed. When assessed over the first 72 h of adipogenesis, MNK-7g decreased P-eIF4E levels, exhibiting a similar potency to MNK-I1, as expected (Figure 3-33B). The expression of C/EBPβ was not affected by MNK-7g, including *Cebpb* mRNA (Figure 3-33A,B), consistent with the effect of MNK-I1 (Figure 3-16). MNK-7g significantly reduced the expression of C/EBPα but not *Cebpa* mRNA levels, in contrast to the effect of MNK-I1 (Figure 3-16). MNK-7g and MNK-I1 therefore appear to reduce C/EBPα expression through different mechanisms: MNK-I1 affects transcription, whilst MNK-7g may affect translation of the *Cebpa* message. In addition, MNK-7g did not affect the induction of *Cebpd* or C/EBPδ protein level, in contrast to MNK-I1 (Figure 3-33A,B). PPARγ, but not *Pparg* mRNA, was reduced at 48 h by MNK-7g, consistent with MNK-I1, however, at 72 h, PPARγ expression had recovered, in contrast to MNK-I1 but consistent with the effect of TG003 (Figure 3-26). When the analysis was extended to cover the entire adipogenic program, C/EBPα and PPARγ expression was reduced on Day 3, but recovered by Day 6, similar to the effect of TG003 (Figures 3-15 and 3-16). Consequently, the expression of downstream targets FABP4, PLIN1 and ATGL was not affected by MNK-7g. Furthermore, lipid accumulation and the extent of adipogenesis, quantified from ORO-stained fields of view (Figure 3-34B,C) and absorbance of eluted ORO (Figure 3-34D) was not significantly affected by MNK-7g, in contrast to TG003 and MNK-I1 (Figures 3-17B-D, 3-25). Dual MNK/CLK inhibition did not consistently impair adipocyte differentiation, suggesting a possible discrepancy between the mechanisms of MNK-7g and MNK-I1, which may be due to non-specific off-target effects. These results also highlight a distinction between the mechanisms of TG003 and MNK-7g, the former of which adversely affected adipogenesis but not the latter. This suggests that CLK activity may not in fact be absolutely required for adipogenesis. Given the relatively low potency of TG003, the apparent effects could be due to the targeting of another kinase.

Interim Conclusion

Selective MNK1/2 inhibition with ETC-206 and eFT508 does not impair adipocyte differentiation, suggesting MNK activity is not required for adipogenesis. There are multiple discrepancies between the effects of MNK-7g and MNK-I1 on adipogenesis, which may be due to off-target effects. There are also major discrepancies between MNK-7g and TG003, the former of which adversely affected adipogenesis but not the latter. Given MNK-7g potently inhibits the CLKs but does not impair adipogenesis, CLK activity may in fact not be absolutely required for adipogenesis.

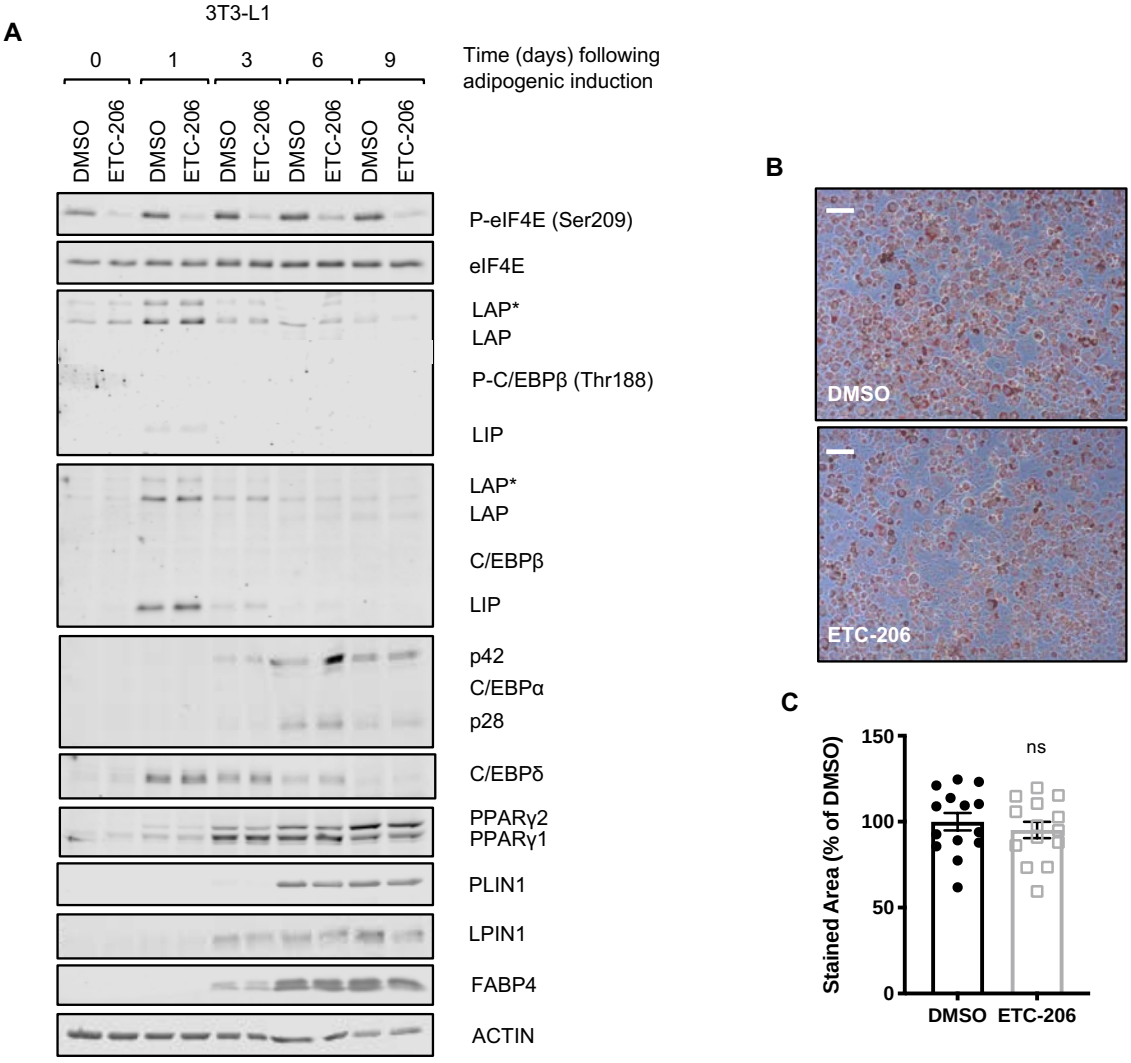

Figure 3-31: Effect of ETC-206 on 3T3-L1 pre-adipocyte differentiation.

3T3-L1 pre-adipocytes were differentiated with adipogenic induction media following pre-treatment with 3 μM ETC-206 or equivalent volume of DMSO. (A) Cell lysates were harvested at the indicated times and analysed by SDS-PAGE using the indicated antibodies; representative immunoblots are shown (n=3). (B) Day 9 differentiated adipocytes were stained with ORO to assess lipid accumulation; representative images are shown, scale bar 0.2 μm. (C) Total stained area was quantified from 6 different fields of view from (B) and is represented as percentage stained area relative to DMSO; data are mean ± SEM; individual data values are plotted (n=2); unpaired t-test (*P < 0.05 **P < 0.01 ***P < 0.001).

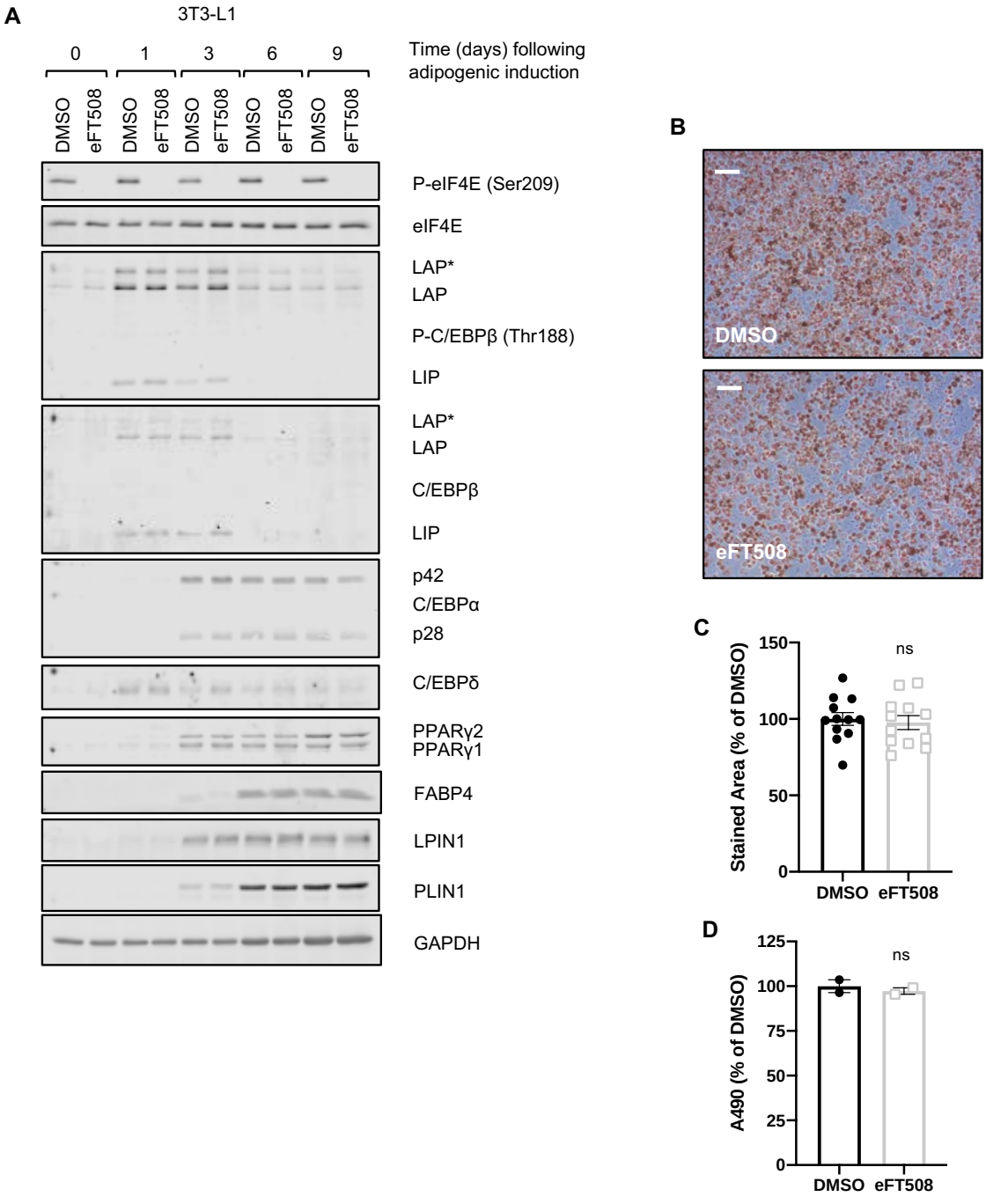
A
3T3-L1
0
1
3
6
9
Time (days) following adipogenic induction
DMSO
eFT508
P-eIF4E (Ser209)
eIF4E
LAP*
LAP
P-C/EBPβ (Thr188)
LIP
LAP*
LAP
C/EBPβ
LIP
p42
C/EBPα
p28
C/EBPδ
PPARγ2
PPARγ1
FABP4
LPIN1
PLIN1
GAPDH
B
DMSO
eFT508
C
Stained Area (% of DMSO)
150
100
50
0
ns
DMSO
eFT508
D
A490 (% of DMSO)
125
100
75
50
25
0
ns
DMSO
eFT508

Figure 3-32: Effect of eFT508 on 3T3-L1 pre-adipocyte differentiation.

3T3-L1 pre-adipocytes were differentiated with adipogenic induction media following pre-treatment with 0.3 μM eFT508 or equivalent volume of DMSO. (A) Cell lysates were harvested at the indicated times and analysed by SDS-PAGE using the indicated antibodies; representative immunoblots are shown (n=3). (B) Day 9 differentiated adipocytes were stained with ORO to assess lipid accumulation; representative images are shown, scale bar 0.2 μm. (C) Total stained area was quantified from 6 different fields of view from (B) and is represented as percentage stained area relative to DMSO; data are mean ± SEM; individual data values are plotted (n=2); unpaired t-test (*P < 0.05 **P < 0.01 ***P < 0.001). (D) ORO eluted from stained cells was quantified by absorbance (A490) and is represented as percentage absorbance relative to DMSO; data are mean ± SEM; individual data values are plotted (n=3); unpaired t-test (*P < 0.05 **P < 0.01 ***P < 0.001).

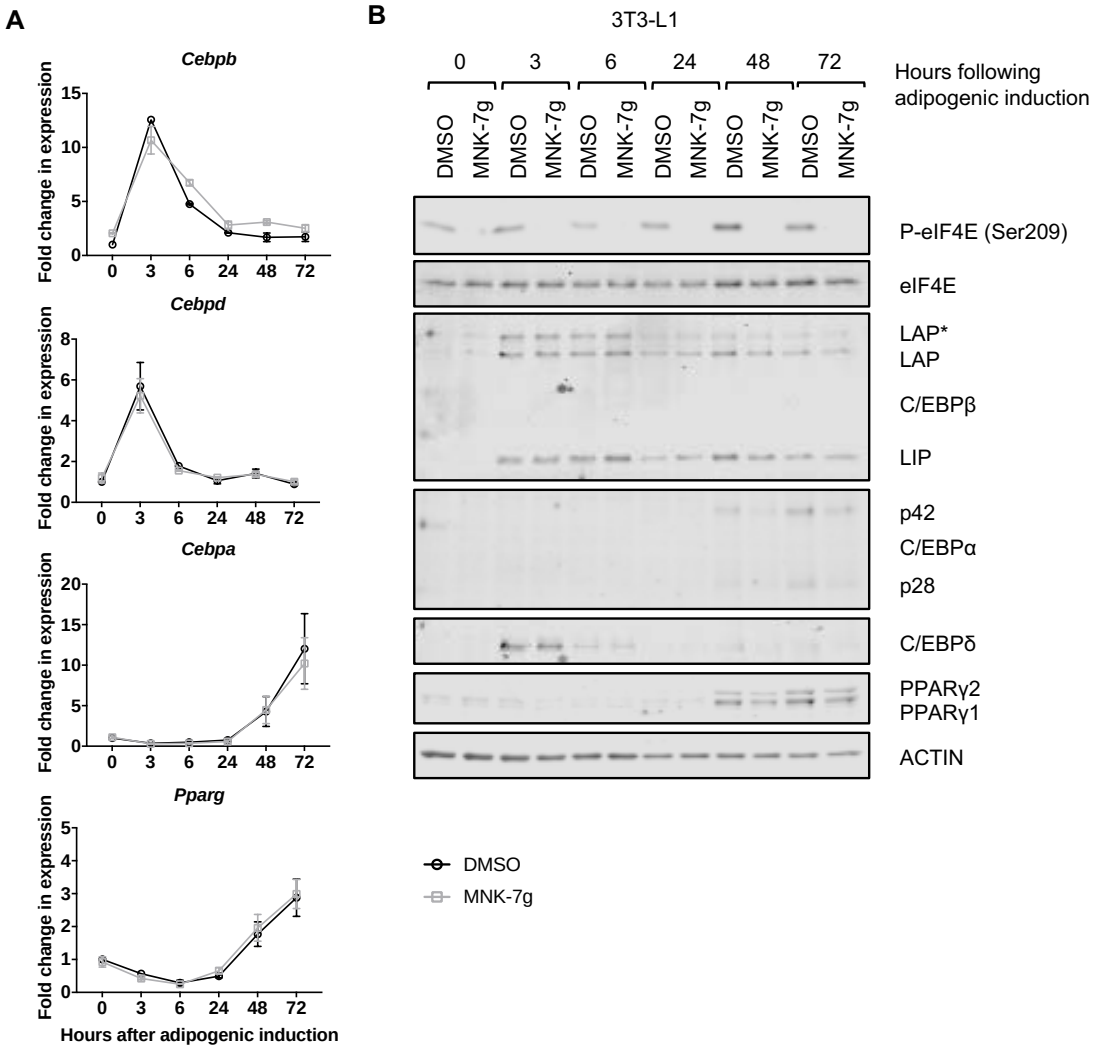

Figure 3-33: Effect of MNK-7g on 3T3-L1 pre-adipocyte differentiation.

3T3-L1 pre-adipocytes were differentiated with adipogenic induction media following pre-treatment with 3 μM MNK-7g or equivalent volume of DMSO. (A) mRNA levels of *Cebpb*, *Cebpd*, *Cebpa* and *Pparg* were assessed by RT-qPCR at the indicated times. Expression levels were normalised to *Nono* and *Hprt* and represented as fold change with respect to Day 0. Data are mean ± SEM; (n=3); 2-way ANOVA (*P < 0.05 **P < 0.01 ***P < 0.001). (B) Cell lysates were harvested at the indicated times and analysed by SDS-PAGE using the indicated antibodies; representative immunoblots are shown (n=2).

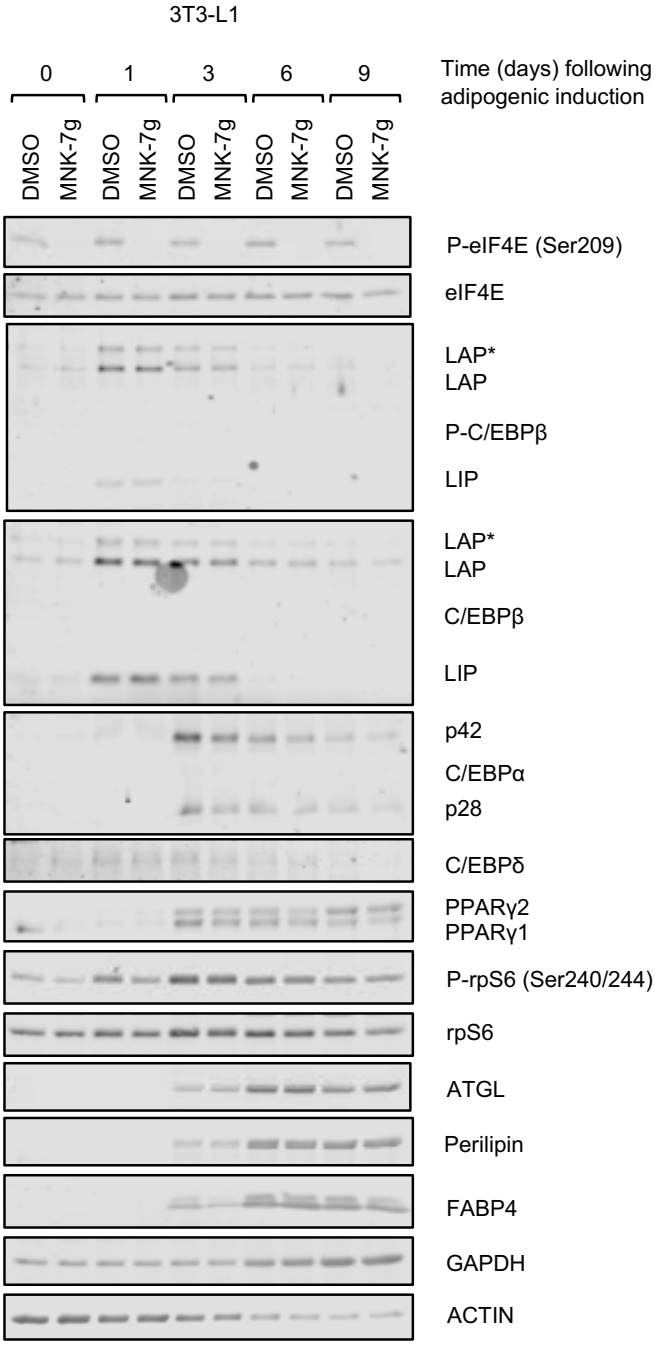
3T3-L1
0
1
3
6
9
Time (days) following adipogenic induction
DMSO
MNK-7g
P-eIF4E (Ser209)
eIF4E
LAP*
LAP
P-C/EBPβ
LIP
LAP*
LAP
C/EBPβ
LIP
p42
C/EBPα
p28
C/EBPδ
PPARγ2
PPARγ1
P-rpS6 (Ser240/244)
rpS6
ATGL
Perilipin
FABP4
GAPDH
ACTIN

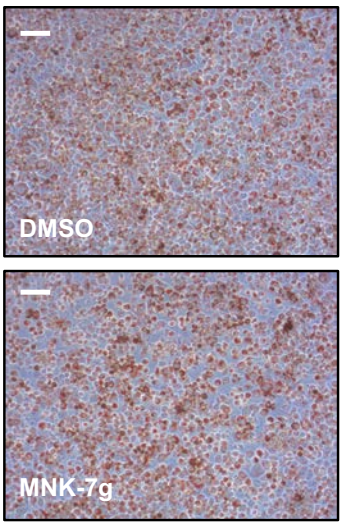
DMSO
MNK-7g

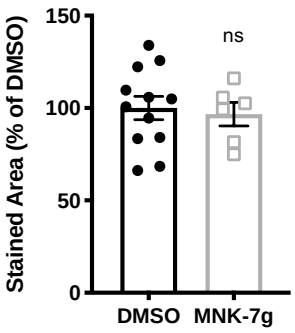
Stained Area (% of DMSO)
150
100
50
0
ns
DMSO
MNK-7g

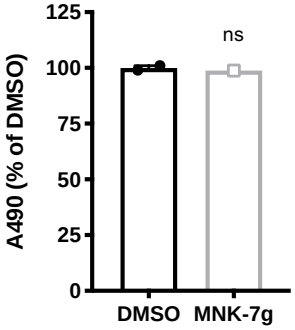
A490 (% of DMSO)
125
100
75
50
25
0
ns
DMSO
MNK-7g

Figure 3-34 Effect of MNK-7g on terminal adipogenesis in 3T3-L1 pre-adipocytes.

3T3-L1 pre-adipocytes were differentiated with adipogenic induction media following pre-treatment with 3 μM MNK-7g or equivalent volume of DMSO. (A) Cell lysates were harvested at the indicated times and analysed by SDS-PAGE using the indicated antibodies; representative immunoblots are shown (n=2). (B) Day 9 differentiated adipocytes were stained with ORO to assess lipid accumulation; representative images are shown, scale bar 0.2 μm. (C) Total stained area was quantified from 6 different fields of view from (B) and is represented as percentage stained area relative to DMSO; data are mean ± SEM; individual data values are plotted (n=2); unpaired t-test (*P < 0.05 **P < 0.01 ***P < 0.001) (D) ORO eluted from stained cells was quantified by absorbance (A490) and is represented as percentage absorbance relative to DMSO; data are mean ± SEM; individual data values are plotted (n=1-2); unpaired t-test (*P < 0.05 **P < 0.01 ***P < 0.001).

Discussion

In this Chapter, the expression and activity of MNK1/2 in 3T3-L1 pre-adipocytes was explored and the question of whether MNK activity is required for adipogenesis was addressed. *Mknk2* (MNK2) levels are induced by hormone induction and increase during adipocyte differentiation (Figures 3-1A and 3-2D). The use of inhibitors with broad specificity (CGP57380 and MNK-I1) impaired expression of adipogenic proteins and lipid accumulation, suggesting that MNK activity is important for adipogenesis (Figures 3-10 and 3-17). However, use of more selective MNK1/2 inhibitors (eFT508 and ETC-206) did not affect adipogenic protein expression or lipid accumulation (Figure 3-31 and 3-32), indicating that MNK1/2 activity is not required for adipogenesis. The disparity in phenotype between broad and selective MNK inhibitors highlights the necessity of using multiple inhibitors to assess kinase function. Finally, this Chapter increased our understanding of how the expression of *Cebpb* and *Cebpd* is regulated during early adipogenesis and provided new insights into the proposed sequence of events that lead to terminal adipogenesis (Figures 3-3 and 3-4).

Here, it was shown that *Mknk2* (MNK2) progressively increased during adipogenesis and is the predominant isoform in mature adipocytes (Figure 3-1A, 3-9) consistent with the *in vivo* expression of MNK1/2 in adipose tissue [3]. For the first time, analysis of the *Mknk2* promoter identified multiple GRE-like elements bound by GR and a single cAMP response element (CRE)-like element bound by CREB, indicating that *Mknk2* expression is regulated through the cAMP and GR signalling pathways (Figure 3-6). During adipogenesis, such pathways are activated immediately upon hormone induction [89,96], suggesting MNK2 up-regulation may be important for adipocyte differentiation. These findings suggest *Mknk2* may be one of a number of other genes up-regulated by CREB and GR to induce or promote adipogenesis [253,254]. However, the function of MNK2 in adipocyte differentiation is likely to be independent of P-eIF4E and therefore kinase activity, given that selective MNK1/2 inhibition did not affect adipogenesis (Figures 3-31 and 3-32). These findings may provide useful insight into the regulation of *Mknk2* in cancer, where MNK2 is typically over-expressed and associated with poor prognosis [255–257].

It was also interesting to observe the differential expression of MNK1/2 in differentiating pre-adipocytes: MNK2 levels were progressively increased whereas MNK1 levels remained stable (Figure 3-1), even though the putative CRE and GRE-like elements identified in *Mknk1* were bound by CREB and GR (Figure 3-5). It is possible the *Mknk1* CRE-like element is constitutively occupied by CREB, as observed in the *Pepck*, *Pcna*, *Ccna* and *c-Fos* promoters [258–261] whereas CREB occupancy on the *Mknk2* CRE is inducible [262]. Based upon their differential regulation, MNK1/2 may perform distinct functions in adipocytes.

The requirement for MNK activity in adipocyte differentiation was investigated using a range of MNK inhibitors. In the first instance, CGP57380, which was previously reported to impair

adipogenesis [3], was found to reduce lipid accumulation and the expression of terminal adipogenic factors C/EBPα and PPARγ by promoting the translation of C/EBPβ-LIP. However, CGP57380 is non-specific (Figures 3-10A and 3-11C) and the effects are likely to be associated with acute inhibition of mTORC1 rather than the MNK1/2 [200,214]. Furthermore, the non-specificity of CGP57380 may extend beyond mTORC1, given it also potently inhibits a number of other kinases [64].

In the second instance, MNK-I1, an apparently more specific inhibitor [65], was found to impair lipid accumulation and adipogenesis (Figure 3-17) without affecting mTORC1 (Figure 3-10C). The impairment in adipogenesis and lipid accumulation was stronger when cells were treated with MNK-I1 prior to adipogenic induction (Figure 3-17) than at the time of induction (Figures 3-12, 3-13 and 3-14) suggesting MNK activity is important for modulating early adipogenic signalling. However, MNK-I1 was discovered to inhibit the activity of CLK1/4 (Figure 3-30), which is thought to be required for regulating an extensive program of alternative splicing needed for cell cycle progression [247]. Unexpectedly, cell cycle progression during MCE was only impaired with MNK-I1 but not TG003 (a CLK1/4 inhibitor), indicating that CLK1/4 activity is not required for cell cycle progression in the context of MCE (Figures 3-21 and 3-27), in contrast to previous findings [247]. TG003 partially impaired adipogenesis (Figures 3-25 and 3-26), whereas MNK-7g, a derivate of MNK-I1 that also inhibits CLK1/4, did not impair adipogenesis (Figure 3-33 and 3-34), indicating that TG003 and MNK-I1 are non-specific and likely target additional kinases that are implicated in adipocyte differentiation. This suggests that neither MNK or CLK activity are required for adipogenesis.

In the final instance selective MNK1/2 inhibitors, eFT508 and ETC-206, were used. Given these compounds are in the process of being assessed for their clinical efficacy [251,252], they are among the most reliable MNK inhibitors currently available. Neither eFT508 nor ETC-206 affected lipid accumulation or the expression of adipogenic proteins, in support of the fact that MNK activity is not actually required for adipogenesis (Figure 3-31 and 3-32). Combined, these findings reveal the inadequacies and lack of specificity of CGP57380 and MNK-I1. It is concerning that a large proportion of the MNK literature has been developed upon the use of sub-optimal inhibitors such as CGP57380 [190]. Therefore, the conclusions and findings of such studies should be interpreted with a high degree of caution. However, even with the best of intentions, developing more potent inhibitors is evidently problematic, as exemplified by MNK-I1 which was found herein to potently inhibit CLK1/4 (Figure 3-30). Recent publications using MNK-I1 which report a role for MNK activity in cancer cell migration and metastasis should be re-interpreted in light of these new findings [65,68,219]. It raises an important point: no kinase inhibitor can be solely relied upon in isolation to draw robust conclusions. This is because inhibitors target the ATP binding domain, a highly conserved region among similar kinases, and therefore have a significant likelihood of inhibiting other related kinases. This Chapter highlights the necessity of

using multiple, structurally distinct inhibitors when assaying the function of kinases. Genetic KO models and siRNA knockdown studies are also of significant value and should be highly considered to complement inhibitor studies.

In this Chapter, new insights into the control of early adipogenesis by C/EBPβ and C/EBPδ were gained. C/EBPβ and C/EBPδ have important and partially redundant roles in adipogenesis, in part by activating expression of PPARγ [96,102,103,150,151]. It is well-established that IBMX directly induces expression of *Cebpb,* as mediated by the binding of CREB to a previously identified CRE (-60/106) [202]. Further analysis of the *Cebpb* promoter however, located an additional CRE-like element at -2343/2398 which was occupied by CREB, albeit to a lesser extent (Figure 3-3). This suggests CREB may regulate *Cebpb* expression from more than one CRE. Notably, and for the first time, DEX was found to directly induce the expression of *Cebpb* (Figure 3-2) through the occupancy of GR at three half-GRE core sequence elements in its proximal and distal promoter (Figure 3-3). Previous reports of DEX-induced *Cebpb* expression have been based on studies in hepatocytes [263], muscle [264] and more recently brown adipocytes [254]; however, this is the first report of DEX-induced *Cebpb* expression in pre-adipocytes and therefore challenges the existing, established model of IBMX-driven *Cebpb* expression.

Further, when DEX was combined with IBMX, it was found to further augment *Cebpb* expression (Figure 3-2). Augmented *Cebpb* induction has been reported in hepatocytes using DEX in combination with either glucagon (a beta-androgenic receptor agonist that increases cAMP) [265] or a cAMP analogue [266]. The combination of DEX and glucagon was shown to facilitate a greater maximal increase and more gradual decline in *Cebpb* levels than was observed with either DEX or glucagon alone [265]. This suggests that IBMX and DEX are both necessary for maximal and sustained C/EBPβ expression and may help to explain why pre-adipocytes incubated in the absence of DEX show diminished expression of C/EBPβ, C/EBPδ and C/EBPα and very little evidence of differentiation whilst pre-adipocytes differentiated in the absence of IBMX show a considerable delay in both the expression of C/EBPβ and in their differentiation [96]. This finding may have implications for other IBMX-driven genes and suggests a complex relationship between CREB and GR-driven gene expression.

It is well-established that DEX directly induces the expression of *Cebpd* [89,96,264], but the location of the GRE has not been previously reported. In this Chapter, two imperfect palindrome 6-bp half-sites separated by three nucleotides were identified in the *Cebpd* proximal promoter (-98), corresponding to a full-length GRE consensus sequence (Figure 3-4). This site was found to be occupied by GR following adipogenic induction, and is therefore likely to be the GRE element responsible for regulating *Cebpd* expression (Figure 3-4). Analysis also identified a half-CRE element in the *Cebpd* promoter (Figure 3-4); however, unlike *Cebpb*, IBMX and DEX did not augment *Cebpd* expression. Rather, IBMX actually impaired *Cebpd* expression suggesting the CRE-

like element may act to negatively regulate *Cebpd* expression. Given that IBMX is present in the initial induction media, such down-regulation of *Cebpd* appears counter-intuitive; however, this may be a mechanism by which cells appropriately modulate expression of *Cebpd* given that C/EBPδ is already very highly expressed after 3 h in the presence of IBMX (Figure 3-1). CREB is typically thought of as a factor that activates gene expression but it can also act to negatively regulate gene expression [267–270]. The regulation of CREB-mediated transcription appears to be gene- and context-specific dependent on the recruitment of co-activators and co-repressors which vary between promoter environments [271,272]. It is hypothesised that CREB may negatively regulate *Cebpd* levels to modulate and balance its expression through interactions and/or recruitment of co-repressors at its promoter environment. However, further investigation is required to better understand the mechanism.

Adipogenesis is understood to involve the regulated induction of C/EBPβ and C/EBPδ, which, in turn, directly induce the expression of PPARγ and in turn, C/EBPα [89,96,150,151,153]. In this Chapter, C/EBPβ was found to occupy response elements in the promoters of both *Cebpa* and *Pparg* after 72 h (Figure 3-18), after which C/EBPα bound to its own promoter and the promoter of *Pparg2* (Figure 3-20). These findings support the view that C/EBPβ induces the expression of PPARγ and C/EBPα [64], and that, once expressed, C/EBPα is responsible for maintaining its own expression [113,120–123] and the expression of PPARγ [153,158]. However, this study did not assess whether the expression of PPARγ precedes that of C/EBPα, as is currently proposed in the consensus model [150–153].

A combination of direct and circumstantial evidence has established that C/EBPα and PPARγ mutually induce the expression of each other [152,153,158]. Whilst the element responsible for binding C/EBPα has been identified in the *Pparg2* promoter [153,158], the element responsible for binding PPARγ in the *Cebpa* promoter had not. In this Chapter, analysis of the *Cebpa* promoter identified a putative PPARE (-125) (Figure 3-18A). This element, however, was not occupied by PPARγ (Figure 3-19A) although the C/EBPREs in *Pparg2* and *Cebpa* were occupied by C/EBPα (Figure 3-20) consistent with the auto-regulation of these genes by C/EBPα [113,120–123,153,158]. Although PPARγ was not found to directly bind the *Cebpa* promoter, it may indeed alter the structural state of the chromatin associated with the *Cebpa* gene by mechanisms that do not involve binding directly to the DNA, such as protein-protein interactions [159].

In conclusion, although *Mknk2* (MNK2) expression is increased during adipogenesis, MNK1/2 activity is not required for adipocyte differentiation. It is shown - for the first time - that during early adipogenesis, *Cebpb* expression is augmented by DEX whilst *Cebpd* expression is under the control of both GR and CREB signalling pathways, the latter acting to modulate its expression. Collectively, findings from this Chapter support the view that C/EBPβ induces the expression of both C/EBPα and PPARγ and that once expressed, C/EBPα is responsible for maintaining its own expression and the expression of PPARγ.

Chapter 4
Role of MNK2 in 3T3-L1 pre-adipocyte differentiation

Introduction

In Chapter 3, the use of selective MNK1/2 inhibitors strongly indicated that MNK activity is not required for adipogenesis (Figure 3-31 – 3-34). Nevertheless, the MNK2 protein remained of particular interest given that it is induced during differentiation (Figure 3-1A) and is the predominant isoform in mature adipocytes [3] (Figure 3-8). Moreover, MNK2-KO mice have blunted weight gain and exhibit the greatest protection from diet-induced obesity [3]. It was therefore hypothesised that the MNK2 protein itself may regulate adipogenesis or indeed metabolism through a function(s) that is independent of its kinase activity.

In investigating additional function(s) of MNK2, it is necessary to understand the interactions that occur with other proteins. MNK2 binds to a docking site in eIF4G through a conserved basic region in its N-terminus, bringing it into close proximity with eIF4E to facilitate its phosphorylation [8,10,24,211,273]. MNK2 tightly associates with activated ERK1/2, to which the high basal activity of MNK2 can be attributed [5,10,61,211]. MNK2 has been reported to interact with mTORC1 to inhibit the phosphorylation of the downstream mTORC1 target, p70S6K (70-kDa ribosomal protein S6 kinase) [53]. Specific interactions of MNK2 with estrogen receptor β (ERβ) [15] and the cytoskeletal-associated protein, plectin [54], have also been reported. MNK2 is predominantly cytoplasmic, owing to unique C-terminal domain features that occlude access of nuclear transport factors to the N-terminal nuclear localisation signal [10,273]. Adipogenesis involves a highly orchestrated transcriptional cascade and so it is possible that these or as yet unidentified MNK2 interactions may be relevant to the control of adipocyte differentiation.

Over several decades, genetic mice models have facilitated the study of genes implicated in adipogenesis and contributed immensely to our understanding of adipocyte biology [274]. Global or adipose-specific gene KO models have been routinely used to study gene function *in vivo*, whilst siRNA-mediated gene knock-down approaches have been used in pre-adipocyte cell models [275]. More recently, the CRISPR-associated protein 9 (Cas9) nuclease has been engineered into an effective RNA-guided gene editing tool (CRISPR-Cas9). CRISPR-Cas9 is now routinely used to generate KO models to study gene function, and the efficacy of CRISPR-Cas9 gene editing has been recently demonstrated in 3T3-L1 pre-adipocytes [276–279]. The use of CRISPR-Cas9 results in complete abrogation of protein expression and eliminates any confounding effects of low-level protein expression that may remain after siRNA knockdown. The generation of a stable KO model by CRISPR-Cas9 is most desirable for assessing loss-of-function phenotypes and is more specific than siRNA-mediated approaches in terms of off-targeting [280].

The aim of this Chapter was to determine the importance of MNK2 as a regulator of adipocyte biology and develop a 3T3-L1-2KO cell model to investigate the role and the underlying mechanisms of MNK2 in adipogenesis and metabolism.

Results

Expression analysis of MNK1/2 in mouse adipose tissue (AT)

The MNKs are expressed across a wide range of tissues, with MNK2 being the predominant isoform in spleen, heart, lung, kidney and testes, and MNK1 predominating in the brain [5]. MNK1/2 are highly expressed in metabolically relevant tissues, particularly skeletal muscle and liver [5], however, MNK2 appears to be the predominant isoform in gonadal AT [3]. To investigate whether MNK2 is similarly expressed across a range of other adipose depots to assess the hypothesis that MNK2 is an important regulator of adipocyte biology, MNK1/2 expression analysis was performed on mice adipose depots.

Mknk1 and *Mknk2* mRNA levels were assessed in omental, subcutaneous, brown scapular and gonadal adipose depots collected from WT C57BL/6 mice (20-week-old). *Mknk2* (MNK2) was highly expressed in omental, gonadal and scapular adipose tissue (AT) and was the predominant isoform in each case (Figure 4-1A,B). In contrast, subcutaneous AT had very low *Mknk2* expression, although it was more abundant than *Mknk1* (Figure 4-1A,B). *Mknk2* expression was also assessed in liver and muscle tissue for reference purposes. *Mknk2* was very highly expressed in muscle where it was the predominant isoform (Figure 4-1A,B), as expected [5]. In liver, *Mknk1* and *Mknk2* levels showed a similar expression profile to subcutaneous AT, suggesting the requirement for MNK activity is comparatively lower in liver. Overall, *Mknk2* (MNK2) was the predominant isoform and highly expressed in all adipose depots, except subcutaneous, supporting the hypothesis that MNK2 is an important regulator of adipocyte biology.

Given that MNK2-KO mice are protected from HFD-induced weight gain [3], it was hypothesised that consuming a HFD may affect MNK1/2 expression. The expression of *Mknk1* and *Mknk2* was therefore assessed in WT mice fed a HFD or regular chow diet for 16-weeks. Compared to a chow diet, *Mknk2* levels were decreased in mice fed the HFD in omental, gonadal and subcutaneous AT, although these differences were not significant (Figure 4-1D). However, in scapular AT, *Mknk2* levels were significantly reduced on the HFD (Figure 4-1D). *Mknk2* levels in liver and muscle were unchanged on the HFD, suggesting *Mknk2* is differentially expressed in AT on a HFD, but most markedly in scapular AT (Figure 4-1D). *Mknk1* levels were not different in liver, muscle, omental, gonadal or scapular AT; however, they were reduced in subcutaneous AT on the HFD, although this change was not significant (Figure 4-1C). The altered expression of *Mknk2* on the HFD indicates MNK2 may respond to changes in dietary composition and adipocyte metabolism may thus be modified accordingly.

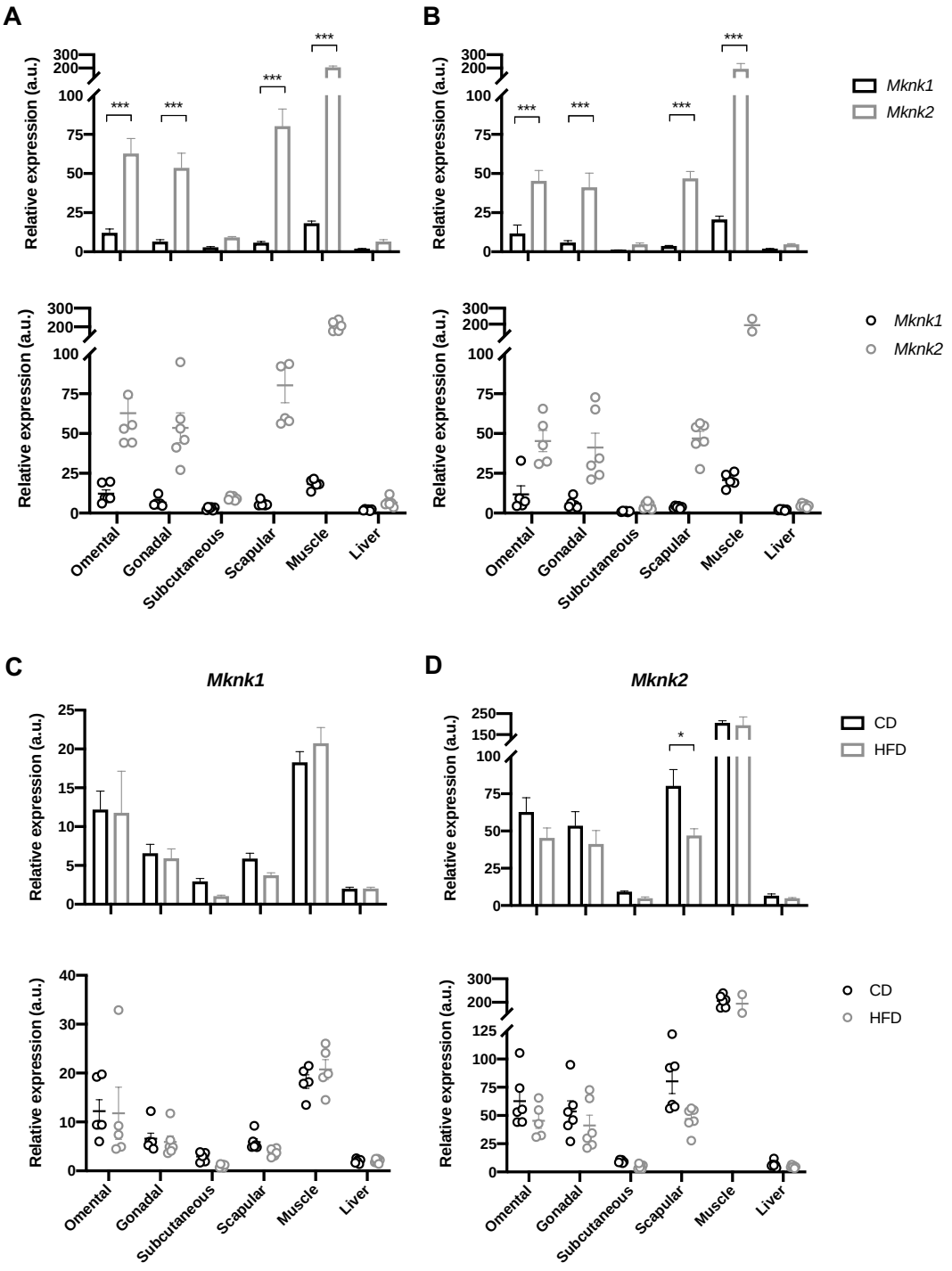
A
B
C
D
Relative expression (a.u.)
Mknk1
Mknk2
CD
HFD
Omental
Gonadal
Subcutaneous
Scapular
Muscle
Liver
***
*

Figure 4-1: *Mknk1/2* adipose tissue expression analysis.

Omental, gonadal, subcutaneous, scapular adipose tissue, muscle and liver were collected from WT C57BL/6 mice fed a (A) chow or (B) HFD for 16-weeks. Levels of *Mknk1* and *Mknk2* mRNA were assessed by RT-qPCR and normalised to *B2m* and *Hprt*. Relative expression levels were calculated using 2-ΔCt. The expression of (C) *Mknk1* and (D) *Mknk2* were compared on separate plots to determine whether expression was differentially expressed on an HFD. Mean ± SEM expression values are presented in the upper panels of each figure (bar graph); values from individual mice (n=5-6 per group) are presented in the lower panels (scatter-plot) with mean ± SEM indicated. 2-way ANOVA (*P < 0.05 **P < 0.01 ***P < 0.001).

Interim Conclusion

Mknk2 (MNK2) is highly expressed and is the predominant isoform in gonadal, omental and brown scapular AT; subcutaneous AT had comparatively lower *Mknk2* expression but was still the predominant isoform. *Mknk2* is differentially expressed in AT on the HFD but most markedly in brown scapular AT.

MNK2-KO CRISPR/Cas9 gene editing strategy

CRISPR-associated protein 9 (Cas9) is an endonuclease that is guided to a specific genomic location by a uniquely-designed single guide RNA (sgRNA) where it induces a double-stranded break (DSB). CRISPR-Cas9 can be harnessed to induce gene KO by designing sgRNAs to anneal within the coding sequence (CDS) of a target gene. The DSB induced by Cas9 cleavage is repaired by the non-homologous end-joining process, which is error-prone and can lead to the insertion or deletion of nucleotides (indels). Indels occurring within a CDS can induce frameshift mutations, premature termination codons (PTCs) and ultimately lead to the production of a truncated peptide. The outcome of this gene-editing strategy can be gene KO, due to the production of a non-functional peptide and/or non-sense mediated decay of the encoding mRNA. The frameshift mutagenesis strategy is routinely applied to generate gene KO where there is a suitable antibody to assay knockdown of the encoded protein. However, in the case of MNK2, there was no suitable antibody available, making this approach less than desirable due to difficulties in validating the KO of MNK2 expression. As an alternative approach, two sgRNAs can be used to generate DSBs and facilitate targeted deletion of particular genomic region [281,282]. This makes screening and validation of the KO more practical as PCR-based approaches can be applied. Therefore, a dual sgRNA approach was applied to KO expression of MNK2 in 3T3-L1 (3T3-L1-2KO).

The *Mknk2* gene contains start codons from which translation can be initiated in exons 2 and 4 (Figure 4-2A). To ensure complete KO of *Mknk2,* it was necessary to design sgRNAs that deleted a region after the second start codon in exon 4. With this in mind, two sgRNAs (*Mknk2* E4 and *Mknk2* E5) were engineered (*see* Materials and Methods) to delete part of the MNK2 catalytic domain containing the glycine-rich loop, a highly conserved region among kinases that is involved in nucleotide binding, substrate recognition and catalysis [283]. The dual sgRNA-induced deletion region corresponds to amino acid residues 30 to 56 of MNK2 and is encoded across exons 4 and 5 of *Mknk2* (Figure 4-2B). Deletion of the intervening exonic and intronic regions between the DSBs was predicted to not only remove the glycine-rich loop but also induce a frameshift in the *Mknk2* CDS, resulting in a truncated peptide that was prematurely terminated in exon 7 (Figure 4-2C, E).

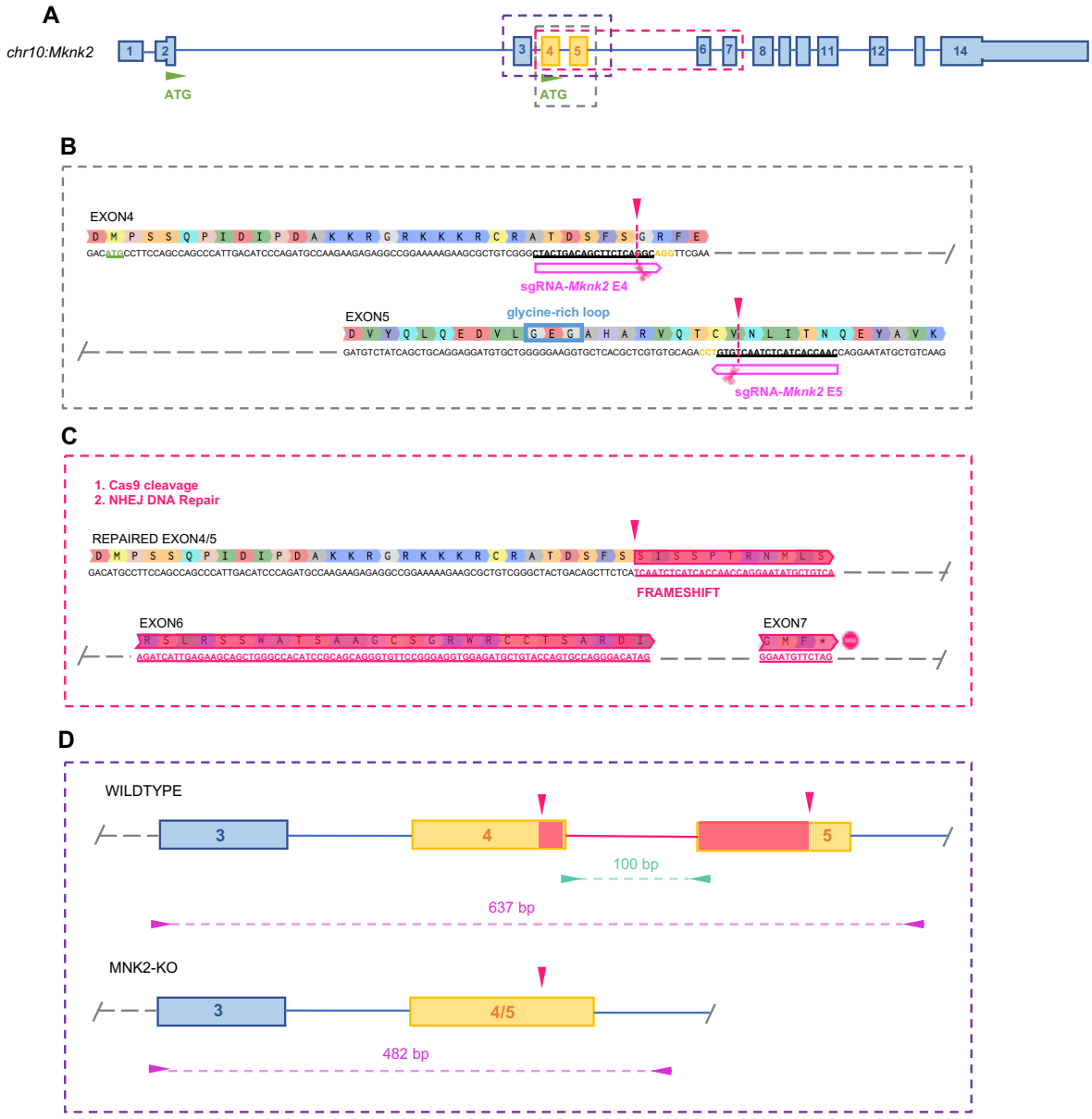

E

MNK2-Knockout Protein Sequence

MPSSQPIDIP DAKKRGRKKK RCRATDSFSS ISSPTRNMLS
RSLRSSWATS AAGCSGRWRC CTSARDIGMF *

MNK2-Wildtype Protein Sequence

MPSSQPIDIP DAKKRGRKKK RCRATDSFSG RFEDVYQLQE
DVLGEGAHAR VQTCVNLITN QEYAVKIIEK QLGHIRSRVF
REVEMLYQCQ GHRNVLELIE FFEEEDRFYL VFEKMRGGSI
LSHIHRRRHF NELEASVVVQ DVASALDFLH NKGIAHRDLK
PENILCEHPN QVSPVKICDF DLGSGIKLNG DCSPISTPEL
LTPCGSAEYM APEVVEAFSE EASIYDKRCD LWSLGVILYI
LLSGYPPFVG HCGSDCGWDR GEACPACQNM LFESIQEGKY
EFPDKDWSHI SFAAKDLISK LLVRDAKQRL SAAQVLQHPW
VQGCAPENTL PTPLVLQRNS CAKDLTSFAA EAIAMNRQLA
QCEEDAGQDQ PVVIRATSRC LQLSPPSQSK LAQRRQRASL
SATPVVLVGD RA*

Figure 4-2: CRISPR-Cas9 *Mknk2* gene KO approach.

(A) Gene structure: *Mknk2* exons are represented as blue boxes, exons targeted for editing are highlighted in yellow and intervening introns represented as solid lines. The location of start codons (ATG) are indicated by green arrows. (B) Grey-box: zoom-in of editing region: DNA and amino acid sequences of *Mknk2* exons 4 and 5 are shown, with the intervening intronic sequence indicated by a dashed line. The sequence of the sgRNAs targeting exons 4 and 5 are bold underlined and the location of predicted Cas9 cleavage sites are depicted with a red line. The glycine-rich loop is highlighted in blue. (C) Red-box: zoom-in of region following Cas9 cleavage and non-homologous end joining repair of exon 4/5 at the indicated junction (red arrow); the predicted DNA and amino acid sequences are depicted, including subsequent exons 6 and 7. The repair is predicted to result in a frameshift and truncated peptide due to a premature termination codon (PTC) in exon 7, as highlighted in red. (D) Purple-box: Zoom in of PCR screening approach: exons 3, 4 and 5 are depicted along with intervening intronic sequences of *Mknk2*. The region targeted for genomic deletion is highlighted in red. External screening primers (purple) flanking the edited region in both WT and MNK2-KO give rise to differently sized amplicons (637 bp WT; 482 bp MNK2-KO). Internal screening primers (green) anneal to sequences within the genomic region targeted for deletion and give rise to a 100 bp amplicon in WT, but no amplicon in MNK2-KO. (E) The predicted amino acid sequence of the truncated MNK2 peptide compared to WT. Amino acid residues affected by the frameshift are highlighted in red.

Construction of GeneART CRISPR-EGFP vector

The GeneART CRISPR vector (Appendix 1) encoding *Streptococcus pyogenes* Cas9 (SpCas9) and the CD4 reporter to facilitate selection by expression of surface CD4 was selected as the method to deliver sgRNA and associated apparatus into 3T3-L1. However, since two sgRNAs required simultaneous delivery into the same cell, a second CRISPR vector with a different reporter was required. Therefore, the CD4 CDS was spliced out and replaced with an enhanced green fluorescent protein (EGFP) CDS, amplified from vector pX458 to generate GeneART CRISPR-EGFP (Appendix 1). The orientation and sequence of the EGFP CDS in the resulting vector was confirmed by Sanger sequencing (Appendix 2).

Annealing and ligation of sgRNA oligonucleotide duplexes

With the CRISPR nuclease vectors constructed, single-stranded DNA oligonucleotides corresponding to sgRNAs *Mknk2* E4 and *Mknk2* E5 were annealed and ligated into GeneART CRISPR and GeneART CRISPR-EGFP at the *Bae*I sgRNA cloning site (*see* Materials and Methods). Vectors containing successfully ligated sgRNA duplexes were screened by sequential *Bae*I-*Eco*RI restriction digestion (Appendix 3). Since sgRNA ligation irreversibly removes the *Bae*I restriction sequence, vectors containing successfully ligated sgRNA duplexes are not cleaved by *Bae*I, but are instead linearised by *Eco*RI, generating a single fragment (>10 kb). Vectors where sgRNA ligation was unsuccessful retain the *Bae*I restriction site and are cleaved at both the *Bae*I and *Eco*RI sites, generating two fragments (~8.0 and ~2.5 kb). sgRNAs *Mknk2* E4 and *Mknk2* E5 were successfully ligated into GeneART CRISPR and GeneART CRISPR-EGFP vectors, respectively, and this was confirmed by Sanger sequencing to ensure DNA sequence and orientation were correct (Appendix 4).

Generation of single-cell $CD4^+/EGFP^+$ 3T3-L1 colonies

The resulting vectors, designated GeneART CRISPR-*Mknk2* E4 and GeneART CRISPR-EGFP-*Mknk2* E5, were simultaneously transfected into 3T3-L1 pre-adipocytes. After 48 h, $CD4^+/EGFP^+$ cells were individually sorted into 384 wells by fluorescence-activated cell sorting (FACS) and propagated over several weeks to generate single-cell colonies. Of the 384 single-cell sorting events, around 10% developed into viable, actively proliferating colonies; 30% entered a state of quiescence, with proliferation halted after multiple rounds of division; no colonies were observed for the remaining (60%) sorting events. Viability staining was not performed as part of the FACS procedure, and it was therefore possible that non-viable cells and/or debris had been sorted into the latter wells where no colonies were observed. It was also possible that viable cells were sorted into these wells, but for reasons unknown, failed to establish and propagate.

Interim Conclusion

A dual sgRNA DSB approach was applied to KO expression of MNK2 in 3T3-L1 pre-adipocytes (3T3-L1-2KO). The deletion corresponds to residues 30-56 of MNK2, which is encoded across exons 4

and 5 of *Mknk2*. sgRNAs were engineered (*Mknk2* E4 and *Mknk2* E5) and successfully ligated into GeneART CRISPR and GeneART CRISPR-EGFP nuclease vectors, respectively, and simultaneously transfected into 3T3-L1 pre-adipocytes. $CD4^+/EGFP^+$ cells were sorted and propagated into single colonies.

External PCR screening of 3T3-L1-2KO colonies

DNA was subsequently isolated from actively proliferating $CD4^+/EGFP^+$ single-cell colonies to screen for the genomic deletion of *Mknk2*. *External* primers flanking the edited region were used to identify clones with WT (637 bp), 2KO sequence (482 bp) or both (Figure 4-2D). Karyotype information of 3T3-L1 was not publicly available, so the number of chromosomal copies of *Mknk2* was unknown. However, from the *External* screen, WT and 2KO amplicons existed in a ratio of 2:1 in heterozygous clones, suggesting 3T3-L1 cells harbour at least three chromosomal copies of the *Mknk2* gene (Figure 4-3A). It was necessary for each chromosomal copy to be edited to ensure the complete KO of MNK2 expression.

From the *External* screen, a number of clones only amplified the 2KO amplicon (1-6B, 1-7B, 1-8E, 2-2E, 2-5C, 2-11D, 3-2G, 3-7C, 4-1E, 4-7C, 4-8C, 4-8E, 4-8F), indicating successful deletion of intervening exonic and intronic regions between the DSBs (Figure 4-3A). These clones were designated homozygous KO ($Mknk2^{-/-}$), as summarised in Table 4-1. A larger number of clones amplified both WT and 2KO amplicons (1-4B, 1-5E, 2-11C, 2-11F, 2-2F, 2-4B, 2-4D, 2-4E, 2-7A, 2-7F, 2-8C, 3-10F, 3-12D, 3-9G, 4-12C, 4-5B, 4-5F, 4-7D, 4-7E), indicating successful deletion of the intervening exonic and intronic regions between the DSBs occurred on some but not all chromosomal copies of *Mknk2*. These clones were therefore designated heterozygous KO ($Mknk2^{+/-}$) (Figure 4-3A, Table 4-1). Finally, a smaller number of clones amplified only the WT amplicon (1-9F, 2-5B, 3-11H and 4-9G), indicating deletion of the intervening sequence had not occurred on any of the chromosomal copies of *Mknk2*. These clones were designated unedited WT ($Mknk2^{+/+}$) (Figure 4-3A, Table 4-1).

In some cases, unexpected editing of the *Mknk2* gene occurred. For example, in the case of clone 1-10D, a fragment larger than the WT amplicon was observed, suggesting a substantial insertion of nucleotides had occurred between the two DSBs (Figure 4-3A). Since only a single fragment was observed, the repair appeared to be consistent across all chromosomal *Mknk2* copies Similarly, in clone 2-2D, the 2KO amplicon along with two larger fragments were amplified, suggesting that on one *Mknk2* chromosomal copy the deletion of the intervening sequence between the DSBs occurred as expected, whilst on the other two copies, large insertions of different sizes had occurred (Figure 4-3A). Both 1-10D and 2-2D were designated homozygous KO ($Mknk2^{-/-}$); however, given that *Mknk2* was not repaired as desired, they were not considered for further analysis (Table 4-1).

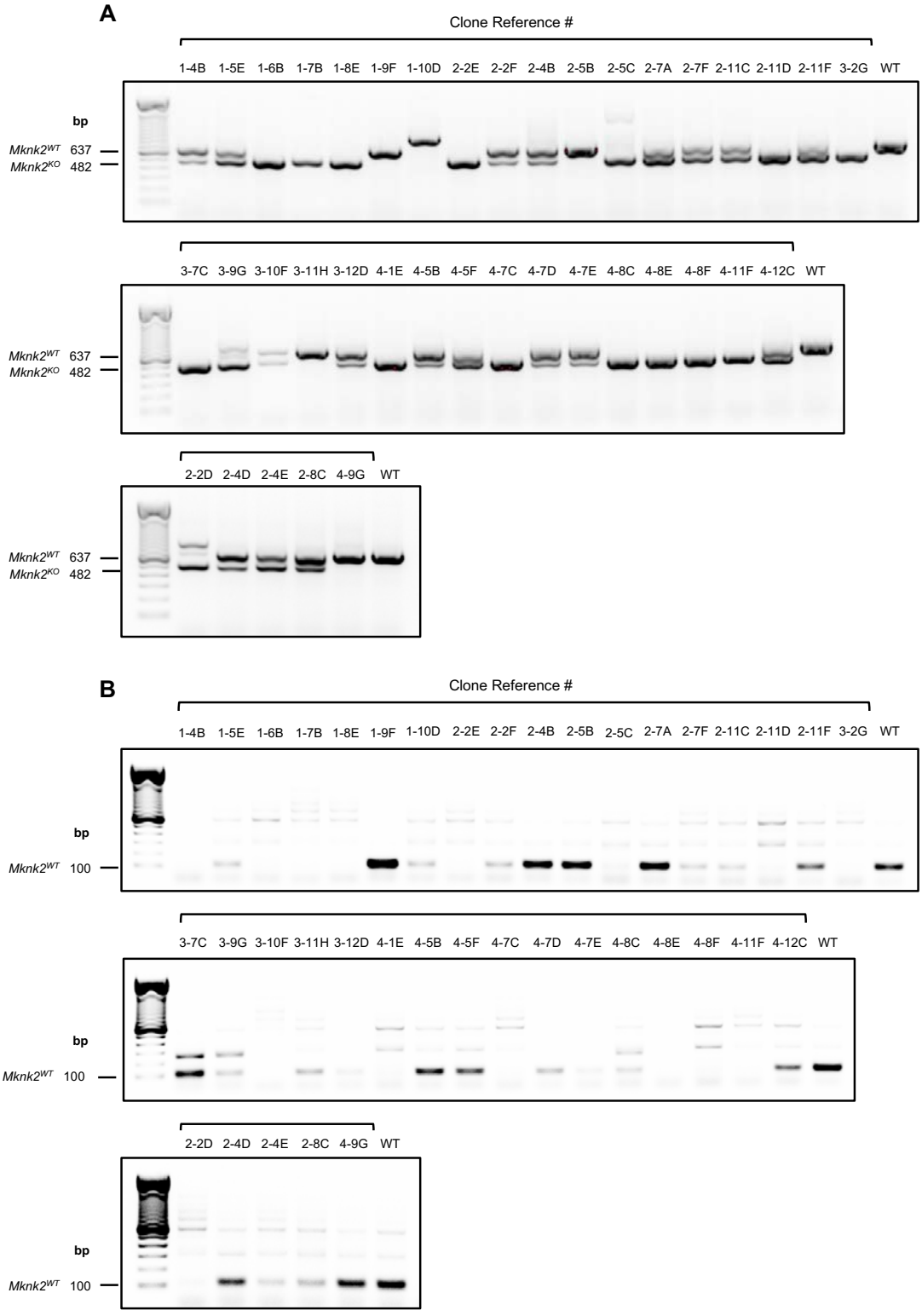
A
Clone Reference #
1-4B 1-5E 1-6B 1-7B 1-8E 1-9F 1-10D 2-2E 2-2F 2-4B 2-5B 2-5C 2-7A 2-7F 2-11C 2-11D 2-11F 3-2G WT
bp
Mknk2WT 637
Mknk2KO 482
3-7C 3-9G 3-10F 3-11H 3-12D 4-1E 4-5B 4-5F 4-7C 4-7D 4-7E 4-8C 4-8E 4-8F 4-11F 4-12C WT
Mknk2WT 637
Mknk2KO 482
2-2D 2-4D 2-4E 2-8C 4-9G WT
Mknk2WT 637
Mknk2KO 482
B
Clone Reference #
1-4B 1-5E 1-6B 1-7B 1-8E 1-9F 1-10D 2-2E 2-2F 2-4B 2-5B 2-5C 2-7A 2-7F 2-11C 2-11D 2-11F 3-2G WT
bp
Mknk2WT 100
3-7C 3-9G 3-10F 3-11H 3-12D 4-1E 4-5B 4-5F 4-7C 4-7D 4-7E 4-8C 4-8E 4-8F 4-11F 4-12C WT
bp
Mknk2WT 100
2-2D 2-4D 2-4E 2-8C 4-9G WT
bp
Mknk2WT 100

Figure 4-3: Genomic screening of *Mknk2*-KO in 3T3-L1 clones.

Genomic DNA from 3T3-L1 CRISPR-Cas9-edited clones was amplified by PCR using (A) external screening primers flanking the edited region of *Mknk2* and (B) internal screening primers within the region targeted for deletion. Fragments were analysed by gel electrophoresis and the predicted amplicon sizes are indicated for WT and 2KO.

Internal PCR screening of 3T3-L1-2KO colonies

PCR screening was then used to validate the deletion of the intervening sequence between the DSBs using *Internal* primers located within the editing region (Figure 4-2D). Clones retaining the intervening *Mknk2* sequence were expected to amplify a 100 bp fragment (WT), whereas clones that had successfully deleted the intervening sequence across all chromosomal *Mknk2* copies were not (2KO).

As expected, homozygous KO clones (*Mknk2*$^{-/-}$) identified from the *External* screen, did not amplify the WT amplicon, confirming the intervening sequence had been deleted across all *Mknk2* chromosomal copies (Figure 4-3B, Table 4-1). Unexpectedly, the homozygous KO clones 3-7C and 4-8C amplified the 100 bp (WT) amplicon, suggesting these clones still harboured at least one WT copy of *Mknk2* (Figure 4-3B). This contrasted with the results of the *External* screen: these clones were, therefore, re-designated as heterozygotes (*Mknk2*$^{+/-}$) (Table 4-1)

As expected, heterozygous KO (*Mknk2*$^{+/-}$) and unedited WT (*Mknk2*$^{+/+}$) clones identified from the *External* screen amplified the WT amplicon, indicating these clones harboured one or more WT copies of *Mknk2* (Figure 4-3B, Table 4-1).

Unexpectedly, in clones 1-4B and 3-10F, the WT amplicon was not amplified in the *Internal* screen, which suggested the intervening *Mknk2* sequence had been successfully deleted (Figure 4-3B). However, this contrasted with the *External* screen, which identified both clones as heterozygotes (Figure 4-3A). This apparent discrepancy may be attributed to a PCR amplification failure. Despite this, given the *External* screen showed that these clones retained at least one WT copy of *Mknk2*, they retained their designation as heterozygotes (*Mknk2*$^{+/-}$) (Table 4-1).

Table 4-1: Summary of 3T3-L1 *Mknk2*-KO genomic screening.

Summary of amplicons generated from the External and Internal genomic screen from Figure 4-3. The final *Mknk2* genotype was determined by considering the type of external and internal amplicons amplified: +/+ homozygous WT; +/- heterozygous KO; -/- homozygous KO. Amplicon(s) corresponding to an insertion event are designated INS.

Clone	External	Internal	Genotype
1-10D	INS	WT	–/–
1-6B	2KO	2KO	–/–
1-7B	2KO	2KO	–/–
1-8E	2KO	2KO	–/–
2-11D	2KO	2KO	–/–
2-2D	2KO/INS	2KO	–/–
2-2E	2KO	2KO	–/–
2-5C	2KO	2KO	–/–
3-2G	2KO	2KO	–/–
4-11F	2KO	2KO	–/–
4-1E	2KO	2KO	–/–
4-7C	2KO	2KO	–/–
4-8E	2KO	2KO	–/–
4-8F	2KO	2KO	–/–
1-4B	WT/2KO	2KO	+/–
1-5E	WT/2KO	WT	+/–
2-11C	WT/2KO	WT	+/–
2-11F	WT/2KO	WT	+/–
2-2F	WT/2KO	WT	+/–
2-4B	WT/2KO	WT	+/–
2-4D	WT/2KO	WT	+/–
2-4E	WT/2KO	WT	+/–
2-7A	WT/2KO	WT	+/–
2-7F	WT/2KO	WT	+/–
2-8C	WT/2KO	WT	+/–
3-10F	WT/2KO	2KO	+/–
3-12D	WT/2KO	WT	+/–
3-7C	2KO	WT	+/–
3-9G	WT/2KO	WT	+/–
4-12C	WT/2KO	WT	+/–
4-5B	WT/2KO	WT	+/–
4-5F	WT/2KO	WT	+/–
4-7D	WT/2KO	WT	+/–
4-7E	WT/2KO	WT	+/–
4-8C	2KO	WT	+/–
1-9F	WT	WT	+/+
2-5B	WT	WT	+/+
3-11H	WT	WT	+/+
4-9G	WT	WT	+/+

Interim Conclusion

External and *Internal* PCR screening of single-cell colonies identified 12 homozygous KO *Mknk2*$^{-/-}$, 21 heterozygous KO *Mknk2*$^{+/-}$ and four homozygous WT *Mknk2*$^{+/+}$. Additionally, two clones had substantial nucleotide insertions between the intervening DSBs and were designated as homozygous KO *Mknk2*$^{-/-}$; however, they were not considered for analysis.

Analysis of P-eIF4E levels in 3T3-L1-2KO clones

The *External* and *Internal* screening process identified 12 homozygous KO (*Mknk2*$^{-/-}$) for further characterisation (Table 4-1). In the absence of a suitable MNK2 antibody, clones were analysed for levels of P-eIF4E, to provide an indirect measure of MNK2 expression, given that MNK2 is the predominant isoform in 3T3-L1 (Figures 3-1 and 3-9). The P-eIF4E/eIF4E ratio of homozygous KO clones was assessed alongside MNK2-KO mouse embryonic fibroblasts (MEFs) (Figure 4-4A,B). Whilst MNK2-KO MEFs had a P-eIF4E/eIF4E ratio of 0.75, clones 1-8E, 2-2E and 4-11F had a much lower ratio (~0.25), followed by 4-7C (0.35), 3-2G (0.45) and 1-7B (0.75), suggesting there was considerable heterogeneity. Despite this, the P-eIF4E/eIF4E ratio in the homozygous KO clones was equal to or below the MNK2-KO MEF ratio, in support of their genotype designation. As cell lysates were collected under non-standardised conditions, the fluctuation in P-eIF4E levels may be attributed to differences in proliferation stage and confluence levels. Therefore, it was not reasonable to interpret the P-eIF4E/eIF4E ratio as a direct measure of the extent of MNK2 KO. Importantly, MNK1 expression was not affected by the KO of MNK2 in any of the clones analysed, consistent with the expression of MNK1 in MNK2-KO MEFs, indicating there was no compensatory increase in MNK1 expression (Figure 4-4).

Validation of 3T3-L1-2KO genotype by Sanger sequencing

Sanger sequencing was performed on DNA isolated from clones 1-6B (Appendix 5), 1-7B (Appendix 6), 1-8E (Appendix 7), 2-2E (Appendix 8), 4-7C (Appendix 10), 4-8E (Appendix 11) and 4-11F (Appendix 12) to validate the partial deletion of exons 4 and 5 and the intervening intronic sequence of *Mknk2*, and confirm their homozygous KO (*Mknk2*$^{-/-}$) genotype. However, sequencing of DNA from clone 3-2G, however, revealed that in addition to deletion of the intervening sequence there was an irregular indel at both sgRNA cut sites on at least one chromosomal copy of *Mknk2* (Appendix 9). Despite the *External* and *Internal* screening results, it was likely that at least one of the chromosomal copies of *Mknk2* had been repaired differently. Therefore, it was decided not to pursue further analysis of this clone to avoid unforeseeable complications.

Interim Conclusion

The P-eIF4E/eIF4E ratio in homozygous *Mknk2*$^{-/-}$ KO clones was equal to or below the MNK2-KO MEF ratio in support of their genotype designation. Deletion of *Mknk2* was confirmed at the gene level by Sanger sequencing in all clones except 3-2G. MNK1 expression was not affected by the KO of MNK2.

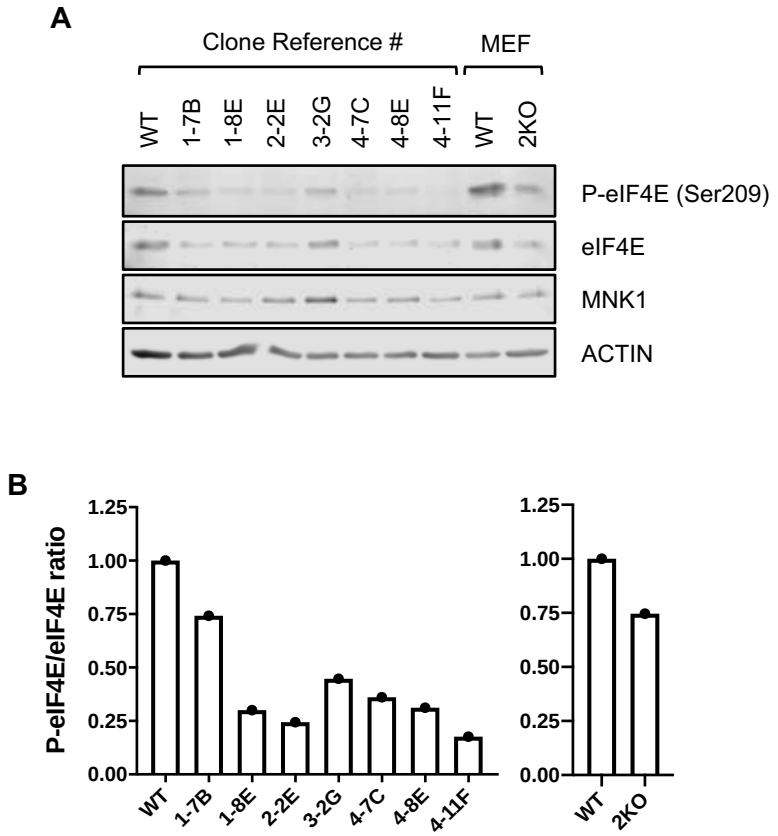

Figure 4-4: Levels of P-eIF4E in 3T3-L1-2KO clones.

(A) Cell lysates of 3T3-L1-2KO pre-adipocyte clones were collected and analysed by SDS-PAGE using the indicated antibodies (n=1). (B) The ratio of P-eIF4E/eIF4E from (A) was quantified, relative to day WT.

Assessment of 3T3-L1-2KO differentiation potential

With the successful generation of 3T3-L1-2KO clones, it was hypothesised that the MNK2 protein may positively regulate adipogenesis by a mechanism(s) that is independent of its kinase activity. To assess the role of MNK2 in adipogenesis, a selection of the homozygous (*Mknk2*$^{-/-}$) KO clones were subjected to adipogenic induction and the extent of their differentiation was assessed by ORO staining. As summarised in Figure 4-5, there was considerable heterogeneity and therefore clones were classified into one of four categories: *non-responsive, impaired, normal* and *enhanced.*

Forty percent of clones were categorised as *non-responsive* (1-6B, 1-8E, 3-2G and 4-8F) as they failed to undergo any morphological change in response to adipogenic induction (Figure 4-5A). Cells in these populations retained fibroblast-like cell morphology and consequently, failed to accumulate lipid (Figure 4-5B). It was suggested that these clones have a major defect in responding to the hormonal signals responsible for inducing the adipogenic program.

Twenty percent of clones (1-7B and 4-8E) were categorised as *impaired* since a significant proportion of cells exhibited non-responsive fibroblast-like morphology, with only a small proportion of cells exhibiting typical adipocyte characteristics (Figure 4-5A). As a result, only a small proportion of cells accumulated lipid and even this was considerably decreased (Figure 4-5B).

In contrast, 20% of clones (2-11D and 4-11F) were categorised as *normal* since almost the entire cell population developed typical and extensive adipocyte characteristics and accumulated comparable levels of lipid to WT (Figure 4-5A,B). Although differentiation appeared normal in both clones, some distinguishing morphological features were evident: 4-11F adipocytes were tightly packed against each other, whereas 2-11D adipocytes were condensed, sparsely populated and carried increased amounts of lipid as if to compensate for an apparently fewer number of cells (Figure 4-5A,B) which may allude to an increase in cell apoptosis.

The final 20% of clones (2-2E and 4-7C) were categorised as *enhanced* since, in addition to exhibiting typical and extensive adipocyte characteristics, they accumulated a greater amount of lipid relative to WT, suggesting their propensity to accumulate lipid was enhanced (Figure 4-5A,B).

Interim Conclusion

There was considerable heterogeneity in the adipogenic propensity of MNK2-KO clones. Clones were classified into one of four categories: *non-responsive, impaired, normal* and *enhanced.* Forty percent of clones were *non-responsive* as they failed to undergo any morphological change; 20% were *impaired* as only a small proportion of cells exhibited typical adipocyte characteristics; 20% were *normal* as they developed extensive adipocyte characteristics and accumulated lipid as expected; and 20% were *enhanced* as they accumulated a greater amount of lipid relative to WT.

A

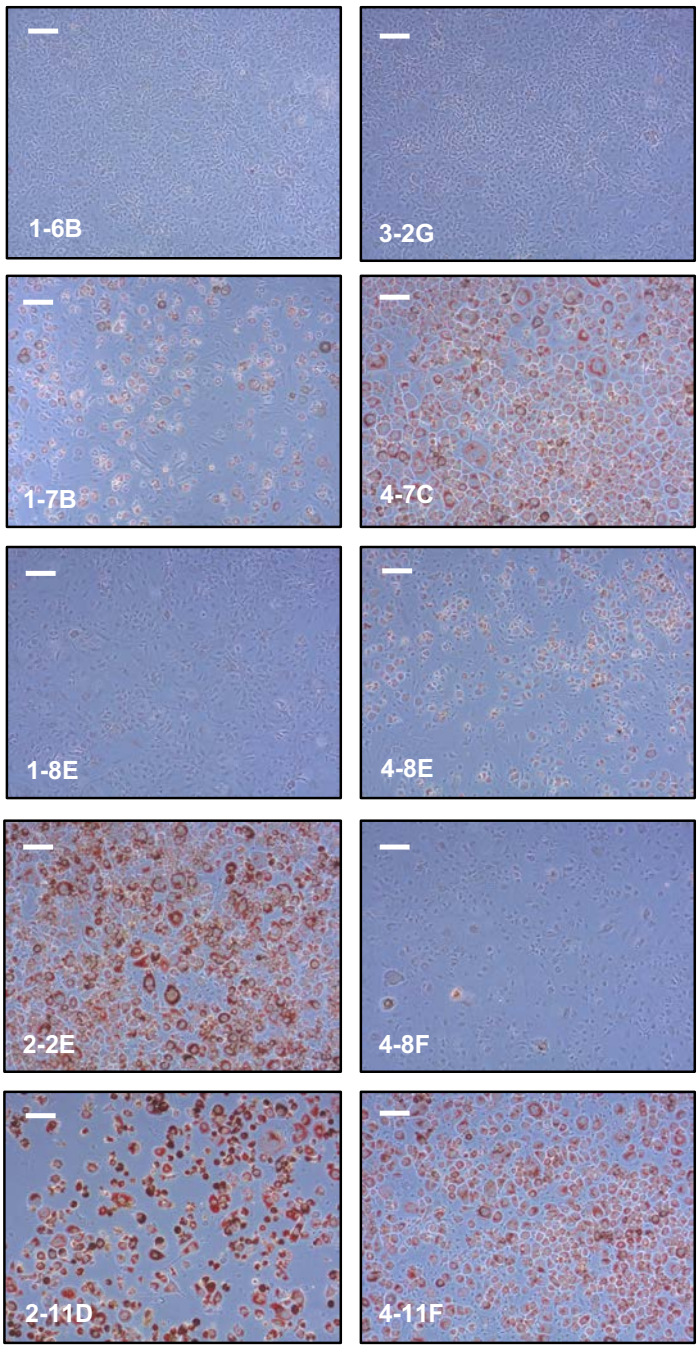
1-6B
3-2G
1-7B
4-7C
1-8E
4-8E
2-2E
4-8F
2-11D
4-11F

B

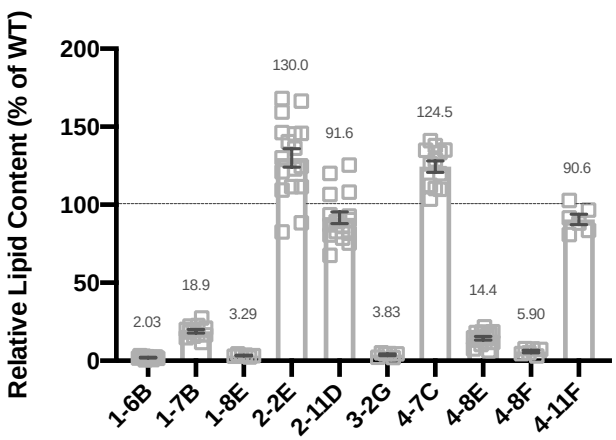
Relative Lipid Content (% of WT)
200
150
100
50
0
2.03
18.9
3.29
130.0
91.6
3.83
124.5
14.4
5.90
90.6
1-6B
1-7B
1-8E
2-2E
2-11D
3-2G
4-7C
4-8E
4-8F
4-11F

Figure 4-5: Comparison of 3T3-L1-2KO adipogenic propensity.

3T3-L1-2KO pre-adipocytes were differentiated with adipogenic induction media and after 9 days stained with ORO to assess lipid accumulation. (A) Representative images are shown, scale bar 0.2 μm. (B) Total stained area was quantified from fields of view from (A) and represented as percentage stained area relative to WT; data are mean ± SEM; individual data values are plotted with mean indicated above.

Effect of clonal selection on adipogenic propensity

The widely-varying phenotypes of 3T3-L1-2KO clones meant that conflicting inferences could be made regarding the function of MNK2, making it difficult to discern its role in adipogenesis. It is known that the adipogenic propensity of 3T3-L1 cells is impaired by high growth confluence and cell passage. Given the CRISPR-Cas9 process of propagating single-cell colonies was conducive to both of these conditions, it was hypothesised that the wide-ranging phenotypes of 3T3-L1-2KO clones may be attributed to this.

To assess this, a heterogenous population of 3T3-L1 cells was serially diluted and subsequently propagated to obtain a single-cell colony (CL). The CL colony was differentiated alongside the original heterogenous 3T3-L1 (WT) population and adipogenic propensity was compared by assessing the expression of adipogenic factors by Western blot (Figure 4-6A). There were no marked or sustained differences in the expression of C/EBPβ, C/EBPδ, C/EBPα or PPARγ between the CL and WT populations, with the exception of slightly elevated C/EBPδ levels and slightly reduced C/EBPα and PPARγ levels on Day 3 in CL. Lipid accumulation, as assessed by ORO staining was not significantly affected in the CL population, although it did trend lower (Figure 4-6B,C). Notably, lipid accumulation was uniform amongst CL adipocytes, whereas it was more heterogenous in WT adipocytes, consistent with the fact that CL adipocytes were derived from a single-cell (Figure 4-6B). Together, these findings suggest that clonal isolation of single-cell colonies is not detrimental to adipogenic propensity and therefore, is unlikely to explain the wide-ranging phenotypes of 3T3-L1-2KO clones. Nevertheless, these findings allude to the fact that slight variations in transcription factor expression and lipid accumulation can occur between cell populations that have been clonally selected. This is likely attributable to the intrinsic genetic variation that exists in the original heterogenous cell line. Thus, it is hypothesised the adipogenic properties of clonally-derived cell populations are constrained to the inherent characteristics of the single-cell that was initially isolated. It was suggested that this so-called *clonal-selection hypothesis* may be responsible for the widely-varying phenotypes of 3T3-L1-2KO clones.

Interim Conclusion

The clonal isolation of single-cell colonies is not detrimental to adipogenic propensity and is unlikely to explain the wide-ranging phenotypes of 3T3-L1-2KO clones. Given the variation in transcription factor expression and lipid accumulation, it is proposed that adipogenic properties of clonally-derived cell populations are constrained to the inherent characteristics of the single-cell that was initially isolated. This so called *clonal-selection hypothesis* may be explain the wide-ranging phenotypes of 3T3-L1-2KO clones.

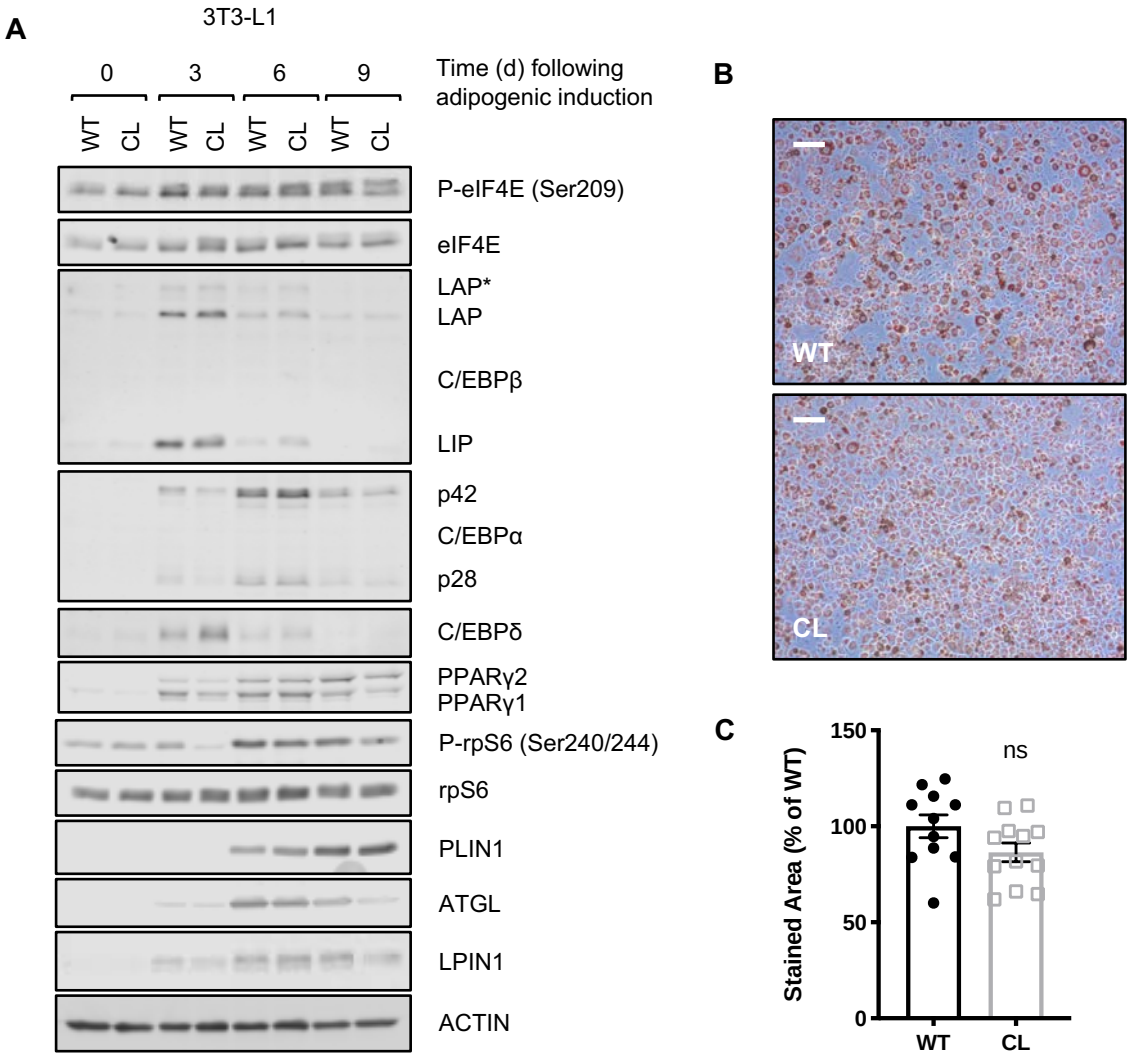

Figure 4-6: Effect of clonal derivation on 3T3-L1 adipogenic propensity.

Non-clonal (WT) and clonally derived (CL) 3T3-L1 pre-adipocytes were differentiated with adipogenic induction media. (A) Cell lysates were harvested at the indicated times and analysed by SDS-PAGE using the indicated antibodies (n=1). (B) Day 9 differentiated adipocytes were stained with ORO to assess lipid accumulation; representative images are shown, scale bar 0.2 µm. (C) Total stained area was quantified from 12 different fields of view from (B) and is represented as percentage stained area relative to WT; data are mean ± SEM; individual data values are plotted (n=2); unpaired t-test (*P < 0.05 **P < 0.01 ***P < 0.001).

Effect of CRISPR-Cas9 methodology on adipogenic propensity

The *clonal selection hypothesis* was subsequently accepted as the major attributing factor for the widely-varying phenotypes of 3T3-L1-2KO clones. However, to support this hypothesis, other existing contributing factors had to be considered. Although propagating single-cell colonies did not adversely affect adipogenic propensity (Figure 4-6), other CRISPR-Cas9 processes, namely vector transfection and FACS, may adversely affect adipogenic propensity. To assess this, clones that had been through CRISPR-Cas9 vector transfection and FACS but had retained *Mknk2*$^{+/+}$ expression were analysed. Two such clones, 1-9F and 2-5B, identified from the screening of 3T3-L1-2KO clones (Figure 4-3, Table 4-1) were differentiated alongside CL pre-adipocytes and the expression of adipogenic transcription factors was assessed by Western blot (Figure 4-7A).

P-eIF4E levels in 1-9F and 2-5B were equivalent to CL, confirming their *Mknk2*$^{+/+}$ genotype. In 2-5B, the expression of C/EBPβ, C/EBPδ, C/EBPα, PPARγ and down-stream targets FABP4 and PLIN1 was not affected with respect to CL, whilst ATGL and LPIN1 were slightly elevated (Figure 4-7A). Crucially, lipid accumulation, as assessed by ORO staining, was not significantly affected (Figure 4-7B,C). In 1-9F, although mostly equivalent to CL levels, there was variability in the expression of C/EBPβ, C/EBPα and PPARγ, which were all slightly reduced, and C/EBPδ which was elevated on Day 3. The reduced expression of these factors likely accounts for the reduction in FABP4 and LPIN1 (Figure 4-7A). P-rpS6 levels in 1-9F and 2-5B were unaffected, suggesting that the expression of adipogenic factors was not likely attributable to altered mTORC1 signalling. Despite these variances, there was no significant differences in lipid accumulation in 1-9F or 2-5B with respect to CL (Figure 4-7B,C), suggesting CRISPR-Cas9 processes do not adversely affect 3T3-L1 adipogenic propensity and are unlikely to explain the wide-ranging phenotypes of MNK2-KO clones.

Interim Conclusion

CRISPR-Cas9 processes do not adversely affect 3T3-L1 adipogenic propensity or lipid accumulation and therefore, are unlikely to explain the widely-varying phenotypes of MNK2-KO clones.

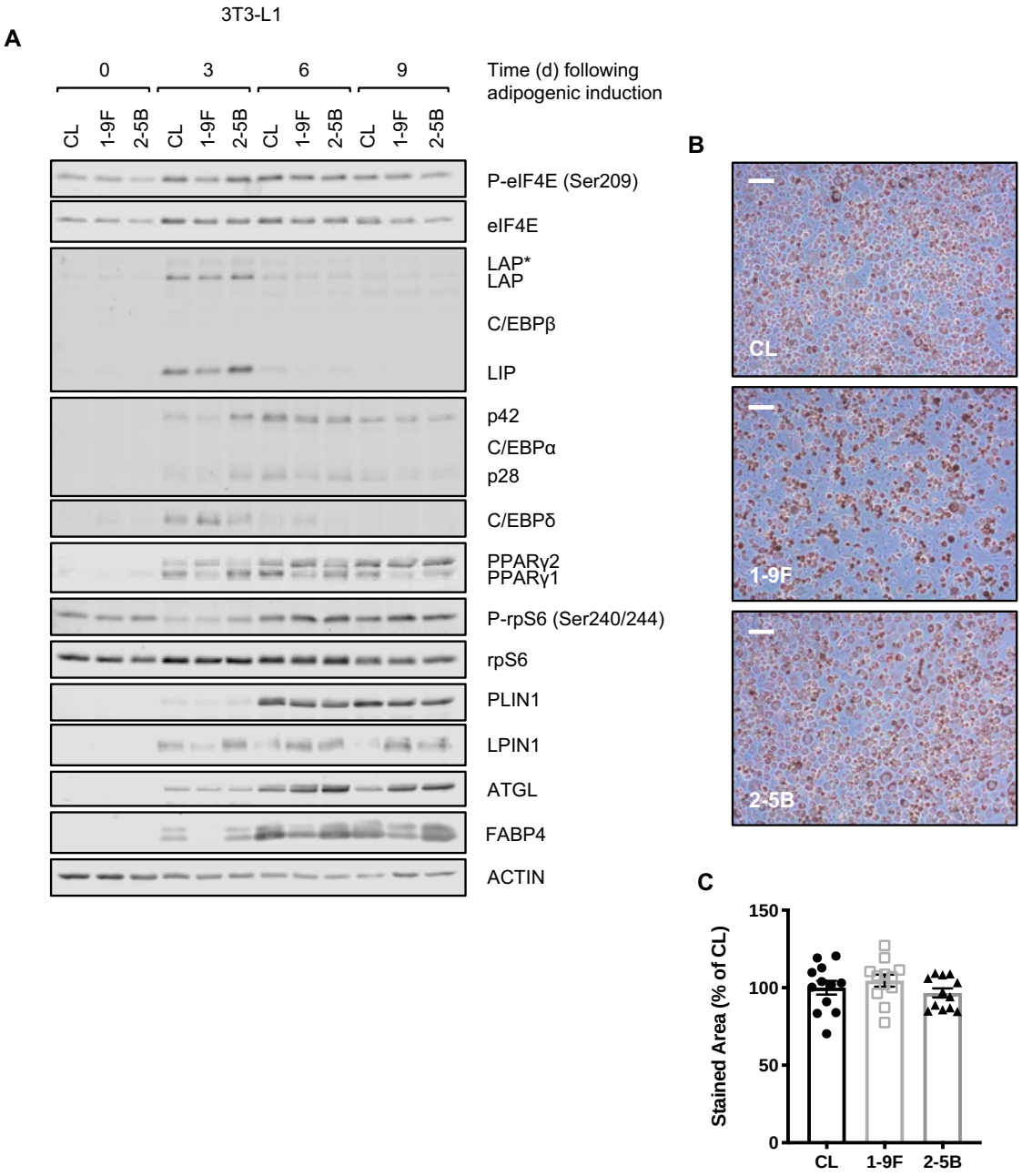
A
3T3-L1
0
3
6
9
Time (d) following adipogenic induction
CL
1-9F
2-5B
P-eIF4E (Ser209)
eIF4E
LAP*
LAP
C/EBPβ
LIP
p42
C/EBPα
p28
C/EBPδ
PPARγ2
PPARγ1
P-rpS6 (Ser240/244)
rpS6
PLIN1
LPIN1
ATGL
FABP4
ACTIN
B
CL
1-9F
2-5B
C
Stained Area (% of CL)
150
100
50
0
CL
1-9F
2-5B

Figure 4-7: Effect of CRISPR-Cas9 methodology on 3T3-L1 adipogenic propensity.

3T3-L1-2KO pre-adipocyte lines 1-9F and 2-5B, identified as retaining WT *Mknk2* expression, were differentiated alongside the clonally-derived (CL) pre-adipocyte line. (A) Cell lysates were harvested at the indicated times and analysed by SDS-PAGE using the indicated antibodies (n=1). (B) Day 9 differentiated adipocytes were stained with ORO to assess lipid accumulation; representative images are shown, scale bar 0.2 μm. (C) Total stained area was quantified from 12 different fields of view from (B) and is represented as percentage stained area relative to CL; data are mean ± SEM; individual data values are plotted (n=2); unpaired t-test (*P < 0.05 **P < 0.01 ***P < 0.001).

Analysis of CRISPR-Cas9 off-targets induced by sgRNAs

The targeting specificity of Cas9 is tightly controlled by the 20 nt sgRNA sequence and the protospacer adjacent motif adjacent to the target sequence; however, potential off-target cleavage can still occur on DNA sequences with even three- to five bp mismatches [281,284–289]. It was hypothesised that off-target Cas9 cleavage may be responsible for the wide-ranging phenotypes of 3T3-L1-2KO clones. The potential for off-target effects induced by Cas9 was heightened given that two sgRNAs were used in the targeting strategy, thereby multiplying the potential for such events. In the case of SpCas9, ~98% of sgRNAs targeting human exons and promoters have at least one off-target site with three or fewer mismatches [290] and it is these sites that are significantly more likely to be cleaved than more dissimilar sites [284,286,288]. Off-target effects of the Cas9 nuclease can be predicted computationally on the basis of sgRNA sequence homology to the target genome [291]. Potential off-targets of sgRNA *Mknk2* E4 and E5 were predicted using *in silico* analysis (crispor.tefor.net). Surprisingly, only a small number of potential off-targets were identified in exonic regions, the majority falling within intergenic or intronic regions (Appendices 13 and 14).

Table 4-2: sgRNA off-targets as predicted *in silico*.

	Gene	Protein Name	Protein Function
***Mknk2* E4**	*Crtc1*	CREB-regulated transcription coactivator 1	Transcriptional coactivator of CREB
	Epsti1	Epithelial-stromal interaction protein 1	Macrophage polarisation
	Iars2	Isoleucine tRNA synthetase	tRNA-amino acid ligation, mRNA translation
	Lhfpl1	Lipoma HMGIC fusion partner-like 1	Translocation partner associated with benign adipose tumours
	Notch2	Neurogenic locus notch homolog 2	Differentiation and development
	Phf13	PHD finger protein 13	Chromosome condensation during mitosis
	Wrnip1	Werner helicase-interacting protein 1	Replication fork complex and modulation of DNA polymerase δ activity
	Fanca	Fanconi anaemia group A protein homolog	DNA repair
***Mknk2* E5**	*Chrac1*	Chromatin accessibility complex protein 1	Chromatin re-organisation
	Arpc3	Actin-related protein 2/3 complex subunit 3	Actin polymerisation
	Stab2	Stabilin-2	Scavenger receptor
	Slc18a2	Synaptic vesicular amine transporter	Synaptic transport of amine neurotransmitters
	Slc1a2	Excitatory amino acid transporter 2	Amino acid transport of glutamate and aspartate
	Tgm4	Protein-glutamine gamma-glutamyltransferase 4	Reproductive biology

The majority of sgRNA off-targets falling within exonic regions were identified in genes that are not directly implicated in adipose function (Table 4-2). For example, protein-glutamine gamma-glutamyltransferase 4 (*Tgm4*) performs specific functions in reproductive biology [292], whilst epithelial-stromal interaction protein 1 (*Epsti1*) is involved in determining macrophage polarisation [293]. CREB-regulated transcription coactivator 1 (*Ctrc1*), as its name suggests, is an important co-activator of CREB but is almost exclusively expressed in the brain [294]. Synaptic vesicular amine transporter (*Slc18a2*) is involved in vesicular transport of neurotransmitters [295], whereas lipoma HMGIC fusion partner-like 1 (*Lhfpl1*) is a gene associated with chromosomal translocations in benign adipose tumours (lipomas); however, its function remains elusive and any effects on adipose function are likely to be limited [296,297].

A subset of off-targets, namely *Phf13*, *Chrac1, Wrnip1* and *Fanca* (Table 4-2), regulate mitotic chromosome condensation, chromatin organisation, and DNA replication and repair, respectively [298–301]. Actin-related protein 2/3 complex subunit 3 (*Arpc3*) promotes actin polymerisation in the nucleus, and regulates gene transcription homology-directed repair but not non-homologous end-joining repair, used for Cas9-induced repair of DSB [302]. Stabillin-2 (*Stab2*) is a scavenger receptor implicated in early endocytic pathways that mediates the endocytosis of hyaluronic acid in immune cells [303]. Isoleucine tRNA synthetase (*Iars2*) is responsible for the ligation of isoleucine to cognate tRNAs, whilst excitatory amino acid transporter 2 (*Slc1a2*) mediates the uptake of glutamate and aspartate into cells [304]. Indirectly, the levels of *Iars2* and *Slc1a2* may regulate mRNA translation and protein synthesis. The *Notch* gene family has been implicated in the regulation of differentiation during development, including adipocytes [305,306]. However, it is believed that the control of adipogenesis is a specific function of *Notch1* but not *Notch2* [305], the latter of which was identified as a potential off-target (Table 4-2).

Therefore, it is suggested that the likelihood of exonic sgRNA off-targets directly affecting adipocyte biology are low, given the affected genes are expressed and perform unrelated functions in different tissues. However, it is possible that some exonic off-targets may interfere with adipocyte differentiation by indirectly affecting key cellular processes such as DNA replication, chromatin organisation and mRNA translation. However, it was beyond the scope of this Chapter to perform detailed off-target genomic screening to examine these possibilities.

In addition to the exonic sgRNA off-targets, a considerable proportion were located within intergenic and intronic regions (Appendices 13 and 14). Typically, cleavage in these regions is less likely to result in loss of gene function, given their location outside the coding sequence. However, a recent report suggests that Cas9 cleavage frequently generates large adjacent genomic deletions which are typically undetectable using conventional screening procedures [307]. These deletions apply to all potential cleavage Cas9 events and, hence, possible ramifications include the deletion of large genomic regions and/or adjacent genes. Considering

the number of predicted exonic, intergenic and intronic sgRNA off-targets, the potential for a CRISPR-Cas9 induced genomic deletion(s) to occur cannot be excluded. Whether large genomic deletions or predicted CRISPR-Cas9 off-targets fully account for the heterogeneity in 3T3-L1-2KO phenotypes is difficult to discern, however, it is useful to consider these effects alongside the *clonal selection hypothesis*.

Interim Conclusion

A small number of sgRNA off-targets were identified that fall within exonic regions. The majority were identified in genes that are not directly implicated in adipose function and the likelihood of a direct effect on adipocyte biology was therefore low. In contrast, a considerable number of off-targets were identified in intergenic and intronic regions. Whilst cleavage at these sites is less likely to result in loss of gene function, the possibility of large adjacent genomic deletions cannot be excluded. Off-target effects are unlikely to fully account for the heterogeneity in 3T3-L1-2KO phenotypes but they should be considered alongside the clonal selection hypothesis.

In order to gain a deeper insight, it was necessary to analyse the phenotypes of the different 3T3-L1-2KO categories in more detail.

Analysis of non-responsive 3T3-L1-2KO clone (1-6B)

To begin, the 'non-responsive' 3T3-L1-2KO clone 1-6B was analysed alongside WT (2-5B) 3T3-L1 cells. Two-day post-confluent pre-adipocytes were subjected to adipogenic induction and the expression of adipogenic transcription factors was assessed by Western blot. As a read-out of MNK2 expression, it was surprising to observe equivalent levels of P-eIF4E in 1-6B and WT cells on Day 0 (Figure 4-8A). This could be due to elevated MNK1 activity, perhaps as a result of increased ERK activation or increased basal mTORC1 activity, as indicated by the increase in P-rpS6 levels (Figure 4-8A). Nevertheless, by Day 1 and throughout the remainder of the differentiation program, P-eIF4E levels were reduced in 1-6B cells consistent with the KO of MNK2, as expected (Figure 4-8A).

Whilst C/EBPβ levels were not affected in 1-6B, C/EBPδ levels were decreased on Day 1 and became elevated on Day 6 (Figure 4-8A), suggesting that MNK2 may regulate C/EBPδ expression. Associated with this was a failure to induce the expression of C/EBPα and PPARγ, which alluded to a potential block in cell cycle progression and MCE, given that CHOP, a dominant-negative regulator of C/EBP protein activity, also failed to increase (Figure 4-8A), which was consistent with findings using MNK-I1 (Figure 3-17A). Consequently, there was very little to no expression of FABP4, PLIN1, ATGL and LPIN1 during terminal adipogenesis and no major morphological changes were apparent in the differentiated cells, which failed to accumulate lipid (Figure 4-8B,C). mTORC1 activity typically increases during adipogenesis [308] as observed previously (Figure 3-1B). However, mTORC1 activity, as assessed by P-rpS6, was notably impaired

throughout differentiation in 1-6B cells, probably reflecting their poor adipogenicity and may suggest an underlying defect in these cells to properly differentiate (Figure 4-8A). The poor adipogenicity may reflect the intrinsic capacity of the original clonally-derived cell to differentiate and/or be due to a CRISPR-Cas9 off-target(s) effect.

Interim Conclusion

Non-responsive clones have dysregulated C/EBPδ expression, which was associated with a failure to induce C/EBPα and PPARγ, their down-stream targets, and accumulate lipid. These cells did not undergo any major morphological changes, which may reflect a defect in the intrinsic capacity of the original clonally-derived cell to differentiate.

Analysis of impaired 3T3-L1-2KO clones (1-7B and 4-8E)

Next, two 'impaired' 3T3-L1-2KO clones, 1-7B and 4-8E, were analysed. As expected, P-eIF4E levels were reduced throughout the differentiation program in both clones, indicating MNK2 expression was knocked-out, as expected (Figures 4-9A, 4-10A). The expression of C/EBPβ was reduced on Days 1 and 3 in 1-7B and 4-8E, suggesting MNK2 may regulate C/EBPβ expression, in contrast to the non-responsive clone 1-6B (Figure 4-8A). Interestingly, C/EBPδ expression was dysregulated in 1-7B but not in 4-8E, suggesting differences amongst clones even in the same category. CHOP levels were lower in 1-7B (Figure 4-9A), suggesting a potential cell cycle defect, consistent with impaired clone 1-6B. However, the most distinguishing characteristic of impaired clones was their failure to induce C/EBPα whilst retaining expression of PPARγ (Figures 4-9A, 4-10A). Consequently, the levels of FABP4, LPIN1, ATGL and PLIN1 were lower during terminal adipogenesis (Figures 4-9A, 4-10A), though not to the same extent as non-responsive clone 1-6B (Figure 4-8A).

There were marked morphological changes that were characteristic of adipocytes in both 1-7B and 4-8E; however, these changes were not uniform across the entire cell population, with many cells still retaining fibroblast morphology (Figures 4-9B, 4-10B). As a result, only a small proportion of cells accumulated lipid and, when quantified, this was reflected as a significant reduction in lipid content (Figures 4-9B,C, 4-10B,C). mTORC1 activity, as assessed by P-rpS6, was notably impaired throughout differentiation in 1-7B and 4-8E cells, probably reflecting their poor adipogenicity (Figures 4-9A, 4-10A). The impaired phenotype of clones 1-7B and 4-8E may be partially attributable to the retention of PPARγ expression; PPARγ is able to drive terminal adipogenic gene expression in the absence of C/EBPα [150,151,309], indicating a level of redundancy which is consistent with the fact that C/EBPα and PPARγ co-occupy adjacent sites on the promoters of their target genes [98,99,310,311]. The phenotypes of impaired clones 1-7B and 4-8E are similar to the effect of MNK-I1 treatment at the time of cocktail addition which was attributed to a block in cell cycle progression (Figure 3-17). Therefore, it was hypothesised that MNK2 may regulate aspects of the cell cycle and MCE required for adipogenesis, at least in these clones.

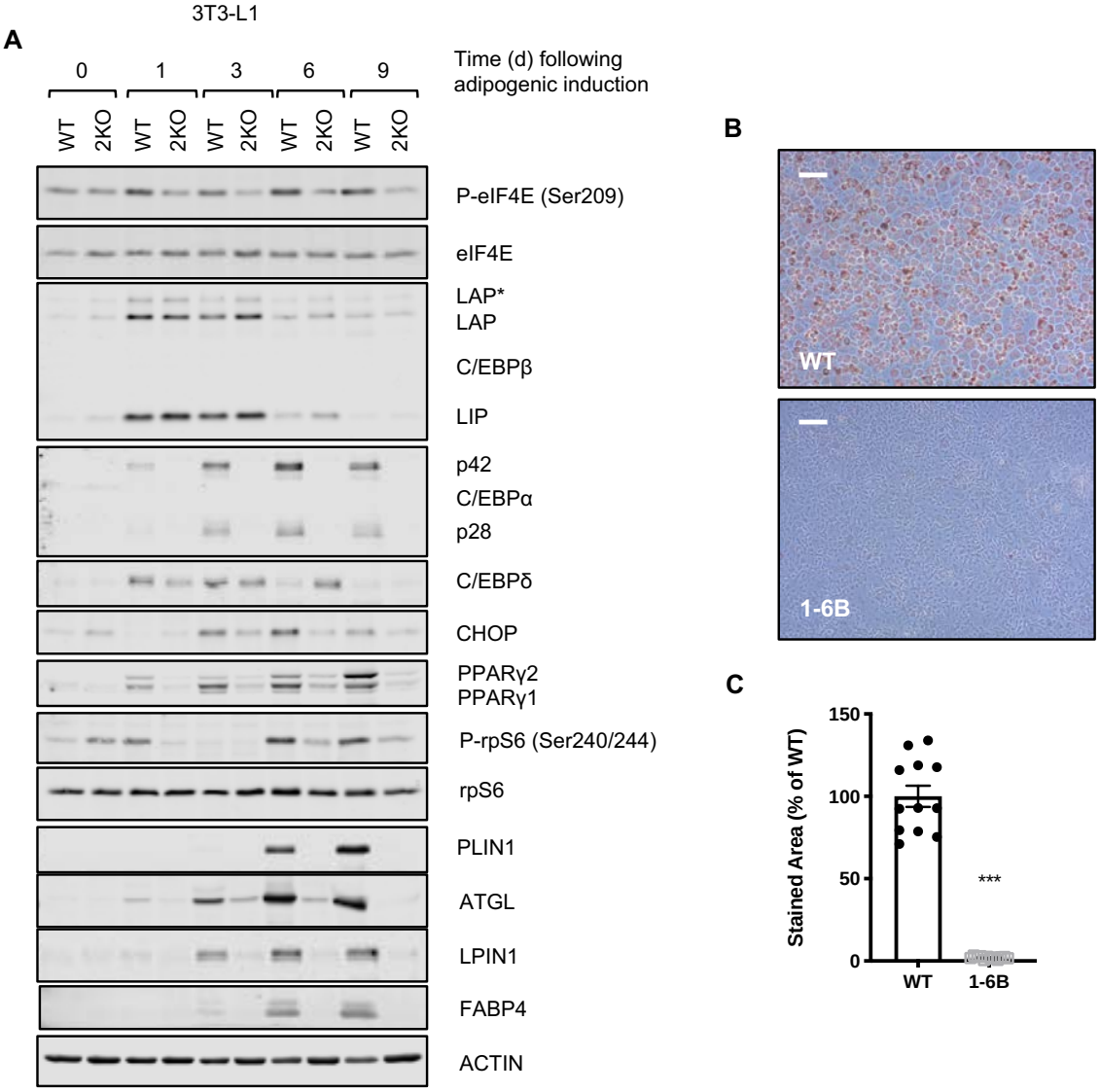

Figure 4-8: Adipogenic differentiation of non-responsive clone (1-6B).

3T3-L1-2KO (1-6B) and WT (2-5B) pre-adipocytes were differentiated with adipogenic induction media. (A) Cell lysates were harvested at the indicated times and analysed by SDS-PAGE using the indicated antibodies (n=1). (B) Day 9 differentiated adipocytes were stained with ORO to assess lipid accumulation; representative images are shown, scale bar 0.2 µm. (C) Total stained area was quantified from 12 different fields of view from (B) and is represented as percentage stained area relative to WT; data are mean ± SEM; individual data values are plotted (n=2); unpaired t-test (*P < 0.05 **P < 0.01 ***P < 0.001).

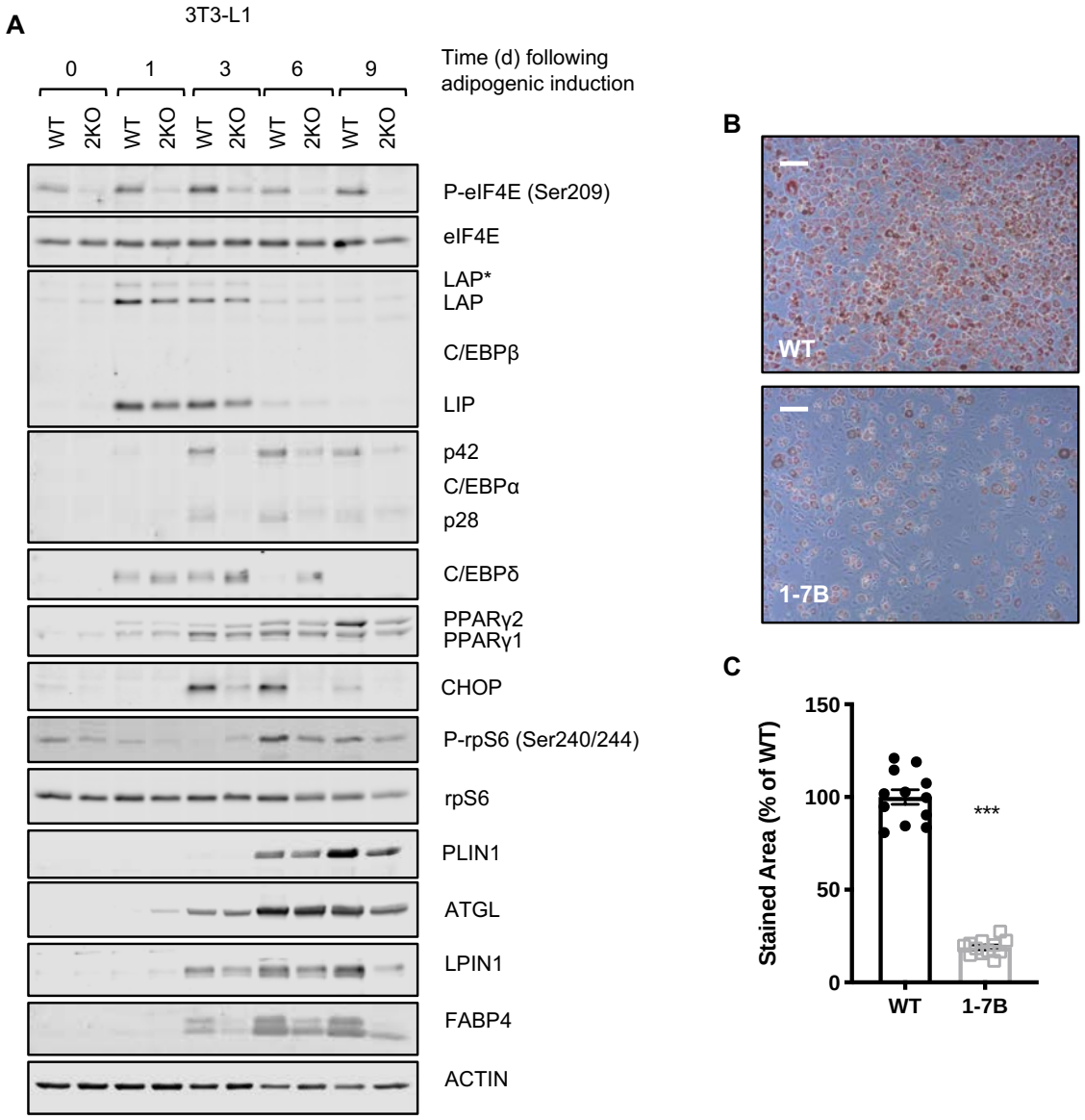

Figure 4-9: Adipogenic differentiation of impaired clone (1-7B).

3T3-L1-2KO (1-7B) and WT (2-5B) pre-adipocytes were differentiated with adipogenic induction media. (A) Cell lysates were harvested at the indicated times and analysed by SDS-PAGE using the indicated antibodies; representative immunoblots are shown (n=3). (B) Day 9 differentiated adipocytes were stained with ORO to assess lipid accumulation; representative images are shown, scale bar 0.2 μm. (C) Total stained area was quantified from 12 different fields of view from (B) and is represented as percentage stained area relative to WT; data are mean ± SEM; individual data values are plotted (n=2); unpaired t-test (*P < 0.05 **P < 0.01 ***P < 0.001).

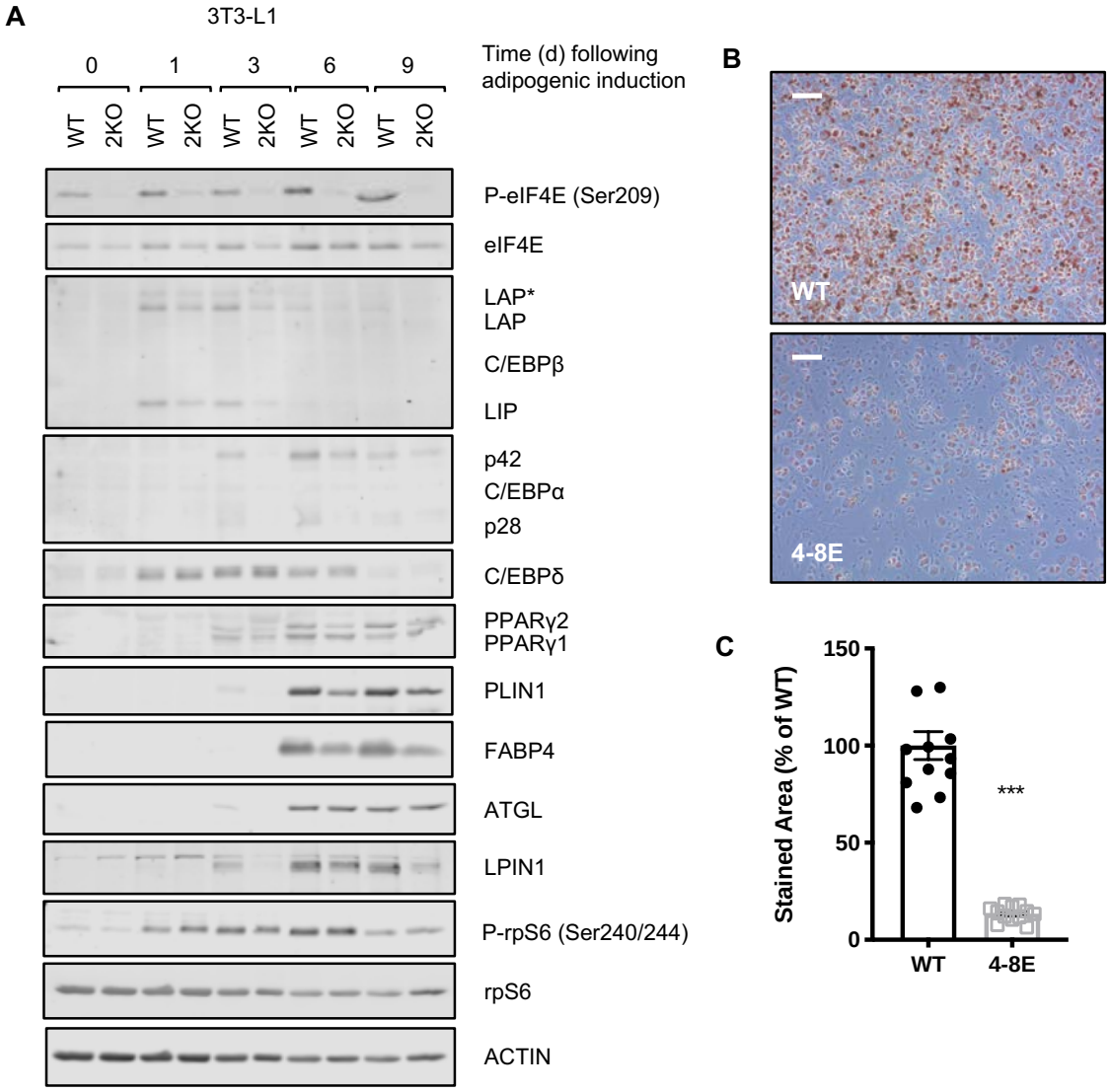

Figure 4-10: Adipogenic differentiation of impaired clone (4-8E).

3T3-L1-2KO (4-8E) and WT (2-5B) pre-adipocytes were differentiated with adipogenic induction media. (A) Cell lysates were harvested at the indicated times and analysed by SDS-PAGE using the indicated antibodies; representative immunoblots are shown (n=2). (B) Day 9 differentiated adipocytes were stained with ORO to assess lipid accumulation; representative images are shown, scale bar 0.2 µm. (C) Total stained area was quantified from 12 different fields of view from (B) and is represented as percentage stained area relative to WT; data are mean ± SEM; individual data values are plotted (n=2); unpaired t-test (*P < 0.05 **P < 0.01 ***P < 0.001).

Interim Conclusion

Impaired clones have reduced expression of C/EBPβ, fail to induce C/EBPα but retain expression of PPARγ. Consequently, the expression of terminal adipogenic proteins was reduced but not completely. Adipocyte morphological changes were not uniform across cell populations, with many cells retaining fibroblast morphology and only a small proportion of cells accumulating lipid. The phenotype is similar to that observed with MNK-I1 treatment, suggesting there may be a cell cycle defect in these clones.

To explore the possibility that MNK2 regulates cell cycle progression and MCE, impaired clone 1-7B was subjected to adipogenic differentiation for a period of 96 h, during which time the expression of adipogenic and cell cycle proteins was assessed by Western blot (Figure 4-11). As expected, P-eIF4E levels were reduced in 1-7B cells and C/EBPα failed to be induced, whilst the expression of PPARγ was retained.

The binding activity of C/EBPβ to DNA is regulated by its phosphorylation on Thr188 (P-C/EBPβ), which primes subsequent phosphorylation on Ser184 and Thr179 [101]. Levels of P-C/EBPβ Thr188 were reduced in 1-7B cells, along with total levels of C/EBPβ, suggesting that although C/EBPβ expression was reduced, its DNA binding activity was not. However, this alone is unlikely to account for the failure to induce C/EBPα expression. Rather, a dysregulation in the cell cycle was hypothesised to be the cause of reduced C/EBPα and therefore, the levels of D-cyclins were assessed. CCND1 levels were basally elevated at 0 h in 1-7B cells and were persistently higher at 18-, 24- and 30 h. Furthermore, the levels of CCND2, CCND3 and $p27^{kip}$ were lower in 1-7B cells. The dysregulation of D-cyclin expression supports an underlying defect in the cell cycle.

To examine the effect of dysregulated D-cyclin expression on mitotic cycling, PI staining was performed across a period of 42 h in 1-7B and WT cells (Figure 4-12A,B). Prior to adipogenic induction (0 h), the proportion of 1-7B and WT cell cycle populations were the same. Concomitant with entry into mitosis after 18 h, there was a shift from G0/1 to S-phase, although the proportion of 1-7B cells in S-phase (5.70%) was significantly lower than in WT cells (18.00%). At 24 h, the transition of cells into S-phase (31.50%) and G2-phase (27.15%) continued in WT cells, however, this transition was significantly blocked in 1-7B cells (S-phase: 13.20%; G2-phase: 8.15%). By 30 h, the proportion of WT cells in S-phase had decreased (11.85%) and was associated with an increased transition of cells into G2-phase (32.30%) or returning to G0/1-phase (47.10%). Since only a small proportion of 1-7B cells had transitioned into S-phase prior to this, a significantly higher proportion of cells were in G0/1-phase (66.85%) at 30 h compared to WT and the proportion of cells transitioning into G2-phase (12.25%) was also significantly lower. By 42 h, WT and 1-7B cell populations had returned to their pre-induction levels, indicating the end of MCE. Together, these results suggest that G1/S cell cycle

progression was impaired in 1-7B cells, similar to the effect of MNK-I1 (Figure 3-21). This suggests MNK2 regulates G1/S transition, however, it is possible that this phenotype is attributable to the clonal selection hypothesis and/or indeed a CRISPR-Cas9 off-target(s).

Interim Conclusion

In impaired clones, the DNA binding activity of C/EBPβ, as assessed by P-Thr188, was not affected, and is therefore unlikely to account for the failure to induce C/EBPα. A cell cycle defect was apparent due to dysregulated expression of D-cyclins which and impaired G1/S phase transition. MNK2 is therefore suggested to regulate G1/S cell cycle progression, however, this phenotype may be attributable to the clonal selection hypothesis and/or a CRISPR-Cas9 off-target(s).

Analysis of normal differentiation 3T3-L1-2KO clones (2-11D and 4-11F)

The phenotypes of non-responsive and impaired clones were contrasted by the phenotype of 'normal' clones 2-11D and 4-11F, in that the expression of C/EBPβ, C/EBPδ, C/EBPα and PPARγ was largely unaffected (Figures 4-13A and 4-14A). As expected, P-eIF4E levels were reduced in both 2-11D and 4-11F. Interestingly, there were some differences in the expression of C/EBPα between 2-11D and 4-11F: C/EBPα levels were elevated in 2-11D on Days 3 and 6, yet reduced on Days 6 and 9 in 4-11F (Figures 4-13A and 4-14A). Notably, the levels of PLIN1, LPIN1 and ATGL reflected the respective expression of C/EBPα, whilst FABP4 was consistently lower in both 2-11D and 4-11F, regardless of C/EBPα and PPARγ levels. The reduction in FABP4 was reflected in a slight (~10%), albeit significant, reduction in lipid accumulation in both clones, as assessed by ORO (Figures 4-13B,C and 4-14B,C). There were also considerable differences in cell morphology, as noted previously (Figure 4-13B and 4-14B), which may be attributed to the clonal selection hypothesis.

Interim Conclusion

Normal clones were characterised by regular expression of C/EBPβ, C/EBPδ, C/EBPα and PPARγ. There were some minor fluctuations in the expression of protein factors and lipid accumulation and distinct differences in cell morphology, however, it is suggested these may be attributable to the clonal selection hypothesis.

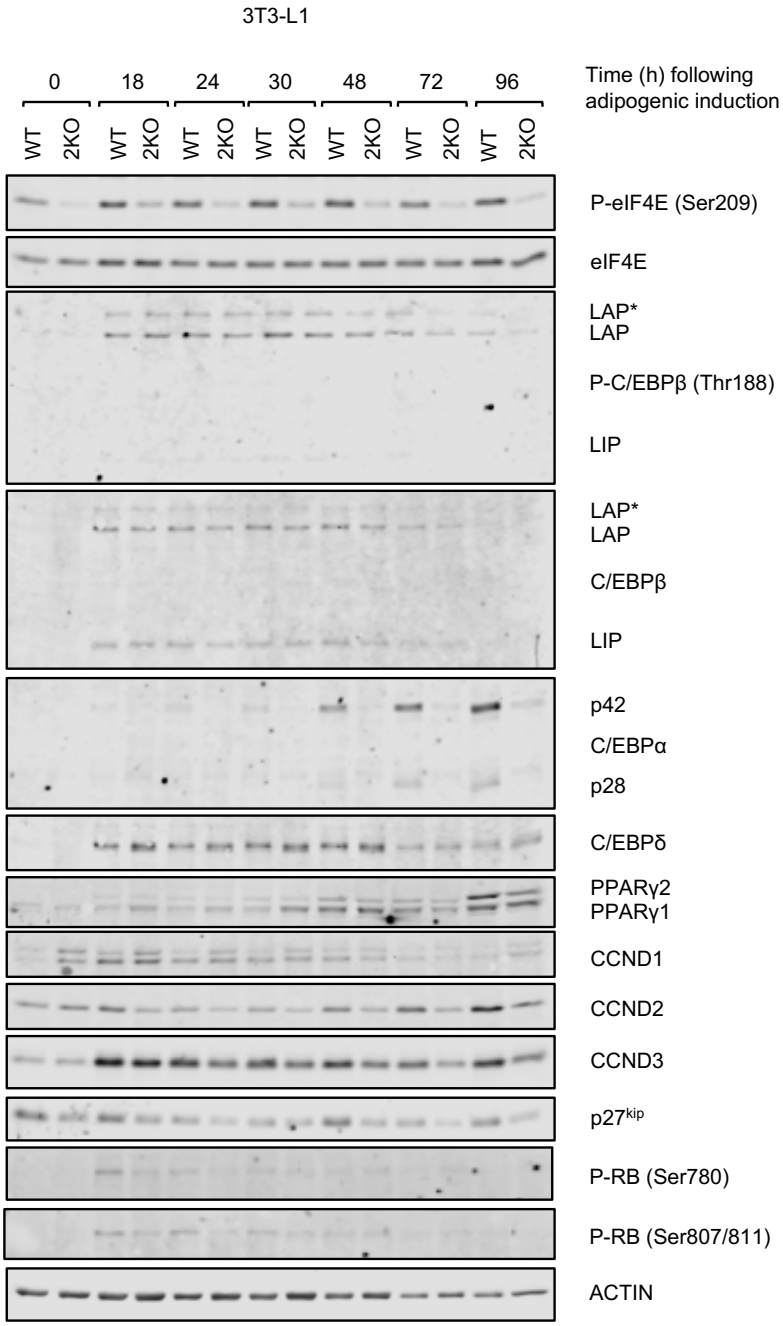

Figure 4-11: Cell cycle factor expression during differentiation of impaired clone (1-7B)

3T3-L1-2KO (1-7B) and WT (2-5B) pre-adipocytes were differentiated with adipogenic induction media. Cell lysates were harvested at the indicated times and analysed by SDS-PAGE using the indicated antibodies (n=1).

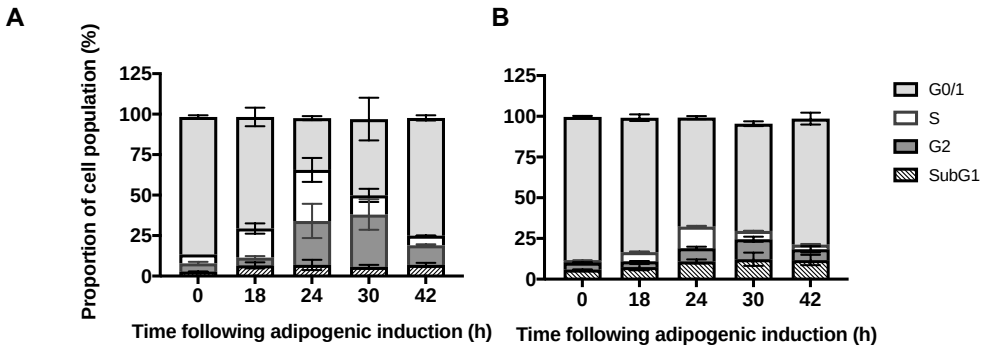

Time (h)	SubG1	G0/1	S	G2
0	2.75	84.90	5.50	5.10
18	6.60	68.90	18.00	4.80
24	6.90	**32.00*** **	**31.50***	**27.15***
30	5.70	**47.10***	11.85	**32.30***
42	6.90	72.80	5.90	12.10

Time (h)	SubG1	G0/1	S	G2
0	5.85	88.20	1.30	4.30
18	7.40	82.50	5.70	3.55
24	10.90	**66.95*** **	**13.20***	**8.15***
30	12.25	**65.85***	5.10	**12.25***
42	11.75	77.45	2.80	6.60

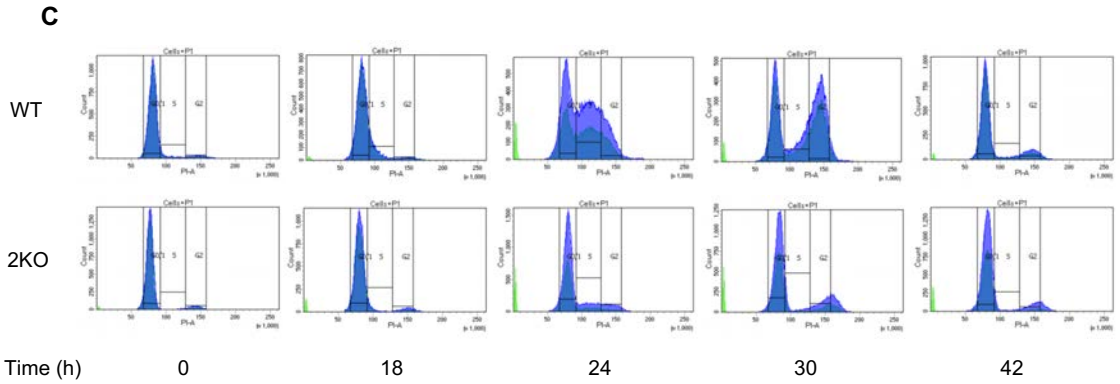

Figure 4-12: Cell cycle analysis of impaired clone (1-7B) during MCE

(A) WT (2-5B) and (B) 2KO (1-7B) pre-adipocytes were differentiated with adipogenic induction media for 42 h, during which cells were harvested at the indicated times, stained with propidium iodide (PI) and analysed by flow cytometry. WT and 2KO cells were gated into Sub G1, G0/1, S and G2 populations, the mean proportions (%) of which are graphed (upper) and detailed in the table (lower). Data are mean ± SEM; n=2; statistically significant differences between WT and 2KO are highlighted; 2-way ANOVA (*P < 0.05 **P < 0.01 ***P < 0.001). (C) Representative flow cytometry panels of WT (upper), 2KO (lower) cells.

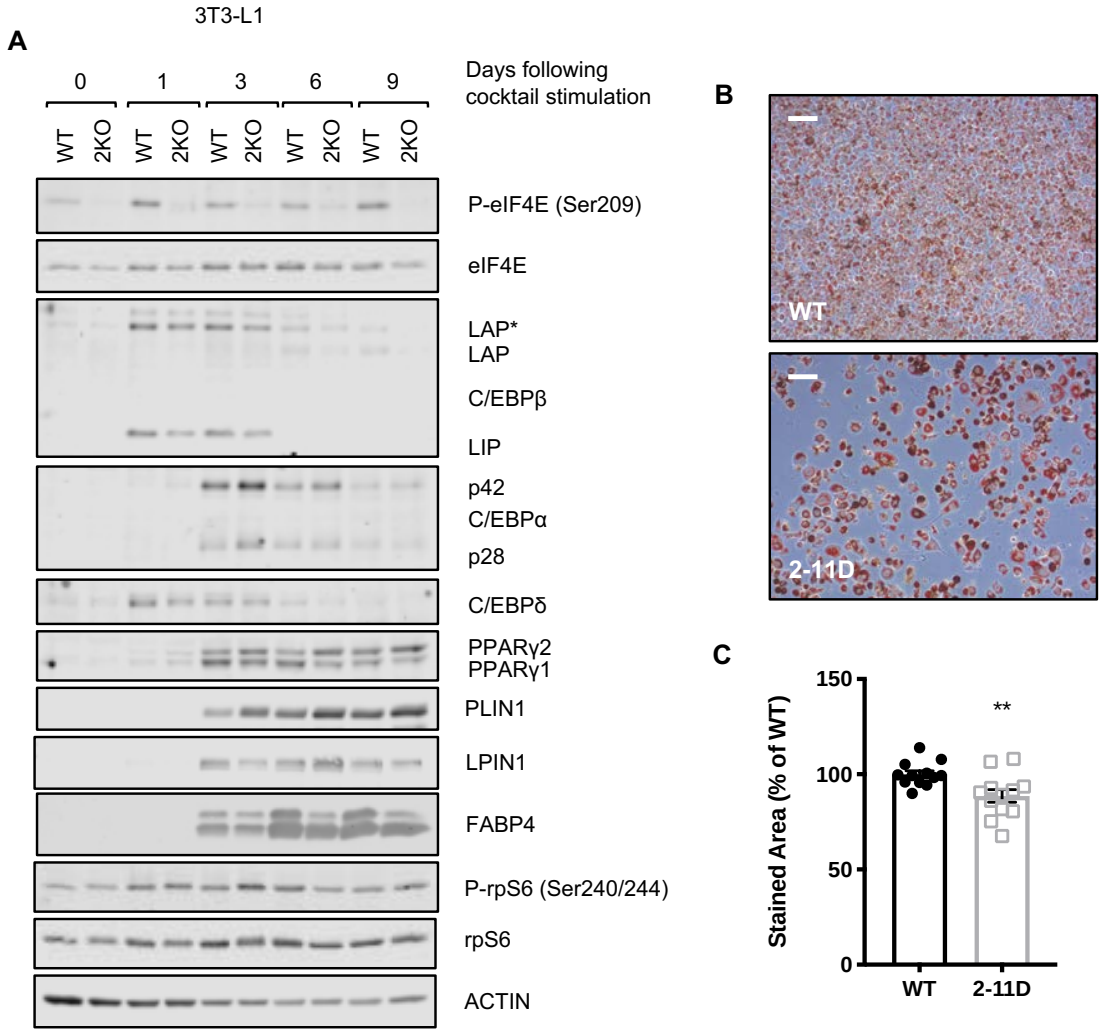

Figure 4-13: Adipogenic differentiation of normal clone (2-11D).

3T3-L1-2KO (2-11D) and WT (2-5B) pre-adipocytes were differentiated with adipogenic induction media. (A) Cell lysates were harvested at the indicated times and analysed by SDS-PAGE using the indicated antibodies; representative immunoblots are shown (n=2). (B) Day 9 differentiated adipocytes were stained with ORO to assess lipid accumulation; representative images are shown, scale bar 0.2 µm. (C) Total stained area was quantified from 12 different fields of view from (B) and is represented as percentage stained area relative to WT; data are mean ± SEM; individual data values are plotted (n=2); unpaired t-test (*P < 0.05 **P < 0.01 ***P < 0.001).

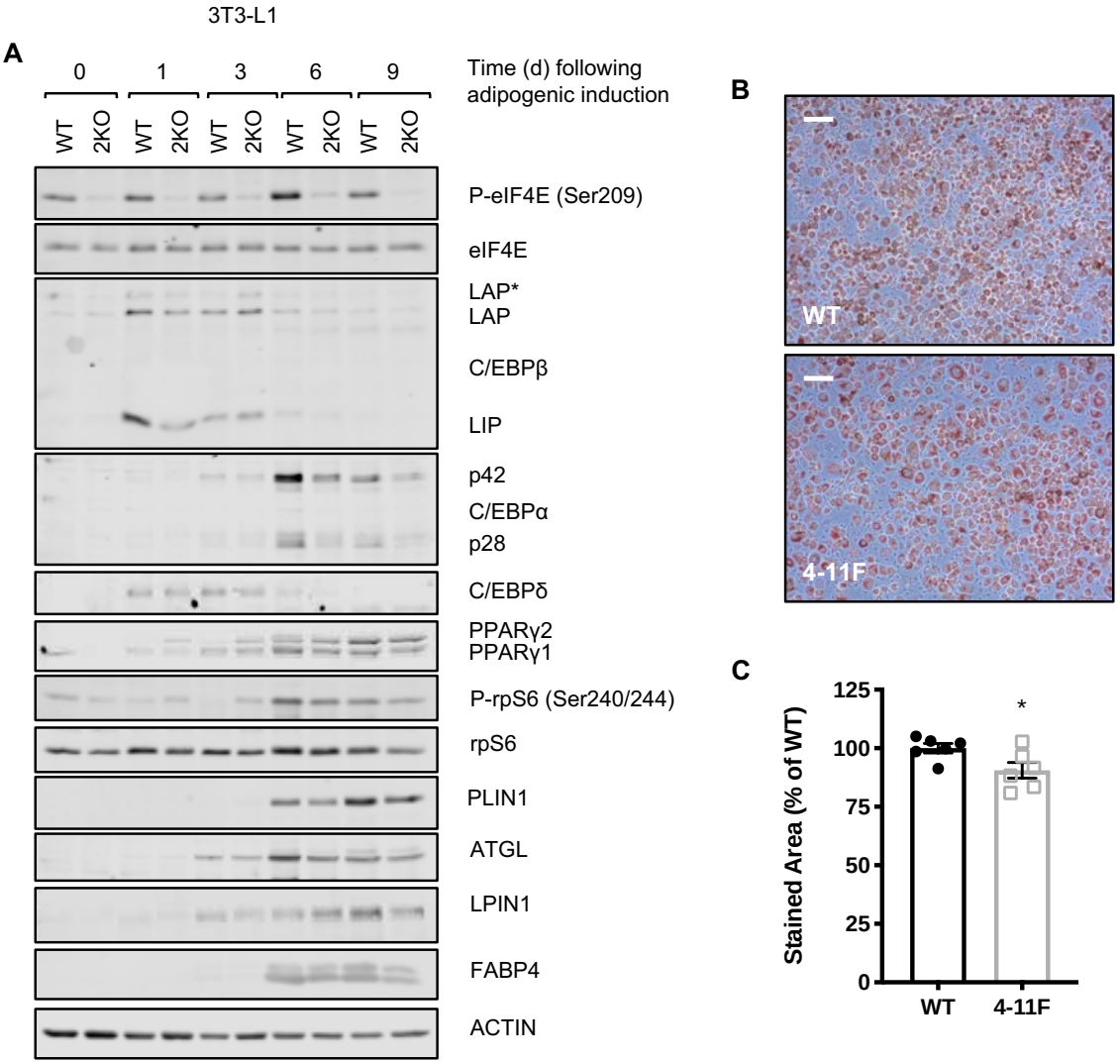

Figure 4-14: Adipogenic differentiation of normal clone (4-11F).

3T3-L1-2KO (4-11F) and WT (2-12C) pre-adipocytes were differentiated with adipogenic induction media. (A) Cell lysates were harvested at the indicated times and analysed by SDS-PAGE using the indicated antibodies; representative immunoblots are shown (n=2). (B) Day 9 differentiated adipocytes were stained with ORO to assess lipid accumulation; representative images are shown, scale bar 0.2 μm. (C) Total stained area was quantified from 6 different fields of view from (B) and is represented as percentage stained area relative to WT; data are mean ± SEM; individual data values are plotted (n=1); unpaired t-test (*P < 0.05 **P < 0.01 ***P < 0.001).

Analysis of enhanced differentiation 3T3-L1-2KO clones (2-2E and 4-7C)

Finally, 'enhanced' clones 2-2E and 4-7C were analysed. As expected, P-eIF4E levels were reduced throughout differentiation, indicating successful KO of MNK2 expression (Figures 4-15A and 4-16A). As observed previously amongst clones in the same category, there were some slight variations in the expression of C/EBPβ and C/EBPδ: in 2-2E, C/EBPβ and C/EBPδ were elevated on Day 1, whereas in 4-7C, they were elevated and reduced, respectively, on Day 3 (Figures 4-15A and 4-16A). As expected, PPARγ remained consistently unaffected in both 2-2E and 4-7C, albeit with some minor variations in C/EBPα expression on Day 3 in both clones (Figures 4-15A and 4-16A). Interestingly, the expression of C/EBPα recovered on day 6 in 4-7C but not 2-2E. Consequently, during terminal differentiation, the levels of PLIN1, ATGL, LPIN1 and FABP4 were modestly reduced in 2-2E (Figures 4-15A and 4-16A). Despite this, a significant increase in lipid accumulation was observed in both 4-7C and 2-2E (~25%), as quantified by ORO staining (Figure 4-15B,C and 4-16B,C). The increase in lipid accumulation is unlikely to be correlated with the expression of C/EBPα and PPARγ. The increase is, however, likely attributable to the clonal selection hypothesis, a reflection of the intrinsic characteristics of the original clonally-selected cell.

Interim Conclusion

Enhanced clones differentiated normally and accumulated significantly more lipid than WT cells. The increase in lipid could not be correlated with the expression of C/EBPα or PPARγ, suggesting it is likely attributable to the clonal selection hypothesis.

Effect of siMknk2 on adipogenesis and lipid accumulation

In light of this analysis, the role of MNK2 in adipogenesis was made very difficult to discern. It was decided that an alternative approach was required to resolve the conflicting phenotypes of 3T3-L1-2KO cells, as it was apparent the clonal derivation of 3T3-L1-2KO cells was obscuring the actual phenotype by restricting analysis to a non-heterogenous population. An siRNA-mediated approach was therefore adopted to allow the heterogeneity of the 3T3-L1 cell-line population to be captured. si*Mknk2* (#1+#2), previously tested for MNK2 knockdown efficacy (Figure 3-8), were transfected into 3T3-L1 cells 72 h prior to adipogenic induction. si*Mknk2* (#1+#2) were re-transfected again on Day 3 of the differentiation program and adipogenic gene expression was assessed by Western blot (Figure 4-17A). As expected, si*Mknk2* transfection decreased both P-eIF4E and *Mknk2* mRNA levels, indicating successful knockdown of MNK2 (Figure 4-17A,F). Notably, the expression of C/EBPβ, C/EBPδ, C/EBPα and PPARγ were not affected by the knockdown of MNK2, nor was the level of P-C/EBPβ, indicating the DNA binding activity of C/EBPβ is not regulated by MNK2 (Figure 4-17A). As C/EBPα and PPARγ expression was normal, the levels of down-stream target genes PLIN1, ATGL and FABP4 were also unaffected (Figure 4-17A), suggesting that MNK2 does not regulate, and is therefore not required for adipogenesis.

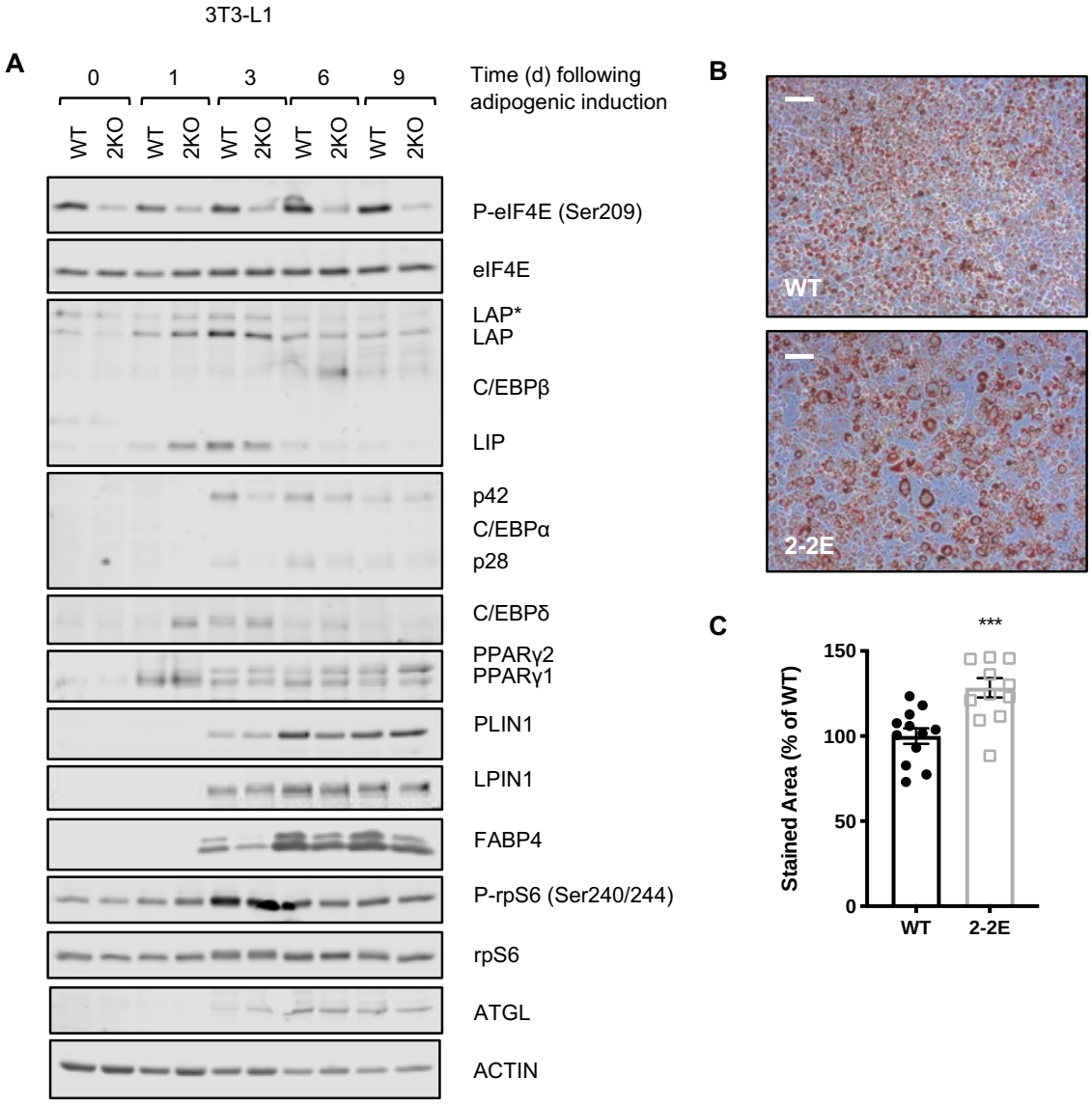

Figure 4-15: Adipogenic differentiation of enhanced clone (2-2E).

3T3-L1-2KO (2-2E) and WT (2-5B) pre-adipocytes were differentiated with adipogenic induction media. (A) Cell lysates were harvested at the indicated times and analysed by SDS-PAGE using the indicated antibodies; representative immunoblots are shown (n=2). (B) Day 9 differentiated adipocytes were stained with ORO to assess lipid accumulation; representative images are shown, scale bar 0.2 μm. (C) Total stained area was quantified from 12 different fields of view from (B) and is represented as percentage stained area relative to WT; data are mean ± SEM; individual data values are plotted (n=2); unpaired t-test (*P < 0.05 **P < 0.01 ***P < 0.001).

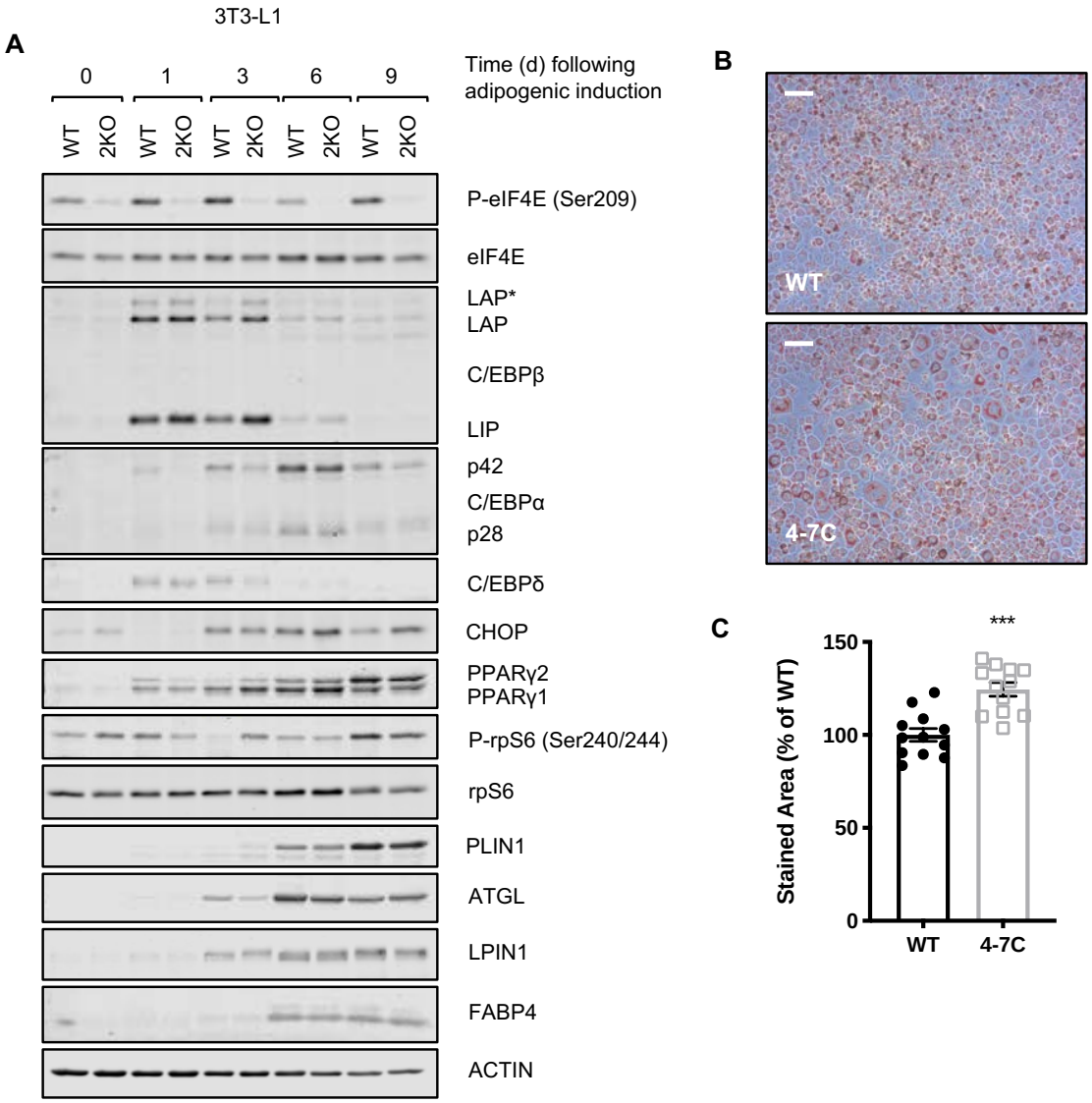

Figure 4-16: Adipogenic differentiation of enhanced clone (4-7C).

3T3-L1-2KO (4-7C) and WT (2-5B) pre-adipocytes were differentiated with adipogenic induction media.(A) Cell lysates were harvested at the indicated times and analysed by SDS-PAGE using the indicated antibodies (n=1). (B) Day 9 differentiated adipocytes were stained with ORO to assess lipid accumulation; representative images are shown, scale bar 0.2 μm. (C) Total stained area was quantified from 12 different fields of view from (B) and is represented as percentage stained area relative to WT; data are mean ± SEM; individual data values are plotted (n=2); unpaired t-test (*P < 0.05 **P < 0.01 ***P < 0.001).

Knock-down of MNK2 did not affect mTORC1 signalling, as assessed by P-rpS6, nor did it alter the expression of CCND1, CCND2 or CCND3 (Figure 4-17A), suggesting that major adipogenic and cell cycle pathways are not regulated by MNK2.

Intriguingly, despite this, lipid accumulation was significantly reduced in si*Mknk2* adipocytes (~40%), as quantified by ORO staining (Figure 4-17C,D) and absorbance of eluted ORO (Figure 4-17E). Since the reduced lipid content could not be directly attributed to a defect in adipogenesis, it was apparent that MNK2 may regulate aspects of lipid metabolism in adipocytes. In terms of metabolism, a decrease in lipid accumulation may be attributable to decreased lipogenesis (lipid synthesis), increased lipolysis (lipid breakdown) or indeed a combination of both. LPIN1 is an enzyme involved in lipogenesis and is responsible for converting phosphatidate to diacylglycerol (DAG) in the synthesis of TAG [312,313] and also acts as a transcriptional activator of genes involved in lipid metabolism [314,315]. Interestingly, LPIN1 expression was reduced by si*Mknk2,* most notably during terminal differentiation (Figure 4-17A), suggesting MNK2 may regulate LPIN1 expression and thereby control adipocyte metabolism.

To examine the robustness and validity of the reduced lipid phenotype, 3T3-L1 cells were individually treated with either si*Mknk2* #1 or #2. As expected, si*Mknk2* #1 and #2 individually decreased P-eIF4E levels, indicating successful knockdown of MNK2 (Figure 4-18A,B). The expression of C/EBPβ, C/EBPδ, C/EBPα and PPARγ was not affected by either si*Mknk2* #1 or #2, nor was the level of P-C/EBPβ (Figure 4-18A,B), as would be expected from the above data. Furthermore, the expression of downstream proteins induced during terminal differentiation (ATGL, FABP4 and GAPDH) were also unaffected, as expected. There was only a minor discrepancy in the effect of si*Mknk2* on PLIN1: its expression was partially reduced by si*Mknk2* #1 on Days 3 and 6 but not by si*Mknk2* #2. Notably, LPIN1 expression was reduced by both si*Mknk2* #1 and #2 and each significantly reduced lipid accumulation, although the effect was greater with si*Mknk2* #2 (~40%) than si*Mknk2* #1 (~30%), as quantified by ORO staining (Figure 4-18C,D); this may be due to the fact that si*Mknk2* #2 more strongly knocks-down MNK2 expression than si*Mknk2* #1 (Figure 3-8C). Nevertheless, these findings strongly implicate MNK2 in the control of adipocyte lipid metabolism, which may impinge on the regulation of LPIN1 expression.

Interim Conclusion

siRNA-mediated knockdown of MNK2 did not affect the expression of adipogenic transcription factors or downstream target genes, suggesting MNK2 does not regulate and is not required for adipogenesis. Knock-down of MNK2 did not affect mTORC1 signalling or the expression of D-cyclins, suggesting major adipogenic and cell cycle pathways are not regulated by MNK2. Despite apparently normal differentiation, there was a significant reduction in lipid accumulation in si*Mknk2* adipocytes, which may be attributed to a reduction in LPIN1 expression.

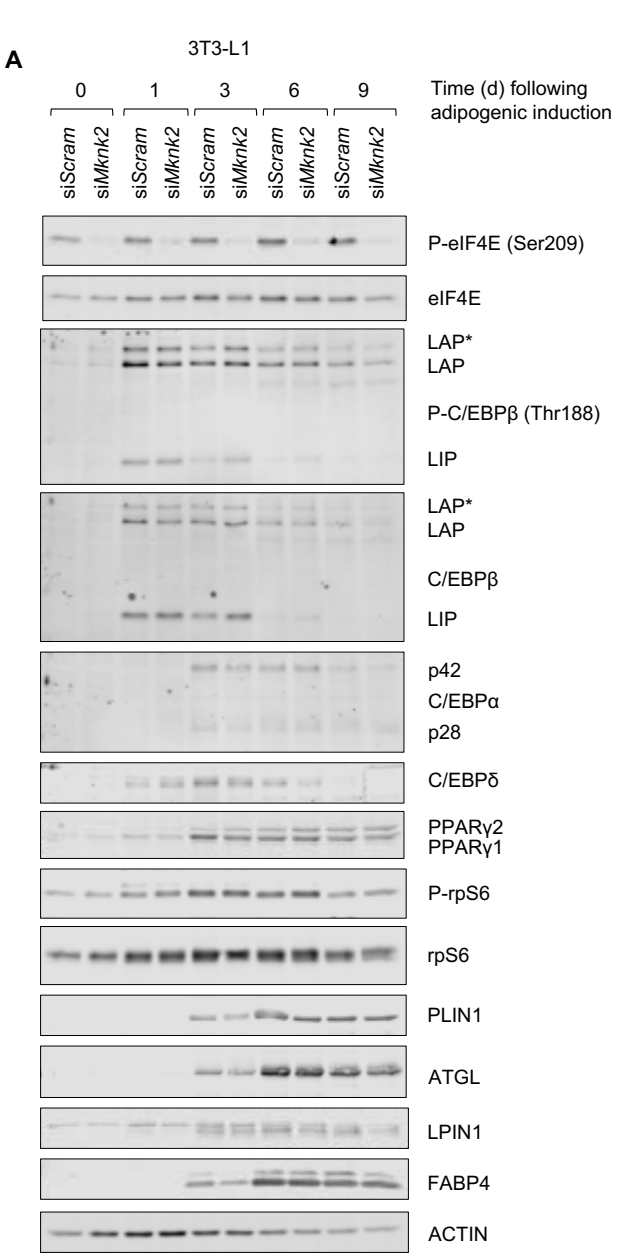
A
3T3-L1
0
1
3
6
9
Time (d) following adipogenic induction
siScram
siMknk2
P-eIF4E (Ser209)
eIF4E
LAP*
LAP
P-C/EBPβ (Thr188)
LIP
LAP*
LAP
C/EBPβ
LIP
p42
C/EBPα
p28
C/EBPδ
PPARγ2
PPARγ1
P-rpS6
rpS6
PLIN1
ATGL
LPIN1
FABP4
ACTIN

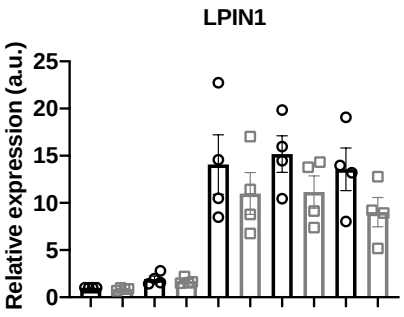
LPIN1
Relative expression (a.u.)
25
20
15
10
5
0

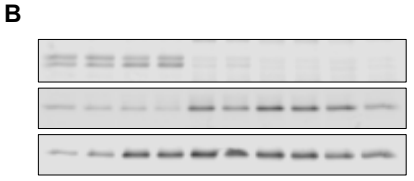
B
CCND1
CCND2
CCND3

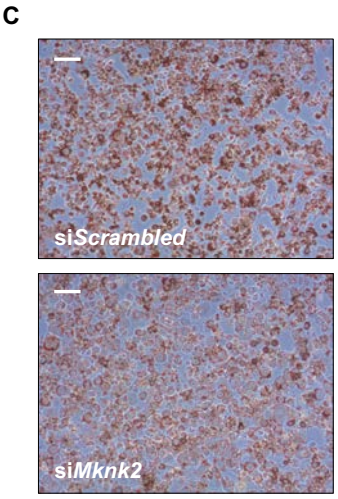
C
siScrambled
siMknk2

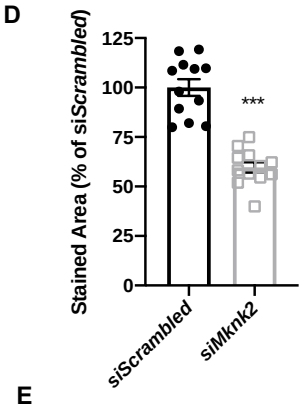
D
Stained Area (% of siScrambled)
125
100
75
50
25
0
***
siScrambled
siMknk2

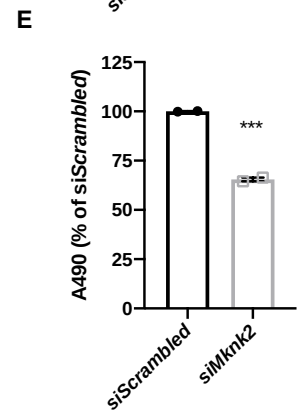
E
A490 (% of siScrambled)
125
100
75
50
25
0
***
siScrambled
siMknk2

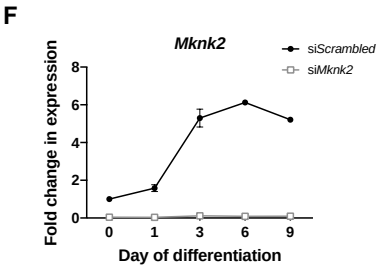
F
Mknk2
siScrambled
siMknk2
Fold change in expression
8
6
4
2
0
0
1
3
6
9
Day of differentiation

Figure 4-17: Effect of *Mknk2* siRNA knockdown on 3T3-L1 adipogenesis.

3T3-L1 pre-adipocytes were pre-transfected with 25 pmol of si*Mknk2* (#1 and #2) or control si*Scrambled*, as indicated 72 h prior to adipogenic induction. (A, B) Cell lysates were harvested at the indicated times and analysed by SDS-PAGE using the indicated antibodies; representative immunoblots are shown (n=4) and the expression of LPIN1 was quantified; data are mean ± SEM. (C) Day 9 differentiated adipocytes were stained with ORO to assess lipid accumulation; representative images are shown, scale bar 0.2 µm. (D) Total stained area was quantified from 12 different fields of view from (C) and is represented as percentage stained area relative to si*Scrambled*; data are mean ± SEM; individual data values are plotted (n=2); unpaired t-test (*P < 0.05 **P < 0.01 ***P < 0.001). (E) ORO eluted from stained cells was quantified by absorbance (A490) and is represented as percentage absorbance relative to si*Scrambled*; data are mean ± SEM; individual data values are plotted (n=2); unpaired t-test (*P < 0.05 **P < 0.01 ***P < 0.001). (F) *Mknk2* mRNA levels were assessed by RT-qPCR at the indicated times. Expression levels were normalised to *Nono* and *Hprt* and represented as fold change with respect to day 0. Data are mean ± SEM; n=3.

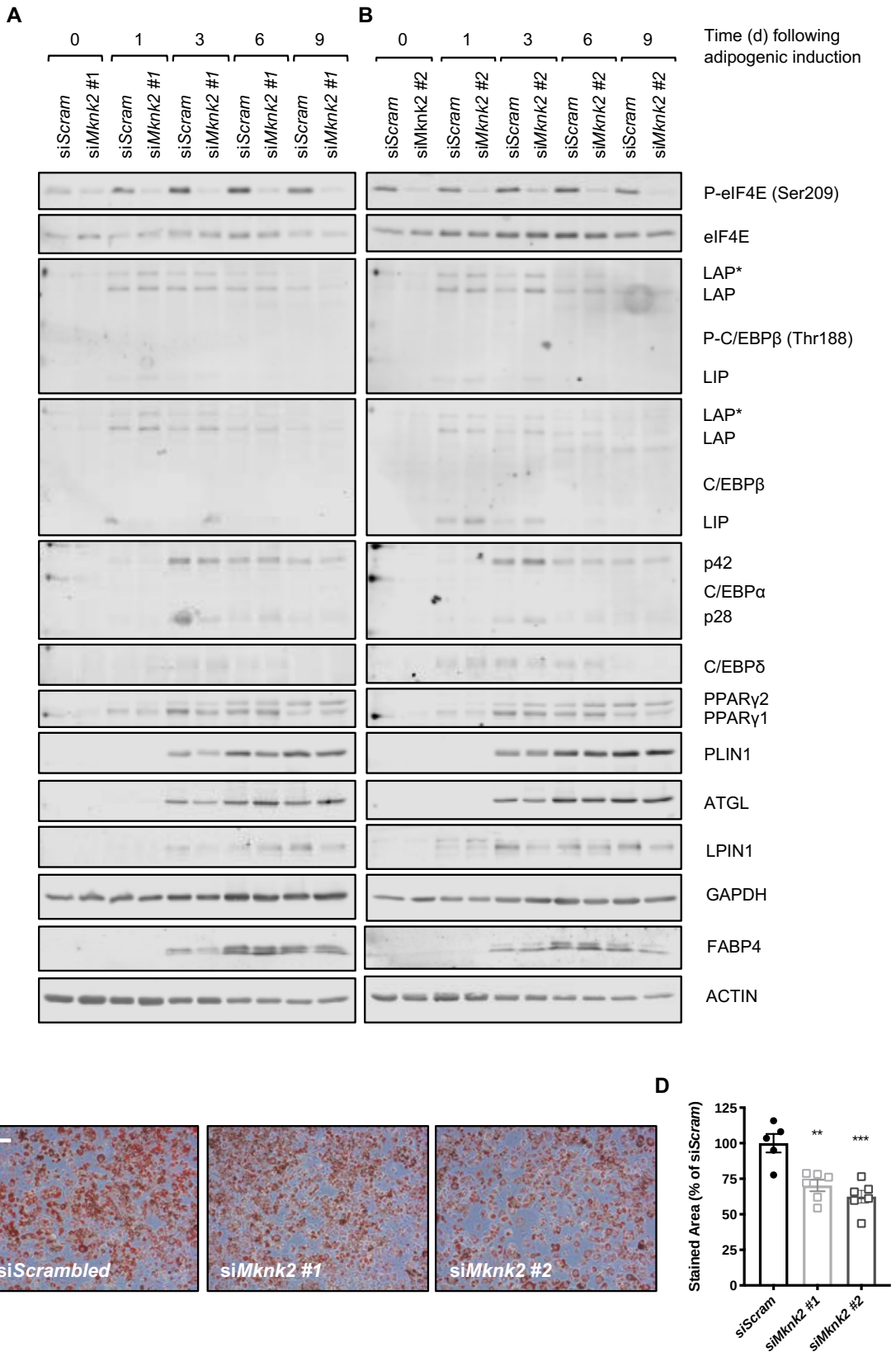
A
B
0
1
3
6
9
Time (d) following adipogenic induction
siScram
siMknk2 #1
siMknk2 #2
P-eIF4E (Ser209)
eIF4E
LAP*
LAP
P-C/EBPβ (Thr188)
LIP
C/EBPβ
p42
C/EBPα
p28
C/EBPδ
PPARγ2
PPARγ1
PLIN1
ATGL
LPIN1
GAPDH
FABP4
ACTIN
C
siScrambled
siMknk2 #1
siMknk2 #2
D
Stained Area (% of siScram)
125
100
75
50
25
0
**
***
siScram
siMknk2 #1
siMknk2 #2

Figure 4-18: Comparison of individual si*Mknk2* on 3T3-L1 adipogenesis.

3T3-L1 pre-adipocytes were pre-transfected with 25 pmol of (A) si*Mknk2* #1 or (B) si*Mknk2* #2, 72 h prior to adipogenic induction with siScrambled as a control. Cell lysates were harvested at the indicated times and analysed by SDS-PAGE using the indicated antibodies (n=1). (C) Day 9 differentiated adipocytes were stained with ORO to assess lipid accumulation; representative images are shown, scale bar 0.2 µm. (D) Total stained area was quantified from 6 different fields of view from (C) and is represented as percentage stained area relative to siScrambled; data are mean ± SEM; individual data values are plotted (n=1); unpaired t-test (*P < 0.05 **P < 0.01 ***P < 0.001).

Discussion

In this Chapter, it was shown that *Mknk2* (MNK2) is the predominant MNK isoform across a range of adipose depots in mice, and that HFD feeding alters its expression, particularly in brown scapular AT (Figure 4-1). Using a CRISPR-Cas9-mediated genomic deletion approach 3T3-L1-2KO cells were successfully generated. However, of the numerous 3T3-L1-2KO lines that were characterised, considerable heterogeneity was evident in their adipogenic propensity; the role of MNK2 in adipogenesis was, therefore, difficult to discern (Figure 4-5). siRNA-mediated knock-down of MNK2 subsequently revealed that MNK2 is not required for adipogenesis, but rather regulates adipocyte lipid metabolism. Adipocytes in which MNK2 was knocked-down by siRNA differentiated normally, but accumulated significantly less lipid than controls which is likely due, at least in part, to a reduction in LPIN1 expression (Figure 4-17).

Comprehensive expression analysis showed that *Mknk2* (MNK2) was highly expressed in omental, gonadal and scapular AT, and predominated over *Mknk1* (MNK1) (Figure 4-1). The expression of gonadal MNK1/2 is consistent with earlier findings [3], suggesting that MNK2 may be important for regulating aspects of adipocyte biology. There was relatively low expression of MNK1/2 in subcutaneous AT (Figure 4-1), suggesting there may be a lower requirement for MNK activity that MNK2 plays a lesser role in this depot.

Considerable heterogeneity was observed amongst the 3T3-L1-2KO clones that were generated using CRISPR-Cas9 (Figure 4-5), which required them to be grouped into different categories, i.e., non-responsive, impaired, normal and enhanced, based on their adipogenic propensity. It was initially hypothesised that the wide-ranging phenotypes were attributable to the clonal isolation of single-cell colonies or CRISPR-Cas9 processes, namely FACS and transfection, however, neither adversely affected 3T3-L1 adipogenic propensity (Figures 4-6 and 4-7).

The widely-differing phenotypes were subsequently hypothesised to be attributed to CRISPR-Cas9 off-target effect(s). However, the likelihood of an off-target cleavage event causing loss of adipocyte function is low, given that the majority of off-targets identified in exonic regions are expressed and perform specific functions in tissues other than adipose (Table 4-2). A large number of potential off-targets were also identified in intergenic and intronic regions (Appendices 13 and 14). Given that two sgRNAs were employed to KO *Mknk2*, the probability of an undesirable cleavage event was increased. Furthermore, with each cleavage event, regardless of whether it is on- or off-target, there is a risk of acquiring large adjacent genomic deletions, often undetectable using conventional screening procedures [307]. These events may result in the deletion of adjacent genes and/or genomic elements, which has the potential to adversely affect adipocyte function. Although the likelihood is low, the effect of CRISPR-Cas9 off-target effects cannot be excluded entirely and may be attributable, to some extent, to the widely-differing phenotype of the 3T3-L1-2KO clones.

Subsequent analysis of 3T3-L1-2KO clones revealed that, even amongst clones in the same category, there was inherent heterogeneity in the expression of adipogenic transcription factors (Figures 4-9, 4-10, 4-13–4-16). This suggests that CRISPR-Cas9 off-targets alone may not sufficiently explain the widely-differing phenotypes. Rather, the *clonal selection hypothesis* was proposed as the leading alternative mechanism by which to explain the widely-differing phenotypes, and assumes inherent heterogeneity (variability) in the original 3T3-L1 cell line population. This variability is normally distributed and determines the inherent adipogenic characteristics of each individual cell in the population. Clonally isolating and propagating single-cell colonies therefore enables the heterogeneity of the population to be captured: 3T3-L1-2KO cells were isolated using clonal selection and their subsequent propagation ensured the population as a whole shared the same genetic and phenotypic characteristics of their predecessors. In this hypothesis, it is possible to imagine how certain intrinsic characteristics may mask and/or distort the interpretation of MNK2 function. This hypothesis is likely sufficient to account for the diversity in 3T3-L1-2KO phenotypes, not only amongst, but within different 3T3-L1-2KO categories. The hypothesis is strengthened when considering that additional diversity may also arise through CRISPR-Cas9 off-targets.

The clonal selection hypothesis identifies a potentially major flaw in the application of CRISPR-Cas9-mediated approaches to studying gene function. This is particularly pertinent to studies involving 3T3-L1 cells where the differentiation phenotype can be highly heterogenous. The fundamental issue with CRISPR-Cas9 lies in the selection of clonal cell populations, which removes the inherent genetic variability of a cell line population, ultimately narrowing interpretations to a single cell. It is increasingly apparent that no two cells are identical, since single-cell analysis has revealed that even in a homogeneous population, there is still cell-to-cell variability [316,317]. It is possible that the isolation of clonally-derived cell populations through CRISPR-Cas9 may lead to erroneous, irrelevant and non-robust interpretations. This is particularly pertinent for cancer cell lines, many of which are highly heterogenous due to high proliferation and mutation rates. Given that CRISPR-Cas9 approaches have been used recently to study adipogenesis in 3T3-L1 pre-adipocytes [276–279] their findings should be interpreted with caution, particularly where data for only one clone is presented.

To resolve the function of MNK2, an alternative siRNA-mediated approach that better captures the inherent heterogeneity of cell populations was used. Knock-down of MNK2 did not affect adipogenesis but rather significantly reduced adipocyte lipid accumulation (Figures 4-17 and 4-18), suggesting that MNK2 regulates adipocyte lipid metabolism, either through decreased lipogenesis, increased lipolysis or indeed a combination of both. Crucially, knockdown of MNK2 reduced the expression of LPIN1, a phosphatidate phosphatase (PAP) enzyme that is responsible for converting phosphatidate to diacylglycerol (DAG) during TAG synthesis [313]. LPIN1 accounts for virtually all PAP activity in adipose tissue [313] and is also involved in the induction

of lipogenic genes [315]. These findings suggest MNK2 may regulate lipogenesis, at least in part, through regulating the expression of LPIN1. These findings should be followed up *ex vivo* using adipose tissue from MNK2-KO mice.

LPIN1 is induced during 3T3-L1 adipogenesis and is thought to be critical for adipocyte development *in vivo* and *in vitro*, as it is required for the expression of PPARγ and C/EBPα [314,318]. LPIN1 is alternatively spliced, producing two isoforms designated LPIN1α and LPIN1β. These isoforms are differentially expressed and exhibit distinct subcellular localisation: LPIN1α is predominantly nuclear and is involved in adipocyte differentiation, whereas LPIN1β is cytoplasmic and has a predominant effect on the induction of lipogenic genes [315]. The expression of PPARγ and C/EBPα was not affected by si*Mknk2* (Figures 4-17 and 4-18) but the expression of LPIN1, especially during terminal adipogenesis, was reduced. Given that LPIN1β is the predominant isoform during the latter stages of adipogenesis [315], it was suggested that MNK2 may promote the expression of LPIN1β either through regulation of alternative splicing or selective mRNA translation. This also raises the possibility that other (metabolic) genes may be similarly regulated by MNK2.

For the first time, it was shown that *Mknk2* (MNK2) expression is differentially expressed (reduced) in adipose tissue on an HFD, most evidently in scapular AT (Figure 4-1). It was suggested that MNK2 expression may therefore be responsive to changes in diet and nutrient composition, which allow it to potentiate changes in adipocyte metabolism. This may help to explain why MNK2-KO mice are protected from HFD-induced weight gain [3]. In light of the abovementioned findings, it is proposed that LPIN1 expression may be reduced in MNK2-KO adipocytes, resulting in decreased lipogenesis and therefore blunting weight gain. Furthermore, given that the greatest differential in MNK2 expression was observed in brown scapular AT, relevant MNK2-mediated metabolic responses may occur in this tissue. Scapular AT has a major function in uncoupling the production of ATP during fatty acid oxidation, which produces heat and thereby 'burns' fat. Promoting the 'browning' of adipose tissue has been recognised as a potential therapeutic strategy to increase energy expenditure and therefore weight loss [319]. Given lipogenesis and lipolysis are reciprocally regulated, it is proposed that the lipolytic activity in scapular AT may be increased in response to the KO of MNK2, thereby increasing the energy expenditure and decreasing adipose tissue mass. Combined, these metabolic changes may sufficiently explain the protection of MNK2-KO mice from HFD-induced weight gain, although follow-up investigation is required.

In conclusion, these findings indicate a role for MNK2 in regulating adipocyte lipid metabolism but not adipogenesis itself. MNK2 promotes lipogenesis independently of its catalytic activity, at least in part by regulating the expression of LPIN1, a key transcriptional activator of lipogenic gene expression. This finding brings us closer to understanding the underlying mechanism(s) that confer protection to MNK2-KO mice from HFD-induced weight gain and sheds new light on the control of cellular metabolism by MNK2 that extend beyond the control of eIF4E phosphorylation.

Chapter 5
MNKs in adipocyte and lipid metabolism

Introduction

Protein phosphorylation is a reversible post-translational modification that is fundamental for cell signalling and the regulation of cell homeostasis. The important catalytic function is mediated by a conserved kinase domain fold, which is highly preserved amongst all protein kinases [52]. Despite this, kinases interact with a surprisingly wide range of binding partners which enable them to perform a range of non-catalytic functions. These include allosterically regulating other kinases and/or proteins, acting as molecular scaffolds to coordinate interactions between different components of signalling pathways, and regulating transcription through interactions with transcription factors or directly with DNA, each of which has been shown to utilise a unique molecular mechanism [52].

Non-catalytic functions are present across all kinase families, including the MAPK family. For example, MAPK-activated protein kinase 2 (MK2) has been shown to interact with the basic helix-loop-helix transcription factor E47 to repress its transactivation activity and modulate gene transcription [320]. ERK2 reportedly acts as a transcriptional repressor by binding to DNA independently of its catalytic activity to repress IFNγ-responsive gene expression [321], whilst in the context of the cell cycle, activated ERK1/2 reportedly dislodges RB from its interaction with Lamin A to promote RB hyper-phosphorylation and cell cycle entry [322]. ERK2 also activates enzymes through allostery: the direct binding of ERK2 to MAPK phosphatase 3 (MKP3) induces a conformational change that markedly enhances MKP3 phosphatase activity, which then inactivates ERK2 [323].

Functional kinase studies are largely concerned with the identification of substrates and understanding the biological response(s) it controls through phosphorylation. Studies are typically facilitated by ATP-competitive kinase inhibitors, which inhibit catalytic kinase activity. However, inhibition of catalytic activity does not always equate to impaired protein activity, since non-catalytic functions can still be performed. It is therefore not surprising that inhibitor and genetic studies can yield vastly different phenotypes (e.g. [324]).

As exemplified in Chapter 3, inhibition of MNK catalytic activity with specific inhibitors did not reduce lipid accumulation, but knock-down of MNK2 expression with siRNA did (Figure 4-17). The fact that adipocytes from MNK2-KO mice failed to increase in size on an HFD [3] supports the hypothesis that non-catalytic functions of MNK2 may be responsible for promoting lipid accumulation, presumably by modulating some aspect(s) of adipocyte metabolism.

The aim of this Chapter was to identify non-catalytic functions of MNK2 pertaining to adipocytes and understand how they may regulate adipocyte metabolism mechanistically.

Results

Adipocytes and the balance of energy metabolism

Broadly speaking, adipocytes are responsible for maintaining whole-body energy homeostasis by balancing the rates of lipid synthesis (lipogenesis) and break-down (lipolysis). Energy balance is achieved, in part, by the regulation of these reciprocal processes by metabolic hormones. Insulin, an anabolic hormone, is elevated upon feeding and promotes the uptake and storage of excess nutrients by activating lipogenic pathways and deactivating lipolysis. Glucagon and other β-androgenic hormones are elevated during fasting and periods of energy demand, and promote the mobilisation of energy stores by activating lipolysis and deactivating lipogenesis.

Lipogenesis is a synthetic process used to store excess nutrients in the form of triacylglycerol (TAG), a stable and compact long-term energy reserve. TAG is synthesised in a series of enzyme-catalysed steps in which three fatty acid (FA) molecules are covalently linked to a glycerol backbone (Figure 5-1). TAG accumulates in so-called 'lipid droplets' which are stabilised by a number of regulatory proteins, most notably, perilipins. FA used in lipogenesis can be acquired *exogenously* from the breakdown of dietary lipids and fat in the small intestine during digestion and/or from the hydrolysis of lipoprotein particles which are synthesised, packaged and delivered into the circulation from the liver. Whilst acting as the key energy trading currency, FA are also key components of signalling pathways and cell membranes. Therefore, in periods of low exogenous FA availability, such as a low-fat diet, it is important for adipocytes to maintain their level of FAs, and this is achieved in a process known as *de novo* lipogenesis (DNL).

In DNL, excess carbohydrates are converted into FAs in a series of enzyme-regulated steps, which are then esterified into TAG (Figure 5-1). It is important to consider that the contribution of *de novo* synthesised FAs is dependent on diet; on a high carbohydrate diet (10% fat; 70% carbohydrate), DNL contributes up to 50% of FAs to plasma lipid, whilst on a typical Western diet (40% fat; 50% carbohydrate), the contribution of DNL to plasma lipids is negligible [325]. It is also important to acknowledge the differences between exogenous and endogenous FA synthetic pathways, and that they do ultimately converge upon TAG synthesis (Figure 5-1). It is becoming increasingly apparent that exogenous and endogenous FAs vary in their composition and consequently can have different biological effects on metabolism [326,327]

In times of energy demand, FAs are sequentially released from TAG by hydrolysis to mobilise energy stores. This process is known as lipolysis and is catalysed by a number of cellular lipases, each exhibiting distinct substrate affinities [328] (Figure 5-1). Adipocyte triacylglycerol lipase (ATGL) has the greatest affinity for TAG and is responsible for hydrolysing the first FA from TAG to produce diacylglycerol (DAG) [328]. Hormone-sensitive lipase (HSL) exhibits high affinity for DAG and is responsible for the hydrolysis of the second FA to produce monoacylglycerol (MAG) [328]. ATGL also exhibits affinity for DAG and can therefore catalyse the second FA hydrolysis

reaction [328]. Monoacylglycerol lipase (MGL), which exhibits affinity only for MAG, hydrolyses the final FA from glycerol [328]. The majority of FAs released from lipolysis are delivered into the circulation for use by energy-demanding tissues for energy production, although a proportion of FAs are re-esterified back into TAG in a process known as 'fatty acid recycling' [329]. The glycerol can readily be used for gluconeogenesis or for energy production via glycolysis.

Effect of MNK2 knockdown on metabolic gene expression

As observed in Chapter 4, MNK2 knock-down decreased the lipid content of adipocytes, suggesting it may regulate an aspect(s) of lipid metabolism (Figure 4-17). To understand which aspect(s) of lipid metabolism was specifically affected by the knockdown of MNK2 and identify pathways that might be subject to its regulation, the expression of genes associated with adipocyte metabolism were assessed by RT-qPCR in differentiating 3T3-L1 pre-adipocytes transfected with si*Mknk2* or si*Scrambled*.

In adipocyte DNL, ATP citrate lyase (*Acly*) catalyses the conversion of citrate to acetyl-CoA which in turn, is converted by acetyl-CoA carboxylase 1 (*Acaca*) to malonyl-CoA, the essential precursor for fatty acid synthase (*Fasn*) which converts it into palmitate (Figure 5-1). *Acly*, *Acaca* and *Fasn*, the rate-limiting enzyme of DNL, were all significantly reduced by si*Mknk2* on Days 6 and 9 (Figure 5-2). This suggests that DNL capacity was significantly reduced by MNK2 knock-down.

A series of enzyme-regulated steps controls the TAG synthetic pathway, in which FFAs become covalently linked to a glycerol backbone (Figure 5-1). Glycerol-3-phosphate acyltransferase (GPAT) enzymes catalyse the addition of the first FFA to glycerol-3-phosphate (G3P), whereas the addition of the second and third FFAs are catalysed by a family of enzymes known as acyl-glycerophosphate acyltransferases (AGPATs) and diacylglycerol-acyltransferases (DGATs), respectively [330]. *Agpat9* (also known as *Gpat3*) is the most relevant GPAT isoform in adipose tissue and catalyses the first of several rate-limiting steps of TAG synthesis [331]. *Dgat1*, and particularly *Dgat2*, are highly expressed in adipose tissue and are responsible for catalysing the final rate-limiting step of TAG synthesis [332,333]. The levels of *Dgat1* and *Dgat2*, but not *Agpat9*, were significantly reduced by si*Mknk2* on Day 6 (Figure 5-2), suggesting the expression of final rate-limiting enzymes of TAG synthesis are regulated by MNK2. A crucial step before the addition of the final FFA involves the conversion of phosphatidate to DAG, which is catalysed by LPIN1 [312]. *Lpin1* levels were significantly reduced by si*Mknk2* on Day 6 (Figure 5-2), consistent with previous results (Figure 4-17). As alluded to previously, LPIN1 is also a transcriptional activator of lipogenic gene expression [315,334] and therefore, it is suggested that the effect of reduced LPIN1 expression may be two-fold: a reduction in the substrate availability for TAG synthesis; and transcriptional down-regulation of lipogenesis.

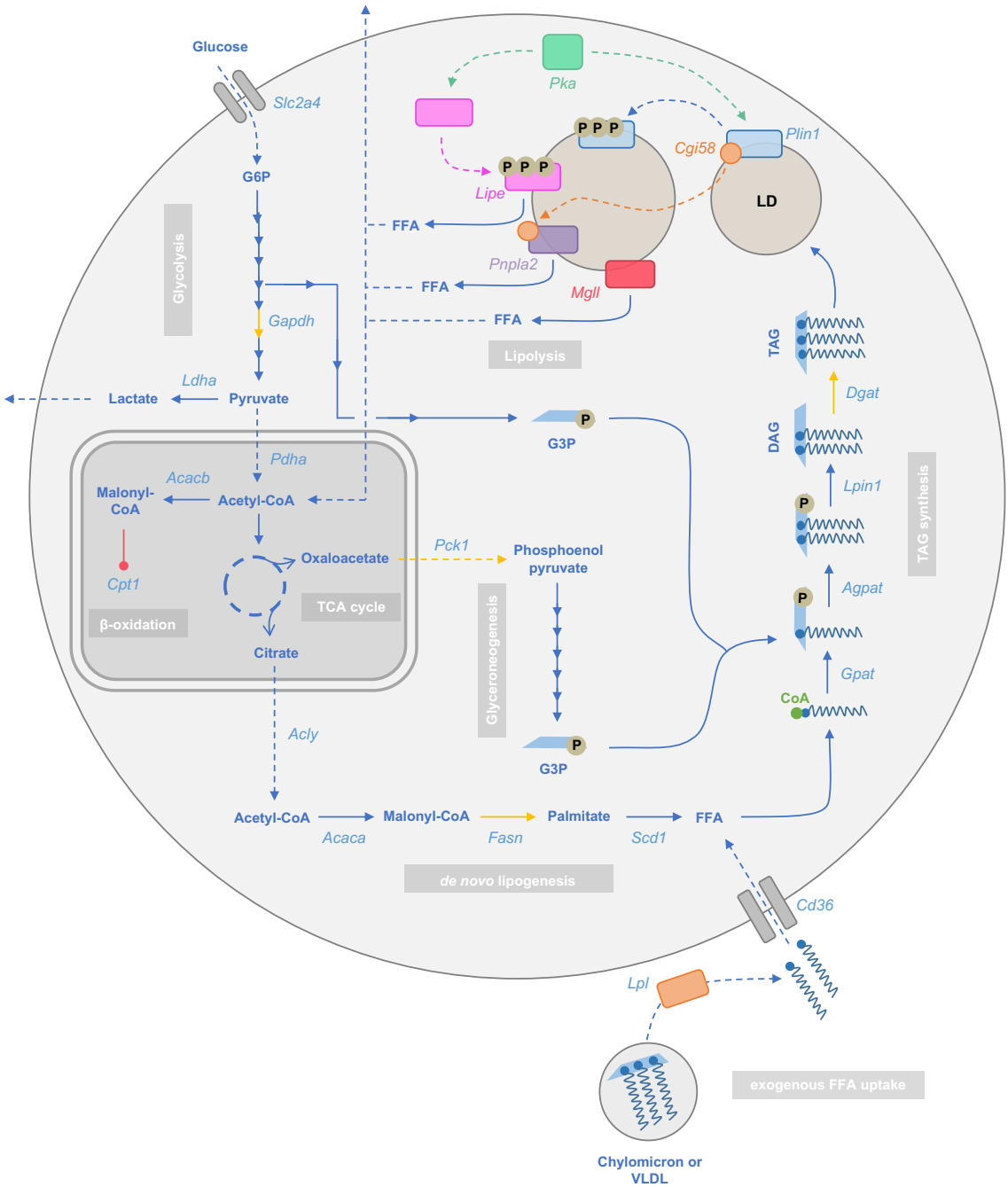

Figure 5-1: Lipogenic and lipolytic pathways in adipocytes.

See text for details.

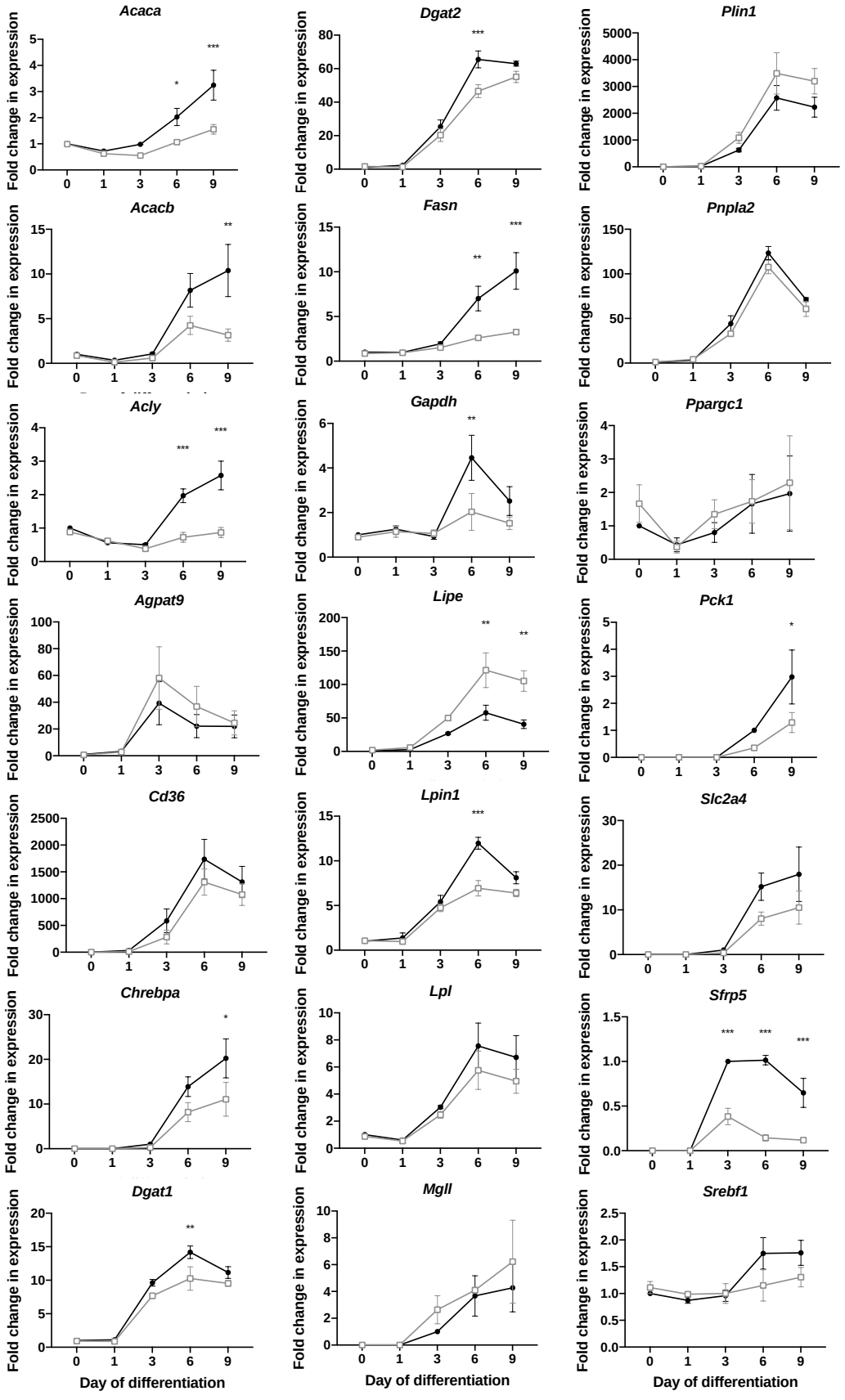
Acaca
Dgat2
Plin1
Acacb
Fasn
Pnpla2
Acly
Gapdh
Ppargc1
Agpat9
Lipe
Pck1
Cd36
Lpin1
Slc2a4
Chrebpa
Lpl
Sfrp5
Dgat1
Mgll
Srebf1
Fold change in expression
Day of differentiation
siScrambled
siMknk2

Figure 5-2: Effect of si*Mknk2* on metabolic gene expression during 3T3-L1 adipogenesis.

3T3-L1 pre-adipocytes were pre-transfected with 25 pmol of si*Mknk2* (#1 and #2) or control si*Scrambled*, as indicated 72 h prior to adipogenic induction. mRNA expression of metabolic genes was assessed by RT-qPCR at the indicated times. Expression levels were normalised to *Nono* and *Hprt* and represented as fold change with respect to Day 0. Data are mean ± SEM; n=3; 2-way ANOVA (*P < 0.05 **P < 0.01 ***P < 0.001).

Acetyl-CoA carboxylase 2 (*Acacb*) is expressed at high levels in adipose tissue [335] and is localised to mitochondria where it is involved in the regulation of fatty acid oxidation [336]. *Acacb* catalyses the synthesis of malonyl-CoA, which inhibits the rate-limiting enzyme of fatty acid oxidation, carnitine palmitoyl-transferase I. *Acacb*$^{-/-}$ mice have increased rates of β-oxidation because they are unable to produce sufficient levels of malonyl-CoA and are thus protected from diet-induced obesity [337]. In si*Mknk2* adipocytes, *Acacb* expression was significantly reduced on Day 9 (Figure 5-2), suggesting the rate of fatty acid oxidation may therefore be increased in these adipocytes, which could account for their reduced lipid content. This may have broader implications in other fatty acid-oxidising tissues, such as the heart and muscle, and may be particularly relevant for understanding the *in vivo* MNK2-KO phenotype in which mice are protected from HFD-induced weight gain.

Expanding on this concept, it was hypothesised that the reduction in lipid accumulation may be attributed to an increase in the metabolic capacity of the adipocytes – a phenomenon known as 'browning'. PPARγ coactivator 1-alpha (*Ppargc1a)* is a marker of brown adipocytes and is responsible for upregulating genes involved in fatty acid uptake and oxidation as well as mitochondrial biogenesis [338]. However, *Ppargc1a* levels were not affected in si*Mknk2* adipocytes (Figure 5-2), suggesting that MNK2 does not regulate the metabolic capacity or 'browning' of adipocytes, at least *in vitro*.

When assessing enzymes involved in lipolytic pathways, si*Mknk2* significantly increased the levels of hormone-sensitive lipase (*Lipe*) which is the key enzyme of DAG hydrolysis. Interestingly, the levels of adipocyte triglyceride lipase (*Pnpla2*) and monoacylglycerol lipase (*Mgll*), which catalyse the hydrolysis of TAG/DAG and MAG, respectively, were not affected by si*Mknk2,* suggesting that MNK2 negatively and selectively regulates the level of *Lipe* in adipocytes (Figure 5-2). The knock-down of MNK2 may therefore increase the rate of lipolysis which likely accounts for the reduction in lipid content.

The lipid droplet surface is complexed with one or more members of the Perilipin family of proteins which help to stabilise the droplet and regulate lipolysis [339]. PLIN1 (*Plin1*) is regarded as the major lipid droplet protein and is central to the regulation of lipolysis in adipocytes. Under basal conditions, PLIN1 is in an unphosphorylated state, whilst HSL and ATGL are localised to the cytoplasm, and the co-activator of ATGL, CGI-58, is sequestered by PLIN1 at the lipid droplet surface. When lipolysis is activated, such as through β-androgenic stimulation, PLIN1, CGI-58 and HSL become phosphorylated by cAMP-dependent protein kinase A and the droplet surface is re-organised to facilitate a considerable increase in lipolysis. P-HSL and ATGL become associated with the lipid droplet and CGI-58 is released from PLIN1 to activate ATGL (Figure 5-1) [339]. Although lipid content was reduced in si*Mknk2* adipocytes, *Plin1* levels were not significantly

affected (Figure 5-2), suggesting the expression of PLIN1, and presumably its control of lipolysis at the lipid-droplet interface, are not regulated by MNK2.

Lipoprotein lipase (*Lpl*) is exogenously expressed in the endothelium and is responsible for the breakdown of TAG in circulating chylomicrons and lipoprotein particles [340]. *Lpl* levels were not significantly affected by si*Mknk2*, although they did trend lower (Figure 5-2). Furthermore, the level of the fatty acid transport protein, *Cd36*, which is responsible for the uptake of exogenous FFAs into adipocytes [341], was not significantly affected by si*Mknk2* but also trended lower (Figure 5-2). This suggests the uptake of exogenous FFAs is unlikely to be regulated by MNK2, which is consistent with the fact that MNK2-KO mice have normal circulating levels of FFAs [3].

Lipid metabolism is in a constant state of flux, where during periods of lipolysis, a considerable proportion of FFAs is re-esterified back into TAG [342]. This 'recycling' of FFAs is thought to be important for regulating lipid homeostasis and FFA release during fasting [329]. G3P is required for the re-esterification of FFA, and indeed the synthesis of TAG from lipogenic pathways described above. However, under conditions where lipolysis is activated, the major source of G3P, glycolysis, is markedly reduced [329]. Glycerol kinase is also expressed at a very low level in adipose tissue, and after complete hydrolysis of TAG, very little of the glycerol backbone can be phosphorylated back to G3P [342]. A necessary metabolic pathway known as glyceroneogenesis allows the synthesis of G3P from non-glucose substrates, such as pyruvate and lactate, when glucose levels are low. Phosphoenolpyruvate carboxykinase 1 (*Pck1*) is the major enzyme regulating glyceroneogenesis [343]. In si*Mknk2* adipocytes, the level of *Pck1* was significantly reduced, suggesting the synthesis of G3P from glyceroneogenesis was significantly impaired, which may reduce the availability of G3P for TAG synthesis and FFA recycling (Figure 5-2). Given expression of *Pck1* is a direct reflection of its activity [344], it is suggested that si*Mknk2* adipocytes may have increased glucose levels and may therefore implicates MNK2 in the control of glucose uptake.

To assess whether glucose uptake was regulated by MNK2, the levels of insulin-responsive glucose transporter GLUT4 (*Slc2a4*) were assessed. Interestingly, the *Slc2a4* levels were not significantly increased in si*Mknk2* adipocytes and in fact they trended lower (Figure 5-2). However, the regulation of glucose transport is considerably more complex than *Slc2a4* expression (reviewed in [345]: GLUT4 resides in intracellular vesicles which translocate to the cellular membrane upon insulin stimulation. Therefore, *Slc2a4* levels may not be the best indicator of glucose uptake. Considering glucose levels modulate the expression of enzymes involved in glycolysis [346], the level of glyceraldehyde-3-phosphate dehydrogenase (*Gapdh*), which is responsible for catalysing the sixth step of glycolysis and exerting control as the most rate-determining step [347], was assessed. Surprisingly, *Gapdh* levels were significantly reduced in si*Mknk2* adipocytes, contrary to what was hypothesised (Figure 5-2) and this was reflected in

reduced GAPDH protein expression (Figure 5-3A). To clarify whether glucose levels were actually substantially elevated in si*Mknk2* adipocytes, quantitative analysis of glucose uptake was subsequently performed, the results of which are presented later in this Chapter.

Interim Conclusion

In si*Mknk2* adipocytes, there was a significant reduction in the expression of genes in DNL and TAG synthetic pathways, namely *Acly, Acaca, Fasn, Dgat1/2* and *Lpin1*. The level of *Acacb*, the activity of which inhibits fatty acid oxidation was also significantly reduced, suggesting si*Mknk2* adipocytes may have increased rates of FFA oxidation. Furthermore, the level of *Lipe* (HSL) was significantly increased by the knock-down of MNK2, suggesting there may be an increase in lipolysis. Combined, it was suggested that these changes in gene expression account for the reduction in lipid accumulation in si*Mknk2* adipocytes.

The level of *Pck1*, which is responsible for the synthesis of G3P via glyceroneogenesis, was significantly reduced, suggesting the availability of G3P for TAG synthesis and lipid recycling may be reduced and account for the reduction in lipid content. Given *Pck1* is negatively regulated by glucose, it was suggested that glucose uptake may be increased in si*Mknk2* adipocytes. MNK2 does not appear to regulate adipocyte browning or the uptake of exogenous FFAs.

Given the changes in metabolic gene expression largely affected genes in lipogenic pathways, it was hypothesised that a transcription factor(s) responsible for the global regulation of lipid metabolism may be regulated by MNK2. Sterol regulatory element-binding protein 1 (*Srebf1*) is known to enhance the transcriptional activity of PPARγ and is thereby linked to the control of expression of genes involved in FFA and lipid metabolism [348–350]. The level of *Srebf1,* however, was not significantly affected by si*Mknk2*, although it did trend lower (Figure 5-2). Carbohydrate response element binding protein (ChREBP) is a lipogenic transcription factor that is activated by carbohydrate feeding [351] and increases during adipocyte differentiation [352–354]. In the context of 3T3-L1 adipocytes, which are cultured in high-glucose media, the study of ChREBP is particularly relevant. In si*Mknk2* adipocytes, the level of *Chrebpa* was significantly reduced, suggesting MNK2 positively regulates ChREBP expression (Figure 5-2). Consistent with these findings, ChREBP depletion in precursor adipocytes has been previously demonstrated to reduce lipid accumulation and partially inhibit adipocyte differentiation [354].

Secreted frizzled-related protein 5 (*Sfrp5*) is protein factor that antagonises Wnt signalling and has been widely implicated in adipocyte biology [355]. *Sfrp5* is induced during adipogenesis and expressed in mature adipocytes [356–359], but is not thought to directly regulate adipogenesis through Wnt signalling [360]. Multiple studies report that *Sfrp5* is highly induced with genetic or diet-induced obesity [358,359,361], although one study reported that *Sfrp5* is actually suppressed under these conditions [357]. In si*Mknk2* adipocytes, *Sfrp5* levels were significantly

reduced (Figure 5-2). *Sfrp5* expression is one of the best *a priori* predictors of adiposity in mice prior to HFD exposure [358] which is consistent with the protection of MNK2-KO mice from HFD-induced weight gain [3].

Effect of siMknk2 on metabolic protein expression

To investigate the functional effect of the gene expression changes induced by the knock-down of MNK2, the levels of key metabolic proteins were assessed by Western blot. Consistent with the decrease in *Fasn* mRNA (Figure 5-2), expression of FASN was significantly decreased in si*Mknk2* adipocytes on Day 9 (Figure 5-3 A,B). This was associated with a significant reduction in ChREBP expression on Days 6 and 9 (Figure 5-3A,B), suggesting that MNK2 regulates lipogenic gene expression by exerting control over ChREBP expression.

LPIN1 expression was significantly reduced in si*Mknk2* adipocytes on Days 3, 6 and 9 in si*Mknk2* adipocytes (Figure 5-3A,B), however, *Lpin1* mRNA was only significantly reduced on Day 6 (Figure 5-2). The discrepancy between mRNA and protein levels suggests MNK2 may regulate LPIN1 expression, as mentioned in Chapter 4.

HSL expression was significantly increased in si*Mknk2* adipocytes on Days 6 and 9 (Figure 5-3A,B), consistent with *Lipe* mRNA levels (Figure 5-2). Crucially the level of ATGL was not significantly affected by si*Mknk2,* supporting the hypothesis that *Lipe* is negatively regulated by MNK2.

The abundance of PLIN1, which regulates lipolytic activity at the lipid droplet interface was unchanged in si*Mknk2* adipocytes (Figure 5-3A,B), consistent with *Plin1* mRNA levels (Figure 5-2). It was therefore suggested that MNK2 does not regulate PLIN1 expression given that the abundance of PLIN1 protein is considered more critical for its regulatory effect, as opposed to its mRNA level [362]. As mentioned previously, GAPDH was reduced by si*Mknk2*, consistent with the reduction in *Gapdh* mRNA levels, suggesting that glycolytic metabolism may, in part, be regulated by MNK2.

Interim Conclusion

Chrebpa levels were significantly reduced in si*Mknk2* adipocytes, suggesting that MNK2 positively regulates *Chrebpa* expression. ChREBP is a transcription factor responsible for regulating lipid metabolism, and its reduction was associated with a reduction in FASN and LPIN1 and a corresponding increase in HSL.

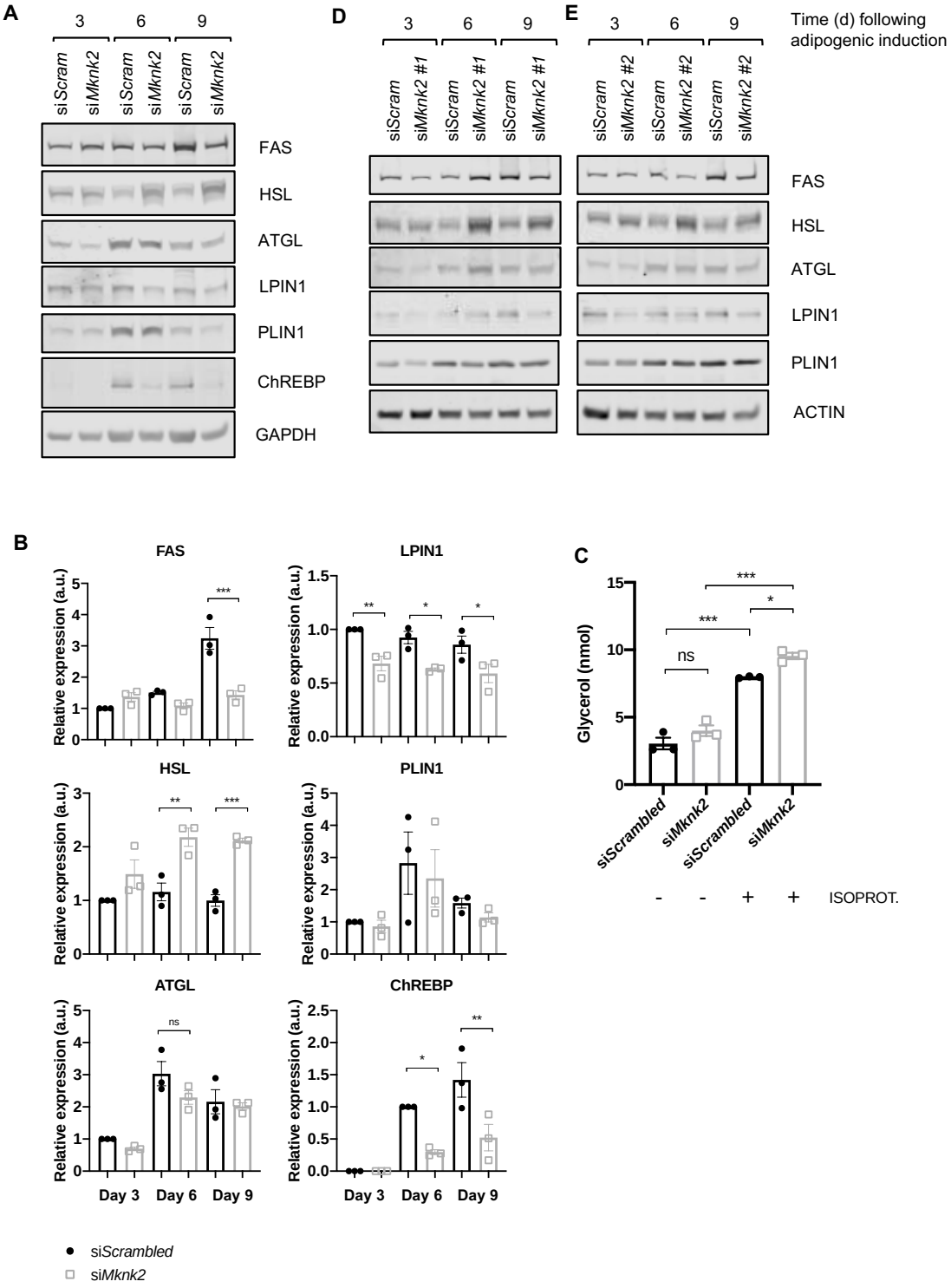
A
3
6
9
siScram
siMknk2
FAS
HSL
ATGL
LPIN1
PLIN1
ChREBP
GAPDH
D
siScram
siMknk2 #1
E
siMknk2 #2
Time (d) following adipogenic induction
ACTIN
B
FAS
LPIN1
HSL
PLIN1
ATGL
ChREBP
Relative expression (a.u.)
Day 3
Day 6
Day 9
siScrambled
siMknk2
C
Glycerol (nmol)
ns
siScrambled
siMknk2
ISOPROT.

Figure 5-3: Effect of si*Mknk2* on metabolic protein expression during 3T3-L1 adipogenesis.
3T3-L1 pre-adipocytes were pre-transfected with 25 pmol of si*Mknk2* (#1 and #2) or control si*Scrambled,* as indicated, 72 h prior to adipogenic induction. (A) Cell lysates were harvested at the indicated times and analysed by SDS-PAGE using the indicated antibodies; representative immunoblots are shown (n=3). (B) Expression levels from (A) were quantified; one-way ANOVA (*P < 0.05 **P < 0.01 ***P < 0.001). (C) Lipolysis assay; glycerol levels were measured in media from Day 9 differentiated adipocytes treated with or without 100 nM isoproterenol (n=3); one-way ANOVA (*P < 0.05 **P < 0.01 ***P < 0.001). (D,E) 3T3-L1 pre-adipocytes were pre-transfected individually with 25 pmol of si*Mknk2* #1 or #2, as indicated with si*Scrambled* as a control. Cell lysates were harvested at the indicated times and analysed by SDS-PAGE using the indicated antibodies; representative immunoblots are shown (n=2).

Effect of siMknk2 on the rate of lipolysis

Given that expression of HSL, the key enzyme responsible for DAG hydrolysis, was elevated in si*Mknk2* adipocytes, it was hypothesised that the overall rate of lipolysis was increased. The rate of basal and stimulated lipolysis was therefore measured in si*Mknk2* and si*Scrambled* 3T3-L1 adipocytes. As expected, the rate of isoproterenol-stimulated lipolysis was significantly increased in si*Mknk2* adipocytes (Figure 5-3C), consistent with elevated expression of HSL; however, the rate of basal lipolysis was not significantly increased (Figure 5-3C). This is consistent with the fact that under basal conditions, PLIN1 acts as a lipid droplet barrier to block access of HSL [363]. This suggests that knock-down of MNK2 increases the rate of stimulated lipolysis associated with elevated HSL expression.

Effect of individual siMknk2 on metabolic gene expression

To examine the robustness and validity of the changes in metabolic gene expression induced by si*Mknk2*, 3T3-L1 cells were treated individually with either si*Mknk2* #1 or #2, and mRNA expression was measured by RT-qPCR. As expected, when si*Mknk2* #1 and #2 were used individually, the levels of *Acaca, Acacb*, *Acly*, *Fasn and Sfrp5*, but not *Lpl,* were significantly reduced (Figure 5-4A). Interestingly, *Lipe* levels were only significantly increased with si*Mknk2* #2 but not si*Mknk2* #1. The levels of *Cd36* trended lower with si*Mknk2* #2 (Figure 5-4A), consistent with earlier findings (Figure 5-2), although they were more significantly reduced with si*Mknk2* #1 (Figure 5-4A). Furthermore, the levels of *Dgat1*, *Dgat2*, *Gapdh* and *Lpin1* were not significantly reduced by si*Mknk2* #1 or #2, as expected; however, *Pnpla2* and *Srebf1* levels were significantly reduced by si*Mknk2* #1 (Figure 5-4A). Notably, *Chrebpa* levels were significantly reduced by si*Mknk2* #1 but not si*Mknk2* #2, somewhat diminishing the robustness and reliability of the MNK2 knockdown phenotype.

To examine these discrepancies further, the level of protein expression was assessed by Western blot as this is a more robust measure of protein function. Despite discrepancies in *Lipe* mRNA levels, both si*Mknk2* #1 and #2 increased HSL expression (Figure 5-3D,E), consistent with earlier findings (Figure 5-2) and supporting the hypothesis that HSL expression is negatively regulated by MNK2. Paradoxically, despite significantly reduced *Pnpla2* levels in si*Mknk2* #1 adipocytes (Figure 5-2), ATGL protein expression was apparently increased (Figure 5-3D) and remained relatively unaffected in si*Mknk2* #2 adipocytes (Figure 5-3E). Consistent with earlier results (Figure 5-2), si*Mknk2* #1 and #2 individually decreased FASN and LPIN1 expression and did not alter PLIN1 levels (Figure 5-3D,E).

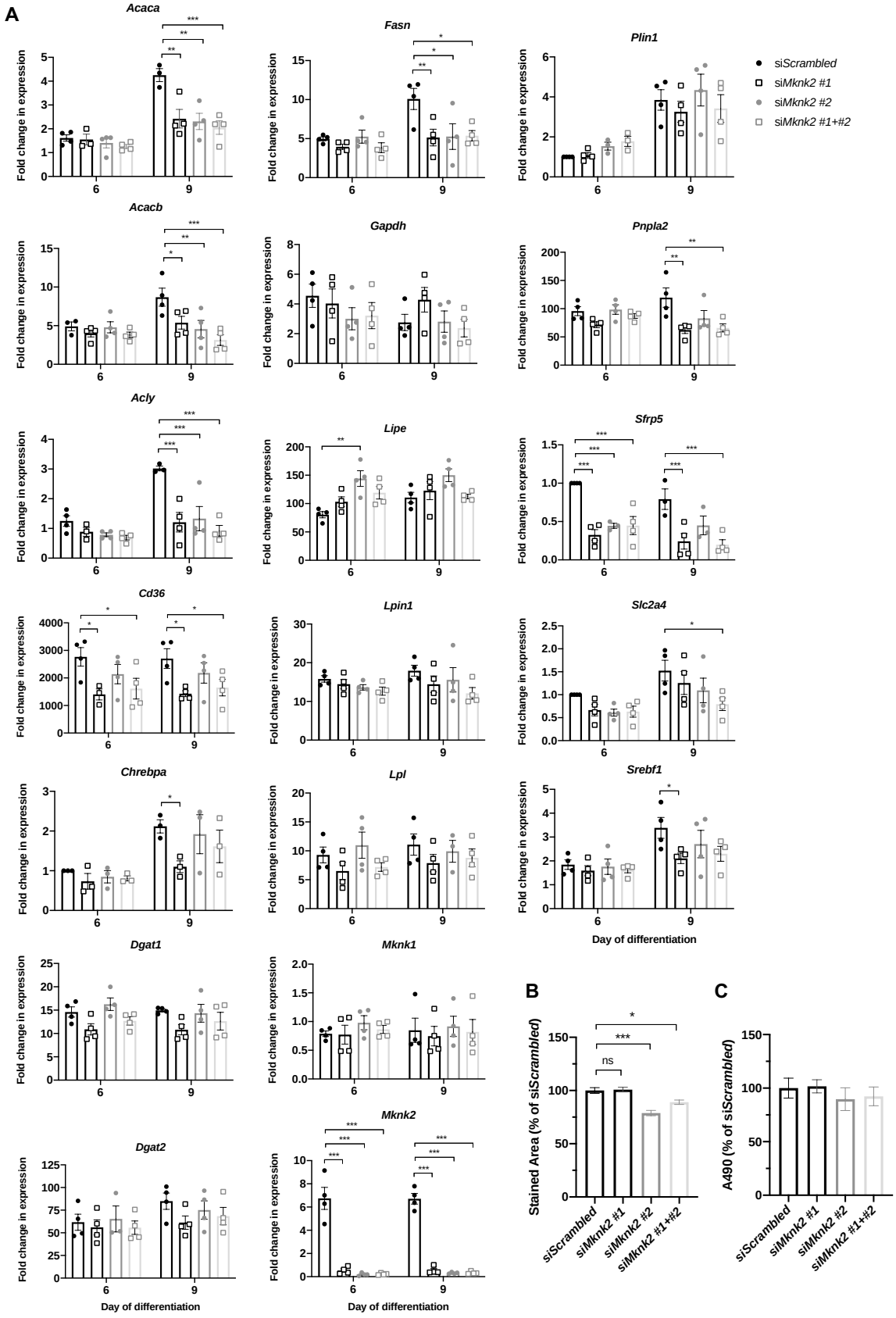
A
Acaca
Fasn
Plin1
Acacb
Gapdh
Pnpla2
Acly
Lipe
Sfrp5
Cd36
Lpin1
Slc2a4
Chrebpa
Lpl
Srebf1
Dgat1
Mknk1
Mknk2
Dgat2
Fold change in expression
Day of differentiation
siScrambled
siMknk2 #1
siMknk2 #2
siMknk2 #1+#2
B
Stained Area (% of siScrambled)
ns
C
A490 (% of siScrambled)

Figure 5-4: Effect of individual si*Mknk2* on metabolic gene expression.

3T3-L1 pre-adipocytes were pre-transfected with 25 pmol of si*Mknk2* #1 and #2 either individually or combined, 72 h prior to adipogenic induction. (A) mRNA expression of metabolic genes was assessed by RT-qPCR at the indicated times. Expression levels were normalised to *Nono* and *Hprt* and represented as fold change with respect to si*Scrambled* on Day 0. Data are mean ± SEM; n=3-4; 2-way ANOVA (*P < 0.05 **P < 0.01 ***P < 0.001). (B) Day 9 differentiated adipocytes were stained with ORO to assess lipid accumulation; the total stained area was quantified from different fields of view and represented as percentage stained area relative to si*Scrambled*; data are mean ± SEM (n=5-6); one-way ANOVA (*P < 0.05 **P < 0.01 ***P < 0.001). (C) ORO eluted from stained cells was quantified by absorbance (A490) and is represented as percentage absorbance relative to si*Scrambled*; data are mean ± SEM; (n=5-6); one-way ANOVA (*P < 0.05 **P < 0.01 ***P < 0.001).

Despite these findings, when lipid accumulation was quantified by ORO staining, it was only significantly reduced in si*Mknk2* (combined) and si*Mknk2* #2, but not si*Mknk2* #1 adipocytes (Figure 5-4B). When the absorbance of eluted ORO was quantified as a secondary measure of lipid accumulation, it trended lower in si*Mknk2* #2 but not si*Mknk2* #1 or si*Mknk2 (combined)* adipocytes (Figure 5-4C). The latter observation was unexpected given that lipid accumulation was consistently reduced on previous occasions (Figure 4-17C-E). The disparity in lipid accumulation between si*Mknk2* adipocytes was unexpected and somewhat further diminished the robustness of the MNK2 knock-down phenotype.

Interim Conclusion

The siRNA-mediated knockdown of MNK2 increased the expression of HSL which was associated with a significant increase in isoproterenol-stimulated lipolysis. Individual siRNA treatments consistently reduced the expression of FASN and LPIN1 and increased HSL, however, *Chrebpa* levels were only significantly reduced by si*Mknk2* #1 and not #2. There were also unexpected discrepancies in the quantification of lipid accumulation between individual siRNA treatments. Therefore, the robustness of the si*Mknk2* phenotype was somewhat diminished.

Gene expression changes in MNK-2KO and double KO (DKO) adipocytes

To determine the biological significance of the gene expression changes in si*Mknk2* adipocytes and their possible implication(s) *in vivo*, adipose tissue from MNK-2KO and -DKO mice was subjected to gene expression analysis (unpublished data), as summarised in Table 5-1. In contrast to si*Mknk2* adipocytes, *Chrebpa* levels were significantly increased, along with *Fasn* and *Acacb* in MNK-DKO adipose tissue. *Slc2a4*, which encodes the GLUT4 glucose transporter and is a predicted target of ChREBP [364] was also significantly increased, although a similar trend was not observed *in vitro*. Despite the increase in *Chrebpa*, the level of *Acaca* was not significantly increased *in vivo*, but *Srebf1,* a lipogenic transcriptional regulator [348], and predicted ChREBP target [364] was.

The level of *Plin1* was significantly elevated in MNK-2KO but not -DKO adipose tissue; however, as mentioned earlier, the levels of PLIN1 protein are more important for its regulatory function, so this increase may not be biologically significant. In contrast to si*Mknk2* adipocytes, the level of *Lipe* in either MNK-2KO or DKO adipose tissue was not significantly increased, suggesting that stimulated lipolysis was unlikely to be increased and account for the reduced lipid content *in vivo*. In support of this, the expression of *Pnpla2* and *Mgll* were also unaffected. The only consistent observation between si*Mknk2* and MNK-DKO adipose tissue was a significant reduction in *Sfrp5* levels, however, the mechanism(s) of how this may regulate and account for the reduced lipid content is unclear. The increase in lipogenic gene transcription in the absence of elevated lipolytic gene expression was expected to increase lipid accumulation; paradoxically, however, DKO mice are protected from HFD-induced weight gain (unpublished data). Given the conflicting gene

expression profiles, it was apparent that the mechanisms responsible for reducing lipid content *in vitro* differ from those that occur *in vivo*.

In light of these findings, how is it that an increase in *Chrebpa* be attributed to a reduction in lipid accumulation *in vivo?* There may be several explanations. In MNK-DKO mice, levels of the adipose 'browning' marker, *Ucp1*, were significantly increased (Table 5-1). ChREBP has been reported to upregulate *Ucp1* levels in white adipose tissue which greatly increased browning capacity and was attributed to a reduction in lipid content *in vivo* [365]. Alternatively, metabolic changes in other tissues and organs where ChREBP is expressed, such as liver [366] may also account for the reduction in lipid accumulation *in vivo*.

The contrasting expression of *Chrebpa in vitro* and *in vivo* is intriguing, but the reason(s) why levels trend in opposite directions is unclear. Nevertheless, these findings strongly implicate MNK2 in the regulation of ChREBP and lipid metabolism, albeit due to different mechanisms likely operating *in vitro* and *in vivo*.

Table 5-1: Comparison of *in vitro* and *in vivo* effects of MNK2 knockdown.

Summary of gene expression trends from 3T3-L1 adipocytes treated with si*Mknk2* #1 and/or #2 *in vitro* and MNK2-KO and MNK-DKO adipose tissue (*in vivo;* unpublished data). Upward and downward arrows indicate the direction of significant trend in mRNA gene expression with respect to si*Scrambled* or WT adipose tissue on chow diet. Horizontal lines indicate no significant trend in expression and in blank boxes, no analysis was performed. Known and predicted ChREBP targets, based on experimental evidence (see Refs), are highlighted in bolded and underlined, respectively. Refs: [1] [367], [2] [367], [3] [367] [4] [364] [5] [368] [6] [365]. Hash ([#]) denotes significant change in expression on the HFD.

	Gene	#1+#2	#1	#2	MNK-2KO	MNK-DKO	Comments and significance
Transcription factors and cell signalling	*Chrebpa*	↓	↓	—		↑	*In vitro* levels decreased; *in vivo* levels increased.
	Lpin1	↓	—	—			Inconsistent effect *in vitro*, other data suggest MNK2 regulates LPIN1
	Sfrp5	↓	↓	↓	↓[#]	↓[#]	*In vitro* and *in vivo* trends are consistent; both associated with reduced adipose lipid content
	Srebf1[4]	—	↓	—		↑	*In vivo* increase reflective of *Chrebpa* levels, but not reflected in increased lipid content. Inconsistent effect *in vitro*
de novo lipogenesis	***Fasn***[1,2]	↓	↓	↓		↑	Levels are correlated with *Chrebpa*
	Acaca[1,2]	↓	↓	↓	—	—	Levels are correlated with *Chrebpa*
	Acly[1]	↓	↓	↓			Levels are correlated with *Chrebpa*
	Pck1[3,4,6]	↓					Decrease may reduce G3P synthesis from glyceroneogenesis
TAG synthesis	*Dgat1*	↓	—	—	—	—	Inconsistent effect; not likely regulated by MNK2
	Dgat2[3,5]	↓	—	—	—	—	Inconsistent effect; not likely regulated by MNK2
	Agpat9[6]	—			—	—	Not likely regulated by MNK2
Browning and FFA oxidation	***Acacb***[1]	↓	↓	↓		↑	Levels are correlated with *Chrebpa*
	Ppargc1a[6]	—			—	—	Mitochondrial biogenesis not likely regulated by MNK2
	Ucp1[6]					↑[#]	Increased browning capacity may account for reduction in lipid
Lipolysis	*Lipe*[4,6]	↑	—	↑	—	—	Increase *in vitro* associated with increased lipolysis; may be negatively regulated by ChREBP; no increase *in vivo*
	Pnpla2[6]	—	↓	—	—	—	Not likely regulated by MNK2
	Mgll	—	—	—			Not likely regulated by MNK2
	Plin1[6]	—	—	—	↑	—	Not likely regulated by MNK2
FFA uptake	*Cd36*	—	↓	—			Inconsistent effect *in vitro*, not likely regulated by MNK2
	Lpl	—	—	—			Not likely regulated by MNK2
Glycolysis	*Slc2a4*[4,6]	—	—	—		↑	*In vivo* increase consistent with *Chrebpa* levels; effect not observed *in vitro*
	Gapdh[4]	↓	—	—			Levels are correlated with *Chrebpa* levels; however, effect is inconsistent

Interim Conclusion

Despite levels trending in opposite directions, the changes in metabolic gene expression that occur *in vitro* and *in vivo* likely centre around the expression of *Chrebpa*. *In vitro*, the level of *Chrebpa* was reduced by si*Mknk2*, and was associated with reduced expression of DNL enzymes (i.e. *Acaca, Acly, Fasn*) and increased expression of *Lipe*. In contrast, *Chrebpa* levels were increased in MNK-DKO adipose tissue (*in vivo*) which was associated with increased DNL enzyme expression but increased levels of the adipose browning marker, *Ucp1*. ChREBP is suggested to up-regulate *Ucp1* to greatly increase the browning capacity of adipose tissue, which may account for lipid reduction.

Effect of eFT508 on metabolic gene expression

Given the metabolic effects described thus far are a result of siRNA-mediated knockdown of MNK2, it was hypothesised that the effects were mediated by a non-catalytic function(s) of MNK2. To assess this, 3T3-L1 pre-adipocytes were subjected to adipogenic differentiation in the presence or absence of the selective MNK1/2 inhibitor eFT508 [59], and the expression of key metabolic genes was assessed by RT-qPCR.

In contrast to si*Mknk2* adipocytes, the levels of *Acaca, Acacb, Acly, Fasn, Dgat1, Dgat2, Sfrp5* and *Gapdh*, were not significantly reduced by eFT508; in fact, some genes were at times marginally or significantly increased (Figure 5-5). Furthermore, the level of *Lipe* was not significantly increased by eFT508, suggesting that the regulation of HSL expression is independent of MNK2 catalytic activity. Interestingly, *Mgll* and *Pnpla2* levels were largely unaffected, except for a significant increase on Day 6 (Figure 5-5).

eFT508 did not significantly affect *Srebf1*, *Slc2a4* or *Cd36* levels, consistent with si*Mknk2* adipocytes, nor did eFT508 affect the expression of *Mknk1* and *Mknk2*. *Plin1* levels were significantly increased by eFT508 on Day 6, however, this discrepancy was unlikely to have any major physiological effect given that PLIN1 protein levels are more critical for their regulatory function than its mRNA. Therefore, given eFT508 did not elicit the same changes in gene expression as observed in si*Mknk2* adipocytes, the observed metabolic changes associated with MNK2 knock-down are suggested to be mediated by a non-catalytic function(s) of MNK2.

Effect of eFT508 on metabolic protein expression and lipolysis

To further support this interpretation, the levels of key metabolic proteins from adipocytes differentiated in the presence of eFT508 were assessed by Western blot (Figure 5-6A,B). As expected, and in contrast to si*Mknk2* adipocytes, the expression of FAS, HSL, LPIN1, ChREBP and GAPDH were not affected by eFT508. Furthermore, despite marginal, but significantly increased *Pnpla2* and *Plin1* levels, eFT508 did not affect the expression of ATGL or PLIN1.

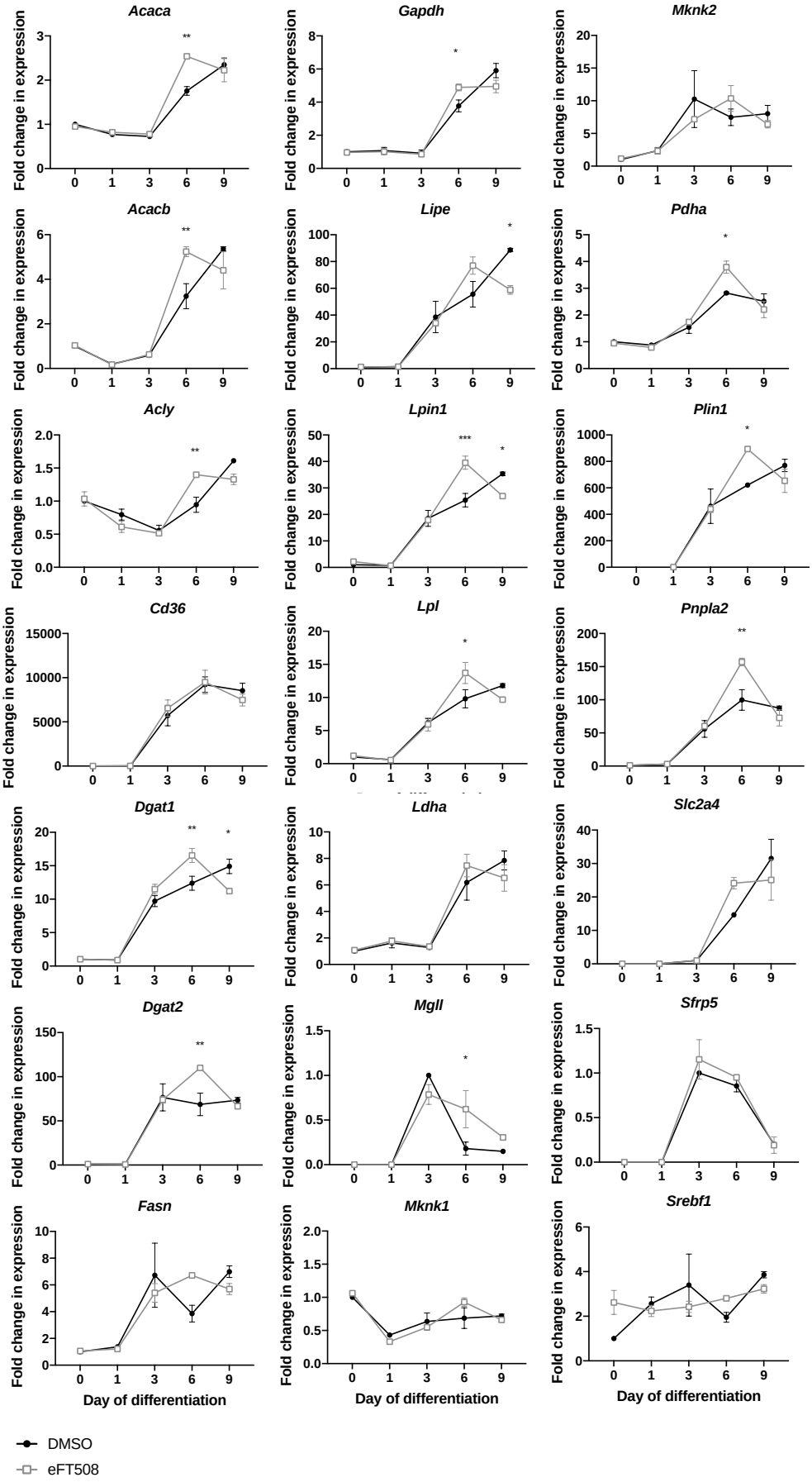
Acaca
Gapdh
Mknk2
Acacb
Lipe
Pdha
Acly
Lpin1
Plin1
Cd36
Lpl
Pnpla2
Dgat1
Ldha
Slc2a4
Dgat2
Mgll
Sfrp5
Fasn
Mknk1
Srebf1
Fold change in expression
Day of differentiation
DMSO
eFT508

Figure 5-5: Effect of eFT508 on metabolic gene expression during 3T3-L1 adipogenesis.

3T3-L1 pre-adipocytes were differentiated with adipogenic induction media following pre-treatment with 0.3 μM eFT508 or equivalent volume of DMSO. mRNA expression of metabolic genes was assessed by RT-qPCR at the indicated times. Expression levels were normalised to *Nono* and *Hprt* and represented as fold change with respect to Day 0. Data are mean ± SEM; n=2; 2-way ANOVA (*P < 0.05 **P < 0.01 ***P < 0.001).

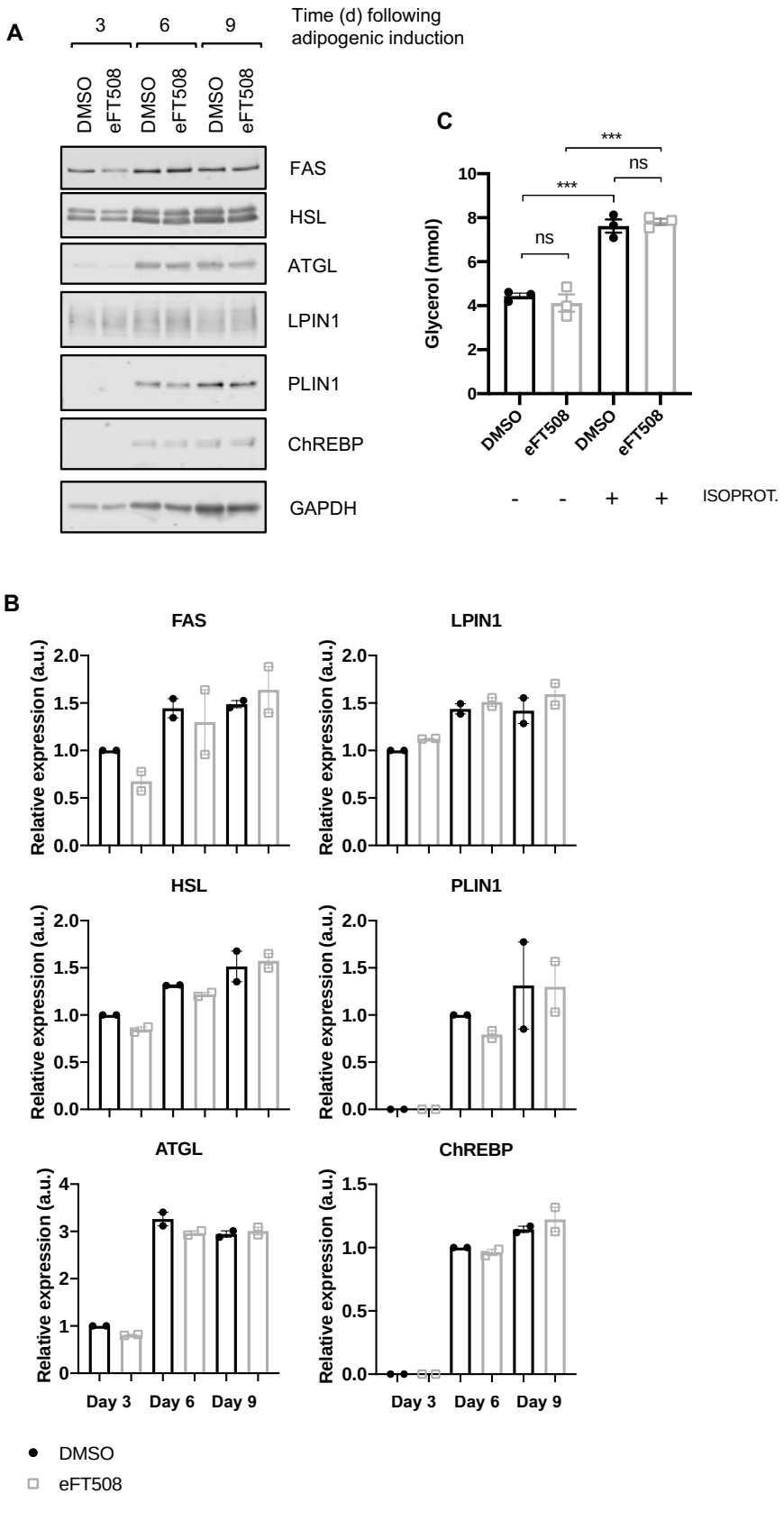
A
3
6
9
Time (d) following adipogenic induction
DMSO
eFT508
DMSO
eFT508
DMSO
eFT508
FAS
HSL
ATGL
LPIN1
PLIN1
ChREBP
GAPDH
C
***
ns
***
ns
Glycerol (nmol)
10
8
6
4
2
0
DMSO
eFT508
DMSO
eFT508
- - + + ISOPROT.
B
FAS
LPIN1
HSL
PLIN1
ATGL
ChREBP
Relative expression (a.u.)
2.0
1.5
1.0
0.5
0.0
4
3
2
1
0
Day 3
Day 6
Day 9
DMSO
eFT508

Figure 5-6: Effect of eFT508 on metabolic protein expression during 3T3-L1 adipogenesis.
3T3-L1 pre-adipocytes were differentiated with adipogenic induction media following pre-treatment with 0.3 μM eFT508 or equivalent volume of DMSO. (A) Cell lysates were harvested at the indicated times and analysed by SDS-PAGE using the indicated antibodies; representative immunoblots are shown (n=2). (B) Expression levels from (A) were quantified; one-way ANOVA (*P < 0.05 **P < 0.01 ***P < 0.001). (C) Lipolysis assay; glycerol levels were measured in media from day 9 differentiated adipocytes treated with or without 100 nM isoproterenol (n=3); one-way ANOVA (*P < 0.05 **P < 0.01 ***P < 0.001).

Finally, given that HSL expression was not elevated by eFT508, it was hypothesised that the rate of lipolysis would also remain unchanged. As expected, and in contrast to si*Mknk2*, eFT508 did not increase the rate of isoproterenol-stimulated or basal lipolysis (Figure 5-6C).

Interim Conclusion

Inhibition of MNK catalytic activity with eFT508 did not result in changes in gene expression or increase the rate of isoproterenol-stimulated lipolysis. These effects are only observed with knockdown of MNK2. It is therefore suggested that these metabolic changes are mediated by a non-catalytic function(s) of MNK2.

Effect of siMknk1 on metabolic gene expression

Given that MNK1 shares considerable protein homology with MNK2 [5] and mediates distinct metabolic effects [3], it was considered that MNK1, like MNK2, may regulate adipocyte metabolism. To assess this hypothesis, 3T3-L1 pre-adipocytes were treated with si*Mknk1* and the levels of key metabolic genes was assessed by RT-qPCR.

As expected in si*Mknk1* adipocytes, the level of *Mknk1* but not *Mknk2*, was significantly reduced, suggesting siRNA-mediated knock-down of MNK1 was effective (Figure 5-7A). In contrast to si*Mknk2* adipocytes, the levels of *Acaca, Acly, Dgat1, Dgat2, Fasn* and *Lpin1* were not significantly decreased in si*Mknk1* adipocytes, suggesting that, unlike MNK2, MNK1 does not regulate the expression of genes involved in DNL and TAG synthetic pathways (Figure 5-7A).

In contrast to si*Mknk2*, the level of *Lipe* was not increased in si*Mknk1* adipocytes, suggesting that, unlike MNK2, MNK1 does not negatively regulate HSL expression (Figure 5-7A). Rather MNK1 is suggested to promote the expression of ATGL, as the level of *Pnpla2* was significantly reduced in si*Mknk1* adipocytes (Figure 5-7A). Unexpectedly, *Chrebpa* levels were significantly reduced in si*Mknk1* adipocytes (Figure 5-7A) but this did not equate to a reduction in ChREBP protein expression (Figure 5-8C) so it is unlikely that MNK1 regulates ChREBP expression.

In contrast to si*Mknk2,* there was no change in the levels of *Slc2a4* or *Gapdh* in si*Mknk1* adipocytes, suggesting that glucose uptake and glycolytic pathways are unlikely to be regulated by MNK1 (Figure 5-7A). However, *Cd36* levels were significantly reduced, suggesting that MNK1 may regulate the uptake of exogenous FFAs (Figure 5-7A).

Consistent with the effects of si*Mknk2*, the levels of *Plin1*, *Srebf1* and *Lpl* were unaffected by si*Mknk1*, and the levels of *Acacb* and *Sfrp5* levels were significantly reduced (Figure 5-7A). Given that *Cd36* is responsible for FFA uptake, *Acacb* activity impairs fatty acid oxidation, and *Sfrp5* is associated with adiposity, a reduction in the expression of these genes would be expected to reduce lipid accumulation. However, paradoxically, when lipid accumulation was quantified by ORO staining and A490 absorbance, it was increased, albeit not significantly (Figure 5-7B-D).

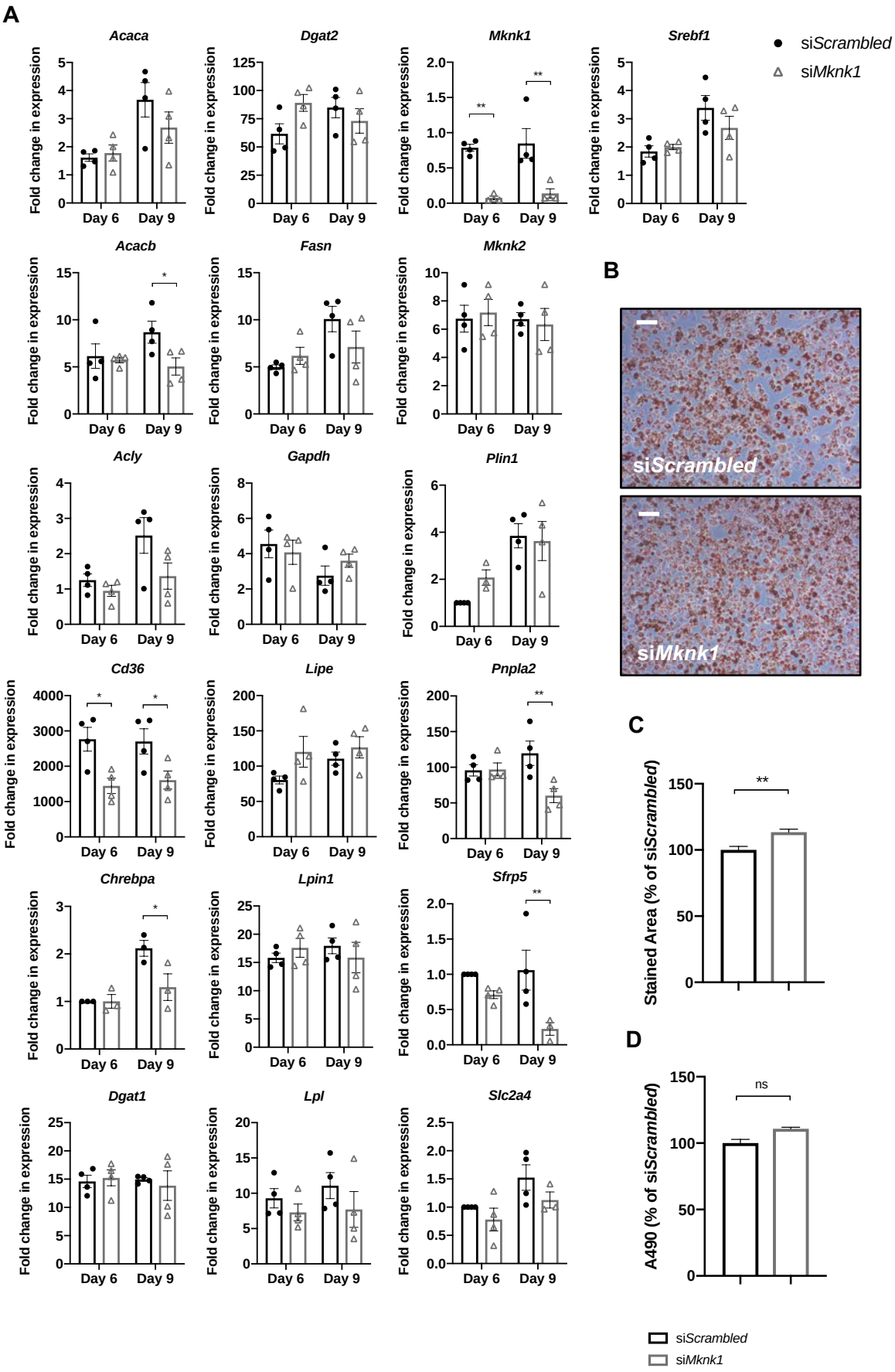
A
Acaca
Dgat2
Mknk1
Srebf1
Acacb
Fasn
Mknk2
Acly
Gapdh
Plin1
Cd36
Lipe
Pnpla2
Chrebpa
Lpin1
Sfrp5
Dgat1
Lpl
Slc2a4
Fold change in expression
Day 6
Day 9
siScrambled
siMknk1
B
siScrambled
siMknk1
C
Stained Area (% of siScrambled)
D
A490 (% of siScrambled)
ns

Figure 5-7: Effect of si*Mknk1* on metabolic gene expression during 3T3-L1 adipogenesis.
3T3-L1 pre-adipocytes were pre-transfected with 25 pmol of si*Mknk1* or control si*Scrambled*, as indicated 72 h prior to adipogenic induction. (A) mRNA expression of metabolic genes was assessed by RT-qPCR at the indicated times. Expression levels were normalised to *Nono* and *Hprt* and represented as fold change with respect to Day 0. Data are mean ± SEM; n=3-4; 2-way ANOVA (*P < 0.05 **P < 0.01 ***P < 0.001). (B) Day 9 differentiated adipocytes were stained with ORO to assess lipid accumulation; representative images are shown, scale bar 0.2 µm. (C) Total stained area was quantified from (B) and is represented as percentage stained area relative to si*Scrambled*; data are mean ± SEM; (n=5-6); one-way ANOVA (*P < 0.05 **P < 0.01 ***P < 0.001). (D) ORO eluted from stained cells was quantified by absorbance (A490) and is represented as percentage absorbance relative to si*Scrambled*; data are mean ± SEM; (n=5-6); one-way ANOVA (*P < 0.05 **P < 0.01 ***P < 0.001).

This discrepancy could be attributed to a reduction in lipolysis as a result of reduced ATGL (*Pnpla2*) expression, which is the key enzyme for initiating lipolysis.

> **Interim Conclusion**
>
> The metabolic effects induced by the knock-down of MNK2 cannot be induced by the knockdown of MNK1; suggesting MNK1 and MNK2 loss-of-function phenotypes are distinct in adipocytes. MNK1 does not regulate genes involved in DNL or TAG synthetic pathways but may increase lipid accumulation through decreasing the expression of ATGL (*Pnpla2*), the key enzyme responsible for regulating lipolysis.

Regulation of ChREBP expression and glucose uptake by MNK2

Given that changes in adipocyte metabolism induced by si*Mknk2* largely affected the expression of genes in lipogenic pathways, it was hypothesised that a change in the activity and/or expression of an underlying transcriptional effector(s) may be responsible. ChREBP regulates lipogenic gene transcription in response to glucose levels in both adipocytes and hepatocytes [351]. Two isoforms of ChREBP are produced from alternative promoters [369]. ChREBPα is present in the cytoplasm and is activated allosterically by the glycolytic intermediates: xylulose-5-phosphate (X5P), glucose-6-phosphate (G6P) and fructose 2,6-bisphosphate (F2,6BP) [351]. Upon activation, ChREBPα translocates to the nucleus where it binds to so-called carbohydrate response elements (ChoRE) in the upstream promoters of target genes, many of which are implicated in fatty acid and glucose metabolism [351]. ChREBPα also activates its own positive-regulatory loop by activating expression of ChREBPβ, a truncated isoform that lacks glucose-sensing and regulatory domains but is a potent transcriptional activator, from an alternative promoter [369]. Earlier, it was shown the mRNA level of *Chrebpa* was significantly reduced in si*Mknk2* adipocytes (Figure 5-2). Importantly and consistent with its mRNA levels, ChREBP protein levels assessed by Western blot, were also significantly reduced (Figure 5-8A).

As alluded to earlier, it was hypothesised that glucose uptake may be regulated by MNK2. Given ChREBP is activated by glucose metabolites, it was necessary to assay glucose uptake as it may account for the reduction in ChREBP levels. Glucose uptake was assayed quantitatively in response to insulin dosage in si*Mknk2* and si*Scrambled* adipocytes: unexpectedly, it was significantly elevated in si*Mknk2* adipocytes, even under basal conditions, suggesting MNK2 may negatively regulate glucose uptake or insulin signalling more broadly (Figure 5-8E). However, its elevated uptake in si*Mknk2* adipocytes was at odds with the reduction in ChREBP expression. This suggests that the reduction in ChREBP levels is likely independent of its activation. Interestingly, at 10 nM insulin, glucose uptake was equivalent in both si*Mknk2* and si*Scrambled* adipocytes (Figure 5-8E).

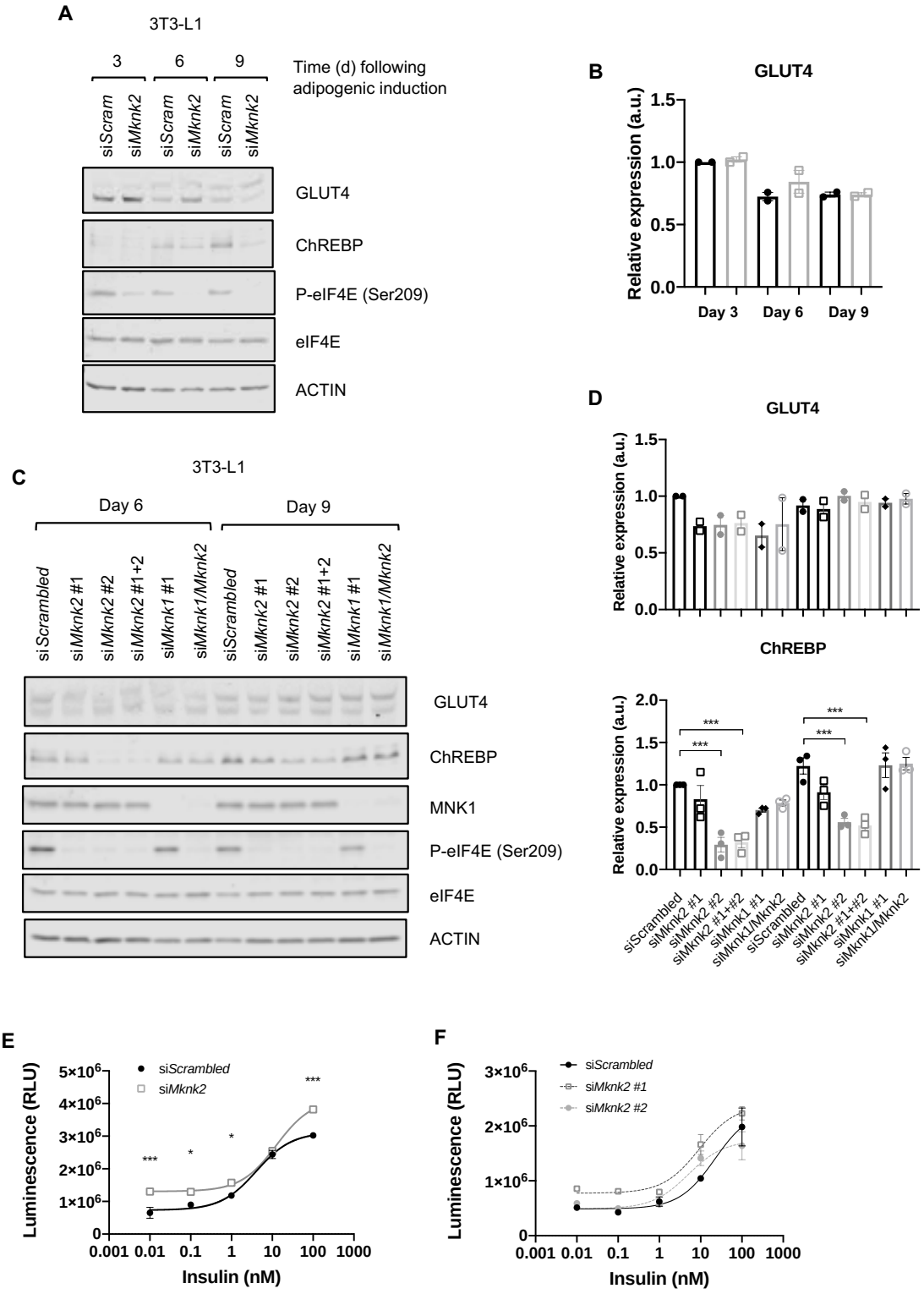
A
3T3-L1
3
6
9
Time (d) following adipogenic induction
siScram
siMknk2
GLUT4
ChREBP
P-eIF4E (Ser209)
eIF4E
ACTIN
B
GLUT4
Relative expression (a.u.)
1.5
1.0
0.5
0.0
Day 3
Day 6
Day 9
C
3T3-L1
Day 6
Day 9
siScrambled
siMknk2 #1
siMknk2 #2
siMknk2 #1+2
siMknk1 #1
siMknk1/Mknk2
GLUT4
ChREBP
MNK1
P-eIF4E (Ser209)
eIF4E
ACTIN
D
GLUT4
Relative expression (a.u.)
ChREBP
Relative expression (a.u.)
2.0
1.5
1.0
0.5
0.0
***
siScrambled
siMknk2 #1
siMknk2 #2
siMknk2 #1+#2
siMknk1 #1
siMknk1/Mknk2
E
Luminescence (RLU)
5×10⁶
4×10⁶
3×10⁶
2×10⁶
1×10⁶
0
siScrambled
siMknk2
***
*
*
***
0.001 0.01 0.1 1 10 100 1000
Insulin (nM)
F
Luminescence (RLU)
3×10⁶
2×10⁶
1×10⁶
0
siScrambled
siMknk2 #1
siMknk2 #2
0.001 0.01 0.1 1 10 100 1000
Insulin (nM)

Figure 5-8: Effect of si*Mknk2* on glucose metabolism in 3T3-L1 adipocytes.

3T3-L1 pre-adipocytes were pre-transfected with 25 pmol of si*Mknk2* (#1 and #2) or control si*Scrambled*, as indicated, 72 h prior to adipogenic induction. (A) Cell lysates were harvested at the indicated times and analysed by SDS-PAGE using the indicated antibodies; representative immunoblots are shown (n=2-3). (B) Total GLUT4 levels were quantified from (A). (C) 3T3-L1 pre-adipocytes were pre-transfected with 25 pmol of si*Mknk2* #1 or #2, individually and combined, si*Mknk1* #1 or si*Mknk1/Mknk2*. as indicated, with si*Scrambled* as a control. Cell lysates were harvested at the indicated times and analysed by SDS-PAGE using the indicated antibodies; representative immunoblots are shown (n=2-3). (D) GLUT4 and ChREBP levels from (C) were quantified. Glucose uptake was measured in Day 9 adipocytes pre-transfected with si*Mknk2* #1 and #2 either (E) combined or (F) individually (n=2-3); 2-way ANOVA (*P < 0.05 **P < 0.01 ***P < 0.001).

Effect of individual siRNA on ChREBP expression and glucose uptake

To examine the robustness and validity of the changes in ChREBP expression and glucose uptake induced by si*Mknk2*, 3T3-L1 cells were treated individually with si*Mknk2* #1 or #2. In contrast to previous results, ChREBP expression was only significantly reduced by si*Mknk2* #2 but not #1 (Figure 5-8C,D); in contrast, glucose uptake was significantly elevated in si*Mknk2* #1 but not si*Mknk2* #2 adipocytes (Figure 5-8E). These data suggest that the si*Mknk2* phenotype is not reproducible with individual siRNA and requires a combination of both si*Mknk2* #1 and #2. Therefore, the MNK2 knock-down phenotype may not be as robust as anticipated initially, as mentioned previously. As expected, si*Mknk1,* did not affect ChREBP expression.

Interim Conclusion

Insulin-responsive glucose uptake was significantly elevated in si*Mknk2* adipocytes, suggesting MNK2 may negatively regulate glucose uptake or insulin signalling more broadly. Glucose uptake was not correlated with ChREBP expression, suggesting the reduction in ChREBP is likely independent of its activation. These results were not reproducible with individual siRNA, suggesting the MNK2 knockdown phenotype may not be as robust as initially anticipated.

Role of MNK2 in the regulation of glycolytic flux

The increase in glucose uptake observed in si*Mknk2* adipocytes was likely to have implications for glycolytic metabolism. Using phenol red as an indicator of growth media acidity, the rate of acidification in differentiating si*Mknk2* adipocytes appeared to be greater than in si*Scrambled* adipocytes (data not shown). It was hypothesised that glycolysis may be occurring at a faster rate in si*Mknk2* adipocytes compared to si*Scrambled*, since increased glycolytic flux would generate more lactic acid and thereby lower the pH of the growth media at a faster rate (Figure 5-1). The level of L-lactate in the growth media of differentiating si*Mknk2* and si*Scrambled* adipocytes was therefore assayed as an indirect measure of glycolytic flux. In support of the hypothesis, L-lactate levels were increased in si*Mknk2* adipocytes compared si*Scrambled*, suggesting increased glycolytic flux (Figure 5-9A).

To account for the increase in glycolytic flux, it was hypothesised that the level of lactate dehydrogenase (*Ldha*), which is responsible for L-lactate production from pyruvate, was increased. However, contrary to the hypothesis, the levels of *Ldha* actually trended lower in si*Mknk2* adipocytes (Figure 5-9B). Subsequently, it was hypothesised that the level of pyruvate dehydrogenase (*Pdha*), which is responsible for the conversion of pyruvate to acetyl-CoA in the mitochondria, was reduced in order to promote the conversion of pyruvate to L-lactate (Figure 5-1). However, *Pdha* levels were not significantly reduced in si*Mknk2* adipocytes (Figure 5-9C). mRNA levels however, may not accurately reflect pyruvate flux given that this process is regulated in a complex manner by insulin and the family of pyruvate dehydrogenase kinases (*Pdks)* [370]. Nevertheless, these findings suggest that pyruvate may be being diverted away

from the citric acid cycle (TCA) (and FFA production) and towards L-Lactate production in si*Mknk2* adipocytes. In light of this, there is a need to examine pyruvate metabolism more closely as it may account, in part, for the reduction in lipid accumulation in these adipocytes. A direct measure of pyruvate to acetyl-CoA flux would be particularly informative.

> **Interim Conclusion**
>
> Lactate levels were elevated in si*Mknk2* adipocytes, suggesting pyruvate may be being diverted away from the TCA cycle and towards L-Lactate production.

Regulation of ChREBP nuclear translocation by MNK2

As shown earlier, the reduction in ChREBP in si*Mknk2* adipocytes was suggested to be independent of its activation. The nuclear translocation of ChREBPα is an important regulatory event that is necessary to induce ChREBPβ and a program of lipogenic and glycolytic gene transcription. The physical interaction of ChREBP with other proteins has been demonstrated to regulate its nuclear translocation: for instance, over-expression of HSL impedes ChREBPα translocation and thereby reduces transcription of lipogenic genes [371].

In si*Mknk2* adipocytes, the reduction in ChREBP was associated with reduced lipogenic gene expression (Figure 5-2), increased lipolysis (Figure 5-3C) and consequently, reduced lipid accumulation (Figure 4-17). Given MNK2, like HSL, is cytoplasmic, it was hypothesised that MNK2 may positively regulate the nuclear translocation of ChREBPα by physical interaction. To assess whether the nuclear translocation of ChREBPα was regulated by MNK2, the occupancy of ChREBP on the ChoRE elements upstream of *Chrebpb* in si*Mknk2* and si*Scrambled* adipocytes was investigated using ChIP. ChREBP regulates transcription by binding to ChoRE elements which are characterised by two E-boxes (CACGTG) separated by five nucleotides [372]. A consensus ChoRE as well as an E-box have been identified upstream of the *Chrebpb* promoter and are believed to be responsible for binding ChREBPα (Figure 5-10A) [369]. Unfortunately, difficulties were encountered when enriching for ChREBP during ChIP and therefore the occupancy of ChREBP on the ChoRE elements of *Chrebpb* could not be assessed (data not shown).

To address the hypothesis in another way, the level of *Chrebpb* mRNA was assayed by RT-qPCR in si*Mknk2* and si*Scrambled* adipocytes. It was hypothesised that if the translocation of ChREBPα was impaired MNK2 knock-down, then a reduction in the level of *Chrebpb* should be detectable. Unfortunately, *Chrebpb* levels were undetectable across all samples assayed, including primary mouse adipose tissue which was used as a positive control (data not shown). The hypothesis was therefore unable to be tested. This was surprising given *Chrebpb* transcript levels were detected in a previous study using the same primers [369].

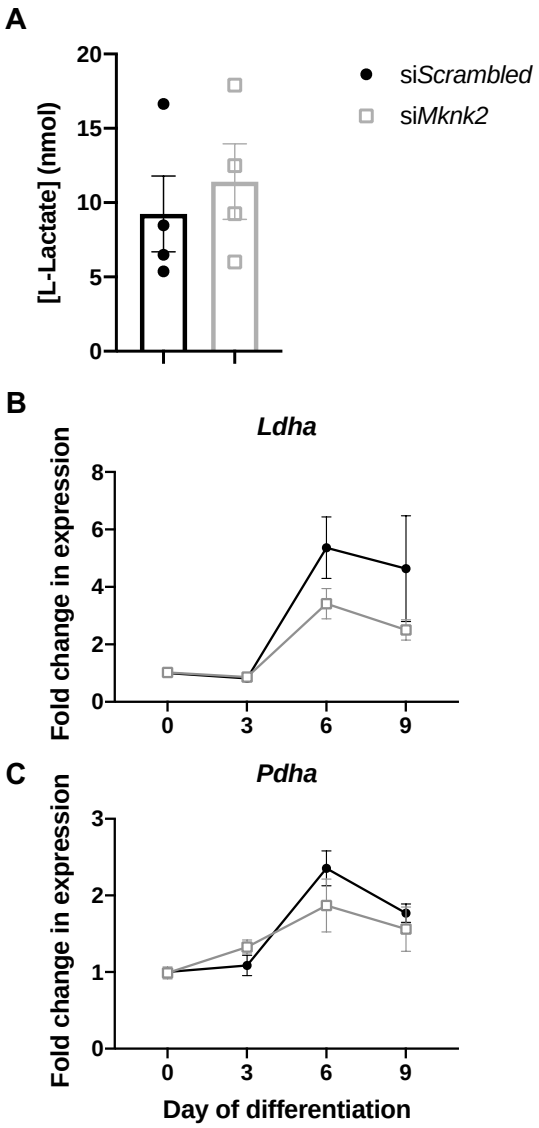

Figure 5-9: Effect of si*Mknk2* on lactate production in 3T3-L1 adipocytes.

3T3-L1 pre-adipocytes were pre-transfected with 25 pmol of si*Mknk2* (#1 and #2) or control si*Scrambled*, as indicated, 72 h prior to adipogenic induction. (A) L-Lactate levels were measured from media isolated from differentiating adipocytes on Day 6 (n=4). mRNA expression of (B) *Ldha* and (C) *Pdha* was assessed by RT-qPCR at the indicated times. Expression levels were normalised to *Nono* and *Hprt* and represented as fold change with respect to Day 0. Data are mean ± SEM; n=3.

Given these difficulties, a less direct approach was used to address the hypothesis. If, as hypothesised, ChREBPα translocation was impaired by MNK2 knock-down, then ChREBP occupancy on downstream target genes should be reduced. ChoRE elements upstream of *Fasn, Acaca* and *Acacb* have been previously identified in a genome-wide ChIP-seq study [364] and herein were precisely mapped to the mouse genome (Figure 5-10C-E). From the same study, ChoRE elements were also identified upstream of the *Eif4e* and *Mknk2* promoters [373], suggesting that the expression of eIF4E and MNK2 may be regulated by ChREBP and thus respond to glycolytic metabolism (Figure 5-10). MNK2 and, to a certain extent, eIF4E were increased during adipogenesis (Figure 3-1), so it was hypothesised that occupancy of ChREBP on their respective ChoRE elements may account for this.

Studies have reported that *Lipe* may be transcriptionally regulated by ChREBP [364,373], and based on these data, a putative ChoRE element upstream of the *Lipe* promoter was identified (Figure 5-10B). To account for the increased level of *Lipe* in si*Mknk2* adipocytes, it was hypothesised that ChREBP may negatively regulate *Lipe* expression through occupation of this ChoRE element. The negative regulation of gene expression by ChREBP has been reported previously [374]. In such cases, ChREBP is thought to promote the recruitment of co-repressors to impair transcriptional activity. If, as hypothesised, ChREBPα translocation was impaired by MNK2 knock-down, the *Lipe* promoter should become de-repressed and lead to increased HSL expression.

The occupancy of ChREBP on the respective ChoRE elements, as depicted in Figure 5-10C-E, was assessed in si*Mknk2* and si*Scrambled* adipocytes by ChIP to investigate the abovementioned hypotheses. However, as before, there were difficulties in enriching for ChREBP and therefore its occupancy could not be properly assessed (data not shown). The hypotheses in question therefore remained unresolved. They are, however, pertinent and relevant to understanding the underlying mechanism(s) of ChREBP regulation and require further experimental effort.

Interim Conclusion

It is hypothesised that MNK2 positively regulates the nuclear translocation of ChREBPα by physical interaction. A ChoRE element was identified in the proximal promoter of *Lipe*, which is hypothesised to bind ChREBP and negatively regulate its expression. Direct and indirect methods were used to assess ChREBPα translocation and its binding to ChoRE elements but were unsuccessful due to technical difficulties.

Site	Sequence
ChoRE +157/174	GCAGATCGCGTGGAGCTCAGGTGAGCAGG
E-box -92/98	GCCATCCACGTGCTAAGG

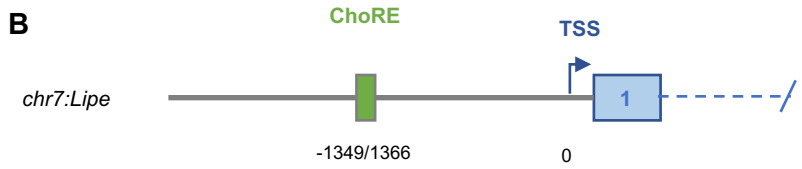

Site	Sequence
ChoRE -1349/1366	GGAACCCATGTGCTAAGCATGCGCTCCTG

Site	Sequence
ChoRE -247/264	CCCGGCCTCGCGCGGGCCACGCGGGGCTC
ChoRE -6922/6939	GGATGGCATGCCTGCAGCGCATGCTGGAA

Site	Sequence
ChoRE -6635/6652	GGTGTCCATGTGAAAACACTGTGGGCAGT

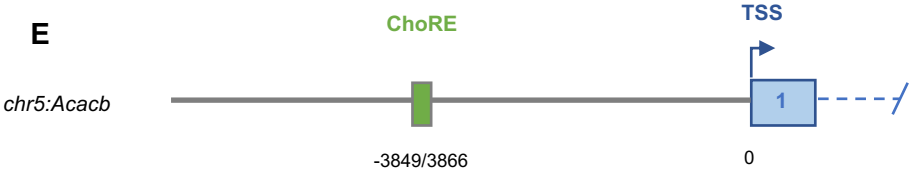

Site	Sequence
ChoRE -3849/3866	AGCCATCATGAGGTTTGCACGTGGCTCCA

Figure 5-10: Identification of ChoRE elements in ChREBP-responsive genes.

Schematics depicting the genomic location of putative carbohydrate response elements (ChoRE) or E-boxes, on the promoters of (A) *Chrebp* (*Mlxipl*) (B) *Lipe* (C) *Fasn* (D) *Acaca* and (E) *Acacb*, relative to the TSS. The DNA sequence of the putative ChoRE and E-box elements are shown; nucleotides corresponding to the core consensus sequence are bold underlined. TSS locations: *Chrebpa* chr5:135,582,760; *Chrebpb* chr5:135,565,789; *Lipe* chr7:26,175,130; *Fasn* chr11:120,685,420; *Acaca* chr11:83,993,336; *Acacb* chr5:114,615,526.

Prediction of MNK2 protein interactions

To understand how MNK2 may physically interact with proteins to regulate lipid metabolism, a functional protein interaction network was generated from the STRING database (string-db.org) [375] to analyse known and predicted interactions with *Mknk2* (MNK2) (Figure 5-11). As expected, *Mknk2* was predicted to interact with *Mapk3* (ERK1), *Mapk1* (ERK2), *Eif4e* (eIF4E), *Eif4e1b* (eIF4E-1B), *Eif4e2* (eIF4E-2), *Mapk14* (p38α) and *Mapk11* (p38β) (Figure 5-13). However, the MNK2 interaction network did not predict interactions with *Chrebp* or *Lipe*. Nevertheless, such interactions cannot be excluded from this analysis alone, as they may be indirect or lacking from the available data, and therefore immunoprecipitation (IP) of MNK2 should be performed to investigate any such interactions.

Earlier, it was mentioned that MNK2 may regulate the expression of LPIN1, since it was differentially expressed in si*Mknk2* adipocytes (Figure 4-17A). From the interaction network, experimental evidence sources suggest that MNK2 may interact with serine/arginine-rich splicing factor (SRSF) 1 (*Srsf1)*, *Srsf5* and SRSF kinase 1 (*Sprk1*) (Figure 5-11), all of which are implicated in the regulation of alternative mRNA splicing. LPIN1α/β splicing is controlled by *Srsf10* (SRSF10) [376], a related splicing factor from the same family. It was therefore hypothesised that the activity of similarly-related *Srsf1, Srsf5* or *Srpk1* or indeed *Srsf10* itself, may be regulated by interaction with MNK2 and this interaction promotes LPIN1β splicing. The predicted interactions of MNK2 with components of the splicing machinery are intriguing given the observations with CLK1/4 and alternative splicing (Chapter 3).

Functional associations with MNK2 were also predicted for C-terminal domain (CTD) small phosphatase-like protein (*Ctdspl)* and CTD small phosphatase protein 1 (*Ctdsp1*), which regulate the activity of RNA polymerase II (RNAPII) (Figure 5-11). During the transcription cycle, the CTD of RNAPII undergoes dynamic phosphorylation and dephosphorylation [377]. The CTD is also required for mRNA processing and binds to processing factors when hyper-phosphorylated [378]. MNK2 interaction with one or both of these partner proteins may therefore modulate the transcriptional and/or the mRNA processing activity of RNAPII.

Co-expression evidence sources predicted a functional association between MNK2 and polymerase I and transcript release factor (PTRF; *Ptrf*), also known as Cavin-1 (Figure 5-11). PTRF is the major structural protein of caveolae, which are specialised membrane invaginations at the surface of adipocyte cell membranes. Caveolae are involved in the uptake of FFA, synthesis of TAG, contain the necessary enzymes for lipolysis and are considered central to adipose function [379]. KO of PTRF has pleiotropic effects on lipid metabolism: adipocytes are smaller, show poor responsiveness to β-adrenergic stimuli and insulin, have a marked inability to take up and store FFAs, whilst animals are remarkably protected from diet-induced obesity [380].

A

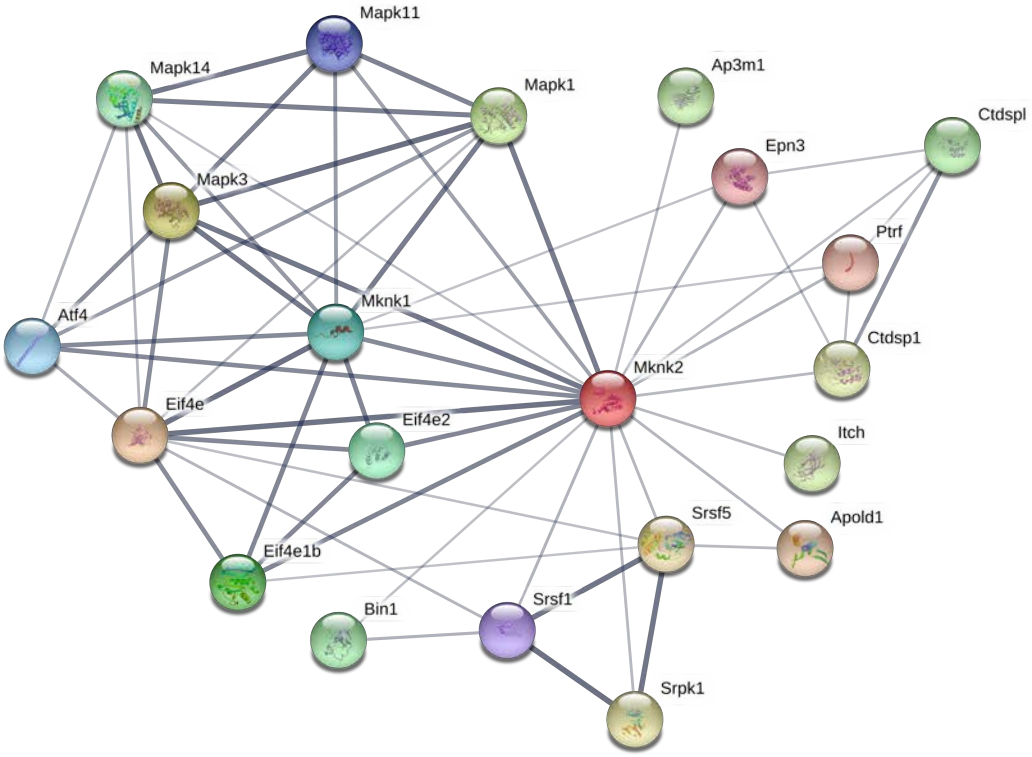
Mapk11
Mapk14
Mapk1
Ap3m1
Ctdspl
Epn3
Mapk3
Ptrf
Mknk1
Atf4
Ctdsp1
Mknk2
Eif4e
Eif4e2
Itch
Srsf5
Apold1
Eif4e1b
Srsf1
Bin1
Srpk1

B

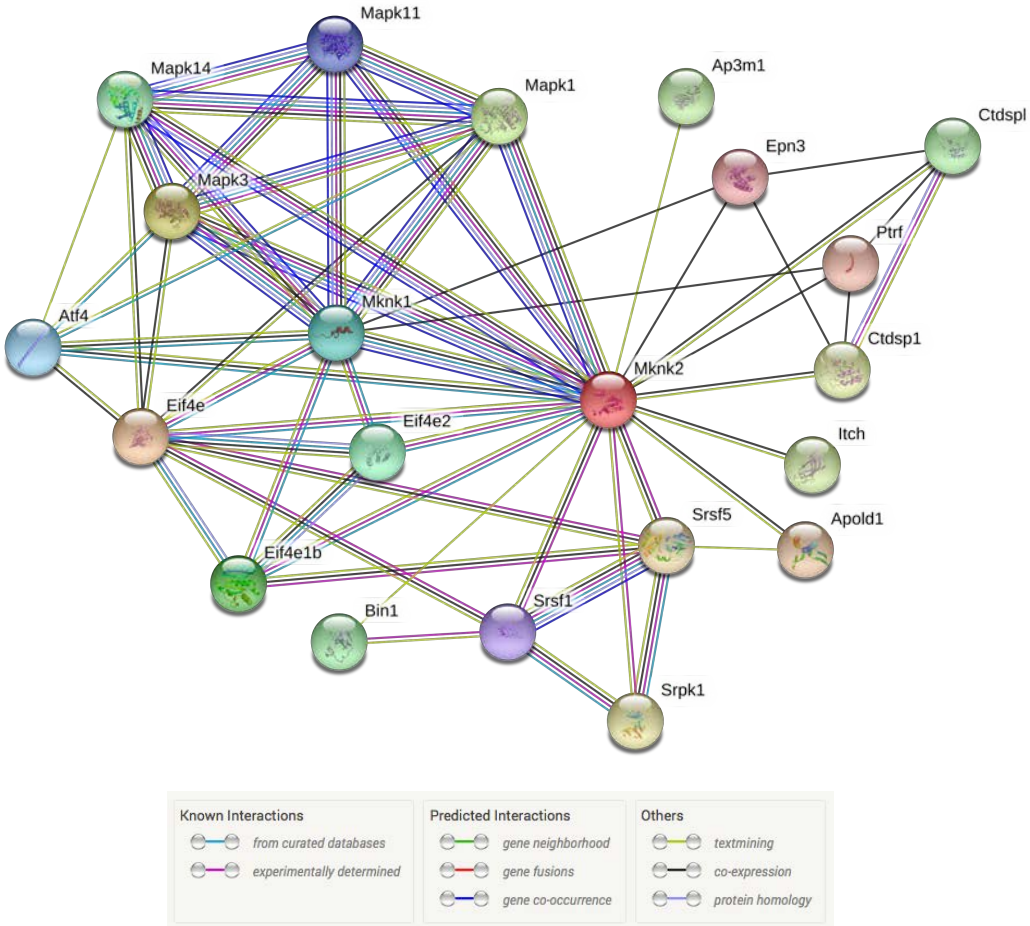
Mapk11
Mapk14
Mapk1
Ap3m1
Ctdspl
Epn3
Mapk3
Ptrf
Mknk1
Atf4
Ctdsp1
Mknk2
Eif4e
Eif4e2
Itch
Srsf5
Apold1
Eif4e1b
Srsf1
Bin1
Srpk1
Known Interactions
from curated databases
experimentally determined
Predicted Interactions
gene neighborhood
gene fusions
gene co-occurrence
Others
textmining
co-expression
protein homology

Figure 5-11: Predicted protein interactions with MNK2.

The STRING database was used to generate an interaction network to predict protein interactions with MNK2. In (A); the thickness of the line indicates the degree of confidence of the protein interaction whilst in (B), the colour of the line indicates the type of evidence for the interaction: known interactions are represented in magenta or pink; predicted interactions in green, red or blue; other associations in lime, black or purple (see key for details).

The structural integrity of caveolae in si*Mknk2* adipocytes was not investigated, so it was not established whether MNK2 regulates caveolae formation. However, given that some of the phenotypic features of PTRF KO are consistent with MNK2-KO animals, and MNK2 is predicted to interact with PTRF, which in turn may affect the function or indeed formation of caveolae.

Less relevant functional associations were predicted from text-mining and co-expression evidence sources (Figure 5-11). Epsin-3 (*Epn3*), is an endocytic clathrin adaptor involved in endocytosis [381] that is exclusively expressed in the stomach [382]. *Ap3m1* is a subunit of the adaptor protein-3 (AP-3) complex associated with the Golgi body that facilitates the intracellular trafficking of membrane-associated proteins [383]. Itchy (*Itch)* is an E3 ubiquitin-protein ligase involved in the control of immune signalling pathways: Itchy-deficient mice display severe immune and inflammatory defects [384], but are remarkably protected from diet induced obesity [385]. Apolipoprotein L domain-containing protein 1 (*Apold1*), also known as vascular early response gene (Verge), is selectively expressed in vascular endothelial cells and platelets where it is involved in developmental angiogenesis and responses to ischaemia [386].

Interestingly, curated database evidence suggested with a reasonable degree of confidence that *Mknk2* interacts with *Atf4* (ATF4) and surprisingly *Mknk1* (MNK1) (Figure 5-11).

Interim Conclusion

No physical interactions were predicted to occur between MNK2, ChREBP and HSL; however, potential interactions cannot be excluded until determined experimentally. MNK2 was predicted to interact with SRSF1, SRSF5 and SRPK1, which are implicated in alternative mRNA splicing. MNK2 may interact with these factors to modulate the splicing of LPIN1. MNK2 may also interact with and modulate the activity of PTRF (Cavin-1), a major structural protein of caveolae which are localised membrane regions involved in FFA uptake, TAG synthesis and lipolysis.

Metabolic changes induced by siMknk2 post-adipogenesis

To investigate the potential of therapeutics used to silence MNK2 expression in adipose tissue, it was important to discern whether the metabolic changes induced by the knock-down of MNK2 could also be induced at later times, for example, in mature or maturing adipocytes. To assess this hypothesis, 3T3-L1 pre-adipocytes were treated with si*Mknk2* or si*Scrambled* either three-days prior to (–3), at the time of (+0), or three-days post-adipogenic induction (+3), during which time metabolic gene expression was assessed by RT-qPCR (Figure 5-12A). As expected, the level of *Mknk2* was significantly reduced on Days 0, 3 and 6 in (–3), (+0) and (+3) in si*Mknk2*-treated cells, respectively, whilst the level of *Mknk1* was not affected in all cases.

In (–3) si*Mknk2*-treated cells, consistent with previous findings (Figure 5-1), the level of *Acaca* and *Acly* were significantly reduced, whilst the level of *Lipe* was significantly increased (Figure 5-

12A). Unexpectedly and in contrast to previous findings, the level of *Acacb, Chrebpa, Dgat1, Dgat2* and *Fasn* trended lower albeit not significantly (Figure 5-12A). The levels of *Cd36*, *Lpin1, Lpl, Mgll, Plin1, Pnpla2* and *Slc2a4* were not significantly affected by (–3) si*Mknk2,* as expected (Figure 5-12A). Lipid accumulation, as assessed by ORO staining, was significantly reduced in (–3) si*Mknk2*-treated adipocytes (Figure 5-12B,C), consistent with earlier findings (Figures 4-17, 5-2, 5-3)

Developing adipocytes treated with (+0) si*Mknk2* showed reduced levels of *Acaca, Acacb, Acly, Chrebpa, Dgat1, Dgat2* and *Fasn*, and elevated levels of *Lipe;* however, these changes were not significant (Figure 5-12A). As expected, the levels of *Cd36*, *Lpin1, Lpl, Mgll, Plin1, Pnpla2* and *Slc2a4* were not significantly affected, consistent with (–3) si*Mknk2* treated adipocytes. In line with these gene expression changes, lipid accumulation also trended lower, although not significantly (Figure 5-12B,C). Therefore, the knock-down of MNK2 at the time of induction (+0) induced the same trends in altered metabolic gene expression, however, the effect was not as strong as treatment prior to induction (–3) si*Mknk2*.

Adipocytes treated with (+3) si*Mknk2* had reduced levels of *Acaca, Acacb, Acly, Chrebpa, Dgat1, Dgat2* and *Fasn*, however, the changes were smaller in magnitude compared to (+0) si*Mknk2*-treated cells; in contrast, *Lipe* was significantly increased (Figure 5-12A). As expected, *Cd36*, *Lpin1, Lpl, Mgll, Plin1, Pnpla2* and *Slc2a4* levels were unaffected. Despite the modest changes in gene expression, lipid accumulation was reduced to an extent similar to (–3) si*Mknk2*-treated cells, suggesting MNK2 knock-down can significantly reduce lipid accumulation, regardless of treatment prior to or post-induction (i.e. in developing or developed adipocytes). However, it was not clear why (+3) treatment induced a stronger reduction in lipid accumulation than (+0) si*Mknk2* adipocytes. The magnitude of the gene expression changes induced by (+3) si*Mknk2* were less than (–3) si*Mknk2*, presumably because the cells had not been exposed to si*Mknk2* for the same duration, or because effects of MNK2 are exerted earlier in the adipogenic program. If given more exposure to si*Mknk2*, it is likely the magnitude of the gene expression changes would increase in subsequent days.

Interim Conclusion

siRNA knockdown of MNK2 at later stages of adipocyte development can induce changes in metabolic gene expression that significantly reduce lipid accumulation. The knock-down of MNK2 expression in adipose tissue has potential as a future therapeutic that can be broadly applied to adipocyte populations and is not restricted to a particular stage of adipocyte development.

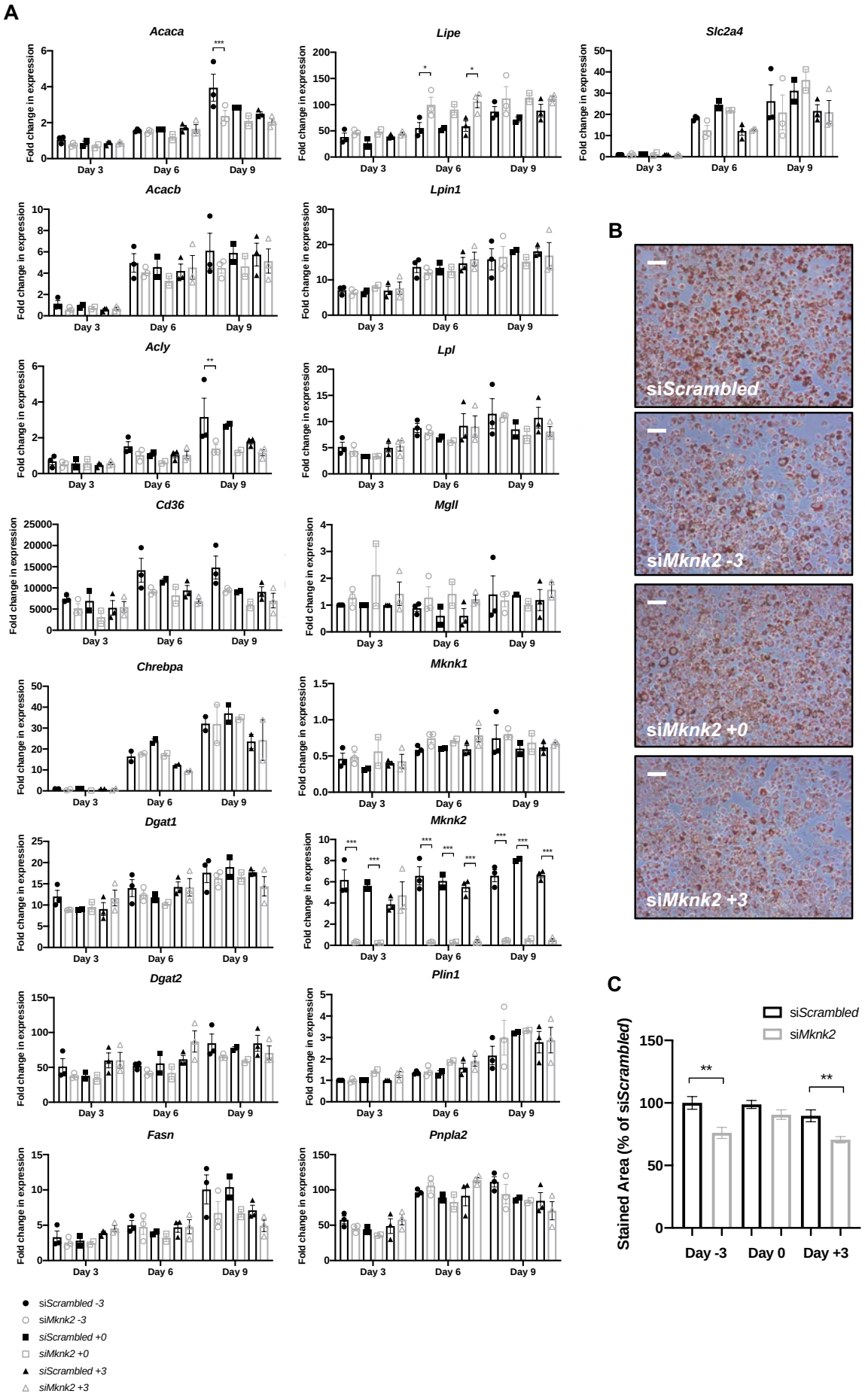
A
Acaca
Lipe
Slc2a4
Acacb
Lpin1
Acly
Lpl
Cd36
Mgll
Chrebpa
Mknk1
Dgat1
Mknk2
Dgat2
Plin1
Fasn
Pnpla2
Fold change in expression
Day 3
Day 6
Day 9
siScrambled -3
siMknk2 -3
siScrambled +0
siMknk2 +0
siScrambled +3
siMknk2 +3
B
siScrambled
siMknk2 -3
siMknk2 +0
siMknk2 +3
C
siScrambled
siMknk2
Stained Area (% of siScrambled)
Day -3
Day 0
Day +3

Figure 5-12: Inducible effects of si*Mknk2* on metabolic gene expression.

3T3-L1 pre-adipocytes were pre-transfected with 25 pmol of si*Mknk2* #1+#2 or si*Scrambled,* either 72 h prior (-3), at the time of (0) or 72 h after adipogenic induction (+3), as indicated. mRNA expression of metabolic genes was assessed by RT-qPCR at the indicated times. Expression levels were normalised to *Nono* and *Hprt* and represented as fold change with respect to Day 0 si*Scrambled*. Data are mean ± SEM; n=2-3; 2-way ANOVA (*P < 0.05 **P < 0.01 ***P < 0.001). (B) Day 9 differentiated adipocytes were stained with ORO to assess lipid accumulation. (C) The total stained area was quantified from different fields of view and represented as percentage stained area relative to si*Scrambled*; data are mean ± SEM (n=2); one-way ANOVA (*P < 0.05 **P < 0.01 ***P < 0.001).

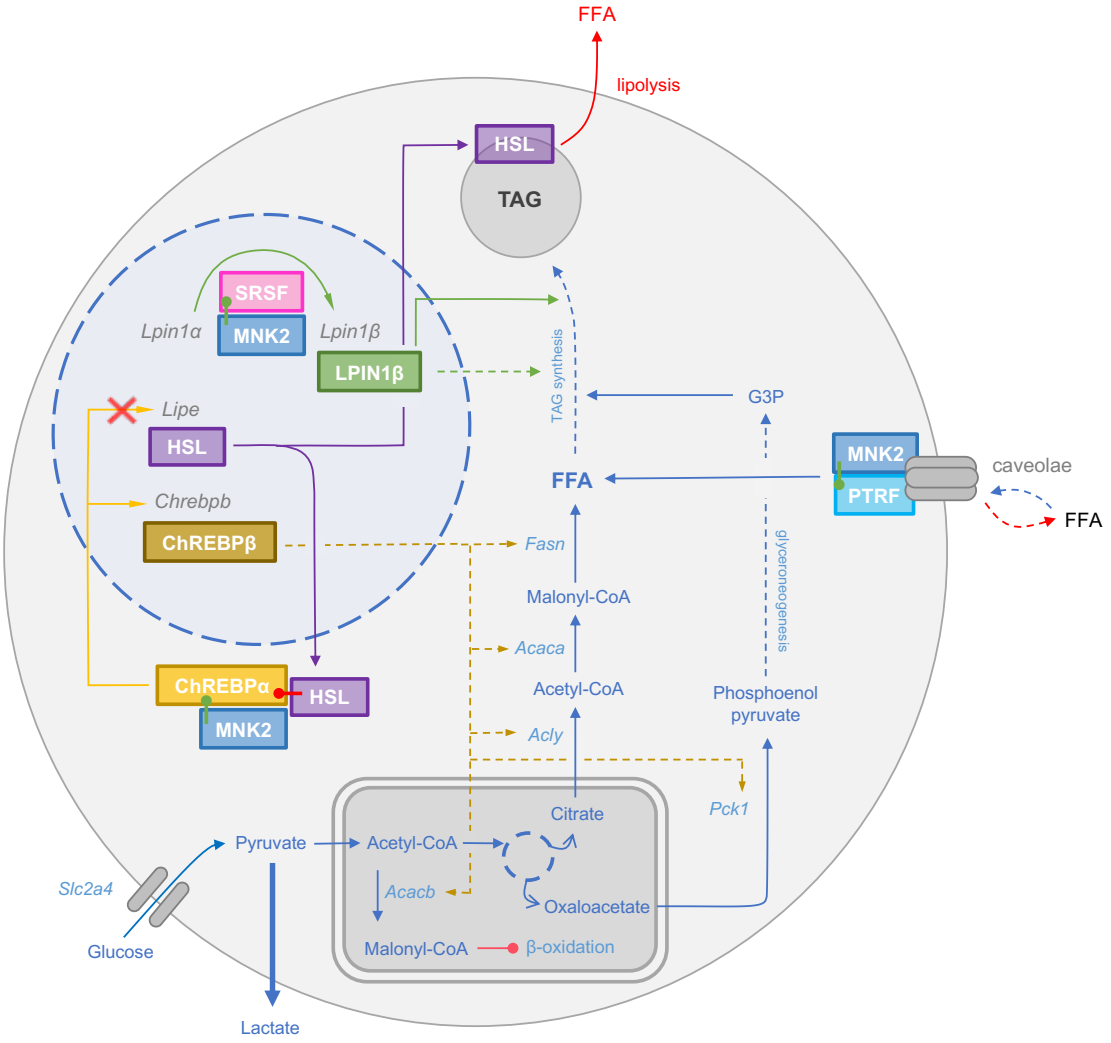
FFA
lipolysis
HSL
TAG
SRSF
MNK2
Lpin1α
Lpin1β
LPIN1β
TAG synthesis
G3P
Lipe
HSL
FFA
MNK2
PTRF
caveolae
FFA
Chrebpb
ChREBPβ
Fasn
Malonyl-CoA
Acaca
glyceroneogenesis
ChREBPα
HSL
MNK2
Acetyl-CoA
Phosphoenol pyruvate
Acly
Pck1
Citrate
Pyruvate
Acetyl-CoA
Slc2a4
Acacb
Oxaloacetate
Glucose
Malonyl-CoA
β-oxidation
Lactate

Figure 5-13: Regulation of 3T3-L1 adipocyte metabolism by MNK2.

Proposed model of how MNK2 regulates adipocyte metabolism *in vitro*. MNK2 is proposed to positively regulate the nuclear translocation of ChREBPα which is responsible for inducing the transcription of *Chrebpb* (solid gold line) and repressing transcription of *Lipe* (red cross). *Chrebpb* is responsible for increasing the transcription of ChoRE responsive genes (dotted gold lines). Upon MNK2 knock-down, ChREBPα translocation is decreased which in turn reduces the expression of DNL genes (*Fasn, Acaca, Acly*), FFA synthesis and their incorporation into TAG. Pyruvate, from glycolysis, is increasingly be diverted away from the citric acid cycle (TCA) and FFA synthesis towards lactate production. The level of *Acacb* may is reduced, thereby increasing mitochondrial β-oxidation and the breakdown of TAG. HSL expression is increased from de-repression of the *Lipe* promoter which increases lipolysis further impeded ChREBP nuclear translocation by direct interaction. MNK2 may interact with and modulate the activity of SRSF factors (SRSF1/5, SPRK10) and in turn regulate LPIN1β splicing. LPIN1β transactivates genes involved in TAG synthesis (dotted green line) and converts phosphatidate to DAG in the second-last step of this pathway (solid green line). MNK2 may also interact with Cavin-1 (PTRF), which is an essential component of caveolae, to regulate FFA uptake, synthesis and breakdown of TAG.

Discussion

This Chapter has investigated whether and how the loss of MNK2 expression alters adipocyte metabolism and reduces lipid accumulation. The knockdown of MNK2 resulted in a significant reduction in the level of genes involved in lipogenic pathways, namely DNL and glyceroneogenesis (Figure 5-2). These changes were attributed to significant reductions in two major lipogenic transcriptional regulators, ChREBP and LPIN1 (Figure 5-3), the latter of which also catalyses the conversion of phosphatidate to (DAG) during the synthesis of TAG. It is proposed that MNK2 positively regulates the nuclear translocation of ChREBPα through a direct or indirect interaction (Figure 5-13). MNK2 is also thought to regulate the splicing of LPIN1β by interacting with components of the alternative splicing machinery which has previously been implicated in LPIN1β alternative splicing [376] (Figure 5-11, 5-13). Loss of MNK2 expression also increased HSL expression and consequently, the rate of isoproterenol-stimulated lipolysis (Figure 5-3). It is proposed that ChREBP negatively regulates the expression of HSL through a putative ChoRE element identified in the upstream promoter of its gene, *Lipe* (Figure 5-10B). Additionally, an MNK2 protein interaction was predicted with Cavin-1 (PTRF), an essential structural component of caveolae (Figure 5-11). It is proposed that MNK2 interacts with PTRF to modulate the activity or indeed assembly of caveolae and this, to some extent, may account for the reduction in lipid content. Importantly, the changes in lipogenic gene expression and the lipid reduction associated with MNK2 knock-down were inducible at later stages of adipocyte development (Figure 5-12), suggesting the changes can be broadly applied to developing adipocyte populations and are not restricted to a certain stage of development. Intriguingly, alternative mechanisms appear to be responsible for reducing lipid content *in vivo* (Table 5-1). MNK-DKO mice have significantly elevated levels of *Chrebpa* and *Ucp1*, and are protected from HFD-induced weight gain despite increases in DNL gene transcription, suggesting they have greater 'browning' capacity.

Previously, the loss of MNK2 expression in adipocytes significantly reduced lipid accumulation (Figure 4-17C-E). In this Chapter, significant reductions in the rate-limiting enzymes of DNL and TAG synthesis, *Fasn* and *Dgat1/2*, respectively, were observed, alongside other genes in these pathways including *Acaca, Acly* and *Lpin1* (Figure 5-2). There was also a significant decrease in *Pck1* (Figure 5-2), the rate-limiting enzyme of glyceroneogenesis which is responsible for regenerating G3P as a substrate for TAG synthesis and lipid recycling. This is consistent with the observation that adipose-specific KO of *Pck1* reduces the amount of stored triglyceride in adipose depots [387]. Consistent with the reduction in lipogenic gene expression was a decrease in *Acacb* (Figure 5-2), the activity of which regulates mitochondrial FFA oxidation [337,388]. *Acacb*$^{-/-}$ mice have increased rates of FFA oxidation, are leaner and protected from diet induced obesity [337,388]. The knockdown of MNK2 is therefore proposed to increase adipocyte FFA oxidation and thereby contribute to the overall reduction in cellular lipid content.

Given that gene expression changes in si*Mknk2* adipocytes broadly affected lipogenic pathways (Figure 5-2), it was proposed that MNK2 regulated upstream regulators. The protein expression of two major lipogenic transcriptional regulators, ChREBP and LPIN1 [315,351,389], was significantly reduced in si*Mknk2* adipocytes (Figure 5-3). The ChREBPα isoform is localised to the cytoplasm and its nuclear translocation (reviewed in [351]) is necessary for full activation of the ChREBP transcriptional program. Direct protein-protein interactions regulate ChREBPα translocation; notably HSL has been shown to physically interact and impede ChREBP nuclear translocation [371]. Given that expression of ChREBP and downstream lipogenic genes were significantly reduced in si*Mknk2* adipocytes (Figure 5-2, 5-3), it was proposed that MNK2 positively regulates ChREBPα nuclear translocation through a direct or indirect interaction. Protein network analyses were unable to predict an interaction of ChREBP with MNK2; however, it must be stressed that this does not exclude the possibility and needs to be assessed experimentally. In terms of the regulation of LPIN1 expression, protein network analyses predicted MNK2 to interact with SRSF1/5 and SRPK1 (Figure 5-11). The predicted interaction with SRSF1 may be attributed to its role in controlling MNK2 alternative splicing in human cells [16]. However, given that LPIN1β splicing is regulated by a related family member, SRSF10 [376], it is proposed that the physical interaction between MNK2 and SRSF1/5, SRPK1 or indeed SRSF10 may promote LPIN1β splicing. The effect of reduced LPIN1β expression on reducing lipid accumulation is likely to be two-fold: reducing lipogenic gene transcription; and the conversion of phosphatidate to (DAG) during TAG synthesis (Figure 5-13).

The knock-down of MNK2 resulted in the up-regulation of *Lipe* (Figure 5-2) which was reflected directly in the elevated expression of HSL (Figure 5-3). HSL is the key enzyme responsible for the hydrolysis of DAG during lipolysis [328]. The elevation in HSL was associated with an increased rate of isoproterenol-stimulated lipolysis (Figure 5-3C), consistent with the way HSL is recruited to the lipid droplet surface under such conditions [339]. Previous reports have identified *Lipe* as a potential transcriptional target of ChREBP [364,365]. Analysis of the proximal promoter region in *Lipe* identified a putative ChoRE element where ChREBP may bind (Figure 5-10B). It is proposed that ChREBP may negatively regulate *Lipe* from this ChoRE, given that HSL expression was inversely correlated with ChREBP in si*Mknk2* adipocytes (Figure 5-3). The effect of elevated HSL expression on reducing lipid accumulation is suggested to be two-fold: in addition to (1) increasing the breakdown of TAG through increased lipolysis, elevated levels of HSL are likely to (2) further impair the nuclear translocation of ChREBPα [371] and thereby establish a feedback loop that further reduces the expression of lipogenic genes (Figure 5-13).

Protein network analyses also predicted a protein interaction between MNK2 and Cavin-1 (PTRF) (Figure 5-11). Cavin-1 is the major structural protein of caveolae, the KO of which results in a marked inability to take up and store FFAs *in vivo* [380]. It is suggested that MNK2

may interact with Cavin-1 to modulate the activity or indeed formation of caveolae. The predicted interaction is not based on experimental evidence and must therefore be assessed experimentally to validate and establish its biological importance. MNK2 protein interactions could be assessed by pulldown of tagged constructs following transfection of 3T3-L1 cells. Similarly, kinase-dead mutant constructs could be used to assess non-catalytic functions of MNK2, as inferred from the differences between the effects of inhibitors and siRNA.

In contrast to the *in vitro* results, *Chrebpa* and the expression of DNL genes were paradoxically increased in MNK-DKO mice *in vivo* (Table 5-1). It remains to be determined where FFAs may be being diverted or utilised to account for the reduction in lipid content *in vivo*. However, given there was a significant increase in *Ucp1* in MNK-DKO adipocytes (Table 5-1), it was suggested that these mice may have increased thermogenic capacity (i.e. ability to 'burn' fat) which may provide protection from HFD-induced weight gain [390]. Experimental evidence suggests ChREBP may transcriptionally regulate *Ucp1* [365], consistent with the expression of *Chrebpa* and *Ucp1* in MNK-DKO mice (Table 5-1). MNK2 may therefore regulate thermogenesis and the 'browning' of adipose tissue *in vivo*.

Intriguingly, the metabolic phenotype of si*Mknk2* adipocytes was not replicated by the knock-down of MNK1 (Figure 5-7). In fact, MNK1 appeared to play an opposing role, particularly in relation to lipolysis: *Pnpla2* (ATGL), the key enzyme responsible for initiating TAG lipolysis, was significantly reduced (Figure 5-7). Despite some reductions in lipogenic gene expression, lipid accumulation was slightly elevated in si*Mknk1* adipocytes, suggesting lipolysis may be reduced, presumably due to the reduction in *Pnpla2* expression. The fact that MNK1/2 differentially regulate the expression of two lipases, suggests there is a perceived role for the MNKs in regulating lipid metabolism. This finding is consistent with the unique roles of MNK1 and MNK2 in regulating responses to an HFD [3], and highlights the importance of designing isoform-selective therapies.

The potential for an MNK2-targeted knockdown therapy was encouraged by the fact that changes in metabolic gene expression and lipid reduction were inducible during later stages of adipocyte development (Figure 5-12). This is important because it suggests that the targeting window for administering therapy is not restricted to a certain developmental stage. However, the development of MNK2 targeted therapies requires more investigation, particularly to determine how decreased lipogenesis and increased lipolysis may (adversely) impact other tissues and organs. Increased lipolysis increases the circulation of FFAs which, under sustained conditions, leads to lipid deposition in metabolically important tissues such as liver and muscle, and can impair insulin signalling [72].

In conclusion, novel insights have been made into the non-catalytic functions of MNK2 that establish it as a key metabolic regulator in adipocytes. *In vitro* knock-down of MNK2 reduces ChREBP and LPIN1 expression, which decreases DNL and glyceroneogenic gene expression and increases isoproterenol-stimulated lipolysis. In contrast, the *in vivo* KO of MNK2 increases *Chrebpa* and *Ucp1* levels, the latter of which is proposed to increase the 'browning' capacity of adipose tissue. It is apparent that both *in vitro* and *in vivo* models impinge on the regulation of ChREBP expression, albeit in contrasting ways. The net outcome of loss of MNK2 expression is reduced adipose lipid content and so MNK2 may be a desirable candidate for interventional weight management therapies.

Chapter 6
Discussion, Future Perspectives and Limitations

Key findings and future work

The studies described in this Thesis were based on the observation that MNK2-KO mice are protected from HFD-induced weight gain. This was attributed to the fact that there were fewer adipocytes in MNK2-KO mice and that they did not increase in size on an HFD [3]. It was hypothesised that adipogenesis may be regulated by MNK activity, in particular by the activity of MNK2, since it is the predominant isoform in adipose tissue [3]. However, using specific MNK inhibitors it was shown that MNK catalytic activity is not actually required for adipogenesis (Figures 3-31, 3-32, 3-34). Therefore, given that its expression was highly induced during adipogenesis (Figure 3-1A), it was proposed that MNK2 may regulate aspects of adipocyte biology. To explore this, MNK2 expression in 3T3-L1 fibroblasts was knocked out using a CRISPR-Cas9 genetic deletion approach (Figure 4-2); however, this yielded widely-differing phenotypes in terms of adipogenic propensity and lipid accumulation, making it difficult to discern the role of MNK2 (Figure 4-5). This was overcome by knocking-down MNK2 in a heterogenous pre-adipocyte population with siRNA. The siRNA-mediated knockdown of MNK2 did not impair adipogenesis but, rather surprisingly reduced adipocyte lipid accumulation (Figure 4-17). Since this phenotype was not observed with MNK inhibition, it was proposed that MNK2 regulates adipocyte metabolism through a novel non-catalytic function(s). Subsequent *in vitro* findings revealed that underlying lipogenic pathways were down-regulated in si*Mknk2* adipocytes, which was ultimately attributed to the down-regulation of two major lipogenic transcriptional regulators, ChREBP and LPIN1 (Figure 5-3). However, in MNK-DKO adipose tissue ChREBP was upregulated along with the adipocyte browning marker, *Ucp1* (Table 5-1) and so it is apparent that alternative mechanisms may account for lipid reduction *in vivo*.

The revelation that adipogenesis does not require MNK catalytic activity, but rather that non-catalytic function(s) of MNK2 are responsible for regulating adipocyte metabolism prompts the questions: *does MNK2 regulate additional biological processes in other cellular contexts?* and *what is the significance of P-eIF4E as a metric of MNK function?* As discussed in Chapter 5, the catalytic activity of a kinase is only one aspect of its biological function; non-catalytic properties determine where the kinase is localised in the cell, which protein(s) with which it interacts, how these interactions govern the activities of the kinase itself and its partner proteins, and whether the protein binds DNA or other cellular components. Given eIF4E is the only *in vivo* validated substrate of the MNKs [13], many studies have focused on P-eIF4E to make interpretations about MNK function. Unfortunately, a large proportion of studies have relied upon the use of inhibitors [62,63] some of which are non-specific [64,65] and may well have led to misleading interpretations. If studies were repeated using more specific inhibitors such as eFT508 [59], *would the same interpretations about MNK function be made?*

Alternative approaches have been used to study P-eIF4E, such as the use of mice or cells expressing the non-phosphorylatable S209A knock-in mutant of endogenous eIF4E [37] and MNK-KO mouse models [13], but there remains great speculation but no general consensus regarding the biological significance of Ser209 phosphorylation (reviewed in [30,32]). *If the focus was shifted away from P-eIF4E and towards investigating the non-catalytic functions of MNK2, what else might be uncovered?* Novel non-catalytic functions of MNK2 were revealed in Chapter 5 (Figure 5-13), and therefore the study of non-catalytic functions in a wider range of cellular contexts warrants more investigation. This may be particularly revealing in cancer lines where MNK2 is over-expressed [255–257], given that such cells are adept at hijacking cellular metabolism for their own survival advantage. This prompts several questions: d*oes over-expression of MNK2 confer a survival advantage for cancer cells and, if so, why? Are the non-catalytic functions of MNK2 in adipocytes relevant in the context of cancer cell biology*? *Could the knockdown of MNK2 be a therapeutic avenue to explore in combination with other cancer therapies?* It is important to keep in mind that there is some therapeutic benefit of MNK inhibition in at least certain types of cancer, as exemplified by the progression of an MNK inhibitor through clinical trials, namely eFT508 [59]. Thus, although MNK catalytic activity does not appear to be relevant in 3T3-L1-derived adipocytes, there does seem to be a function for MNK activity in mature adipocytes in mice.

Future work required

Investigate whether the likely non-catalytic functions of MNK2 are relevant in other cellular and biological contexts, such as cancer and/or identify additional non-catalytic functions that are yet to be identified.

In Chapter 5, it was shown that the knock-down of MNK2 decreased the expression of rate-limiting enzymes of *de novo* lipogenic and glyceroneogenic pathways (Figures 5-2, 5-3), and increased stimulated lipolysis (Figure 5-3C). These changes were attributed to a reduction in the lipogenic transcriptional regulator, ChREBP (Figure 5-3); it is possible, but untested, that MNK2 may regulate its nuclear translocation (Figure 5-13). Furthermore, the expression of LPIN1 was reduced (Figure 5-3); LPIN1 is a bi-functional protein that regulates the transcription of lipogenic genes and catalyses the conversion phosphatidate to DAG during TAG synthesis [315,389]. MNK2 is predicted to interact with members of the SRSF splicing factor family (Figure 5-11) which may promote splicing of the LPIN1β mRNA (Figure 6-1). This is because another related splicing factor, SRSF10, has already been implicated in the regulation of LPIN1 splicing [376]. The knockdown of MNK2 up-regulated HSL expression and increased isoproterenol-stimulated lipolysis (Figure 5-3), and this is thought to be due to the fact that *Lipe* is under negative regulation of ChREBP which binds to a putative ChoRE located in its proximal promoter (Figure 5-10B). Given that HSL directly interacts with ChREBP to impede its nuclear translocation [367], it would be important to determine whether the loss of MNK2 expression

further impedes the nuclear translocation of ChREBP, as hypothesised. Furthermore, MNK2 has been predicted to interact with PTRF (Cavin-1), a key structural component of caveolae, responsible for FFA uptake, TAG synthesis and TAG breakdown (Figure 5-11). It is proposed that MNK2 may regulate the stability, assembly and/or function of caveolae and thereby affect these functions (Figure 6-1).

Future work required

The proposed mechanisms of the *in vitro* model require investigation; it is important to assess whether ChREBP nuclear translocation is regulated by MNK2, and if so whether its occupancy on downstream targets (of DNL) are reduced. It will also be important to investigate whether the *Lipe* promoter is regulated by ChREBP and assess whether the increase in HSL further impedes its nuclear translocation. Furthermore, the interaction of MNK2 with PTRF and SRSF1/5 should be assessed and if so, then investigate how these interactions are responsible for regulating metabolism.

The incidence of being overweight and obesity are at epidemic levels and will continue to rise on their current trajectory if unimpeded. Both are risk-factors for the development of chronic diseases such as type-2 diabetes, cardiovascular disease and cancer [185]. Therefore, the principle of reducing the lipid content of adipose tissue is therapeutically desirable. Both the *in vitro* and *in vivo* models share a consistent phenotype in that the knockdown or KO of MNK2 reduces adipose lipid content. The fact that ChREBP, a key upstream regulator of DNL and lipid metabolism, was differentially expressed in the two models (i.e. affected by the loss of MNK2) (Table 5-1) suggests that the regulation of adipocyte metabolism by MNK2 may fall largely on this factor. Whilst ChREBP and associated DNL genes were downregulated *in vitro* by the knockdown of MNK2, ChREBP was actually up-regulated *in vivo* in MNK-DKO adipose tissue along with DNL genes and, interestingly, a protein of importance for non-shivering thermogenesis (which uses metabolic energy, i.e. ATP) *Ucp1* (Table 5-1). It is therefore pertinent to clarify these contrasting observations concerning levels of ChREBP: in simple terms, *why does the knock-down of MNK2 increase or decrease ChREBP levels in different models?* Our laboratory has performed and is currently conducting parallel studies using MNK-KO mice models to investigate this further. It is essential that underlying core mechanistic details are established to decide whether to develop a potential MNK2-targeted therapy and, if so, how to achieve this.

There are surprising advantages to increasing ChREBP expression in adipose tissue: over-expression of a constitutively active form of ChREBP (ChREBP-OX) specifically in adipose tissue reduces adiposity, improves insulin sensitivity and decreases fatty liver, whilst simultaneously promoting the 'browning' of adipose tissue [365]. The study predicted *Ucp1* to be a ChREBP target as it was up-regulated in WAT of ChREBP-OX animals, consistent with our *in vivo* findings (Table 5-1). Promoting adipose tissue 'browning' is an attractive therapeutic strategy for

decreasing lipid burden, as it is associated with metabolic changes that consume ATP and 'burn' fat reserves [390]. In contrast, lowering ChREBP expression in adipose tissue, whilst it may appear a good idea in principle to reduce lipid burden, actually has adverse effects on metabolism more broadly [327]. The loss of ChREBP reduces adipose DNL which in turn increases glucose levels, and over time animals develop insulin resistance. The liver, being the principal glycaemic regulator and only other major organ performing DNL, becomes overwhelmed and FFA synthesis must proceed at elevated levels. Excess DNL in the liver leads to deposition of FFAs and the promotion of fatty liver, which can lead to cirrhosis and even necessitate liver transplants. Other lipodystrophic effects also occur, leading to many undesirable metabolic consequences [327]. Therefore, it would seem that increasing ChREBP expression in adipose tissue would be the most attractive in a therapeutic perspective to deliver improved metabolic health outcomes.

Future work required

The increased 'browning' phenomenon predicted to occur in MNK-DKO mice should be followed up to determine whether *Ucp1* is a direct target of ChREBP and whether the expression of other browning markers are similarly regulated.

ChREBP has a well-defined role in liver, much like adipose tissue [391–395]. In fact, given that liver is the major glycaemic regulator [396], the function of ChREBP in regulating whole-body lipid metabolism is perhaps arguably more important here than in adipose tissue. In Chapter 5 it was proposed that the knockdown of MNK2 impairs the nuclear translocation of ChREBP which in turn reduces both the transcription of DNL genes and lipid content (Figure 6-1). If MNK2 were to regulate ChREBP translocation in the same manner in liver, then presumably liver DNL would be down-regulated as well. Whilst this may instinctively appear a good idea to reduce lipid burden, it may have unintended consequences for lipid metabolism. This would of course be dependent on diet, since the synthesis of liver FFAs would be most affected on a high carbohydrate diet as opposed to an HFD, where the principal source of FFAs is exogenous (dietary). Similarly, given that MNK2 is suggested to regulate the splicing and reduce the expression of LPIN1 in adipose tissue, it may well do the same in liver. Unlike adipose tissue, however, LPIN2, not LPIN1, is the predominant isoform and accounts for the majority of phosphatidate phosphatase activity during TAG synthesis [313]. Liver-specific KO of LPIN2 has been shown to significantly reduce body fat mass [334]. Therefore, based on this and its similarity to the *in vivo* phenotype of MNK2-KO mice, it is possible that pleiotropic or combinational effects of MNK2 KO in different organs may contribute to the protection from HFD-induced weight gain. It would be important to discern the role of MNK2 specifically in the liver and the effect of its knockdown on lipid metabolism. Floxed *Mknk2* mice have recently been made available to generate conditional MNK2-KO mice with KO only, e.g. in liver or fat to

discern the contributions made by MNK2 to metabolism in other tissues; i.e. *does the loss of adipose NK2 affect lipid metabolism in the liver?*

It is widely acknowledged that adipose tissue is composed of a heterogenous cell population and adipose depots specialise in performing distinct functions. Owing to differences in adipose depot biology, the effect of MNK2 knock-down may be more advantageous in certain adipose depots or combinations of depots over others. It would therefore be worthwhile to investigate the role of MNK2 in specific adipose depots to help inform the design of therapies, i.e. where they should be directed. Again, conditional MNK2-KO mice would be of significant importance here.

Future work required

Conditional MNK2-KO mouse models should be used to investigate the effect of MNK2 knockdown in the liver and selected adipose depots to assess the overall contribution of MNK2 to lipid metabolism in these organs.

In terms of developing an MNK2-targeted therapy, it would be important to assess the effect of MNK2 knock-down in human-derived adipocytes. At this stage, it would be important to assess the metabolic changes that occur and whether they resemble the *in vitro* or *in vivo* models, or some combination of both. It is also apparent that different dietary compositions affect the response and activity of ChREBP [327,369], so how might *different diets affect metabolism in response to MNK2 knockdown? Would an MNK2-targeted therapy be more responsive under an HFD or high-carbohydrate conditions?* Whilst in-roads have been made into understanding the non-catalytic functions of murine MNK2, there is an additional layer of complexity in that a second MNK2 isoform (MNK2b) is expressed in humans. MNK2b lacks a MAPK-binding domain, which accounts for its low activity [10]. MNK2b is also predominantly nuclear as opposed to MNK2, which is primarily cytoplasmic [10]. The different sub-cellular localisations of these MNK2 variants imply that the isoforms perform distinct functions, as has indeed been previously reported [17].

Future work required

Once the mechanistic details of the *in vitro* and *in vivo* models have been clarified, particularly concerning ChREBP, it will be appropriate to assess whether the findings can be translated into human tissues using human-derived adipocytes. This would be an important demonstration of the therapeutic potential of MNK2 to modify adipocyte metabolism in a beneficial manner in humans. Additional mouse studies could be performed to investigate how diet composition affects ChREBP-regulated metabolism in MNK2-KO mice. This will help to identify the dietary conditions most conducive and efficacious for therapy.

Adipose tissue is a major regulator of whole-body energy homeostasis and so mechanisms that perturb the homeostatic balance may have adverse consequences. It is therefore important to assess the long-term health implications of an MNK2-targeted therapy and investigate possible adverse side-effects, particularly related to global lipid metabolism, e.g. whether circulating levels of FFAs become elevated to precipitate the development of insulin resistance. Finding an optimal homeostatic balance in adipocytes and indeed other potentially-targeted organs (e.g. liver) would be a critical step for developing an MNK2 targeted therapy. However, other important considerations remain, such as the duration, timing and dosage of MNK2 knock-down in humans. It will also be important to identify the margin for error of MNK2 knockdown: whether complete knockdown is required for therapeutic benefit, or whether the same benefit can be achieved through the partial knock-down of MNK2.

> **Future work required**
>
> Investigate the long-term metabolic health implications of a potentially-targeted MNK2 therapy in animals and identify possible effects in other potentially-targeted organs. Investigate the duration, timing and dosage of MNK2 knock-down for which the desired therapeutic benefit can be achieved.

Future perspectives

In this Thesis, a deeper understanding of MNK2 biology has been achieved, for example, in relation to revealing its likely non-catalytic functions and how they regulate adipocyte metabolism. However, to better understand how these functions operate mechanistically, further investigation is required as identified above. Briefly, given the central role ChREBP appears to play in both *in vitro* and *in vivo* models, it will be essential to understand how differential ChREBP expression accounts for reduced lipid accumulation and identify which model is applicable to human adipose biology. As mentioned previously, the mechanisms involved appear to be distinct and therefore, could have marked outcomes for metabolism (i.e. depending on whether ChREBP expression is increased or decreased). Moreover, inter-organ effects may be contributing to the *in vivo* phenotype and so it will be important to understand to what extent MNK2 plays a role in other organs, particularly the liver, and its role in specific adipose depots, as this will ultimately guide therapy design. Considering ChREBP is regulated by metabolites downstream of carbohydrate metabolism, dietary composition will inevitably impact on the conditions that are most conducive and efficacious for MNK2 targeted therapy. Many unknowns still exist at this early stage as to the potential consequences such a therapy may have on metabolism at an organismal level, particularly if applied over a long duration.

Limitations

The findings from this Thesis are restricted to a (widely-used) murine *in vitro* model of adipogenesis. The contrasting findings related to ChREBP *in vitro* and *in vivo* may imply a limitation of the *in vitro* model in that it is unable to capture the heterogeneity and complexity of interactions that exist in adipose tissue *in vivo*. Thus, it is conceivable that the findings described in this Thesis do not translate directly to human adipose tissue and may be made more complicated by the expression of an additional MNK2 isoform, MNK2b. Nevertheless, this Thesis presents clear new data that prompts further study of MNK2 both *in vitro* and *in vivo*.

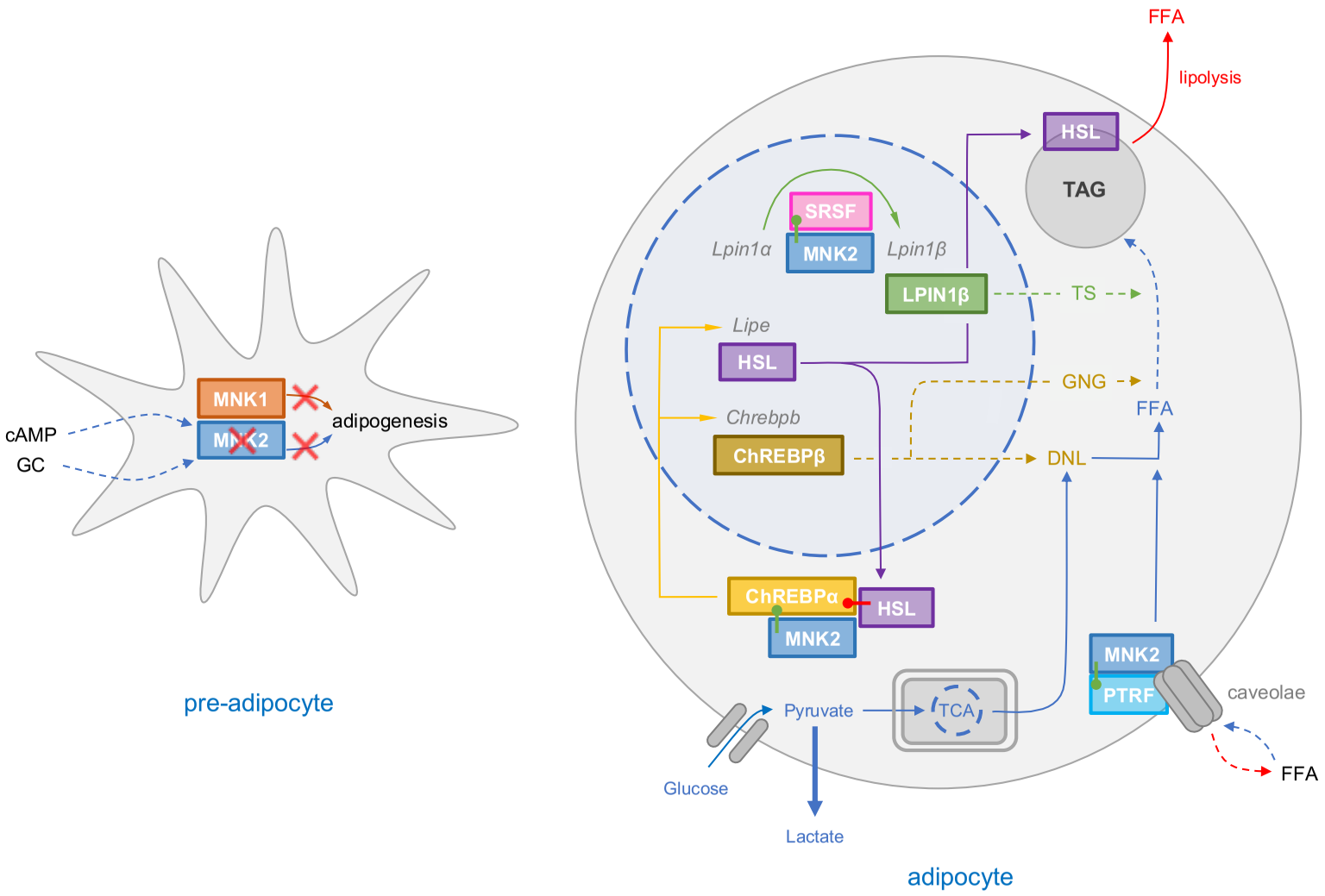
FFA
lipolysis
HSL
TAG
SRSF
MNK2
Lpin1α
Lpin1β
LPIN1β
TS
Lipe
HSL
GNG
FFA
Chrebpb
ChREBPβ
DNL
ChREBPα
HSL
MNK2
MNK2
PTRF
caveolae
Pyruvate
TCA
Glucose
Lactate
FFA
MNK1
MNK2
adipogenesis
cAMP
GC
pre-adipocyte
adipocyte

Figure 6-1: Graphical abstract of thesis findings.

MNK2 is induced during early adipogenesis through glucocorticoid and cAMP signalling. However, MNK1/2 catalytic activity (i.e. phosphorylation of eIF4E, as depicted by (P)) is not required for adipogenesis and proceeds normally in the absence of MNK2 expression. MNK2 is the predominant isoform in adipose tissue and is proposed to play a role in mature adipocytes. siRNA-mediated knock-down of MNK2 reduces adipocyte lipid accumulation *in vitro*. MNK2 is proposed to positively regulate the nuclear translocation of ChREBPα which induces *Chrebpb* and the transcription of ChoRE responsive genes regulating de novo lipogenesis (DNL) and glyceroneogenesis (GNG) (dotted gold lines); as well as repressing *Lipe*. Therefore, when ChREBPα translocation is reduced, DNL and GNG are reduced, which reduces FFA synthesis and their incorporation into TAG. Pyruvate, from glycolysis, is increasingly diverted away from the citric acid cycle (TCA) and converted to lactate. The *Lipe* promoter becomes de-repressed which increases HSL expression: HSL increases lipolysis and interacts with ChREBP to further impede the translocation of ChREBP. MNK2 may interact and modulate the activity of SRSF factors (SRSF1/5, SPRK10) which may regulate LPIN1β splicing. LPIN1β transactivates genes involved in TAG synthesis (TS: dotted green line) and acts as a phosphatidate phosphatase in the second-last step of this pathway. MNK2 may also interact with Cavin-1 (PTRF), an essential component of caveolae which are specialised membrane structures involved in FFA uptake, TAG synthesis and TAG breakdown.

Appendices

Appendix 1: Generation of GeneART CRISPR-EGFP vector.

(1) The CD4 CDS was spliced out of the parent GeneART CRISPR vector by *Eco*RI and *Age*I restriction digestion. (2) EGFP CDS was amplified from pX458 by PCR using EGFP Fwd and EGFP Rev primers with flanking restriction sites. (3) The EGFP CDS was ligated into the GeneART CRISPR backbone, generating GeneART CRISPR-EGFP.

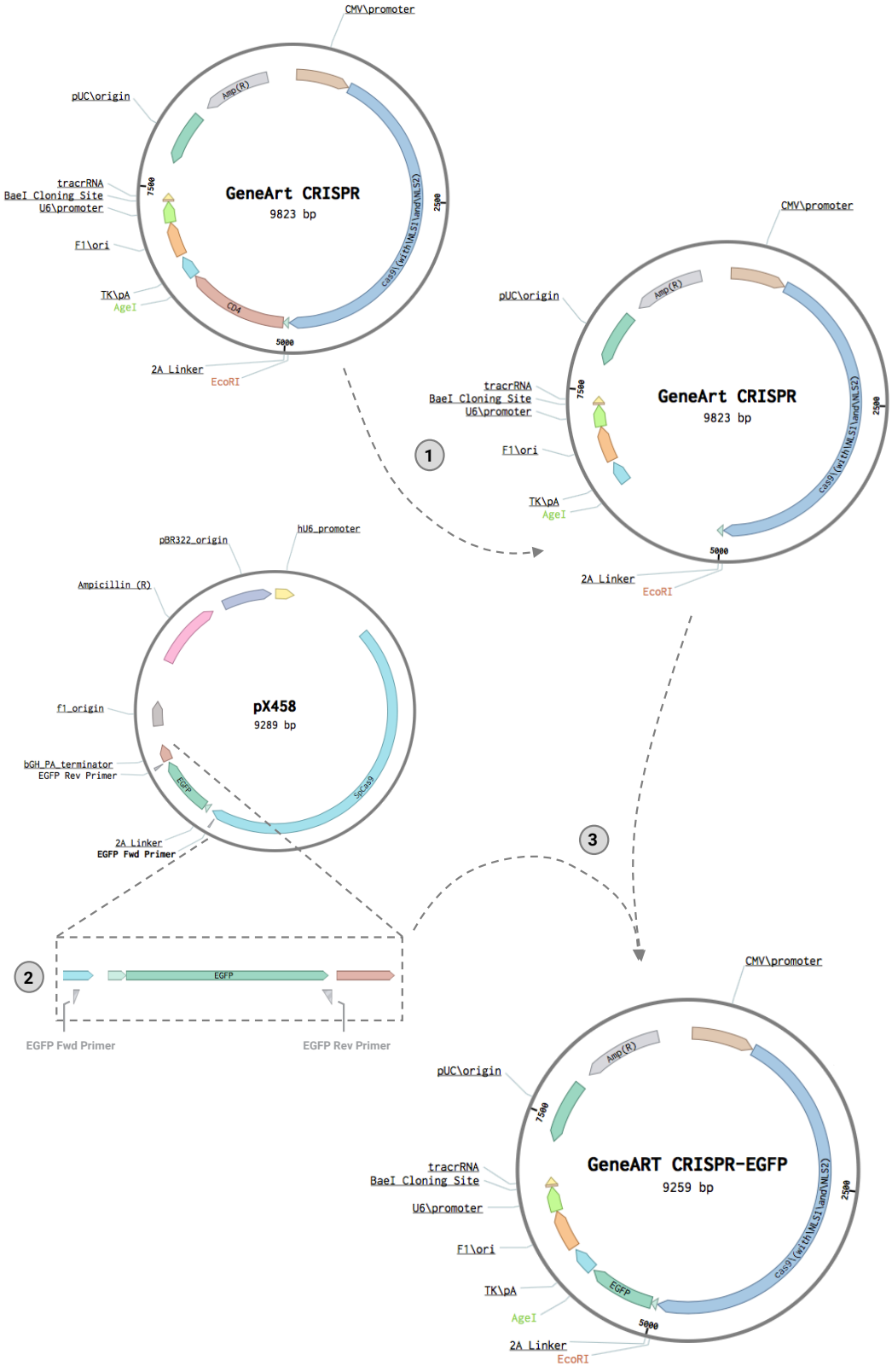

Appendix 2: Sanger sequencing alignment of the EGFP CDS and flanking regions of the GeneART CRISPR-EGFP vector.

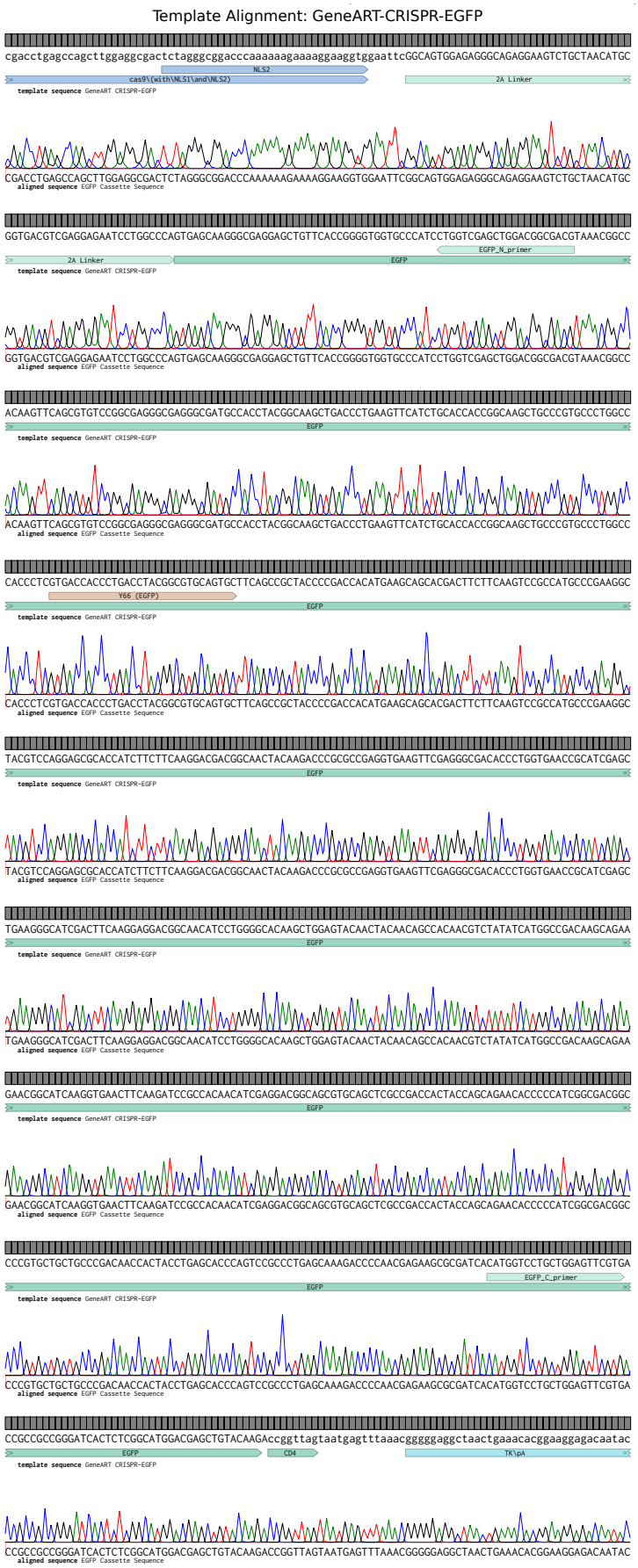

Appendix 3: Ligation of *Mknk2* E4 and *Mknk2* E5 sgRNAs into GeneART CRISPR vectors.

(A) Sequential *Bae*I and *Eco*RI restriction digestion was used to confirm ligation of sgRNA into *Bae*I sgRNA cloning site. Vectors with successfully ligated sgRNA are digested by *Eco*RI only and appear as a single fragment (green). Vectors with unsuccessfully ligated sgRNA are digested by both *Bae*I and *Eco*RI and appear as two fragments (red). Diagnostic digests for GeneART CRISPR-EGFP-Mknk2-E5 (lanes 3-5) and GeneART CRISPR-Mknk2-E4 (lanes 8-10) are represented alongside negative (*Bae*I+*Eco*RI) and positive controls (*Eco*RI) for the respective parent vectors (lanes 1-2 and 6-7). GeneRuler 1 kb ladder was used; size of fragments as indicated. Vector maps of (C) GeneART CRISPR-EGFP-Mknk2-E5 and (D) GeneART CRISPR-Mknk2-E4 display key coding sequences and location of *Eco*RI restriction site.

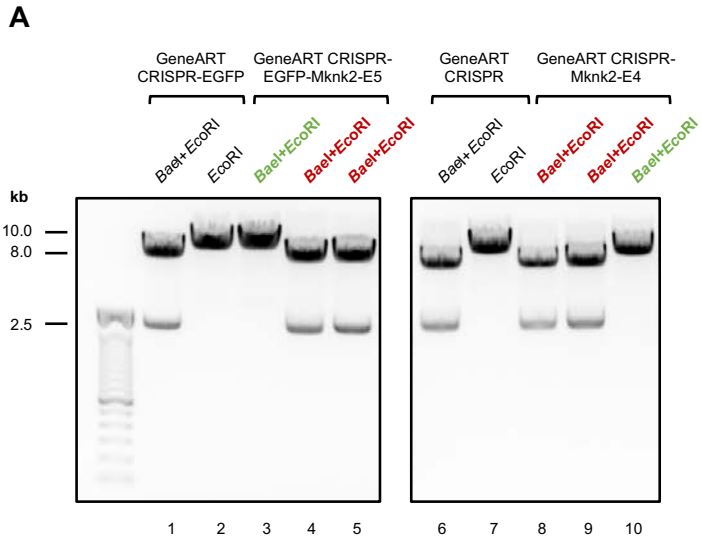
A
GeneART CRISPR-EGFP
GeneART CRISPR-EGFP-Mknk2-E5
GeneART CRISPR
GeneART CRISPR-Mknk2-E4
BaeI+EcoRI
EcoRI
BaeI+EcoRI
BaeI+EcoRI
BaeI+EcoRI
BaeI+EcoRI
EcoRI
BaeI+EcoRI
BaeI+EcoRI
BaeI+EcoRI
kb
10.0
8.0
2.5
1 2 3 4 5 6 7 8 9 10

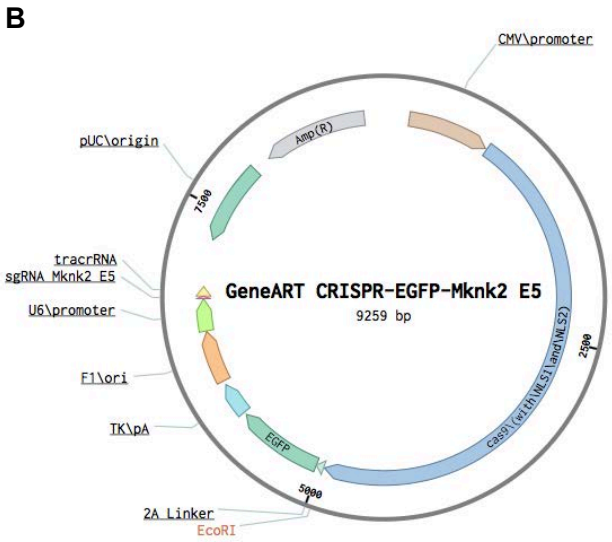
B
CMV\promoter
pUC\origin
Amp(R)
tracrRNA
sgRNA Mknk2 E5
U6\promoter
F1\ori
TK\pA
2A Linker
EcoRI
GeneART CRISPR-EGFP-Mknk2 E5
9259 bp
EGFP
Cas9(w1th\NLS1\and\NLS2)

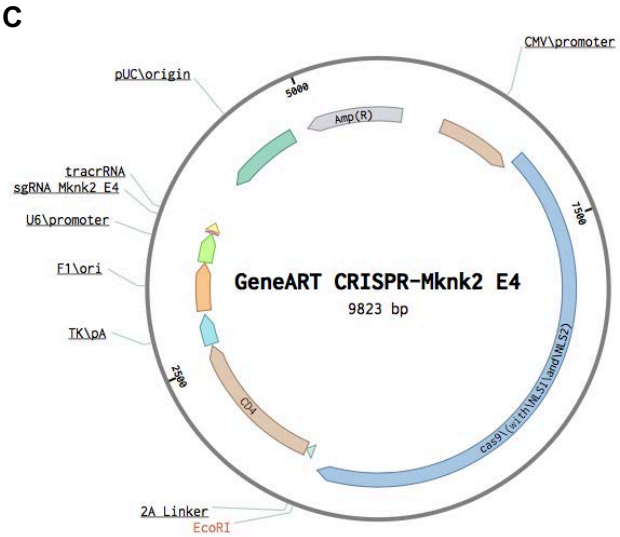
C
CMV\promoter
pUC\origin
Amp(R)
tracrRNA
sgRNA Mknk2 E4
U6\promoter
F1\ori
TK\pA
2A Linker
EcoRI
GeneART CRISPR-Mknk2 E4
9823 bp
CD4
Cas9(w1th\NLS1\and\NLS2)

Appendix 4: Verification of sgRNA cloning.

Sanger sequencing alignment of region flanking the sgRNA cloning site of (A) GeneART CRISPR-*Mknk2*-E4 and (B) GeneART CRISPR-EGFP-*Mknk2*-E5

A

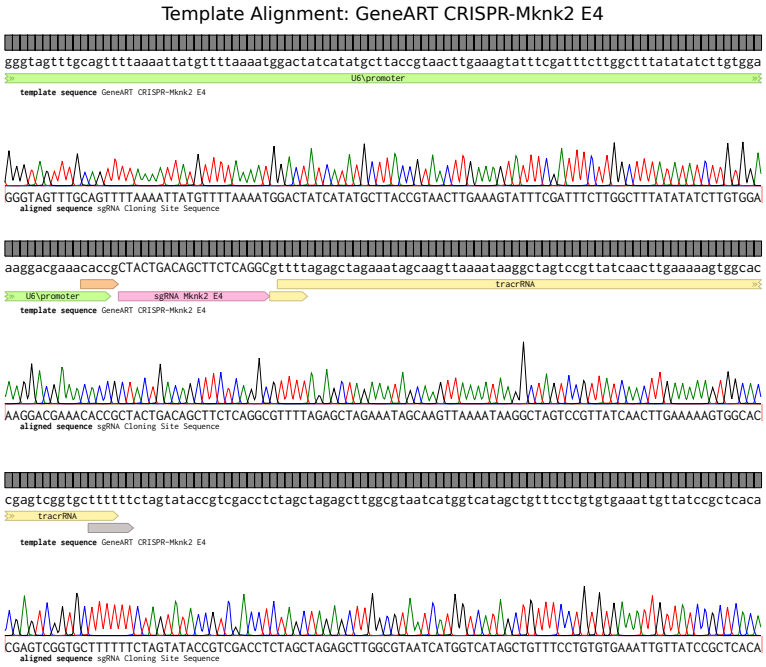

B

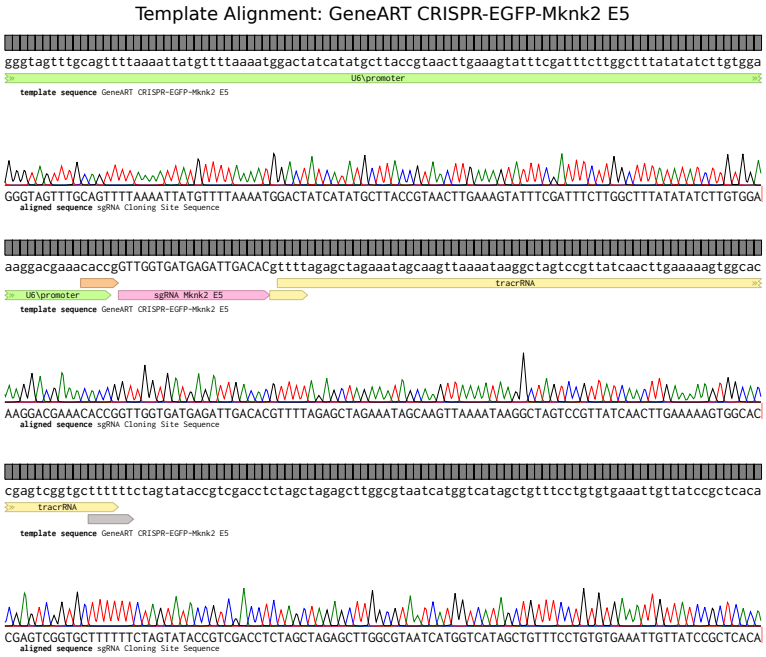

Appendix 5: Sanger sequencing alignment of Clone 1-6B.

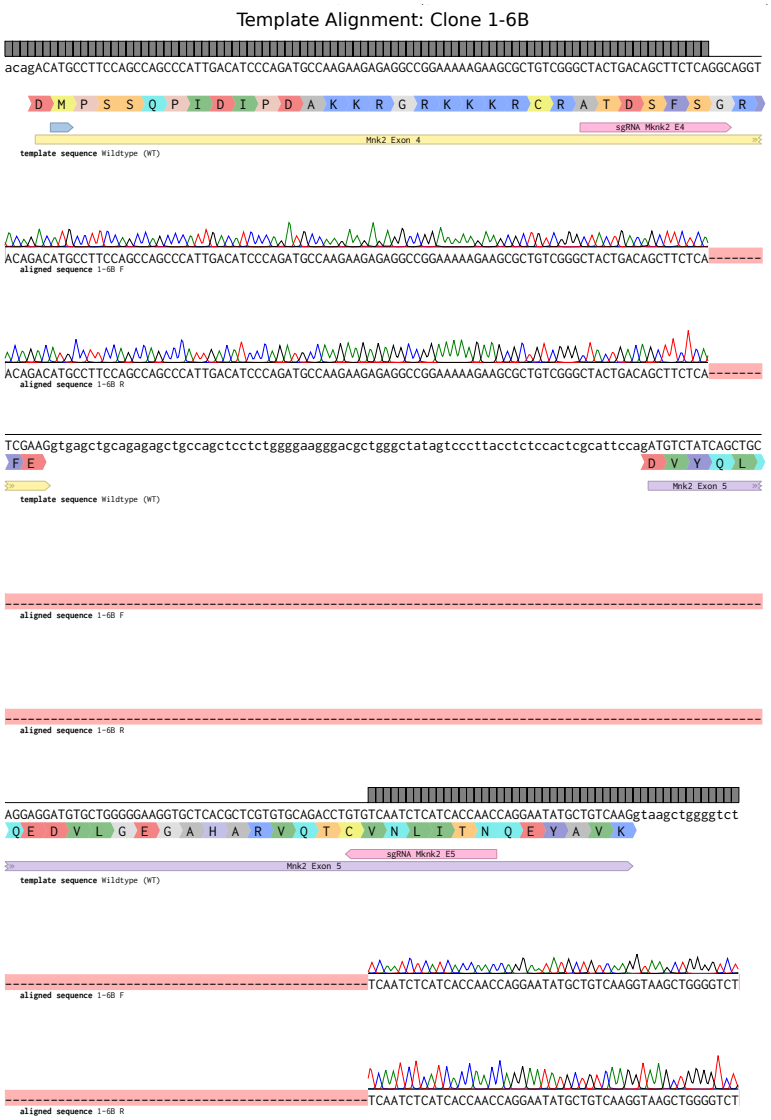

Appendix 6: Sanger sequencing alignment of Clone 1-7B.

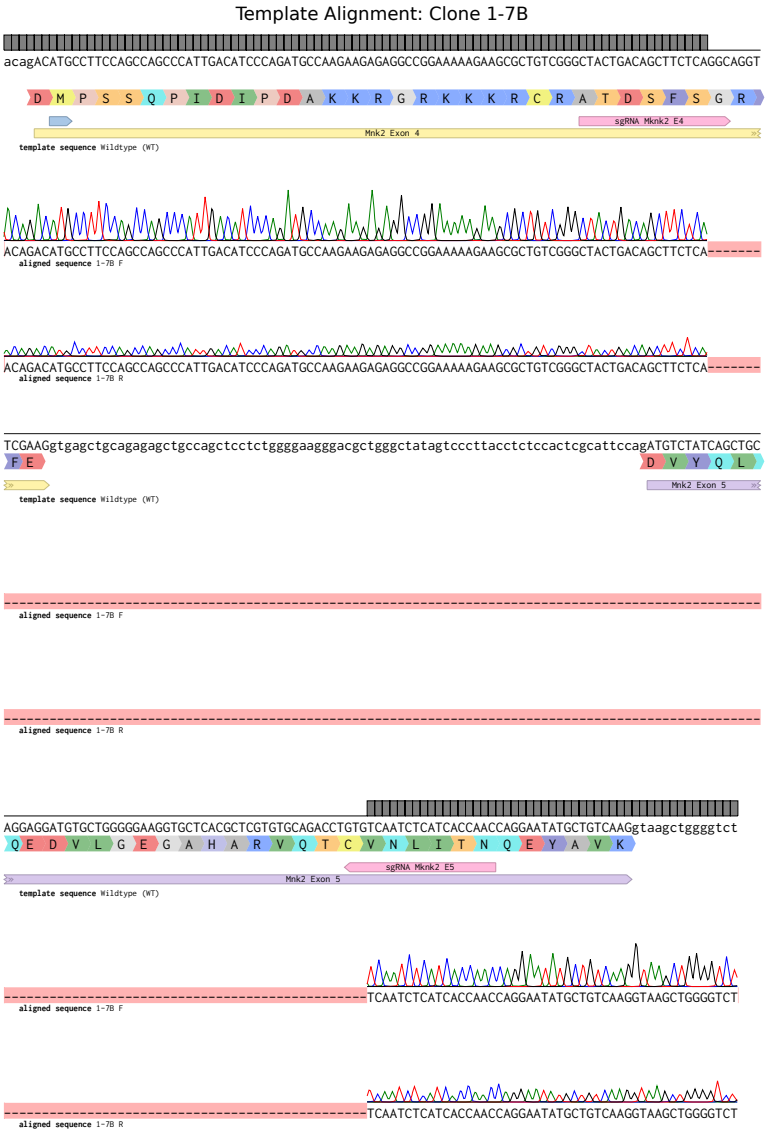

Appendix 7: Sanger sequencing alignment of Clone 1-8E.

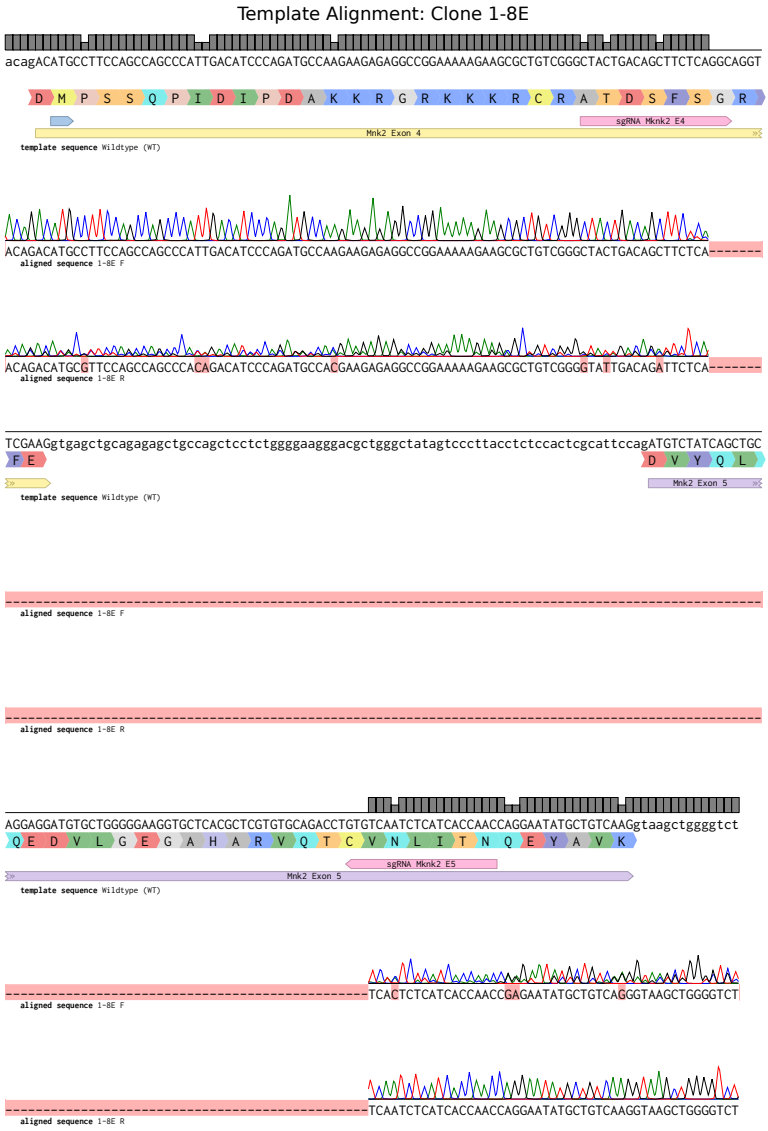

Appendix 8: Sanger sequencing alignment of Clone 2-2E.

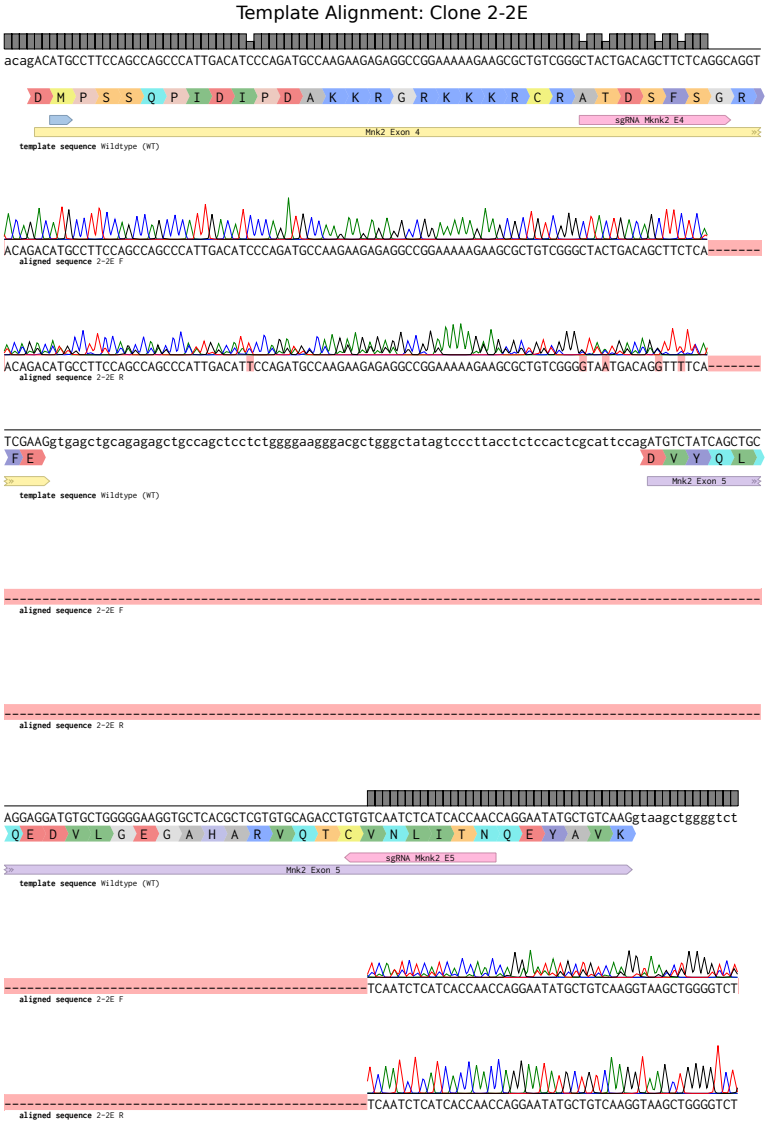

Appendix 9: Sanger sequencing alignment of Clone 3-2G.

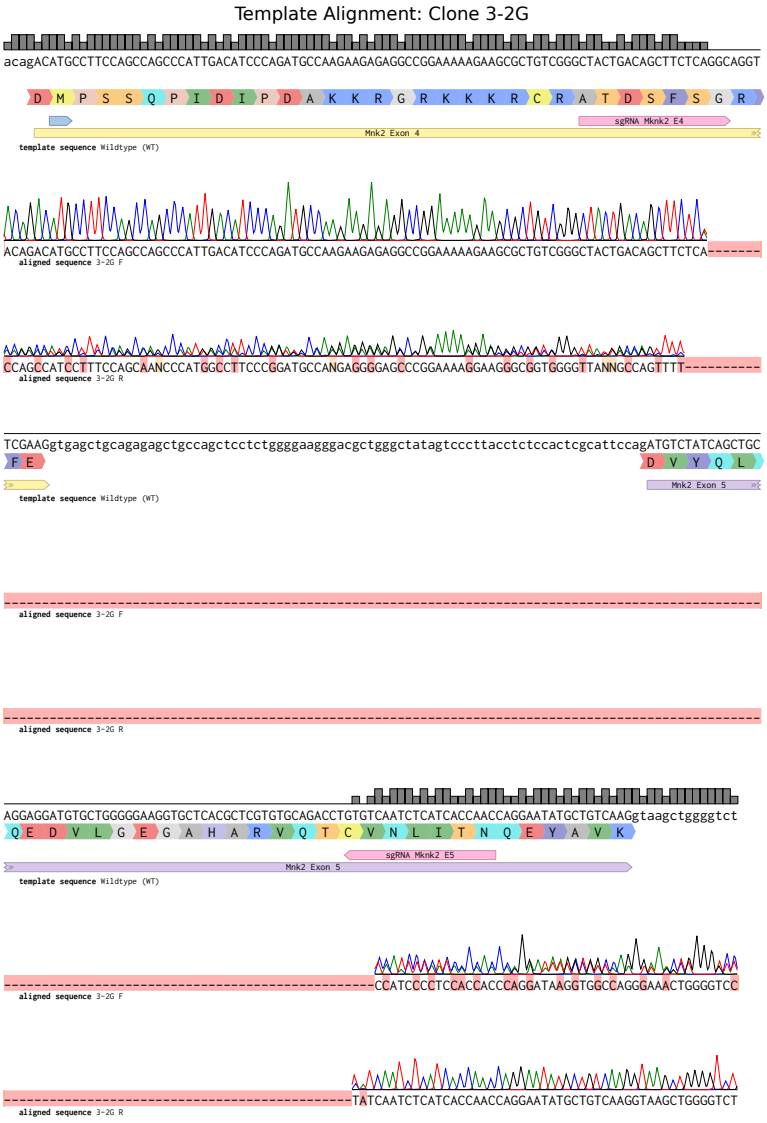

Appendix 10: Sanger sequencing alignment of Clone 4-7C.

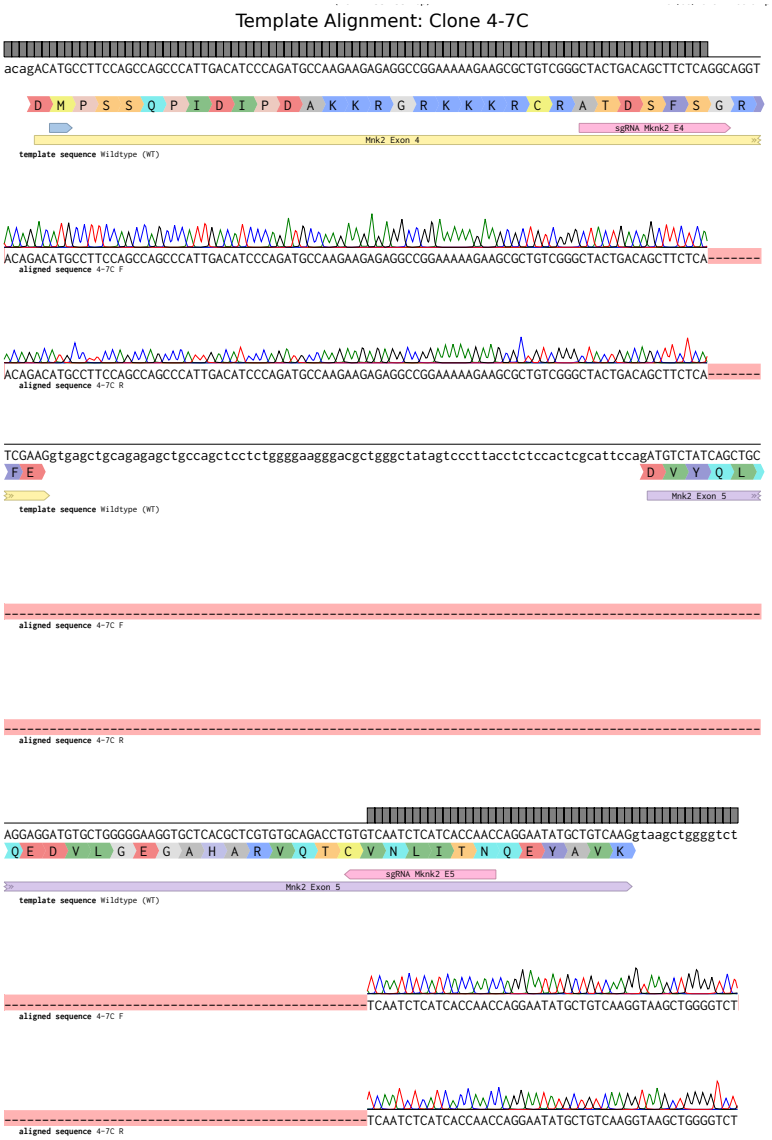

Appendix 11: Sanger sequencing alignment of Clone 4-8E.

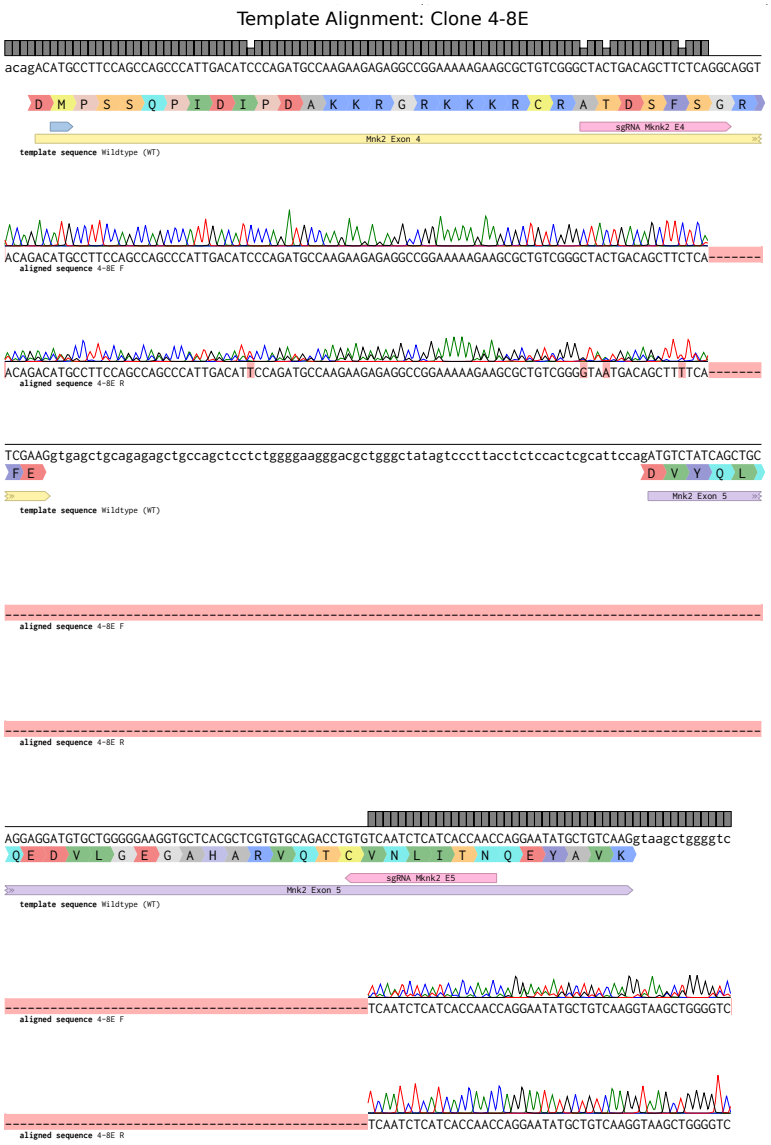

Appendix 12: Sanger sequencing alignment of Clone 4-11F.

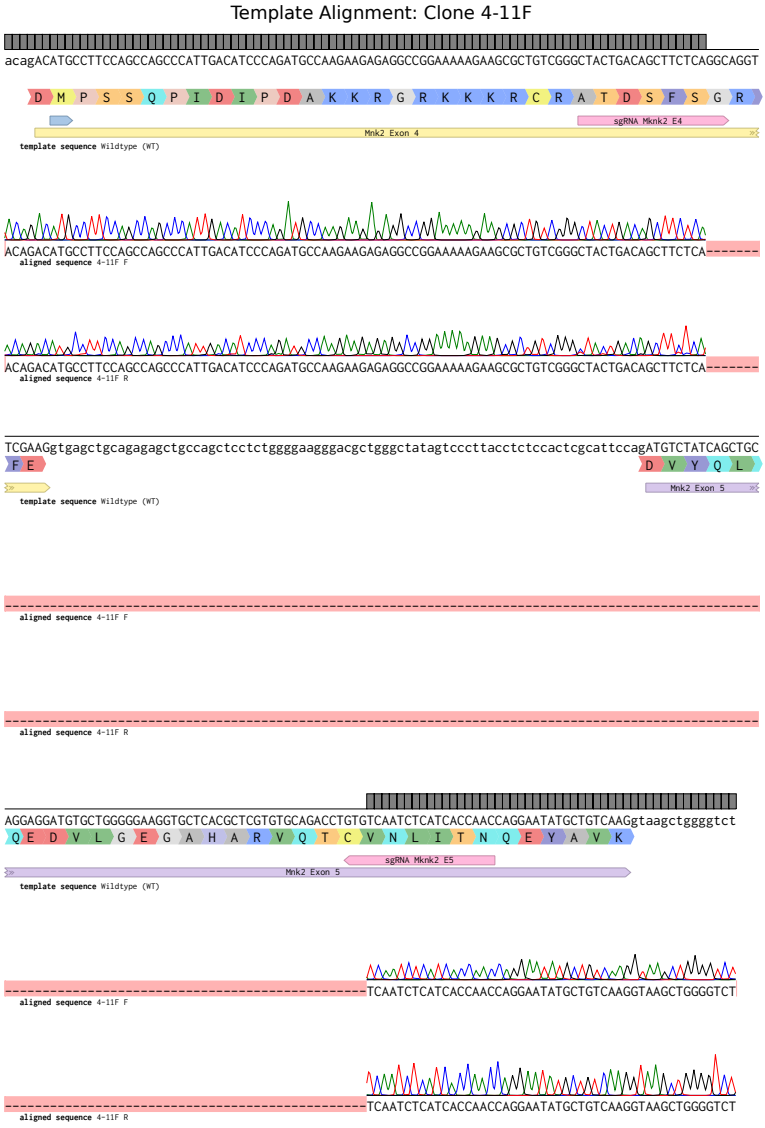

Appendix 13: Off-targets of sgRNA *Mknk2* E4.

Sorted from exonic, intergenic to intronic.

Gene Locus	Chr	Off-target sequence	Mismatches	Position
exon:Crtc1	chr8	CCACAGACAGCTTCTCTAGCGGG	4	.*..*.....**..
exon:Epsti1	chr14	CCACTTACACCTTCACAGGCCGG	4	.*...*...*....*.....
exon:Gm13117	chr4	TTGCTGAGAGCTTCTCAGGCTGA	3	*.*....*.....
exon:Iars2	chr1	CTTCTGCCTTCTTCTCAGGCTGG	4	..*...*.**.....
exon:Lhfpl1	chrX	CTTCTCACAGCTTGTCAGACAGG	4	..*..*.......*....*.
exon:Notch2	chr3	CCTCTGCCAGGTTCTCAGGCTGG	4	.**...*...*.....
exon:Phf13	chr4	CTGCTGACCCCTGCTCAGGCTGG	4	..*.....**..*.....
exon:Wrnip1	chr13	CTCCTCTCAGCTCCTCAGGCAGG	4	..*..**.....*.....
exon:Zfp276/Fanca	chr8	CTGCAGACAGCTTATCGGGCTGG	4	..*.*.......*..*...
intergenic:1110008E08Rik-Gm23406	chr16	CTTCTGCCAGCTCCTCTGGCGGG	4	..*...*.....*...*...
intergenic:1700019D03Rik-Mstn	chr1	TTACTGACTGATTCTCAGGCTGG	3	*.......*.*.....
intergenic:1700021A07Rik-1700020N01Rik	chr10	CTACTGAGATCTTCTCATGGAGG	4	.......*.*.......*.*
intergenic:2410076I21Rik-Hcn4	chr9	CTTCTGAGAGCTTCACATGCTGG	4	..*....*......*..*..
intergenic:2900072N19Rik-Phf21a	chr2	CTAAGGAGAGCTTGTCAGGCTGG	4	...**..*.....*.....
intergenic:4930505M18Rik-Zfp536	chr7	TAACTGCCAACTTCTCAGGCTGG	4	**....*..*.....
intergenic:4930547C10Rik-4930552N02Rik	chr4	CTAATGACAGTTTCCCAGGAAGG	4	...*......*...*....*
intergenic:4930583I09Rik-Gm25344	chr17	CTACTGACTTCTTCTCACCCTGG	4	........**.......**.
intergenic:9230109A22Rik-Basp1	chr15	CTACTGACACCCTCTGAGGCTGG	3	.........*.*...*....
intergenic:AC154801.1-BC040587	chr16	ATACTCAAAGCTTCTCAGGATGG	4	*....*.*.....*
intergenic:Ankrd50-Gm24462	chr3	CTAATGACAGCTCCTCAGCTAGG	4	...*........*.....**
intergenic:Arhgap12-Kif5b	chr18	CTACTGACAGATTCAGAGGAAGG	4	.........*...**...*
intergenic:C330008G21Rik-Ptprt	chr2	CTCCTGACAACTTCTCAGATAGG	4	..*......*........**
intergenic:Cadm1-Nxpe2	chr9	CTACTGATAGCTTCTCAGGTAGA	2	.......*.....*
intergenic:Ccser1-Gm22212	chr6	CTTCAGGCAGCATCTCAGGCGGG	4	..*.*.*....*.....
intergenic:Chordc1-Naalad2	chr9	TTACTAACAGCTTCTCAGCTAGG	4	*....*.....**
intergenic:Clstn2-4921534H16Rik	chr9	CTACTGACAACCTCTCATCCTGG	4	.........*.*.....**.
intergenic:Cntnap2-Gm25161	chr6	CTTCTGAGAGGGTCTCAGGCTGG	4	..*....*..**.....
intergenic:Col4a3-n-R5s213	chr1	CTACTGGCTTCTTCTCTGGCTGG	4	......*.**......*...
intergenic:Csrp2bp-Zfp133-ps	chr2	CTACTCTCAGCTTCTGAGGTGGG	4	.....**.......*...*
intergenic:D330020A13Rik/B4galnt3-Ccdc77	chr6	CTACCAAGAGCTTCTCAGGGAGG	4	....**.*.....*
intergenic:Emp1-Gm25136	chr6	CTACTAACATCCTCTGAGGCTGG	4	.....*...*.*...*....
intergenic:Fam155a-Gm10217	chr8	CTGCTAATAGCTTCTCAGGAGGG	4	..*..*.*.....*
intergenic:Fam19a2-Gm23777	chr10	CTACTGACAAATGCTCAGGTGGG	4	.........**.*......*
intergenic:Fcf1-Ylpm1	chr12	CTTCTAACAGCTTCTCAGGCAGG	2	..*..*.....
intergenic:Fut8-Gm24070	chr12	CTATTGTGAGCTTCTCAGGCAAG	3	...*..**.....
intergenic:Gabrq-Magea9-ps	chrX	CTTCTGCCAGCTCCTCAGACAGG	4	..*...*.....*.....*.
intergenic:Gm10258-Mecom	chr3	CTGCTGACAGCTTCTCAGCTAGG	3	..*.....**
intergenic:Gm12017-Gm12018	chr11	GTGCTGACAGATTCTCAGGGAGG	4	*.*.......*.....*

intergenic:Gm12037-Gm12038	chr11	GTACAGACAGCTCCTCAGGATGG	4	*...*.......*.....*
intergenic:Gm12287-Gm12288	chr11	CCAGTGACAGTTTCTCAGGAAGG	4	.*.*.....*.......*
intergenic:Gm12325-Gm12326	chr11	CTGCTGACAGCTGGCCAGGCAGG	4	..*.........***.....
intergenic:Gm13468-Gm13481	chr2	ATAGTGACAAGTTCTCAGGCAGG	4	*..*.....**.........
intergenic:Gm13861-Cald1	chr6	CTTCTCACAGTTTCTAAGGCTGG	4	..*..*....*....*....
intergenic:Gm14589-Gm1862	chrX	CCACTGACAGTCTCTCAGGAAGG	4	.*........**.......*
intergenic:Gm14731-Rplp1-ps1	chrX	CTAGTAACAGCTTCTCATTCAGG	4	...*.*..........**.
intergenic:Gm14947-Gm14940	chrX	ACACTAACTGCTTCTCAGGCAGG	4	**...*..*..........
intergenic:Gm15407-Katnal1	chr5	CTACTGACAGCTTGTGAGGAGGG	3	............*.*...*
intergenic:Gm15501-Gm5899	chr7	CTGCTGACTGGTTCTCAGTCGGG	4	..*.....*.*.......*.
intergenic:Gm15766-Gm6288	chr6	CTACTGACAGCTTCCCAAGCAGG	2	............*..*..
intergenic:Gm16231-St6galnac5	chr3	CTGCAGACTGCTTCACAGGCAGG	4	..*.*...*.....*.....
intergenic:Gm17131-Tmem132d	chr5	CAGCAGACAGCTTCTGAGGCTGG	4	.**.*.........*....
intergenic:Gm2018-4932411E22Rik	chr11	CTACTGAAAGGTTCTCAGGAGGG	3	.......*..*........*
intergenic:Gm20618-Gm5873	chr6	CTACTGAGAACTGCTCAGGGAGG	4	.......*.*..*......*
intergenic:Gm22032-Gm22895	chr15	CTACTGAGTTCTTCTCAGGATGG	4	.......***........*
intergenic:Gm22103-Gm14638	chrX	CCACTGACAGTCTCTCAGGAAGG	4	.*........**.......*
intergenic:Gm22914-Skap2	chr6	CTACTGACAACGTCTGCGGCTGG	4	.........*.*...**...
intergenic:Gm23097-Dync2h1	chr9	CTACTGACAGTGTCTTAGTCAGG	4	..........**...*..*.
intergenic:Gm23315-Rprm	chr2	CTACTTAGAGCTTCCCAGGATGG	4	.....*.*......*....*
intergenic:Gm23342-Myt1l	chr12	CTACGGACACCCTCTGAGGCTGG	4	....*....*.*...*....
intergenic:Gm23615-Pdzd4	chrX	TTCCTGTCTGCTTCTCAGGCAGG	4	*.*...*.*...........
intergenic:Gm23796-Gm23831	chr3	CGACTGACAGCTTCTAAGAGAGG	4	.*.............*..**
intergenic:Gm24295-Mef2c	chr13	CTACTGACAGCTCATCAGCTTGG	4	............**....**
intergenic:Gm24371-BC024582	chr4	GTACTGCCAGCCTCTCAGCCTGG	4	*.....*....*......*.
intergenic:Gm24383-Kcnc4	chr3	ATTCTGACAGCTTCTCAGGCAGG	2	*.*..................
intergenic:Gm25267-Il15	chr8	CTACACACAGGCTCTCAGGCTGG	4	....**....**........
intergenic:Gm25270-Gm12974	chr4	AAGCTGTCAGCTTCTCAGGCTGG	4	***...*.............
intergenic:Gm25297-Dlk1	chr12	CTGGTGACAGCTTCTCAGAGGGG	4	..**............**
intergenic:Gm25401-Mir100	chr9	CTACAGACAGCTCAGCAGGCTGG	4	....*.......***.....
intergenic:Gm25431-Ighmbp2	chr19	CTGCTGACAGCTTTTCAGAGGGG	4	..*.........*....**
intergenic:Gm25839-4930587A21Rik	chr1	CTACTGTCTGCTCCTCAGCCAGG	4	......*.*...*.....*.
intergenic:Gm26022-Chl1	chr6	CTACAGACAACTTATCTGGCTGG	4	....*....*...*..*...
intergenic:Gm26042-Tbx19	chr1	CTACAGACAGCTCAACAGGCTGG	4	....*.......***.....
intergenic:Gm26100-Ccdc7	chr8	CTTTTGAGAGCTTCTCAAGCTGG	4	..**...*.........*..
intergenic:Gm5507-Redrum	chr18	CTACTGAAAGATACTCAGACGGG	4	.......*..*.*.....*.
intergenic:Gm6226-Ube3a	chr7	CTACTTAGAGCATCTTAGGCAGG	4	.....*.*...*...*....
intergenic:Gm7222-Gm15018	chrX	CTACCAACAGCTTCTCAAGAAGG	4	....**..........*.*
intergenic:Gm7816-Gm2810	chr5	CTGCTTACAGCTTCACAGCCTGG	4	..*..*........*...*.
intergenic:Gm8349-Arhgef26	chr3	CTACCTACTGCTTCTCAGCCAGG	4	....**..*.........*.
intergenic:Gm9002-Kifc5c-ps	chr10	CTACTTACAGCCTCACCGGCTGG	4	.....*.....*..*.*...
intergenic:Grin3a-Gm12458	chr4	CCACAGACAGCTTCTGATGCTGG	4	.*..*.........*.*..

intergenic:Grm5-Ctsc	chr7	CCTCTGACAGCTTCCCAGTCAGG	4	.**.....*...*.
intergenic:Gse1-Gm26971	chr8	GTACTCACAGCCTCACAGGCTGG	4	*....*.....*..*.....
intergenic:Gzmk-BC067074	chr13	CTAATGTCTGCTTCTCAGGCAGA	3	...*..*.*.....
intergenic:Hat1-Gm23166	chr2	CTCCTGAGTGCTTCTGAGGCAGG	4	..*....**.....*....
intergenic:Hdac9-4921508M14Rik	chr12	CTACACATAGCTACTCAGGCTGG	4	....**.*....*.....
intergenic:Hmgb3-Gpr50	chrX	CTACTGACATCTGCCAAGGCAGG	4	.....*..*.**....
intergenic:Igbp1b-Gm25434	chr6	CTTCTGACATCTAGTCAGGCAGG	4	..*.....*..**.....
intergenic:Igkv12-98-Igkv10-96	chr6	CTTCAGAGAGCTTCTCAGGCCAG	3	..*.*..*.....
intergenic:Lbx1-Btrc	chr19	CAACTGACAGCTTCTCCAGAAGG	4	.*.....**.*
intergenic:Litaf-Gm26268	chr16	CTATTGTCAGCTTCTGAGGCAGG	3	...*..*.....*....
intergenic:Lrch2-Gm16400	chrX	CTCCTGACAGCATCTGAGGCAGG	3	..*.....*...*....
intergenic:Mbd2-Dcc	chr18	CAACTGAAAGCATCTCAGTCAGG	4	.*.....*...*.....*.
intergenic:Mir802-Setd4	chr16	CTACCCATAGCTCCTCAGGCAGG	4	....**.*....*.....
intergenic:Mki67-Gm9341	chr7	CTGCTGACAGCTTAACAGGCGGG	3	..*.....**.....
intergenic:mmu-mir-6394-Gm15412	chr7	CTTCTGAAAGCTTTTCATGCTGG	4	..*....*.....*...*..
intergenic:Mycs-Gm14366	chrX	CTGCTGACACCCTCTCAGGCTGA	3	..*.....*.*.....
intergenic:Ncor2-Scarb1	chr5	CCACTGGTAGCTACTCAGGCTGG	4	.*....**....*.....
intergenic:Nmd3-Sptssb	chr3	ATACTCACACCTTCTCAGGACGG	4	*....*...*.....*
intergenic:Ntrk2-Agtpbp1	chr13	TTTCTGACAGCTTCTCTGGGTGG	4	*.*.....*..*
intergenic:Papd4-Gm2076	chr13	ATAGTAATAGCTTCTCAGGCAGG	4	*..*.*.*.....
intergenic:Pard3-mmu-mir-21c	chr8	CAACTGAAAGCTTCTTAGACCGG	4	.*.....*.....*..*.
intergenic:Pitx2-Enpep	chr3	CTACTGACAGGGTATCAGGGAGG	4	.....**.*.....*
intergenic:Ppp1r14c-Iyd	chr10	CTACTGACAGCCTGTTATGCAGG	4	.....*.*.*.*..
intergenic:Prkcd-Rft1	chr14	CTGCAGGCAGCTTCTCAGGCAGA	3	..*.*.*.....
intergenic:Prl2c2-Prl2c5	chr13	CTAAGGGCAGCTTCTGAGGCTGG	4	...**.*.....*....
intergenic:Rasgef1a-Csgalnact2	chr6	CTCATGCCAGCTTCGCAGGCAGG	4	..**..*.....*.....
intergenic:Rgs17-Gm10945	chr10	AAAAGGACAGCTTCTCAGGCAGA	4	**.**.....
intergenic:Rmnd5a-Rnf103	chr6	CTGCAGACAGCTTCTCAGTTAGG	4	..*.*.....**
intergenic:Rpl7a-ps10-Trim42/Gm15891	chr9	CTGCTGGCAACTCCTCAGGCTGG	4	..*...*..*..*.....
intergenic:Rybp-Gm23234	chr6	CTCCTGACAGCGCCTCAAGCCGG	4	..*.....**....*..
intergenic:Sema5b-Gm5963	chr16	CCACTGACAGCCCCTCAGCCTGG	4	.*.....**.....*.
intergenic:Slc38a4-Amigo2	chr15	CTAATGGAAACTTCTCAGGCCGG	4	...*..**.*.....
intergenic:Slco6c1-D1Ertd622e	chr1	CTCCTGAGAACTTCTCAGGCAAG	4	..*....*.*.....
intergenic:Sptlc1-Msx2	chr13	CTAATGGCTGCTTCTCAGGGTGG	4	...*..*.*.....*
intergenic:Srgap2-Gm24273	chr1	CTACTGACAGCAGCTCTGTCTGG	4	.....**...*.*.
intergenic:Suv39h2-Hspa14	chr2	CTAGTGACATTTTCTCCGGCAGG	4	...*.....**.....*...
intergenic:Tln2-Mir190	chr9	CTTGTGACAGTGTCTCAGGCTGG	4	..**.....**.....
intergenic:Tmem47-Gm14754	chrX	CCAGAGAGAGCTTCTCAGGCCAG	4	.*.**..*.....
intergenic:Tpbg-Ube2cbp	chr9	TTTCTTACAGCCTCTCAGGCTGG	4	*.*..*.....*.....
intergenic:Trub1-Atrnl1	chr19	ATACTGGCATCTACTCAGGCAGG	4	*.....*..*..*.....
intergenic:Tssc1-Gm23342	chr12	CTACTGATAGATTCTAGGGCAGG	4	.....*..*....**...
intergenic:Ttc32-Gm7099	chr12	CTCCTGACCTCTTCTCAGGGAGG	4	..*.....**.....*

intergenic:Vash1-Angel1	chr12	CCACTGACAGCATGTCAGGGTGG	4	.*.....*.*.....*
intergenic:Yipf6-Gm14813	chrX	CTATTCAAAGCTGCTCAGGCTGG	4	...*.*.*....*.....
intron:1700007B14Rik	chr8	GTACTGTCTGCTTCTCTGGCAGG	4	*.....*.*.....*...
intron:4930588K23Rik	chr16	CTGCTGACAGGTTCTCAGGAAGG	3	..*.....*.....*
intron:Adal	chr2	CTCCTCAAAGCTTCTCAGTCTGG	4	..*..*.*.....*.
intron:Adamts20	chr15	CTCCTGCCAGCTTTTCTGGCAGG	4	..*...*.....*..*...
intron:Als2cr11	chr1	CTATTGACAGCTGCTCAAGAAGG	4	...*.....*....*.*
intron:Ano10	chr9	CTGCTGACAGTTTCTCAGAATGG	4	..*.....*.....**
intron:Antxr1	chr6	CTACTGACTGCTTGGCAGGCAGG	3	.....*....**.....
intron:Asap1	chr15	CTACAGACAACTTCAAAGGCAGG	4	....*....*....**....
intron:Atp1a1	chr3	CTACTATCAGCTTCTCAGAGAGG	4	.....**.....**
intron:Bin1	chr18	CTACTGATACAATCTCAGGCAGG	4	.....*.***.....
intron:C130079G13Rik	chr3	CTACTGATATTTTCTCAGGAAGG	4	.....*.**.....*
intron:Camta1	chr4	CTGCTGACAGCTGGACAGGCTGG	4	..*.....***.....
intron:Clpb	chr7	CCACTGAGGCCTTCTCAGGCTGG	4	.*.....***.....
intron:Cnnm3	chr1	CTGCGGGCAGCTTCCCAGGCTGG	4	..*.*.*.....*.....
intron:Daam2	chr17	CACCTGCCAGATTCTCAGGCTGG	4	.**...*...*.....
intron:Dcc	chr18	TTACCAACAGCTTCTCAGCCAGG	4	*...**.....*.
intron:Dcc	chr18	CCACTGACATCTTGTCAGGCAGG	3	.*.....*...*.....
intron:Dcdc5	chr2	CAACTTACAGCCTCACAGGCTGG	4	.*...*.....*..*.....
intron:Efhc2	chrX	AAGCTGACAGCTTCTCAGACAGG	4	***.....*.
intron:Elmo1	chr13	CTTCTGAGAACTTCCCAGGCTGG	4	..*....*.*....*.....
intron:Epha6	chr16	CTACGGACAGCTTGTCTGTCAGG	4	....*.....*..*.*.
intron:Esrrg	chr1	TTTCTCACAGATTCTCAGGCTGG	4	*.*..*....*.....
intron:Fam129a	chr1	CTGCTCACAGCTCCTCAGTCGGG	4	..*..*.....*.....*.
intron:Gm12092	chr11	CTACCAACAGCTTCTCAGGTAGG	3	....**.....*
intron:Gm12239	chr11	CTACCAACAGCTTCTTAGCCAGG	4	....**.....*..*.
intron:Gm16630	chr6	CTAATCACAGCTCCTCAGGCTGG	3	...*.*.....*.....
intron:Gm2382	chr9	CTTCTGACAGCTTCGCAGGGAGG	3	..*.....*....*
intron:Gm9530	chr1	CTACTCTCAGTTTCTCAGGATGG	4	.....**...*.....*
intron:Gmds	chr13	CTACTAACAGATTCTGAGGAAGG	4	.....*....*....*...*
intron:Gtpbp10	chr5	CAACTGACAACTTCCCATGCTGG	4	.*.....*....*..*..
intron:Hck	chr2	CTAGTGACTGCTTCACAGCCTGG	4	...*....*.....*...*.
intron:Hecw1	chr13	ATAGTGACAGGTTTTCAGGCAGG	4	*..*.....*..*.....
intron:Immt	chr6	CTACACTCAGATTCTCAGGCAGG	4	....***...*.....
intron:Impdh2	chr9	CTACTGGCTGCCTCTCAGGAGGG	4	.....*.*..*.....*
intron:Itgb2	chr10	GTTCTGACAGCTACTCGGGCTGG	4	*.*.....*...*...
intron:Kansl3	chr1	TTACTGACAGCTTCTAAGCCCGG	3	*.....*..*.
intron:Kcnd3	chr3	CTTCTGCCTGCCTCTCAGGCAGG	4	..*...*.*..*.....
intron:Kcnh1	chr1	CTCCTGACAGCTTCTGAAGTAGG	4	..*.....*.*.*
intron:Klhl29	chr12	CTCCTGGCTGCCTCTCAGGCAGG	4	..*...*.*..*.....
intron:Klhl5	chr5	CTGCTGACAGATTCCCAGACAGG	4	..*.....*...*...*.

intron:Klhl7	chr5	CTGCGGACAGCTACTCATGCTGG	4	..*.*.....*....*..
intron:Lrfn2	chr17	CTCCTTACAGCTCCTCAGCCAGG	4	..*..*.....*.....*.
intron:Magi2	chr5	CTATAGACAGATCCTCAGGCTGG	4	...**.....*.*.....
intron:Mical3	chr6	CTACAGGCATCTTCTCAGGCAGA	3	....*.*..*.....
intron:Mkln1os	chr6	CAACTGCCAGCTTCTCTGCCGGG	4	.*....*.....*.*.
intron:Mprip	chr11	CTCCTGAGAGCTTCTCTGGGTGG	4	..*....*.....*..*
intron:Mthfs	chr9	CTTCTGACAGCTTCGCAGGGAGG	3	..*.....*....*
intron:Myeov2	chr1	CTACTGACTGCTTCCCAGCACGG	4	.....*.....*...**
intron:Myh6	chr14	CCACTGAGAACTTCCCAGGCTGG	4	.*.....*.*....*.....
intron:Ndufa10	chr1	GTAGTGACAGCTCCTCTGGCAGG	4	*..*.....*...*...
intron:Ofcc1	chr13	GTGCAGACAGCTTCTCAGGTTGG	4	*.*.*.....*
intron:Ofcc1	chr13	TTAGTGAGATCTTCTCAGGCAGA	4	*..*...*.*.....
intron:Pigk	chr3	CTACTGACAGCATTTCATGAAGG	4	.....*.*...*.*
intron:Prdm16	chr4	CTGCTGACAGTTTCTGAGCCCGG	4	..*.....*....*..*.
intron:Prep	chr10	CAACTGACAGCTTCTGAGGGAGG	3	.*.....*...*
intron:Ret	chr6	CTACTGATAGGTTCTCAGAGAGG	4	.....*..*.....**
intron:Slc25a21	chr12	TTCCTGACAGCTTCTTTGGCAGG	4	*.*.....**...
intron:Slc9a8	chr2	CTGGTCAGAGCTTCTCAGGCTGG	4	..**.*.*.....
intron:Stox1	chr10	CTACAGACAATCTCTCAGGCAGG	4	....*....***.....
intron:Themis	chr10	CTACTAATAGCTTCTCATCCAGG	4	.....*.*.....**.
intron:Tmem132d	chr5	CTACTGACAGCTCATAAGGTGGG	4	.....**.*...*
intron:Tmem2	chr19	CTACTGTCAGCCACCCAGGCTGG	4	.....*....**.*.....
intron:Ubash3b	chr9	CTGCTGACACATTCTCAGGTTGG	4	..*.....**.....*
intron:Vgll4	chr6	CTGCAGAGAGCTGCTCAGGCAGG	4	..*.*..*....*.....
intron:Zfat	chr15	CTCCTGAGAGCTCCTGAGGCAGG	4	..*....*....*..*....
intron:Zmiz2	chr11	TTACTGACTGCCTCTCAGCCTGG	4	*.....*..*.....*.

Appendix 14: Off-targets of sgRNA *Mknk2* E5.

Sorted from exonic, intergenic to intronic.

Gene Locus	Chr	Off-target sequence	Mismatches	Position
exon:Ago2/Chrac1	chr15	GCAGGTGATGAAATTTACACAGG	4	.**.....*...*....
exon:Arpc3	chr5	GCTGGTGCTCAGATTGACAGCGG	4	.*.....*.*.....*
exon:Gm16268/Stab2	chr10	GTTGGTGCTGATAATGTCACTGG	4	.....*...*.*..*...
exon:Slc18a2	chr19	GTTGGTGAGGAGCTGGACAGTGG	4	.....*...*.*....*
exon:Slc1a2	chr2	GGTGGAGATGAGATTAACAATGG	4	.*...*.....*...*
exon:Tgm4	chr9	GTTGATGATGAGATGGTCATTGG	4	....*.....*.*..*
intergenic:1700020N15Rik-Ids	chrX	ATGGGTGATGAGATCAACACTGG	4	*.*.....**....
intergenic:3100003L05Rik-Gm21957	chr7	GCTGGTGATGAGTTTTACAAAGG	4	.*.....*..*...*
intergenic:4930417H01Rik-4930580A09Rik	chr2	GTTGGTGATGAGAGAAAAACGGG	4	.....***.*..
intergenic:4930448E22Rik-Gm22659	chr9	GTTTGTGATGACAGTGACAGTGG	4	...*.....*.*.....*
intergenic:4930529M08Rik-Insm1	chr2	TTTGCTGATGAGTTTGACCCAGG	4	*...*.....*.....*.
intergenic:4930564D02Rik-1700095B22Rik	chr3	GTTTGTGATCAGTTTGTCACTGG	4	...*.....*..*...*...
intergenic:4930579C12Rik-Bcl2a1b/Mthfs	chr9	TGTGCTGCTGAGATTGACACCAG	4	**..*..*.....
intergenic:5430425J12Rik-Slc12a7	chr13	GTAGGTGATGGGAGTGACCCAGG	4	..*.....*..*....*.
intergenic:A1bg-Gm24696	chr15	TTTGGGGATGAGATAGCCACTGG	4	*....*.....*.*...
intergenic:A430105J06Rik-Gm3809	chr1	GTTGGTGATGTGGATAACACAGG	4	.....*.**.*....
intergenic:A930031H19Rik-Gm25261	chr4	GTTGGTTGAGTGATTGACACAGG	4	.....***.*.....
intergenic:Anapc10-Hhip	chr8	GTTGGTGCTGAGCCTGGCACAGG	4	.....*....**..*...
intergenic:Apol10a-Apol11a	chr15	GTTGGTGAGCAGATGCACACAGG	4	.....**....**....
intergenic:Apol11b-Apol7e	chr15	GTTGGTGAGCAGATGCACACAGG	4	.....**....**....
intergenic:B430319H21Rik-Gm12285	chr11	GCTGGGGAGGAGATGGACACTGG	4	.*...*..*.....*.....
intergenic:BC048507-Mtrr	chr13	GATGCTGATGAGATGGACAGAGG	4	.*..*.....*....*
intergenic:Btbd11-Pwp1	chr10	GTTGGTGATGGGGGTGACATAGG	4	.....*.**.....*
intergenic:Ccl1-Tmem132e	chr11	GATGGTGATGAGAACCACACTGG	4	.*.....***....
intergenic:Cdh13-Gm24035	chr8	CTTGGTGATGAGGTCAACACTGG	4	*.....*.**....
intergenic:Crhr2-Inmt	chr6	GTGGGTGGTGGGAATGACACAGG	4	..*....*..*..*.....
intergenic:Dtx1-Oas2	chr5	AGTGTTGATGAGATTGACAGTGG	4	**..*.....*
intergenic:Eif3s6-ps1-Gm11995	chr11	GTGAGAGATGAGATTGACAATGG	4	..**.*.....*
intergenic:Frk-Gm26341	chr10	GATGGAGATAAGATAGACACAGG	4	.*...*...*....*.....
intergenic:Gm10295-Mctp2	chr7	GAAGGTGATAAGATTGACACTAG	3	.**.....*.....
intergenic:Gm10571-Gm23845	chr4	GGTGGTTATGAGAATGTCACAGG	4	.*....*.....*..*...
intergenic:Gm11779-Gm11782	chr4	TTTGGAGATGAGTTTTACACAGG	4	*....*.....*..*....
intergenic:Gm11935-Rngtt	chr4	GTAGGAGATGAGACTGAGACTGG	4	..*..*.....*...*..
intergenic:Gm12243-4933424L21Rik	chr11	GTGGGTAATGACATTAACACAGG	4	..*...*....*...*....
intergenic:Gm12674-Gm12673	chr4	GTTCATGATGAAACTGACACTGG	4	...**.....*.*.....
intergenic:Gm13018-Prdm2	chr4	GATGCTGATGAGACTGACAGAGG	4	.*..*.....*.....*
intergenic:Gm13835-AB041803	chr6	GGTGGTGGTGAGATTTACTCTGG	4	.*.....*.....*..*.

intergenic:Gm14264-Dok5	chr2	GTTCGTGAAGAGATAGTCACAGG	4	...*....*.....*.*...
intergenic:Gm14714-Gm5398	chrX	GTTGGTGAAGAGATTGCATCAGG	4	........*.......***.
intergenic:Gm15208-Bcl11b	chr12	CTGTGTGATGAGATGGACACAGG	4	*.**.........*.....
intergenic:Gm15381-Gm24647	chr15	GGCGGTGCTGAGATTCACACAGG	4	.**....*.......*....
intergenic:Gm15496-Kcnmb2	chr3	GTTGTTGATTAGATGGTCACTGG	4	....*....*....*.*...
intergenic:Gm15501-Gm5899	chr7	GTGGGTGCTGAGATTGAACCTGG	4	..*....*.........**.
intergenic:Gm16330-Npy5r	chr8	GTTGGAGATGATATTGACACTGG	2	.....*.....*........
intergenic:Gm1815-Zfp353-ps	chr8	GCTGTTGATGAGATTCACAGAGG	4	.*..*.........*...*
intergenic:Gm20646-Mrps9	chr1	TTTGGTGCTGAGATTGAACCAGG	4	*......*.........**.
intergenic:Gm22211-Gm6181	chr7	ATTGGTACTGTGATTGACACTGG	4	*.....**..*.........
intergenic:Gm22211-Gm6181	chr7	GTTTGTGATGAGAATGATATTGG	4	...*.........*...*.*
intergenic:Gm22308-Cbfa2t2-ps1	chr5	GTTGGTGGTGAGGTTTTCACGGG	4	.......*....*..**...
intergenic:Gm22418-AC167724.1	chr6	ATTGGTGATGATATTGCCAAAGG	4	*..........*....*..*
intergenic:Gm22507-Trhde	chr10	GTTGTTGATCAGATTTACAATGG	4	....*....*.....*...*
intergenic:Gm22798-Cog6	chr3	GGTGGTGATGACAATGACAATGG	4	.*.........*.*.....*
intergenic:Gm23162-Runx1t1	chr4	GTTGGTGCTGAGAATGGAACAGG	4	.......*.....*..**..
intergenic:Gm23511-Gm22480	chr3	GTTGTTGATTAGATGGTCACTGG	4	....*....*....*.*...
intergenic:Gm23591-Speer2	chr16	CTTGCTGGTGAGATTGAAACTGG	4	*...*..*.........*..
intergenic:Gm23677-Maf	chr8	GTTGCTCATGAGATTGACTCAGG	3	....*.*...........*.
intergenic:Gm23735-Fndc3a	chr14	TTTGATGATGAGATTGTCAAAGG	4	*...*...........*..*
intergenic:Gm23911-Gm26288	chr7	GTTGGTGAGGTGACTGACAGTGG	4	........*.*..*.....*
intergenic:Gm24292-Wac	chr18	GTTGATGAAGTGCTTGACACAGG	4	....*...*.*.*.....
intergenic:Gm24634-Gm17366	chr14	TTTGGTCATGGGATTTACACTGG	4	*.....*...*....*....
intergenic:Gm24795-Gm8609	chr16	GTTGTTGATGAGATGGAAATGGG	4	....*.........*..*.*
intergenic:Gm25127-Gm9912	chr3	GCTGGAGCTGAGATTGAGACAGG	4	.*...*.*.........*..
intergenic:Gm25169-Efnb2	chr8	GTTGGTGTTGGGATTGGCCCTGG	4	.......*..*.....*.*.
intergenic:Gm25344-Tmem232	chr17	GTTGCTGATTAGTTTGACTCTGG	4	....*....*..*.....*.
intergenic:Gm25442-Gm25696	chr3	GTTGTTGATTAGATGGACACTGG	3	....*....*....*.....
intergenic:Gm25519-Gm5548	chr3	GTTGGTGAGGATATTGAAAGAGG	4	........*..*.....*.*
intergenic:Gm25684-Gm9966	chr7	GTTGAAGATGGGATAGACACAGG	4	....**....*...*.....
intergenic:Gm25977-Gm11875	chr4	CCTGGTGATGAGAGTGACTCAGG	4	**..........*....*.
intergenic:Gm26878-Fendrr	chr8	GTTGATGGTGAGATTGAAAATGG	4	....*..*.........*.*
intergenic:Gm2694-4933402J07Rik	chr8	GTTGGGGATGGGATTGAGGCTGG	4	.....*....*......**.
intergenic:Gm4822-Tpm3-rs7	chr14	GTTGGCTATGATATTGTCACTGG	4	.....**....*....*...
intergenic:Gm6634-Gm8604	chr3	GTTGGTGAAGATGTTGAGACAGG	4	........*..**....*..
intergenic:Gm7847-Gm23674	chr18	GTTGGTGATGATTTTGCTACTGG	4	...........**...**..
intergenic:Gm9621-Gm24200	chr9	GCTGCTTATGTGATTGACACAGG	4	.*..*.*...*.........
intergenic:Gprin1-Sncb	chr13	GTCGGTGATGTGATAGACACAGG	3	..*.......*...*.....
intergenic:Hdac4-Ndufa10	chr1	GCTGATGATGTGATTGACACAGG	3	.*..*.....*.........
intergenic:Icam5-Zglp1	chr9	GTTGGTAAAGTGATTGCCACAGG	4	......*.*.*.....*...
intergenic:Klrg1-Gm25304	chr6	ATTGGTGCTGAGACTGAGACAGG	4	*......*.....*...*..
intergenic:Mir5112-4930445N18Rik	chr18	CTCAGTGATGAGATTGACACCAG	3	*.**................

intergenic:Mrap2-4922501C03Rik	chr9	GATGGTGATGGGTTTGAGACAGG	4	.*.....*.*....*..
intergenic:n-R5s70-Xaf1	chr11	GCTGGTGATGAGAAAGACAGAGG	4	.*.....**....*
intergenic:Ndufv1-Gstp1	chr19	CTTGGTGCTGAGCTTGACACTAG	3	*.....*....*.....
intergenic:Neil3-Vegfc	chr8	GTAAGTGAAGGGATTGACACTGG	4	..**....*.*.....
intergenic:Nr4a3-Stx17	chr4	GTTGTTGTTGATATTGAGACAGG	4	....*..*...*.....*..
intergenic:Pbx1-Pbx1/AC096625.1	chr1	GTTGGTGTTGAGTTTGTCAGAGG	4	.......*....*...*..*
intergenic:Pced1b-Rpap3	chr15	GTTGGTGAGGAGAAGGACAAAGG	4	........*....**....*
intergenic:Pola1-Gm14780	chrX	GTTGATGCTGTGATTGACACTAG	3	....*..*..*.....
intergenic:Rap2a-Gm17613	chr14	GTTGGTGATGATAGTGACGGAGG	4	.....*.*....**
intergenic:Rbm27-Pou4f3	chr18	GTAGGTGATGAGAGTGAAATGGG	4	..*.....*...*.*
intergenic:Rpl17-ps4-Tnc	chr4	GTTGGTTATGAGGATGACACAGG	3	......*.....**.....
intergenic:Rsl24d1-Gm5745	chr9	GTGGGTGCTGGGATTGAAACTGG	4	..*....*..*.....*..
intergenic:Samd4-mmu-mir-378c	chr14	ATTGGTGATGAAAGGGACACTGG	4	*.....*.**.....
intergenic:Slc16a7-Lrig3	chr10	TGTGGTCATGAGATTGAGACAGG	4	**....*.....*..
intergenic:Smad5-Trpc7	chr13	GATGATGATGAGTTTGTCACTGG	4	.*..*.....*...*...
intergenic:Srpk2-Gm24009	chr5	GTTTGTAATGAGATTGACAGAGG	3	...*..*.....*
intergenic:Tcf21-Eya4	chr10	GGTGGTGATGAGGTACACACTGG	4	.*.....*.**....
intergenic:Tfcp2l1/Gm23497-Gli2	chr1	GTTGTTGTTGAGGTTGAGACAGG	4	....*..*....*....*..
intergenic:Tmem179-Inf2	chr12	GTCGGTGTTGAAGTTGACACAGG	4	..*....*...**.....
intergenic:Trbv21-Trbv23	chr6	GATGGGGATGATAATGACACAGG	4	.*...*.....*.*.....
intergenic:Tshz2/Gm26883-Gm26883	chr2	GGTGGTGATGAACATGACACTGG	4	.*.....***.....
intergenic:Vdac3-ps1-Pou6f2	chr13	CTTGGTAATGAGGGTGACACAGG	4	*.....*.....**.....
intergenic:Veph1-Shox2	chr3	GTGGTTGATGAGGTTGACCCAGG	4	..*.*.....*.....*.
intergenic:Zfp637-Zfp239	chr6	GGTGGTGGTGAAATTGACACAAG	3	.*.....*...*.....
intergenic:Zfp746-Gm16630	chr6	GCTGATGAAGAGATAGACACTGG	4	.*..*...*.....*.....
intron:A330043C09Rik	chr2	GGTGATGATGAGAGTGACAGAGG	4	.*..*.....*.....*
intron:Aftph	chr11	GGTGATGCTAAGATTGACACTAG	4	.*..*..*.*.....
intron:Agbl1	chr7	GTTGGTGATGGGGTTGAGGCAGG	4	.....*.*....**.
intron:Anks1b	chr10	GCTGGTGATGAGATAGGCATTGG	4	.*.....*.*..*
intron:Arhgap26	chr18	GGTGCTGAGGGGATTGACACTGG	4	.*..*...*.*.....
intron:Car10	chr11	ATTGGTGATGATATTGACCTGGG	4	*.....*.....**
intron:Ccdc150	chr1	GTTGTTGATGGGTTTGACACTGG	3	....*.....*.*.....
intron:Cdkl5	chrX	GATGGTGGTGAGATGGAGACAGG	4	.*.....*.....*..*..
intron:Col4a2	chr8	GTGGGTGAGGAGATTGGCAGAGG	4	..*.....*.....*..*
intron:Ctnna3	chr10	GTTGCTGATGAGAAAGGCACAGG	4	....*.....**.*...
intron:Dlg1	chr16	GTTGGTTCTCAGCTTGACACAGG	4	.....**.*..*.....
intron:Epb4.1l1	chr2	GTTTCTGATGAGATTTACTCAGG	4	...**.....*..*.
intron:Epb4.1l4b	chr4	GTGGGTGATGAGTCTGACACGGG	3	..*.....**.....
intron:Ext1	chr15	ATTGGTGATGGAGTTGACACAGG	4	*.....***.....
intron:Gm14486	chr2	GTTGGTGCTGGGAATGAAACGGG	4	.....*..*..*...*..
intron:Gm1527	chr3	GTTGTTGATTAGATGGTCACTGG	4	....*....*....*.*...
intron:Gpc6	chr14	TTTAGTGATGAGATTGACTCCAG	3	*..*.....*.

intron:Immp2l	chr12	GTTGGTGATGAGGCTGAGATTGG	4	...........**...*.*
intron:Kif4	chrX	GTTGGGGATGAGAACGACATGGG	4	.....*.......**....*
intron:Map3k14	chr11	GGTGGTGATGAGGTCGAAACGGG	4	.*.........*.*..*..
intron:Myo1f	chr17	GTTGGTGGTGAGGATGACAATGG	4	.......*....**.....*
intron:Pacrg	chr17	CTGGGTGATGAGATTGACAAAGA	3	*.*..............*
intron:Piezo1	chr8	GTTGGTGAGGAGCCTGACCCAGG	4	........*...**....*.
intron:Plcl1	chr1	GATGGAGGTGAGATTCACACCGG	4	.*...*.*.......*....
intron:Ppp1r37	chr7	GTTGCTGGGGAGATGGACACAGG	4	....*..**.....*.....
intron:Prkaca	chr8	GGTGGTGATGGGCTTGGCACAGG	4	.*........*.*...*...
intron:Prkar1b	chr5	GGTGGTGATGCCTTTGACACTGG	4	.*........***.......
intron:Prkch	chr12	GCTGGGGTTGAGATAGACACTGG	4	.*...*.*......*.....
intron:Prkcq	chr2	GGTGGTGATGAGACTGGCACTGG	3	.*...........*..*...
intron:Prkg1	chr19	GATGATGCTGAGATTGACAGTGG	4	.*..*..*...........*
intron:Prune2	chr19	GCTGGTGATTAGATGCACACAGG	4	.*.......*....**....
intron:Psmd14	chr2	GTTGGTGATCTGACTGGCACAGG	4	.........**..*..*...
intron:Rnf13	chr3	GCTGGTGGTGGGACTGACACAGG	4	.*.....*..*..*......
intron:Rps6kb1	chr11	GTTGGTGGTGATAGTGAGACGGG	4	.......*...*.*...*..
intron:Skap2	chr6	GTGGGTGCTGTGATTGACATGGG	4	..*....*..*........*
intron:Sntb2	chr8	GTGGGTAATGAGATTGAGCCGGG	4	..*...*..........**.
intron:Sorcs2	chr5	GTTGGTAAAGGGATGGACACTGG	4	......*.*.*...*.....
intron:Sox5	chr6	GTTGGTGAAGAGACTGAGATGGG	4	........*....*...*.*
intron:Specc1	chr11	GTTGTTCATCAGATTCACACCGG	4	....*.*..*.....*....
intron:Tcerg1l	chr7	GATGGTGATGATATTGATAATGG	4	.*.........*.....*.*
intron:Tnn	chr1	GTGGGGGATGAGACTGATACTGG	4	..*..*.......*...*..
intron:Ube3c	chr5	CTTGGTGATGGTTTTGACACTGG	4	*.........***.......

References

1 Bendz, C. and Lake, S. (2002) Method for identification of agents for the treatment of diabetes, Patent WO/2002/103361.

2 Steuernagel, A., Eulenberg, K., Brönner, G., Ciossek, T., Rudolph, B., Rudolph, D., Belgore, F., Jäkel, S. and Meyer, C. (2003) MNK kinase homologous proteins involved in the regulation of energy homeostasis and organelle metabolism, Patent WO/2003/037362.

3 Moore, C. E. J., Pickford, J., Cagampang, F. R., Stead, R. L., Tian, S., Zhao, X., Tang, X., Byrne, C. D. and Proud, C. G. (2016) MNK1 and MNK2 mediate adverse effects of high-fat feeding in distinct ways. Sci Rep **6**, 23476.

4 Fukunaga, R. and Hunter, T. (1997) MNK1, a new MAP kinase-activated protein kinase, isolated by a novel expression screening method for identifying protein kinase substrates. EMBO J **16**, 1921–1933.

5 Waskiewicz, A. J., Flynn, A., Proud, C. G. and Cooper, J. A. (1997) Mitogen-activated protein kinases activate the serine/threonine kinases Mnk1 and Mnk2. EMBO J **16**, 1909–1920.

6 O'Loghlen, A., González, V. M., Jurado, T., Salinas, M. and Martín, M. E. (2007) Characterization of the activity of human MAP kinase-interacting kinase Mnk1b. BBA **1773**, 1416–1427.

7 Scheper, G. C., Morrice, N. A., Kleijn, M. and Proud, C. G. (2001) The Mitogen-Activated Protein Kinase Signal-Integrating Kinase Mnk2 Is a Eukaryotic Initiation Factor 4E Kinase with High Levels of Basal Activity in Mammalian Cells. Mol Cell Biol **21**, 743–754.

8 Waskiewicz, A. J., Johnson, J. C., Penn, B., Mahalingam, M., Kimball, S. R. and Cooper, J. A. (1999) Phosphorylation of the Cap-Binding Protein Eukaryotic Translation Initiation Factor 4E by Protein Kinase Mnk1 In Vivo. Mol Cell Biol **19**, 1871–1880.

9 Goto, S., Yao, Z. and Proud, C. G. (2009) The C-terminal domain of Mnk1a plays a dual role in tightly regulating its activity. Biochem J **423**, 279–290.

10 Scheper, G. C., Parra, J. L., Wilson, M., Kollenburg, B. van, Vertegaal, A. C. O., Han, Z.-G. and Proud, C. G. (2003) The N and C Termini of the Splice Variants of the Human Mitogen-Activated Protein Kinase-Interacting Kinase Mnk2 Determine Activity and Localization. Mol Cell Biol **23**, 5692–5705.

11 Flynn, A. and Proud, C. G. (1995) Serine 209, Not Serine 53, Is the Major Site of Phosphorylation in Initiation Factor eIF-4E in Serum-treated Chinese Hamster Ovary Cells. J Biol Chem **270**, 21684–21688.

12 Wang, X., Flynn, A., Waskiewicz, A. J., Webb, B. L. J., Vries, R. G., Baines, I. A., Cooper, J. A. and Proud, C. G. (1998) The Phosphorylation of Eukaryotic Initiation Factor eIF4E in Response to Phorbol Esters, Cell Stresses, and Cytokines Is Mediated by Distinct MAP Kinase Pathways. J Biol Chem **273**, 9373–9377.

13 Ueda, T., Watanabe-Fukunaga, R., Fukuyama, H., Nagata, S. and Fukunaga, R. (2004) Mnk2 and Mnk1 Are Essential for Constitutive and Inducible Phosphorylation of Eukaryotic Initiation Factor 4E but Not for Cell Growth or Development. Mol Cell Biol **24**, 6539–6549.

14 O'Loghlen, A., González, V. M., Piñeiro, D., Pérez-Morgado, M. I., Salinas, M. and Marťın, M. E. (2004) Identification and molecular characterization of Mnk1b, a splice variant of human MAP kinase-interacting kinase Mnk1. Exp Cell Res **299**, 343–355.

15 Slentz-Kesler, K., Moore, J. T., Lombard, M., Zhang, J., Hollingsworth, R. and Weiner, M. P. (2000) Identification of the Human Mnk2 Gene (MKNK2) through Protein Interaction with Estrogen Receptor β. Genomics **69**, 63–71.

16 Karni, R., Stanchina, E. de, Lowe, S. W., Sinha, R., Mu, D. and Krainer, A. R. (2007) The gene encoding the splicing factor SF2/ASF is a proto-oncogene. Nat Struct Mol Biology **14**.

17 Maimon, A., Mogilevsky, M., Shilo, A., Golan-Gerstl, R., Obiedat, A., Ben-Hur, V., Lebenthal-Loinger, I., Stein, I., Reich, R., Beenstock, J., et al. (24AD) Mnk2 Alternative Splicing Modulates the p38-MAPK Pathway and Impacts Ras-Induced Transformation. Cell Reports **7**, 501–513.

18 Yoon, S. and Seger, R. (2006) The extracellular signal-regulated kinase: Multiple substrates regulate diverse cellular functions. Growth Factors **24**, 21–44.

19 Yamamoto, T., Ebisuya, M., Ashida, F., Okamoto, K., Yonehara, S. and Nishida, E. (2006) Continuous ERK Activation Downregulates Antiproliferative Genes throughout G1 Phase to Allow Cell-Cycle Progression. Curr Biol **16**, 1171–1182.

20 Brown, J. R., Nigh, E., Lee, R. J., Ye, H., Thompson, M. A., Saudou, F., Pestell, R. G. and Greenberg, M. E. (1998) Fos Family Members Induce Cell Cycle Entry by Activating Cyclin D1. Mol Cell Biol **18**, 5609–5619.

21 Dhillon, A. S., Hagan, S., Rath, O. and Kolch, W. (2007) MAP kinase signalling pathways in cancer. Oncogene **26**, 1210421.

22 Gingras, A.-C., Raught, B. and Sonenberg, N. (1999) eIF4 Initiation Factors: Effectors of mRNA Recruitment to Ribosomes and Regulators of Translation. Annu Rev Biochem **68**, 913–963.

23 Sonenberg, N. and Hinnebusch, A. G. (2009) Regulation of translation initiation in eukaryotes: mechanisms and biological targets. Cell **136**, 731–45.

24 Pyronnet, S., Imataka, H., Gingras, A., Fukunaga, R., Hunter, T. and Sonenberg, N. (1999) Human eukaryotic translation initiation factor 4G (eIF4G) recruits Mnk1 to phosphorylate eIF4E. EMBO J **18**, 270–279.

25 Shveygert, M., Kaiser, C., Bradrick, S. S. and Gromeier, M. (2010) Regulation of Eukaryotic Initiation Factor 4E (eIF4E) Phosphorylation by Mitogen-Activated Protein Kinase Occurs through Modulation of Mnk1-eIF4G Interaction. Mol Cell Biol **30**, 5160–5167.

26 Pause, A., Belsham, G. J., Gingras, A.-C., Donzé, O., Lin, T.-A., Lawrence, J. C. and Sonenberg, N. (1994) Insulin-dependent stimulation of protein synthesis by phosphorylation of a regulator of 5'-cap function. Nature **371**, 762–767.

27 Marcotrigiano, J., Gingras, A.-C., Sonenberg, N. and Burley, S. K. (1999) Cap-Dependent Translation Initiation in Eukaryotes Is Regulated by a Molecular Mimic of eIF4G. Mol Cell **3**, 707–716.

28 Haghighat, A., Mader, S., Pause, A. and Sonenberg, N. (1995) Repression of cap-dependent translation by 4E-binding protein 1: competition with p220 for binding to eukaryotic initiation factor-4E. EMBO J **14**, 5701–5709.

29 Hara, K., Yonezawa, K., Kozlowski, M. T., Sugimoto, T., Andrabi, K., Weng, Q.-P., Kasuga, M., Nishimoto, I. and Avruch, J. (1997) Regulation of eIF-4E BP1 Phosphorylation by mTOR. J Biol Chem **272**, 26457–26463.

30 Scheper, G. C. and Proud, C. G. (2002) Does phosphorylation of the cap-binding protein eIF4E play a role in translation initiation? Eur J Biochem **269**, 5350–5359.

31 Marcotrigiano, J., Gingras, A.-C., Sonenberg, N. and Burley, S. K. (1997) Cocrystal Structure of the Messenger RNA 5′ Cap-Binding Protein (eIF4E) Bound to 7-methyl-GDP. Cell **89**, 951–961.

32 Proud, C. G. (2015) Mnks, eIF4E phosphorylation and cancer. BBA Gene Regul Mech **1849**, 766–773.

33 Koromilas, A. E., Lazaris-Karatzas, A. and Sonenberg, N. (1992) mRNAs containing extensive secondary structure in their 5′ non-coding region translate efficiently in cells overexpressing initiation factor eIF-4E. EMBO J **11**, 4153–4158.

34 Korneeva, N. L., Song, A., Gram, H., Edens, M. A. and Rhoads, R. E. (2016) Inhibition of Mitogen-activated Protein Kinase (MAPK)-interacting Kinase (MNK) Preferentially Affects Translation of mRNAs Containing Both a 5′-Terminal Cap and Hairpin. J Biol Chem **291**, 3455–3467.

35 Amorim, I. S., Kedia, S., Kouloulia, S., Simbriger, K., Gantois, I., Jafarnejad, S. M., Li, Y., Kampaite, A., Pooters, T., Romanò, N., et al. (2018) Loss of eIF4E phosphorylation engenders depression-like behaviors via selective mRNA translation. J Neurosci Official J Soc Neurosci **38**, 2118–2133.

36 Wendel, H.-G., Silva, R. L. A., Malina, A., Mills, J. R., Zhu, H., Ueda, T., Watanabe-Fukunaga, R., Fukunaga, R., Teruya-Feldstein, J., Pelletier, J., et al. (2007) Dissecting eIF4E action in tumorigenesis. Gene Dev **21**, 3232–3237.

37 Furic, L., Rong, L., Larsson, O., Koumakpayi, I. H., Yoshida, K., Brueschke, A., Petroulakis, E., Robichaud, N., Pollak, M., Gaboury, L. A., et al. (2010) eIF4E phosphorylation promotes tumorigenesis and is associated with prostate cancer progression. PNAS **107**, 14134–14139.

38 Truitt, M. L., Conn, C. S., Shi, Z., Pang, X., Tokuyasu, T., Coady, A. M., Seo, Y., Barna, M. and Ruggero, D. (2015) Differential Requirements for eIF4E Dose in Normal Development and Cancer. Cell **162**, 59–71.

39 Topisirovic, I., Ruiz-Gutierrez, M. and Borden, K. L. B. (2004) Phosphorylation of the Eukaryotic Translation Initiation Factor eIF4E Contributes to Its Transformation and mRNA Transport Activities. Cancer Res **64**, 8639–8642.

40 Culjkovic, B., Topisirovic, I., Skrabanek, L., Ruiz-Gutierrez, M. and Borden, K. L. B. (2005) eIF4E promotes nuclear export of cyclin D1 mRNAs via an element in the 3′UTR. J Cell Biology **169**, 245–256.

41 Han, J., Brown, T. and Beutler, B. (1990) Endotoxin-responsive sequences control cachectin/tumor necrosis factor biosynthesis at the translational level. J Exp Medicine **171**, 465–475.

42 Buxade, M., Ramirez-Alvarado, M., Fernandez-Troy, N., MacKenzie, S., Casaroli-Marano, R. P., Vilella, R. and Espel, E. (2001) Integrating signals from T-cell receptor and serum by T cells enhance translation of tumour necrosis factor-alpha. Immunology **102**, 416–425.

43 Hoffmeyer, A., Grosse-Wilde, A., Flory, E., Neufeld, B., Kunz, M., Rapp, U. R. and Ludwig, S. (1999) Different Mitogen-activated Protein Kinase Signaling Pathways Cooperate to Regulate Tumor Necrosis Factor α Gene Expression in T Lymphocytes. J Biol Chem **274**, 4319–4327.

44 Buxadé, M., Parra, J. L., Rousseau, S., Shpiro, N., Marquez, R., Morrice, N., Bain, J., Espel, E. and Proud, C. G. (2005) The Mnks Are Novel Components in the Control of TNFα Biosynthesis and Phosphorylate and Regulate hnRNP A1. Immunity **23**, 177–189.

45 Buxadé, M., Morrice, N., Krebs, D. L. and Proud, C. G. (2008) The PSF·p54nrb Complex Is a Novel Mnk Substrate That Binds the mRNA for Tumor Necrosis Factor α. J Biol Chem **283**, 57–65.

46 Mason, J. M., Morrison, D. J., Basson, M. A. and Licht, J. D. (2006) Sprouty proteins: multifaceted negative-feedback regulators of receptor tyrosine kinase signaling. Trends Cell Biol **16**, 45–54.

47 Kim, H. J. and Bar-Sagi, D. (2004) Modulation of signalling by Sprouty: a developing story. Nat Rev Mol Cell Bio **5**, 441–450.

48 DaSilva, J., Xu, L., Kim, H. J., Miller, W. T. and Bar-Sagi, D. (2006) Regulation of Sprouty Stability by Mnk1-Dependent Phosphorylation‡. Mol Cell Biol **26**, 1898–1907.

49 Edwin, F., Anderson, K. and Patel, T. B. (2010) HECT Domain-containing E3 Ubiquitin Ligase Nedd4 Interacts with and Ubiquitinates Sprouty2. J Biol Chem **285**, 255–264.

50 Funk, C. D. (2001) Prostaglandins and Leukotrienes: Advances in Eicosanoid Biology. Science **294**, 1871–1875.

51 Hefner, Y., Börsch-Haubold, A. G., Murakami, M., Wilde, J. I., Pasquet, S., Schieltz, D., Ghomashchi, F., Yates, J. R., Armstrong, C. G., Paterson, A., et al. (2000) Serine 727 Phosphorylation and Activation of Cytosolic Phospholipase A2 by MNK1-related Protein Kinases. J Biol Chem **275**, 37542–37551.

52 Kung, J. E. and Jura, N. (2016) Structural Basis for the Non-catalytic Functions of Protein Kinases. Structure **24**, 7–24.

53 Hu, S.-I., Katz, M., Chin, S., Qi, X., Cruz, J., Ibebunjo, C., Zhao, S., Chen, A. and Glass, D. J. (2012) MNK2 Inhibits eIF4G Activation Through a Pathway Involving Serine-Arginine-Rich Protein Kinase in Skeletal Muscle. Sci Signal **5**.

54 Bouameur, J.-E., Schneider, Y., Begre, N., Hobbs, R. P., Lingasamy, P., Fontao, L., Green, K. J., Favre, B. and Borradori, L. (2013) Phosphorylation of serine 4642 in the C-terminus of plectin

by MNK2 and PKA modulates its interaction with intermediate filaments. J Cell Sci **126**, 4195–4207.

55 Svitkina, T. M., Verkhovsky, A. B. and Borisy, G. G. (1996) Plectin sidearms mediate interaction of intermediate filaments with microtubules and other components of the cytoskeleton. J Cell Biology **135**, 991–1007.

56 Manning, G., Whyte, D. B., Martinez, R., Hunter, T. and Sudarsanam, S. (2002) The Protein Kinase Complement of the Human Genome. Science **298**, 1912–1934.

57 Jauch, R., Jäkel, S., Netter, C., Schreiter, K., Aicher, B., Jäckle, H. and Wahl, M. C. (2005) Crystal Structures of the Mnk2 Kinase Domain Reveal an Inhibitory Conformation and a Zinc Binding Site. Structure **13**, 1559–1568.

58 Matsui, Y., Yasumatsu, I., Yoshida, K., Iimura, S., Ikeno, Y., Nawano, T., Fukano, H., Ubukata, O., Hanzawa, H., Tanzawa, F., et al. (2018) A novel inhibitor stabilizes the inactive conformation of MAPK-interacting kinase 1. Acta Crystallogr Sect F Struct Biology Commun **74**, 156–160.

59 Reich, S. H., Sprengeler, P. A., Chiang, G. G., Appleman, J. R., Chen, J., Clarine, J., Eam, B., Ernst, J. T., Han, Q., Goel, V. K., et al. (2018) Structure-based Design of Pyridone-Aminal eFT508 Targeting Dysregulated Translation by Selective Mitogen-activated Protein Kinase Interacting Kinases 1 and 2 (MNK1/2) Inhibition. J Med Chem **61**, 3516–3540.

60 Kannan, S., Pradhan, M. R., Cherian, J., Joseph, T. L., Poh, Z. Y., Yan, Y. H., Melvyn, H., Boping, L., Jeffrey, H., Nacro, K., et al. (2017) Small Molecules Targeting the Inactive Form of the Mnk1/2 Kinases. Acs Omega **2**, 7881–7891.

61 Parra, J. L., Buxadé, M. and Proud, C. G. (2005) Features of the Catalytic Domains and C Termini of the MAPK Signal-integrating Kinases Mnk1 and Mnk2 Determine Their Differing Activities and Regulatory Properties. J Biol Chem **280**, 37623–37633.

62 Tschopp, C., Knauf, U., Brauchle, M., Zurini, M., Ramage, P., Glueck, D., New, L., Han, J. and Gram, H. (2000) Phosphorylation of eIF-4E on Ser 209 in Response to Mitogenic and Inflammatory Stimuli Is Faithfully Detected by Specific Antibodies. Mol Cell Biology Res Commun **3**, 205–211.

63 Konicek, B. W., Stephens, J. R., McNulty, A. M., Robichaud, N., Peery, R. B., Dumstorf, C. A., Dowless, M. S., Iversen, P. W., Parsons, S., Ellis, K. E., et al. (2011) Therapeutic Inhibition of MAP Kinase Interacting Kinase Blocks Eukaryotic Initiation Factor 4E Phosphorylation and Suppresses Outgrowth of Experimental Lung Metastases. Cancer Res **71**, 1849–1857.

64 Bain, J., Plater, L., Elliott, M., Shpiro, N., Hastie, C. J., Mclauchlan, H., Klevernic, I., Arthur, J. S. C., Alessi, D. R. and Cohen, P. (2007) The selectivity of protein kinase inhibitors: a further update. Biochem J **408**, 297–315.

65 Beggs, J. E., Tian, S., Jones, G. G., Xie, J., Iadevaia, V., Jenei, V., Thomas, G. and Proud, C. G. (2015) The MAP kinase-interacting kinases regulate cell migration, vimentin expression and eIF4E/CYFIP1 binding. Biochem J **467**, 63–76.

66 Teo, T., Yang, Y., Yu, M., Basnet, S. K. C., Gillam, T., Hou, J., Schmid, R. M., Kumarasiri, M., Diab, S., Albrecht, H., et al. (2015) An integrated approach for discovery of highly potent and selective Mnk inhibitors: Screening, synthesis and SAR analysis. Eur J Med Chem **103**, 539–550.

67 Yu, M., Li, P., Basnet, S. K. C., Kumarasiri, M., Diab, S., Teo, T., Albrecht, H. and Wang, S. (2015) Discovery of 4-(dihydropyridinon-3-yl)amino-5-methylthieno[2,3-d]pyrimidine derivatives as potent Mnk inhibitors: synthesis, structure–activity relationship analysis and biological evaluation. Eur J Med Chem **95**, 116–126.

68 Jin, X., Merrett, J., Tong, S., Flower, B., Xie, J., Yu, R., Tian, S., Gao, L., Zhao, J., Wang, X., et al. (2018) Design, synthesis and activity of Mnk1 and Mnk2 selective inhibitors containing thieno[2,3-d]pyrimidine scaffold. Eur J Med Chem **162**, 735–751.

69 Santag, S., Siegel, F., Wengner, A. M., Lange, C., Bömer, U., Eis, K., Pühler, F., Lienau, P., Bergemann, L., Michels, M., et al. (2017) BAY 1143269, a novel MNK1 inhibitor, targets oncogenic protein expression and shows potent anti-tumor activity. Cancer Lett **390**, 21–29.

70 Tang, Q. Q. and Lane, M. D. (2012) Adipogenesis: From Stem Cell to Adipocyte. Annu Rev Biochem **81**, 715–736.

71 Shepherd, P. R., Gnudi, L., Tozzo, E., Yang, H., Leach, F. and Kahn, B. B. (1993) Adipose cell hyperplasia and enhanced glucose disposal in transgenic mice overexpressing GLUT4 selectively in adipose tissue. J Biol Chem **268**, 22243–6.

72 Lafontan, M. (2013) Adipose tissue and adipocyte dysregulation. Diabetes Metab **40**, 16–28.

73 Tang, Q.-Q., Otto, T. C. and Lane, M. D. (2003) Mitotic clonal expansion: A synchronous process required for adipogenesis. PNAS **100**, 44–49.

74 Bowers, R. R., Kim, J. W., Otto, T. C. and Lane, M. D. (2006) Stable stem cell commitment to the adipocyte lineage by inhibition of DNA methylation: Role of the BMP-4 gene. PNAS **103**, 13022–13027.

75 Huang, H., Song, T.-J., Li, X., Hu, L., He, Q., Liu, M., Lane, M. D. and Tang, Q.-Q. (2009) BMP signaling pathway is required for commitment of C3H10T1/2 pluripotent stem cells to the adipocyte lineage. PNAS **106**, 12670–5.

76 Tang, Q.-Q., Otto, T. C. and Lane, M. D. (2004) Commitment of C3H10T1/2 pluripotent stem cells to the adipocyte lineage. PNAS **101**, 9607–9611.

77 Huang, H.-Y., Hu, L.-L., Song, T.-J., Li, X., He, Q., Sun, X., Li, Y.-M., Lu, H.-J., Yang, P.-Y. and Tang, Q.-Q. (2010) Involvement of cytoskeleton-associated proteins in the commitment of C3H10T1/2 pluripotent stem cells to adipocyte lineage induced by BMP2/4. Mol Cell Proteom **10**.

78 Komiya, Y. and Habas, R. (2008) Wnt signal transduction pathways. Organogenesis **4**, 68–75.

79 Davis, L. A. and Nieden, N. I. zur. (2008) Mesodermal fate decisions of a stem cell: the Wnt switch. Cell Mol Life Sci **65**, 2658–2674.

80 Green, H. and Kehinde, O. (1975) An established preadipose cell line and its differentiation in culture II. Factors affecting the adipose conversion. Cell **5**, 19–27.

81 Green, H. and Kehinde, O. (1976) Spontaneous heritable changes leading to increased adipose conversion in 3T3 cells. Cell **7**, 105–113.

82 Green, H. and Meuth, M. (1974) An established pre-adipose cell line and its differentiation in culture. Cell **3**, 127–133.

83 MacDougald, O. A. and Lane, M. D. (1995) Transcriptional Regulation of Gene Expression During Adipocyte Differentiation. Annu Rev Biochem **64**, 345–373.

84 Student, A. K., Hsu, R. Y. and Lane, M. D. (1980) Induction of fatty acid synthetase synthesis in differentiating 3T3-L1 preadipocytes. J Biol Chem **255**, 4745–50.

85 Green, H. and Kehinde, O. (1974) Sublines of mouse 3T3 cells that accumulate lipid. Cell **1**, 113–116.

86 Coleman, R. A., Reed, B. C., Mackall, J. C., Student, A. K., Lane, M. D. and Bell, R. M. (1978) Selective changes in microsomal enzymes of triacylglycerol phosphatidylcholine, and phosphatidylethanolamine biosynthesis during differentiation of 3T3-L1 preadipocytes. J Biol Chem **253**, 7256–61.

87 Day, C. (1999) Thiazolidinediones: a new class of antidiabetic drugs. Diabetic Med **16**, 179–192.

88 Zebisch, K., Voigt, V., Wabitsch, M. and Brandsch, M. (2012) Protocol for effective differentiation of 3T3-L1 cells to adipocytes. Anal Biochem **425**, 88–90.

89 Cao, Z., Umek, R. M. and McKnight, S. L. (1991) Regulated expression of three C/EBP isoforms during adipose conversion of 3T3-L1 cells. Gene Dev **5**, 1538–1552.

90 Landschulz, W., Johnson, P. and McKnight, S. (1989) The DNA binding domain of the rat liver nuclear protein C/EBP is bipartite. Science **243**, 1681–1688.

91 Christy, R. J., Yang, V. W., Ntambi, J. M., Geiman, D. E., Landschulz, W. H., Friedman, A. D., Nakabeppu, Y., Kelly, T. J. and Lane, M. D. (1989) Differentiation-induced gene expression in 3T3-L1 preadipocytes: CCAAT/enhancer binding protein interacts with and activates the promoters of two adipocyte-specific genes. Gene Dev **3**, 1323–1335.

92 Kaestner, K. H., Christy, R. J. and Lane, M. D. (1990) Mouse insulin-responsive glucose transporter gene: characterization of the gene and trans-activation by the CCAAT/enhancer binding protein. PNAS **87**, 251–255.

93 Cheneval, D., Christy, R. J., Geiman, D., Cornelius, P. and Lane, M. D. (1991) Cell-free transcription directed by the 422 adipose P2 gene promoter: activation by the CCAAT/enhancer binding protein. PNAS **88**, 8465–8469.

94 Samuelsson, L., Strömberg, K., Vikman, K., Bjursell, G. and Enerbäck, S. (1991) The CCAAT/enhancer binding protein and its role in adipocyte differentiation: evidence for direct involvement in terminal adipocyte development. EMBO J **10**, 3787–3793.

95 Lin, F. T. and Lane, M. D. (1992) Antisense CCAAT/enhancer-binding protein RNA suppresses coordinate gene expression and triglyceride accumulation during differentiation of 3T3-L1 preadipocytes. Gene Dev **6**, 533–544.

96 Yeh, W. C., Cao, Z., Classon, M. and McKnight, S. L. (1995) Cascade regulation of terminal adipocyte differentiation by three members of the C/EBP family of leucine zipper proteins. Gene Dev **9**, 168–181.

97 Tang, Q.-Q. and Lane, M. D. (1999) Activation and centromeric localization of CCAAT/enhancer-binding proteins during the mitotic clonal expansion of adipocyte differentiation. Gene Dev **13**, 2231–2241.

98 Siersbæk, R., Baek, S., Rabiee, A., Nielsen, R., Traynor, S., Clark, N., Sandelin, A., Jensen, O. N., Sung, M.-H., Hager, G. L., et al. (2014) Molecular Architecture of Transcription Factor Hotspots in Early Adipogenesis. Cell Reports **7**, 1434–1442.

99 Siersbæk, R., Nielsen, R., John, S., Sung, M., Baek, S., Loft, A., Hager, G. L. and Mandrup, S. (2011) Extensive chromatin remodelling and establishment of transcription factor 'hotspots' during early adipogenesis. EMBO J **30**, 1459–1472.

100 Wiper-Bergeron, N., Salem, H. A., Tomlinson, J. J., Wu, D. and Haché, R. J. G. (2007) Glucocorticoid-stimulated preadipocyte differentiation is mediated through acetylation of C/EBPβ by GCN5. PNAS **104**, 2703–2708.

101 Tang, Q.-Q., Grønborg, M., Huang, H., Kim, J.-W., Otto, T. C., Pandey, A. and Lane, M. D. (2005) Sequential phosphorylation of CCAAT enhancer-binding protein β by MAPK and glycogen synthase kinase 3β is required for adipogenesis. PNAS **102**, 9766–9771.

102 Tang, Q.-Q., Otto, T. C. and Lane, M. D. (2003) CCAAT/enhancer-binding protein β is required for mitotic clonal expansion during adipogenesis. PNAS **100**, 850–855.

103 Tanaka, T., Yoshida, N., Kishimoto, T. and Akira, S. (1997) Defective adipocyte differentiation in mice lacking the C/EBPβ and/or C/EBPδ gene. EMBO J **16**, 7432–7443.

104 Patel, Y. M. and Lane, M. D. (2000) Mitotic Clonal Expansion During Preadipocyte Differentiation: Calpain-Mediated Turnover of p27. J Biol Chem **275**, 17653–17660.

105 Zhang, J.-W., Tang, Q.-Q., Vinson, C. and Lane, M. D. (2004) Dominant-negative C/EBP disrupts mitotic clonal expansion and differentiation of 3T3-L1 preadipocytes. PNAS **101**, 43–47.

106 Moitra, J., Mason, M. M., Olive, M., Krylov, D., Gavrilova, O., Marcus-Samuels, B., Feigenbaum, L., Lee, E., Aoyama, T., Eckhaus, M., et al. (1998) Life without white fat: a transgenic mouse. Gene Dev **12**, 3168–3181.

107 Kim, J. -w, Tang, Q.-Q., Li, X. and Lane, M. D. (2007) Effect of phosphorylation and S-S bond-induced dimerization on DNA binding and transcriptional activation by C/EBPbeta. PNAS **104**, 1800–1804.

108 Giacinti, C. and Giordano, A. (2006) RB and cell cycle progression. Oncogene **25**, 5220–5227.

109 Chen, P. L., Riley, D. J., Chen, Y. and Lee, W. H. (1996) Retinoblastoma protein positively regulates terminal adipocyte differentiation through direct interaction with C/EBPs. Gene Dev **10**, 2794–2804.

110 Chen, P. L., Riley, D. J., Chen-Kiang, S. and Lee, W. H. (1996) Retinoblastoma protein directly interacts with and activates the transcription factor NF-IL6. PNAS **93**, 465–469.

111 Cole, K. A., Harmon, A. W., Harp, J. B. and Patel, Y. M. (2004) Rb regulates C/EBPβ-DNA-binding activity during 3T3-L1 adipogenesis. Am J Physiol Cell Physiol **286**, C349–C354.

112 Lin, F. T. and Lane, M. D. (1994) CCAAT/enhancer binding protein alpha is sufficient to initiate the 3T3-L1 adipocyte differentiation program. PNAS **91**, 8757–8761.

113 Christy, R. J., Kaestner, K. H., Geiman, D. E. and Lane, M. D. (1991) CCAAT/enhancer binding protein gene promoter: binding of nuclear factors during differentiation of 3T3-L1 preadipocytes. PNAS **88**, 2593–2597.

114 Kaestner, K. H., Ntambi, J. M., Kelly, T. J. and Lane, M. D. (1989) Differentiation-induced gene expression in 3T3-L1 preadipocytes. A second differentially expressed gene encoding stearoyl-CoA desaturase. J Biol Chem **264**, 14755–61.

115 Wang, N., Finegold, M., Bradley, A., Ou, C., Abdelsayed, S., Wilde, M., Taylor, L., Wilson, D. and Darlington, G. (1995) Impaired energy homeostasis in C/EBP alpha knockout mice. Science **269**, 1108–1112.

116 MacDougald, O. A., Cornelius, P., Liu, R. and Lane, M. D. (1995) Insulin Regulates Transcription of the CCAAT/Enhancer Binding Protein (C/EBP) alpha, beta and delta Genes in Fully-differentiated 3T3-L1 Adipocytes. J Biol Chem **270**, 647–654.

117 Jiang, M.-S., Tang, Q.-Q., McLenithan, J., Geiman, D., Shillinglaw, W., Henzel, W. J. and Lane, M. D. (1998) Derepression of the C/EBPα gene during adipogenesis: Identification of AP-2α as a repressor. PNAS **95**, 3467–3471.

118 Tang, Q.-Q., Jiang, M.-S. and Lane, M. D. (1999) Repressive Effect of Sp1 on the C/EBPα Gene Promoter: Role in Adipocyte Differentiation. Mol Cell Biol **19**, 4855–4865.

119 Tang, Q.-Q., Jiang, M.-S. and Lane, M. D. (1997) Repression of transcription mediated by dual elements in the CCAAT/enhancer binding protein gene. PNAS **94**, 13571–13575.

120 Lin, F. T., MacDougald, O. A., Diehl, A. M. and Lane, M. D. (1993) A 30-kDa alternative translation product of the CCAAT/enhancer binding protein alpha message: transcriptional activator lacking antimitotic activity. PNAS **90**, 9606–9610.

121 Legraverend, C., Antonson, P., Flodby, P. and Xanthopoulos, G. (1993) High level activity of the mouse CCAAT/enhancer binding protein (C/EBPα) gene promoter involves autoregulation and several ubiquitous transcription factors. Nucleic Acids Res **21**, 1735–1742.

122 Timchenko, N., Wilson, D. R., Taylor, L. R., Abdelsayed, S., Wilde, M., Sawadogo, M. and Darlington, G. J. (1995) Autoregulation of the human C/EBP alpha gene by stimulation of upstream stimulatory factor binding. Mol Cell Biol **15**, 1192–1202.

123 Tang, Q.-Q., Zhang, J.-W. and Lane, M. D. (2004) Sequential gene promoter interactions by C/EBPβ, C/EBPα, and PPARγ during adipogenesis. Biochem Bioph Res Co **318**, 213–218.

124 Ron, D. and Habener, J. F. (1992) CHOP, a novel developmentally regulated nuclear protein that dimerizes with transcription factors C/EBP and LAP and functions as a dominant-negative inhibitor of gene transcription. Gene Dev **6**, 439–453.

125 Tang, Q.-Q. and Lane, M. D. (2000) Role of C/EBP homologous protein (CHOP-10) in the programmed activation of CCAAT/enhancer-binding protein-β during adipogenesis. PNAS **97**, 12446–12450.

126 Batchvarova, N., Wang, X. Z. and Ron, D. (1995) Inhibition of adipogenesis by the stress-induced protein CHOP (Gadd153). EMBO J **14**, 4654–4661.

127 Williams, S. C., Cantwell, C. A. and Johnson, P. F. (1991) A family of C/EBP-related proteins capable of forming covalently linked leucine zipper dimers in vitro. Gene Dev **5**, 1553–1567.

128 Nishio, Y., Isshiki, H., Kishimoto, T. and Akira, S. (1993) A nuclear factor for interleukin-6 expression (NF-IL6) and the glucocorticoid receptor synergistically activate transcription of the rat alpha 1-acid glycoprotein gene via direct protein-protein interaction. Mol Cell Biol **13**, 1854–1862.

129 Vallejo, M., Ron, D., Miller, C. P. and Habener, J. F. (1993) C/ATF, a member of the activating transcription factor family of DNA-binding proteins, dimerizes with CAAT/enhancer-binding proteins and directs their binding to cAMP response elements. PNAS **90**, 4679–4683.

130 LeClair, K. P., Blanar, M. A. and Sharp, P. A. (1992) The p50 subunit of NF-kappa B associates with the NF-IL6 transcription factor. PNAS **89**, 8145–8149.

131 Descombes, P., Chojkier, M., Lichtsteiner, S., Falvey, E. and Schibler, U. (1990) LAP, a novel member of the C/EBP gene family, encodes a liver-enriched transcriptional activator protein. Gene Dev **4**, 1541–1551.

132 Descombes, P. and Schibler, U. (1991) A liver-enriched transcriptional activator protein, LAP, and a transcriptional inhibitory protein, LIP, are translated from the same mRNA. Cell **67**, 569–579.

133 Lechner, S., Mitterberger, M. C., Mattesich, M. and Zwerschke, W. (2013) Role of C/EBPβ-LAP and C/EBPβ-LIP in early adipogenic differentiation of human white adipose-derived progenitors and at later stages in immature adipocytes. Differentiation **85**, 20–31.

134 Hamm, J. K., Park, B. H. and Farmer, S. R. (2001) A Role for C/EBPβ in Regulating Peroxisome Proliferator-activated Receptor γ Activity during Adipogenesis in 3T3-L1 Preadipocytes. J Biol Chem **276**, 18464–18471.

135 Qian, S.-W., Li, X., Zhang, Y.-Y., Huang, H.-Y., Liu, Y., Sun, X. and Tang, Q.-Q. (2010) Characterization of adipocyte differentiation from human mesenchymal stem cells in bone marrow. BMC Dev Biol **10**, 47.

136 Ossipow, V., Descombes, P. and Schibler, U. (1993) CCAAT/enhancer-binding protein mRNA is translated into multiple proteins with different transcription activation potentials. PNAS **90**, 8219–8223.

137 Tontonoz, P., Hu, E. and Spiegelman, B. M. (1994) Stimulation of adipogenesis in fibroblasts by PPARγ2, a lipid-activated transcription factor. Cell **79**, 1147–1156.

138 Rosen, E. D., Hsu, C.-H., Wang, X., Sakai, S., Freeman, M. W., Gonzalez, F. J. and Spiegelman, B. M. (2002) C/EBPα induces adipogenesis through PPARγ: a unified pathway. Gene Dev **16**, 22–26.

139 Hamm, J. K., Jack, A. K. E., Pilch, P. F. and Farmer, S. R. (1999) Role of PPARgamma in Regulating Adipocyte Differentiation and Insulin-Responsive Glucose Uptake. Ann NY Acad Sci **892**, 134–145.

140 Fajas, L., Auboeuf, D., Raspé, E., Schoonjans, K., Lefebvre, A.-M., Saladin, R., Najib, J., Laville, M., Fruchart, J.-C., Deeb, S., et al. (1997) The Organization, Promoter Analysis, and Expression of the Human PPARγ Gene. J Biol Chem **272**, 18779–18789.

141 Zhu, Y., Alvares, K., Huang, Q., Rao, M. S. and Reddy, J. K. (1993) Cloning of a new member of the peroxisome proliferator-activated receptor gene family from mouse liver. J Biol Chem **268**, 26817–20.

142 Tontonoz, P., Hu, E., Graves, R. A., Budavari, A. I. and Spiegelman, B. M. (1994) mPPAR gamma 2: tissue-specific regulator of an adipocyte enhancer. Gene Dev **8**, 1224–1234.

143 Zhu, Y., Qi, C., Korenberg, J. R., Chen, X. N., Noya, D., Rao, M. S. and Reddy, J. K. (1995) Structural organization of mouse peroxisome proliferator-activated receptor gamma (mPPAR gamma) gene: alternative promoter use and different splicing yield two mPPAR gamma isoforms. PNAS **92**, 7921–7925.

144 Mueller, E., Drori, S., Aiyer, A., Yie, J., Sarraf, P., Chen, H., Hauser, S., Rosen, E. D., Ge, K., Roeder, R. G., et al. (2002) Genetic Analysis of Adipogenesis through Peroxisome Proliferator-activated Receptor γ Isoforms. J Biol Chem **277**, 41925–41930.

145 Zhang, J., Fu, M., Cui, T., Xiong, C., Xu, K., Zhong, W., Xiao, Y., Floyd, D., Liang, J., Li, E., et al. (2004) Selective disruption of PPAR 2 impairs the development of adipose tissue and insulin sensitivity. PNAS **101**, 10703–10708.

146 Barak, Y., Nelson, M. C., Ong, E. S., Jones, Y. Z., Ruiz-Lozano, P., Chien, K. R., Koder, A. and Evans, R. M. (1999) PPARγ Is Required for Placental, Cardiac, and Adipose Tissue Development. Mol Cell **4**, 585–595.

147 Rosen, E. D., Sarraf, P., Troy, A. E., Bradwin, G., Moore, K., Milstone, D. S., Spiegelman, B. M. and Mortensen, R. M. (1999) PPARγ Is Required for the Differentiation of Adipose Tissue In Vivo and In Vitro. Mol Cell **4**, 611–617.

148 Koutnikova, H., Cock, T.-A., Watanabe, M., Houten, S. M., Champy, M.-F., Dierich, A. and Auwerx, J. (2003) Compensation by the muscle limits the metabolic consequences of lipodystrophy in PPARγ hypomorphic mice. PNAS **100**, 14457–14462.

149 Medina-Gomez, G., Gray, S. L., Yetukuri, L., Shimomura, K., Virtue, S., Campbell, M., Curtis, R. K., Jimenez-Linan, M., Blount, M., Yeo, G. S. H., et al. (2007) PPAR gamma 2 Prevents Lipotoxicity by Controlling Adipose Tissue Expandability and Peripheral Lipid Metabolism. PloS Genet **3**, e64.

150 Wu, Z., Xie, Y., Bucher, N. L. and Farmer, S. R. (1995) Conditional ectopic expression of C/EBP beta in NIH-3T3 cells induces PPAR gamma and stimulates adipogenesis. Gene Dev **9**, 2350–2363.

151 Wu, Z., Bucher, N. L. and Farmer, S. R. (1996) Induction of peroxisome proliferator-activated receptor gamma during the conversion of 3T3 fibroblasts into adipocytes is mediated by C/EBPbeta, C/EBPdelta, and glucocorticoids. Mol Cell Biol **16**, 4128–4136.

152 Elberg, G., Gimble, J. M. and Tsai, S. Y. (2000) Modulation of the Murine Peroxisome Proliferator-activated Receptor γ2 Promoter Activity by CCAAT/Enhancer-binding Proteins. J Biol Chem **275**, 27815–27822.

153 Clarke, S. L., Robinson, C. E. and Gimble, J. M. (1997) CAAT/Enhancer Binding Proteins Directly Modulate Transcription from the Peroxisome Proliferator-Activated Receptor γ2 Promoter. Biochem Bioph Res Co **240**, 99–103.

154 Tontonoz, P. and Spiegelman, B. M. (2008) Fat and Beyond: The Diverse Biology of PPARγ. Annu Rev Biochem **77**, 289–312.

155 Miyata, K. S., McCaw, S. E., Marcus, S. L., Rachubinski, R. A. and Capone, J. P. (1994) The peroxisome proliferator-activated receptor interacts with the retinoid X receptor in vivo. Gene **148**, 327–330.

156 Siersbæk, R., Nielsen, R. and Mandrup, S. (2010) PPARγ in adipocyte differentiation and metabolism – Novel insights from genome-wide studies. Febs Lett **584**, 3242–3249.

157 Lefterova, M. I., Haakonsson, A. K., Lazar, M. A. and Mandrup, S. (2014) PPARγ and the global map of adipogenesis and beyond. Trends Endocrinol Metabolism **25**, 293–302.

158 Wu, Z., Rosen, E. D., Brun, R., Hauser, S., Adelmant, G., Troy, A. E., McKeon, C., Darlington, G. J. and Spiegelman, B. M. (1999) Cross-Regulation of C/EBPα and PPARγ Controls the Transcriptional Pathway of Adipogenesis and Insulin Sensitivity. Mol Cell **3**, 151–158.

159 Zuo, Y., Qiang, L. and Farmer, S. R. (2006) Activation of CCAAT/Enhancer-binding Protein (C/EBP) α Expression by C/EBPβ during Adipogenesis Requires a Peroxisome Proliferator-activated Receptor-γ-associated Repression of HDAC1 at the C/ebpα Gene Promoter. J Biol Chem **281**, 7960–7967.

160 Rosen, E. D. and MacDougald, O. A. (2006) Adipocyte differentiation from the inside out. Nat Rev Mol Cell Bio **7**, 885–896.

161 Deschênes, J., Bourdeau, V., White, J. H. and Mader, S. (2007) Regulation of GREB1 Transcription by Estrogen Receptor α through a Multipartite Enhancer Spread Over 20 kb of Upstream Flanking Sequences. J Biol Chem **282**, 17335–17339.

162 Lefterova, M. I., Zhang, Y., Steger, D. J., Schupp, M., Schug, J., Cristancho, A., Feng, D., Zhuo, D., Stoeckert, C. J., Liu, X. S., et al. (2008) PPARγ and C/EBP factors orchestrate adipocyte biology via adjacent binding on a genome-wide scale. Gene Dev **22**, 2941–2952.

163 Schmidt, S. F., Jørgensen, M., Chen, Y., Nielsen, R., Sandelin, A. and Mandrup, S. (2011) Cross species comparison of C/EBPα and PPARγ profiles in mouse and human adipocytes reveals interdependent retention of binding sites. BMC Genomics **12**, 152.

164 Nielsen, R., Pedersen, T. Å., Hagenbeek, D., Moulos, P., Siersbæk, R., Megens, E., Denissov, S., Børgesen, M., Francoijs, K.-J., Mandrup, S., et al. (2008) Genome-wide profiling of PPARγ:RXR and RNA polymerase II occupancy reveals temporal activation of distinct metabolic pathways and changes in RXR dimer composition during adipogenesis. Gene Dev **22**, 2953–2967.

165 Chang, F., Steelman, L. S., Shelton, J. G., Lee, J. T., Navolanic, P. M., Blalock, W. L., Franklin, R. and McCubrey, J. A. (2003) Regulation of cell cycle progression and apoptosis by the Ras/Raf/MEK/ERK pathway (Review). Int J Oncol **22**, 469–80.

166 Benito, M., Porras, A., Nebreda, A. and Santos, E. (1991) Differentiation of 3T3-L1 fibroblasts to adipocytes induced by transfection of ras oncogenes. Science **253**, 565–568.

167 Sale, E. M., Atkinson, P. G. and Sale, G. J. (1995) Requirement of MAP kinase for differentiation of fibroblasts to adipocytes, for insulin activation of p90 S6 kinase and for insulin or serum stimulation of DNA synthesis. EMBO J **14**, 674–684.

168 Camp, H. S. and Tafuri, S. R. (1997) Regulation of Peroxisome Proliferator-activated Receptor γ Activity by Mitogen-activated Protein Kinase. J Biol Chem **272**, 10811–10816.

169 Hu, E., Kim, J. B., Sarraf, P. and Spiegelman, B. M. (1996) Inhibition of Adipogenesis Through MAP Kinase-Mediated Phosphorylation of PPARγ. Science **274**, 2100–2103.

170 Hanlon, M., Sturgill, T. W. and Sealy, L. (2001) ERK2- and p90 Rsk2 -dependent Pathways Regulate the CCAAT/Enhancer-binding Protein-β Interaction with Serum Response Factor. J Biol Chem **276**, 38449–38456.

171 Saba-El-Leil, M. K., Vella, F. D. J., Vernay, B., Voisin, L., Chen, L., Labrecque, N., Ang, S.-L. and Meloche, S. (2003) An essential function of the mitogen-activated protein kinase Erk2 in mouse trophoblast development. EMBO Rep **4**, 964–968.

172 Pagès, G., Guérin, S., Grall, D., Bonino, F., Smith, A., Anjuere, F., Auberger, P. and Pouysségur, J. (1999) Defective Thymocyte Maturation in p44 MAP Kinase (Erk 1) Knockout Mice. Science **286**, 1374–1377.

173 Bost, F., Aouadi, M., Caron, L., Even, P., Belmonte, N., Prot, M., Dani, C., Hofman, P., Pages, G., Pouyssegur, J., et al. (2005) The Extracellular Signal-Regulated Kinase Isoform ERK1 Is Specifically Required for In Vitro and In Vivo Adipogenesis. Diabetes **54**, 402–411.

174 Donzelli, E., Lucchini, C., Ballarini, E., Scuteri, A., Carini, F., Tredici, G. and Miloso, M. (2011) ERK1 and ERK2 are involved in recruitment and maturation of human mesenchymal stem cells induced to adipogenic differentiation. J Mol Cell Biol **3**, 123–131.

175 Engelman, J. A., Lisanti, M. P. and Scherer, P. E. (1998) Specific Inhibitors of p38 Mitogen-activated Protein Kinase Block 3T3-L1 Adipogenesis. J Biol Chem **273**, 32111–32120.

176 Engelman, J. A., Berg, A. H., Lewis, R. Y., Lin, A., Lisanti, M. P. and Scherer, P. E. (1999) Constitutively Active Mitogen-activated Protein Kinase Kinase 6 (MKK6) or Salicylate Induces Spontaneous 3T3-L1 Adipogenesis. J Biol Chem **274**, 35630–35638.

177 Takenouchi, T., Takayama, Y. and Takezawa, T. (2004) Co-treatment with dexamethasone and octanoate induces adipogenesis in 3T3-L1 cells. Cell Biol Int **28**, 209–216.

178 Patel, N. G., Holder, J. C., Smith, S. A., Kumar, S. and Eggo, M. C. (2003) Differential Regulation of Lipogenesis and Leptin Production by Independent Signaling Pathways and Rosiglitazone During Human Adipocyte Differentiation. Diabetes **52**, 43–50.

179 Wang, X.-Z. and Ron, D. (1996) Stress-Induced Phosphorylation and Activation of the Transcription Factor CHOP (GADD153) by p38 MAP Kinase. Science **272**, 1347–1349.

180 Yang, T. T. C., Xiong, Q., Enslen, H., Davis, R. J. and Chow, C.-W. (2002) Phosphorylation of NFATc4 by p38 Mitogen-Activated Protein Kinases. Mol Cell Biol **22**, 3892–3904.

181 Ho, I.-C., Kim, J. H.-J., Rooney, J. W., Spiegelman, B. M. and Glimcher, L. H. (1998) A potential role for the nuclear factor of activated T cells family of transcriptional regulatory proteins in adipogenesis. PNAS **95**, 15537–15541.

182 Tamura, K., Sudo, T., Senftleben, U., Dadak, A. M., Johnson, R. and Karin, M. (2000) Requirement for p38α in Erythropoietin Expression. Cell **102**, 221–231.

183 Huse, O., Hettiarachchi, J., Gearon, E., Nichols, M., Allender, S. and Peeters, A. (2017) Obesity in Australia. Obes Res Clin Pract **12**, 29–39.

184 Abarca-Gómez, L., Abdeen, Z. A., Hamid, Z. A., Abu-Rmeileh, N. M., Acosta-Cazares, B., Acuin, C., Adams, R. J., Aekplakorn, W., Afsana, K., Aguilar-Salinas, C. A., et al. (2017) Worldwide trends in body-mass index, underweight, overweight, and obesity from 1975 to 2016: a pooled analysis of 2416 population-based measurement studies in 128·9 million children, adolescents, and adults. Lancet **390**, 2627–2642.

185 Australian Institute of Health and Welfare (2020) Overweight and obesity: an interactive insight, *https://www.aihw.gov.au/reports/overweight-obesity/overweight-and-obesity-an-interactive- insight*, accessed 19 February 2020.

186 Australian Institute of Health and Welfare (2015) Australian Burden of Disease Study: impact and causes of illness and death in Australia 2015, Canberra, Australia.

187 House of Representatives Standing Committee on Health and Ageing (2009) Weighing it up: Obesity in Australia, Printing and Publishing Office, Department of House of Representatives, Canberra, Australia.

188 Arsenijevic, T., Grégoire, F., Delforge, V., Delporte, C. and Perret, J. (2012) Murine 3T3-L1 adipocyte cell differentiation model: validated reference genes for qPCR gene expression analysis. PLoS One **7**.

189 Xie, J., Merrett, J. E., Jensen, K. B. and Proud, C. G. (2019) The MAP kinase-interacting kinases (MNKs) as targets in oncology. Expert Opin Ther Tar **23**, 187–199.

190 Joshi, S. and Platanias, L. C. (2014) Mnk kinase pathway: Cellular functions and biological outcomes. World J Biol Chem **5**, 321–333.

191 Joshi, S. and Platanias, L. C. (2015) Mnk kinases in cytokine signaling and regulation of cytokine responses. Biomol Concepts **6**, 85–85.

192 Bost, F., Aouadi, M., Caron, L. and Binétruy, B. (2005) The role of MAPKs in adipocyte differentiation and obesity. Biochimie **87**, 51–56.

193 Farmer, S. R. (2006) Transcriptional control of adipocyte formation. Cell Metab **4**, 263–273.

194 Magun, R., Burgering, B. M., Coffer, P. J., Pardasani, D., Lin, Y., Chabot, J. and Sorisky, A. (1996) Expression of a constitutively activated form of protein kinase B (c- Akt) in 3T3-L1 preadipose cells causes spontaneous differentiation. Endocrinology **137**, 3590–3593.

195 Xu, J. and Liao, K. (2004) Protein Kinase B/AKT 1 Plays a Pivotal Role in Insulin-like Growth Factor-1 Receptor Signaling Induced 3T3-L1 Adipocyte Differentiation. J Biol Chem **279**, 35914–35922.

196 Kohn, A. D., Summers, S. A., Birnbaum, M. J. and Roth, R. A. (1996) Expression of a Constitutively Active Akt Ser/Thr Kinase in 3T3-L1 Adipocytes Stimulates Glucose Uptake and Glucose Transporter 4 Translocation. J Biol Chem **271**, 31372–31378.

197 Armoni, M., Harel, C., Karni, S., Chen, H., Bar-Yoseph, F., Ver, M. R., Quon, M. J. and Karnieli, E. (2006) FOXO1 Represses Peroxisome Proliferator-activated Receptor-γ1 and -γ2 Gene Promoters in Primary Adipocytes. J Biol Chem **281**, 19881–19891.

198 Nakae, J., Kitamura, T., Kitamura, Y., Biggs, W. H., Arden, K. C. and Accili, D. (2003) The Forkhead Transcription Factor Foxo1 Regulates Adipocyte Differentiation. Dev Cell **4**, 119–129.

199 Inoki, K., Li, Y., Zhu, T., Wu, J. and Guan, K.-L. (2002) TSC2 is phosphorylated and inhibited by Akt and suppresses mTOR signalling. Nat Cell Biol **4**, 648–657.

200 Zhang, H. H., Huang, J., Düvel, K., Boback, B., Wu, S., Squillace, R. M., Wu, C.-L. and Manning, B. D. (2009) Insulin Stimulates Adipogenesis through the Akt-TSC2-mTORC1 Pathway. PLoS One **4**, e6189.

201 Manning, B. D. and Cantley, L. C. (2007) AKT/PKB Signaling: Navigating Downstream. Cell **129**, 1261–1274.

202 Zhang, J.-W., Klemm, D. J., Vinson, C. and Lane, M. D. (2004) Role of CREB in Transcriptional Regulation of CCAAT/Enhancer-binding Protein β Gene during Adipogenesis. J Biol Chem **279**, 4471–4478.

203 Zhang, X., Odom, D. T., Koo, S.-H., Conkright, M. D., Canettieri, G., Best, J., Chen, H., Jenner, R., Herbolsheimer, E., Jacobsen, E., et al. (2005) Genome-wide analysis of cAMP-response element binding protein occupancy, phosphorylation, and target gene activation in human tissues. PNAS **102**, 4459–4464.

204 Schiller, B. J., Chodankar, R., Watson, L. C., Stallcup, M. R. and Yamamoto, K. R. (2014) Glucocorticoid receptor binds half sites as a monomer and regulates specific target genes. Genome Biol **15**, 418.

205 Mayr, B. and Montminy, M. (2001) Transcriptional regulation by the phosphorylation-dependent factor CREB. Nat Rev Mol Cell Bio **2**, 35085068.

206 Oakley, R. H. and Cidlowski, J. A. (2013) The biology of the glucocorticoid receptor: New signaling mechanisms in health and disease. J Allergy Clin Immun **132**, 1033–1044.

207 Ryden, T. A. and Beemon, K. (1989) Avian retroviral long terminal repeats bind CCAAT/enhancer-binding protein. Mol Cell Biol **9**, 1155–1164.

208 Osada, S., Yamamoto, H., Nishihara, T. and Imagawa, M. (1996) DNA Binding Specificity of the CCAAT/Enhancer-binding Protein Transcription Factor Family. J Biol Chem **271**, 3891–3896.

209 Palmer, C. N. A., Hsu, M.-H., Griffin, K. J. and Johnson, E. F. (1995) Novel Sequence Determinants in Peroxisome Proliferator Signaling. J Biol Chem **270**, 16114–16121.

210 Flynn, A. and Proud, G. (1996) Insulin-stimulated phosphorylation of initiation factor 4E is mediated by the MAP kinase pathway. **389**, 162.

211 Scheper, G. C., Morrice, N. A., Kleijn, M. and Proud, C. G. (2001) The Mitogen-Activated Protein Kinase Signal-Integrating Kinase Mnk2 Is a Eukaryotic Initiation Factor 4E Kinase with High Levels of Basal Activity in Mammalian Cells. Mol Cell Biol **21**, 743–754.

212 Lane, M. D., Tang, Q.-Q. and Jiang, M.-S. (1999) Role of the CCAAT Enhancer Binding Proteins (C/EBPs) in Adipocyte Differentiation. Biochem Bioph Res Co **266**, 677–683.

213 Yeh, W. C., Bierer, B. E. and McKnight, S. L. (1995) Rapamycin inhibits clonal expansion and adipogenic differentiation of 3T3-L1 cells. PNAS **92**, 11086–11090.

214 Cho, H. J., Park, J., Lee, H. W., Lee, Y. S. and Kim, J. B. (2004) Regulation of adipocyte differentiation and insulin action with rapamycin. Biochem Bioph Res Co **321**, 942–948.

215 Brown, M. C. and Gromeier, M. (2017) MNK Controls mTORC1:Substrate Association through Regulation of TELO2 Binding with mTORC1. Cell Reports **18**, 1444–1457.

216 Ali, E. M. H., Abdel-Maksoud, M. S. and Oh, C.-H. (2019) Thieno[2,3-d]pyrimidine as a promising scaffold in medicinal chemistry: Recent advances. Bioorgan Med Chem **27**, 1159–1194.

217 Taylor, S., Murfin, S., Coulter, S., Jaekel, S., Aicher, B., Kelter, A.-R., Krämer, J., Kirchhoff, C., Scheel, A. and Wölcke, J. (2006) Thienopyrimidines for pharmaceutical compositions, Patent WO/2006/136402.

218 Aicher, B., Coulter, S., Jaekel, S., Kelter, A.-R., Murfin, S., Reuter, T. and Taylor, S. (2007) Thienopyrimidines having MNK1 /MNK2 inhibiting activity for pharmaceutical compositions, Patent WO/2007/115822A1

219 Tian, S., Wang, X. and Proud, C. G. (2017) Oncogenic MNK signalling regulates the metastasis suppressor NDRG1. Oncotarget **5**, 46121.

220 Chresta, C. M., Davies, B. R., Hickson, I., Harding, T., Cosulich, S., Critchlow, S. E., Vincent, J. P., Ellston, R., Jones, D., Sini, P., et al. (2010) AZD8055 Is a Potent, Selective, and Orally Bioavailable ATP-Competitive Mammalian Target of Rapamycin Kinase Inhibitor with In vitro and In vivo Antitumor Activity. Cancer Res **70**, 288–298.

221 Shao, D. and Lazar, M. A. (1997) Peroxisome Proliferator Activated Receptor γ, CCAAT/Enhancer-binding Protein α, and Cell Cycle Status Regulate the Commitment to Adipocyte Differentiation. J Biol Chem **272**, 21473–21478.

222 Wang, Z., Frederick, J. and Garabedian, M. J. (2002) Deciphering the Phosphorylation “Code” of the Glucocorticoid Receptor in Vivo. J Biol Chem **277**, 26573–26580.

223 Zhu, Y., Qi, C., Korenberg, J. R., Chen, X. N., Noya, D., Rao, M. S. and Reddy, J. K. (1995) Structural organization of mouse peroxisome proliferator-activated receptor gamma (mPPAR gamma) gene: alternative promoter use and different splicing yield two mPPAR gamma isoforms. Proc National Acad Sci **92**, 7921–7925.

224 Tang, Q. Q. and Lane, M. D. (1999) Activation and centromeric localization of CCAAT/enhancer-binding proteins during the mitotic clonal expansion of adipocyte differentiation. Cold Spring Harbor Laboratory Press **13**, 2231.

225 Adams, P. D. and Kaelin, W. G. (1995) Transcriptional control by E2F. Semin Cancer Biol **6**, 99–108.

226 Hitomi, M. and Stacey, D. W. (1999) Cyclin D1 production in cycling cells depends on Ras in a cell-cycle-specific manner. Curr Biol **9**, 1075-S2.

227 Lavoie, J. N., L'Allemain, G., Brunet, A., Müller, R. and Pouysségur, J. (1996) Cyclin D1 Expression Is Regulated Positively by the p42/p44MAPK and Negatively by the p38/HOGMAPK Pathway. J Biol Chem **271**, 20608–20616.

228 Ohtani, K., DeGregori, J. and Nevins, J. R. (1995) Regulation of the cyclin E gene by transcription factor E2F1. PNAS **92**, 12146–12150.

229 Klein, E. A. and Assoian, R. K. (2008) Transcriptional regulation of the cyclin D1 gene at a glance. J Cell Sci **121**, 3853–3857.

230 Ji, P., Jiang, H., Rekhtman, K., Bloom, J., Ichetovkin, M., Pagano, M. and Zhu, L. (2004) An Rb-Skp2-p27 Pathway Mediates Acute Cell Cycle Inhibition by Rb and Is Retained in a Partial-Penetrance Rb Mutant. Mol Cell **16**, 47–58.

231 Alexander, K. and Hinds, P. W. (2001) Requirement for p27KIP1 in Retinoblastoma Protein-Mediated Senescence. Mol Cell Biol **21**, 3616–3631.

232 Blanchard, P.-G., Festuccia, W. T., Houde, V. P., St-Pierre, P., Brûlé, S., Turcotte, V., Côté, M., Bellmann, K., Marette, A. and Deshaies, Y. (2012) Major involvement of mTOR in the PPARγ-induced stimulation of adipose tissue lipid uptake and fat accretion. J Lipid Res **53**, 1117–1125.

233 Festuccia, W. T., Laplante, M., Brûlé, S., Houde, V. P., Achouba, A., Lachance, D., Pedrosa, M. L., Silva, M. E., Guerra-Sá, R., Couet, J., et al. (2009) Rosiglitazone-induced heart remodelling is associated with enhanced turnover of myofibrillar protein and mTOR activation. J Mol Cell Cardiol **47**, 85–95.

234 Bacquer, O. L., Petroulakis, E., Paglialunga, S., Poulin, F., Richard, D., Cianflone, K. and Sonenberg, N. (2007) Elevated sensitivity to diet-induced obesity and insulin resistance in mice lacking 4E-BP1 and 4E-BP2. J Clin Invest **117**, 387–396.

235 Fang, M.-Z., Lee, M.-H., Lee, Y.-S., Kim, Y.-C. and Lee, B.-M. (2002) Low Expression of Cyclin D2 in G2/M-Arrested and Transformed Proliferating Balb/3T3 Cells. J Vet Med Sci **64**, 201–205.

236 Phelps, D. E. and Xiong, Y. (1998) Regulation of cyclin-dependent kinase 4 during adipogenesis involves switching of cyclin D subunits and concurrent binding of p18INK4c and p27Kip1. Am Assoc Cancer Res **9**, 595–610.

237 Fu, M., Rao, M., Bouras, T., Wang, C., Wu, K., Zhang, X., Li, Z., Yao, T.-P. and Pestell, R. G. (2005) Cyclin D1 Inhibits Peroxisome Proliferator-activated Receptor γ-mediated Adipogenesis through Histone Deacetylase Recruitment. J Biol Chem **280**, 16934–16941.

238 Fu, M., Wang, C., Rao, M., Wu, X., Bouras, T., Zhang, X., Li, Z., Jiao, X., Yang, J., Li, A., et al. (2005) Cyclin D1 Represses p300 Transactivation through a Cyclin-dependent Kinase-independent Mechanism. J Biol Chem **280**, 29728–29742.

239 Wang, C., Pattabiraman, N., Zhou, J. N., Fu, M., Sakamaki, T., Albanese, C., Li, Z., Wu, K., Hulit, J., Neumeister, P., et al. (2003) Cyclin D1 Repression of Peroxisome Proliferator-Activated Receptor γ Expression and Transactivation. Mol Cell Biol **23**, 6159–6173.

240 Aguilar, V., Annicotte, J.-S., Escote, X., Vendrell, J., Langin, D. and Fajas, L. (2010) Cyclin G2 regulates adipogenesis through PPAR gamma coactivation. Endocrinology **151**, 5247–54.

241 Sarruf, D. A., Iankova, I., Abella, A., Assou, S., Miard, S. and Fajas, L. (2005) Cyclin D3 Promotes Adipogenesis through Activation of Peroxisome Proliferator-Activated Receptor γ. Mol Cell Biol **25**, 9985–9995.

242 Fiszbein, A. and Kornblihtt, A. R. (2017) Alternative splicing switches: Important players in cell differentiation. Bioessays **39**.

243 Zhou, Z. and Fu, X.-D. (2013) Regulation of splicing by SR proteins and SR protein-specific kinases. Chromosoma **122**, 191–207.

244 Roscigno, R. F. and Garcia-Blanco, M. A. (1995) SR proteins escort the U4/U6.U5 tri-snRNP to the spliceosome. RNA **1**, 692–706.

245 Colwill, K., Pawson, T., Andrews, B., Prasad, J., Manley, J. L., Bell, J. C. and Duncan, P. I. (1996) The Clk/Sty protein kinase phosphorylates SR splicing factors and regulates their intranuclear distribution. EMBO J **15**, 265–275.

246 Lin, J.-C. (2015) Impacts of Alternative Splicing Events on the Differentiation of Adipocytes. Int J Mol Sci **16**, 22169–22189.

247 Dominguez, D., Tsai, Y.-H., Weatheritt, R., Wang, Y., Blencowe, B. J. and Wang, Z. (2016) An extensive program of periodic alternative splicing linked to cell cycle progression. eLife **5**.

248 Ninomiya, K., Kataoka, N. and Hagiwara, M. (2011) Stress-responsive maturation of Clk1/4 pre-mRNAs promotes phosphorylation of SR splicing factor. J Cell Biology **195**, 27–40.

249 Uzor, S., Zorzou, P., Bowler, E., Porazinski, S., Wilson, I. and Ladomery, M. (2018) Autoregulation of the human splice factor kinase CLK1 through exon skipping and intron retention. Gene **670**, 46–54.

250 Muraki, M., Ohkawara, B., Hosoya, T., Onogi, H., Koizumi, J., Koizumi, T., Sumi, K., Yomoda, J., Murray, M. V., Kimura, H., et al. (2004) Manipulation of Alternative Splicing by a Newly Developed Inhibitor of Clks. J Biol Chem **279**, 24246–24254.

251 Yang, H., Chennamaneni, L. R., Ho, M. W. T., Ang, S. H., Tan, E. S. W., Jeyaraj, D. A., Yeap, Y. S., Liu, B., Ong, E. H., Joy, J. K., et al. (2018) Optimization of Selective Mitogen-Activated Protein Kinase Interacting Kinases 1 and 2 Inhibitors for the Treatment of Blast Crisis Leukemia. J Med Chem **61**, 4348–4369.

252 Falchook, G. S., Infante, J. R., Meric-Bernstam, F., Miller, L. L., Morison, K., Vallner, D., Sperry, S., Goel, V., Chiang, G. G., Webster, K., et al. (2017) A phase 1 dose escalation study of eFT508, an inhibitor of mitogen-activated protein kinase-interacting serine/threonine kinase-1 (MNK-1) and MNK-2 in patients with advanced solid tumors. J Clin Oncol **35**, 2579–2579.

253 Reusch, J. E. B., Colton, L. A. and Klemm, D. J. (2000) CREB Activation Induces Adipogenesis in 3T3-L1 Cells. Mol Cell Biol **20**, 1008–1020.

254 Park, Y.-K. and Ge, K. (2017) Glucocorticoid Receptor Accelerates, but Is Dispensable for, Adipogenesis. Mol Cell Biol **37**.

255 Guo, Z., Peng, G., Li, E., Xi, S., Zhang, Y., Li, Y., Lin, X., Li, G., Wu, Q. and He, J. (2017) MAP kinase-interacting serine/threonine kinase 2 promotes proliferation, metastasis, and predicts poor prognosis in non-small cell lung cancer. Sci Rep **7**, 10612.

256 Chrestensen, C. A., Shuman, J. K., Eschenroeder, A., Worthington, M., Gram, H. and Sturgill, T. W. (2007) MNK1 and MNK2 Regulation in HER2-overexpressing Breast Cancer Lines. J Biol Chem **282**, 4243–4252.

257 Bell, J. B., Eckerdt, F. D., Alley, K., Magnusson, L. P., Hussain, H., Bi, Y., Arslan, A. D., Clymer, J., Alvarez, A. A., Goldman, S., et al. (2016) MNK Inhibition Disrupts Mesenchymal Glioma Stem Cells and Prolongs Survival in a Mouse Model of Glioblastoma. Mol Cancer Res **14**, 984–993.

258 Nichols, M., Weih, F., Schmid, W., DeVack, C., Kowenz-Leutz, E., Luckow, B., Boshart, M. and Schütz, G. (1992) Phosphorylation of CREB affects its binding to high and low affinity sites: implications for cAMP induced gene transcription. EMBO J **11**, 3337–3346.

259 Sibinga, N. E. S., Wang, H., Perrella, M. A., Endege, W. O., Patterson, C., Yoshizumi, M., Haber, E. and Lee, M.-E. (1999) Interferon-γ-mediated Inhibition of Cyclin A Gene Transcription Is Independent of Individual cis-Acting Elements in the Cyclin A Promoter. J Biol Chem **274**, 12139–12146.

260 Tommasi, S. and Pfeifer, G. P. (1999) In Vivo Structure of Two Divergent Promoters at the Human PCNA Locus. J Biol Chem **274**, 27829–27838.

261 Dey, A., Nebert, D. W. and Ozato, K. (1991) The AP-1 Site and the cAMP- and Serum Response Elements of the c-fos Gene Are Constitutively Occupied In Vivo. DNA Cell Biol **10**, 537–544.

262 Wölfl, S., Martinez, C. and Majzoub, J. A. (1999) Inducible Binding of Cyclic Adenosine 3′,5′-Monophosphate (cAMP)-Responsive Element Binding Protein (CREB) to a cAMP-Responsive Promoter in Vivo. Mol Endocrinol **13**, 659–669.

263 Campos, S. P. and Baumann, H. (1992) Insulin is a prominent modulator of the cytokine-stimulated expression of acute-phase plasma protein genes. Mol Cell Biol **12**, 1789–1797.

264 Yang, H., Mammen, J., Wei, W., Menconi, M., Evenson, A., Fareed, M., Petkova, V. and Hasselgren, P. (2005) Expression and activity of C/EBPβ and δ are upregulated by dexamethasone in skeletal muscle. J Cell Physiol **204**, 219–226.

265 Matsuno, F., Chowdhury, S., Gotoh, T., Iwase, K., Matsuzaki, H., Takatsuki, K., Mori, M. and Takiguchi, M. (1996) Induction of the C/EBP Gene by Dexamethasone and Glucagon in Primary-Cultured Rat Hepatocytes. J Biochem **119**, 524–532.

266 Tönjes, R. R., Xanthopoulos, K. G., Darnell, J. E. and Paul, D. (1992) Transcriptional control in hepatocytes of normal and c14CoS albino deletion mice. EMBO J **11**, 127–133.

267 Lamph, W. W., Dwarki, V. J., Ofir, R., Montminy, M. and Verma, I. M. (1990) Negative and positive regulation by transcription factor cAMP response element-binding protein is modulated by phosphorylation. PNAS **87**, 4320–4324.

268 Liu, N., Wei, K., Xun, Y., Yang, X., Gan, S., Xiao, H., Xiao, Y., Yan, F., Xie, G., Wang, T., et al. (2015) Transcription factor cyclic adenosine monophosphate responsive element binding protein negatively regulates tumor necrosis factor alpha-induced protein 1 expression. Mol Med Rep **12**, 7763–7769.

269 Wang, G., Cheng, Z., Liu, F., Zhang, H., Li, J. and Li, F. (2015) CREB is a key negative regulator of carbonic anhydrase IX (CA9) in gastric cancer. Cell Signal **27**, 1369–1379.

270 Chen, W.-K., Kuo, W.-W., Hsieh, D. J.-Y., Chang, H.-N., Pai, P.-Y., Lin, K.-H., Pan, L.-F., Ho, T.-J., Viswanadha, V. P. and Huang, C.-Y. (2015) CREB Negatively Regulates IGF2R Gene Expression and Downstream Pathways to Inhibit Hypoxia-Induced H9c2 Cardiomyoblast Cell Death. Int J Mol Sci **16**, 27921–27930.

271 Johannessen, M., Delghandi, M. P. and Moens, U. (2004) What turns CREB on? Cell Signal **16**, 1211–1227.

272 Naqvi, S., Martin, K. J. and Arthur, J. S. C. (2014) CREB phosphorylation at Ser 133 regulates transcription via distinct mechanisms downstream of cAMP and MAPK signalling. Biochem J **458**, 469–479.

273 Parra-Palau, J.-L., Scheper, G. C., Wilson, M. L. and Proud, C. G. (2003) Features in the N and C Termini of the MAPK-interacting Kinase Mnk1 Mediate Its Nucleocytoplasmic Shuttling. J Biol Chem **278**, 44197–44204.

274 Sarjeant, K. and Stephens, J. M. (2012) Adipogenesis. Csh Perspect Biol **4**.

275 Isidor, M. S., Winther, S., Basse, A. L., Petersen, M. C. H., Cannon, B., Nedergaard, J. and Hansen, J. B. (2015) An siRNA-based method for efficient silencing of gene expression in mature brown adipocytes. Adipocyte **5**, 175–185.

276 Teodoro, J. S., Rolo, A. P., Carvalho, R. A. and Palmeira, C. M. (2018) P-319 Exploring the role of the bile acid receptor TGR5 in bile acid mediated obesity control: New insights from a CRISPR/Cas9 adipocyte model. Free Radical Bio Med **120**, S141.

277 Helsley, R. N., Sui, Y., Park, S., Liu, Z., Lee, R. G., Zhu, B., Kern, P. A. and Zhou, C. (2016) Targeting IκB kinase β in Adipocyte Lineage Cells for Treatment of Obesity and Metabolic Dysfunctions. Stem Cells **34**, 1883–1895.

278 J, B. and Das, A. (2019) An edible fungi Pleurotus ostreatus inhibits adipogenesis via suppressing expression of PPAR γ and C/EBP α in 3T3-L1 cells: In vitro validation of gene knock out of RNAs in PPAR γ using CRISPR spcas9. Biomed Pharmacother **116**, 109030.

279 Ishijima, Y., Ohmori, S., Uneme, A., Aoki, Y., Kobori, M., Ohida, T., Arai, M., Hosaka, M. and Ohneda, K. (2019) The Gata2 repression during 3T3-L1 preadipocyte differentiation is dependent on a rapid decrease in histone acetylation in response to glucocorticoid receptor activation. Mol Cell Endocrinol **483**, 39–49.

280 Boettcher, M. and McManus, M. T. (2015) Choosing the Right Tool for the Job: RNAi, TALEN, or CRISPR. Mol Cell **58**, 575–85.

281 Cong, L., Ran, F. A., Cox, D., Lin, S., Barretto, R., Habib, N., Hsu, P. D., Wu, X., Jiang, W., Marraffini, L. A., et al. (2013) Multiplex Genome Engineering Using CRISPR/Cas Systems. Science **339**, 819–823.

282 Chen, F., Pruett-Miller, S. M., Huang, Y., Gjoka, M., Duda, K., Taunton, J., Collingwood, T. N., Frodin, M. and Davis, G. D. (2011) High-frequency genome editing using ssDNA oligonucleotides with zinc-finger nucleases. Nat Methods **8**, 753.

283 Bossemeyer, D. (1994) The glycine-rich sequence of protein kinases: a multifunctional element. Trends Biochem Sci **19**, 201–205.

284 Hsu, P. D., Scott, D. A., Weinstein, J. A., Ran, F. A., Konermann, S., Agarwala, V., Li, Y., Fine, E. J., Wu, X., Shalem, O., et al. (2013) DNA targeting specificity of RNA-guided Cas9 nucleases. Nat Biotechnol **31**, nbt.2647.

285 Cho, S. W., Kim, S., Kim, Y., Kweon, J., Kim, H. S., Bae, S. and Kim, J.-S. (2014) Analysis of off-target effects of CRISPR/Cas-derived RNA-guided endonucleases and nickases. Genome Res **24**, 132–141.

286 Fu, Y., Foden, J. A., Khayter, C., Maeder, M. L., Reyon, D., Joung, J. K. and Sander, J. D. (2013) High-frequency off-target mutagenesis induced by CRISPR-Cas nucleases in human cells. Nat Biotechnol **31**, 822–826.

287 Cradick, T. J., Fine, E. J., Antico, C. J. and Bao, G. (2013) CRISPR/Cas9 systems targeting β-globin and CCR5 genes have substantial off-target activity. Nucleic Acids Res **41**, 9584–9592.

288 Pattanayak, V., Lin, S., Guilinger, J. P., Ma, E., Doudna, J. A. and Liu, D. R. (2013) High-throughput profiling of off-target DNA cleavage reveals RNA-programmed Cas9 nuclease specificity. Nat Biotechnol **31**, 839–843.

289 Cho, S. W., Kim, S., Kim, J. M. and Kim, J.-S. (2013) Targeted genome engineering in human cells with the Cas9 RNA-guided endonuclease. Nat Biotechnol **31**, 230.

290 Bolukbasi, M. F., Gupta, A. and Wolfe, S. A. (2016) Creating and evaluating accurate CRISPR-Cas9 scalpels for genomic surgery. Nat Methods **13**, 41–50.

291 Zhang, X.-H., Tee, L. Y., Wang, X.-G., Huang, Q.-S. and Yang, S.-H. (2015) Off-target Effects in CRISPR/Cas9-mediated Genome Engineering. Mol Ther Nucleic Acids **4**, e264.

292 Tseng, H.-C., Lin, H.-J., Gandhi, P. S. S., Wang, C.-Y. and Chen, Y.-H. (2008) Purification and identification of transglutaminase from mouse coagulating gland and its cross-linking activity among seminal vesicle secretion proteins. J Chromatogr B **876**, 198–202.

293 Kim, Y.-H., Lee, J.-R. and Hahn, M.-J. (2018) Regulation of inflammatory gene expression in macrophages by epithelial-stromal interaction 1 (Epsti1). Biochem Bioph Res Co **496**, 778–783.

294 Altarejos, J. Y., Goebel, N., Conkright, M. D., Inoue, H., Xie, J., Arias, C. M., Sawchenko, P. E. and Montminy, M. (2008) The Creb1 coactivator Crtc1 is required for energy balance and fertility. Nat Med **14**, 1112–1117.

295 Rilstone, J. J., Alkhater, R. A. and Minassian, B. A. (2013) Brain Dopamine–Serotonin Vesicular Transport Disease and Its Treatment. New Engl J Medicine **368**, 543–550.

296 Petit, M. M. R., Schoenmakers, E. F. P. M., Huysmans, C., Geurts, J. M. W., Mandahl, N. and Ven, W. J. M. V. de. (1999) LHFP, a Novel Translocation Partner Gene ofHMGICin a Lipoma, Is a Member of a New Family ofLHFP-like Genes. Genomics **57**, 438–441.

297 Huang, C., Guo, J., Liu, S., Shan, Y., Wu, S., Cai, Y. and Yu, L. (2004) Isolation, Tissue Distribution and Prokaryotic Expression of a Novel Human X-linked Gene LHFPL1. DNA Sequence **15**, 299–302.

298 Kinkley, S., Staege, H., Mohrmann, G., Rohaly, G., Schaub, T., Kremmer, E., Winterpacht, A. and Will, H. (2009) SPOC1: a novel PHD-containing protein modulating chromatin structure and mitotic chromosome condensation. J Cell Sci **122**, 2946–2956.

299 Poot, R. A., Dellaire, G., Hülsmann, B. B., Grimaldi, M. A., Corona, D. F. V., Becker, P. B., Bickmore, W. A. and Varga-Weisz, P. D. (2000) HuCHRAC, a human ISWI chromatin remodelling complex contains hACF1 and two novel histone-fold proteins. EMBO J **19**, 3377–3387.

300 Tsurimoto, T., Shinozaki, A., Yano, M., Seki, M. and Enomoto, T. (2005) Human Werner helicase interacting protein 1 (WRNIP1) functions as a novel modulator for DNA polymerase δ. Genes Cells **10**, 13–22.

301 Benitez, A., Liu, W., Palovcak, A., Wang, G., Moon, J., An, K., Kim, A., Zheng, K., Zhang, Y., Bai, F., et al. (2018) FANCA Promotes DNA Double-Strand Break Repair by Catalyzing Single-Strand Annealing and Strand Exchange. Mol Cell **71**, 621-628.e4.

302 Schrank, B. R., Aparicio, T., Li, Y., Chang, W., Chait, B. T., Gundersen, G. G., Gottesman, M. E. and Gautier, J. (2018) Nuclear ARP2/3 drives DNA break clustering for homology-directed repair. Nature **559**, 61–66.

303 Harris, E. N. and Cabral, F. (2019) Ligand Binding and Signaling of HARE/Stabilin-2. Biomol **9**, 273.

304 Kirschner, M. A., Copeland, N. G., Gilbert, D. J., Jenkins, N. A. and Amara, S. G. (1994) Mouse Excitatory Amino Acid Transporter EAAT2: Isolation, Characterization, and Proximity to Neuroexcitability Loci on Mouse Chromosome 2. Genomics **24**, 218–224.

305 Garcés, C., Ruiz-Hidalgo, M. J., Mora, J. F. de, Park, C., Miele, L., Goldstein, J., Bonvini, E., Porrás, A. and Laborda, J. (1997) Notch-1 Controls the Expression of Fatty Acid-activated Transcription Factors and Is Required for Adipogenesis. J Biol Chem **272**, 29729–29734.

306 Nueda, M.-L., González-Gómez, M.-J., Rodríguez-Cano, M.-M., Monsalve, E.-M., Díaz-Guerra, M. J. M., Sánchez-Solana, B., Laborda, J. and Baladrón, V. (2018) DLK proteins modulate NOTCH signaling to influence a brown or white 3T3-L1 adipocyte fate. Sci Rep **8**, 16923.

307 Adikusuma, F., Piltz, S., Corbett, M. A., Turvey, M., McColl, S. R., Helbig, K. J., Beard, M. R., Hughes, J., Pomerantz, R. T. and Thomas, P. Q. (2018) Large deletions induced by Cas9 cleavage. Nature **560**, E8–E9.

308 Yoon, M.-S., Zhang, C., Sun, Y., Schoenherr, C. J. and Chen, J. (2013) Mechanistic target of rapamycin controls homeostasis of adipogenesis. J Lipid Res **54**, 2166–2173.

309 Wu, Z., Xie, Y., Morrison, R. F., Bucher, N. L. and Farmer, S. R. (1998) PPARgamma induces the insulin-dependent glucose transporter GLUT4 in the absence of C/EBPalpha during the conversion of 3T3 fibroblasts into adipocytes. J Clin Invest **101**, 22–32.

310 Madsen, M. S., Siersbæk, R., Boergesen, M., Nielsen, R. and Mandrup, S. (2014) Peroxisome Proliferator-Activated Receptor γ and C/EBPα Synergistically Activate Key Metabolic Adipocyte Genes by Assisted Loading. Mol Cell Biol **34**, 939–954.

311 Siersbæk, R., Nielsen, R. and Mandrup, S. (2012) Transcriptional networks and chromatin remodeling controlling adipogenesis. Trends Endocrinol Metab **23**, 56–64.

312 Han, G.-S. and Carman, G. M. (2010) Characterization of the Human LPIN1-encoded Phosphatidate Phosphatase Isoforms. J Biol Chem **285**, 14628–14638.

313 Donkor, J., Sariahmetoglu, M., Dewald, J., Brindley, D. N. and Reue, K. (2007) Three Mammalian Lipins Act as Phosphatidate Phosphatases with Distinct Tissue Expression Patterns. J Biol Chem **282**, 3450–3457.

314 Péterfy, M., Phan, J., Xu, P. and Reue, K. (2001) Lipodystrophy in the fld mouse results from mutation of a new gene encoding a nuclear protein, lipin. Nat Genet **27**, 121.

315 Péterfy, M., Phan, J. and Reue, K. (2005) Alternatively Spliced Lipin Isoforms Exhibit Distinct Expression Pattern, Subcellular Localization, and Role in Adipogenesis. J Biol Chem **280**, 32883–32889.

316 Raj, A. and Oudenaarden, A. van. (2008) Nature, Nurture, or Chance: Stochastic Gene Expression and Its Consequences. Cell **135**, 216–226.

317 Eldar, A. and Elowitz, M. B. (2010) Functional roles for noise in genetic circuits. Nature **467**, 167.

318 Phan, J., Péterfy, M. and Reue, K. (2004) Lipin Expression Preceding Peroxisome Proliferator-activated Receptor-γ Is Critical for Adipogenesis in Vivo and in Vitro. J Biol Chem **279**, 29558–29564.

319 Jung, S. M., Sanchez-Gurmaches, J. and Guertin, D. A. (2018) Brown Adipose Tissue Development and Metabolism. Hand Exp Pharmacol 3–36.

320 Neufeld, B., Große-Wilde, A., Hoffmeyer, A., Jordan, B. W., Chen, P., Dinev, D., Ludwig, S. and Rapp, U. R. (2000) The serine/threonine kinases 3pK and MAPKAP kinase 2 interact with the basic HLH transcription factor E47 and repress its transcriptional activity. J Biol Chem **275**, 20239–20242.

321 Hu, S., Xie, Z., Onishi, A., Yu, X., Jiang, L., Lin, J., Rho, H., Woodard, C., Wang, H., Jeong, J.-S., et al. (2009) Profiling the human protein-DNA interactome reveals ERK2 as a transcriptional repressor of interferon signaling. Cell **139**, 610–22.

322 Rodríguez, J., Calvo, F., José, González, M., Casar, B., Andrés, V. and Crespo, P. (2010) ERK1/2 MAP kinases promote cell cycle entry by rapid, kinase-independent disruption of retinoblastoma-lamin A complexes. J Cell Biology **191**, 967–79.

323 Camps, M., Nichols, A., Gillieron, C., Antonsson, B., Muda, M., Chabert, C., Boschert, U. and Arkinstall, S. (1998) Catalytic Activation of the Phosphatase MKP-3 by ERK2 Mitogen-Activated Protein Kinase. Science **280**, 1262–1265.

324 Kotlyarov, A., Yannoni, Y., Fritz, S., Laass, K., Telliez, J.-B., Pitman, D., Lin, L.-L. and Gaestel, M. (2002) Distinct Cellular Functions of MK2. Mol Cell Biol **22**, 4827–4835.

325 Lehner, R. and Quiroga, A. D. (2016) Biochemistry of Lipids, Lipoproteins and Membranes (Sixth Edition), pp 149–184.

326 Yore, M. M., Syed, I., Moraes-Vieira, P. M., Zhang, T., Herman, M. A., Homan, E. A., Patel, R. T., Lee, J., Chen, S., Peroni, O. D., et al. (2014) Discovery of a class of endogenous mammalian lipids with anti-diabetic and anti-inflammatory effects. Cell **159**, 318–32.

327 Vijayakumar, A., Aryal, P., Wen, J., Syed, I., Vazirani, R. P., Moraes-Vieira, P. M., Camporez, J. P., Gallop, M. R., Perry, R. J., Peroni, O. D., et al. (2017) Absence of Carbohydrate Response Element Binding Protein in Adipocytes Causes Systemic Insulin Resistance and Impairs Glucose Transport. Cell Reports **21**, 1021–1035.

328 Frühbeck, G., Méndez-Giménez, L., Fernández-Formoso, J.-A., Fernández, S. and Rodríguez, A. (2014) Regulation of adipocyte lipolysis. Nutr Res Rev **27**, 63–93.

329 Forest, C., Tordjman, J., Glorian, M., Duplus, E., Chauvet, G., Quette, J., Beale, E. G. and Antoine, B. (2003) Fatty acid recycling in adipocytes: a role for glyceroneogenesis and phosphoenolpyruvate carboxykinase. Biochem Soc Trans **31**, 1125–1129.

330 Wang, H., Airola, M. V. and Reue, K. (2017) How lipid droplets “TAG” along: Glycerolipid synthetic enzymes and lipid storage. BBA Mol Cell Biol Lipids **1862**, 1131–1145.

331 Cao, J., Li, J.-L., Li, D., Tobin, J. F. and Gimeno, R. E. (2006) Molecular identification of microsomal acyl-CoA:glycerol-3-phosphate acyltransferase, a key enzyme in de novo triacylglycerol synthesis. PNAS **103**, 19695–19700.

332 Liu, Q., Siloto, R. M. P., Lehner, R., Stone, S. J. and Weselake, R. J. (2012) Acyl-CoA:diacylglycerol acyltransferase: molecular biology, biochemistry and biotechnology. Prog Lipid Res **51**, 350–77.

333 Cao, H. (2018) Identification of the major diacylglycerol acyltransferase mRNA in mouse adipocytes and macrophages. BMC Biochem **19**, 11.

334 Kajimoto, K., Suemitsu, E., Sato, Y., Sakurai, Y. and Harashima, H. (2016) Liver-Specific Silencing of Lipin1 Reduces Fat Mass as Well as Hepatic Triglyceride Biosynthesis in Mice. Biological Pharm Bulletin **39**, 1653–1661.

335 Castle, J. C., Hara, Y., Raymond, C. K., Garrett-Engele, P., Ohwaki, K., Kan, Z., Kusunoki, J. and Johnson, J. M. (2009) ACC2 is expressed at high levels in human white adipose and has an isoform with a novel N-terminus [corrected]. PLoS One **4**, e4369.

336 Abu-Elheiga, L., Brinkley, W. R., Zhong, L., Chirala, S. S., Woldegiorgis, G. and Wakil, S. J. (2000) The subcellular localization of acetyl-CoA carboxylase 2. PNAS **97**, 1444–1449.

337 Abu-Elheiga, L., Oh, W., Kordari, P. and Wakil, S. J. (2003) Acetyl-CoA carboxylase 2 mutant mice are protected against obesity and diabetes induced by high-fat/high-carbohydrate diets. PNAS **100**, 10207–10212.

338 Cheng, C.-F., Ku, H.-C. and Lin, H. (2018) PGC-1α as a Pivotal Factor in Lipid and Metabolic Regulation. Int J Mol Sci **19**, 3447.

339 Kimmel, A. R. and Sztalryd, C. (2016) The Perilipins: Major Cytosolic Lipid Droplet–Associated Proteins and Their Roles in Cellular Lipid Storage, Mobilization, and Systemic Homeostasis. Annu Rev Nutr **36**, 471–509.

340 Chang, C. L. (2019) Lipoprotein lipase. Curr Opin Clin Nutr **22**, 111–115.

341 Ibrahimi, A. and Abumrad, N. A. (2002) Role of CD36 in membrane transport of long-chain fatty acids. Curr Opin Clin Nutr **5**, 139–145.

342 Reshef, L., Olswang, Y., Cassuto, H., Blum, B., Croniger, C. M., Kalhan, S. C., Tilghman, S. M. and Hanson, R. W. (2003) Glyceroneogenesis and the Triglyceride/Fatty Acid Cycle. J Biol Chem **278**, 30413–30416.

343 Ballard, F. J., Hanson, R. W. and Leveille, G. A. (1967) Phosphoenolpyruvate carboxykinase and the synthesis of glyceride-glycerol from pyruvate in adipose tissue. J Biol Chem **242**, 2746–50.

344 Foufelle, F., Gouhot, B., Perdereau, D., Girard, J. and Ferre, P. (1994) Regulation of lipogenic enzyme and phosphoenolpyruvate carboxykinase gene expression in cultured white adipose tissue. Eur J Biochem **223**, 893–900.

345 Huang, S. and Czech, M. P. (2007) The GLUT4 Glucose Transporter. Cell Metab **5**, 237–252.

346 Girard, J., Ferré, P. and Foufelle, F. (1997) Mechanisms by which carbohydrates regulate expression of genes for glycolytic and lipogenic enzymes. Ann Rev Nutr **17**, 325–352.

347 Shestov, A. A., Liu, X., Ser, Z., Cluntun, A. A., Hung, Y. P., Huang, L., Kim, D., Le, A., Yellen, G., Albeck, J. G., et al. (2014) Quantitative determinants of aerobic glycolysis identify flux through the enzyme GAPDH as a limiting step. eLife **3**, e03342.

348 Kim, J. B. and Spiegelman, B. M. (1996) ADD1/SREBP1 promotes adipocyte differentiation and gene expression linked to fatty acid metabolism. Gene Dev **10**, 1096–1107.

349 Kim, J. B., Wright, H. M., Wright, M. and Spiegelman, B. M. (1998) ADD1/SREBP1 activates PPARγ through the production of endogenous ligand. PNAS **95**, 4333–4337.

350 Sul, H. S., Latasa, M.-J., Moon, Y. and Kim, K.-H. (2000) Regulation of the Fatty Acid Synthase Promoter by Insulin. J Nutrition **130**, 315S-320S.

351 Abdul-Wahed, A., Guilmeau, S. and Postic, C. (2017) Sweet Sixteenth for ChREBP: Established Roles and Future Goals. Cell Metab **26**, 324–341.

352 He, Z., Jiang, T., Wang, Z., Levi, M. and Li, J. (2004) Modulation of carbohydrate response element-binding protein gene expression in 3T3-L1 adipocytes and rat adipose tissue. Am J Physiol-Endoc Met **287**, E424–E430.

353 Pozo, C. H. del, Vesperinas-García, G., Rubio, M.-Á., Corripio-Sánchez, R., Torres-García, A. J., Obregon, M.-J. and Calvo, R. M. (2011) ChREBP expression in the liver, adipose tissue and differentiated preadipocytes in human obesity. Biochimica Et Biophysica Acta Bba - Mol Cell Biology Lipids **1811**, 1194–1200.

354 Witte, N., Muenzner, M., Rietscher, J., Knauer, M., Heidenreich, S., Nuotio-Antar, A. M., Graef, F. A., Fedders, R., Tolkachov, A., Goehring, I., et al. (2015) The Glucose Sensor ChREBP Links De Novo Lipogenesis to PPARγ Activity and Adipocyte Differentiation. Endocrinology **156**, 4008–4019.

355 Christodoulides, C., Lagathu, C., Sethi, J. K. and Vidal-Puig, A. (2009) Adipogenesis and WNT signalling. Trends Endocrinol Metabolism **20**, 16–24.

356 Mori, H., Prestwich, T. C., Reid, M. A., Longo, K. A., Gerin, I., Cawthorn, W. P., Susulic, V. S., Krishnan, V., Greenfield, A. and Macdougald, O. A. (2012) Secreted frizzled-related protein 5 suppresses adipocyte mitochondrial metabolism through WNT inhibition. J Clin Investigation **122**, 2405–16.

357 Ouchi, N., Higuchi, A., Ohashi, K., Oshima, Y., Gokce, N., Shibata, R., Akasaki, Y., Shimono, A. and Walsh, K. (2010) Sfrp5 is an anti-inflammatory adipokine that modulates metabolic dysfunction in obesity. Science **329**, 454–7.

358 Koza, R. A., Nikonova, L., Hogan, J., Rim, J.-S., Mendoza, T., Faulk, C., Skaf, J. and Kozak, L. P. (2006) Changes in Gene Expression Foreshadow Diet-Induced Obesity in Genetically Identical Mice. PLoS Genet **2**, e81.

359 Lagathu, C., Christodoulides, C., Virtue, S., Cawthorn, W. P., Franzin, C., Kimber, W. A., Nora, E. D., Campbell, M., Medina-Gomez, G., Cheyette, B. N. R., et al. (2008) Dact1, a nutritionally regulated preadipocyte gene, controls adipogenesis by coordinating the Wnt/beta-catenin signaling network. Diabetes **58**, 609–19.

360 Wang, R., Hong, J., Liu, R., Chen, M., Xu, M., Gu, W., Zhang, Y., Ma, Q., Wang, F., Shi, J., et al. (2014) SFRP5 acts as a mature adipocyte marker but not as a regulator in adipogenesis. J Mol Endocrinol **53**, 405–415.

361 Okada, Y., Sakaue, H., Nagare, T. and Kasuga, M. (2009) Diet-induced up-regulation of gene expression in adipocytes without changes in DNA methylation. Kobe J Medical Sci **54**, E241-9.

362 Hall, A. M., Brunt, E. M., Chen, Z., Viswakarma, N., Reddy, J. K., Wolins, N. E. and Finck, B. N. (2010) Dynamic and differential regulation of proteins that coat lipid droplets in fatty liver dystrophic mice. J Lipid Res **51**, 554–563.

363 Souza, S. C., Vargas, L. M. de, Yamamoto, M. T., Lien, P., Franciosa, M. D., Moss, L. G. and Greenberg, A. S. (1998) Overexpression of Perilipin A and B Blocks the Ability of Tumor Necrosis Factor α to Increase Lipolysis in 3T3-L1 Adipocytes. J Biol Chem **273**, 24665–24669.

364 Poungvarin, N., Chang, B., Imamura, M., Chen, J., Moolsuwan, K., Sae-Lee, C., Li, W. and Chan, L. (2015) Genome-Wide Analysis of ChREBP Binding Sites on Male Mouse Liver and White Adipose Chromatin. Endocrinology **156**, 1982–94.

365 Nuotio-Antar, A. M., Poungvarin, N., Li, M., Schupp, M., Mohammad, M., Gerard, S., Zou, F. and Chan, L. (2015) FABP4-Cre Mediated Expression of Constitutively Active ChREBP Protects Against Obesity, Fatty Liver, and Insulin Resistance. Endocrinology **156**, 4020–32.

366 Ortega-Prieto, P. and Postic, C. (2019) Carbohydrate Sensing Through the Transcription Factor ChREBP. Frontiers Genetics **10**, 472.

367 Jeong, Y.-S., Kim, D., Lee, Y. S., Kim, H.-J., Han, J.-Y., Im, S.-S., Chong, H. K., Kwon, J.-K., Cho, Y.-H., Kim, W. K., et al. (2011) Integrated Expression Profiling and Genome-Wide Analysis

of ChREBP Targets Reveals the Dual Role for ChREBP in Glucose-Regulated Gene Expression. PLoS One **6**, e22544.

368 Shin, E., Bae, J.-S., Han, J.-Y., Lee, J., Jeong, Y.-S., Lee, H.-J., Ahn, Y.-H. and Cha, J.-Y. (2016) Hepatic DGAT2 gene expression is regulated by the synergistic action of ChREBP and SP1 in HepG2 cells. Anim Cells Syst **20**, 7–14.

369 Herman, M. A., Peroni, O. D., Villoria, J., Schön, M. R., Abumrad, N. A., Blüher, M., Klein, S. and Kahn, B. B. (2012) A novel ChREBP isoform in adipose tissue regulates systemic glucose metabolism. Nature **484**, 333.

370 Holness, M. J. and Sugden, M. C. (2003) Regulation of pyruvate dehydrogenase complex activity by reversible phosphorylation. Biochem Soc T **31**, 1143–1151.

371 Morigny, P., Houssier, M., Mairal, A., Ghilain, C., Mouisel, E., Benhamed, F., Masri, B., Recazens, E., Denechaud, P.-D., Tavernier, G., et al. (2018) Interaction between hormone-sensitive lipase and ChREBP in fat cells controls insulin sensitivity. Nat Metabolism **1**, 1.

372 Shih, H.-M., Liu, Z. and Towle, H. C. (1995) Two CACGTG Motifs with Proper Spacing Dictate the Carbohydrate Regulation of Hepatic Gene Transcription. J Biol Chem **270**, 21991–21997.

373 Ishii, S., IIzuka, K., Miller, B. C. and Uyeda, K. (2004) Carbohydrate response element binding protein directly promotes lipogenic enzyme gene transcription. PNAS **101**, 15597–15602.

374 Noordeen, N. A., Khera, T. K., Sun, G., Longbottom, E. R., Pullen, T. J., Xavier, G. da S., Rutter, G. A. and Leclerc, I. (2010) Carbohydrate-Responsive Element-Binding Protein (ChREBP) Is a Negative Regulator of ARNT/HIF-1β Gene Expression in Pancreatic Islet β-Cells. Diabetes **59**, 153–160.

375 Szklarczyk, D., Morris, J. H., Cook, H., Kuhn, M., Wyder, S., Simonovic, M., Santos, A., Doncheva, N. T., Roth, A., Bork, P., et al. (2016) The STRING database in 2017: quality-controlled protein-protein association networks, made broadly accessible. Nucleic Acids Res **45**, D362–D368.

376 Li, H., Cheng, Y., Wu, W., Liu, Y., Wei, N., Feng, X., Xie, Z. and Feng, Y. (2014) SRSF10 Regulates Alternative Splicing and Is Required for Adipocyte Differentiation. Mol Cell Biol **34**, 2198–2207.

377 Kamenski, T., Heilmeier, S., Meinhart, A. and Cramer, P. (2004) Structure and Mechanism of RNA Polymerase II CTD Phosphatases. Mol Cell **15**, 399–407.

378 Hirose, Y. and Manley, J. L. (2000) RNA polymerase II and the integration of nuclear events. Gene Dev **14**, 1415–29.

379 Pilch, P. F. and Liu, L. (2011) Fat caves: caveolae, lipid trafficking and lipid metabolism in adipocytes. Trends Endocrinol Metab **22**, 318–24.

380 Ding, S.-Y., Lee, M.-J., Summer, R., Liu, L., Fried, S. K. and Pilch, P. F. (2014) Pleiotropic effects of cavin-1 deficiency on lipid metabolism. J Biol Chem **289**, 8473–83.

381 Rosenthal, J. A., Chen, H., Slepnev, V. I., Pellegrini, L., Salcini, A. E., Fiore, P. P. D. and Camilli, P. D. (1999) The Epsins Define a Family of Proteins That Interact with Components of the Clathrin Coat and Contain a New Protein Module. J Biol Chem **274**, 33959–33965.

382 Ko, G., Paradise, S., Chen, H., Graham, M., Vecchi, M., Bianchi, F., Cremona, O., Fiore, P. P. D. and Camilli, P. D. (2010) Selective high-level expression of epsin 3 in gastric parietal cells, where it is localized at endocytic sites of apical canaliculi. PNAS **107**, 21511–6.

383 Dell'Angelica, E. C. (2009) AP-3-dependent trafficking and disease: the first decade. Curr Opin Cell Biol **21**, 552–9.

384 Melino, G., Gallagher, E., Aqeilan, R. I., Knight, R., Peschiaroli, A., Rossi, M., Scialpi, F., Malatesta, M., Zocchi, L., Browne, G., et al. (2008) Itch: a HECT-type E3 ligase regulating immunity, skin and cancer. Cell Death Differ **15**, 1103–12.

385 Marino, A., Menghini, R., Fabrizi, M., Casagrande, V., Mavilio, M., Stoehr, R., Candi, E., Mauriello, A., Moreno-Navarrete, J. M., Gomez-Serrano, M., et al. (2013) ITCH Deficiency Protects From Diet-Induced Obesity. Diabetes **63**, 550–561.

386 Regard, J. B., Scheek, S., Borbiev, T., Lanahan, A. A., Schneider, A., Demetriades, A.-M., Hiemisch, H., Barnes, C. A., Verin, A. D. and Worley, P. F. (2004) Verge: A Novel Vascular Early Response Gene. J Neurosci **24**, 4092–4103.

387 Olswang, Y., Cohen, H., Papo, O., Cassuto, H., Croniger, C. M., Hakimi, P., Tilghman, S. M., Hanson, R. W. and Reshef, L. (2002) A mutation in the peroxisome proliferator-activated receptor -binding site in the gene for the cytosolic form of phosphoenolpyruvate carboxykinase reduces adipose tissue size and fat content in mice. PNAS **99**, 625–630.

388 Abu-Elheiga, L., Matzuk, M. M., Abo-Hashema, K. A. H. and Wakil, S. J. (2001) Continuous Fatty Acid Oxidation and Reduced Fat Storage in Mice Lacking Acetyl-CoA Carboxylase 2. Science **291**, 2613–2616.

389 Reue, K. and Zhang, P. (2007) The lipin protein family: Dual roles in lipid biosynthesis and gene expression. Febs Lett **582**, 90–96.

390 Betz, M. J. and Enerbäck, S. (2017) Targeting thermogenesis in brown fat and muscle to treat obesity and metabolic disease. Nat Rev Endocrinol **14**, 77–87.

391 Iizuka, K., Bruick, R. K., Liang, G., Horton, J. D. and Uyeda, K. (2004) Deficiency of carbohydrate response element-binding protein (ChREBP) reduces lipogenesis as well as glycolysis. PNAS **101**, 7281–7286.

392 Yamashita, H., Takenoshita, M., Sakurai, M., Bruick, R. K., Henzel, W. J., Shillinglaw, W., Arnot, D. and Uyeda, K. (2001) A glucose-responsive transcription factor that regulates carbohydrate metabolism in the liver. PNAS **98**, 9116–9121.

393 Ma, L., Tsatsos, N. G. and Towle, H. C. (2005) Direct Role of ChREBP-Mlx in Regulating Hepatic Glucose-responsive Genes. J Biol Chem **280**, 12019–12027.

394 Uyeda, K. and Repa, J. J. (2006) Carbohydrate response element binding protein, ChREBP, a transcription factor coupling hepatic glucose utilization and lipid synthesis. Cell Metab **4**, 107–110.

395 Ma, L., Robinson, L. N. and Towle, H. C. (2006) ChREBP-Mlx Is the Principal Mediator of Glucose-induced Gene Expression in the Liver. J Biol Chem **281**, 28721–28730.

396 Sharabi, K., Tavares, C. D. J., Rines, A. K. and Puigserver, P. (2015) Molecular pathophysiology of hepatic glucose production. Mol Aspects Med **46**, 21–33.